ROBUST ADAPTIVE CONTROL FOR A CLASS OF NONLINEAR SYSTEMS WITH UNCERTAINTIES OF UNKNOWN BOUNDS

COMMANDE ROBUSTE ADAPTATIVE POUR UNE CLASSE DE SYSTÈMES NON LINÉAIRES AVEC DES INCERTITUDES DE BORNES INCONNUES

A Thesis Submitted to the Division of Graduate Studies
of the Royal Military College of Canada
by

Jiang Zhu, B.Eng., M.A.Sc.

In Partial Fulfillment of the Requirements for the Degree of
Doctor of Philosophy in Mechanical and Aerospace Engineering

November, 2016

Acknowledgments

I am very grateful to my supervisor Professor Karim Khayati. Thank you for your guidance, support and patience for the research work reported in this thesis.

I would also like to acknowledge the assistance of my colleagues and friends Debbie Fisher, Peter Jansen and Yingchun Bai. Thank you for your critical help and advice.

My foremost thanks goes to my family, my wife, my lovely daughters, my parents and my sister for their encouragement and support throughout my studies.

Abstract

Zhu, Jiang Ph.D. student, Royal Military College of Canada, September 2016. *Robust Adaptive Control for a Class of Nonlinear Systems with Uncertainties of Unknown Bounds*. Supervised by Dr. Karim Khayati, Ph.D., P.Eng., Associate Professor.

Although linear control theory has been applied in industry successfully over a long period, it has been found to be inadequate in many physical systems having nonlinear properties such as friction, hysteresis, backlash, and saturation. To deal with the nonlinear systems with uncertainties of unknown bounds, adaptive sliding mode control (ASMC) techniques with integral and modified integral adaptation law have been introduced during the past two decades. However, the integral type adaptation laws have a weakness that they can not achieve fast response to the uncertainties and lower chattering simultaneously.

The dissertation first reviews the general idea of ASMC techniques for nonlinear systems with uncertainties of unknown bounds. The necessary and sufficient conditions are discussed. It shows that any positive definite monotonic function of the sliding variable can be used in the integral adaptation law. Moreover, a special type of function is proposed to smooth the chattering.

The dissertation then investigates the convergence and boundedness in the existing classic ASMC techniques. By applying a new Lyapunov method and a new majorant curve approach, it successfully proves the finite-time convergence (FTC) of the sliding variable and uniformly ultimately bounded (UUB) convergence of the switching gain. Moreover, it deduces a new formula for reaching time estimation (RTE). The new RTE shows the relationship that the reaching time is inversely proportional to the square root of the designed integral parameter. The explicit relationship indicates that the classic ASMC techniques cannot achieve fast response and lower chattering simultaneously. Thus, it reveals the inherent reason of the slow response existing in the classic ASMC techniques with integral adaptation laws.

In order to thoroughly resolve the trade-offs involved in system response to the uncertainties and chattering attenuation, a new adaptation law, integral-exponential reaching law, of first order ASMC for nonlinear uncertain systems of uncertainties is proposed. The new algorithm combines the classic integral reaching law with an exponential term. With the newly added exponential term, the system responds to the uncertainties quickly. Moreover, it reduces the final switching gain. Thus, the lower chattering level is achieved simultaneously. Moreover, the new design can deal with the uncertainties bounded with not only unknown constant bounds but also polynomial bounds in the norm of the states.

Illustrative simulations are provided to help understand the existing and the proposed ASMC adaptation processes. The proposed designs are then numerically verified upon different real nonlinear dynamic systems such as a variable-length pendulum, a two-degree-of-freedom (2-DOF) experimental helicopter and a 5-DOF robotic manipulator. Moreover, the experiments are conducted on the 2-DOF experimental helicopter-model-based setup to compare the proposed designs with the existing ASMC designs and the common proportional-integral-derivative (PID) designs. Both numerical and experimental results show that the new proposed ASMC designs for nonlinear dynamic systems with uncertainties of unknown bounds can significantly improve the robustness of the systems and reduce the chattering level compared to currently existing ASMC designs.

Keywords: nonlinear systems, uncertainties of unknown bounds, adaptive sliding mode control, integral-exponential adaptation law, robustness, reaching time estimation, chattering attenuation.

Résumé

Jiang Zhu, doctorant, collège militaire royal du Canada, septembre 2016. Commande robuste adaptative pour une classe de systèmes non linéaires avec des incertitudes de bornes inconnues. Supervisé par M. Karim Khayati, Ph.D., P.Eng., Professeur agrégé.

Bien que la théorie de commande linéaire a été appliquée avec succès dans l'industrie longtemps, elle a été jugée insuffisante dans de nombreux systèmes physiques ayant des propriétés non linéaires tels que le frottement, l'hystérésis, le jeu, et la saturation. Pour faire face aux systèmes non linéaires avec des incertitudes de limites inconnues, des techniques de commande par mode de glissement adaptatif (CMGA) avec des lois d'adaptations intégrales simplifiées et modifiées ont été introduites durant les deux dernières décennies. Cependant, les lois d'adaptation de type intégral ont des faiblesses; elles ne peuvent pas garantir une réponse rapide aux incertitudes et des niveaux de bruit bas simultanément.

La présente thèse examine d'abord l'idée générale des techniques de CMGA appliquées aux systèmes non linéaires avec des incertitudes de limites inconnues. Les conditions nécessaires et suffisantes sont discutées. On montre que toute fonction définie positive monotone par rapport à la variable de glissement peut être utilisée dans la loi d'adaptation intégrale. En plus, un type de fonctions est proposé pour atténuer le niveau de bruit.

La thèse étudie par la suite la convergence et bornitude dans les techniques classiques existantes de CMGA. En appliquant une nouvelle méthode de Lyapunov et une nouvelle approche de la courbe de majorants, on prouve avec succès la convergence à temps finie de la variable de glissement et de celle uniformément bornée du gain de commutation . En outre, on déduit une nouvelle formule pour évaluer l'estimation du temps convergence (ETC). La nouvelle relation d'ETC montre que cette durée est inversement proportionnelle à la racine carrée du paramètre d'adaptation choisi. La relation explicite indique que les techniques classiques de CMGA ne peuvent pas obtenir une réponse

rapide et des niveaux de bruits réduits simultanément. Ainsi, cette thèse révèle la raison intrinsèque de la réponse lente existant dans les techniques de CMGA classiques avec les lois d'adaptation intégrale.

Afin de résoudre complètement les compromis impliqués dans la réponse des systèmes incertains et l'atténuation des bruits, une nouvelle loi d'adaptation, dite intégral/exponentielle, pour la classe de CMGA de premier ordre pour les systèmes non linéaires incertains, est proposée. Le nouvel algorithme combine la loi d'adaptation intégrale classique avec un terme exponentiel. Avec la composante exponentielle nouvellement ajoutée, le système répond aux incertitudes plus rapidement tout en réduisant le gain de commutation final. En plus, le niveau de bruit dans la commande proposée est inférieur à ceux réalisé avec les anciennes approches. En outre, la nouvelle conception peut faire face aux incertitudes limitées non seulement avec les limites constantes inconnues, mais aussi des limites à base de polynômes.

Des simulations simplifiées, pour illustrer et comprendre le processus d'adaptation des CMGA existants et proposés, sont fournies. Les conceptions proposées sont ensuite numériquement vérifiées sur des systèmes dynamiques non linéaires réels différents, comme un pendule de longueur variable, un modèle à deux degrés de liberté (2-ddl) d'hélicoptère expérimental et un modèle de robot manipulateur à 5-ddl. Finalement, des expériences réelles sont menées sur le modèle simulateur à 2-ddl d'hélicoptère expérimental comparant les résultats de l'approche proposé avec la principale méthode de CMGA existante et la commande PID conventionnelle. Les deux résultats numériques et expérimentaux montrent que la nouvelle approche concept de CMGA conçue pour les systèmes dynamique non linéaires incertains avec des incertitudes des limites inconnues peuvent améliorer considérablement la robustesse du système et réduire le niveau de bruit par rapport aux concepts de CMGA existants actuellement.

Mots-clés : systèmes non linéaires, incertitudes avec des limites inconnues, commande par mode de glissement adaptatif, loi d'adaptation intégrante/exponentielle, robustesse, estimation du temps de convergence, atténuation de bruit.

Statement of Contributions

Statement of Contributions

The major contributions of the research work presented in this thesis are summarised as follows:

- *A large class of nonlinear dynamic systems to be stabilized.* Since the proposed ASMC designs aim to stabilize nonlinear systems with uncertainties of unknown bounds not necessarily constant, these systems represent a large class of dynamic systems and are very close to real mechanical dynamic systems. The successful application on a 2-DOF experimental helicopter-based model could be extended to a wide class of nonlinear dynamic systems.

- *Generalization of the adaptation function, smoothing technique.* Based on the analysis of the necessary and sufficient conditions for the classic ASMC designs, the generalization of the adaptation function is found. Moreover, functions for smoothing the chattering phenomenon are proposed.

- *New proofs for the convergence in a UUB sense of the switching gain and FTC of the sliding variable, new formula for RTE and new property characterizing the ASMC action.* The UUB switching gain and the FTC of the sliding variable for the integral-adaptation based ASMC are analysed by identifying the existence of two phases, a *compensating phase* and a *reaching phase* during the adaptation process. A new Lyapunov function and a new majorant curve methods are adopted to prove the FTC property. Moreover, a completely new formula for reaching time estimation is deduced with high accuracy. The new formula also reveals the fact that the conventional integral-type ASMC designs have

an inherent weakness in terms of robustness and chattering level.

- *New ASMC method called integral-exponential adaptation law, with simultaneous robustness and lower chattering.* A new ASMC methodology using an integral-exponential adaptation law is proposed. It perfectly resolves the weakness of the conventional ASMC, *i.e.*, by applying the new algorithm, the robustness to the perturbations and the minimum admissible switching gain (resulting lower level chattering) are achieved simultaneously.

- *New ASMC method for nonlinear systems with uncertainties of unknown polynomial bounds.* The new ASMC algorithm not only can deal with uncertainties of unknown constant bounds, the thesis also proves that the new algorithm is the first ASMC method to deal with uncertainties of unknown polynomial bounds of the norm of the system states.

- Numerical and experimental results successfully demonstrated the discussed properties and the new proposed design.

List of Papers

Peer-Reviewed Journal Papers

1. **Jiang Zhu** and Karim Khayati. Applications of Adaptive Sliding Model Control for Nonlinear Systems with Uncertainties of Unknown Polynomial Bounds. In review in *Transactions of the Institute of Measurement and Control*, 2016.

2. Karim Khayati and **Jiang Zhu**. Nonlinear Adaptive Observer for Electromechanical Systems – Asymptotic and Exponential Stability Designs. In review in *International Journal of Adaptive Control and Signal Processing*, 2016.

3. **Jiang Zhu** and Karim Khayati. On New Adaptive Sliding Model Control for MIMO Nonlinear Systems with Uncertainties of Unknown Bounds. *International Journal of Robust and Nonlinear Control*, DOI: 10.1002/rnc.3608, 2016.

4. **Jiang Zhu** and Karim Khayati. Adaptive Sliding Mode Control - Convergence and Gain Boundedness Revisited. *International Journal of Control*, 89(4):801-814, 2016.

5. **Jiang Zhu** and Karim Khayati. A New Approach for Adaptive Sliding Model Control – integral-exponential Gain Law. *Transactions of the Institute of Measurement and Control*, 38(4):385-394, 2016.

6. **Jiang Zhu** and Karim Khayati. LMI-based Adaptive Observers for Nonlinear Systems. *International Journal of Mechanical Engineering and Mechatronics*, pages 50-60, 2012. doi:10.11159/ijmem.2012.006.

Conference Papers, Posters and Proceedings

1. **Jiang Zhu** and Karim Khayati. Robust, Smooth and Fast ASMC – Application to Robot Manipulators. *The 24th International Congress of Theoretical and Applied Mechanics (ICTAM 2016)*, Montreal, Quebec, Canada, 2016.

2. **Jiang Zhu** and Karim Khayati. On ASMC Design for Robotic Manipulators. *The 29th Annual IEEE Canadian Conference on Electrical and Computer Engineering (CCECE 2016)*, Vancouver, British Columbia, Canada, 2016.

3. **Jiang Zhu** and Karim Khayati. Application of Adaptive Sliding Mode Control with integral-exponential Adaptation Law to Mechanical Manipulators. *IEEE 3rd International Conference on Control, Decision and Information Technologies*, Malta, 2016.

4. **Jiang Zhu** and Karim Khayati. New Algorithms of Adaptive Switching Gain for Sliding Mode Control: Part II – Real Case. *IEEE 2nd International Conference on Control, Decision and Information Technologies*, pages 447-452, Metz, France, 2014.

5. **Jiang Zhu** and Karim Khayati. New Algorithms of Adaptive Switching Gain for Sliding Mode Control: Part I – Ideal Case. *IEEE 2nd International Conference on Control, Decision and Information Technologies*, pages 441-446, Metz, France, 2014.

6. **Jiang Zhu** and Karim Khayati. Adaptive Sliding Mode Control with Smooth Switching Gain. *The 27th IEEE Canadian Conference on Electrical and Computer Engineering (CCECE2014)*, pages 893-898, Toronto, Canada, 2014.

7. **Jiang Zhu** and Karim Khayati. On Adaptive Sliding Mode Control Switching Gain Comments and Alternative Design. *Proceedings of The Canadian Society for Mechanical Engineering International Congress 2014*, Toronto, Canada, 2014.

8. Karim Khayati and **Jiang Zhu**. Adaptive Observer for a Large Class of Nonlinear System with Exponential Convergence of Parameter Estimation. *2013 International Conference on Control, Decision and Information Technologies*, Hammamet, Tunisia, 2013.

9. Karim Khayati and **Jiang Zhu**. On Exponentially Stable Nonlinear Adaptive Observer. *International Conference on Mechanical Engineering and Mechatronics*, Ottawa, Canada, 2012.

10. **Jiang Zhu** and Karim Khayati. On Robust Nonlinear Adaptive Observer - LMI Design. *International Conference on Mechanical Engineering and Mechatronics*, Ottawa, Canada, 2012.

11. Karim Khayati and **Jiang Zhu**. Nonlinear Adaptive Observer Design for an Electromechanical Rotative Plant. *23rd Canadian Congress of Applied Mechanics*, pages 656-660, Vancouver, Canada, 2011.

12. **Jiang Zhu** and Karim Khayati. Adaptive Observer for a Class of Second Order Nonlinear Systems. *International Conference on Communications, Computing and Control Application*, Hammamet, Tunisia, 2011.

Contents

List of Tables

List of Figures

Nomenclature

ϵ	Thickness of the boundary layer in real adaptive sliding mode control
ϕ	Pitch angle
ψ	Yaw angle
Σ	Ideal sliding surface (or manifold)
σ	Sliding variable
Σ^*	Sliding manifold
Σ_δ	Real sliding manifold
Σ_ϵ	Target sliding manifold
ε	Thickness of the boundary layer in smooth sliding mode control
K	Switching gain
2-DOF	Two-degree-of-freedom
3-D	Three-dimensional
AC	Asymptotic convergence
ADRC	Active disturbance rejection control
AS	Asymptotically stable
ASAO	Asymptotically stable adaptive observer
ASMC	Adaptive sliding mode control
CMC	Control matching condition
DOF	Degree-of-freedom
EC	Exponential convergence
ES	Exponentially stable
ESAO	Exponentially stable adaptive observer
FTC	Finite-time convergence

HOSMC High-order sliding mode control

IEG Integral-exponential gain

IEG-ASMC Integral-exponential-gain based adaptive sliding mode control

IG Integral gain

IG-ASMC Integral-gain based adaptive sliding mode control

ISG Integral switching gain

LMI Linear matrix inequality

MIMO Multiple inputs multiple outputs

MRAC Model reference adaptive control

P0Y0 Pitch and yaw stabilization at zero position

P0Yv Pitch stabilization at zero position and yaw trajectory tracking

P10Y10 Pitch and yaw stabilization at 10° position

PE Persistent excitation

PID Proportional-integral-derivative

PvY0 Pitch trajectory tracking and yaw stabilization at zero position

PvYv Pitch and yaw trajectories tracking

RAC Robust adaptive control

RC Robust control

RMS Root mean square

RTE Reaching time estimation

SMC Sliding mode control

SMCPE Sliding mode control with perturbation estimation

TSM Terminal sliding mode

UUB Uniformly ultimately bounded

VHOS Very-high-order state

1 Introduction

1.1 Uncertain Nonlinear Systems

Although linear control theory has been applied in industry successfully over a long period, it has been found to be inadequate in many physical systems having nonlinear properties such as Coulomb friction, hysteresis, backlash, and saturation [1]. These nonlinarities often cause undesirable behaviour when linear controllers are applied. To obtain acceptable performaces of nonlinear systems, the design of nonlinear controllers has attracted researchers over the past few decades [2–6]. Usually nonlinear dynamics may be modelled via physical or chemical laws, and the parameters of nonlinear systems can be tested priorly. If the parameters are constant and calibrated precisely, the exact shape of the nonlinear functions are known. However, the system parameters may be uncertain because of mode parameter errors and possibly wrong experimental testing methods. Parameters may also be slowly time-varying, for instance, the overall mass of an aircraft in flying condition decreases slowly due to fuel consumption. Such uncertainties in nonlinear systems are classified as *uncertain parameters*. In many mechanical systems, some nonlinearities such as external disturbances, measure noises or backlash cannot be modelled exactly. Moreover, some nonlinearities such as high order terms in Taylor expansion are ignored. These types of uncertainties are called *uncertain nonlinear functions*, *uncertain nonlinearities* or simply *uncertainties*. Usually, the uncertainties are assumed to be bounded in different ways. Sometimes, they are assumed to be bounded within some constants. They may also be assumed to be bounded within some affine functions or higher order (polynomial) functions. Most conventional robust controllers are designed based on the knowledge of the bounds. Specifically, the values of the constants or the parameters of the affine functions must be known *a priori*. The most conservative situation is that knowledge of the bounds are unknown *a priori*, for example, an unmanned-aerial-vehicle flying through a snow storm.

1.2 Techniques for Uncertain Nonlinear Systems

Among the techniques dealing with nonlinear systems with uncertainties, two major classes of control methods can be classified, according to the method of dealing with the uncertain dynamics, as adaptive control and robust control [7, 8].

To deal with parametric uncertainties, techniques of adaptive control have been introduced over the past few decades. In this case, the uncertainties are parameterized in terms of unknown parameters. These uncertain parameters are estimated by adaptive laws and then used in controllers directly or indirectly. In a more extensive adaptive scheme, the controller might be also learning certain unknown nonlinear functions through some neural network training [9]. Usually, the adaptive control method requires that the uncertainties are parameterizable, *i.e.*, the knowledge of the explicit form of the nonlinearities are known *a priori* though the parameters of these nonlinearities are unknown. Moreover, the persistent excitation (PE) is a necessary condition in most adaptive control techniques to ensure the convergence of parameter estimation.

Robust control, on the other hand, characterizes the uncertain nonlinearities as perturbations. The robust controller is designed to work well in spite of these perturbations if these perturbations are within some bounds. Thus, the uncertainties are usually assumed to be bounded by some *a priori* known constants in the state vector norm [10]. Most conventional linear and nonlinear robust control techniques such as H-infinity loop shaping, linear-quadratic-Gaussian control, quantitative feedback theory, conventional sliding mode control (SMC) and high-order sliding mode control (HOSMC) are designed based on the knowledge of the bounds of uncertainties. In fact, the designed feedback gain in the above techniques must be greater than the bounds of the lumped uncertainties such that it will ultimately compensate for these uncertainties.

However, in most cases, such perturbation bounds are unknown and rarely estimated *a priori*. Thus, the conventional robust control algorithms face a dilemma: If the designed feedback gain is based on underestimated bounds of the actual uncertainties, the system may become unstable, and, if the designed feedback gain is based on an overestimation of the actual uncertainty bounds, the system may encounter high chattering and consume 'unnecessary' high energy.

To solve the problem of nonlinear systems with uncertainties of unknown bounds, techniques of SMC with perturbation estimation (SMCPE) [11] and active disturbance rejection control (ADRC) [12] were proposed to estimate

the bounds of uncertainties and then reject them. Both techniques of SMCPE and ADRC require a differentiator to obtain knowledge of the system's high order state (*e.g.*, acceleration). The differentiator required for these methods also amplifies the noise in the input signals and may create further uncertainties and large errors. Without using differentiators and without using the knowledge of the explicit form of the nonlinearities, another nonlinear control technique, the ASMC, has been introduced during the past two decades to design a feedback gain adaptively compensating for the lumped uncertainties [10,11,13–19]. These ASMC designs commonly use an integral adaptation law to compensate for the uncertainties of unknown constant bounds. The uncertainties may also be assumed to be bounded by affine functions with unknown parameters. To deal with these nonlinearities, ASMC with a modified integral adaptation law was introduced. However, some problems exist in these ASMC techniques. First, the chattering phenomenon is still observed during the adaptation process and the feedback gain is still overestimated; second, the stability analysis is not complete and the FTC property is not proven adequately; third, the convergence rate is still not understood quantitatively, *i.e.*, no one reveals the quantitative relationship between the convergence rate and the designed parameter.

So far, all the existing ASMC techniques dealing with the nonlinear systems with uncertainties bounded by unknown constants or unknown affine functions (*e.g.*, [10, 16]) have integral and modified integral adaptation laws. Despite the nonlinear systems with uncertainties bounded by some unknown constants or unknown affine functions, other common kinds of uncertain systems still exist. For instance, if the system's parameters are unknown, the Duffing dynamics (*i.e.*, mechanical systems with softening springs) and the tunnel-diode circuit dynamics contain uncertainties bounded by polynomials [1]. Moreover, according to Taylor's theorem, most continuous nonlinearities can be approximated by polynomials. A new question then arises: how to control the nonlinear dynamical systems with uncertainties bounded by unknown polynomials. This question and the weakness found in the existing ASMC techniques motivate the new ASMC design discussed in this dissertation.

1.3 Motivations and Problem Statement

Despite the recent vast advances on the subject of ASMC, limitations still exist. One drawback in the existing ASMC methods is that the controller responds to the external perturbation relatively slowly. Consequently, the

system state may be driven far away from its equilibrium point. Another limitation is that the gain is still overestimated during the adaptation process. Therefore, the chattering phenomenon is still observed during the adaptation process. Investigation of the existing ASMC techniques, to find the hidden reason why they have these limitations, comes out as the first motivation of the dissertation.

During the sliding mode, the system shows robustness to both parametric uncertainties and unknown nonlinear functions. However, the discontinuity across sliding surfaces often leads to control chattering when involving high frequency control activity which may excite the neglected high-frequency dynamics. Although smoothing techniques such as the traditional boundary-layer-based ones [20] preserve the transient performance at large, there is a trade-off between the control bandwidth and the tracking precision. New smoothing ASMC techniques are required leading to the second motivation.

The third motivation comes from the parameter uncertainties as well as uncertain nonlinearities. Sometimes, the parameters in mechanical systems are not provided truly or could not be fully reliable. For example, in the Quanser 2-DOF helicopter 2006 manual [21], six major mistakes were found and these mistakes caused the provided parameters a drift greatly from their true values. Consequently, it is extremely difficult to stabilize the 2-DOF helicopter by using the provided but wrong parameters. Moreover, the nonlinearities in the 2-DOF helicopter are quadratic functions of the system states. Combined with unknown parameters, the system is under uncertainties bounded within unknown-parameter quadratic functions of the system states. No existing ASMC controller can deal with this kind of uncertainties. Thus, new ASMC techniques must be developed.

Motivated by the practical requirement of solving the above problems and through literature searches, we aim to design a new robust adaptive controller using new ASMC techniques to stabilize a large class of nonlinear systems which have uncertainties with unknown constant or polynomial bounds. This leads to the objectives of the thesis.

1.4 Objectives

The objectives of the undertaken research are stated as follows.

- *ASMC Framework*. The first objective is to analyse the framework of the general ASMC designs. Sufficient and necessary conditions must be analysed before proposing the smoothing techniques in classic ASMC.

- *ASMC Properties.* The second objective is to investigate classic ASMC properties. Specifically, the FTC property of the sliding variable and the boundedness of the switching gain must be accurately addressed. Moreover, the reaching time estimation of the ASMC must be given as accurately as possible.
- *New ASMC Design for Nonlinear System with Uncertainties of Unknown Constant Bounds.* The new design must have simultaneous robustness of fast response to the external perturbation and small variation of the state to the equilibrium, and minimum admissible switching gain resulting in minimum chattering level and minimum energy consumption.
- *New ASMC Design for Nonlinear System with Uncertainties of Unknown Polynomial Bounds.* Not only for uncertainties of unknown constant bounds, the new ASMC design must also deal with uncertainties of unknown polynomial bounds. The details of the adaptation law as well as the controller design must be given.
- *Applications.* All designs need to be tested numerically through MATLAB Simulink first. Then, they must be demonstrated experimentally through an electro-mechanical setup, *i.e.*, a 2-DOF experimental helicopter model plant available in the Instrumentation Laboratory in the Department of Mechanical and Aerospace Engineering.

1.5 Methodology

Based on the analysis of the existing techniques, the dissertation proposes new ASMC designs for a large class of nonlinear systems with uncertainties of unknown bounds. This study is carried out as follows

- Analysis of stability will be based on Lyapunov stability theorems. The majorant curve of differential inequalities will be first-time introduced to prove the FTC property and estimate the maximum reaching time.
- A newly developed boundary layer method will be adopted to prevent the wind-up without sacrificing the stability in real implementation.
- An exponential term will be introduced to the new design to speed up the system response to the various uncertainties and reduce the final switching gain. The classic integral adaptation law will be kept as a part of the new design to compensate for the uncertainties of unknown constant bounds and to guarantee the FTC of the feedback system.
- The performance of the designed control schemes will be simulated by MATLAB software and then implemented on a real nonlinear system, *i.e.*, the 2-DOF experimental helicopter model to demonstrate the effectiveness of our design.

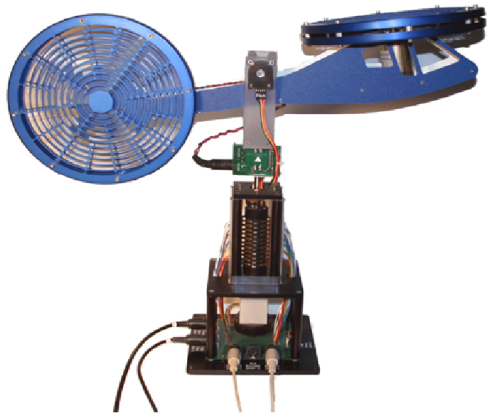

Figure 1.1: Quanser 2DOF helicopter [21]

1.6 Apparatus and Software

The performance of the control schemes were simulated first. The experimental works were carried out on a 2-DOF experimental helicopter which is available in the Instrumentation Laboratory, Mechanical and Aerospace Engineering, RMC. Specifically,

• MATLAB software with Simulink including Control and Simmechanics toolboxes – The MATLAB software is used for design, simulation and control.

• 2-DOF experimental helicopter made by Quanser – The Quanser 2-DOF Helicopter model, shown in 1.1, is mounted on a fixed base with two propellers that are driven by DC motors, respectively. The front propeller controls the elevation of the helicopter nose about the pitch axis and the back propeller controls the side to side motions of the helicopter about the yaw axis. The pitch and yaw angles are measured using high-resolution encoders. By using a slip-ring, the yaw angle can rotate freely 360 degrees [21]. This model, with uncertain parameters, limited output and highly coupled nonlinearities between the pitch dynamics and the yaw dynamics, is a typical representative of the large class of nonlinear systems we intend to control.

1.7 Outline of the Thesis

The rest of the thesis is organized into seven chapters:

Chapter 2 gives a review of the literature regarding the main subjects treated in this thesis.

Chapter 3 models the 2-DOF helicopter-model setup. It first introduces the common nonlinear systems models. Then, it briefly presents the concept of transformation matrices and Lagrangian mechanics. Based on the transformation matrices and Lagrangian mechanics of the 2-DOF helicopter-model setup, the kinematic and nonlinear dynamic equations of the helicopter model are developed. Some corrections to the manual 2006 of [21] are pointed out. The methods of parameter validation are discussed. New designs of adaptive observers are proposed to estimate the parameters.

Chapter 4 presents the framework of ASMC. The concepts of stabilities are introduced first following the basic structures of SMC. The ASMC techniques are then presented in terms of equivalent control method, the discussion of sufficient and necessary conditions and the *ideal* and *real* ASMC. As a result, the extension of the switching function as well as the techniques of smoothing ASMC is proposed. The application of the proposed smooth techniques is conducted via simulations and experiments on a reduced dynamics of the 1-DOF helicopter model.

Chapter 5 investigates the properties of the classic integral-based ASMC techniques. The upper-bound of the switching gain and the FTC of the ASMC are proven through the analysis of the two phases: the compensating phase and the reaching phase, existing in the ASMC process. Two approaches of using a new Lyapunov function and of using a majorant curve are developed to prove the FTC property. Along with the FTC proof, a completely new formula for RTE is deduced. Simulations and experiments are performed to verify the two phases and the new formula of RTE.

Chapter 6 develops a new algorithm of ASMC for nonlinear systems with uncertainties of unknown constant bounds. An exponential term is combined with the integral-based adaptation law to speed up the system response to various uncertainties and reduce the final switching gain. The new algorithm for the scalar case and ideal ASMC is discussed first for the sake of simplicity. Then, the new method is extended to real ASMC and multi-input-multi-output (MIMO) nonlinear systems. Simulations are conducted on a variable-length pendulum and the 2-DOF helicopter model. Experimental

stabilizations of the equilibrium point are performed to compare the proposed new design to the traditional PID laws and the existing ASMC with IG laws.

Chapter 7 further proves that the new ASMC design is capable of stabilizing nonlinear systems with uncertainties of unknown polynomial bounds on the norm of the states. The corresponding MIMO ASMC controller designs for the two cases of the uncertain input parameters are provided. The applications of the proposed new ASMC design to the trajectory tracking control of a 5-link robotic manipulator are simulated via Simmechanics toolbox of MATLAB with comparisons to the existing ASMC and the traditional PID control. Experimental trajectory tracking control are performed on the 2-DOF helicopter model to compare the proposed new ASMC with the existing ASMC.

Chapter 8 presents a summary of this thesis, and proposes some recommendations arising from the different subjects discussed in the thesis.

2 Literature Review

2.1 Robust Adaptive Control

The robust adaptive control has extensive literature full of different techniques for the design, analysis, and performance, covering many applications [7, 14, 22–31]. In 1960s, adaptive pole placement schemes, model reference controls, a dual control idea and dynamic programming were suggested by Kalman [32], Osburn *et al.* [33], Fel'dbaum [34] and Bellman [35], respectively. The introduction of state space techniques and Lyapunov-based stability theory contributed to the research in the 1970s and 1980s [6,7,22,36]. The concepts of Lyapunov redesign have been used to develop a wide class of *model reference adaptive control* (MRAC) schemes with good stability properties [7, 27, 37]. However, controversies that the adaptive schemes of the two decades could easily become unstable in the presence of small disturbances [38] were found. The nonrobust behavior of adaptive control motivated many researchers to study the concept of the *robust adaptive control* (RAC), whose objective was to design an adaptive controller to be also robust by guaranteeing signal boundedness in the presence of'reasonable' classes of unmodeled dynamics and bounded disturbances as well as performance error bounds that are of the order of the modeling errors [6, 39]. In view of the importance of PE property in adaptive systems, Narendra and Annaswamy [23] demonstrated that the degree of persistent excitation would determine whether or not the system would be robust in the presence of specified disturbances. Boyd and Sastry [22] used Generalized Harmonic Analysis to show the necessary and sufficient conditions for the parameter convergence in MRAC of linear systems, that is, if the reference signal'contains enough frequencies' then the parameter vector converges to its correct value. For most applications such as tracking error control, the reference input (or desired output trajectory) normally does not satisfy the PE condition. By introducing δ-modification [40] and ϵ-modification [6] in the adaptation law in linear systems, Ioannou *et al.* demonstrated that a semi-global boundedness result is

guaranteed in the presence of unmodeled dynamics provided that the input is PE.

When trying to extend the RAC from linear systems to nonlinear systems, the linearization of nonlinear systems were considered first with specific problems such as the control of robot manipulators [29]. Since robot dynamics are described by a set of highly coupled nonlinear differential equations with parametric uncertainties such as the payload, the control of such a system is challenging. Many methods, such as the computed torque method [41] and RAC scheme using reference trajectory information rather than the actual state [42, 43], are applied. For the uncertainty-constrained schemes, the control matching condition(CMC) were assumed to develop a feedback control scheme for a class of nonlinear plants with parametric and dynamic uncertainties (loosely speaking, the CMC implies that control and uncertainty enter the system dynamics via the same channel) [44]. By applying the properties of a novel Lyapunov function introduced by [45], feedback linearization designs [46] and output-feedback designs [47] were studied. To relax the restrictions on nonlinearities existing in the feedback-linearization-based adaptive controllers, an RAC with backstepping is introduced in [8]. For a class of nonlinear systems transformable to a parametric strict-feedback canonical form, a systematic design of globally stable and asymptotically tracking adaptive controllers was presented in [48]. Other than the above discussed RC and RAC techniques, a nonlinear control method, the SMC technique, has been gained much attention during the past decades for its robustness and finite time convergence.

2.2 SMC and ASMC

Sliding mode control, or SMC, is a nonlinear control method that forces the system trajectories to reach a *sliding manifold* (also, called *sliding surface*) in a finite time and to stay on or 'slide' along the manifold thereafter by applying a discontinuous control signal [49]. This method has gained much attention for its robustness in terms of parameter variations that occur in the control channel and the finite time convergence (FTC) to the sliding surface [5, 8, 10, 11, 13, 16, 17, 19, 39, 49–57]. The state-feedback control law is not a continuous function of time. Instead, it can switch from one continuous structure to another based on the current position in the state space. Hence, SMC is a variable structure control method. The multiple control structures are designed so that trajectories always move toward an adjacent region with a different control structure, and so that the ultimate trajectory will not exist

entirely within one control structure. Instead, it will slide along the boundaries of the control structures. The motion of the system as it slides along these boundaries is called a sliding mode and the geometrical locus consisting of the boundaries is called the sliding surface or sliding hypersurface [1]. In the context of modern control theory, any variable structure system, like a system under SMC, may be viewed as a special case of a hybrid dynamical system as the system flows through a continuous state space and also moves through different discrete control modes [1]. In a conventional SMC design, *a priori* knowledge of the bounds on system uncertainties has to be acquired to compensate for these uncertainties. As a result, the control gain tends to be overestimated, which may excite the unmodeled dynamics and induce poor tracking performance and undesirable chattering [13, 58]. This scenario happens, in particular, when the estimate of the uncertainty bounds is inaccurate, or very weak.

To suppress the chattering phenomenon which is commonly observed in SMC, different techniques have been used, such as the boundary layer method [49, 52], the HOSMC [18, 50, 59], the terminal sliding mode [60], the filtered switching function [13, 61] and the exponential reaching law [56] methods. Also, [62] deployed a chain of PID sliding surfaces. However, in all of these approaches, knowledge of the uncertainty bounds is required.

To overcome the drawback of overestimation in a conventional SMC scheme and to deal with uncertainties of unknown bounds, on the one hand, the SMCPE design [11, 63, 64] and active disturbance rejection control (ADRC) [12] were proposed to estimate the values of uncertainties and then reject them. In SMCPE, the modeling uncertainties and disturbances are estimated on-line by properly utilizing the feedback from the present position and velocity sensing devices as well as the control decisions. Different SMCPE controllers have been designed such as SMCPE with PID sliding surface [11], SMCPE with a PI feedforward compensator [64], SMCPE by solving a set of partial differential equations [65], *etc.* Such SMCPE designs often require the information of very-high-order state (VHOS), *e.g.*, the acceleration. In fact, when only low-order state, *e.g.*, the position is measured, the SMCPE and ADRC usually has to estimate the VHOS, either by the differentiation method or by the observer method [11, 12], to estimate the perturbation. When the noise and error exist in low-order state measurement, SMCPE and ADRC may encounter the risk of large estimation errors and result in a degraded performance. In fact, the differentiator often required for these methods amplifies the noisy input signals and creates further uncertainties and large errors.

On the other hand, to avoid the risk of estimating VHOS in SMCPE and ADRC, the design of an ASMC with a time-varying switching gain (using

an integral adaptation law) dynamically compensating for the perturbation was introduced [10,11,13,14,16,17,19,49,66–71]. The time-varying switching gain is designed to adaptively compensate for the lumped uncertainties. Most ASMC techniques use integral-type adaptation laws. The pure integral adaptation law is often used in an *ideal* sliding mode where the system trajectory is constrained on the sliding surface for all time after reaching this surface. However, the overshoot is still large at the beginning of the adaptation process and the chattering still exists in the control input and the system trajectories before the end of the adaptation process. The efficiency of this sliding mode structure has been demonstrated using an observer-based control design for mechanical systems with uncertainties reducing significantly the levels of chatter and improving accuracy [72]. In particular, within the case of a *real* sliding mode, the sliding variable is generally non-zero due to measurement noise, sampled computation or imperfect switching action. As a result, the switching gain will be always increasing and become unbounded whenever the sliding variable is not identically equal to zero. To avoid this phenomenon of unbounded or overestimated switching gain, ASMC techniques for *real* SMC were suggested using integral-type adaptation law with some modifications. Motivated by the σ-modification used in the adaptive control, [10] proposed an ASMC scheme with σ-modification method. ASMC techniques using a dead zone method can be found in [11,14]. For the ASMC designs, the thorough analysis for stabilities is still lacking. In [73], it is shown that, by using integral-type adaptation law, the systems with uncertainties of unknown constant bounds have finite-time stability (*i.e.*, the systems are stabilized in finite time). However, the system response to the perturbation is relatively slow and, even though the overestimation is avoided somehow, the chattering phenomenon is still observed. Since the magnitude of the switching gain is proportional to the magnitude of the chattering level [61], a possible adaptation law is to reduce this switching gain to the minimum admissible value. The method suggested in [13] evaluates the disturbance magnitude once the sliding mode occurs. It uses a low-pass filter to tune the switching gain in the control and allows a decrease in the switching gain once the sliding mode is established. Therefore, the gain adaptation law does not overestimate the magnitude of the perturbations. However, it still requires knowledge of the bounds of perturbations, and the use of a low-pass filter introduces a time delay which affects the transient phenomenon. Most recently, the control gain in [16,17,74] depends on the distance from the sliding variable to a discontinuity surface referred to as a boundary layer which is different from the conventional boundary lay used to replace the switching function, often, a signum function, so that the switching gain is reduced gradually when the

sliding variable is inside the boundary layer. To avoid the wind-up in the process of gain adaptation, [16] suggests that the boundary layer parameter should be large enough or tuned dynamically with the switching gain.

The ASMC is also improved with the application to HOSMC. In [61], the authors apply ASMC to "super-twisting" algorithm, and in [18] ASMC is combined with a second-order SMC. The improved algorithms successfully reduced the switching gain so that the chattering level is lowered. However, in [18], the exact robust differentiator is required and the design fits mainly for *ideal* sliding mode; while in [13, 16, 17, 19, 61], the system response is relatively slow at the beginning of the presence of perturbations. Since the sliding surface is mostly designed such that the system state is stable when the trajectory is on the surface, a slow response to the sliding variable variation may encounter a serious stability problem. To achieve fast response and chattering-free property, asymptotic reaching laws rather than ASMC can be found as the form of power reaching law [5] and an exponential reaching law [56]. However, they either lose the robustness when system states are around the sliding surface [5] or require *a priori* knowledge of the uncertainty bounds [56].

For the uncertainties in the nonlinear systems, many assumptions were made. Mostly, the uncertainties are assumed to be bounded within some unknown constants or affine function of the norm of the state with unknown coefficients. To deal with uncertainties of unknown bounds, the integral adaptation law has been often used [11,13–19,75–78] over the past two decades. Also, uncertainties bounded by affine functions have been treated using an ASMC design with "improved" integral adaptation laws [10, 61, 79–81] . Despite the nonlinear systems with uncertainties bounded by some unknown constants or unknown affine functions, other common kinds of uncertain systems still exist. For instance, if the system's parameters are unknown, the Duffing dynamics (*i.e.*, mechanical systems with softening springs) and the tunnel-diode circuit dynamics contain uncertainties bounded by polynomials [1]. Moreover, according to Taylor's theorem, most continuous nonlinearities can be approximated by polynomials. Thus, the uncertainties bounded with some unknown polynomials exist. However, most the existing ASMC techniques only deal with the nonlinear systems with uncertainties bounded by constants or affine functions.

2.3 Applications to Robot Systems

Robotic manipulators play an important role in modern industry. The control of rigid manipulators has gained much attention during the past decades.

Since the rigid manipulators often face significant difficulties related to highly nonlinear, time-varying and coupled dynamic behavior, and external disturbance, numerous control methods, from linear to nonlinear control, adpative to robust control, and model-based to fuzzy and neural network control, have been widely applied to these complex dynamics [20, 42, 43, 56, 60, 79, 81–86]. In particular, the SMC attracts much attention for its robustness in terms of parameter variations that occur in the control channel and its FTC property [39, 60]. In a conventional SMC design, *a priori* knowledge of the bounds on system uncertainties has to be acquired to compensate for these uncertainties [60, 87]. As a result, the control action tends to be overestimated and may excite the unmodeled dynamics inducing poor tracking performance and undesirable chattering [13]. To deal with these issues in the controller design for robotic manipulators, [56] introduced an exponential reaching law, [87, 88] used a continuous terminal sliding mode (TSM) control, and [11, 62] deployed a chain of PID sliding surfaces. However, the exponential reaching law [56] and the continuous TSM [87, 88] require knowledge of the upper bounds of the uncertainties. To deal with uncertainties of unknown bounds, ASMC techniques has been also applied to the control of robotic manipulators with an integral-type adaptation law [10, 11, 79, 80, 83]. In particular, a high order integral-type adaptation law was designed in [79] for nonlinear systems with uncertainties bounded by some high order polynomial functions with unknown parameters.

3 Modelling and Validation of 2-DOF Experimental Helicopter-Model Setup

In this Chapter, we first present some commonly used nonlinear system models. Then, we briefly introduce the space transformation matrices and Euler-Lagrange method in Section 3.2. In Section 3.3, the kinematic and dynamic equations of the experimental helicopter-model setup will be analyzed based on the space transformation matrices and the Euler-Lagrange method. Some discrepancies, between the description of the dynamics given in this chapter and the one shown in the 2006 manual of the setup [21], will be pointed out. The parameter validations are discussed in Section 3.4 where the parameter estimation methods, based on adaptive observers with asymptotic and exponential stabilizations, are briefly presented with simulation demonstrations.

3.1 Nonlinear System Modeling

In this section, we briefly present the main models of nonlinear dynamic systems. Usually, nonlinear dynamics are modelled via various (physical, chemical, mechanical, and/or electrical) laws, and can be expressed as

$$\dot{x} = a(x, u, t) \tag{3.1a}$$

$$y = c(x, u, t) \tag{3.1b}$$

where $t \in \mathbb{R}$ is the time, $x \in \mathbb{R}^n$ the state vector, $u \in \mathbb{R}^m$ the input vector, and $y \in \mathbb{R}^p$ the output. $a(x, u, t)$ and $c(x, u, t)$ are nonlinear functions in $\mathbb{R}^n$ and $\mathbb{R}^p$, respectively. The following special form, called a control/input affine system with uncertainties [1], is commonly used to deal with different control objectives (*e.g.*, stabilization)

$$\dot{x} \quad = \quad f(x, t) + g(x, t) \cdot u \tag{3.2}$$

where $x \in \chi$ is the state vector, with $\chi \subset \mathbb{R}^n$ a domain containing the origin, and $u \in \mathbb{R}^m$ the input vector. The vector $f(x,t) \in \mathbb{R}^n$ and the matrix $g(x,t) \in \mathbb{R}^{n\times m}$ are nonlinear time-varying smooth functions containing parametric uncertainties and external disturbances [14,16,51,74,89,90]. In general, the bounds of these uncertainties are unknown *a priori*. The model (3.2) represents a large class of nonlinear dynamics on which different designs and analyses discussed in this thesis will be based.

Example 3.1. Most mechanical dynamic systems involve position, velocity and acceleration. One general form of this kind of dynamics is

$$D(q)\ddot{q} + C(q,\dot{q})\dot{q} + g(q) = \tau + \tau_d \tag{3.3}$$

where $q \in \mathbb{R}^n$ refers to the position, $\tau \in \mathbb{R}^m$ the input vector (of torques and forces) and τ_d input disturbance vector (such as unknown friction torques). $D(q)$ is the inertia matrix, $C(q,\dot{q})\dot{q}$ the vector of Coriolis and centrifugal forces, and $g(q)$ the vector of gravitational forces [91]. Based on the fact that $D(q)$ is regular [52, 85], the dynamics (3.3) can be rewritten in the standard state-space form (3.2) with $u = \tau$, $x = [x_1^T, x_2^T]^T = [q^T, \dot{q}^T]^T$, The nonlinear field functions of (3.3) are given by

$$f(x) = \begin{bmatrix} x_2 \\ D^{-1}(x_1)\cdot\big[-C(x_1,x_2)x_2 - g(x_1) + \tau_d\big] \end{bmatrix} \tag{3.4}$$

and

$$g(x) = \begin{bmatrix} 0 \\ D^{-1}(x_1) \end{bmatrix} \tag{3.5}$$

respectively.

When the system has linearly joined unknown parameters, (3.1) can be written in state-space representaion with known and unmeasurable nonlinearities [92]

$$\dot{x} = Ax + f_m(y,u) + B\big[f_u(x,u) + f_r(x,u)\theta\big] \tag{3.6a}$$
$$y = Cx \tag{3.6b}$$

with $A \in \mathbb{R}^{n\times n}$, $B \in \mathbb{R}^{n\times r}$ and $C \in \mathbb{R}^{p\times n}$. $x \in \mathbb{R}^n$ designates the state vector, $u \in \mathbb{R}^m$ the input vector, $y \in \mathbb{R}^p$ the output, and $\theta \in \mathbb{R}^q$ the vector of unknown constant parameters. $f_m(y,u)$, $f_u(x,u)$ and $f_r(x,u)$ are nonlinear functions in $\mathbb{R}^n$, $\mathbb{R}^r$ and $\mathbb{R}^{r\times q}$, respectively. The usefulness for this representation will be highlighted later when we discuss the parameter estimation.

3.2 Modelization Tools

3.2.1 Space Transformation

The movement of a body in a three-dimensional (3-D) Euclidean space changes its positions and orientations by translation and rotation. The motion of a rotation and a translation can be represented by a rotation matrix and a translation matrix, respectively. To calculate the position of a mass after some movements in a 3-D space, we use homogeneous transformation matrices containing homogeneous coordinates so that translations can be seamlessly intermixed with rotations [93]. The homogeneous coordinates of a 3-D $(x, y, z)^T$ are represented as a vector $(x, y, z, 1)^T$ of dimension four. The translation matrix containing homogeneous coordinates $(l_x, l_y, l_z, 1)^T$ is described as [93]

$$Trans_{(l_x,l_y,l_z)} = \begin{bmatrix} 1 & 0 & 0 & l_x \\ 0 & 1 & 0 & l_y \\ 0 & 0 & 1 & l_z \\ 0 & 0 & 0 & 1 \end{bmatrix} \tag{3.7}$$

Then, after a 3-D translation, the new coordinates $(x_1, y_1, z_1, 1)^T$ of a point vector expressed in the base coordinate system can be obtained from the multiplication of the translation matrix with its original coordinates $(x_0, y_0, z_0, 1)^T$, as

$$\begin{aligned} (x_1, y_1, z_1, 1)^T &= Trans_{(l_x,l_y,l_z)}(x_0, y_0, z_0, 1)^T \\ &= \begin{bmatrix} 1 & 0 & 0 & l_x \\ 0 & 1 & 0 & l_y \\ 0 & 0 & 1 & l_z \\ 0 & 0 & 0 & 1 \end{bmatrix} \begin{bmatrix} x_0 \\ y_0 \\ z_0 \\ 1 \end{bmatrix} = \begin{bmatrix} x_0 + l_x \\ y_0 + l_y \\ z_0 + l_z \\ 1 \end{bmatrix} \end{aligned} \tag{3.8}$$

Similarly, the affine rotation matrices are expanded from their general rotation matrices. The affine rotation matrices for the rotations about x, y and z axes with angles θ, ϕ and ψ, respectively, are defined as [93]

$$Rot_{(x,\theta)} = \begin{bmatrix} 1 & 0 & 0 & 0 \\ 0 & \cos\theta & -\sin\theta & 0 \\ 0 & \sin\theta & \cos\theta & 0 \\ 0 & 0 & 0 & 1 \end{bmatrix} \tag{3.9}$$

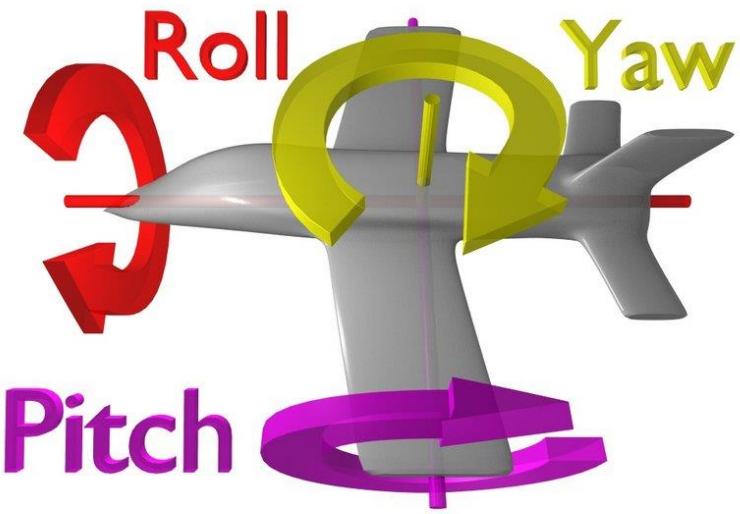

Figure 3.1: Pitch, yaw and roll rotations (adapted from the internet)

$$Rot_{(y,\phi)} = \begin{bmatrix} \cos\phi & 0 & \sin\phi & 0 \\ 0 & 1 & 0 & 0 \\ -\sin\phi & 0 & \cos\phi & 0 \\ 0 & 0 & 0 & 1 \end{bmatrix} \tag{3.10}$$

and

$$Rot_{(z,\psi)} = \begin{bmatrix} \cos\psi & -\sin\psi & 0 & 0 \\ \sin\psi & \cos\psi & 0 & 0 \\ 0 & 0 & 1 & 0 \\ 0 & 0 & 0 & 1 \end{bmatrix} \tag{3.11}$$

3.2.2 Definition of Pitch, Yaw and Roll

An aircraft in flight is free to rotate in three dimensions. In particular, the three rotations are defined, from the pilot's view, as (see Figure 3.1) [94]:

- *pitch*, nose up or down about an axis running from the pilot's left to right in a piloted aircraft;
- *yaw*, nose right or left about an axis running from top to bottom; and
- *roll*, rotation about an axis drawn through the body of the vehicle from tail to nose in the normal direction of flight.

Thus, we know the positive angles of pitch, yaw and roll based on the right-hand rule

- pitch positive, nose up
- yaw positive, nose right
- roll positive, left wing up and right wing down

The axes are alternatively designated as lateral, vertical, and longitudinal. These definitions were analogously applied to spacecraft when the first manned spacecraft were designed in the late 1950s [95]. However, we only use pitch and yaw throughout this thesis.

3.2.3 Lagrangian Mechanics

As a reformulation of classical mechanics, Lagrangian mechanics is widely used to solve mechanical problems in physics and engineering [96]. It is ideal for systems with conservative forces [96]. Instead of forces, Lagrangian mechanics uses the energies in the system. The central quantity of Lagrangian mechanics is the Lagrangian, a function which summarizes the dynamics of the entire system. The Lagrangian for a system of particles can be defined by [96]

$$L = T - V \tag{3.12}$$

where

$$T = \frac{1}{2}\sum_{i=1}^{N} m_i v_i^2 \tag{3.13}$$

is the total kinetic energy and V the potential energy of the system. The Lagrange's equations are defined as [96]

$$\frac{\mathrm{d}}{\mathrm{d}t}\frac{\partial L}{\partial \dot{q}_j} - \frac{\partial T}{\partial q_j} = Q_j \tag{3.14}$$

where Q_j are the generalized forces, q_j the generalized coordinates and $\dot{q}_j$ the generalized velocities.

3.3 Modelling of 2-DOF Experimental Helicopter Model

To validate the effectiveness of the proposed control schemes that will be discussed in this thesis, we consider a 2-DOF helicopter simulator model actuated with two propellers as shown in Figure 1.1 [21]. The front propeller controls

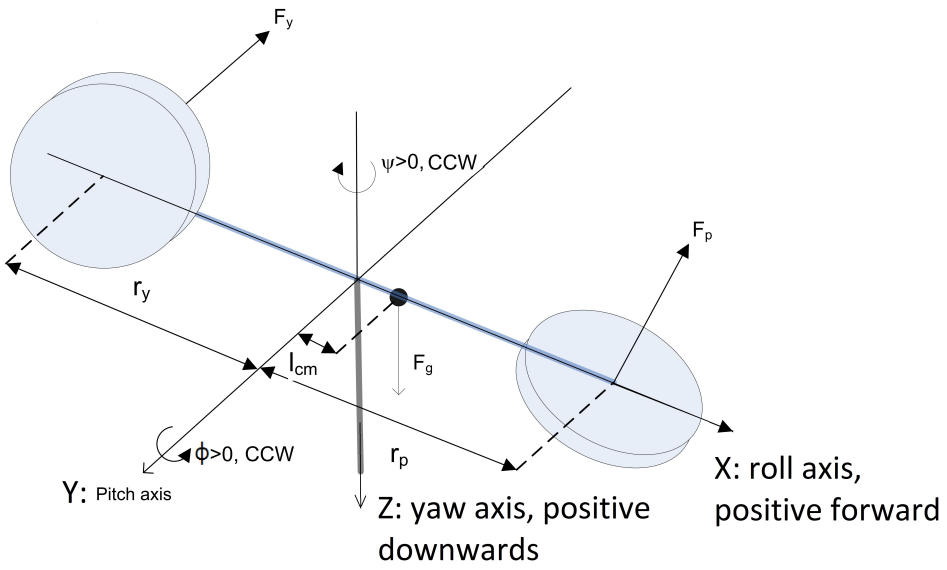

Figure 3.2: Correct pitch and yaw [21]

the elevation of the helicopter nose about the pitch axis and the back propeller controls the side to side motions of the helicopter about the yaw axis. A computer equipped with a QuaRC-Simulink configuration and a data acquisition board is installed to control and monitor the plant in real-time and in designing the controller through Simulink of MATLAB. The 2-DOF helicopter simulator model is provided by Quanser Company. The 2006 manual version provides some details of modelling. However, the modelling methods in the 2006 manual are not all correct. In this section, we investigate the modelling of the helicopter simulator in more detail.

3.3.1 Base Coordinate System

Based on the definitions of pitch, yaw and roll discussed in subsection 3.2.2, we define [21] the pitch-yaw-roll coordinates as (see Figure 3.2) [95]

- X (roll) axis – positive forward, through nose of aircraft
- Y (pitch) axis – positive to right of X axis
- Z (yaw) axis – positive downwards, perpendicular to X-Y plane

The $X-Y-Z$ coordinate system is the base coordinate system in the following discussion dealing with the kinematics of the setup.

3.3.2 Kinematics

To analyse the kinematics of the helicopter, we consider the following movements

- Step 1: the center of mass moves from the origin with a distance l_{cm} along the X-direction.
- Step 2: the center of mass rotates about Y (pitch) axis with angle ϕ.
- Step 3: the center of mass rotates about Z (yaw) axis with angle ψ.

Step 1 can be represented by an affine transformation (translation) matrix in the form of (3.7) as

$$Trans_{(l_{cm},0,0)} = \begin{bmatrix} 1 & 0 & 0 & l_{cm} \\ 0 & 1 & 0 & 0 \\ 0 & 0 & 1 & 0 \\ 0 & 0 & 0 & 1 \end{bmatrix} \tag{3.15}$$

Steps 2 and 3 can be represented by the affine transformation (rotation) matrices $Rot_{(z,\psi)}$ and $Rot_{(y,\phi)}$ in the forms of (3.10) and (3.11), respectively. Thus, the total transformation matrix can be obtained by multiplying the three individual translation and rotation matrices as [93]

$$\begin{aligned} T_{transf} &= Rot_{(z,\psi)} Rot_{(y,\phi)} Trans_{(l_{cm},0,0)} \\ &= \begin{bmatrix} \cos\psi & -\sin\psi & 0 & 0 \\ \sin\psi & \cos\psi & 0 & 0 \\ 0 & 0 & 1 & 0 \\ 0 & 0 & 0 & 1 \end{bmatrix} \begin{bmatrix} \cos\phi & 0 & \sin\phi & 0 \\ 0 & 1 & 0 & 0 \\ -\sin\phi & 0 & \cos\phi & 0 \\ 0 & 0 & 0 & 1 \end{bmatrix} \begin{bmatrix} 1 & 0 & 0 & l_{cm} \\ 0 & 1 & 0 & 0 \\ 0 & 0 & 1 & 0 \\ 0 & 0 & 0 & 1 \end{bmatrix} \\ &= \begin{bmatrix} \cos\psi\cdot\cos\phi & -\sin\psi & \cos\psi\cdot\sin\phi & \cos\psi\cdot\cos\phi\cdot l_{cm} \\ \sin\psi\cdot\cos\phi & \cos\psi & \sin\psi\cdot\sin\phi & \sin\psi\cdot\cos\phi\cdot l_{cm} \\ -\sin\phi & 0 & \cos\phi & -\sin\phi\cdot l_{cm} \\ 0 & 0 & 0 & 1 \end{bmatrix} \end{aligned} \tag{3.16}$$

Using the transformation matrix (3.16), the homogeneous position of the center of mass after the three movements can be obtained (in the base coordinate system O_{XYZ})

$$\begin{bmatrix} x_{cm} \\ y_{cm} \\ z_{cm} \\ 1 \end{bmatrix} = Transf \begin{bmatrix} 0 \\ 0 \\ 0 \\ 1 \end{bmatrix} = \begin{bmatrix} l_{cm}\cdot\cos\psi\cdot\cos\phi \\ l_{cm}\cdot\sin\psi\cdot\cos\phi \\ -l_{cm}\cdot\sin\phi \\ 1 \end{bmatrix} \tag{3.17}$$

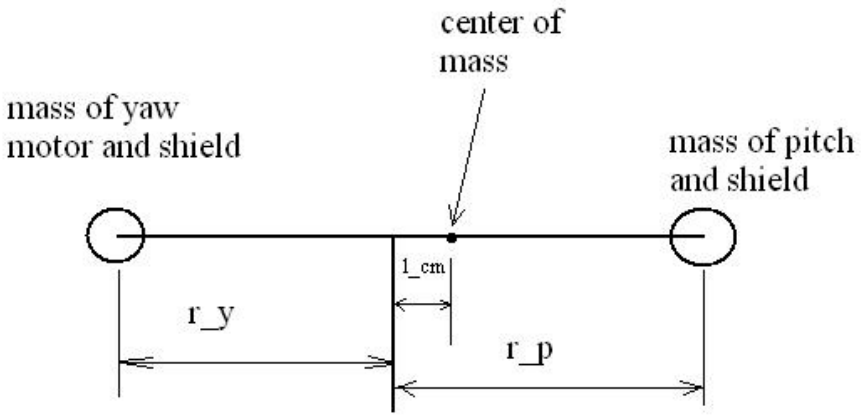

Figure 3.3: Center of mass [21]

Note that the actual position vector is simply obtained by removing the fourth element of the homogeneous position vector, *i.e.*,

$$\begin{pmatrix} x_{cm} \\ y_{cm} \\ z_{cm} \end{pmatrix} = \begin{pmatrix} l_{cm} \cdot \cos\psi \cdot \cos\phi \\ l_{cm} \cdot \sin\psi \cdot \cos\phi \\ -l_{cm} \cdot \sin\phi \end{pmatrix} \tag{3.18}$$

Remark 3.1. l_{cm} is the center of mass where the system should statically balance at the point. Based on Figure 3.3, the center of mass is calculated as follows: if the mass of the body is negligible,

$$(m_p + m_{shield})(r_p - l_{cm}) = (m_y + m_{shield})(r_y + l_{cm})$$

which yields

$$l_{cm} = \frac{(m_p + m_{shield})r_p \ - \ (m_y + m_{shield})r_y}{m_p + m_y + 2m_{shield}} \tag{3.19}$$

where m_p, m_y and m_{shield} represents the mass of pitch rotor (or front rotor), yaw rotor (or rear rotor) and the shield. r_p and r_p are the distances of the pitch rotor and yaw rotor to the pivot, respectively.

If the mass of the body is not negligible,

$$\begin{aligned}&(m_p + m_{shield})(r_p - l_{cm}) + \big[m_{body}\frac{r_p - l_{cm}}{r_p + r_y}\big]\frac{r_p - l_{cm}}{2} \\ &= (m_y + m_{shield})(r_y + l_{cm}) + \big[m_{body}\frac{r_y + l_{cm}}{r_p + r_y}\big]\frac{r_y + l_{cm}}{2}\end{aligned} \tag{3.20}$$

which yields

$$l_{cm} = \frac{(m_p + m_{shield})r_p \ - \ (m_y + m_{shield})r_y + m_{body}\dfrac{r_p^2 - r_y^2}{2(r_p + r_y)}}{m_p + m_y + 2m_{shield} + m_{body}} \tag{3.21}$$

The Equations (3.19) and (3.21) correct the equation calculating the center of mass in [21] where its form is similar to (3.19) but with a positive sign '+' replacing the negative sign '−' in the numerator of (3.19).

Taking the time derivative of the position vector (3.18), we obtain the velocity vector of the center of mass.

$$\begin{pmatrix} \dot{x}_{cm} \\ \dot{y}_{cm} \\ \dot{z}_{cm} \end{pmatrix} = \begin{pmatrix} -l_{cm}\big(\dot{\psi}\sin\psi\cdot\cos\phi + \dot{\phi}\cdot\cos\psi\cdot\sin\phi\big) \\ l_{cm}\big(\dot{\psi}\cos\psi\cdot\cos\phi - \dot{\phi}\cdot\sin\psi\cdot\sin\phi\big) \\ -\dot{\phi}\cdot\cos\phi\cdot l_{cm} \end{pmatrix} \tag{3.22}$$

where $\dot{x}_{cm}$, $\dot{y}_{cm}$ and $\dot{z}_{cm}$ are the linear velocities of the center of mass. $\dot{\phi}$ and $\dot{\psi}$ are the angular velocities about the pitch and yaw axes, respectively.

Remark 3.2. The transformation matrix (3.16), the position vector (3.18) and the velocity vector (3.22) are now different from the results obtained in [21].

3.3.3 Kinematic and Potential Energy

To develop the dynamic equations of the helicopter, we apply the Lagrangian equation (3.14). First, we calculate the Lagrangian L which is the difference of the kinematic energy T and the potential energy V.

The total kinetic energy is the sum of the rotational kinetic energies acting from the pitch, $T_{r,p}$, and from the yaw, $T_{r,y}$, along with the translational kinetic energy generated by moving the center of mass, T_t, defined as

$$T = T_{r,p} + T_{r,y} + T_t \tag{3.23}$$

The pitch rotational energy $T_{r,p}$ and yaw rotational energy $T_{r,y}$ are

$$T_{r,p} = \frac{1}{2}\cdot J_p\cdot\dot{\phi}^2 \tag{3.24}$$

and

$$T_{r,y} = \frac{1}{2} \cdot J_y \cdot \dot{\psi}^2 \tag{3.25}$$

where J_p and J_y are the equivalent moments of inertia of the pitch and yaw, respectively. The equivalent moments of inertia about the pitch axis and the yaw axis can be calculated as follows [21]

$$J_p = J_{rotor,p} + J_{body,p} + J_{m,p} + J_{m,y} \tag{3.26}$$

and

$$J_y = J_{rotor,y} + J_{body,y} + J_{m,p} + J_{m,y} + J_{shaft} \tag{3.27}$$

where $J_{rotor,p}$ (*resp.*, $J_{rotor,y}$) is the pitch (*resp.*, yaw) rotors moment of inertia, $J_{body,p}$ (*resp.*, $J_{body,y}$) is the moment of inertia of the helicopter body about its center-of-mass, $J_{m,p}$ (*resp.*, $J_{m,y}$) is the moment of inertia of pitch (*resp.*, yaw) motor and guard assembly about pivot, and J_{shaft} is the moment of inertia of the yaw shaft. Moreover, [21]

$$J_{body,p} = \frac{m_{body,p} L_{body}^2}{12} + m_{body,p} \cdot l_{cm}^2 \tag{3.28a}$$

$$J_{body,y} = \frac{m_{body,y} L_{body}^2}{12} + m_{body,y} \cdot l_{cm}^2 \tag{3.28b}$$

$$J_{shaft} = \frac{m_{shaft} r_{shaft}^2}{2} \tag{3.28c}$$

where $m_{body,p}$ (*resp.*, $m_{body,y}$) is the equivalent mass of the helicopter body about the pitch (*resp.*, yaw), m_{shaft} the mass of the yaw shaft, L_{body} the length of the helicopter body and r_{shaft} the radius of the yaw shaft. We use the approximations (3.28a) and (3.28b) since l_{cm} is very small compared to L_{body}.

Remark 3.3. The Equations (3.28) are slightly different from those in [21]

The translational kinetic energy is obtained from the mass and the linear velocity of the helicopter (3.22), as

$$T_t = \frac{1}{2} m_{heli} \left(\sqrt{\dot{x}_{cm}^2 + \dot{y}_{cm}^2 + \dot{z}_{cm}^2} \right)^2 \tag{3.29}$$

where m_{heli} is the mass of the helicopter given by

$$m_{heli} = m_p + m_y + m_{body} + 2 \cdot m_{shield} \tag{3.30}$$

Substituting (3.22) into (3.29), the translational kinetic energy is obtained

$$T_t = \frac{1}{2} m_{heli} \cdot l_{cm}^2 \cdot \left(\dot{\psi}^2 \cdot \cos^2 \phi + \dot{\phi}^2\right) \tag{3.31}$$

Thus, we have the total kinetic energy

$$T = \frac{1}{2} \cdot J_p \cdot \dot{\phi}^2 + \frac{1}{2} \cdot J_y \cdot \dot{\psi}^2 + \frac{1}{2} m_{heli} \cdot l_{cm}^2 \cdot \left(\dot{\psi}^2 \cdot \cos^2 \phi + \dot{\phi}^2\right) \tag{3.32}$$

The potential energy due to gravity is

$$\begin{aligned} V &= m_{heli} \cdot g \cdot (-z_{cm}) \\ &= m_{heli} \cdot g \cdot l_{cm} \cdot \sin \phi \end{aligned} \tag{3.33}$$

where g is the gravitational acceleration and z_{cm} the position of the center of mass on Z_0-axis. We use negative z_{cm} here because the positive z direction is downwards. The Lagrangian L is the difference between the kinetic and potential energy of the system. Substituting (3.32) and (3.33) into (3.12), we obtain the Lagrangian [96].

$$\begin{aligned} L = &\frac{1}{2} \cdot J_p \cdot \dot{\phi}^2 + \frac{1}{2} \cdot J_y \cdot \dot{\psi}^2 + \frac{1}{2} m_{heli} \cdot l_{cm}^2 \cdot \left(\dot{\psi}^2 \cdot \cos^2 \phi + \dot{\phi}^2\right) \\ &- m_{heli} \cdot g \cdot l_{cm} \cdot \sin \phi \end{aligned} \tag{3.34}$$

In the following, we use (3.34) to derive the dynamics of motion of the helicopter model.

3.3.4 Nonlinear Equation of Motion

Choosing the generalized coordinates

$$q = [q_1, \ \ q_2]^T = [\phi, \ \ \psi]^T \tag{3.35}$$

the Euler-Lagrange equations (3.14) of the 2-DOF helicopter become

$$\frac{\partial}{\partial t} \frac{\partial L}{\partial \dot{\phi}} - \frac{\partial}{\partial \phi} L = Q_p \tag{3.36a}$$

$$\frac{\partial}{\partial t} \frac{\partial L}{\partial \dot{\psi}} - \frac{\partial}{\partial \psi} L = Q_y \tag{3.36b}$$

where Q_p and Q_y are the generalized forces on pitch and yaw respectively. Using (3.34), we have

$$\frac{\partial L}{\partial \phi} = -\cos \phi \cdot (\dot{\psi}^2 \cdot l_{cm} \cdot \sin \phi + g) \cdot m_{heli} \cdot l_{cm} \tag{3.37}$$

and

$$\frac{\partial}{\partial t}\frac{\partial L}{\partial \dot{\phi}} = (J_p + m_{heli} \cdot l_{cm}^2)\ddot{\phi} \tag{3.38}$$

Now, by substituting (3.37) and (3.38) into (3.36a), we obtain

$$(J_p + m_{heli} \cdot l_{cm}^2)\ddot{\phi} + m \cdot g \cdot l_{cm} \cdot \cos\phi + m_{heli} \cdot l_{cm}^2 \cdot \dot{\psi}^2 \cos\phi \sin\phi = Q_p \tag{3.39}$$

where $\ddot{\phi}$ is the pitch angular acceleration. Similarly, we determine the terms of (3.36b) using (3.34) to obtain

$$(J_y + m_{heli} \cdot l_{cm}^2 \cos^2\phi)\ddot{\psi} - 2m_{heli} \cdot l_{cm}^2 \cdot \dot{\phi} \cdot \dot{\psi} \cos\phi \sin\phi = Q_y \tag{3.40}$$

where $\ddot{\psi}$ is the yaw angular acceleration.

The generalized forces are the total forces from the propellers and the viscous damping given by [96]

$$Q_p = K_{pp}V_p + K_{py}V_y - B_p\dot{\phi} \tag{3.41}$$

and

$$Q_y = K_{yp}V_p + K_{yy}V_y - B_y\dot{\psi} \tag{3.42}$$

where V_p and V_y are the applied torques on pitch and yaw rotations, respectively. B_p (*resp.*, B_y) is the viscous damping about pitch (*resp.*, yaw) axis, K_{pp} (*resp.* K_{py}) the thrust torque constant acting on the pitch axis from the pitch (*resp.*, yaw) motor/propeller, K_{yy} (*resp.*, K_{yp}) the thrust torque constant acting on the yaw axis from the yaw (*resp.*, pitch) motor/propeller.

Substituting (3.41) and (3.42) into Euler-Lagrange expression (3.39) and (3.40), we obtain the nonlinear equations of motion

$$\begin{aligned}(J_p + m_{heli} \cdot l_{cm}^2)\ddot{\phi} =& K_{pp}V_p + K_{py}V_y - B_p\dot{\phi} - m_{heli} \cdot g \cdot l_{cm} \cdot \cos\phi \\ &- m_{heli} \cdot l_{cm}^2 \cdot \dot{\psi}^2 \cdot \cos\phi \sin\phi \qquad (3.43a)\\ (J_y + m_{heli} \cdot l_{cm}^2 \cos^2\phi)\ddot{\psi} =& K_{yp}V_p + K_{yy}V_y - B_y\dot{\psi} \\ &+ 2m_{heli} \cdot l_{cm}^2 \cdot \dot{\phi} \cdot \dot{\psi} \cdot \cos\phi \sin\phi \qquad (3.43b)\end{aligned}$$

Note that the terms $\dot{\psi}^2 \cdot \sin\phi\cos\phi$, $\dot{\phi} \cdot \dot{\psi} \cdot \sin\phi\cos\phi$ and $m_{heli} \cdot g \cdot l_{cm} \cdot \cos\phi$, shown in (3.43a) and (3.43b), are typical nonlinear dynamics with quadratic polynomial and trigonometric functions of the system state. Thus, the helicopter-model setup is a typical nonlinear dynamic system. However, if the pitch angle

keeps strictly constant, *i.e.*, $\dot{\phi} = 0$, the setup can be considered as a linear dynamic system.

In the following, for the sake of simplicity, we use m (instead of m_{heli}) and l (instead of l_{cm}) to represent the mass of the helicopter and the center of the mass, respectively.

The equations (3.43a) and (3.43b) can be packaged in the matrix form (recall (3.3))

$$D(q)\ddot{q} + C(q,\dot{q})\dot{q} + g(q) = B\tau \tag{3.44}$$

where $q = [\phi, \psi]^T \in \mathbb{R}^2$ refers to the position and $\tau = [V_p, V_y]^T \in \mathbb{R}^2$ the input torque. The matrix $D(q)$ is the inertia matrix, $C(q,\dot{q})\dot{q}$ the vector of Coriolis and centrifugal forces, $g(q)$ the vector of gravitational forces, and B the input matrix [91].

$$D(q) = \begin{bmatrix} J_p + m \cdot l^2 & 0 \\ 0 & J_y + m \cdot l^2 \cos^2\phi \end{bmatrix} \tag{3.45}$$

$$C(q,\dot{q}) = \begin{bmatrix} B_p & m \cdot l^2 \cdot \dot{\psi} \cos\phi \sin\phi \\ -2m \cdot l^2 \cdot \dot{\psi} \cos\phi \sin\phi & B_y \end{bmatrix} \tag{3.46}$$

$$g(q) = \begin{bmatrix} m \cdot g \cdot l \cdot \cos\phi \\ 0 \end{bmatrix} \tag{3.47}$$

and

$$B = \begin{bmatrix} K_p p & K_p y \\ K_y p & K_y y \end{bmatrix} \tag{3.48}$$

Let $x_1 = \phi$, $x_2 = \psi$, $x_3 = \dot{\phi}$ and $x_4 = \dot{\psi}$ be the measurable states and $u = [u_1 \ u_2]^T = [V_p \ V_y]^T$ the input vector. The dynamics (3.43a) and (3.43b) can be rewritten in the form of (recall (3.2))

$$\dot{x} \ = \ f(x,t) + g(x,t) \cdot u \tag{3.49}$$

where the nonlinear uncertain dynamics are given by

$$f(x,t) = \big[x_3, \ x_4, \ f_1(x), \ f_2(x)\big]^T \tag{3.50}$$

and

$$g(x,t) = \big[g_1(x,t), \ g_2(x,t)\big] \tag{3.51}$$

Table 3.1: Some nominal values of the model parameters [21]

Parameters	Values	Units	Parameters	Values	Units
$m_{m,p}$	0.292	kg	$m_{m,y}$	0.128	kg
$m_{body,p}$	0.633	kg	$m_{body,y}$	0.667	kg
m_{shield}	0.167	kg	m_{shaft}	0.151	kg
J_p	0.038	$\mathrm{kg}\cdot\mathrm{m}^2$	J_y	0.043	$\mathrm{kg}\cdot\mathrm{m}^2$
K_{pp}	0.204	$\mathrm{N}\cdot\mathrm{m/V}$	K_{py}	0.007	$\mathrm{N}\cdot\mathrm{m/V}$
K_{yp}	0.022	$\mathrm{N}\cdot\mathrm{m/V}$	K_{yy}	0.072	$\mathrm{N}\cdot\mathrm{m/V}$
B_p	0.800	N/V	B_y	0.318	N/V
l	0.054*	m	L_{body}	0.280	m
m	1.3872	kg	g	9.810	$\mathrm{m/sec}^2$

* In [21], $l = 0.186$ m.

with

$$f_1(x) = \frac{-B_p x_3 - mgl\cos x_1 - ml^2 \sin x_1 \cos x_1 \cdot x_4^2}{J_p + ml^2} \tag{3.52}$$

$$f_2(x) = \frac{-B_y x_4 + 2ml^2 \sin x_1 \cos x_1 \cdot x_3 x_4}{J_y + ml^2 \cos^2 x_1} \tag{3.53}$$

$$g_1(x,t) = \big(0,\ 0,\ \frac{K_{pp}}{J_p + ml^2},\ \frac{K_{yp}}{J_y + ml^2\cos^2 x_1}\big)^T \tag{3.54}$$

and

$$g_2(x,t) = \big(0,\ 0,\ \frac{K_{py}}{J_p + ml^2},\ \frac{K_{yy}}{J_y + ml^2\cos^2 x_1}\big)^T \tag{3.55}$$

3.4 Model Parameters

3.4.1 Provided Values

Some of the numerical values of the helicopter model are provided by [21] (see Table 3.1, except parameter l). These values were obtained by static experiments and by calculations. However, the calculations are not always correct. For example, the center of mass in [21] is calculated using

$$l_{cm} = \frac{(m_p + m_{shield})r_p \ + \ (m_y + m_{shield})r_y}{m_p + m_y + 2m_{shield}} \tag{3.56}$$

which is different from the Equations (3.19) and (3.21). The resulting value of l_{cm} is then very different.

Another example is the calculations of the moments of inertia $J_{body,p}$, $J_{body,y}$ and J_{shaft} in [21]:

$$J_{body,p} = \frac{m_{body,p} L_{body}^2}{12} \tag{3.57a}$$

$$J_{body,y} = \frac{m_{body,y} L_{body}^2}{12} \tag{3.57b}$$

$$J_{shaft} = \frac{m_{shaft} L_{shaft}^2}{3} \tag{3.57c}$$

which are different from (3.28). Thus, it is necessary to estimate the parameters again. In fact, a dynamic estimation method based on adaptive observer techniques is designed to estimate the unknown constant parameters [92,97–102]. These techniques are based on the state-space representation (3.6) where the unknown constant parameters are set as the linearly joined vector θ.

3.4.2 Parameterization

Let $x_1 = \phi$, $x_2 = \psi$, $x_3 = \dot{\phi}$ and $x_4 = \dot{\psi}$ be the state variables, $u = [u_1 \;\; u_2]^T = [V_p \;\; V_y]^T$ the input vector and $y = [x_1 \;\; x_2]^T$ the output vector (*i.e.*, measurable states), the dynamics (3.43a) and (3.43b) can also be written in the form of state-space representation (3.6), where the matrices A, B and C are given by:

$$A = \begin{pmatrix} 0 & 0 & 1 & 0 \\ 0 & 0 & 0 & 1 \\ 0 & 0 & 0 & 0 \\ 0 & 0 & 0 & 0 \end{pmatrix}, \; B = \begin{pmatrix} 0 & 0 \\ 0 & 0 \\ 1 & 0 \\ 0 & 1 \end{pmatrix}, \; C = \begin{pmatrix} 1 & 0 & 0 & 0 \\ 0 & 1 & 0 & 0 \end{pmatrix} \tag{3.58}$$

Assuming that the parameters J_p, J_y, K_{pp}, $\cdots$ *etc.*, are uncertain, we have $f_m(y,u) = 0$ and $f_u(x,u) = 0$. The unmeasured nonlinear term, often called regression function, with uncertain parameters is written as

$$f_r(x,u)\theta = \begin{bmatrix} \dfrac{K_{pp}u_1 + K_{py}u_2}{J_p + ml^2} + f_1(x) \\ \dfrac{K_{yp}u_1 + K_{yy}u_2}{J_y + ml^2 \cos^2 x_1} + f_2(x) \end{bmatrix} \tag{3.59}$$

To deal with the nonlinear parameterization depicted in (3.59), an approximation resulting in uncertain bounded terms is used to develop the modeling

scheme. If we denote by $a = \dfrac{1}{J_y + ml^2}$, we notice actually that $ml^2 a \sin^2 x_1 \ll 1$ (from the provided values *a priori*), we apply the Taylor series decomposition to the nonlinear parameter dependent term $\dfrac{1}{J_y + ml^2 \cos^2 x_1}$ as

$$\begin{aligned} \frac{1}{J_y + ml^2 \cos^2 x_1} &= \frac{a}{1 - ml^2 a \sin^2 x_1} \\ &= a\big(1 + \mathcal{O}(\sin^2 x_1)\big) \\ &\approx a \end{aligned} \tag{3.60}$$

where $\mathcal{O}(\sin^2 x_1) \triangleq ml^2 a \sin^2 x_1 + m^2 l^4 a^2 \sin^4 x_1 + m^3 l^6 a^3 \sin^6 x_1 + \dots$ is very small. We use this approximation to linearize the yaw dynamics (3.59) *w.r.t.* its independent parameters. We can also use a second order extended form of the approximation instead of the reduced approximation (limited to the constant $a = \dfrac{1}{J_y + ml^2}$) for the sake of accuracy.

Using (3.60), the components of the unknown parameter vector $\theta \in \mathbb{R}^9$ are $\theta_1 = \dfrac{K_{pp}}{J_p + ml^2}$, $\theta_2 = \dfrac{K_{py}}{J_p + ml^2}$, $\theta_3 = \dfrac{B_p}{J_p + ml^2}$, $\theta_4 = \dfrac{mgl}{J_p + ml^2}$, $\theta_5 = \dfrac{ml^2}{J_p + ml^2}$, $\theta_6 = aK_{yp}$, $\theta_7 = aK_{yy}$, $\theta_8 = aB_y$ and $\theta_9 = aml^2$, respectively. Note that, given the validated values of θ_1 to θ_9 and any two correct values of Table 3.1 (for instance, $g = 9.81$ m/sec^2 and $m = 1.3872$ kg), we can derive all of the remaining model parameters in Table 3.1.

Also, the nonlinear function $f_r(x, u) \in \mathbb{R}^{2\times 9}$ containing unmeasured states has the form

$$f_r(x, u) = \begin{bmatrix} f_{r1}(x, u) & 0 \\ 0 & f_{r2}(x, u) \end{bmatrix} \tag{3.61}$$

with $f_{r1}(x, u) = \begin{bmatrix} u_1 & u_2 & -x_3 & -\cos x_1 & \frac{-x_4^2 \sin 2x_1}{2} \end{bmatrix}$ and $f_{r2}(x, u) = \begin{bmatrix} u_1 & u_2 & -x_4 & x_3 x_4 \sin 2x_1 \end{bmatrix}$.

3.4.3 Validation – Parameter Estimation

Adaptive observer techniques are designed to estimate the unknown constant parameters. In particular, the designs of the adaptive observer with asymptotic and exponential convergences are proposed in [92]. These schemes will be briefly introduced in the following.

Consider the state representation (3.6). For the forthcoming designs, we consider the following assumptions [97–100]

Assumption 3.1. *The matrix B is a* strict *full-column-rank matrix, that is* $\mathrm{rk}(B) = r < n$*, the output vector y does not recover the whole states of x, that is $m < n$, and the pair (A, C) is observable.*

Assumption 3.2. *There exist matrices Φ and Ψ of $\mathbb{R}^{n\times p}$ chosen, s.t.*

$$\Psi CB = 0 \tag{3.62}$$

and

$$\Phi C + \Psi CA = I_n \tag{3.63}$$

Assumption 3.3. *The vector of unknown constant parameters θ is bounded with*

$$\|\theta\| < \beta_0 \tag{3.64}$$

Assumption 3.4. *The functions f_u and f_r are continuously bounded and Lipschitz in x, with*

$$\|f_u(x,u) - f_u(\hat{x},u)\| \leq \beta_u \|x - \hat{x}\| \tag{3.65}$$

and

$$\|f_r(x,u) - f_r(\hat{x},u)\| \leq \beta \|x - \hat{x}\| \tag{3.66}$$

Assumption 3.5. *The input vector u is of class $\mathcal{C}_1$ (i.e., continuous and differentiable function having continuous derivatives). In addition, u is required to fulfill the PE condition.*

These hypotheses are commonly used in related research and can characterize adequately many real plants [98, 102–107]. In particular, by setting up Assumptions 3.1 and 3.2, one can neutralize the following inappropriate observer forms: form 1, where B is right invertible (*i.e.*, B regular square matrix or full-row-rank), and form 2, where C is a full-column rank matrix. In fact, with form 1, there always exists a transformation reducing the number of channels within the parameter matching term $Bf_r(x,u)\theta$, by reducing and/or combining the elements of $f_r(x,u)\theta$ to lower r under the number of states n, while with form 2, the output vector y would recover the whole state vector x. Moreover, we notice, from (3.62) of Assumption 3.2, that in the case where the columns of B lie in the null space of C, *i.e.*, $CB = 0$, Ψ and Φ will be selected based on the equality requirement (3.63) only. However, when $CB \neq 0$, Assumption 3.2 requires the selection of a matrix Ψ in the null space of C, *i.e.*, $\Psi C = 0$, then we select Φ *s.t.* $\Phi C = I$. This statement remains strenuous. Otherwise, we select Ψ simply in the null space of CB,

i.e., $\Psi \cdot (CB) = 0$, and Φ *s.t.* (3.63) holds. Later, when we deal with the exponentially stable adaptive observer design, the condition (3.63) of Assumption 3.2 will be slightly relaxed from [97,100,102] enrolling a wider set of dynamics. In fact, we substitute the following conditions for the constraint (3.63), as

Assumption 3.2.s. *There exist matrices Φ and Ψ of $\mathbb{R}^{n\times m}$ chosen, s.t. (3.62) holds and $\tilde{B} = \big(\Phi C + \Psi CA\big)B$ is full-column rank.*

Note that, from Assumptions 3.1 and 3.2.*s*, $\big(\Phi C + \Psi CA\big)$ can be either regular (that is, there exist Φ and Ψ *s.t.* (3.63) holds), or singular.

Adaptive Observer with Asymptotic Stability

The design of a nonlinear adaptive observer for the nonlinear dynamics, generalizes a concept introduced and widely discussed in [92, 97, 100]. Known as an asymptotically stable adaptive observer (ASAO), the detailed proof of the asymptotic stability of the overall scheme is discussed using appropriate Lyapunov function and linear matrix inequality (LMI) frameworks. Based on the dynamics (3.6), we propose the following full-order nonlinear observer

$$\dot{\hat{x}} = A\hat{x} + f_m(y,u) + B\big[f_u(\hat{x},u) + f_r(\hat{x},u)\hat{\theta}\big] + L\big(y - C\hat{x}\big) \tag{3.67}$$

coupled with the adaptation law

$$\dot{\breve{\theta}} = \big[G(t)^T P\big(\Phi + \Psi CL\big) - \dot{G}(t)^T P\Psi\big] \cdot \big(y - C\hat{x}\big) \tag{3.68}$$

$$\hat{\theta} = \breve{\theta} + G(t)^T P\Psi \cdot \big(y - C\hat{x}\big) \tag{3.69}$$

with

$$G(t) = Bf_r(\hat{x},u)Q \tag{3.70}$$

where $Q = Q^T > 0$ and L are matrices of $\mathbb{R}^{q\times q}$ and $\mathbb{R}^{n\times p}$, respectively. Φ and Ψ are matrices of $\mathbb{R}^{n\times p}$, and $\dot{G}(t)$ the total time derivative of G. The following result discusses the conditions that guarantee the convergence of the estimates of both the states and parameters to their actual values [97–100].

Proposition 3.1 (LMI-based ASAO Design)**.** *Under Assumptions 3.1-3.5, for $\delta = \beta_u + \beta_0\beta > 0$, if there exist matrices $P = P^T > 0$ in $\mathbb{R}^{n\times n}$ and W in $\mathbb{R}^{n\times p}$, s.t.*

$$\begin{pmatrix} PA + A^TP - WC - C^TW^T & PB & I_n \\ B^TP & -\frac{1}{\delta}I_p & 0 \\ I_n & 0 & -\frac{1}{\delta}I_n \end{pmatrix} < 0 \tag{3.71}$$

and if $Bf_r(x,u)$ respects the PE condition, that is, there exist positive scalars α_1, α_2 and t_0, s.t. $\forall t$

$$\alpha_1 I_q \leq \int_t^{t_0+t} f_r^T(u,x) B^T B f_r(x,u) d\tau \leq \alpha_2 I_q \tag{3.72}$$

then the adaptive observer (3.67)–(3.70) for the system (3.6), with the observer gain matrix $L = P^{-1}W$, is asymptotically stable, that is, the state estimate error $\tilde{x}$ and the parameter estimate error $\tilde{\theta}$ tend both to zero as $t \to \infty$.

Proof. See [92] (Refer to Appendix C.2). □

A robust adaptive observer version derived from this scheme has been investigated in [99, 100]. In the following, a modified form is proposed to investigate the exponential stability of the entire dynamics (state and parameter estimates).

Adaptive Observer with Exponential Stability

The following design of a nonlinear adaptive observer for the nonlinear dynamics is derived from the scheme presented above. The detailed proof of the exponential stability of the overall dynamics is based on the Lyapunov theory. We consider the model dynamics (3.6). We modify the previous adaptive observer scheme to ensure the exponential convergence of both the state and parameter estimates. We use appropriate change of variables and Lyapunov function candidates to extend the scenario introduced first in [102] and subdue the weaknesses depicted therein. In the following, this new form will be referred to as expoentially stable adaptive observer (ESAO).

We propose the full-order nonlinear observer

$$\dot{\breve{x}} = A\hat{x} + f_m(u,y) + B\big[f_u(\hat{x},u) - \Lambda\Gamma(t)\hat{\theta}\big] + L\big(y - C\hat{x}\big) \tag{3.73}$$

$$\hat{x} = \breve{x} + B\Gamma(t)\hat{\theta} \tag{3.74}$$

where $\Gamma(t) \in \mathbb{R}^{r\times q}$ is defined as

$$\dot{\Gamma} = \Lambda\Gamma + f_r(\hat{x},u) \tag{3.75}$$

with $\Lambda \in \mathbb{R}^{r\times r}$ any Hurwitz matrix, coupled with the adaptation law

$$\dot{\breve{\theta}} = \Big[G(t)^T P\big(\Phi + \Psi CL\big) - \dot{G}(t)^T P\Psi\Big] \cdot \big(y - C\hat{x}\big) \tag{3.76}$$

$$\hat{\theta} = \breve{\theta} + G(t)^T P\Psi \cdot \big(y - C\hat{x}\big) \tag{3.77}$$

where $P = P^T > 0$ is a matrix of $\mathbb{R}^{n\times n}$, L, Φ and Ψ matrices of $\mathbb{R}^{n\times p}$, and $G(t) \in \mathbb{R}^{n\times q}$ is defined by

$$G(t) = P^{-1}\Upsilon\tilde{B}\Gamma(t)Q \tag{3.78}$$

with $\Upsilon = \Upsilon^T > 0$ in $\mathbb{R}^{n\times n}$, $Q = Q^T > 0$ in $\mathbb{R}^{q\times q}$ and $\tilde{B} = \big(\Phi C + \Psi CA\big)B$. Finally, $\dot{G}(t)$ denotes the total time derivative of G.

Proposition 3.2 (LMI-based ESAO Design – Form 1)**.** *Under Assumptions 3.1, 3.2.s, 3.3-3.5, if there exist matrices $P = P^T > 0$, $\Upsilon = \Upsilon^T > 0$ in $\mathbb{R}^{n\times n}$, $W \in \mathbb{R}^{n\times p}$, s.t.*

$$\begin{pmatrix} \mathcal{T}(P,W) & \mathcal{S}_\Lambda(P,W,\Upsilon) & PB & I_n & 0 \\ \mathcal{S}_\Lambda^T(P,W,\Upsilon) & -2\tilde{B}^T\Upsilon\tilde{B} & 0 & 0 & B^T \\ B^TP & 0 & -\frac{1}{2\delta}I_p & 0 & 0 \\ I_n & 0 & 0 & -\frac{1}{\delta}I_n & 0 \\ 0 & B & 0 & 0 & -\frac{1}{\delta}I_n \end{pmatrix} < 0 \tag{3.79}$$

with $\mathcal{T}(P,W) = PA + A^TP - WC - C^TW^T$, $\mathcal{S}_\Lambda(P,W,\Upsilon) = PAB - WCB - PB\Lambda - \big(\Phi C + \Psi CA\big)^T\Upsilon\tilde{B}$, Φ and Ψ in $\mathbb{R}^{n\times p}$, $\Lambda \in \mathbb{R}^{r\times r}$ any Hurwitz matrix, $\delta = \beta_u + \beta_0\beta > 0$, and if Γ is PE, that is, there exist positive scalars α_0 and t_0, s.t. $\forall t$ [106–108]

$$\alpha_0 t_0 I_q \leq \int_t^{t+t_0} \Gamma(\tau)^T\Gamma(\tau)d\tau \tag{3.80}$$

then the state estimation error vector $\tilde{x}$ and the parameter estimate error vector $\tilde{\theta}$ of the nonlinear adaptive observer (3.73)–(3.78), designed for the nonlinear system (3.6), tend to zero exponentially as $t \to \infty$. The closed-loop observer gain matrix L is computed as $L = P^{-1}W$.

Proof. See [92] (Refer to Appendix C.2). □

Corollary 3.1 (LMI-based ESAO Design – Form 2)**.** *Under Assumptions 3.1, 3.2.s, 3.3-3.5, if there exist matrices $P = P^T > 0$, $\Upsilon = \Upsilon^T > 0$ in $\mathbb{R}^{n\times n}$, $R \in \mathbb{R}^{r\times r}$ and $W \in \mathbb{R}^{n\times p}$, s.t.*

$$\begin{pmatrix} B^T\mathcal{T}(P,W)B & \mathcal{S}(P,R,W,\Upsilon) & B^TPB & B^T & 0 \\ \mathcal{S}^T(P,R,W,\Upsilon) & -2\tilde{B}^T\Upsilon\tilde{B} & 0 & 0 & B^T \\ B^TPB & 0 & -\frac{1}{2\delta}I_p & 0 & 0 \\ B & 0 & 0 & -\frac{1}{\delta}I_n & 0 \\ 0 & B & 0 & 0 & -\frac{1}{\delta}I_n \end{pmatrix} < 0 \tag{3.81}$$

and

$$R + R^T < 0 \tag{3.82}$$

with $\tilde{B} = \big(\Phi C + \Psi C A\big)B$, $\mathcal{T}(P, W) = PA + A^T P - WC - C^T W^T$, $\mathcal{S}(P, R, W, \Upsilon) = B^T PAB - B^T WCB - R - \tilde{B}^T \Upsilon \tilde{B}$, Φ *and* Ψ *in* $\mathbb{R}^{n\times p}$, $\delta = \beta_u + \beta_0 \beta > 0$, *and if* Γ *is PE, then the state estimation error vector* $\tilde{x}$ *and the parameter estimate error vector* $\tilde{\theta}$ *of the nonlinear adaptive observer (3.73)–(3.78), designed for the nonlinear system (3.6), tend to zero exponentially as* $t \to \infty$. *The closed-loop observer gain matrix* L *is computed as* $L = P^{-1}W$ *and the Hurwitz matrix* $\Lambda = \big(B^T PB\big)^{-1} R \in \mathbb{R}^{r\times r}$ *exists for any full-column rank matrix* B *and* $P = P^T > 0$. $Q = Q^T > 0$ *can be freely selected in* $\mathbb{R}^{q\times q}$.

Proof. See [92] (Refer to Appendix C.2). □

Further discussions of these designs are given in [92]. Also, these new approaches are exhaustively elaborated from backgrounds to advanced features in [97–102]. To keep consistency and entire forms of the present thesis on its main research subject dealing with robust adaptive sliding mode control techniques (discussed in the following chapters), the study on these adaptive observers is presented concisely. The validation of such techniques follows.

3.4.4 Simulation Results

The techniques of adaptive observer are tested on the 2-DOF helicopter simulator model [21]. We assume that all the input and state signals are bounded. The values of the actual parameters characterizing the simulated helicopter-based dynamics are determined in [21] and shown in Table 3.1. Moreover, the terms $\sin\phi\cos\phi\cdot\dot{\psi}^2$ and $\sin\phi\cos\phi\cdot\dot{\phi}\dot{\psi}$, shown in (3.43a) and (3.43b) respectively, are not globally Lipschitz functions in the state variables. Nevertheless, we consider the terms depicted above as Lipschitz since in practice they are bounded based on the boundedness of the states (any function, which is not globally Lipschitz, can be referred to as a weak Lipschitz function if it is bounded). The matrices Φ and Ψ are simply computed from the matrix equality (3.63) as

$$\Phi = \begin{pmatrix} 1 & 0 \\ 0 & 1 \\ 0 & 0 \\ 0 & 0 \end{pmatrix}, \ \Psi = \begin{pmatrix} 0 & 0 \\ 0 & 0 \\ 1 & 0 \\ 0 & 1 \end{pmatrix} \tag{3.83}$$

The computation of the ASAO gains L and P is based on the LMI design of the asymptotic stability (refer to Proposition 3.1). Meanwhile, the observer gains

L, P, Υ and Λ of the ESAO scheme are computed based on the exponential stability (refer to Corollary 3.1). The observer and adaptation law parameters of the ASAO (3.67)–(3.70) are

$$P = \begin{pmatrix} 4471.1 & 0 & -25.6 & 0 \\ 0 & 4471.1 & 0 & -25.6 \\ -25.6 & 0 & 1.2 & 0 \\ 0 & -25.6 & 0 & 1.2 \end{pmatrix} \tag{3.84a}$$

$$L = \begin{pmatrix} 23.9 & 0 \\ 0 & 23.9 \\ 3984.2 & 0 \\ 0 & 3984.2 \end{pmatrix} \tag{3.84b}$$

The observer and adaptation law parameters of the ESAO (3.73)–(3.78) are therefore selected as

$$P = \begin{pmatrix} 6595.9 & 0 & -20.6 & 0 \\ 0 & 6595.9 & 0 & -20.6 \\ -20.6 & 0 & 0.8 & 0 \\ 0 & -20.6 & 0 & 0.8 \end{pmatrix} \tag{3.85a}$$

$$L = \begin{pmatrix} 28.4 & 0 \\ 0 & 28.4 \\ 8776.3 & 0 \\ 0 & 8776.3 \end{pmatrix} \tag{3.85b}$$

$$\Lambda = \begin{pmatrix} -4395.6 & 0 \\ 0 & -4395.6 \end{pmatrix} \tag{3.85c}$$

$$\Upsilon = \begin{pmatrix} 6061.6 & 0 & 0 & 0 \\ 0 & 6061.6 & 0 & 0 \\ 0 & 0 & 3425.9 & 0 \\ 0 & 0 & 0 & 3425.9 \end{pmatrix} \tag{3.85d}$$

and

$$Q = \mathrm{diag}(20,\ 20,\ 20,\ 20,\ 400,\ 20,\ 400,\ 2000,\ 200) \tag{3.86}$$

for both ASAO and ESAO schemes. The computation of the observer gains, in both cases, are cast as LMI problems which can easily be solved by using the interior point optimization method implemented in the MATLAB software using the LMI control toolbox [109]. While the selection of the adaptation matrix Q, which is significant for the algorithms regarding the parameter estimation performance (rate and accuracy), is freely adjusted, it is reduced to a positive diagonal matrix (more simply, can be any positive scalar multiplying

the identity matrix). In fact, the parametrization and the implementation of the proposed algorithms remain moderately easier (less laborious) than many other algorithms for similar adaptive observer problems (see *e.g.* [107, 110–114]).

Consider the input signals $u_1 = 3.4+2.7\sin(4.3\pi t)+4.0\sin(3.0\pi t+0.4\pi)+3.7\sin(2.0\pi t+0.4\pi)+3.2\sin(0.4\pi t)+1.9\sin(0.3\pi t)$ and $u_2 = 1.0+3.1\sin(5.1\pi t-0.25\pi)+2.7\sin(3.1\pi t-0.5\pi)+2.5\sin(1.7\pi t+0.4\pi)+3.3\sin(\pi t+0.5\pi)+2.3\sin(0.6\pi t+0.5\pi)$ which result in sufficient PE signals. The simulation results for the estimation of the parameters and states are shown in Figures 3.4-3.14. It can be seen that both the state and the parameter estimates converge to their actual values accurately. However, the transient responses of the ESAO design are more satisfactory than those of the ASAO (see Figure 3.4–3.12). The estimation errors of the states are demonstrated within a very short time (see Figures 3.13 and 3.14). Indeed, their convergences are much faster than the parameter estimates. Note that we use the ASAO and ESAO schemes by considering the effect of the uncertainty approximations negligible. It should be pointed out that the effect of the approximation uncertainty due to the nonlinear parameter dependency within the yaw dynamics is well rejected and cannot be distinguished in the different estimation results shown. However, to deal with any external perturbation or any modeling uncertainty, given by $d(x,t)$ added to the system dynamics (3.6), the different adaptive observers discussed above can be extended to robust ASAO and ESAO designs based on any H_∞ minimization of the loop transfer from the lumped uncertainty amount $d(x,t)$ to the estimate errors (for instance, $\tilde{x}$). In addition, such multi-objective designs can be investigated under further LMI constraints encountering specific transient performances and robustness properties. Some experimental results are tentatively obtained by the implementation of the ESAO scheme (refer to Figures B.1-B.11 in Appendix B.1). Further adjustments of the freely selected parameters (*e.g.*, Q) will most probably improve the accuracy of estimation. But also, the inaccuracy depicted there justifies the requirement for robust control techniques for systems with uncertainties poorly evaluated (principal objective investigated in this thesis).

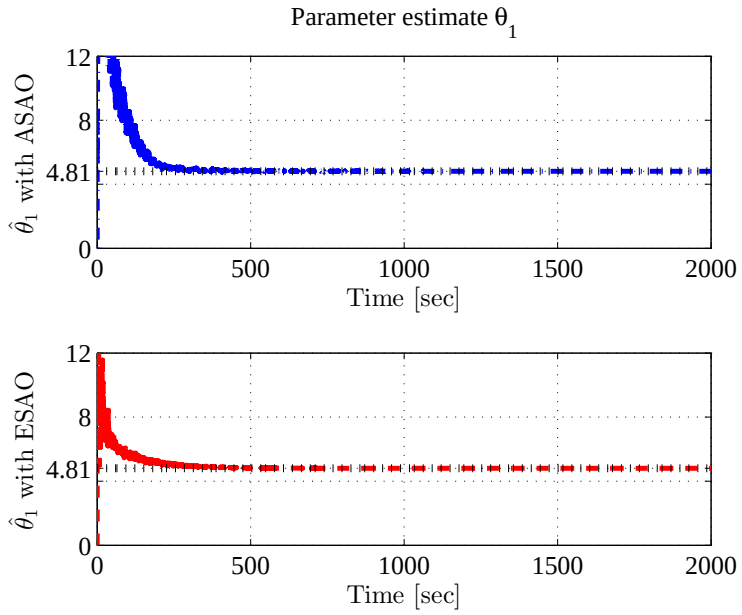

Figure 3.4: Estimate of parameter θ_1

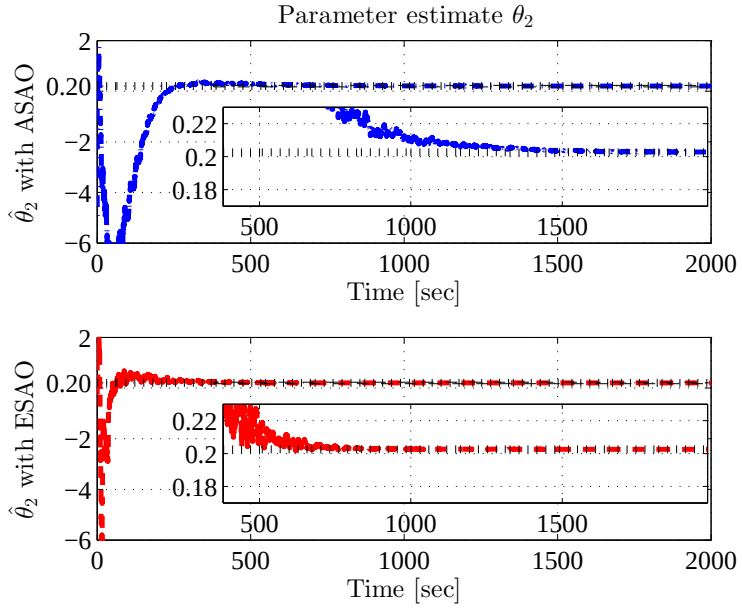

Figure 3.5: Estimate of parameter θ_2

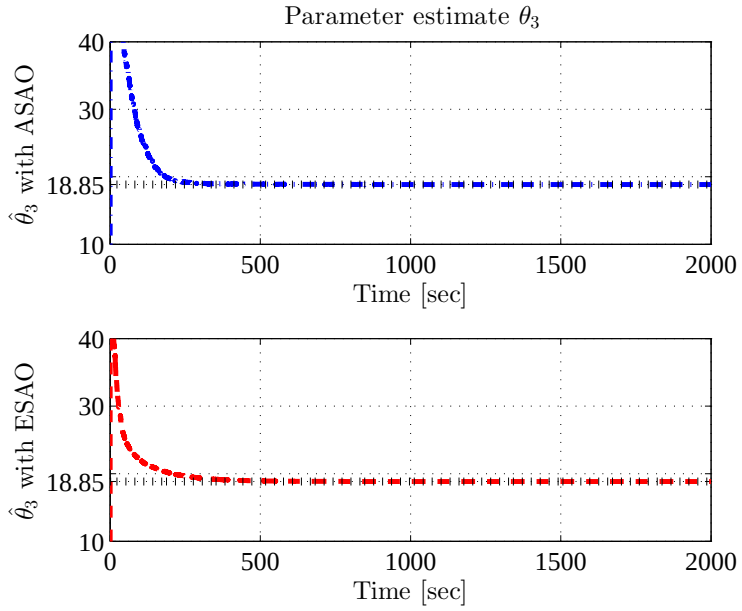

Figure 3.6: Estimate of parameter θ_3

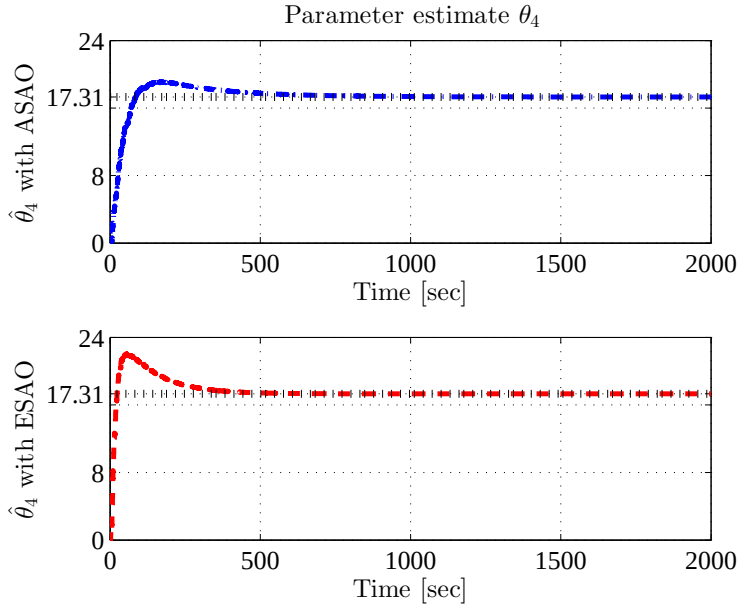

Figure 3.7: Estimate of parameter θ_4

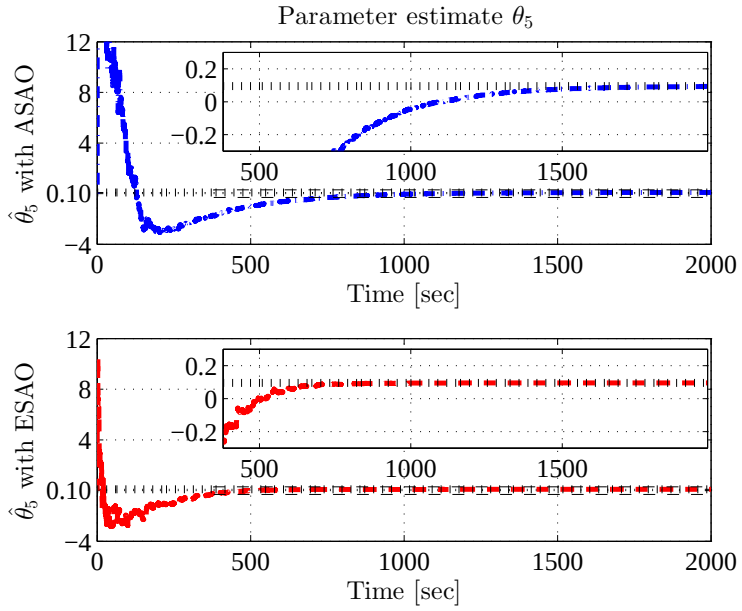

Figure 3.8: Estimate of parameter θ_5

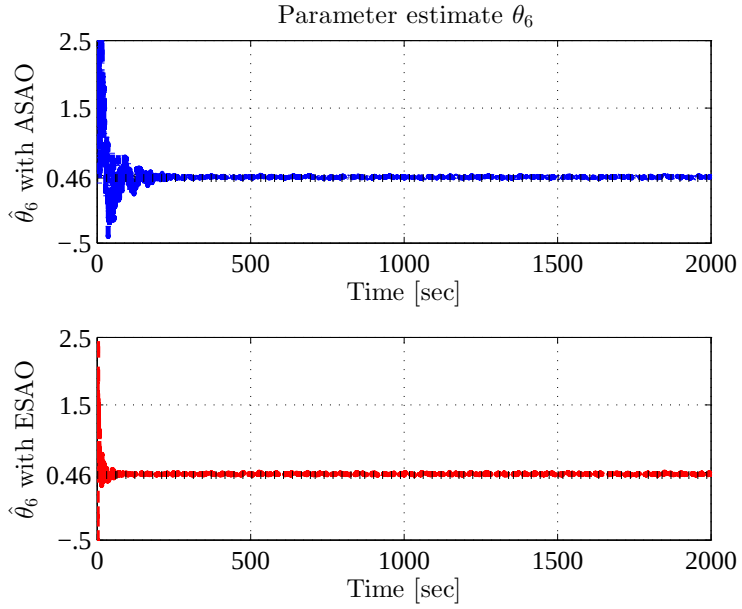

Figure 3.9: Estimate of parameter θ_6

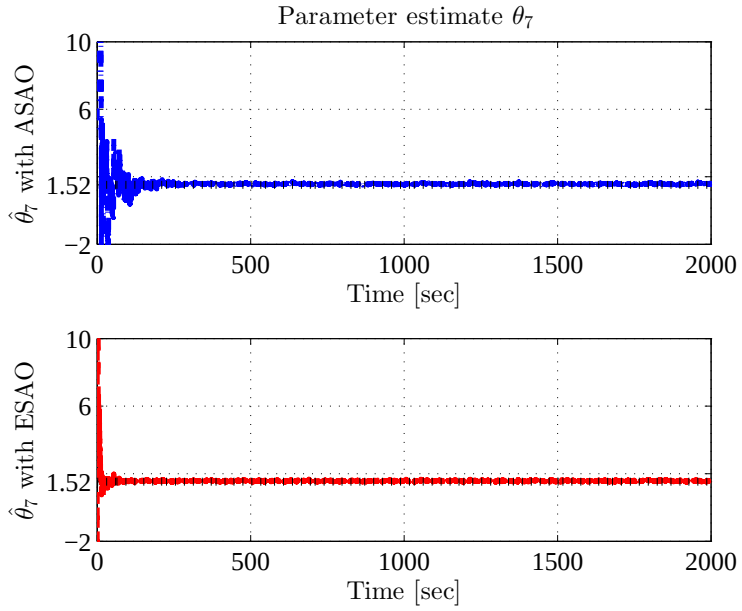

Figure 3.10: Estimate of parameter θ_7

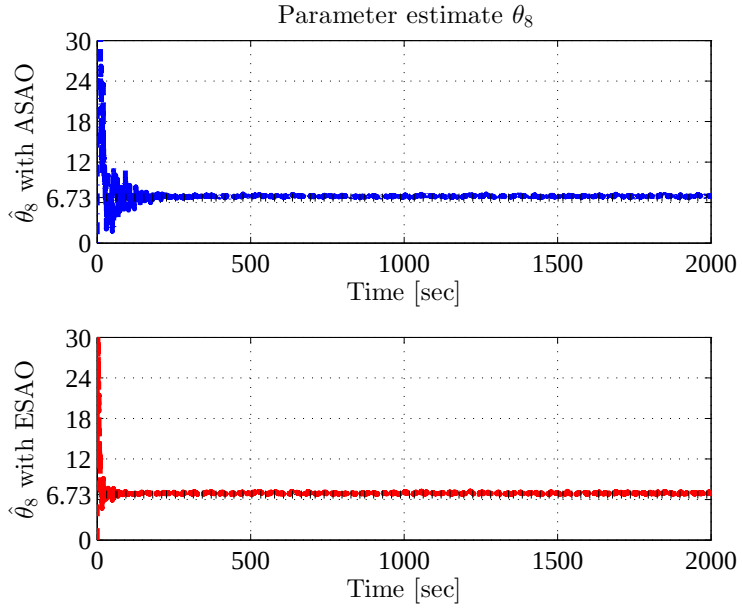

Figure 3.11: Estimate of parameter θ_8

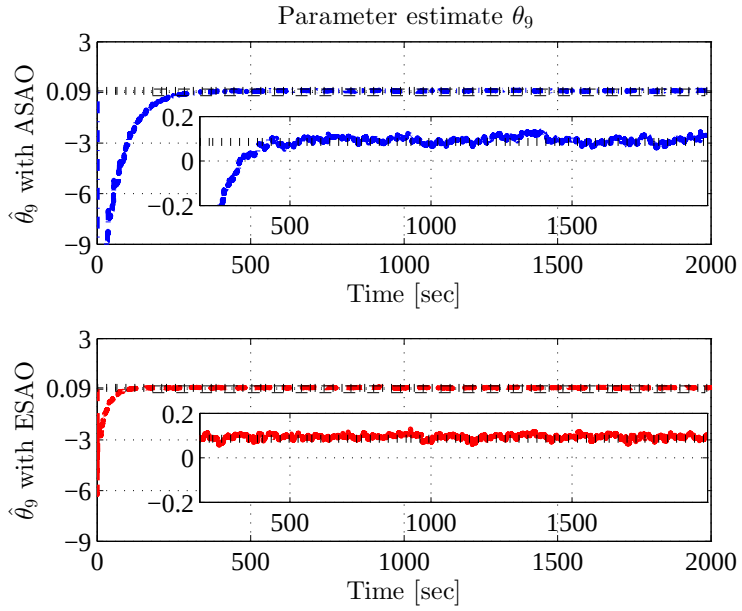

Figure 3.12: Estimate of parameter θ_9

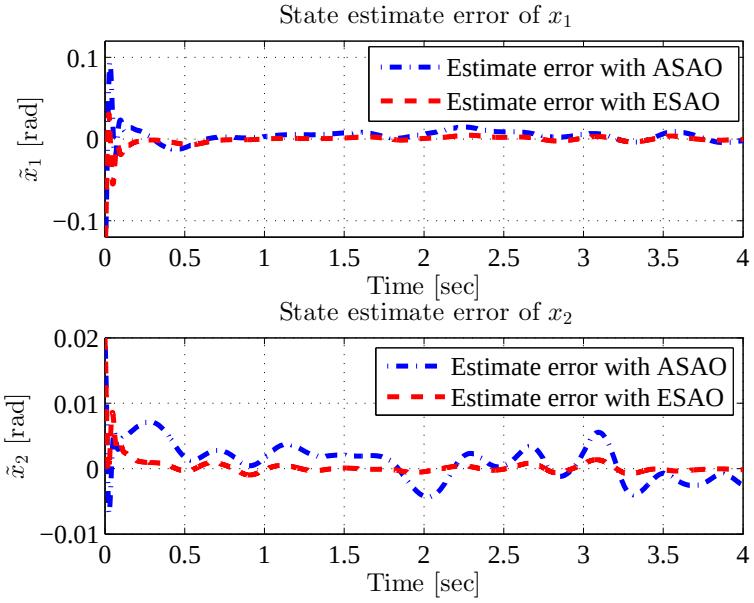

Figure 3.13: State estimate errors x_1 and x_2

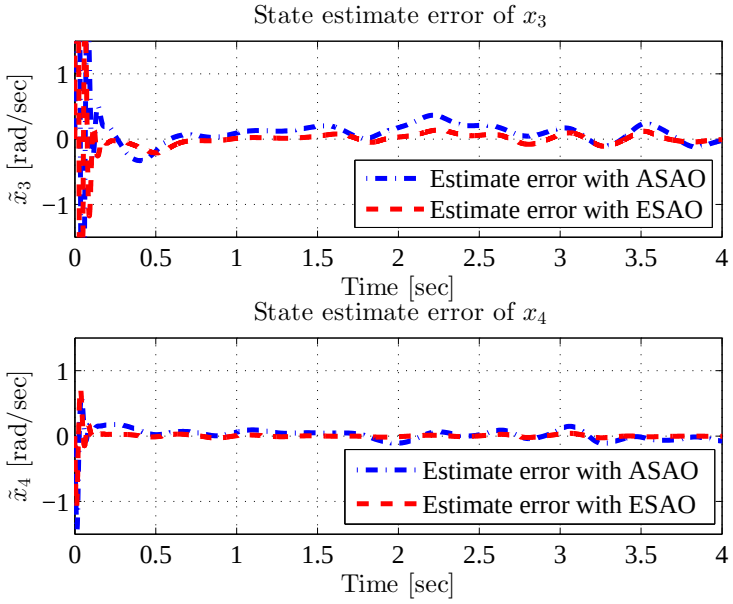

Figure 3.14: State estimate errors of x_3 and x_4

3.5 Conclusion

This chapter models the 2-DOF experimental helicopter-based setup and validates the model parameters. The nonlinear dynamics of the helicopter model are derived based on space transformation and Lagrangian mechanics. The validations of the parameters are discussed. Techniques of adaptive observer with asymptotic and exponential designs are provided to validate the unknown constant parameters of the setup. Simulation results on the 2-DOF experimental helicopter model setup demonstrate the effectiveness of the adaptive observer designs.

The dynamics of the setup containing quadratic and trigonometric functions of the system states with uncertain parameters is a typical nonlinear uncertain system. When the setup with uncertain parameters is close to its equilibrium state, it can be treated as a nonlinear system with uncertainties of unknown constant bounds. When the system states are far from the equilibrium states, the uncertainties are bonded with some quadratic polynomials of the system states.

More details in terms of motivations, objectives, novelties, pros and cons of this chapter contents are presented in Table 3.2.

Table 3.2: Chapter 3 Recap

Motivation(s)	- Modeling and parameterization of the principal setup to validate the different control approaches discussed in the current thesis.
Objective(s)	- Parameter estimation of nonlinear dynamics with unmeasurable regression matrix (*i.e.*, matching with the unknown parameter vector).
Novelty(ies)	- New nonlinear adaptive observer schemes - Asymptotic stability *vs.* exponential stability based design.
Pro(s)	- LMI-based design. - Applicability to electromechanical dynamics. - Extendible to perturbed dynamics (robustness). - Exponential stability of both state and parameter estimate dynamics.
Con(s)	- Uneven adjustment of adaptation law gains (as most of adaptive schemes). - PE condition still required.

4 Adaptive Sliding Mode Control – General Framework

As discussed in Chapter 3, constant parameters of the nonlinear uncertain dynamic systems can be obtained by static experiments, calculations and adaptive observer techniques. However, for unknown time-varying uncertainties (*e.g.*, unknown time-varying parameters and unknown external disturbances), robust control techniques are required. In this chapter, we introduce the general framework of a robust control technique – ASMC. Stability types will be presented first. Then, the conventional SMC model will be discussed. Based on the analysis of the necessary and sufficient conditions for the FTC of ASMC, an extension of the integral adaptation law is proposed for the ASMC design. The relevant mathematical definitions and theorems can be found in Appendix A and can also be seen in [1, 49, 115]. Some propositions are reported in [116–118].

4.1 Types of Stability

The stability definitions and theorems can be found in many textbooks. Some of them used in this dissertation are mainly from [1]. Given any dynamic system with some equilibria (refer to A.1 of Appendix A), roughly speaking, an equilibrium is stable if all solutions starting at nearby points remain nearby. If all solutions of a stable system are ultimately bounded, it is UUB. It is asymptotically stable (AS) or asymptotically converges to the equilibrium if all solutions starting at nearby points not only stay nearby, but also tend to the equilibrium as time approaches infinity [1]. If all the solutions of an AS system converge to its equilibrium with some exponential rate, the equilibrium is exponentially stable (ES) or the solutions converge exponentially. It is finite-time stable or stable with FTC to the equilibrium if all solutions starting at nearby points tend to the equilibrium in finite time interval [49]. Figure 4.1

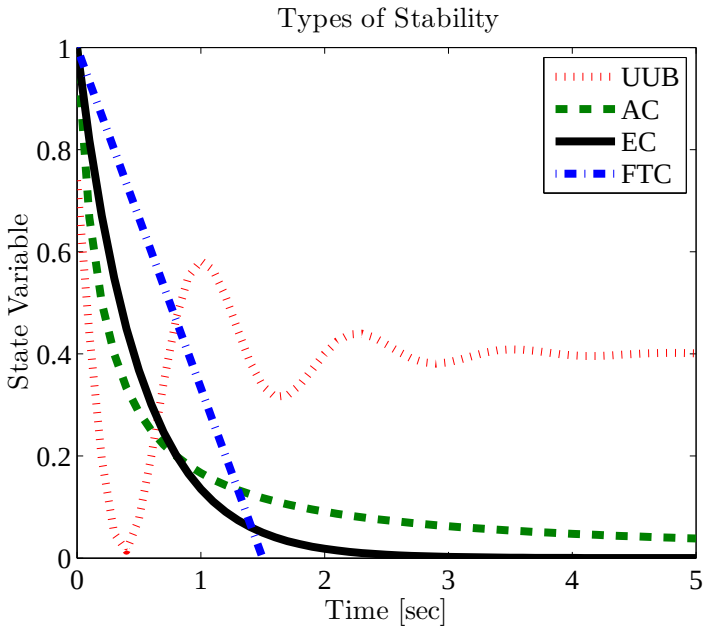

Figure 4.1: Different convergences: asymptotic convergence (AC), exponential convergence (EC), FTC, and convergence in UUB sense. The equilibrium point is at the origin

shows these different stabilities (convergences). For the nonlinear systems with uncertainties, the stability analysis is mainly based on Lyapunov's stability theorem and other Lemmas such as Barbalat's Lemma, LaSalle's Invariance Principle, Comparison Lemma and Fillipov Integration. They can be found in many books (*e.g.* [1, 119]). Also, they are partially presented in Appendix A.

4.2 Sliding Mode Control

4.2.1 Motivation Example

Consider the following nonlinear scalar dynamics:

$$\dot{x} = a \cos x + bu \tag{4.1}$$

where a and b are uncertain parameters and u the control input. Consider the two cases

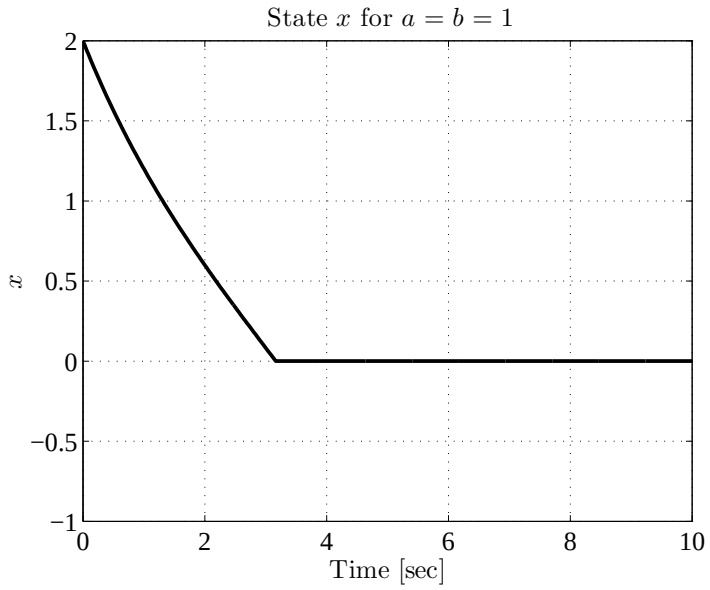

Figure 4.2: Closed-loop switching control response of (4.1)-(4.3) – Case 1

- Case 1: a and b are constants with $b > 0$. For instance, $a = 1$ and $b = 1$.
- Case 2: a and b are uncertain varying terms. For instance, $a = \sin t$ and $b = 1 + 0.25 \sin 3t$.

For both cases, the following feedback control will stabilize the state x to zero in finite time.

$$u = -1.5 \operatorname{sgn}(x) \tag{4.2}$$

where $\operatorname{sgn}(\cdot)$ is the signum function defined as follows

$$\operatorname{sgn}(x) := \begin{cases} -1 & \text{if} \quad x < 0 \\ 0 & \text{if} \quad x = 0 \\ 1 & \text{if} \quad x > 0 \end{cases} \tag{4.3}$$

The time-responses of the closed-loop system are shown in Figures 4.2 and 4.3. This is an example of a typical SMC design. From this example, we can see two main properties of SMC:

- The system is *robust* against the uncertainties that can be time invariant (constant) or varying.

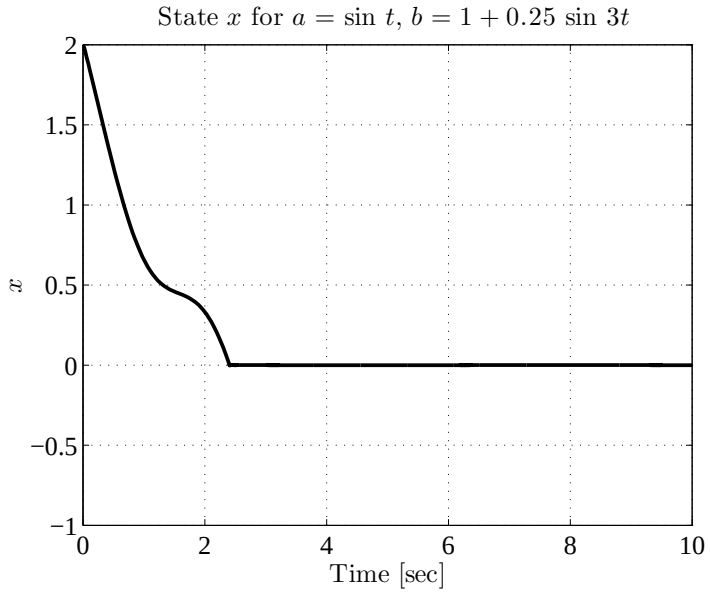

Figure 4.3: Closed-loop switching control response of (4.1)-(4.3) – Case 2

- The system is stabilized to its equilibrium point in *finite time*.

To achieve these two properties, we use a switching function $\text{sign}(\cdot)$ in the feedback control, $u = -K\text{sign}(x)$, with the switching gain $K = 1.5$. In this example, the feedback gain K is designed greater than the magnitudes of the lumped uncertainties, *i.e.*, $u > \dfrac{|a|}{b}$ such that the state x can be stabilized to zero in finite time no matter whether the uncertainties are constant or time-varying.

Typically, the SMC is a nonlinear control method that forces the trajectories to reach a *sliding manifold* [1] (also, called *sliding hypersurface*) in finite time and to stay on the manifold thereafter. The sliding manifold can be simply an equilibrium state of the system (as in the above example, $x = 0$) or any designed variable dynamics (usually the system state has asymptotic stability when the system is on this surface). The state-feedback control law in SMC switches from one continuous structure to another based on the current position in the state space. Hence, the control signal in classic SMC is discontinuous. In Figure 4.4, system trajectories reach the sliding surface in finite time and then stay on or slide along this surface. The main strength of SMC is its robustness in terms of non-sensitivity to parameter variations that enter

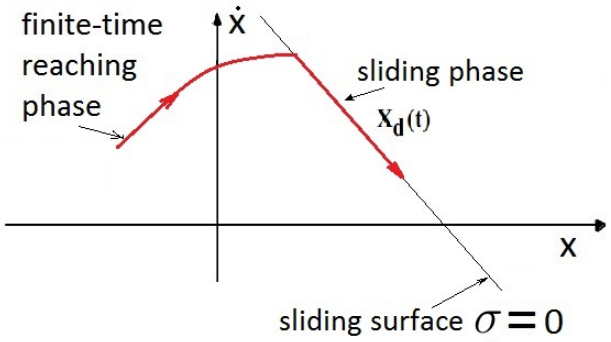

Figure 4.4: Ideal Sliding Mode [52]: Phase plane trajectory of a system being stabilized by any SMC. After the initial reaching phase, the system state (red) *slides* along the *sliding surface* $\sigma = 0$ (black)

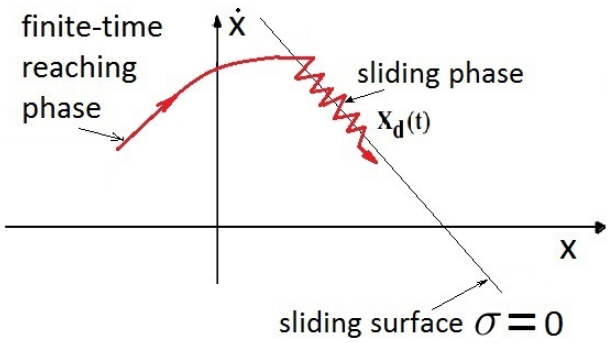

Figure 4.5: Real Sliding Mode [52]: Phase plane trajectory of a system being stabilized by any SMC. After the initial reaching phase, the system state (red) *slides* along the vicinity of the *sliding surface* $\sigma = 0$ (black)

into the control channel, *i.e.*, CMC, and FTC to the sliding surface. In real implementations of SMC, however, the generally non-deterministic switching control signal causes the system to 'chatter' in a tight neighborhood of the sliding surface. In addition to chatter, energy loss, plant damage, and excitation of unmodeled dynamics may also occur [1, 61, 120]. In Figure 4.5, system states (red) chatter along the sliding surface as the system asymptotically approaches the origin. Thus, in the real implementation of SMC, smooth techniques must be adopted.

4.2.2 SMC Scheme

Consider the nonlinear dynamic system (3.2). Defining a *sliding variable* (also called *sliding function*, *switching variable*, *switching function*, or *sliding quantity*) $\sigma(x,t) \in \mathbb{R}^m$ that represents a kind of distance at which the states x are away from a sliding surface, then we have:

- $\sigma(x,t) \neq 0$, when the state is outside the sliding surface
- $\sigma(x,t) = 0$, when the state is on the sliding surface

Mathematically, the variable σ is a continuous function, and the set

$$\Sigma = \{x \in \chi \mid \sigma(x,t) = 0\} \tag{4.4}$$

is non-empty and is locally an integral set in the sense of Filippov [16, 53].

Definition 4.1. The set Σ is called *sliding surface* (*sliding manifold*) [16, 53].

The sliding surface $\sigma(x,t) = 0$ is a designed state mode where the system state on this mode is stable or has a desired behaviour. For example, we can select

$$\sigma(x,t) = x + \dot{x} \tag{4.5}$$

that is, $\sigma = 0$ yields $x = x_0 e^{-t}$,

$$\sigma(x,t) = K_P \cdot x + K_I \int_0^t x d\tau + K_D \cdot \dot{x} \tag{4.6}$$

$$\sigma(x,t) = e = x - x_{desired} \tag{4.7}$$

and

$$\sigma(x,t) = K_P \cdot e + K_I \int_0^t e d\tau + K_D \cdot \dot{e} \tag{4.8}$$

The system state on the sliding surface (4.5) has an exponential stability. The sliding surface can also be designed as a PID form (4.6) in the state or a function of the trajectory error (4.7) or (4.8).

Definition 4.2. The motion on Σ is called *sliding mode* [16, 53, 120]

Therefore, the control objectives of SMC are such that:

1. The system is capable of reaching $\sigma(x,t) = 0$ in finite time from any initial condition.

2. Having reached the surface $\sigma(x,t) = 0$, the system stays on it.

Ideally, the system state slides along the sliding surface $\sigma = 0$ exactly. However, in real implementation, the system state can not stay on the sliding surface exactly due to measurement and computation imperfections. Instead, the state slides along the vicinity of the sliding surface $\sigma = 0$ in *real sliding mode*.

Definition 4.3. *Ideal sliding mode:* The motion of the system as it takes place strictly on the constraint manifold $\sigma = 0$ [53].

Definition 4.4. *Real sliding mode:* The motion of the system as it takes place on the *sliding manifold* $|\sigma| \leq \delta$ with $\delta > 0$, *i.e.*, it slides along the vicinity of the sliding surface $\sigma = 0$ [53].

Figures 4.4 and 4.5 show the ideal sliding mode and real sliding mode respectively.

4.2.3 Switching Feedback Control Law

To fulfil the objectives of SMC, we first consider the feedback control law based on Lyapunov redesign. Let us first write the sliding variable dynamics. Recall the nonlinear dynamics (3.2) introduced in Chapter 3,

$$\dot{x} \quad = \quad f(x,t) + g(x,t) \cdot u \tag{4.9}$$

From (4.9), we have

$$\begin{aligned} \dot{\sigma}(x,t) &= \frac{\partial \sigma}{\partial t} + \frac{\partial \sigma}{\partial x} \cdot \dot{x} \\ &= \frac{\partial \sigma}{\partial t} + \frac{\partial \sigma}{\partial x} \cdot f(x,t) + \frac{\partial \sigma}{\partial x} \cdot g(x,t) u \end{aligned} \tag{4.10}$$

That is,

$$\dot{\sigma}(x,t) = \Psi(x,t) + \Gamma(x,t) \cdot u \tag{4.11}$$

where $\Psi(x,t) = \dfrac{\partial \sigma}{\partial t} + \dfrac{\partial \sigma}{\partial x} \cdot f(x,t)$ and $\Gamma(x,t) = \dfrac{\partial \sigma}{\partial x} \cdot g(x,t)$ are nonlinear time-varying smooth functions containing parametric uncertainties and external

disturbances [16, 51, 74, 90]. In the following, the arguments of these scalar-valued functions (*i.e.*, x and t in σ, Ψ and Γ) will be omitted occasionally for the sake of simplicity. In (4.11), the control input u appears in the first order derivative of the sliding variable. Thus, the *relative degree* of the system is equal to one [53].

Definition 4.5. The dynamic system (4.9) has a *relative degree* of r if the control input appears on the $r-$th order derivative of the sliding variable σ [53].

Most mechanical systems have a relative degree of one. We also consider that the target nonlinear systems have a relative degree of one throughout the dissertation, *i.e.*, we only consider the first order SMC.

Consider a Lyapunov candidate function

$$V = \frac{1}{2}\sigma^T(t)\sigma(t) \tag{4.12}$$

Using (4.11), the time derivative of V is

$$\begin{aligned} \dot{V} &= \sigma^T \dot{\sigma} \\ &= \sigma^T[\Psi + \Gamma u] \end{aligned} \tag{4.13}$$

A sufficient condition for the existence of a sliding mode is that $\dot{V}$ is less than zero, *i.e.*, the feedback control law $u(x)$ is chosen such that σ and $\dot{\sigma}$ have opposite signs. We present two ideas.

One way is to select $u(x)$ such that

$$\dot{\sigma} = -\mu \cdot \mathbf{sgn}(\sigma) \tag{4.14}$$

where $\mathbf{sgn}(\cdot)$ is the signum vector function in $\mathbb{R}^m$ defined as $[\mathrm{sgn}(\sigma_1), \cdots, \mathrm{sgn}(\sigma_m)]^T$. Assume that $\Gamma(x,t)$ is non-singular. Then, we can find the feedback control u by rewriting (4.14),

$$\Psi + \Gamma u = -\mu \cdot \mathbf{sgn}(\sigma) \tag{4.15}$$

We take

$$u = -\Gamma^{-1}\Big[\Psi + \mu \cdot \mathbf{sgn}(\sigma)\Big] \tag{4.16}$$

From (4.16), one can see that the control u requires the exact knowledge of $\Psi(x,t)$ and $\Gamma(x,t)$. By choosing the control (4.16), we have the following lemma.

Lemma 4.1. *Consider the nonlinear uncertain system* (4.9) *with the sliding variable dynamics* (4.11) *controlled by* (4.16)*. A sliding mode can be established in finite time with the maximum reaching time t_r estimated as*

$$t_r = \frac{\sqrt{2V(0)}}{\mu} \tag{4.17}$$

where $\sqrt{2V(0)} = |\sigma(0)|$ is the initial state.

Proof. Denoting by $\|\sigma\|_p = (|\sigma_1|^p + |\sigma_2|^p + \cdots + |\sigma_m|^p)^{1/p}$ for any integer $p \geq 1$, the l_p-norm of any vector $\sigma \in \mathbb{R}^m$. In particular, when $p = 1$, we have $\|\sigma\|_1 = |\sigma_1| + |\sigma_2| + \cdots + |\sigma_m|$. We have $\forall \sigma \in \mathbb{R}^m$, $\|\sigma\|_2 \leq \|\sigma\|_1 \leq \sqrt{m}\|\sigma\|_2$ [121]. Substituting (4.14) into (4.13), we obtain

$$\begin{aligned} \dot{V} &= -\mu\sigma^T \cdot \mathbf{sgn}(\sigma) \\ &= -\mu\|\sigma\|_1 \\ &\leq -\mu\|\sigma\|_2 \\ &\leq -\mu\sqrt{2V} \end{aligned} \tag{4.18}$$

This result implies that the trajectories always approach the sliding surface with the speed $\dot{\sigma} \cdot \mathrm{sgn}(\sigma) \equiv \dfrac{d}{dt}|\sigma|$ toward the switching surface fixed by μ [122]. In fact, from (4.18), we have, for $\sigma \neq 0$ (*i.e.*, $V \neq 0$),

$$\frac{d\sqrt{V}}{dt} \leq -\frac{\mu}{\sqrt{2}} \tag{4.19}$$

Integrating both sides of (4.19) from 0 to $t \geq 0$, we have

$$\sqrt{V(t)} \leq -\frac{\sqrt{2}\mu}{2}t + \sqrt{V(0)} \tag{4.20}$$

The inequality (4.20) implies that the positive function $\sqrt{V}$ will decrease with a rate at least $\dfrac{\mu}{\sqrt{2}}$ and reach zero with a maximum reaching time t_r estimated as (4.17) [1, 49, 61]. □

Alternatively, we select $u(x)$ such that

$$\frac{d}{dt}|\sigma| \leq -\mu \tag{4.21}$$

For the sake of simplicity, we consider a single sliding variable dynamic (*i.e.*, $m = 1$). The objective (4.21) implies that the positive term $|\sigma|$ will be decreasing at a rate of at least μ per second and, therefore, reaches the sliding surface $|\sigma| = 0$ in finite time from any bounded initial value $|\sigma(0)|$. Considering the case $\sigma \neq 0$, (4.21) can be rewritten as

$$\frac{d}{dt}|\sigma| = \dot{\sigma} \cdot \mathrm{sgn}(\sigma) \leq -\mu \tag{4.22}$$

Then, substituting (4.11) into (4.22), we obtain

$$\Psi \cdot \mathrm{sgn}(\sigma) + \Gamma \cdot \mathrm{sgn}(\sigma) \cdot u \leq -\mu \tag{4.23}$$

We assume Γ is positive definite. Denote by $\bar{\Psi}$ the upper bound of $|\Psi|$ and $\underline{\Gamma}$ the lower bound of Γ, *i.e.*,

$$|\Psi| \leq \bar{\Psi} \tag{4.24}$$

and

$$0 < \underline{\Gamma} \leq \Gamma \tag{4.25}$$

Noticing that $\mathrm{sgn}(\sigma) \cdot \mathrm{sgn}(\sigma) = 1$ for $\sigma \neq 0$, one can verify that by taking

$$u = -K\mathrm{sgn}(\sigma) \tag{4.26}$$

with the switching gain K large enough

$$K \geq \frac{\bar{\Psi} + \mu}{\underline{\Gamma}} \tag{4.27}$$

then (4.21) will be met and the sliding variable will reach the sliding surface in finite time.

Lemma 4.2. *Consider the nonlinear uncertain system* (4.9) *with the sliding variable dynamics* (4.11) *controlled by* (4.26) *satisfying* (4.27)*. A sliding mode can be established in finite time with the maximum reaching time t_r estimated as*

$$t_r \leq \frac{|\sigma(0)|}{\mu} \tag{4.28}$$

Proof. Integrating both sides of (4.21) from 0 to $t \geq 0$, we obtain

$$|\sigma(t)| \leq -\mu t + |\sigma(0)| \tag{4.29}$$

The inequality (4.29) implies that the positive amount $|\sigma|$ will decrease with a rate at least μ and will reach zero with a maximum reaching time t_r estimated as (4.28) [1]. □

It can be seen that the first SMC design (4.16) requires a full knowledge of the uncertainties Ψ and Γ, while in the second method (*i.e.*, equations (4.26) and (4.27)) the upper bound of $|\Psi|$ and the lower bound of Γ, must be given.

The above results using conventional SMC show that the knowledge of the bounds of the uncertainties must be *a priori* known so that a constant switching gain can be selected to ensure the FTC. For the nonlinear system with uncertainties of unknown bounds, ASMC techniques are developed trying to design a time-varying switching gain K such that it can compensate for the uncertainties dynamically.

4.3 ASMC – Equivalent Control Method

Given the dynamics (4.9) with the sliding variable dynamics (4.11), if we know the nominal values of the uncertainties Ψ and Γ, it is usually a good choice to apply the *equivalent control* first [49]. For the sake of simplicity, we consider in the following the scalar dynamics, *i.e.*, $m = 1$.

Separating Ψ and Γ into nominal and uncertain parts, *i.e.*$\Psi \triangleq \hat{\Psi} + \tilde{\Psi}$ and $\Gamma \triangleq \hat{\Gamma} + \tilde{\Gamma}$ with $\hat{\Psi}$ (*resp.*, $\hat{\Gamma}$) and $\tilde{\Psi}$ (*resp.*, $\tilde{\Gamma}$) representing the nominal and uncertain values respectively, the sliding variable dynamics is then written as

$$\dot{\sigma} = \hat{\Psi} + \tilde{\Psi} + (\hat{\Gamma} + \tilde{\Gamma})u \tag{4.30}$$

By using the equivalent control method, the control input consists of two parts:

$$u = u_{eq} + u_{sw} \tag{4.31}$$

where u_{eq} represents the equivalent control part and u_{sw} the switching control part. The equivalent control u_{eq} is obtained by solving the following equation

$$\dot{\sigma} = \hat{\Psi} + \hat{\Gamma} u_{eq} = 0 \tag{4.32}$$

i.e., by assuming that the uncertainties $\tilde{\Psi}$ and $\tilde{\Gamma}$ are zero and by letting the sliding variable dynamics be at equilibrium. The equivalent control is then obtained

$$u_{eq} = -\hat{\Gamma}^{-1}\hat{\Psi} \tag{4.33}$$

The term u_{eq} compensates for the nominal parts of the nonlinear system. It determines the behaviour of the nominal system restricted to the switching surface. The term u_{sw} represents the switching part to compensate the effect

of the uncertainties $\tilde{\Psi}$ and $\tilde{\Gamma}$, and drives the system trajectories toward the switching surface until intersection occurs [10]. Substituting (4.31) with u_{eq} defined by (4.33) into (4.30), we obtain

$$\dot{\sigma} = \left(\tilde{\Psi} - \tilde{\Gamma}\hat{\Gamma}^{-1}\hat{\Psi}\right) + \Gamma u_{sw} \tag{4.34}$$

The term $\left(\tilde{\Psi} - \tilde{\Gamma}\hat{\Gamma}^{-1}\hat{\Psi}\right)$ in (4.34) is fully uncertain. The dynamics (4.34) has a similar form as (4.11). Indeed, the intermediate control u_{sw} can be treated in the same way as (4.26), *i.e.*,

$$u_{sw} = -K(t) \cdot \mathrm{sgn}(\sigma) \tag{4.35}$$

Substituting (4.33) and (4.35) into (4.31), we obtain the final control input

$$u = -\hat{\Gamma}^{-1}\hat{\Psi} - K(t) \cdot \mathrm{sgn}(\sigma) \tag{4.36}$$

In most electro-mechanical dynamic systems, we know some nominal values. Thus, in real implementation of ASMC, the control has the form (4.36) since the compensator (4.33) would help to reduce the magnitudes of the eventual SMC structure. Without loss of generality and for the sake of simplicity for the rest of the chapter, we assume that Ψ *is fully uncertain*, *i.e.*, $\hat{\Psi} = 0$, so that the control is reduced to its switching structure, *i.e.*, $u \equiv u_{sw}$. In other words, we focus on the design of the time-varying switching gain in order to suppress the uncertainties.

4.4 ASMC - Sufficient and Necessary Conditions

As discussed above, for the case of unknown nominal values of the uncertainties, the corresponding control input (4.36) eventually turns to the form of (4.35) which has only a switching part. Thus, for simplicity, we consider that for the sliding variable dynamics (4.11) the uncertainty Ψ is fully unknown. Therefore the control input only has a switching part, *i.e.*,

$$u = -K(t) \cdot \mathrm{sgn}(\sigma) \tag{4.37}$$

The objective of ASMC is to design a time-varying switching gain $K(t)$ so that the sliding variable $\sigma(x,t)$ can be stabilized to zero in finite time. In this section, we discuss the ASMC conditions which are slightly different from the previous publications (*e.g.*, [123, 124]). These conditions must satisfy the two main requirements of ASMC (4.37) for any dynamics (4.11). First, the control $u(t)$ compensates for any bounded perturbation $\frac{\Psi}{\Gamma}$, standardly. Second, after

compensating for $\frac{\Psi}{\Gamma}$, the sliding mode can be established in finite time. For the dynamics (4.11) subject to the control (4.37), we consider the case of *ideal sliding* ASMC, where the sliding mode is said to be established when $\sigma = 0$ for all time after reaching the designed manifold.

Substituting (4.37) into (4.11), we obtain the sliding variable dynamics in terms of the switching gain $K(t)$

$$\dot{\sigma} = \Psi - \Gamma K(t) \cdot \mathrm{sgn}(\sigma) \tag{4.38}$$

4.4.1 Sufficient Condition

The following result discusses a "minimum" conditional statement to be tied to the existence of a sliding mode.

Lemma 4.3. *Consider the nonlinear uncertain system* (4.9) *with the sliding variable dynamics* (4.11) *controlled by* (4.37). *Given the scalars* $t^* \geq 0$ *and* $\varepsilon > 0$ *small, for any varying (or dynamically changing) switching gain* $K(t)$ *satisfying*

$$K(t) \geq \frac{|\Psi|}{\Gamma} + \varepsilon \tag{4.39}$$

for all $t \geq t^*$, *a sliding mode can be established in finite time* $t_r \geq t^*$.

Proof. Noticing $|\sigma| = \sigma \cdot \mathrm{sgn}(\sigma)$ for $\sigma \neq 0$, assuming (4.25) and combining (4.38) and (4.39), we have for $t \geq t^*$

$$\begin{aligned} \frac{d}{dt}|\sigma| &= \dot{\sigma} \cdot \mathrm{sgn}(\sigma) \\ &= \Psi \mathrm{sgn}(\sigma) - \Gamma K \\ &\leq -\varepsilon \underline{\Gamma} \end{aligned} \tag{4.40}$$

where $\underline{\Gamma}$ is the positive lower bound of Γ introduced in (4.25). By integrating the differential inequality (4.40) between t^* and $t \geq t^*$, we obtain

$$|\sigma| \leq |\sigma(t^*)| - \underline{\Gamma}\varepsilon(t - t^*) \tag{4.41}$$

Thus, $|\sigma| \to 0$ in finite time. In addition, an upper-bound of the reaching time is estimated as

$$t_r \leq t^* + \frac{|\sigma(t^*)|}{\underline{\Gamma}\varepsilon} \tag{4.42}$$

for given $t^* \geq 0$ and $\varepsilon > 0$. □

Roughly, from the sufficient condition (4.39) of Lemma 4.3, t^* refers to the so-called compensating phase, when the switching gain compensates completely for the lumped uncertainties, while the reaching phase time frame can be depicted from the second term of the right member of (4.42), *i.e.*, $\frac{|\sigma(t^*)|}{\Gamma\varepsilon}$. The concept of these two phases will be discussed more extensively in Section 4.6. The second phase is sensitively monitored by the given positive scalar ε; which has an impact on the overall reaching time performance. The requirement for (4.39) establishing the sliding mode in form (4.37) for the dynamics (4.11) can be relaxed. In fact, (4.39) demonstrates that the aimed gain value would be slightly greater than the instantaneous uncertainty magnitude in order to hold an optimum sliding mode in terms of compensating performance. These conditions convey some conservativeness in computing undesirable high gains as in the case of conventional SMC [13, 58]. The following counter-example illustrates this limitation.

Example 4.1. Consider a single mass $m = 1$ in kg, moving on a horizontal surface with an initial velocity $\sigma(0) > 0$ under a static frictional resistance of $-2\text{sgn}(\sigma)$, in N, and an applied force u in the form of bang-bang controller (*i.e.*, feedback controller switching abruptly between two states) as $u = -K\text{sgn}(\sigma)$. The velocity feedback dynamics can be stated as $\dot{\sigma} = -2\text{sgn}(\sigma) + u = -(2 + K)\text{sgn}(\sigma)$. For such dynamics, written in form (4.38), we note that $\frac{|\Psi|}{\Gamma} = 2$. Obviously, we verify that any constant or varying switching gain $K > -2$ (*e.g.*, $K = 1$, $K = \sin\sigma$, provided that it is greater than -2) can guarantee the existence of a sliding mode and $\sigma \to 0$ in finite time from any initial velocity $\sigma(0) > 0$. In conclusion, the condition (4.39) introduced above, $K > \frac{|\Psi|}{\Gamma} = 2$, is no longer required in this case.

4.4.2 Necessary and Sufficient Condition

Now, we present diversely a result treating a necessary and sufficient condition for any sliding mode to be guaranteed using appropriate ASMC gain dynamics. To this end, we substitute the expression $\Psi\text{sgn}(\sigma)$ for the term $|\Psi|$ in (4.39), *i.e.*,

$$K(t) \geq \frac{\Psi\text{sgn}(\sigma)}{\Gamma} + \varepsilon \tag{4.43}$$

Lemma 4.4. *Consider the nonlinear uncertain system* (4.9) *with the sliding variable dynamics* (4.11) *controlled by* (4.37). *Given $\sigma \neq 0$, a sliding mode*

can be established in finite time if, and only if, there exist $t^* \geq 0$ *and* $\varepsilon > 0$ *such that a switching gain* $K(t)$*, satisfying* (4.43) *for all* $t \geq t^*$*, exists.*

Proof. First, we discuss the sufficient condition. Using (4.25), we combine (4.38) and (4.43) to obtain, for $t \geq t^*$,

$$\begin{aligned} \sigma\dot{\sigma} &\leq \Psi\sigma - \Gamma K|\sigma| \\ &\leq \Psi\sigma - \big[\Psi \mathrm{sgn}(\sigma) + \varepsilon\Gamma\big]|\sigma| \\ &\leq -\varepsilon\underline{\Gamma}|\sigma| \end{aligned} \tag{4.44}$$

Then, taking $V = \sigma^2$ a Lyapunov function, its time derivative satisfies for $t \geq t^*$ and $\sigma \neq 0$,

$$\frac{1}{2}\dot{V} \leq -\varepsilon\underline{\Gamma}\sqrt{V} \tag{4.45}$$

That is,

$$\frac{d}{dt}\sqrt{V} \leq -\varepsilon\underline{\Gamma} \tag{4.46}$$

By integrating the above differential inequality between t^* and $t \geq t^*$ and following (4.40)–(4.42), we obtain $\sqrt{V} = |\sigma| \to 0$ in finite time with the upper-bound of the reaching time estimated as $t_r \leq t^* + \dfrac{|\sigma(t^*)|}{\underline{\Gamma}\varepsilon}$.

Now, let us prove the necessary condition. We assume that $\forall t \geq 0$, $K(t)$ satisfies $K(t) \leq \dfrac{\Psi \mathrm{sgn}(\sigma)}{\Gamma}$. Then, from (4.38), we obtain $\dot{\sigma}\mathrm{sgn}(\sigma) = \dfrac{d}{dt}|\sigma| \geq 0$, that is, $|\sigma|$ never decreases as $t \to \infty$, and no FTC exists if (4.43) does not hold. Thus, we show indirectly (*i.e.*, by contradiction) that the existence of FTC solution for (4.11), controlled by (4.37), results in (4.43). □

The sufficient condition (4.43) refers to the compensating phase. Even though the conditions (4.39) and (4.43) remain hard to employ physically for the design of ASMC gain dynamics (as uncertainties are actually unknown), they show signs of interest in determining guidelines for best instantaneous uncertainty compensation. In [16], the authors have presumably introduced and discussed the ASMC design from the concept cast by (4.39). The condition (4.43) is seemingly performing the same objective. More preferably, it should improve somewhat the use of the gain dynamics (to optimum), and relaxing the older condition (4.39). To justify the subtlety of (4.43), one can see from (4.38) that when σ and Ψ have different signs, any nonzero gain value would be enough to realize the move of σ toward the sliding surface, naturally.

4.5 Existing ASMC

Assuming that the perturbations present in any dynamic system have unknown bounds *a priori*, ASMC will be designed using a switching gain dynamically changing with the sliding variable. One idea is that the gain keeps increasing whenever the sliding variable is nonzero, reducing its rate as the sliding variable is bordering the sliding surface, and finally stops increasing as soon as $\sigma = 0$ [17, 61, 125, 126].

4.5.1 Ideal ASMC

For the ASMC with *ideal sliding* mode, the integral adaptation law is commonly used to define the time-varying switching gain [10, 11, 13, 14, 16, 17, 19, 49, 66, 67].

$$\dot{K}(t) = \alpha \cdot |\sigma| \tag{4.47}$$

where $\alpha > 0$ is a tuning parameter. We state the following results.

Lemma 4.5. *For the uncertain system described in* (4.9) *with the sliding dynamics* (4.11) *controlled by* (4.37) *with the switching gain adaptation law* (4.47)*, the gain K has an upper bound, i.e., there exists a positive constant K^* so that $\forall t > 0$.*

$$K \leq K^* \tag{4.48}$$

Proof. See Appendix A.4 □

Theorem 4.1. *Consider the nonlinear uncertain system* (3.2) *with the sliding variable dynamics* (4.11) *controlled by* (4.37)*. Given $\sigma \neq 0$, a sliding mode can be established in finite time if the switching gain $K(t)$ is defined as* (4.47)*.*

Proof. See Appendix A.5 □

4.5.2 Real ASMC

For the ASMC with *real sliding* mode, the integral adaptation law with modified boundary-layer is commonly used to define the time-varying switching gain [10, 11, 13, 14, 16, 17, 19, 67]. The following form of the adaptation law is commonly used.

$$\dot{K}(t) = \alpha \cdot |\sigma| \cdot \text{sgn}(|\sigma| - \epsilon) \tag{4.49}$$

where $\alpha > 0$ is a tuning parameter.

Theorem 4.2. *Consider the nonlinear uncertain system* (4.9) *with the sliding variable dynamics* (4.11) *controlled by* (4.37). *Given* $|\sigma| > \epsilon$, *a sliding mode can be established in finite time, that is,* $|\sigma|$ *tends to the domain* $|\sigma| < \epsilon$ *in finite time, if the switching gain* $K(t)$ *is defined as* (4.49).

Proof. Refer to Theorem 4 of [16]. The proof is based on Lyapunov stability criterion. Define the switching gain adaptation error $\tilde{K} = K - K^*$, where K^* is an upper bound value of K defined in (4.48). Indeed, from Lemma 4.5, there always exists a constant K^* *s.t.* $\tilde{K} < 0 \ \forall t > 0$, *i.e.*, $\tilde{K} = -|\tilde{K}|$. Given the closed-loop system (4.37) with (4.49), consider the following Lyapunov candidate function

$$V = \frac{1}{2}\sigma^2 + \frac{1}{2\gamma}\tilde{K}^2 \tag{4.50}$$

with $\gamma > 0$. Since Ψ and Γ are bounded, there exist $\bar{\Psi}$ and $\underline{\Gamma}$ *s.t.* $\big|\Psi\big| \leq \bar{\Psi}$ and $\underline{\Gamma} \leq \Gamma$ (refer to (4.24) and (4.25)). Noting that K^* is constant and $K(t) > 0 \forall t > 0$, the time derivative of V is

$$\begin{aligned}
\dot{V} &= \sigma\dot{\sigma} + \frac{1}{\gamma}\tilde{K}\dot{K} \\
&= \sigma\big[\Psi - \Gamma K \text{sgn}(\sigma)\big] + \frac{1}{\gamma}\tilde{K}\alpha \cdot |\sigma| \cdot \text{sgn}(|\sigma| - \epsilon) \\
&\leq |\sigma|(\bar{\Psi} - \underline{\Gamma}K) + \frac{1}{\gamma}\tilde{K}\alpha \cdot |\sigma| \cdot \text{sgn}(|\sigma| - \epsilon) + |\sigma|\underline{\Gamma}K^* - |\sigma|\underline{\Gamma}K^* \\
&\leq -|\sigma|\big[-\bar{\Psi} + \underline{\Gamma}K^*\big] + \frac{1}{\gamma}\tilde{K}\alpha \cdot |\sigma| \cdot \text{sgn}(|\sigma| - \epsilon) - |\sigma|\underline{\Gamma}\tilde{K} \\
&\leq -|\sigma|\big[-\bar{\Psi} + \underline{\Gamma}K^*\big] - \beta_K|\tilde{K}| - |\tilde{K}| \cdot \\
&\quad \big[\frac{\alpha}{\gamma} \cdot |\sigma| \cdot \text{sgn}(|\sigma| - \epsilon) - |\sigma|\underline{\Gamma} - \beta_K\big]
\end{aligned} \tag{4.51}$$

for any $\beta_K > 0$. Note that there always exists K^* *s.t* $\beta_\sigma \triangleq -\bar{\Psi} + \underline{\Gamma}K^* > 0$ [16]. Then, two cases arise.

Case 1: $|\sigma| > \epsilon > 0$, *i.e.*, $\text{sgn}(|\sigma| - \epsilon) = 1$, if we select $\gamma < \dfrac{\alpha\epsilon}{\underline{\Gamma}\epsilon + \beta_K}$ and $\beta = \min(\beta_\sigma, \beta_K\sqrt{\gamma})$, then

$$\dot{V} \leq -\beta \cdot (2V)^{1/2} \tag{4.52}$$

Therefore, a finite time convergence to a domain $|\sigma| \leq \epsilon$ is guaranteed from any initial condition $|\sigma(0)| > \epsilon > 0$, and the reaching time can be estimated [1]

$$t_F \leq \frac{\sqrt{2}V(0)^{1/2}}{\beta} \tag{4.53}$$

Case 2: $|\sigma| \leq \epsilon$, $\dot{V}$ would be sign indefinite and the stability inside the boundary layer is not certain [16]. Therefore, the sliding variable $|\sigma|$ can increase over the boundary layer. As soon as $|\sigma| > \epsilon$, the Lyapunov stability (refer to (4.50) and (4.52)) is established again and $|\sigma|$ is attracted to the boundary layer (*i.e.*, $|\sigma| < \epsilon$). □

Remark 4.1. The purpose of the boundary layer principle in (4.49) is to provide a decreasing phase of switching gain so that its overestimation could be avoided. This scheme is different from the traditional boundary layer whose purpose is to replace the signum function by a smooth switching action.

4.6 Extension of Integral Adaptation Law

Given the nonlinear uncertain system (4.9) with the sliding variable dynamics (4.11) controlled by (4.37), a general ASMC design with integral adaptation law is introduced below based on the necessary and sufficient condition (4.43) discussed in Lemma 4.4.

Proposition 4.1. *If the gain $K(t)$, in* (4.37)*, is designed explicitly as*

$$K(t) = \int_0^t G(|\sigma|)d\tau \tag{4.54}$$

where $G(|\sigma|)$ is any strictly positive non-decreasing function in its argument $|\sigma| \neq 0$ satisfying $G(0) = 0$, then the sliding variable $\sigma \to 0$ in finite time.

Proof. First, we investigate the existence of a compensating phase during which the lumped perturbation will be eventually compensated by the proposed switching gain. Then, we discuss the existence of a reaching phase.

Compensating phase: For any perturbation greater than the switching gain, eventually

$$\frac{\Psi \text{sgn}(\sigma)}{\Gamma} > K(t) \tag{4.55}$$

we have, from (4.38),

$$\sigma\dot{\sigma} = \Psi\sigma - \Gamma K|\sigma| > 0 \tag{4.56}$$

Thus, $|\sigma|$ is increasing and, from (4.54), $K(t)$ is increasing also with a rate $G(|\sigma|) > 0$. Since Ψ and Γ are bounded, there always exists a finite time $t^* \geq 0$ so that $K(t^*)$ compensates $\dfrac{\Psi \mathrm{sgn}(\sigma)}{\Gamma}$, *i.e.*,

$$K(t^*) = \frac{\Psi(t^*)\mathrm{sgn}(\sigma)}{\Gamma(t^*)} \tag{4.57}$$

Insofar as the non-decreasing $K(t)$ reacts and compensates for *any* perturbation greater than it, we state, without loss of generality, $K(t) > \dfrac{\Psi \mathrm{sgn}(\sigma)}{\Gamma}$ for all $t > t^*$. *Hint:* In a future time, if the level of perturbation exceeds the switching gain, the latter reacts and compensates again which means that the compensating instant t^* always exists.

Reaching phase: As far as $K(t) > \dfrac{\Psi \mathrm{sgn}(\sigma)}{\Gamma}$ for $t > t^*$, there always exists $\varepsilon > 0$ *s.t.*(4.43) holds. Then, from Lemma 4.4, the system trajectory moves into the reaching phase and $\sigma = 0$ is established in finite time. Moreover, the maximum reaching time is estimated as $t_r \leq t^* + \dfrac{|\sigma(t^*)|}{\underline{\Gamma}\varepsilon}$ □

The existing compensating and reaching phases referred to above will be thoroughly discussed in the next Chapter. Alternatively, the form (4.54) can be presented implicitly as [117]

$$\dot{K}(t) = G(|\sigma|) \tag{4.58}$$

Figure 4.6 shows the ideal case for which the sliding variable $|\sigma|$, its corresponding reshaped variable $G(|\sigma|)$ and the switching gain $K(t)$ change with time t under perturbation $|\Psi/\Gamma|$. At time t_0, the switching gain $K(t_0)$ compensates for lumped perturbation $|\Psi(t_0)/\Gamma(t_0)|$ and the sliding variable σ starts decreasing. At time t^*, $K(t^*)$ completely compensates for maximum perturbation $\max|\Psi(t)/\Gamma(t)|$.

Ideally, by reaching the sliding surface, *i.e.*, $\sigma = 0$, the trajectory will remain on the surface thereafter and the switching gain $K(t)$ will stop increasing (refer to (4.58)). However, in practice, σ could not remain exactly zero due to sampling time delay, calculation error and measurement noise. Thus, $K(t)$ may keep increasing for any small deviation from the sliding surface, *i.e.*,

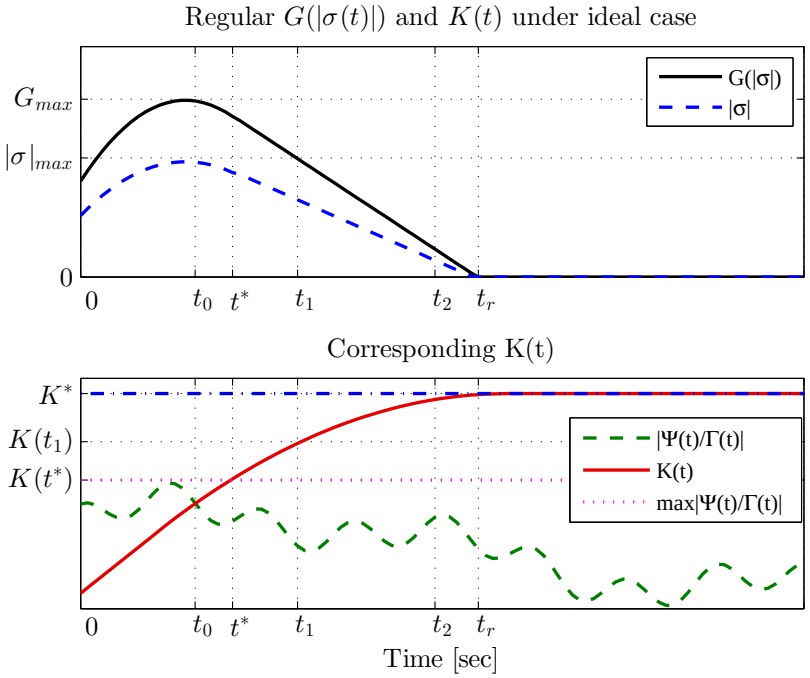

Figure 4.6: Ideal case for sliding variable $|\sigma|$, reshaped one $G(|\sigma|)$ and switching gain $K(t)$ *vs.* time under perturbation $|\Psi/\Gamma|$

$\sigma \neq 0$. To overcome this problem, [13] and [61] propose a low-pass filter to slowly decrease the switching gain whenever σ reaches zero. Also a boundary layer method is provided in [16] and [17]. Here, we propose a modified boundary layer method with smoother adaptation shape about the boundary layer. In Figure 4.7, $G(|\sigma|)$ is quite smaller than $|\sigma|$ when the trajectory is around the boundary layer. This shape will allow reducing the "large jump" of the switching gain dynamics which may force the trajectory to jump over the opposite limit of the boundary layer. In other words, the risks, that the sliding variable σ never gets inside the boundary layer and the switching gain $K(t)$ keeps increasing, will be minimized by choosing appropriately the gain function $G(|\sigma|)$.

The dynamics (4.58) represents a standard form of a switching gain law. The term $G(|\sigma|)$ in (4.58) generally refers to the varying rate of increase of the compensation gain, and then, it affects the ASMC reaction during the compensating and reaching time frames. In particular, this function is chosen as

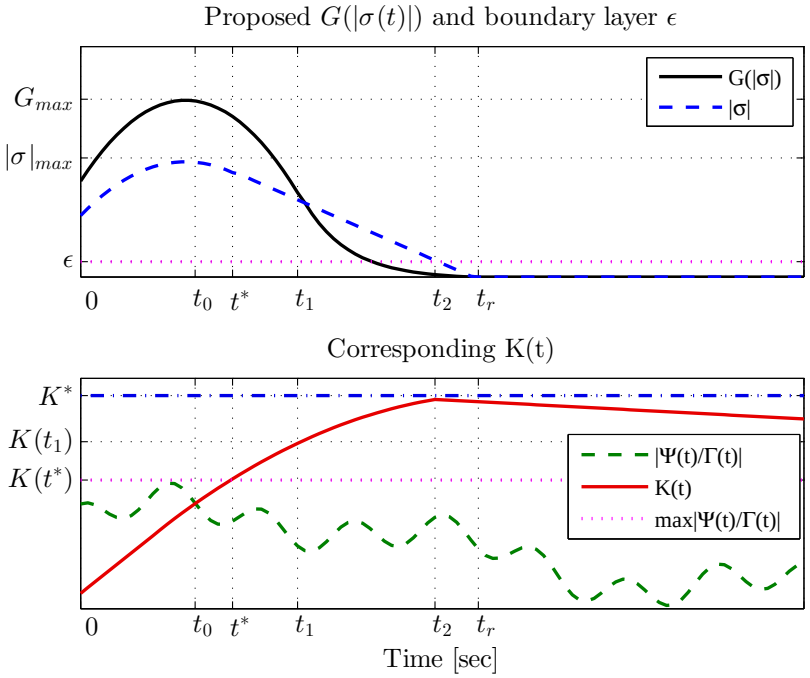

Figure 4.7: Sliding variable $|\sigma|$, reshaped function $G(|\sigma|)$ and switching gain $K(t)$ *vs.* time under perturbation $|\Psi/\Gamma|$ for the proposed method

$G(|\sigma|) = \alpha|\sigma|$ with $\alpha > 0$ in [11,14–17,19], and (4.58) becomes (4.47) for *ideal* ASMC [115]. In general, we emphasize the selection of $G(|\sigma|)$ from numerous function candidates that respect the necessary and sufficient conditions for ASMC discussed above. More details can be seen in [73,116]. The adaptation law (4.47) is able to control the nonlinear uncertain system (4.9). However, the result of (4.47) exhibits relatively slow response at the beginning stage so that the sliding variable is leaving the sliding surface forced by perturbations. It also maintains relatively high value (because K is non-decreasing) after the sliding mode has been built and thus produces relatively high chattering levels. The selection of the form of the rate function $G(|\sigma|)$ allows the tuning of the chattering level according to the desired accuracy/stability performance.

Remark 4.2. It is reasonable to develop an adaptation method so that the magnitude could be reduced to a minimum admissible value whenever the sliding mode is established. The idea is to choose the terminal condition for the adaptation process as: "When $K(t)$ completely compensates for the

perturbation $\frac{\Psi(t)}{\Gamma(t)}$, it would stop increasing." But, since the magnitude of the perturbation is unknown, we could not directly use this threshold. However, we note that the accomplished compensation implies the time derivative of $|\sigma|$, denoted by $\frac{d}{dt}|\sigma| \equiv \dot{\sigma} \cdot \mathrm{sgn}(\sigma)$ (or, equivalently the derivative of σ^2, $\frac{d}{dt}\sigma^2$), is negative. This objective can be achieved by a negative threshold of the time derivative of $|\sigma|$ as [125]

$$\dot{K} = \begin{cases} 0 & \text{if } \dot{\sigma} \cdot \mathrm{sgn}(\sigma) \leq -V_\sigma \\ \bar{K} \cdot G\big(|\sigma|\big) & \text{otherwise} \end{cases} \tag{4.59}$$

where $V_\sigma > 0$ represents the threshold amplitude of the time derivative of $|\sigma|$, $K(0) > 0$ and $\bar{K} > 0$.

4.7 Techniques of Smoothing SMC: Alternative Switching Gain

Since the chattering phenomenon is mainly due to the discontinuous switching across the sliding surface, it may be attenuated by introducing a smooth function to replace the discontinuous $\mathrm{sgn}(\,\cdot\,)$ function. Another way is to select an appropriate integral function $G(|\sigma|)$ based on the previous discussion of the necessary and sufficient conditions.

4.7.1 Existing Method: Replacement of Signum Function

Traditionally, some smooth functions have been proposed to replace the signum function. If a continuous function satisfies

1. $F(\sigma) \approx 1$ when $\sigma \geq \varepsilon > 0$,
2. $F(\sigma) \approx -1$ when $\sigma \leq -\varepsilon < 0$, and
3. $F(\sigma)$ very small when $-\varepsilon < \sigma < \varepsilon < 0$

with $\varepsilon > 0$ is the width of the boundary layer, then $F(\sigma)$ can be the candidate function to replace the signum function and the trajectory will be sliding along the adjacent of the sliding surface instead of the ideal sliding surface $\sigma = 0$. The true trajectory may not smoothly follow $|\sigma(x,t)| \leq \varepsilon$, but it will always return to this *layer* $|\sigma(x,t)| \leq \varepsilon$ after leaving it. One candidate of the smooth function is the commonly used saturation function

$$F(\sigma) = \begin{cases} \dfrac{\sigma}{|\sigma|} & \text{if} \quad |\sigma| \geq \varepsilon \\ \dfrac{\sigma}{\varepsilon} & \text{if} \quad |\sigma| < \varepsilon \end{cases} \tag{4.60}$$

where $\varepsilon > 0$ represents the width of the boundary layer. The expression (4.60) is a continuous function with a discontinuous derivative. Another candidate of the smooth function is

$$F(\sigma) = \frac{2}{\pi} \tan^{-1}(\frac{\sigma}{\varepsilon}) \tag{4.61}$$

This function is continuously differentiable. It can replace the signum function $\text{sgn}(\cdot)$ if ε is sufficiently small. In practice, we do not want $F(\sigma)$ to completely work as $\text{sgn}(\cdot)$. Instead, we want some transient performance, that is, when the trajectory enter the *layer* $|\sigma(x,t)| \leq \varepsilon$, the speed $|\dot{\sigma}|$ also slows down.

4.7.2 Alternative Switching Gain

Upon the extended integral function, one can have many choices from which to select this integral function appropriately. In [116, 117], $G(|\sigma|)$ is selected to be quite a bit smaller than $|\sigma|$ when the trajectory is around the boundary layer. The switching gain rate changes smoothly along the boundary layer and the chattering phenomenon due to switching dynamics can be reduced substantially. In other words, the risk that the sliding variable σ never gets inside the boundary layer or that the switching gain $K(t)$ keeps increasing will be avoided by choosing the gain rate function $G(|\sigma|)$ appropriately [117]. For instance, the adaptation law can be modified as

$$\dot{K} = \alpha \cdot |\sigma| \cdot \big[\frac{2}{\pi} \cdot \tan^{-1}(\sigma^4)\big] \cdot \text{sgn}(|\sigma| - \epsilon) \tag{4.62}$$

with $K(0) > 0$, $\alpha > 0$ and $\epsilon > 0$ being small [117]. The increment or decrement of K tends to be smaller while $\big(|\sigma| - \epsilon\big) \to 0$ (*i.e.* as $|\sigma|$ approaches ϵ from the outside or the inside of the boundary layer).

Another candidate function for G can be simply chosen as $|\sigma|^r$ with $r > 1$ and the adaptation law will be

$$\dot{K} = \alpha \cdot |\sigma|^r \cdot \text{sgn}(|\sigma| - \epsilon) \tag{4.63}$$

with $K(0) > 0$, $\alpha > 0$, $r > 1$ and $\epsilon > 0$ be very small. Then, one has the following proposition, similar to Theorem 4 of [16].

Proposition 4.2. *Given the uncertain system* (4.9) *with the sliding variable* σ *given by* (4.11) *and controlled by* (4.37) *with the switching gain adaptation law* (4.63)*, for any initial trajectory outside the boundary layer, i.e.,* $|\sigma(0)| > \epsilon > 0$*, there exists a finite time* $t_F > 0$ *so that a real sliding mode is established for all* $t > t_F$*.*

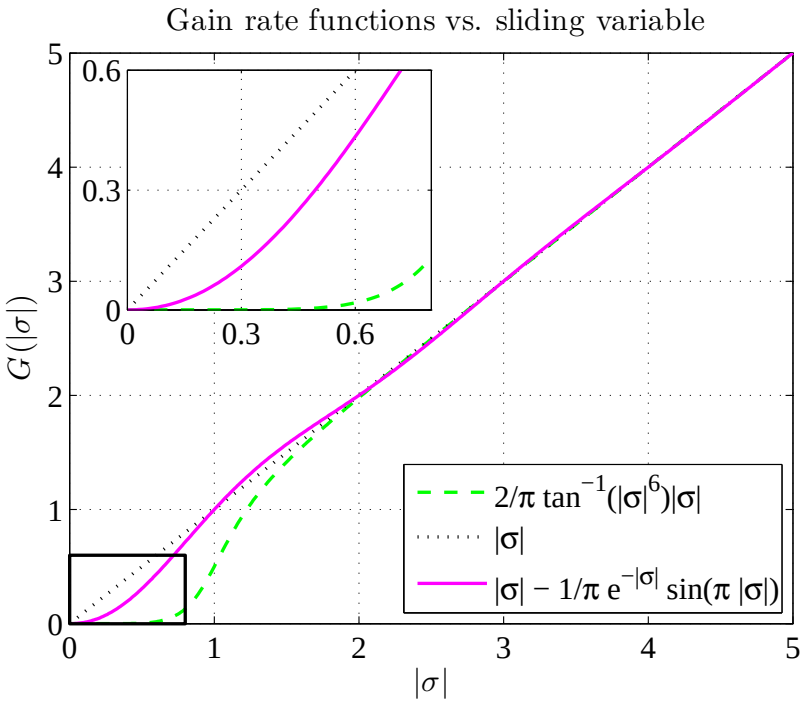

Figure 4.8: Different gain rate functions $G(|\sigma|)$

Proof. Since the integral function is positive definite in its argument $|\sigma|$, the proof is ended by applying Proposition 4.1. □

The proposed adaptation laws (4.62) and (4.63) provide new choices to control the smoothness of the switching gain about the boundary layer. These equations show that $\dot{K}$ (in other words, the increment or decrement of K) tends to be smaller while $|\sigma|$ approaches ϵ from the outside or the inside of the boundary layer, *i.e.* as $|\sigma| \to \epsilon$. To illustrate this property, refer to the zoomed frame in Figure 4.8 which shows different gain rate function $G(|\sigma|)$ shapes with reduced levels about any small value of ϵ. Thus, the switching gain changes smoothly along the boundary layer and the chattering phenomenon due to switching gain adaptation can be suppressed substantially.

Remark 4.3. It should also be pointed out that the boundary layer ϵ for the switching gain adaptation is different from the boundary layer ε used in the continuous function to replace the discontinuous $\mathrm{sgn}(\cdot)$ function. The thickness ϵ of the boundary layer in switching gain adaptation (4.62) and

(4.63) may be time-varying (*e.g.*, depending on the sliding variable in [16]) whereas the thickness ε of the boundary layer in the traditional smoothing functions (4.60) and (4.61) is usually fixed.

Remark 4.4. Similar to the negative threshold of $\dot{\sigma} \cdot \mathrm{sgn}(\sigma)$ discussed in [125], the adaptation law for the real ASMC can be stated as [126]

$$\dot{K} = \begin{cases} 0 & \text{if } \dot{\sigma} \cdot \mathrm{sgn}(\sigma) \leq -V_\sigma \text{ and } |\sigma| > \epsilon \\ \bar{K} \cdot G\big(|\sigma|\big)\mathrm{sgn}\big(|\sigma| - \epsilon\big) & \text{otherwise} \end{cases} \tag{4.64}$$

where $K(0) > 0$, $\bar{K} > 0$ and $V_\sigma > 0$.

Remark 4.5. The designs introduced in [125, 126] (refer to Remarks 4.2 and 4.4) require knowledge of the rate of the sliding dynamics. However, $\dot{\sigma}$ is not always available. Instead, we can use any dynamic observer (*e.g.*, high gain, sliding-mode-based one) or a derivative filter to estimate $\dot{\sigma}$. Since $\dot{\sigma}$ is not directly measured, we use a low-pass derivative filter, denoted by $\dot{\sigma}_f$, to replace $\dot{\sigma}$, as $\dot{\sigma}_f = \big[\frac{\omega_c^2 s}{s^2 + 2\zeta\omega_c s + \omega_c^2}\big]\sigma$, with ω_c and ζ given cut-off frequency and damping ratio, respectively [126]. The low-pass filtered signal $\dot{\sigma}_f$ blocks the high frequency white noise. It also provides some time delay . The latter is not always harmful. It may slow down the system response, and during a time period after completely compensating the perturbations, it allows slightly the increase of $K(t)$. In other words, it provides higher feedback control gain to speed up the convergence of σ. This time delay balances the reaching time t_r of FTC and the maximum switching gain $K(t)$. First, if is too large, $K(t)$ will increase. Then, t_r is reduced. More chattering may appear or the system accuracy may be sacrificed. Second, if is too small, the maximum value of $K(t)$ would be just equal to the compensated perturbation magnitude. Then, t_r is increased, the chattering is much lower and the accuracy is improved. Thus, when the control objective requires systems with high accuracy and low chatter, it will be used to guarantee small . Such a delay should rather be too small than too large because the system trajectories are globally UUB with excellent accuracy and compressed chattering phenomenon even t_r is "slow".

Remark 4.6. The problem of delayed response (due to low-pass filtered signal $\dot{\sigma}_f$) can be fixed by adding a speed threshold (refer to nonzero V_σ in (4.64)). The negative speed threshold $-V_\sigma$ controls the rate of FTC for σ. It also helps to eliminate the phenomenon of delayed system response caused by time delay τ_d at the beginning of compensating phase [126].

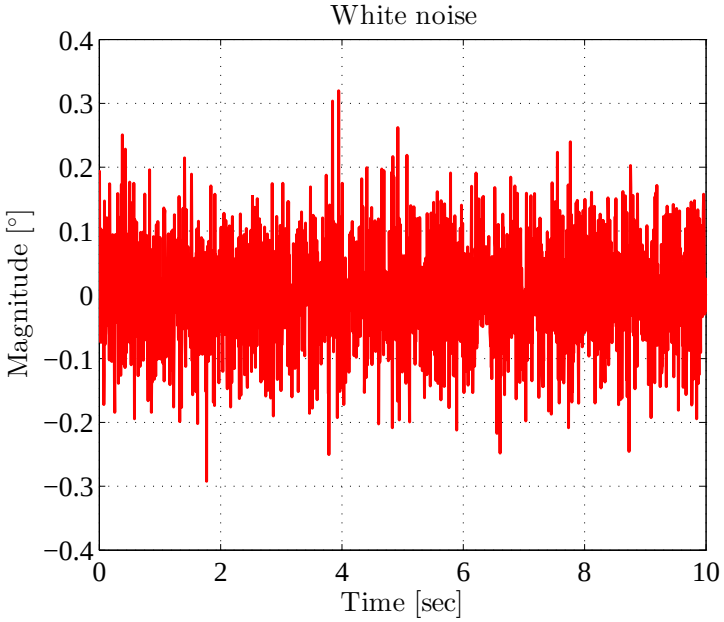

Figure 4.9: Simulations: White noise in position measurement

4.8 Applications

To illustrate the ideas discussed in this Chapter, simulations and experiments are implemented. The simulation results are obtained by applying the proposed algorithm (4.63), while the proposed algorithm (4.62) is tested experimentally.

4.8.1 Simulation Results

We consider the equation of only the pitch motion of the experimental helicopter model setup (refer to Figure 1.1 in Section 1.6 of Chapter 1, Introduction and Figure 3.2) with external disturbances. That is, the yaw motion inhibits while the rear motor is stopped. Rewriting (3.43a) with $\dot{\psi} = 0$ and adding an external disturbance, we obtain

$$\ddot{\phi} = \frac{K_{pp}u - B_p\dot{\phi} - mgl\cos\phi}{J_p + ml^2} + w(t) \tag{4.65}$$

where $w(t)$ denotes the external disturbance. Note that all the parameters J_p, m, l, K_{pp} and B_b are bounded but may be time-varying. Let $x_1 = \phi$, $x_2 = \dot{\phi}$

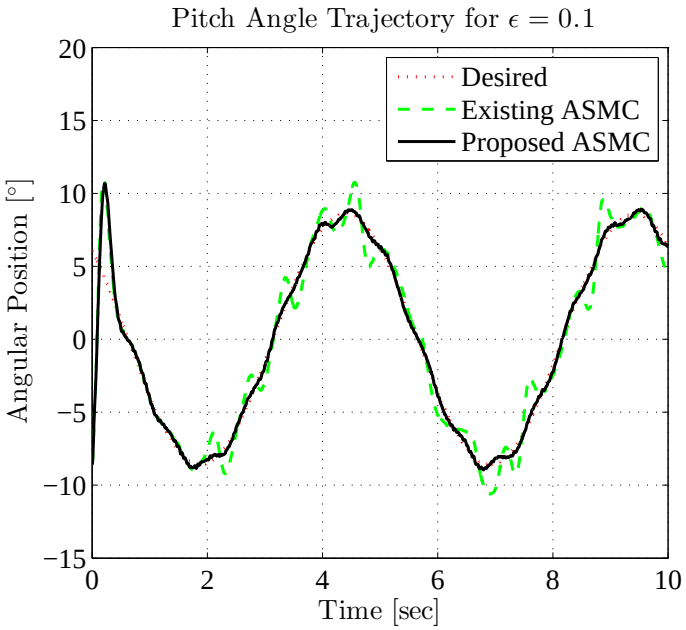

Figure 4.10: Simulations: Desired and actual trajectories for $\epsilon = 0.1$

and $u = V_p$. The state space representation is

$$\dot{x} = \begin{bmatrix} x_2 \\ -\theta_2 x_2 - \theta_3 \cos x_1 + \omega(t) \end{bmatrix} + \begin{bmatrix} 0 \\ \theta_1 \end{bmatrix} u \tag{4.66}$$

where $\theta_1 = \dfrac{K_{pp}}{J_p + ml^2}$, $\theta_2 = \dfrac{B_p}{J_p + ml^2}$, and $\theta_3 = \dfrac{mgl}{J_p + ml^2}$ are uncertain parameters. Given $\hat{\theta}_1$, $\hat{\theta}_2$ and $\hat{\theta}_3$ their nominal values, and $\tilde{\theta}_1$, $\tilde{\theta}_2$ and $\tilde{\theta}_3$ their corresponding variations, respectively, (4.66) can be written in form

$$\dot{x} = \hat{f}(x) + \hat{g}(x)u + [0, d(t)]^T \tag{4.67}$$

where

$$d(t) = \tilde{\theta_1} u - \tilde{\theta_2} x_2 - \tilde{\theta_3} \cos x_1 + \omega(t) \tag{4.68}$$

is the lumped perturbation.

Assuming that the pitch angle tracks a continuously differentiable trajectory x_{1d} and denoting by $e_p = x_1 - x_{1d}$ the tracking error, a PID sliding surface can be built as [11]

$$\sigma = K_p e_p + K_i \int e_p d\tau + K_d \dot{e}_p \tag{4.69}$$

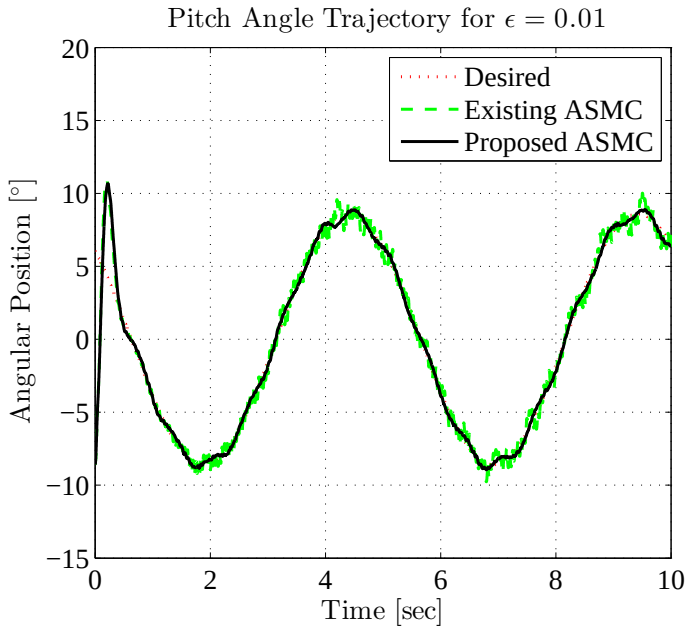

Figure 4.11: Simulations: Desired and actual trajectories for $\epsilon = 0.01$

This PID sliding surface implies a transfer function from the sliding variable σ to the tracking error e_p as

$$\frac{e_p(s)}{\sigma(s)} = \frac{s}{K_d s^2 + K_p s + K_i} \tag{4.70}$$

Differentiating the sliding variable σ *w.r.t.* time and substituting (4.66), we obtain the sliding dynamics in the form (4.11) with

$$\Gamma = K_d \cdot \theta_1 \tag{4.71}$$

$$\begin{aligned}\Psi =& K_p \cdot (x_2 - \dot{x}_{1d}) + K_i \cdot (x_1 - x_{1d}) - K_d \cdot \ddot{x}_{1d} + \\ & K_d \cdot \big[- \theta_2 x_2 - \theta_3 \cos x_1 + \omega(t) \big]\end{aligned} \tag{4.72}$$

The nominal values of Γ and Ψ and their uncertainties are

$$\hat{\Gamma} = K_d \cdot \hat{\theta}_1 \tag{4.73}$$

$$\begin{aligned}\hat{\Psi} =& K_p \cdot (x_2 - \dot{x}_{1d}) + K_i \cdot (x_1 - x_{1d}) - K_d \cdot \ddot{x}_{1d} \\ & + K_d \cdot \big[- \hat{\theta}_2 x_2 - \hat{\theta}_3 \cos x_1 \big]\end{aligned} \tag{4.74}$$

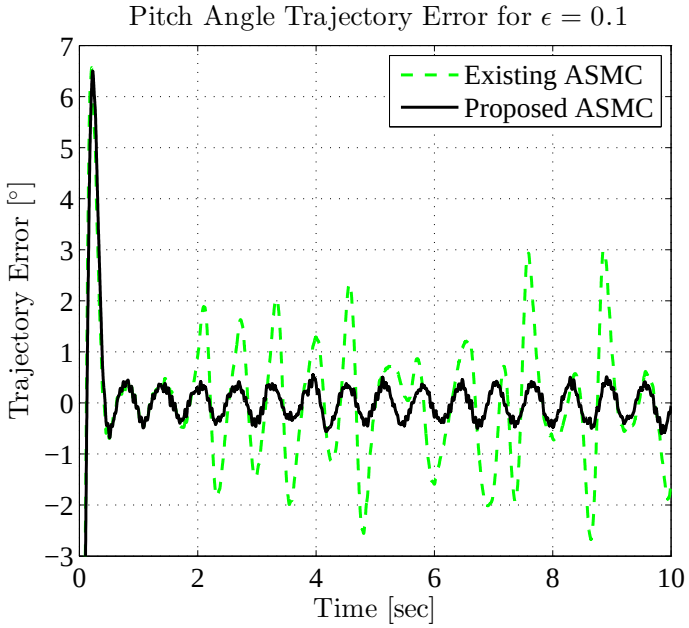

Figure 4.12: Simulations: Position errors for $\epsilon = 0.1$

Table 4.1: Parameter nominal values and variations for the simulations

Nominal Values		Time-Varying Uncertainties	
$\hat{\theta}_1$	5	$\tilde{\theta}_1$	$0.1\hat{\theta}_2 \sin(0.6t)$
$\hat{\theta}_2$	0.2	$\tilde{\theta}_2$	$0.2\hat{\theta}_2 \sin(0.5t)$
$\hat{\theta}_3$	20	$\tilde{\theta}_3$	$0.3\hat{\theta}_3 \sin(0.43t)$

and

$$\tilde{\Psi} = K_d \cdot d(t) \tag{4.75}$$

Information for the simulations is listed in Table 4.1 which gives the nominal values and time-varying uncertainties of the parameters. Table 4.2 shows the desired trajectory, initial value, ASMC parameters and the sampling period T_s. The external disturbance $w(t)$ in (4.66) is roughly set as $w(t) = 6.15 \sin(10t)$.

To be closer to the actual experimental implementation, a white noise is added to the position measurement (see Figure 4.9), and the input signal is saturated at ± 24 volt [21].

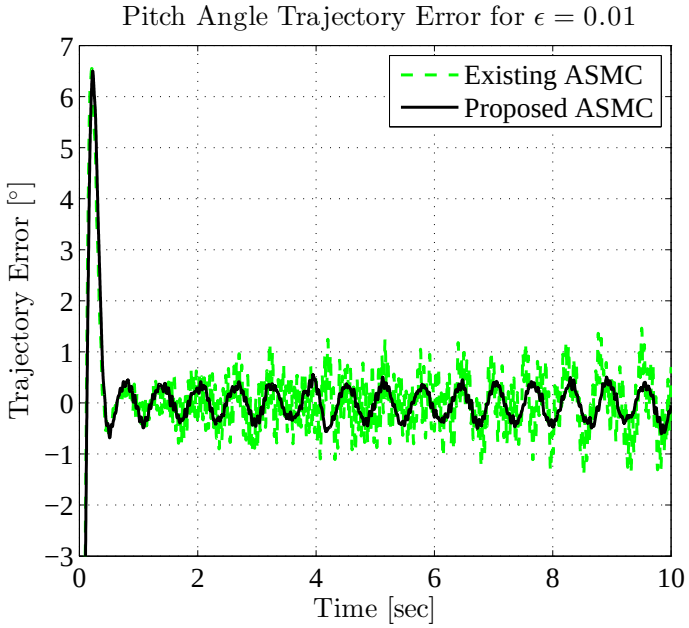

Figure 4.13: Simulations: Position errors for $\epsilon = 0.01$

Table 4.2: Desired trajectory, initial values and ASMC parameters

$x_{1,desired}$	$x_1(0)$	$x_2(0)$	$\hat{K}_{pp}(0)$	α	ρ	T_s
$0.15\sin(1.25t + \frac{3}{4}\pi)$	-0.15	0	100	0.1	0.01	0.005

The proposed smooth ASMC is compared with the existing ASMC design, introduced in [16]

$$K = \begin{cases} \alpha|\sigma| \cdot \text{sgn}(|\sigma| - \epsilon) & \text{if } K > \rho \\ \rho & \text{if } K \leq \rho \end{cases} \tag{4.76}$$

using different fixed values of the parameter ϵ. The desired and actual trajectories are shown in Figure 4.10 for $\epsilon = 0.1$ and Figure 4.11 for $\epsilon = 0.01$. The error performances are shown in Figures 4.12 and 4.13, respectively. The corresponding control input $u(t)$ is shown in Figure 4.16 and Figure 4.17, while Figure 4.14 and Figure 4.15 show the switching gain adaptation evolution in time, respectively. When ϵ is tuned from a relatively large value of 0.1 to a smaller value 0.01, one can see that accuracy is improved for both algorithms; however, the control gain K of the existing ASMC keeps increasing rapidly

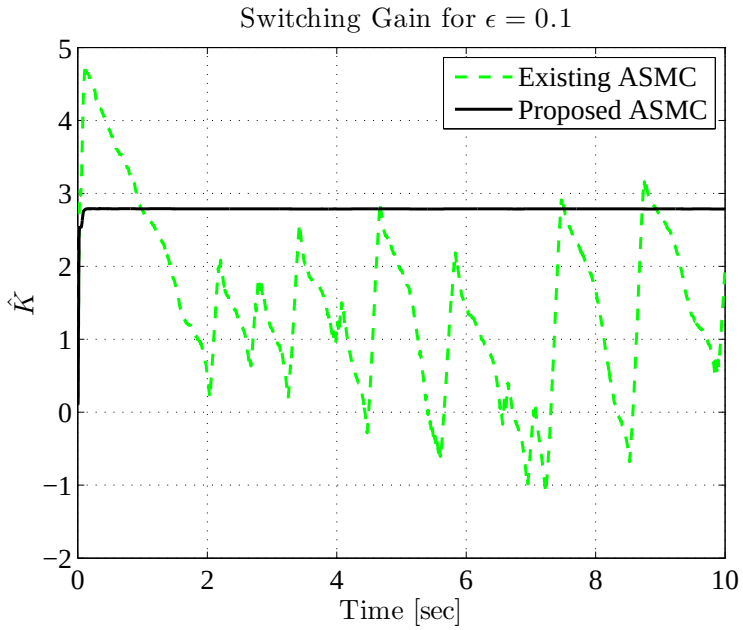

Figure 4.14: Switching gain $K(t)$ for $\epsilon = 0.1$

and becomes unstable (see Figure 4.15) and the corresponding control $u(t)$ of the ASMC becomes saturated. In contrast, the switching gain K and the control $u(t)$ of the proposed smooth ASMC keep a good, and definitely, optimal pace of progress.

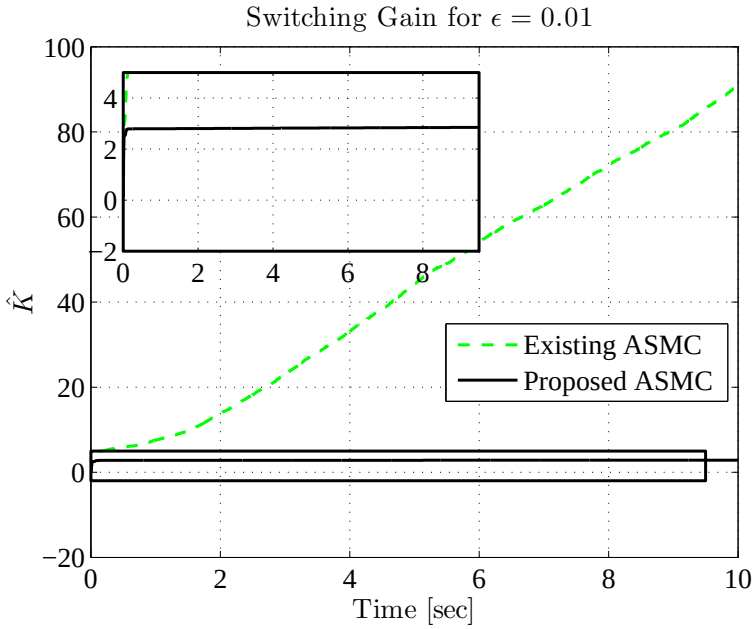

Figure 4.15: Simulations: Switching gain $K(t)$ for $\epsilon = 0.01$

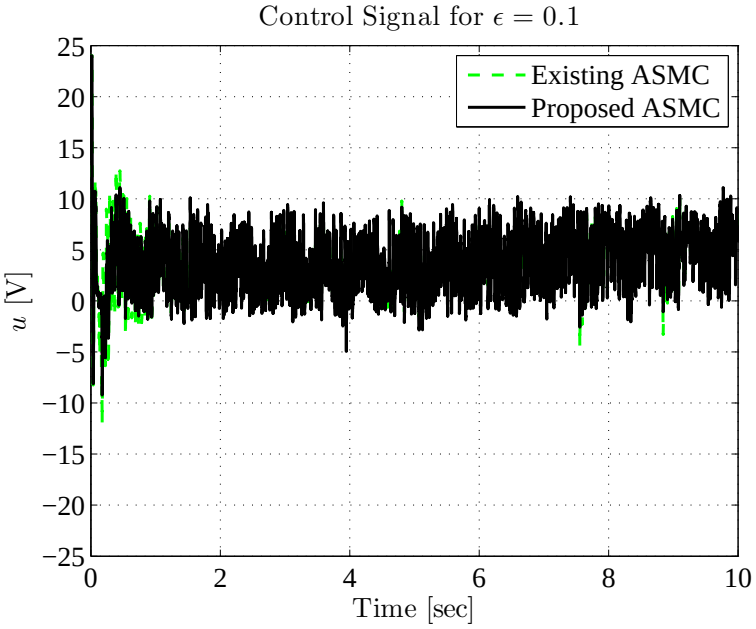

Figure 4.16: Simulations: Control $u(t)$ for $\epsilon = 0.1$

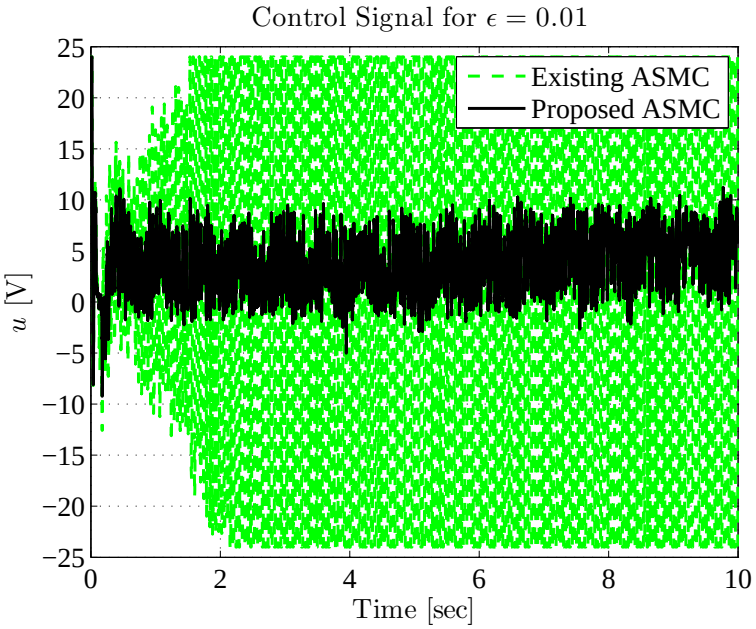

Figure 4.17: Simulations: Control $u(t)$ for $\epsilon = 0.01$

Table 4.3: Nominal values of the model parameters [21] for the experiments

Parameters	Values	Units
$\hat{J}_p$	0.038	$\mathrm{kg \cdot m^2}$
$\hat{K}_{pp}$	0.204	$\mathrm{N \cdot m/V}$
$\hat{K}_{yp}$	0.022	$\mathrm{N \cdot m/V}$
$\hat{B}_p$	0.800	N/V
$\hat{l}$	0.054	m
$\hat{m}$	1.3872	kg

4.8.2 Experimental Results

Experiments are carried out on the actual helicopter model setup (see Figure 1.1 in Chapter 1, Introduction). We consider its 1-DOF body mounted on a fixed base with a front propeller that is driven by a DC motor (refer to Section 1.6 for further details about the description of this setup). We rewrite the dynamic model of the rotating body about the pitch axis with perturbations and parameter uncertainties as

$$\hat{J}\ddot{x} = \hat{K}_{pp}u - \hat{B}_p\dot{x} - \hat{m}g\hat{l}\cos x + d(t) \tag{4.77}$$

with $d(t) = \omega(t) + \tilde{K}u - \tilde{J}\ddot{x} - \tilde{B}_p\dot{x} + (mgl - \hat{m}g\hat{l})\cos x$. $J = J_p + ml^2$ is the lumped moment of inertia about the rotating pivot, x, $\dot{x}$ and $\ddot{x}$ are the displacement angle, velocity and acceleration, respectively. $\omega(t)$ represents the unmodeled dynamics, uncertainties and external disturbances. The given parameters have been roughly estimated, *i.e.*, of known constant values $\hat{J}$, $\hat{K}_{pp}$, $\hat{B}_p$, $\hat{m}$ and $\hat{l}$, with unknown uncertainties, *i.e.*, $\tilde{J}$, $\tilde{K}_{pp}$, $\tilde{B}_p$, $\tilde{m}$ and $\tilde{l}$. Parameter values are shown in Table 4.3

We apply the adaptation law (4.62) during the experiments. Results of the response of a step input signal are shown in Figures 4.18-4.21. One can see that the accuracy is improved (see Figure 4.18) and the magnitude and the chattering level of the control input are reduced (see Figure 4.19). These phenomena resulted from the improved accuracy of sliding variable (see Figure 4.20) and reduced switching gain (see Figure 4.21), respectively.

Figures 4.22-4.26 show the responses of a sine wave trajectory tracking. One can see that the accuracy is also improved (see Figures 4.22 and 4.23 for tracking accuracy and Figure 4.25 for sliding variable accuracy) and the switching gain is reduced as well (see Figure 4.26). Moreover, the magnitude

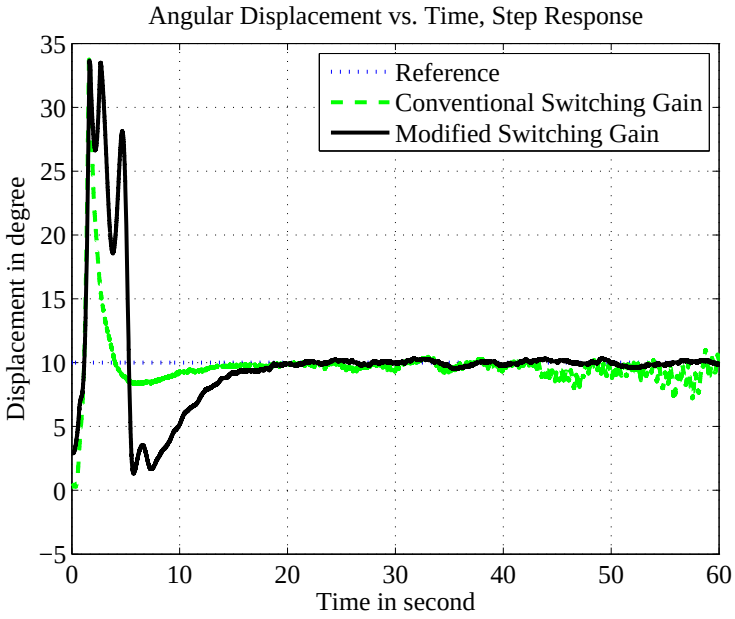

Figure 4.18: Experimental step response results: Angle displacement

and the chattering level of the control input are slightly reduced (see Figure 4.24).

The performances with more experiments obtained using different widths of the boundary layer ϵ, *i.e.*, $\epsilon = 10^{-3}$, $\epsilon = 10^{-1}$ and ϵ-tuning [16], are summarized in Table 4.4 for the error root-mean-square (RMS) and error peak in % of maximum displacement and in Table 4.5 for the control input. From Table 4.4, one can see that, comparing to the algorithm given in [16], the error RMS with the proposed algorithm is reduced from 29% up to 76% for step response and from 28% up to 74% for sine wave trajectory tracking. Also the peaks errors are reduced $16\% - 82\%$ by using the proposed method. Table 4.5 summarizes the performance of the control inputs. By applying the proposed algorithm, both Input RMS and Input Average values are improved for fixed $\epsilon = 10^{-3}$. However, there is no significant improvement for fixed $\epsilon = 10^{-1}$ and ϵ-tuning in terms of robustness and the magnitudes of the control inputs.

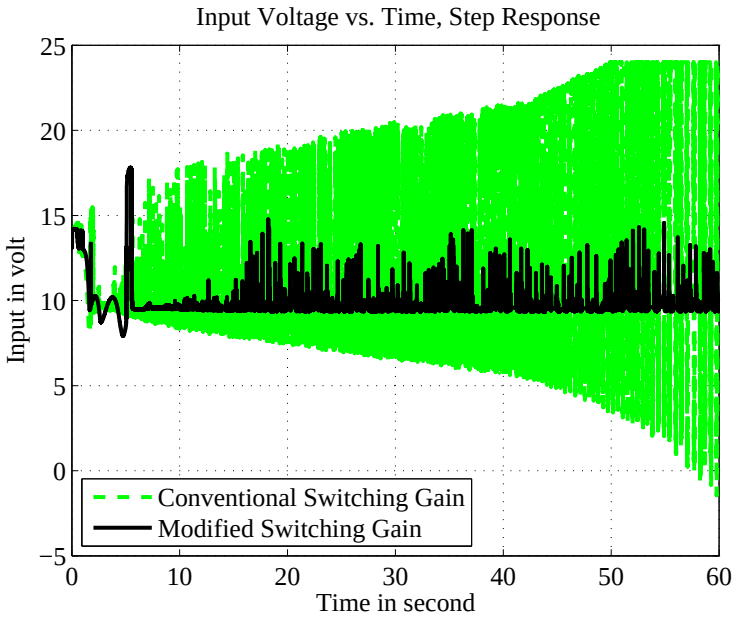

Figure 4.19: Experimental step response results: Input voltage

Table 4.4: Recap: Experimental results – Error RMS and peak values in % of maximum displacement

Performance	Error RMS		Error Peak	
Switch. Gain Design	of [16]	Proposed	of [16]	Proposed
Input Signal	Step			
$\epsilon = 10^{-3}$	8.1	**1.9**	27.9	**5.1**
$\epsilon = 10^{-1}$	1.7	**1.2**	8.1	**4.2**
ϵ-tunning	1.4	**1.0**	3.7	**2.8**
Input Signal	Sine			
$\epsilon = 10^{-3}$	9.0	**2.3**	30.9	**5.8**
$\epsilon = 10^{-1}$	3.8	**3.8**	7.3	**7.9**
ϵ-tunning	3.6	**2.6**	7.7	**6.5**

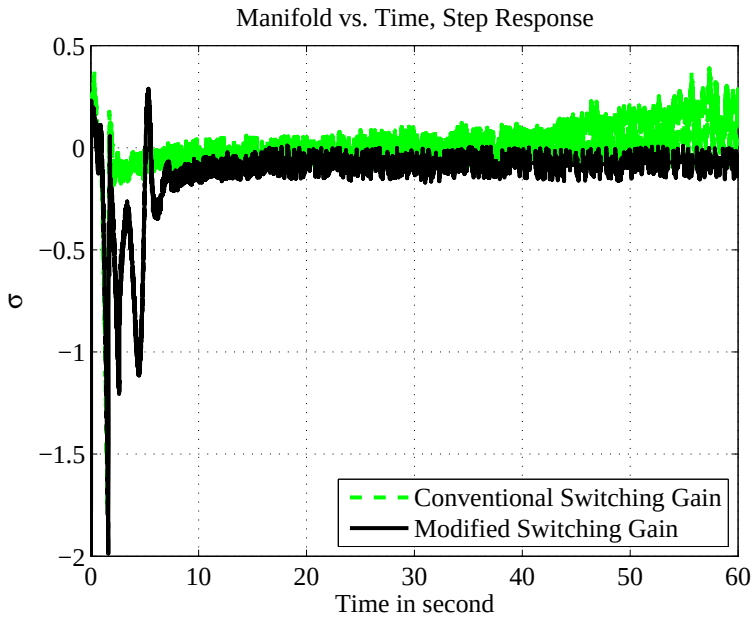

Figure 4.20: Experimental step response results: Sliding variable

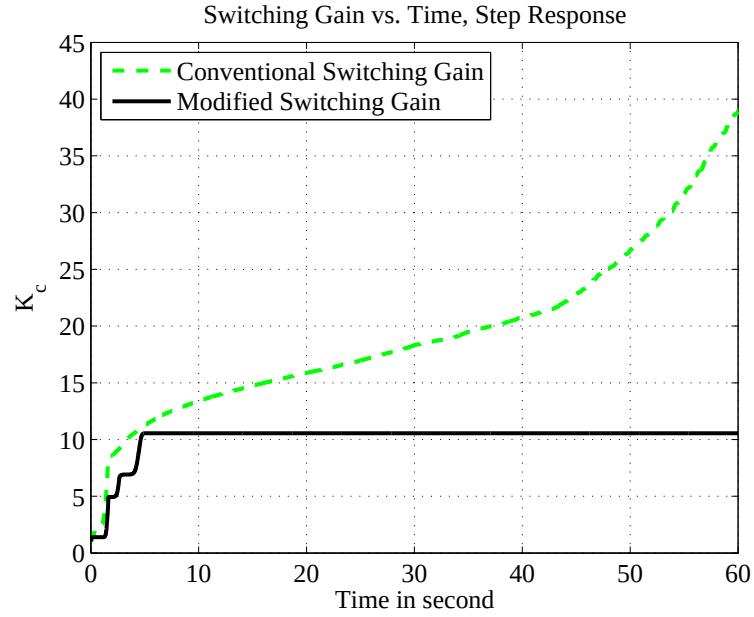

Figure 4.21: Experimental step response results: Switching gain

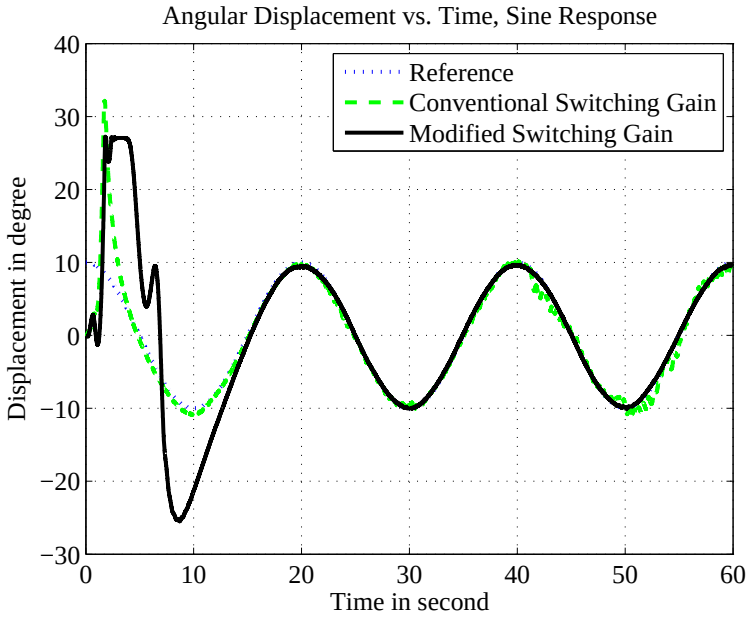

Figure 4.22: Experimental sine response results: Tracking performance

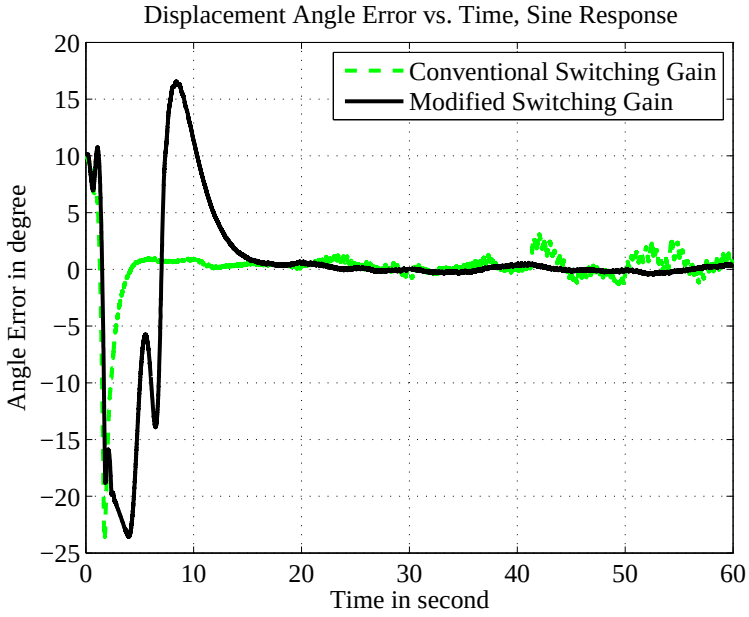

Figure 4.23: Experimental sine response results: Tracking error

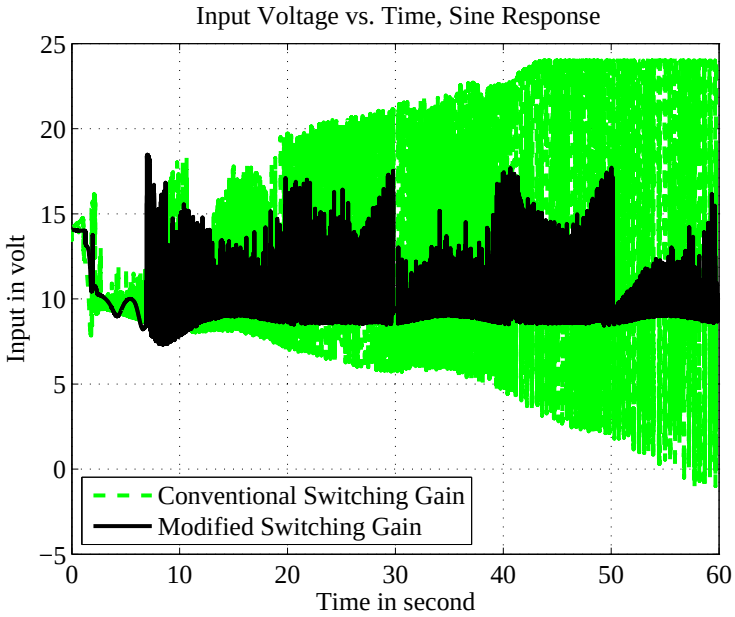

Figure 4.24: Experimental sine response results: Input voltage

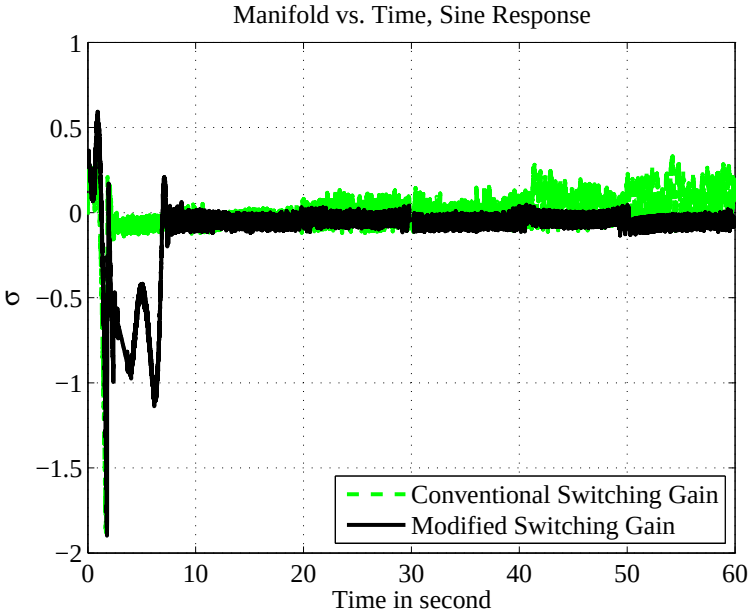

Figure 4.25: Experimental sine response results: Sliding variable

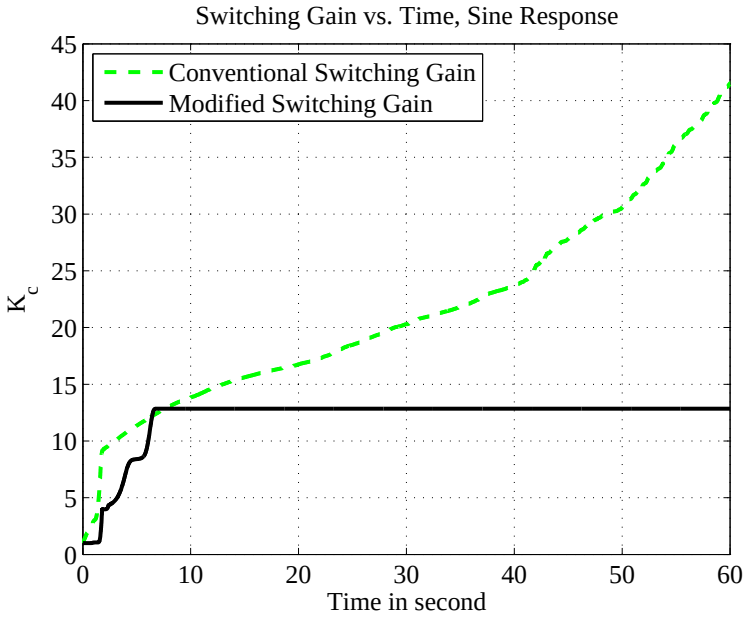

Figure 4.26: Experimental sine response results: Switching gain

Table 4.5: Recap: Experimental results – Input performance in Volt

Input Performance	Input RMS		Input Mean	
Switch. Gain Design	of [16]	Proposed	of [16]	Proposed
Input Signal	Step			
$\epsilon = 10^{-3}$	8.1	**1.9**	16.8	**9.6**
$\epsilon = 10^{-1}$	1.7	**1.2**	9.8	**9.8**
ϵ-tunning	1.4	**1.0**	9.7	**9.7**
Input Signal	Sine			
$\epsilon = 10^{-3}$	19.2	**9.9**	17.7	**9.8**
$\epsilon = 10^{-1}$	9.6	**9.6**	9.6	**9.6**
ϵ-tunning	9.4	**9.7**	9.4	**9.6**

4.9 Conclusions

In this chapter, the framework of SMC and ASMC are presented with the discussion of necessary and sufficient conditions. As a result, the integral adaptation law is extended. Based on these discussions, a modified ASMC design with a smooth adaptation of the switching gain is proposed for nonlinear systems with unknown uncertainties. The algorithm is developed based on the idea of smoothing the adaptation gain change along the boundary layer without sacrificing the system response performance. Compared to the algorithm given in [16], accuracy is improved and the chattering phenomenon is further suppressed. Numerical simulations and experimental results demonstrate the proposed design for both ideal and real ASMC. However, the magnitudes of the control inputs and the robustness (overshoot) do not show significant improvement for the proposed design. These phenomena will be discussed in Chapter 5, while new ASMC designs to solve these problems will be given in Chapter 6 and 7. More details in terms of motivations, objectives, novelties, pros and cons of this chapter are presented in Table 4.6.

Table 4.6: Chapter 4 Recap

Motivation(s)	- Control of perturbured and nonlinear dynamics with limited knowledge of the uncertainty levels. - Investigation of new frameworks of SMC with various dynamical switching gain laws.
Objective(s)	- Study of the existing laws. - Advantages and limitations of most common ASMC design (widely used in literature).
Novelty(ies)	- New necessary and sufficient conditions for establishment of any sliding mode. - Extended integral adaptation laws proposed to smooth the switching control along the boundary.
Pro(s)	- FTC, one of the most important characteristic of SMC but often ignored when designing the ASMC, is pointed out and tentatively fixed. - Chattering phenomenon and control performance are improved with the proposed forms of adaptation laws.
Con(s)	- Large overshot still exists. - Uncommon and highly nonlinear function forms of the modified gain laws. - Diversity of the smoothing function could be source of ambivalence.

5 Adaptive Sliding Mode Control – Properties

This chapter reviews the main ASMC designs for nonlinear systems with finite uncertainties of unknown bounds. Different statements of convergence referring to UUB property, AC and FTC for ASMC shown in recent papers are analyzed. Weaknesses and incomplete proofs apropos FTC are pointed out. Thereafter, a new approach is proposed to successfully demonstrate FTC of the *sliding variable*. We identify a compensating phase and a reaching phase during the ASMC process as two separate stages characterizing the sliding mode dynamics. A new explicit form for estimating the upper-bound reaching time is provided for any bounded perturbation. Finally, numerical and experimental applications are performed to convey the discussed results.

5.1 Introduction

FTC of the sliding variable to zero is one of the two main features that SMC deserves and differs from other control methods [19]. From a stability point of view, FTC is distinctive from the other two forms: AC (including EC) and convergence in UUB sense. Since FTC refers to the time required to build the sliding mode, it directly affects the overall system response [1, 39, 49]. Moreover, under certain conditions, dynamics with FTC properties exhibit better rejection of bounded perturbations than the Lipschitzian ES systems [123].

The main idea in ASMC is that the switching gain is designed to be time-varying so that it dynamically compensates for the perturbations. In the various ASMC designs established in the literature, a core algorithm, based on integral switching gain (ISG), is commonly deployed to deal with uncertainties of unknown bounds. For ASMC designs utilizing ISG (we call them IG-ASMC designs), three different statements of sliding variable convergence

(in the UUB sense, AC and FTC) have been acknowledged over the past decade. The AC of the sliding variable to zero was stated in [10, 11, 15]. Recently, the authors discussed in [16] the FTC of the sliding variable for *ideal* ASMC design, and in [17], the UUB sliding variable and the switching gain adaptation error for *real sliding* using a boundary-layer-based ASMC were investigated. In [79, 127], the authors obtained FTC result of the designed sliding variable; however, the switching gain adaptation error only has AC property. In [14, 16, 18, 19], the authors state that both the sliding variable and the switching gain adaptation error converge to zero in finite time. However, the main result of [14] could not sustain authentically the FTC of both the sliding variable and adaptation gain. The discussed problem in [14] considered a Lyapunov function in two independent variables, the sliding variable and the switching gain adaptation error, differing from the required condition on the time derivative of this Lyapunov function, and then discrediting the effectiveness of the original result in this case. The reader can refer to Theorem 4.2 in [123] and its applications in [116, 117, 128] for further understanding of this argumentative result. In [16,18,19], when dealing with ideal sliding mode, deficiencies exist in the estimated reaching time. According to the given formulas, this reaching time tends to infinity as the sliding variable approaches zero, and there is no guarantee of FTC in [16, 19]. Hence, the convergence can only be achieved over an infinite time interval (which is indeed intrinsic to AC property rather than FTC).

Roughly speaking, for the ASMC designs presented over the past decade, researchers either have not referred to FTC (have shown only AC, *e.g.*, in [10,11,15] and UUB performances in [17]) or have stated FTC results encountering weaknesses (*e.g.*, [14,16–19]). These limits will be discussed thoroughly leading to the three main contributions of this chapter. First, it demystifies the confusion of convergence types in ASMC designs applied for uncertain systems with unknown bounds. It overcomes weaknesses and inadequate statements depicted from existing ASMC designs discussed above. We revisit the FTC of the sliding variable to zero in these ASMC designs by demonstrating the existence of a compensating phase and a reaching phase during the sliding process. Second, a new Lyapunov-based FTC property is discussed. A majorant curve approach is proposed to prove FTC. Along with the new proof, a new formula of RTE, different from any existing result, is provided. This new explicit RTE formulates simply the relationship between the reaching time and the switching gain.

This chapter focuses on the completeness of convergence and RTE in ASMC designs in recent years. In Section 5.2, we present some mathematical preliminaries and state the control problem. Section 5.3 analyzes deficiencies

(in terms of sliding variable convergence) depicted in existing statements of ASMC designs for the *ideal* case. A new framework, introducing results about switching gain boundedness and estimating finite reaching time, is proposed in Section 5.4 and represents the main contribution of this paper. The implementation of real ASMC is discussed in Section 5.5. A tutorial example and experimental results are shown in Section 5.6 to verify the effectiveness of the new formula of RTE and the improvement of the modified reaching law for real ASMC designs, while Section 5.7 concludes this chapter.

5.2 Mathematical Preliminaries and Problem Statement

In this section, we first present some properties that can be retrieved from [1,11,123]. Then, we state the control problem and assumptions for nonlinear systems with finite uncertainties of unknown bounds.

5.2.1 Mathematical Preliminaries

Useful definitions of the AC, UUB and FTC are presented in Appendix A (refer to Section A.3.1)

Given a second order dynamic system

$$\dot{x} = f_1(x, y) \tag{5.1a}$$

$$\dot{y} = f_2(x, y) \tag{5.1b}$$

where $f_i : \chi \to \mathbb{R}$, $i = 1, 2$, is Lipschitzian in (x, y) on an open neighborhood χ of the origin $(0, 0)$ which is an equilibrium point for (5.1). Consider the Lyapunov function

$$V = ax^2 + by^2 \tag{5.2}$$

where $a > 0$ and $b > 0$. V is positive definite.

Lemma 5.1. *If there exists $c > 0$ s.t. $\forall (x, y) \in D \subseteq \chi$*

$$\dot{V} \leq -c|x| \tag{5.3}$$

then, for any $x(0) \neq 0$, $x \to 0$ asymptotically and y is stable.

Proof. Integrating both sides of (5.3), we have

$$\begin{aligned}\int_0^t |x| d\tau &\leq \frac{V(0) - V(t)}{c} \\ &\leq \frac{V(0)}{c}\end{aligned} \tag{5.4}$$

First, based on Theorem 4.18 of [1], we obtain, from (5.2) and (5.3), x and y UUB. Then, as $t \to \infty$, from (5.4), the non-negative integral is always less than $\frac{V(0)}{c}$. So, $\lim_{t\to\infty} \int_0^t |x| d\tau$ exists and is finite. By Barbalat's Lemma [1], it yields that $\lim_{t\to\infty} |x| = 0$. □

The above Lemma indicates well the AC of $x \to 0$ for any $x \neq 0$. However, the AC of $y \to 0$ is not guaranteed. Actually, as $V(t)$ decreases (by referring to $\dot{V} \leq -c|x|$), x converges to zero and y is stable [1], *i.e.*, y can be AS or UUB. Moreover, the FTC of both dynamics to zero is not necessarily true. Indeed, this statement can be validated by the following example.

Example 5.1. First, given the nominal dynamic system

$$\dot{x} = -2x \tag{5.5a}$$

$$\dot{y} = -x - y \tag{5.5b}$$

with $x(0) \neq 0$ and $\frac{y(0)}{x(0)} \geq 1$. We have

$$x(t) = e^{-2t} x(0) \tag{5.6a}$$

$$y(t) = e^{-t} y(0) + (e^{-2t} - e^{-t}) x(0) \tag{5.6b}$$

For any $x(0) > 0$ and $-\frac{y(0)}{x(0)} + 1 < 0$, we have $x(t) \neq 0$ and $y(t) \neq 0$ $\forall t \geq 0$. From (5.6a) and (5.6b), $x(t)$ and $y(t)$ converge to zero infinitely (exponentially as $t \to \infty$). In addition, by selecting $V = x^2 + y^2$ which satisfies (5.2), we have

$$\begin{aligned}\dot{V} &= 2x\dot{x} + 2y\dot{y} \\ &= -4x^2 - 2xy - 2y^2\end{aligned} \tag{5.7}$$

Note, from (5.6a), that $x(t) > 0$. Assuming $x(0) \neq 0$ and $\dfrac{y(0)}{x(0)} > 1$, from (5.6b), we write $y(t) = x(t) + e^{-t}\big(y(0) - x(0)\big)$, and we obtain

$$\begin{aligned}\dot{V} &\leq -2y^2 \\ &\leq -2x^2 - 2e^{-t}\big(y(0) - x(0)\big)x(t) - e^{2t}\big(y(0) - x(0)\big)^2 \\ &\leq -\big(y(0) - x(0)\big)^2\frac{|x(t)|}{x(0)} \end{aligned} \tag{5.8}$$

verifying (5.3). It is clear that x and y are ES, but no FTC is guaranteed.

Now, consider the perturbed system

$$\dot{x} = -2x \tag{5.9a}$$

$$\dot{y} = -x - y + d \tag{5.9b}$$

with d unknown positive constant. We have x is ES and y UUB but there is no FTC of these dynamics (refer to Appendix A.6 for more details).

Lemma 5.2. *Given the Lyapunov function* (5.2)*, if there exists a non-negative function $h(x, y)$ in x and y s.t.*

$$\dot{V} \leq -h(x, y) \tag{5.10}$$

then $h(x, y) \to 0$ as $t \to \infty$. In particular,

- *If $h(x, y) = c|xy|$, with $c > 0$, we obtain $|x| \to 0$ or $|y| \to 0$ as $t \to \infty$.*
- *If $h(x, y) = c_1|x| + c_2|xy|$, for $c_1 > 0$ and $c_2 > 0$, we have $|x| \to 0$ and y is UUB as $t \to \infty$.*

Proof. Similar to Lemma 5.1. □

Note that Lemma 5.2 represents a general form of Lemma 5.1 regarded as a factor in the Lyapunov function distinction studying the stability statement of the problem of SMC that will be discussed in the following subsection.

Lemma 5.3. *(refer to [123]) Given the Lyapunov function* (5.2)*, if there exist real scalars $t^* \geq 0$, $k > 0$ and $0 < \lambda < 1$, s.t. $\forall t \geq t^*$*

$$\dot{V}(x, y) + kV^{\lambda}(x, y) \leq 0 \tag{5.11}$$

then, the dynamics (5.1) *is finite-time stable. Moreover, the settling time satisfies*

$$t_r \leq \frac{V(x_0, y_0)^{1-\lambda}}{k(1-\lambda)} + t^* \tag{5.12}$$

for all $(x, y) \in \mathbb{R}^2 \backslash \{(0, 0)\}$.

Note that Lemma 5.3 is a simple extension of a classical FTC theorem (where $t^* = 0$) in SMC designs [1, 39, 49].

5.2.2 Problem Statement of SMC Scheme

Recall the uncertain dynamic system

$$\dot{x} \quad = \quad f(x,t) + g(x,t)u, \quad x(0) = x_0 \tag{5.13}$$

where $x \in \chi$ is the state vector, with χ as a domain of $\mathbb{R}^n$ containing the origin, and $u \in \mathbb{R}$ the input signal. Let $x = 0$ be an equilibrium point for (5.13). Functions $f(x,t)$ and $g(x,t)$, containing parameter uncertainties and external disturbances, are bounded in $\chi \times \mathbb{R}^+$ [52]. The bounds of $f(x,t)$ and $g(x,t)$ are unknown with $g(x,t) \neq 0$ in $\chi \times \mathbb{R}^+$ [16]. Recall the sliding variable dynamics with a relative degree equal to 1 *w.r.t.* u

$$\dot{\sigma}(x,t) = \Psi(x,t) + \Gamma(x,t)u, \quad \sigma(x_0,0) = \sigma_0 \tag{5.14}$$

where the scalar functions $\Psi(x,t)$ and $\Gamma(x,t)$ are bounded. The sign of Γ remains the same. In fact, without loss of generality, it will be assumed to be strictly positive, *i.e.*,

$$0 < \underline{\Gamma} \leq \Gamma(x,t) \leq \bar{\Gamma} \tag{5.15}$$

with $\underline{\Gamma}$ and $\bar{\Gamma}$ representing the lower and upper bounds of Γ, respectively, whose values are unknown *a priori* [16].

5.3 ASMC Law and Existing Results

In this section, we recall some recent results, introduced in [10, 11, 13–19], and we analyze the sliding variable convergence and RTE statements as shown in these references. The incurred deficiencies in these works will be highlighted, eventually.

5.3.1 ASMC Law

As discussed in Chapter 4, for the case where the uncertainties are fully unknown, the feedback control $u(t)$ in SMC is defined as

$$u(t) = -K(t) \cdot \mathrm{sgn}(\sigma) \tag{5.16}$$

where $\mathrm{sgn}(\cdot)$ refers to the signum function. In particular, with classic SMC design, the switching gain K is a constant scalar which is designed to be

sufficiently large so that it can compensate for the uncertainties [39,52]. However, the ASMC techniques are designed as further SMC structures without knowledge of the bounds of uncertainties *a priori*. The forms introduced in [10,11,13–19] use time-varying gain $K(t)$ to adaptively compensate for the lumped uncertainties. We substitute (5.16) into (5.14)

$$\dot{\sigma} = \Psi - \Gamma K \text{sgn}(\sigma), \quad \sigma(x(0), 0) = \sigma_0 \tag{5.17}$$

Among the numerous ASMC designs shown during the past decade (*e.g.*, [10,11,13–19]), a common gain adaptation law under the *ideal sliding* case is stated as ISG law (recall integral adaptation law for ideal ASMC discussed in Chapter 3)

$$\dot{K} = \alpha|\sigma|, \quad K(0) = K_0 \tag{5.18}$$

with $\alpha > 0$ representing the gain of the adaptation law. Note that in the case of *ideal* ASMC, the sliding mode is said to be established when $\sigma = 0$ for all time after reaching the required manifold, and the switching control time interval can be infinitely small.

Remark 5.1. For a *real* ASMC, the law (5.18) will force K to increase constantly without bound since σ will never be identically zero due to inherent processing delays, finite sampling rates, measurement errors, noises, *etc.* Thus for *real* ASMC, the law (5.18) should be changed to other forms. For instance, in [16], this integral gain (IG) adaptation law for real ASMC is given by (refer to Chapter 4),

$$\dot{K} = \alpha|\sigma| \cdot \text{sgn}(|\sigma| - \varepsilon) \tag{5.19}$$

to provide the ability that K reduces its value after σ entering a small boundary layer (*i.e.*, $|\sigma| \leq \epsilon$). However, we consider mainly the *ideal sliding* ASMC in this chapter to analyse the boundedness, FTC, and RTE for the sake of simplicity.

5.3.2 Comments on Existing Results

Essentially, two different statements about the sliding variable convergence (referring to AC and FTC) have been discussed in [10,11,14–19] for the case of *ideal* ASMC design (5.16) and (5.18). To prove these statements, for a presumed maximum gain K^* compensating for the overall lumped uncertainties, the authors have commonly used the following Lyapunov candidate function

$$V = \frac{1}{2}\sigma^2 + \frac{1}{2\gamma}\tilde{K}^2 \tag{5.20}$$

where σ is the sliding variable, $\tilde{K} = K - K^*$ the gain error and γ a positive scalar. In the following, the first Theorem states the FTC of the designed ASMC, while the second one shows the AC performance.

Remark 5.2. K^* is defined as a presumed maximum gain to which K converges. Some researchers defined K^* as the maximum value of Ψ/Γ. However, during the adaptation process, K mostly converges to a value greater than $|\Psi/\Gamma|_{max}$ (refer to the numerical illustration discussed later in Section 5.6.1 of this chapter); it is also possible that K converges to a value less than $|\Psi/\Gamma|$ (refer to Example 4.1 in Chapter 4). There is no reason that K converges to the upper-bound of Ψ/Γ. Such a statement implies that defining K^* as the upper-bound of Ψ/Γ will make the Lyapunov candidate function (5.20) deficient.

Theorem 5.1. *(refer to [14, 16–19]) Given the nonlinear uncertain system* (5.13) *with the sliding variable dynamics* (5.14) *controlled by* (5.16) *and* (5.18)*, both the sliding variable σ and the switching gain error $\tilde{K}$ converge to zero in finite time.*

As will be shown later, this statement of FTC for both arguments, σ and $\tilde{K}$, would be true. In the following we discuss the ways (*i.e.*, steps taken in order to achieve this particular end) addressed in the cited references. On the one hand, in [14], the authors use the Lyapunov function (5.20) and conduct to the inequality

$$\dot{V} \leq -\beta_1 |\sigma| \tag{5.21}$$

for some $\beta_1 > 0$ and all $t > 0$, where $\dot{V}$ is the time derivative of V. Then, they conclude the FTC of the dynamics. According to Lemma 5.1 introduced above, we can only state that $\sigma \to 0$ asymptotically and $\tilde{K}$ is UUB. The example 5.1 discussed in Subsection 5.2.1 is definitely a counterexample of the analysis demonstrated in [14]. On the other hand, the determination of FTC for both σ and $\tilde{K}$ presented in [16, 18, 19] is different from that in [14]. Given the Lyapunov candidate function (5.20), the authors conclude that for all $t > 0$, the inequality

$$\dot{V} \leq -\beta_\sigma |\sigma| - \beta_k |\tilde{K}| \tag{5.22}$$

holds for $\beta_\sigma > 0$, $\beta_k = \big(-\underline{\Gamma} + \frac{\alpha}{\gamma} \big) \cdot |\sigma| > 0$ and $0 < \gamma < \frac{\alpha}{\underline{\Gamma}}$, leading to FTC of the sliding variable [18]. In addition, a maximum reaching time is estimated

as

$$t_r \leq \frac{\sqrt{2V(0)}}{\beta_2} \tag{5.23}$$

with $\beta_2 = \min(\beta_\sigma, \beta_k\sqrt{\gamma})$. In this case, the idea of FTC of V, as well as of its arguments σ and $\tilde{K}$, is not well conveyed in [16, 18, 19]. In fact, one can see that as $|\sigma|$ approaches zero $\beta_k \to 0$ and $\beta_2 \to 0$ too, and from (5.23), the reaching time t_r tends to ∞, actually. Thus, there is no guarantee of FTC for both σ and $\tilde{K}$. Alternatively, (5.22) can be rewritten as

$$\dot{V} \leq -\beta_\sigma|\sigma| - \beta_{\sigma k}|\sigma| \cdot |\tilde{K}| \tag{5.24}$$

with $\beta_{\sigma k} = \big(-\underline{\Gamma} + \frac{\alpha}{\gamma}\big) > 0$. So, according to Lemma 5.2 discussed above, we can only state that $\sigma \to 0$ asymptotically and $\tilde{K}$ is UUB. Finally, in [17], the authors admit first the AC of the sliding variable $\sigma \to 0$. Then, they state intuitively the FTC of σ. Roughly, they notice that if the condition (5.22) is satisfied and if the design parameter α, introduced in (5.18), is selected sufficiently large, as

$$\alpha > \beta_{\sigma,t_2} \cdot \max|\Psi| \tag{5.25}$$

for some positive scalar β_{σ,t_2} which is predetermined and correlated with σ and some instant t_2 (referring to the finite time when the maximum value of the lumped uncertainty occurs), then the FTC of σ can be guaranteed [17]. In fact, since β_{σ,t_2} is difficult to estimate, the requirement for a sufficiently large α would affect the design (5.18) and may cause the switching gain to be extremely high. Although the FTC result is true, the discussed proof remains injudicious, and the intuitive investigation of FTC in [17] relies on high gain design, as far as the maximum lumped uncertainty is unknown (rather than the SMC which requires knowledge of such upper-bounds of uncertainties, *i.e.*, $\max|\Psi|$) or by sacrificing an extra time consumption (refer to the parameter t_2 introduced above) to adjust the switching gain.

Theorem 5.2. *(refer to [10,11,15]) For the nonlinear uncertain system* (5.13) *with the sliding variable dynamics* (5.14) *controlled by* (5.16) *and* (5.18)*, the sliding variable* $\sigma \to 0$ *asymptotically.*

Using the Lyapunov function (5.20), assuming that there exists $\beta_1 > 0$ so that (17) holds for all $t > 0$. Then, the proof is basically ended by Lemma 5.1. As opposed to the results on FTC and their deficiencies, the AC result

of Theorem 5.2 is well stated in numerical form of the references [10, 11, 15]. However, Theorem 5.2 does not reveal the FTC result, often presented as the aimed statement for the convergence of the sliding variable σ and the dynamic gain error $\tilde{K}$.

In summary, the results discussed in [14,16,17,19] support poorly the FTC statement, while the works conducted in [10,11,15] do not conclude the FTC. In the following section, we will prove properly that both the sliding variable σ and the gain error $\tilde{K}$, in the nonlinear uncertain systems (5.13) with the sliding variable dynamics (5.14) controlled by (5.16) and (5.18), have FTC to zero. Moreover, a new formula, different from any existing equation, will be deduced to estimate the upper-bound of reaching time t_r.

5.4 Upper-Bound of Switching Gain and FTC – New Framework

In this section, we first recall Lemma 1 of [16] (see Lemma 2.1 of [19] as well). The proof will be discussed in detail in light of further evidence on the boundedness property of the switching gain dynamics. Then, based on the revised proof, we demonstrate the FTC of the sliding variable σ to zero by showing the existence of a finite-time *compensating phase* and the existence of a finite-time *reaching phase*. During the *compensating phase*, any perturbation will be eventually compensated in finite time by the switching gain. Also, the sliding variable will stop increasing its value at the end of the *compensating phase*. During the *reaching phase* the sliding variable will reach the sliding surface in finite time. Moreover, we introduce a new form to estimate the upper-bound of the maximum reaching time.

5.4.1 Upper-Bound of Switching Gain

The following Lemma states the boundedness of the switching gain.

Lemma 5.4. *(refer to Lemma 2.1 in [19] and Lemma 1 in [16]) Consider the nonlinear uncertain system* (5.13) *with the sliding variable dynamics* (5.14) *controlled by* (5.16) *and* (5.18) *with* $K(0) > 0$*. The gain* $K(t)$ *has an upper-bound, i.e., there exists a finite positive constant* K^* *so that* $\forall t > 0$

$$K(t) \leq K^* \tag{5.26}$$

Proof. From (5.18), $\forall t \geq 0$, $\dot{K}(t) \geq 0$, *i.e.*, $\forall t_1 > 0$ and $t_2 > t_1$, we have $K(t_2) \geq K(t_1) > 0$. $K(t)$ is a monotonically continuous function. Two cases may arise.

Case 1 (finite limit) *i.e.*, $K(t) \to K_\infty$ as $t \to \infty$, for a given finite constant $K_\infty > 0$. Thus, it always exists $K^* > 0$ *s.t.* $K^* \geq K_\infty$ and, $\forall t > 0$, $K(t) \leq K_\infty \leq K^*$.

Case 2 (infinite limit) *i.e.*, $K(t) \to \infty$ as $t \to \infty$. Then, there exist $\alpha_k > 0$ and $t_1 > 0$ *s.t.* $\forall t \geq t_1$

$$\frac{\max|\Psi|}{\underline{\Gamma}} + \frac{\alpha_k}{\underline{\Gamma}} \leq K(t) \tag{5.27}$$

that is,

$$\max|\Psi| - \underline{\Gamma} K(t) \leq -\alpha_k \tag{5.28}$$

Now, consider the Lyapunov function $V = \sigma^2$. Using (5.17) and (5.28), we obtain $\forall t \geq t_1$

$$\dot{V} \leq -2\alpha_k \sqrt{V} \tag{5.29}$$

Then, $|\sigma| \to 0$ in finite time (by applying Lemma 5.3 introduced in subsection 5.2.1). Let t_2 be the time at which σ reaches zero. Then, for all $t \geq t_2$, we have $\dot{K}(t) = \alpha|\sigma| = 0$, *i.e.*, $K(t)$ stops increasing for all $t \geq t_2$. Thus, $K(t)$ is upper-bounded, which is a contradiction of the statement of Case 2. Thus, we conclude that $K(t)$ is finitely bounded. □

5.4.2 Existence of Compensating Phase

In the ASMC processes, there usually exist two phases: compensating phase and reaching phase [73]. The *compensating phase* is the phase during which the control $u(t)$ is automatically increasing and corresponding to the increase of unknown perturbations $\frac{\Psi}{\Gamma}$. This phase continues until the moment when the control $u(t)$ completely compensates for the perturbation $\frac{\Psi}{\Gamma}$ for all future time (see Figure 5.1). Such an event refers to the end of the compensating phase, and then, the beginning of the reaching phase. At this moment, the time rate of the sliding variable is non-positive, *i.e.*, $\frac{d|\sigma|}{dt} \leq 0$. The *converging phase*, identified also as *reaching phase*, is the phase during which the sliding

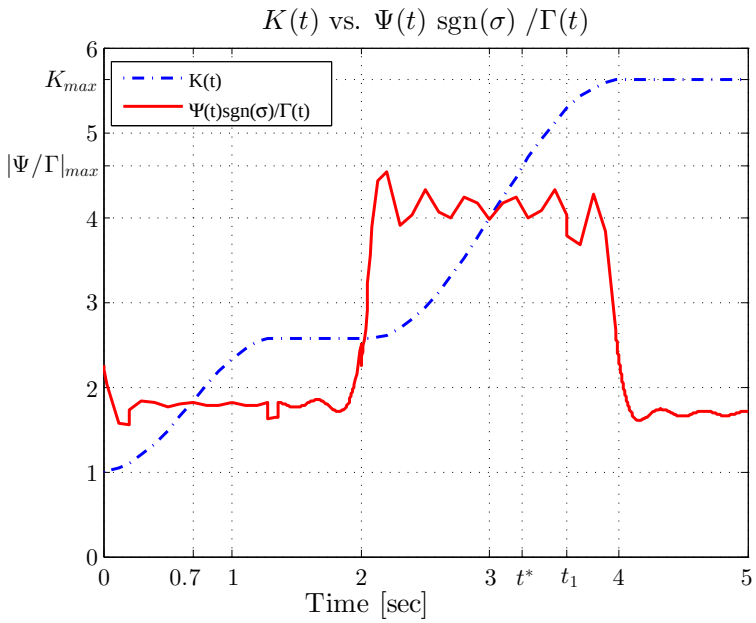

Figure 5.1: Illustration of the switching gain K for a given lumped perturbation $\frac{\Psi}{\Gamma}$. The ASMC between $t = 0$ and $t = t^*$ is in *compensating phase* mode. The *reaching phase* corresponds to the time period from $t = t^*$ to $t \approx 4$ (in sec).

variable is forced to reach the sliding surface (see Figure 5.1). Based on the idea of the aforementioned proof of upper-bounded switching gain, we will demonstrate that both phases exist in ideal ASMC processes under unknown bounded perturbations. We deal with the ASMC dynamics as follows. The compensating phase is first presented in Lemma 5.5; then the reaching phase is discussed in Theorems 5.3 and 5.4.

Lemma 5.5. *(Existence of compensating phase [73]) Given the nonlinear uncertain system* (5.13) *with the sliding variable dynamics* (5.14) *controlled by* (5.16) *and* (5.18)*, there exists a time t^* so that for all $t \geq t^*$*

$$K(t^*) \geq \frac{\Psi sgn(\sigma)}{\Gamma} \tag{5.30}$$

Proof. It is based on the same idea and procedure of the proof of Lemma 5.4. □

Since $K(t)$ keeps growing whenever $\sigma \neq 0$ (refer to gain dynamics (5.18)), there exists a positive time interval $\Delta t > 0$ and a positive scalar $\kappa > 0$ so that the following inequality holds

$$K(t) \geq K(t^*) + \kappa \geq \frac{\Psi \text{sgn}(\sigma)}{\Gamma} + \kappa \tag{5.31}$$

for all $t \geq t^* + \Delta t$. Lemma 5.5 implies that, for $\sigma \neq 0$, the monotonically growing gain $K(t)$ will completely compensate for the lumped perturbations at the time instant t^* so that (5.30) holds for all $t \geq t^*$. In other words, there always exists t^* so that (5.30) holds for all future time $t \geq t^*$. Obviously, the inequality (5.30) holding for $t \geq t^*$ can be extended to any time $t \geq 0$. Lemma 5.5 demonstrates the existence of a *compensating phase* in the ASMC process and t^* represents the compensating time (refer to *compensating phase* in Figure 5.1). Considering $\Gamma > 0$, note that, from (5.31), we have

$$\Gamma K \geq \Psi \text{sgn}(\sigma) + \Gamma \kappa \tag{5.32}$$

Remark 5.3. It should be pointed out that, during the adaptation process, $K(t^*)$ only compensates for $\dfrac{\Psi \text{sgn}(\sigma)}{\Gamma}$. $K(t^*)$ can be smaller than $\left|\dfrac{\Psi}{\Gamma}\right|$ (see Example 4.1 in Chapter 4.

Particular Case: Let us consider the *compensating phase*, for t between 0 and t^*. For simplicity, assume constant perturbations and uncertainties (*i.e.*, Ψ and Γ are constants) occur (or take form) at $t = 0$. The compensating phase implies that, if the uncertainties cause $|\sigma|$ initially increasing, K will eventually compensate for such uncertainties. Thus, during the compensating phase, $\text{sgn}(\sigma) = \text{sgn}(\sigma_0)$ and $\Psi \text{sgn}(\sigma) = \Psi \text{sgn}(\sigma_0) > \Gamma K$. If $\Psi \text{sgn}(\sigma) = \Psi \text{sgn}(\sigma_0) \leq \Gamma K$, technically there is no compensating phase or the compensating time $t^* = 0$. We have

$$\frac{d}{dt}|\sigma| = \dot{\sigma} \text{sgn}(\sigma) = \Psi \text{sgn}(\sigma_0) - \Gamma K > 0 \tag{5.33}$$

Differentiating both sides of (5.33) and noticing (5.18), we have

$$\frac{d^2}{dt^2}|\sigma| = -\Gamma \alpha |\sigma| \tag{5.34}$$

It has a general solution

$$|\sigma| = c \sin(\sqrt{\Gamma \alpha} \cdot t + \Phi) \tag{5.35}$$

where c and Φ are constant. To determine Φ, we integrate both sides of (5.18) from 0 to t and apply (5.35). We obtain

$$K(t) = K_0 + \frac{\alpha c}{\sqrt{\Gamma\alpha}}[\cos\Phi - \cos(\sqrt{\Gamma\alpha}\cdot t + \Phi)] \tag{5.36}$$

where K_0 is the initial value of K. Thus, (5.33) becomes

$$\frac{d}{dt}|\sigma| = \Psi\text{sgn}(\sigma_0) - \Gamma\Big[K_0 + \frac{\alpha c}{\sqrt{\Gamma\alpha}}[\cos\Phi - \cos(\sqrt{\Gamma\alpha}\cdot t + \Phi)]\Big] \tag{5.37}$$

Also, from (5.35), we have

$$\frac{d}{dt}|\sigma| = c\sqrt{\Gamma\alpha}\cos(\sqrt{\Gamma\alpha}\cdot t + \Phi) \tag{5.38}$$

Equating the right sides of (5.37) and (5.38), we obtain

$$c\sqrt{\Gamma\alpha}\cos\Phi = \Psi\text{sgn}(\sigma_0) - \Gamma K_0 \tag{5.39}$$

Moreover, from (5.35), we have for $t = 0$

$$|\sigma_0| = c\sin\Phi \tag{5.40}$$

Combine (5.39) and (5.40) to write

$$\tan\Phi = \frac{|\sigma_0|\sqrt{\Gamma\alpha}}{\Psi\text{sgn}(\sigma_0) - \Gamma K_0} \tag{5.41}$$

At the end of the compensating phase, the perturbations $\frac{\Psi\text{sgn}(\sigma)}{\Gamma}$ are compensated by the gain K and $\frac{d}{dt}|\sigma| = 0$ (refer to dynamics (5.33)). In other words, $|\sigma|$ reaches its maximum distance from the sliding surface (*i.e.*, $\sin(\sqrt{\Gamma\alpha}t + \Phi) = 1$ in (5.35)). Then, the compensating time t^* can be estimated by letting $\sqrt{\Gamma\alpha}t^* + \Phi = \frac{\pi}{2}$, *i.e.*,

$$t^* = \frac{\pi - 2\Phi}{2\sqrt{\Gamma\alpha}} \tag{5.42}$$

with $\Phi = \arctan\big(\frac{|\sigma_0|\sqrt{\Gamma\alpha}}{\Psi\text{sgn}(\sigma_0) - \Gamma K_0}\big)$ obtained from (5.41).

5.4.3 FTC of the Closed-Loop ASMC System – Lyapunov Approach

In [10, 11, 14, 16–19], the stability of ASMC design is based on the Lyapunov analysis by using the candidate positive definite function (5.20). As discussed in Section 5.3, however, the results can only conclude AC thoroughly, but not FTC. In the following, we propose a new Lyapunov candidate function, novelly contributing to prove FTC of $\sigma \to 0$, as

$$V = (|\sigma| + |\tilde{K}|)^2 = \sigma^2 + 2|\sigma||\tilde{K}| + \tilde{K}^2 \tag{5.43}$$

Obviously, V is continuous and positive definite and it is differentiable almost everywhere (except at the origin, *i.e.*, $\sigma = 0$ and $\tilde{K} = 0$).

Theorem 5.3. *Given the nonlinear uncertain system* (5.13) *with the sliding variable dynamics* (5.14) *controlled by* (5.16) *and* (5.18)*, the sliding variable* $\sigma \to 0$ *in finite time. Moreover, the upper-bound of the settling time can be estimated as [73]*

$$t_r \leq \frac{\sqrt{V(\sigma_0, \tilde{K}_0)}}{\underline{\Gamma}\kappa} + t' \tag{5.44}$$

for some positive scalars κ *and* t'*.* σ_0 *and* $\tilde{K}_0$ *designate the initial values of* σ *and* $\tilde{K}$*, respectively, and* $\underline{\Gamma}$ *is the lower bound of* Γ*.*

Proof. Considering the Lyapunov candidate function (5.43), its time derivative is

$$\dot{V} = 2\sigma\dot{\sigma} + 2\frac{d|\sigma|}{dt}|\tilde{K}| + 2|\sigma|\frac{d|\tilde{K}|}{dt} + 2|\tilde{K}|\frac{d}{dt}|\tilde{K}| \tag{5.45}$$

Notice that, for $\sigma \neq 0$, we have $|\sigma| = \sigma\text{sgn}(\sigma)$, $\frac{d}{dt}|\sigma| = \Psi\text{sgn}(\sigma) - \Gamma K$, and, for $\tilde{K} \neq 0$, $\tilde{K} = K - K^* = -|\tilde{K}|$ (refer to (5.26) in Lemma 5.4) then $\frac{d}{dt}|\tilde{K}| = -\dot{K}$. Consider t^* the time instant when the compensating phase is reached (refer to Lemma 5.5). Then, from (5.32) and (5.45), the time derivative, along the trajectories of (5.17) and (5.18), for $t \geq t' = t^* + \Delta t$, $\sigma \neq 0$ and $\tilde{K} \neq 0$, is

$$\begin{aligned}
\dot{V} &= -2|\sigma|\big[\Gamma K - \Psi\text{sgn}(\sigma)\big] - 2\big[\Gamma K - \Psi\text{sgn}(\sigma)\big]|\tilde{K}| - 2\alpha|\sigma|^2 - 2\alpha|\sigma| \cdot |\tilde{K}| \\
&\leq -2|\sigma|\Gamma\kappa - 2\Gamma\kappa|\tilde{K}| - 2\alpha|\sigma|^2 - 2\alpha|\sigma||\tilde{K}| \\
&\leq -2\Gamma\kappa \cdot \Big(|\sigma| + |\tilde{K}|\Big) \\
&\leq -2\underline{\Gamma}\kappa\sqrt{V}
\end{aligned} \tag{5.46}$$

Then, the proof is ended by applying Lemma 5.3. □

With the new approach, the settling time depends on the initial state and system parameters. It does not depend on the magnitude of the sliding variable $|\sigma|$, which is different from the FTC discussed in [16, 18, 19].

5.4.4 FTC of the Closed-Loop ASMC System – Majorant Curve Approach

The Lyapunov-based approach of Theorem 5.3 has successfully proven the FTC occurred during the reaching phase that follows the compensating phase. However, it is difficult to practically estimate the reaching time because of the difficulty to calculate κ and the initial gain error $\tilde{K}_0$. In this subsection, we propose a new approach (contributing to a new analysis framework of the ASMC problem) to prove the existence of the reaching phase and to give a new formula of RTE. Based on Lemma 5.5, we have the following Theorem.

Theorem 5.4. *(*Existence of reaching phase *[73]) Given the nonlinear uncertain system* (5.13) *with the sliding variable dynamics* (5.14) *controlled by* (5.16) *and* (5.18)*, the sliding variable* $\sigma \to 0$ *and switching gain error* $\tilde{K} \to 0$ *in finite time. Moreover, the maximum reaching time of* σ *to sliding surface can be estimated as*

$$t_r \leq \frac{\pi}{2\sqrt{\underline{\Gamma}\alpha}} + t^* \tag{5.47}$$

where t^* *is the compensating time defined in Lemma 5.5,* α *the designed adaptation gain rate introduced in* (5.18) *and* $\underline{\Gamma} > 0$ *the lower-bound of* Γ*.*

Proof. We refer to the *reaching phase* and we integrate (5.18) between 0 and any instant $t \geq t^*$ to obtain

$$K(t) = K(t^*) + \int_{t^*}^{t} \alpha|\sigma| d\tau \tag{5.48}$$

Since $\sigma = 0$ represents the establishment of the sliding mode (*i.e.*, the objective of ASMC), we consider only $\sigma > 0$ or $\sigma < 0$. Using Lemma 5.5 and noticing that (5.17) is equivalent to $\dfrac{d|\sigma|}{dt} = \Psi \text{sgn}(\sigma) - \Gamma K$, we obtain from (5.30) and

(5.48)

$$\frac{d|\sigma|}{dt} = \Psi \mathrm{sgn}(\sigma) - \Gamma K(t^*) - \Gamma \int_{t^*}^{t} \alpha |\sigma| d\tau$$
$$\leq -\underline{\Gamma}\alpha \int_{t^*}^{t} |\sigma| d\tau \tag{5.49}$$

The above differential inequality shows that the positive amount $|\sigma(t)|$ is decreasing with a time-varying rate of at least $\underline{\Gamma}\alpha \int_{t^*}^{t} |\sigma| d\tau$. From (5.49), we derive the following limit case for the time evolution of σ (*i.e.*, the worst in terms of time response rate) which depends on the initial condition of the reaching phase. In fact, the trajectory of $|\sigma|$ geometrically lies below the majorant curve [53, 89] of $|\sigma|$ governed by

$$\frac{d|\sigma|}{dt} = -\underline{\Gamma}\alpha \int_{t^*}^{t} |\sigma| d\tau \tag{5.50}$$

Then, the reaching time can be generically estimated by solving (5.50) with the limit conditions $|\sigma(t^*)| = |\sigma^*|$ and $|\dot{\sigma}(t^*)| = 0$. The explicit formula of the majorant curve can be written as

$$|\sigma(t)| = |\sigma^*| \cos\left(\sqrt{\underline{\Gamma}\alpha} \cdot (t - t^*)\right) \tag{5.51}$$

The sliding variable σ reaches 0 when the argument of the cosine function (5.51) reaches $\frac{\pi}{2}$ from 0 (initial value corresponding to $t = t^*$). Thus, the upper-bound of RTE, $t_r - t^*$, is written as

$$t_r - t^* \leq \frac{\pi}{2\sqrt{\underline{\Gamma}\alpha}} \tag{5.52}$$

Note that (5.52) is evaluated by letting $|\sigma(t)| = 0$ in (5.51). Moreover, from (5.18), K stops increasing as soon as σ reaches zero. Thus, $\tilde{K}$ reaches zero at the same time that σ reaches zero. □

From (5.47), the estimation of the maximum reaching time comprises two time frames. First, the interim, limited by t^* (*i.e.*, from $t = 0$ to $t = t^*$), is the time period of compensating phase where the switching gain $K(t)$ value is increasing to be sufficiently large to completely compensate for the perturbation. The second frame, with a maximum magnitude of $\frac{\pi}{2\sqrt{\underline{\Gamma}\alpha}}$, is the time period of reaching phase, *i.e.*, the maximum time required to force the sliding variable σ to reach zero from $\sigma^* = \sigma(t^*)$. Note, from (5.52), that the reaching

phase interval from t^* to t_r depends neither on $\sigma(t^*)$ (*i.e.*, the initial value of σ during the reaching phase), nor on the maximum uncertain perturbation, $\max|\Psi|$. More specifically, no matter whether $\sigma(t^*)$ and $|\Psi|$ are small or large, we figure $t_r - t^* \leq \frac{\pi}{2\sqrt{\underline{\Gamma}\alpha}}$. Let us recall that this term represents an upper-bound or a maximum value of the "slowest" sliding variable dynamics. The new result of reaching time (5.47) represents a better estimate than the existing ones given in [16,19] (*e.g.*, refer to (5.23)) by making its upper-bound value tightened thoroughly.

In summary, the FTC property of ASMC design is obtained by demonstrating the existence of a compensating phase (refer to Lemma 5.5) and a reaching phase (refer to Theorem 5.3 and 5.4) during the ASMC process [73]. Even though the estimation of the FTC was estimated differently in [16] (refer to (5.23) discussed above), explicit forms of the sliding variable and switching gain dynamics, as introduced in [16] *w.r.t.* the "worst" case of uncertainties and perturbations, can be adapted to obtain the estimated reaching time (5.47). Along with the discussions and proofs introduced above, new formulas to estimate specifically the upper-bounds of both compensating and reaching periods are derived (see (5.42) and (5.47)). Finally, we note that (5.42) remains valid only for the particular case of uncertainties with constant amplitudes, and despite the fact that it is a limited scenario, it is considered as an instructive case study to interpret the dynamics of any ASMC. Acknowledging its benefit, a maximum range of FTC for this particular case can be computed from (5.42) and (5.47), as $t_r \leq \frac{\pi - \Phi}{\sqrt{\underline{\Gamma}\alpha}}$.

5.5 Implementation of Real ASMC

For a *real sliding mode*, as discussed in Chapter 4 (refer to Subsection 4.5.2) the law (5.18) would force K to increase constantly without bound since σ would rarely be "identically" zero due to inherent processing delays, finite sampling rate, measurement errors and noise [16]. Thus, the switching gain (5.18) has been modified for *real* ASMC using boundary-layer-dependent gain laws [16, 17, 117]. With such forms, the control gain K reduces its value after σ entering a small boundary layer (*i.e.*, $|\sigma| \leq \epsilon$).The thickness of the boundary layer ϵ in switching gain adaptation may be fixed or time-varying (*e.g.*, depending on the gain K and the sampling time T_s) according to [16,116].

5.5.1 Existing Real ASMC

We recall the real ASMC design with discontinuous gain rate at the layer limit ϵ as [16].

$$\dot{K} = \alpha|\sigma| \cdot \text{sgn}(|\sigma| - \epsilon) \tag{5.53}$$

The FTC of this ASMC design has been proven by choosing the Lyapunov candidate function $V = \frac{1}{2}\sigma^2 + \frac{1}{2\gamma}\tilde{K}^2$ with $\tilde{K} = K - K^*$ for appropriate $\gamma > 0$ (refer to (5.20)). Moreover, the maximum reaching time has been estimated as [16, 74]

$$t_r \leq \frac{\sqrt{2V(0)}}{\beta_2} \tag{5.54}$$

where $\beta_2 = \min\{\beta_\sigma, \beta_k\sqrt{\gamma}\}$ with $\beta_\sigma > 0$ and $0 < \beta_k < (-1 + \frac{\alpha}{\gamma}) \cdot |\sigma|$. Once again, since β_k is constrained by $|\sigma|$, the RTE suffers from some weakness. First, according to (5.54), t_r depends on the sliding variable σ, which in turn depends on the boundary layer ϵ. In fact, to achieve fast response, *i.e.*, reduced t_r, it requires large values of $|\sigma|$, which in turn implies a large thickness of the boundary layer and poor accuracy. More recently, in [17], the gain rate continuously alternate at the layer limit ϵ as

$$\dot{K} = \alpha \cdot \big(|\sigma| - \epsilon\big) \tag{5.55}$$

However, the proof for FTC of σ to the boundary layer $|\sigma| \leq \epsilon$ is not provided. Note that the boundary layer used in (5.53) and (5.55) is different from the traditional boundary layer that counts originally for the input signal of the conventional SMC [1, 52].

5.5.2 Alternative Switching Gain Law for Real ASMC

Based on the aforementioned ASMC schemes, we consider the following general ASMC design for the *real case* using the boundary-layer method.

$$\dot{K} = \alpha \cdot G(|\sigma|) \cdot \text{sgn}(|\sigma| - \epsilon) \tag{5.56}$$

where $G(|\sigma|)$ is a positive definite function in its argument $|\sigma|$ [73, 116, 117]. Upon this general design, one can have many choices to select this switching function appropriately [116, 117]. Recall the modified adaptation law, discussed in Chapter 4, as

$$\dot{K} = \alpha \cdot |\sigma| \cdot \big[\frac{2}{\pi} \cdot \tan^{-1}(\sigma^4)\big] \cdot \text{sgn}(|\sigma| - \epsilon) \tag{5.57}$$

with $K(0) > 0$, $\alpha > 0$, and $\epsilon > 0$ being small [117]. The increment or decrement of K tends to be smaller while $\big(|\sigma| - \epsilon\big) \to 0$ (*i.e.*, as $|\sigma|$ approaches ϵ from the outside or the inside of the boundary layer).

5.5.3 FTC of Real ASMC

For the real ASMC design based on switching gains (5.53) and (5.55), the sliding variable converges to its targeted domain in finite time. However, the proof of FTC and the maximum RTE are different from [16] and (5.54).

Proposition 5.1. *Given the nonlinear uncertain system* (5.13) *with the sliding variable dynamics* (5.14) *controlled by* (5.16)*, if the switching gain is designed as* (5.53) *or* (5.55)*, the sliding variable σ converges to a domain $|\sigma| < \epsilon$ in finite time. Moreover, the maximum reaching time can be estimated as* $t_r \leq \dfrac{\pi}{2\sqrt{\underline{\Gamma}\alpha}} + t^*$.

Proof. See Appendix A.7 □

Note that the definitions of t^*, α and $\underline{\Gamma}$ are the same as those of (5.47). Obviously, the same results can be obtained with the algorithm (5.55) (or (5.57), eventually). The proofs using (5.53) and (5.55) are similar to the proof of Theorem 5.4, while the one using (5.57) is similar to the proof of Theorem 5.3.

5.6 Simulation and Experimental Illustrations

5.6.1 Numerical Illustration of an *Ideal* ASMC

Consider a simple scalar dynamics with uncertainties

$$\dot{\sigma} = \Psi(t) + \Gamma(t) \cdot u \tag{5.58}$$

where $\Psi(t)$ is an unknown-bound perturbation, $\Gamma(t) > 0$ is a time-varying uncertain parameter and u is the control input. The control objective is to stabilize the state σ at the origin, *i.e.*, $\sigma = 0$. $\Psi(t)$ and $\Gamma(t)$ are chosen as

$$\begin{aligned}\Psi(t) =& -1.6 + 0.7\delta(t-0.5) + 5.4\delta(t-2.5) + 0.5\delta(t-2.7) - 0.5\delta(t-3.8) + \\ & 0.5\delta(t-3.9) - 0.5\delta(t-4.5) \ + 0.5\delta(t-4.6) - 0.3\delta(t-6.1) \end{aligned} \tag{5.59a}$$

$$\Gamma(t) = 2 + \sum_{n=0}^{n=5} \frac{1}{2n+1} \sin\big(\frac{(2n+1)\pi(t-2.5)}{2}\big) \tag{5.59b}$$

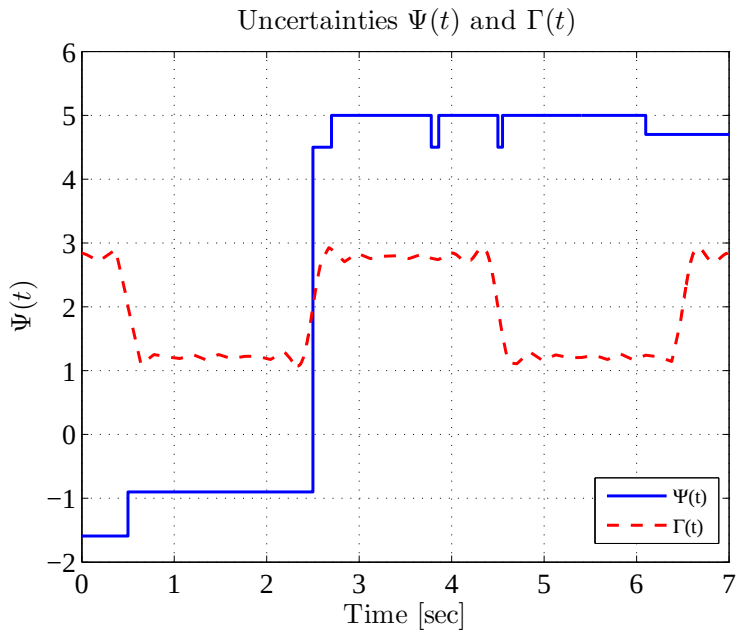

Figure 5.2: Uncertainties $\Psi(t)$ and $\Gamma(t)$ used in the simulation.

where $\delta(t-t_i)$ is a shifted unit step function which has a value of 0 up to time $t = t_i$ and a value of 1 thereafter (see Figure 5.2). The control parameters used in simulations to establish and discuss the sliding mode are $K(0) = 0.3$, $\sigma(0) = 0.6$, $\alpha = 2$, 4, 10 and 20, respectively.

Roughly, the lumped perturbation can be split into three levels $(\Psi/\Gamma)_{0\sim 2.5}$, $(\Psi/\Gamma)_{2.5\sim 4.5}$ and $(\Psi/\Gamma)_{4.5\sim\infty}$ for time intervals $0 \sim 2.5$, $2.5 \sim 4.5$ and $4.5 \sim \infty$, respectively. Figure 5.3 shows the evolutions of perturbation Ψ/Γ, sliding variable σ and switching gain K during the adaptation process for $\alpha = 2$. During the adaptation procedure, the switching gain $K(t)$ is tuned automatically without *a priori* knowledge of the bounds of Ψ and compensates for the three levels of perturbations at time instants $t_{c,1}$, $t_{c,2}$ and $t_{c,3}$, respectively. Note, during the time interval $0 \sim 2.5$, the sliding variable first reaches zero at $t_{r,0}$ due to $K(t)_{0\sim t_{r,0}} \geq \big(\frac{\Psi \mathrm{sgn}(\sigma)}{\Gamma}\big)_{0\sim t_{r,0}}$ even though $K^*_{0\sim t_{r,0}} < \big|\frac{\Psi}{\Gamma}\big|_{0\sim t_{r,0}}$. This phenomenon shows the possibility that σ can reach zero even though K keeps some value less than the upper bounds of Ψ/Γ. A real Example 4.1 in Chapter 4 also shows that $K \to K^*$ less than $\sup\big|\Psi/\Gamma\big|$. After $t_{r,0}$, σ becomes negative because the lumped perturbation is greater than the switching gain,

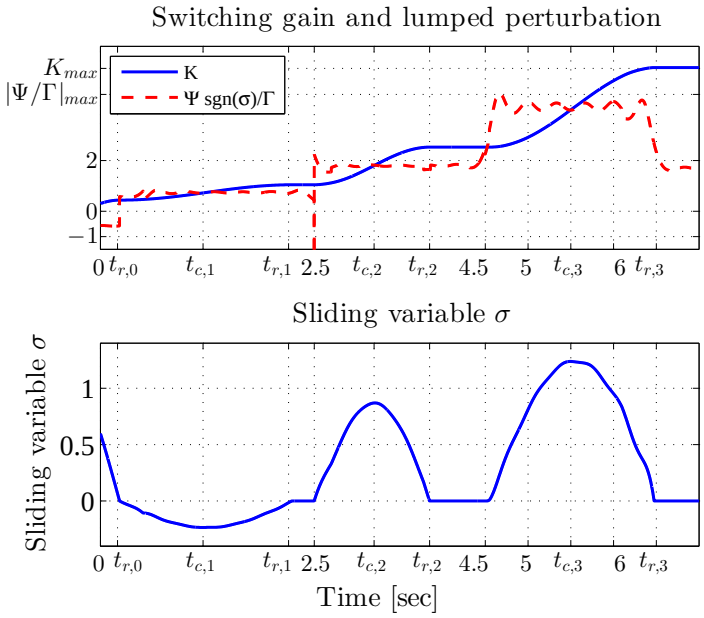

Figure 5.3: Simulations: sliding variable σ, lumped perturbation Ψ/Γ, and switching gain K for $\alpha = 2$.

i.e., $\big(\frac{\Psi \text{sgn}(\sigma)}{\Gamma}\big)_{0\sim t_{c,1}} \geq K(t)_{0\sim t_{c,1}} > 0$. Also, during the time interval $0 \sim t_{r,1}$, K monotonically increases its value until it compensates for the perturbation $\big(\frac{\Psi \text{sgn}(\sigma)}{\Gamma}\big)_{0\sim t_{c,1}}$ at $t_{c,1}$. After the first compensating time $t_{c,1}$, of the first perturbation level, $K(t)_{t_{c,1}\sim 2.5} \geq \big(\frac{\Psi \text{sgn}(\sigma)}{\Gamma}\big)_{t_{c,1}\sim 2.5} > 0$ forces $\sigma \to 0$ at $t_{r,1}$. Similarly, for the perturbation levels, $\big(\Psi/\Gamma\big)_{2.5\sim 4.5}$ and $\big(\Psi/\Gamma\big)_{4.5\sim\infty}$ (during the time intervals $2.5 \sim 4.5$ and $4.5 \sim \infty$, respectively), the switching gain $K(t)$ is tuned automatically and compensates for the two levels of perturbations at time instants $t_{c,2}$ and $t_{c,3}$, and forces σ to reach the sliding surface at $t_{r,2}$ and $t_{r,3}$, respectively. As discussed in Subsection 5.4.2, for any perturbation, K will compensate for it. From Figure 5.4, one can see that the reaching time is reducing while α increases its value. The switching gain $K(t)$ is proportional to α. $K(t)$ increases its value faster as α is larger. For the cases where α has a value of 10 or 20 (see Figure 5.4), the negative perturbation (occuring first) has been completely compensated by $K(t)$ when σ for the first time reaches zero and stays on the surface thereafter during the negative perturbation. So, different from the cases of $\alpha = 2$ and $\alpha = 4$, there is no

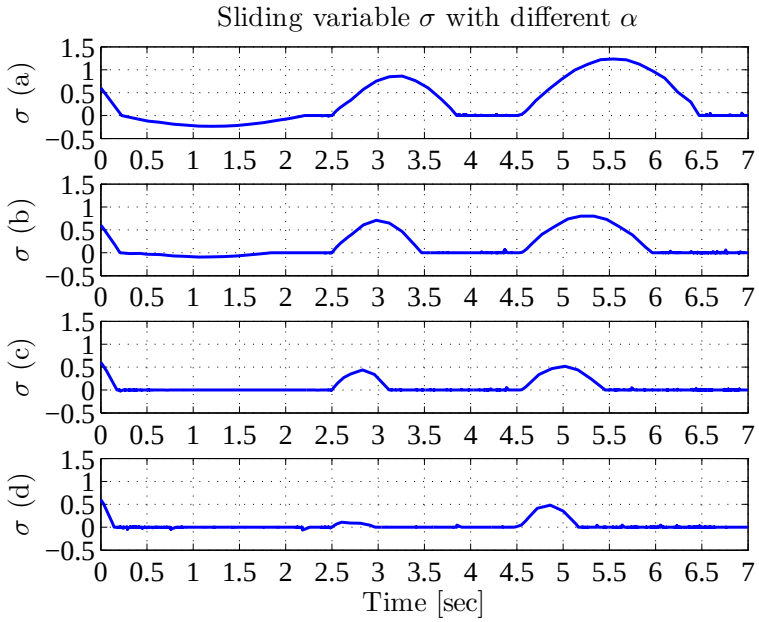

Figure 5.4: Simulations: trajectories of sliding variable σ with different values of α: (a) $\alpha = 2$, (b) $\alpha = 4$, (c) $\alpha = 10$ and (d) $\alpha = 20$.

compensating-reaching phases reacting to the first perturbation for the cases of $\alpha = 10$ and $\alpha = 20$. The relationship between the reaching time during the *reaching phase*, *i.e.*, $t_r - t^*$, and α is shown in Figure 5.5. The reaching time is approximately proportional to $\frac{1}{\sqrt{\alpha}}$, which demonstrates the effectiveness of the new form of RTE (5.47).

5.6.2 Experimental Illustration of a *Real* ASMC

Experiments were conducted on the experimental helicopter-model designed by Quanser Inc. [21] (see Figure 1.1 in Chapter 1 and Figure 3.2 in Chapter 3 and refer to Section 1.6 for further details about the description of this setup) to test the relationship of the reaching time and parameter α of the *real* ASMC (5.19) introduced in [16], and the improvement of the modified ASMC design discussed in this chapter (refer to (5.57)). To illustrate a single input ASMC design, we consider the pitch dynamics entirely uncertain (*i.e.*, can be written in form (5.13), controlled with the front motor voltage u, while the body can independently move about the yaw axis). This motion provides perturbation

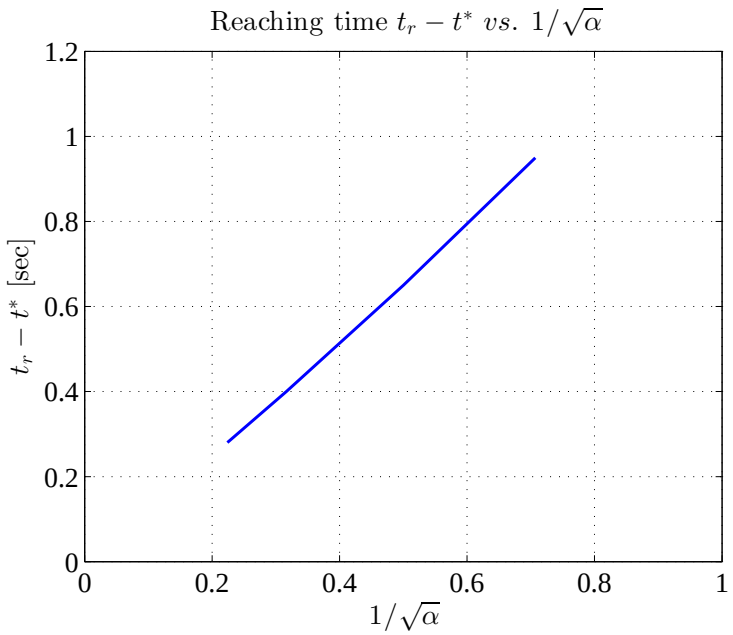

Figure 5.5: Simulations: reaching time $t_r - t^*$ (*i.e.*, reaching phase) *vs.* $\dfrac{1}{\sqrt{\alpha}}$.

effects on the controlled pitch dynamics. More details about the dynamics of this model has been presented in the application section of Chapter 4 (refer to dynamic model (3.43a) and Table 3.1 in Chapter 3. The pitch angle ϕ and rate $\dot{\phi}$ are measurable. The sliding variable is defined as $\sigma = \dot{\phi} + \phi + \frac{1}{2}\int_0^t \phi(\tau)d\tau$. The boundary layer thickness ϵ is settled to $4T_sK$, *i.e.*, varying with $K(t)$ [16]. The sampling period is chosen as $T_s = 5 \cdot 10^{-3}$ sec [21].

Figure 5.6 shows the convergence of the sliding variable σ by applying the real ASMC law (5.19) with different values of the parameter α. One can see that the reaching time t_r reduces as α increases. However the relationship of t_r and α is not inversely proportional. In fact, it can be seen from Figure 5.7 that t_r is roughly inversely proportional to $\sqrt{\alpha}$ which verifies Proposition 5.1. The experimental performances of the real ASMC designs (5.19) and (5.57) are shown in Figures 5.8-5.10. We can see that the accuracy is improved (see Figure 5.8) with the modified switching gain design (5.57) and the control chattering level is also reduced (see Figure 5.9) compared to the switching gain design (5.19). These improvements are due to the reduced switching gain amplitudes (see Figure 5.10) when applying the algorithm (5.57). In

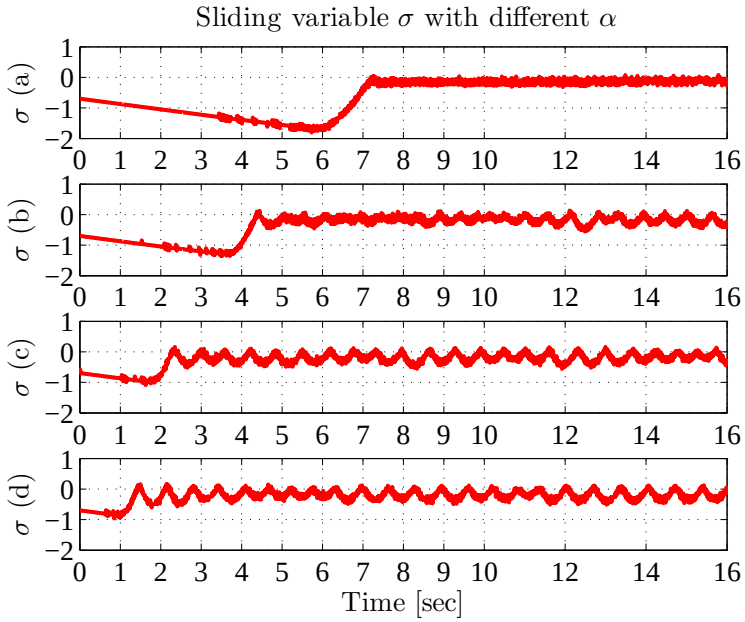

Figure 5.6: Experiments: Sliding variable with different values of α: (a) $\alpha = 1$, (b) $\alpha = 2$, (c) $\alpha = 5$ and (d) $\alpha = 10$.

fact, we note that the chattering level is proportional to the magnitude of the switching gain [61].

We also note, from Figure 5.6, that the reaching time cannot be reduced too small. Otherwise, the chattering level will be increased (see Figure 5.6 (d)). This can be explained by the new form of RTE (5.47) where a too small value of $\frac{1}{\sqrt{\alpha}}$ requires an extremely large α. For example, to reduce the reaching time $t_r - t^*$ to its 10th value, the control parameter α must be roughly increased 100 times. As a result, the system responds to the perturbations relatively slowly by using the existing ASMC gain law (5.19) or the alternative gain law (5.57) (see Figure 5.8). In other words, the system is not very robust while using the integral-based gain law (5.19) or (5.57).

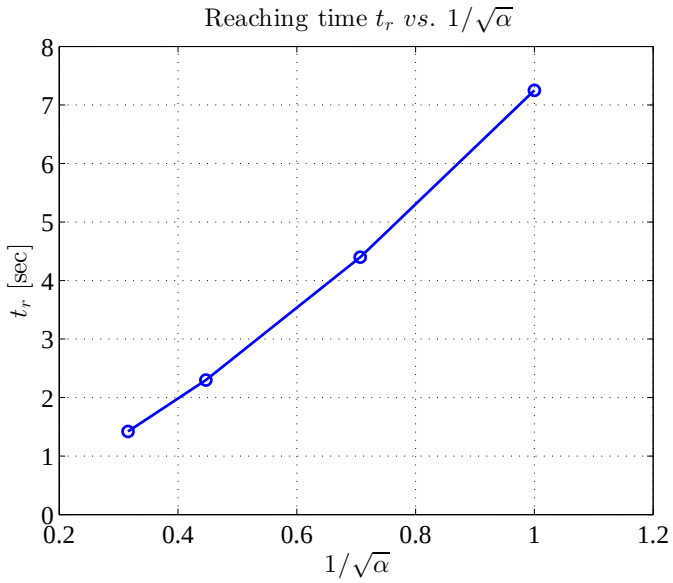

Figure 5.7: Experiments: Overall reaching time t_r *vs.* $\dfrac{1}{\sqrt{\alpha}}$.

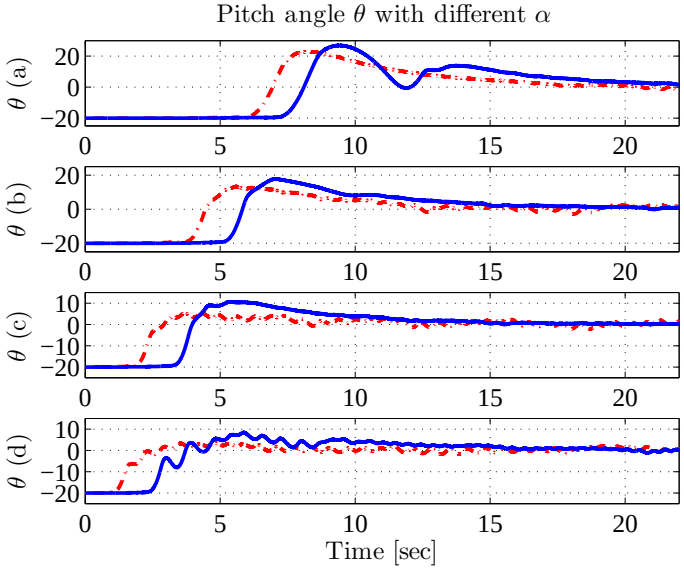

Figure 5.8: Experiments: Pitch angle results using algorithm (5.19) in green dash-dot line and modified algorithm (5.57) in blue solid line, for different values of α: (a) $\alpha = 1$, (b) $\alpha = 2$, (c) $\alpha = 5$ and (d) $\alpha = 10$.

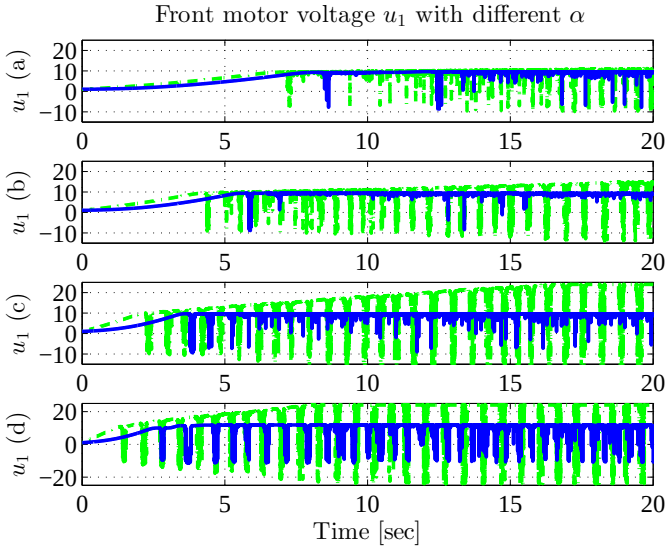

Figure 5.9: Experiments: Front motor voltage u results using algorithm (5.19) in green dash-dot line and modified algorithm (5.57) in blue solid line, for different values of α: (a) $\alpha = 1$, (b) $\alpha = 2$, (c) $\alpha = 5$ and (d) $\alpha = 10$.

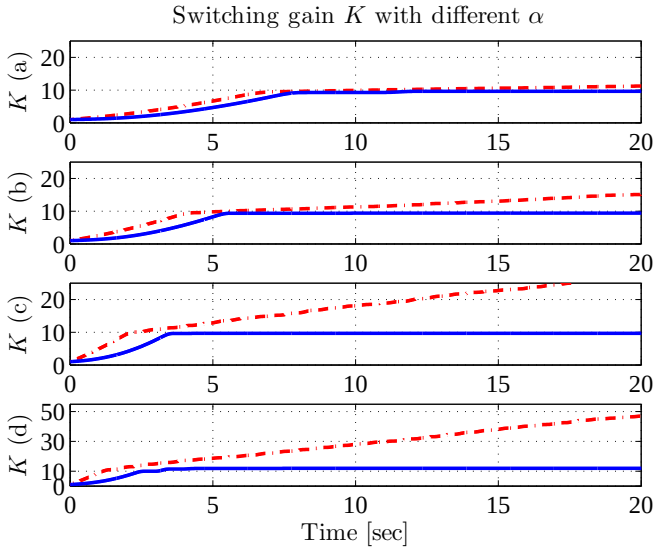

Figure 5.10: Experiments: Switching gain K results using algorithm (5.19) in green dash-dot line and modified algorithm (5.57) in blue solid line, for different values of α: (a) $\alpha = 1$, (b) $\alpha = 2$, (c) $\alpha = 5$ and (d) $\alpha = 10$.

5.7 Conclusions

The main ASMC designs for nonlinear systems with unknown bounded uncertainties under *ideal sliding mode* case are analyzed. Deficiencies in the proofs and statements of ASMC designs of some recent contributions depicted in papers and books are pointed out (*e.g.*, [14, 16, 17, 52]). The behaviour of the sliding variable is revisited with a new concept demonstrating the existence of compensating and reaching phases during the ASMC process. The FTC results for the sliding variable and the switching gain error are proven via a new Lyapunov approach and a novel majorant curve approach. Along with the latest new proof, a new form for RTE is provided and explicitly reveals the influence of ASMC conditions (the gain α of the adaptation law and the lower bound of the uncertainty Γ) on the upper-bound of the reaching time. A tutorial example shows the different phases (*i.e.*, compensating and reaching periods). Then, with these numerical simulations, the experimental results on a 1-DOF subsystem of the helicopter-model setup demonstrate the effectiveness of the new form of RTE.

The simulation and experimental results also show that, by using the existing or the proposed gain law, the system responds to the perturbations relatively slowly and the magnitudes of the control inputs (or the switching gain) are relatively high. In other words, the system is not very robust and the switching gain is overestimated for the integral-type adaptation gain laws (the alternative gain law is an integral type adaptation gain law). The phenomena can be explained by the new form of RTE where the reaching time cannot be reduced too small. To further improve the robustness and reduce the magnitudes of the switching gain, new approaches of ASMC designs will be proposed in the following chapter.

More details in terms of motivations, objectives, novelties, pros and cons of this chapter are presented in Table 5.1.

Table 5.1: Chapter 5 Recap

Motivation(s)	- Evaluate the properties of the common adaptation law for ASMC: FTC and gain boundedness. - Application of the existing ASMC design.
Objective(s)	- Investigation of stability, FTC and robustness properties. - Evaluation of the existing ASMC design.
Novelty(ies)	- New mathematical lemmas are analysed for proof of the ASMC stability. - A new concept demonstrates the existence of compensating and reaching phases during the ASMC process. - A new Lyapunov approach and a novel majorant curve method are provided to prove the FTC of the existing IG-ASMC. - A new form for RTE is provided and explicitly reveals the influence of ASMC conditions.
Pro(s)	- Final gain magnitudes of the existing IG-ASMC are relaxed with the epsilon tuning method. - The FTC of the existing IG-ASMC is novelly proven. - The weaknesses of less robustness and chattering phenomena existing in IG-ASMC are pointed out and explained with the new form of RTE.
Con(s)	- The system with IG-ASMC responds to the perturbations relatively slowly. - The switching gains in IG-ASMC are still overestimated during the adaptation process. - No solution provided regarding the weaknesses discussed above.

6 Adaptive Sliding Mode Control for Nonlinear Systems with Uncertainties of Unknown Constant Bounds – New Design

This chapter proposes a new approach for ASMC designs. The goal is to obtain robust, smooth, and fast transient performance for nonlinear systems with finite uncertainties of unknown bounds and limited available inputs so that the phenomena of the slow response and the gain overestimation in most ASMC designs can be greatly improved. Based on the sufficient conditions, we introduce an integral-exponential adaptation law targeting the reduction of the chatter levels of the sliding mode by significantly reducing the gain overestimation while simultaneously speeding up the system response to the uncertainties [118]. An illustrative example, numerical simulations on a variable-length pendulum and a 2DOF helicopter model dynamics [21], as well as experiments on the helicopter-based setup are performed to convey the discussed results. This chapter is organized as follows. The overall context of the new proposed ASMC design is introduced in Section 6.1. In Section 6.2, we state the control problem and necessary assumptions, and we discuss the continuous equivalent control. Section 6.3 first reviews the extended ASMC design discussed in chapter 4 and three existing asymptotic reaching laws along with a new simple exponential reaching law. Then, it proposes an ASMC design with a new gain adaptation, called integral-exponential adaptation law, for scalar case and ideal sliding mode (we call the design as IEG-ASMC design). Section 6.4 develops the systematic ASMC designs using the proposed integral-exponential adaptation law with a boundary-layer for real sliding mode. Simulations and

experiments on a 2-DOF model device are discussed in Section 6.5, while Section 6.6 concludes this Chapter.

6.1 Introduction

As discussed in the previous chapters, most ASMC designs have an integral type adaptation law. However, for the ASMC designs with integral-type adaptation laws, the system response to the perturbation is relatively slow; moreover, even the overestimation is avoided somehow, the chattering phenomenon is still observed. Since the magnitude of the switching gain is proportional to the magnitude of chattering level [61], a possible adaptation law is to reduce this switching gain to the minimum admissible value. Most recently, the control gain in [16, 17] depends on the distance from the sliding variable to a discontinuity surface (or a boundary layer which is different from the conventional boundary layer used to replace the signum function) so that the switching gain is reduced gradually when the sliding variable is inside the boundary layer. The ASMC is also improved with the application to HOSMC. In [61], the authors apply ASMC using a "super-twisting" algorithm and in [18] ASMC is combined with second-order SMC. The improved algorithms successfully reduced the switching gain so that the chattering level is suppressed. However, in [18], the exact robust differentiator is required and the design fits mainly for the *ideal* sliding mode; while in [13,16,17,19,61], the system response is relatively slow at the beginning of the perturbation process. Since the sliding surface is mostly designed such that the system state is stable when the trajectory is on the surface, a slow response to the sliding variable variation may encounter a serious stability problem. To achieve fast response and chattering-free property, asymptotic reaching laws rather than ASMC can be found in the form of the power reaching law [5] and exponential reaching law [56]. However, they either lose the robustness when system states are around the sliding surface [5] or require *a priori* knowledge of the uncertainty bounds [56].

The objective in this chapter is to propose a novel systematic ASMC approach for nonlinear systems with finite but unknown uncertainties. The control only appears in the first-order sliding mode, then the differentiator is not required. Using the new design, the system reacts quickly to the perturbation so that the overshoot is reduced, and the switching gain and the chattering level are further lowered. To investigate adequately the stabilization of ASMC designs, the FTC will be briefly discussed in terms of *compensating phase* and *reaching phase* during the ASMC process. To overcome the slow

response in the existing *real* ASMC process, in particular, during the compensating phase, and to simultaneously reduce the overall switching gain, an integral-exponential gain (IEG) adaptation law combined with a boundary-layer scheme will be proposed Finally, the new algorithm will be demonstrated numerically and experimentally.

6.2 On ASMC Design Problem

In this section, we first state the control problem and assumptions for nonlinear systems with finite uncertainty of unknown bounds. Then, we recall some existing *real* ASMC designs.

6.2.1 Problem Statement and Assumptions

Recall the uncertain nonlinear dynamics

$$\dot{x} \quad = \quad f(x,t) + g(x,t) \cdot u \tag{6.1}$$

where $x \in \chi$ is the state vector, with $\chi \subset \mathbb{R}^n$ a domain containing the origin, and $u \in \mathbb{R}^m$ the control input with $m \leq n$. The vector $f(x,t) \in \mathbb{R}^n$ and the matrix $g(x,t) \in \mathbb{R}^{n \times m}$ are nonlinear time-varying smooth functions containing parametric uncertainties and external disturbances [14, 16, 51, 74, 89, 90]. The bounds of these uncertainties are unknown *a priori*. Solutions of dynamics (7.1) with discontinuous right-hand side are defined in the sense of Fillipov [119]. Let $\hat{f}(x,t)$ and $\hat{g}(x,t)$ be the known nominal parts of the vector fields $f(x,t)$ and $g(x,t)$, respectively, while $\tilde{f}(x,t)$ and $\tilde{g}(x,t)$ denote their corresponding uncertain, bounded and unknown parts. Thus, we can write

$$f(x,t) = \hat{f}(x,t) + \tilde{f}(x,t) \tag{6.2}$$

and

$$g(x,t) = \hat{g}(x,t) + \tilde{g}(x,t) \tag{6.3}$$

respectively. We assume [129]

Assumption 6.1. *The uncertain term $\tilde{f}(x,t)$ is norm-upper-bounded as*

$$\|\tilde{f}(x,t)\| \leq f_M \tag{6.4}$$

for some unknown constant $f_M \geq 0$.

Assumption 6.2. *The uncertain term $\tilde{g}(x,t)$ is norm-lower-bounded as*

$$0 < g_m \leq \|\tilde{g}(x,t)\| \tag{6.5}$$

for some unknown constant $g_m > 0$.

Let $x = 0$ be an equilibrium point for (6.1). Consider $\sigma(x,t) \in \mathbb{R}^m$ a measurable sliding vector composed of smooth functions in $\chi \times [0,\infty]$. We recall the targeted manifold $\Sigma = \{x \in \chi \; s.t. \; \|\sigma(x,t)\| = 0\}$ as the '*ideal sliding* mode set', and we introduce $\Sigma_\delta = \{x \in \chi \; s.t. \; \|\sigma(x,t)\| \leq \delta\}$, with $\delta > 0$, as the '*real sliding* mode set' [115]. Moreover, we define for some $\delta \geq \epsilon > 0$, the manifold $\Sigma\epsilon = \{x \in \chi \; s.t. \; \|\sigma(x,t)\| \leq \epsilon\}$ as the "*target* manifold". Recall that σ is designed such that, as soon as the vector $x(t)$ reaches the set Σ_δ in finite time $t = t_r > 0$ and belongs to it thereafter, *i.e.*, $\forall t \in [t_r, \infty]$, the dynamics (6.1) has to be stable in the *real sliding* mode. In addition, the relative degree of (6.1) is given as $r = [1, 1, \cdots, 1]^T_{1\times m}$ [74] (Recall the sliding variable dynamics (4.11)), that is, the total time derivative of σ satisfies

$$\dot{\sigma}(x,t) = \Psi(x,t) + \Gamma(x,t) \cdot u \tag{6.6}$$

with $\Psi(x,t) = \dfrac{\partial \sigma}{\partial t} + \dfrac{\partial \sigma}{\partial x} \cdot f(x,t)$ and $\Gamma(x,t) = \dfrac{\partial \sigma}{\partial x} \cdot g(x,t)$ [74].

In the following, the arguments x and t of all the given vector fields (*i.e.*, σ, Ψ, Γ, *etc.*) will be omitted for simplicity. Let Ψ and Γ can be defined by nominal values ($\hat{\Psi}$ and $\hat{\Gamma}$) and uncertain amounts ($\tilde{\Psi}$ and $\tilde{\Gamma}$), respectively, as

$$\Psi = \hat{\Psi} + \tilde{\Psi} \quad \text{and} \quad \Gamma = \hat{\Gamma} + \tilde{\Gamma} \tag{6.7}$$

We call Ψ "fully uncertain" if its nominal value is unknown or unreliable, (*i.e.*, $\hat{\Psi} = 0$ and $\Psi = \tilde{\Psi}$). Based on Assumptions 6.1 and 6.2, we assume that

Assumption 6.3. *The uncertain vector $\tilde{\Psi} \in \mathbb{R}^m$ is norm-upper-bounded as*

$$\|\tilde{\Psi}\| \leq \Psi_M \tag{6.8}$$

where $\Psi_M \geq 0$ is unknown a priori.

Assumption 6.4. *The uncertain matrix $\Gamma \in \mathbb{R}^{m\times m}$ is positive definite in the wider sense, that is, its symmetric part Γ_s defined by*

$$\Gamma_s = \frac{1}{2}\big(\Gamma + \Gamma^T\big) \tag{6.9}$$

is positive definite in the regular meaning [130]. In particular, if $m = 1$, the scalar term Γ is lower-bounded as

$$0 < \underline{\Gamma} \leq \Gamma \tag{6.10}$$

We notice that Assumptions 6.3 and 6.4 can be roughly considered as the results of the Assumptions 6.1 and 6.2. For instance, if the sliding function is designed as a PI transfer relation in the state vector x defined by (7.1), *i.e.*, $\sigma = K_p x + K_i \int_0^t x d\tau$, then the sliding mode dynamics can be written as $\dot{\sigma} = K_p \dot{x} + K_i x$. Thus, from (6.2) and (6.3), the nominal and uncertain values of Ψ and Γ can be obtained as $\hat{\Psi} = K_p \hat{f} + K_i x$, $\tilde{\Psi} = K_p \tilde{f}$, $\hat{\Gamma} = K_p \hat{g}$ and $\tilde{\Gamma} = K_p \tilde{g}$, respectively. Indeed, based on Assumptions 6.1 and 6.2, the assumptions of the inequalities (6.8) and (6.10) can be easily satisfied in this case.

6.2.2 Equivalent Control

For given nominal values of both Ψ and Γ known and reliable, it is often recommended to apply the so-called equivalent control (Refer to Section 4.3 in Chapter 4) to eliminate the known nonlinear term. Consider the compensator [16, 61]

$$u = u_{eq} + u_s \tag{6.11}$$

where the equivalent control u_{eq} is designed to compensate for $\hat{\Psi}$ using $\hat{\Gamma}$, and corresponds to the control action when all uncertainties vanish. The term u_s compensates the uncertain dynamics. We define.

$$u_{eq} = -\hat{\Gamma}^{-1}\hat{\Psi} \quad \text{and} \quad u_s = \hat{\Gamma}^{-1} v \tag{6.12}$$

Given (6.7), we substitute (6.11) and (6.12) into (6.6)

$$\dot{\sigma} = \underbrace{\left(\tilde{\Psi} - \tilde{\Gamma}\hat{\Gamma}^{-1}\hat{\Psi}\right)}_{\Psi_{eq}} + \underbrace{\left(I + \tilde{\Gamma}\hat{\Gamma}^{-1}\right)}_{\Gamma_{eq}} v \tag{6.13}$$

The newly obtained terms Ψ_{eq} and Γ_{eq} are 'residual' uncertainties with unknown bounds. However, if the nominal values are sufficiently reliable (close to their actual values), the magnitudes of the new bounds for Ψ_{eq} and Γ_{eq} are supposed to be smaller than those for Ψ and Γ in (6.6). As a result, the control performance is supposed to be better as well. From (6.13), one can see that the newly obtained uncertain term Ψ_{eq} has fully unknown bounds. In other words, for any first order nonlinear dynamic system, in form (6.6), with uncertainties of unknown bounds, essentially we face the problem of bounded uncertain dynamics with unknown bounds. From (6.11) and (6.12), one can also see that $u(v)$ and $v(u)$ are bijective. Without loss of generality and for simplicity, we consider that Ψ is fully uncertain (without any reliable nominal values), *i.e.*, $\Psi \triangleq \tilde{\Psi}$, provided that Γ is nonsingular.

6.3 New integral-exponential Reaching Law for Ideal ASMC – Scalar Case

Two important considerations in targeted ASMC design including fast response and low chattering will be required. In this section, we first recall two used switching schemes: integral adaptation laws and asymptotic reaching laws. Then, we introduce our new design, called *integral-exponential adaptation law* [129].

Consider the uncertain nonlinear system (6.1) and the sliding variable dynamics (6.6) with $m = 1$. When the uncertainties are fully unknown (*i.e.*, the nominal values are not available), we recall the feedback control

$$u = -K \cdot \text{sgn}(\sigma) \tag{6.14}$$

6.3.1 Integral Adaptation Laws for Ideal Sliding

Given the nonlinear uncertain system (6.1) with the sliding variable dynamics (6.6) controlled by (6.14), we recall the extended ASMC design with integral adaptation law based on the necessary and sufficient condition (4.43) discussed in Lemma 4.4 (refer to Section 4.4 in Chapter 4),

$$K(t) = \int_0^t G(|\sigma|)d\tau \tag{6.15}$$

Alternatively, the form (6.15) can be presented implicitly as [117]

$$\dot{K}(t) = G(|\sigma|) \tag{6.16}$$

In particular, this function is chosen as $G(|\sigma|) = \alpha|\sigma|$ with $\alpha > 0$, that is, (6.16) becomes [11, 14–17, 19]

$$\dot{K} = \alpha|\sigma| \tag{6.17}$$

for *ideal* ASMC [115]. As analysed in Theorem 5.4, the reaching time of (6.17) can be estimated as $t_r \leq \dfrac{\pi}{2\sqrt{\underline{\Gamma}\alpha}} + t^*$ with t^* the compensating time defined in Lemma 5.5 (refer to Section 5.4 in Chapter 5). Based on the FTC analysis, the reaching time can be tuned by the design parameter α. In fact, it is inversely proportional to the *square root* of α. This *square root* limits the effort of α. For example, to reduce the reaching time t_r to its 10th value, the design parameter α is required to increase its value 100 times. This implies that, in

the existing ASMC designs with integral adaptation law (*e.g.*, (6.17)) t_r cannot be reduced significantly and the system response to perturbations is relatively slow. Moreover, the switching gain K still increases during the reaching phase even though it has already compensated for the lumped perturbation after the compensating phase. This fact introduces the undesirable overestimation of K and, consequently, high level of chattering [61].

6.3.2 Asymptotic Reaching Law

To suppress the chattering phenomena, asymptotic reaching laws were introduced [5, 56, 60, 131]. Two approaches have been used: *affine* and *power switching function gains* given by [5, 60]

$$K(\sigma) = K_0 + K_1|\sigma| \tag{6.18}$$

with $K_0,\ K_1 > 0$, and

$$K(\sigma) = K_0|\sigma|^{\gamma} \tag{6.19}$$

with $0 < \gamma < 1$, respectively. These gains called reaching laws increase the reaching speed when the state is far away from the switching surface, and reduce the rate when the state is near the surface. The application of these laws results in FTC with low chattering. However, the reaching law (6.18) requires *a priori* knowledge of the bounds of the uncertainties [5,60]. The form (6.19) rapidly decreases its feedback gain and thus reduces the robustness of the controller near the sliding surface. To overcome the drawbacks of (6.19), an *exponential reaching law* is proposed in [56]

$$K(\sigma) = -\frac{K_0}{\delta_0 + (1-\delta_0)e^{-\gamma_1|\sigma|^p}} \tag{6.20}$$

with $K_0 > 0$, $0 < \delta_0 < 1$, $\gamma_1 > 0$ and p a strictly positive integer. The result of the exponential reaching law (6.20) exhibits fast response, low chattering and robustness near the sliding surface. However, it still requires *a priori* knowledge of the bounds of the uncertainties. Otherwise, the robustness might be lost if $K_0 < \dfrac{\Psi \mathrm{sgn}(\sigma)}{\Gamma}$, the feedback is even unstable if $\dfrac{K_0}{\delta_0} < \dfrac{\Psi \mathrm{sgn}(\sigma)}{\Gamma}$, and the chattering level might be too high if $K_0 >> \dfrac{\Psi \mathrm{sgn}(\sigma)}{\Gamma}$.

6.3.3 Simple Exponential Law

To overcome these limitations and to keep the advantage from this exponential form, (6.19) and (6.20) can be fitted in terms of properties as

$$K(\sigma) = K_0 e^{\gamma_1 |\sigma|^p} \tag{6.21}$$

with $\gamma_1 > 0$ and p a strictly positive integer. This form continues intensively to take advantage of the form (6.20) without requiring knowledge of the uncertainty upper-bounds. Also, it equips the same advantages of (6.18) and (6.19).

Proposition 6.1. *Consider the nonlinear uncertain system* (6.1)*, with the sliding variable dynamics* (6.6)*, controlled by* (6.14) *and* (6.21)*. The sliding variable σ converges to*

- 0 *in finite time if there exists $\eta > 0$ s.t. $K_0 \geq \dfrac{\Psi sgn(\sigma)}{\Gamma} + \eta$ for all $t \geq 0$.*
- *a domain $|\sigma| \leq \left[\dfrac{1}{\gamma_1} \ln(\dfrac{|\Psi|}{\underline{\Gamma} K_0})\right]^{1/p}$ asymptotically otherwise.*

Proof. For the case when $K_0 \geq \dfrac{\Psi \text{sgn}(\sigma)}{\Gamma} + \eta$, we have, from (6.6) and (6.14),

$$\frac{d}{dt}|\sigma| = \Psi \text{sgn}(\sigma) - \Gamma K_0 e^{\gamma_1 |\sigma|^p} \leq -\eta \underline{\Gamma} \tag{6.22}$$

From the differential inequality (6.22), we obtain

$$|\sigma(t)| \leq |\sigma(0)| - \eta \underline{\Gamma} t \tag{6.23}$$

that is, $|\sigma(t)| = 0$ at most after $t_r = \dfrac{|\sigma(0)|}{\eta \underline{\Gamma}}$.

For the case when $|\sigma| > \left[\dfrac{1}{\gamma_1} \ln(\dfrac{|\Psi|}{\underline{\Gamma} K_0})\right]^{1/p}$, we have, from (6.6) and (6.14),

$$\begin{aligned} \frac{d}{dt}|\sigma| &= \Psi \text{sgn}(\sigma) - \Gamma K_0 e^{\gamma_1 |\sigma|^p} \\ &< \Psi \text{sgn}(\sigma) - \Gamma \frac{|\Psi|}{\underline{\Gamma}} \\ &< 0 \end{aligned} \tag{6.24}$$

Then, $|\sigma|$ converges to the domain $|\sigma| \leq \left[\dfrac{1}{\gamma_1} \ln(\dfrac{|\Psi|}{\underline{\Gamma} K_0})\right]^{1/p}$, asymptotically [1]. □

Proposition 6.1 provides rather a new asymptotic reaching law than an ASMC law. Comparing to the simple feedback law "$u = -K_0\sigma$" where σ is only converging to the domain $|\sigma| \leq \dfrac{|\Psi|}{\underline{\Gamma}K_0}$, the ASMC (6.14) with (6.21) could confine the sliding variable σ closer to the sliding surface $\sigma = 0$ by tuning γ_1 and p. With this new law, σ will never diverge because it is UUB even the bounds of uncertainties are unknown. Thus, it improves the exponential law (6.20) introduced in [56]. However, it still requires *a priori* knowledge of the bounds of the uncertainties to assure FTC of σ to zero.

6.3.4 integral-exponential Adaptation Law

In order to overcome the drawbacks of the aforementioned reaching laws and simultaneously keep their advantages, we introduce a new reaching law combining an integral adaptation term with an exponential term as

$$\begin{cases} \dot{\breve{K}}(\sigma) &= G(|\sigma|) \\ K(\sigma) &= \breve{K}(\sigma) + \gamma_0(e^{\gamma_1|\sigma|^p} - 1) \end{cases} \tag{6.25}$$

where $\gamma_0 > 0$, $\gamma_1 > 0$, p is a strictly positive integer and $G(|\sigma|)$ is a positive definite function of $|\sigma|$ [116]. To simply illustrate the new design, we use $G(|\sigma|) = \alpha|\sigma|$ [129], *i.e.*,

$$\begin{cases} \dot{\breve{K}}(\sigma) &= \alpha|\sigma| \\ K(\sigma) &= \breve{K}(\sigma) + \gamma_0(e^{\gamma_1|\sigma|^p} - 1) \end{cases} \tag{6.26}$$

To illustrate the new design more simply, we remove the tuning parameters γ_1 and p and replace γ_0 with $\beta > 0$ [129], *i.e.*,

$$\begin{cases} \dot{\breve{K}}(\sigma) &= \alpha|\sigma| \\ K(\sigma) &= \breve{K}(\sigma) + \beta(e^{|\sigma|} - 1) \end{cases} \tag{6.27}$$

Theorem 6.1. *Consider the nonlinear uncertain system* (6.1)*, with the sliding variable dynamics* (6.6)*, controlled by* (6.14)*. If the gain $K(t)$ is designed as* (6.25)*, then the sliding variable $\sigma \to 0$ in finite time.*

Proof. In this new design, there still exist a compensating phase and a reaching phase. Thus, the proof refers to the one of Proposition 4.1 (refer to Section 4.6 in Chapter 4) with a slight difference. We briefly state:

Compensating phase: Since $\breve{K}$ keeps growing whenever $\sigma \neq 0$, $\gamma_0(e^{\gamma_1|\sigma|^p} - 1) > 0$ and any lumped perturbation $\dfrac{\Psi \mathrm{sgn}(\sigma)}{\Gamma}$ is bounded. There always exist a time instant $t^* \geq 0$ and positive scalar $\eta > 0$ *s.t.* for all $t \geq t^*$

$$K(t) \geq \frac{\Psi \mathrm{sgn}(\sigma)}{\Gamma} + \eta \tag{6.28}$$

Reaching phase: From Lemma 4.4 (refer to Section 4.4 in Chapter 4), the system trajectory moves into *reaching phase* and $\sigma = 0$ is established in finite time. Moreover, the upper-bound of reaching time is estimated as $t_r \leq \dfrac{|\sigma(t^*)|}{\underline{\Gamma}\varepsilon} + t^*$ □

Remark 6.1. Theorem 6.3 can be exactly the same when we use (6.26) or (6.27).

The new design (6.25) (in particular, (6.27)) has two parts. The first part, integration term $\breve{K}(\sigma)$, provides the ability to compensate for uncertainties with unknown bounds and forces the sliding variable to converge to the sliding surface in finite time. Compared to the well-known ASMC law (6.17), the new algorithm (6.25) adds an exponential term which has the following properties.

On the one hand, the exponential term $\gamma_0(e^{\gamma_1|\sigma|^p} - 1)$ provides an extra but sufficiently high gain when the state is far away (*i.e.*, $|\sigma|$ is large) from the sliding surface. Then, K (with the exponential term) reaches and compensates for the lumped perturbation $\dfrac{\Psi \mathrm{sgn}(\sigma)}{\Gamma}$ more quickly than $\breve{K}$ alone (*i.e.*, law (6.17) or K without an exponential term). Thus, the compensating time t^* is reduced; the leaving σ from the sliding surface (because of $\dfrac{\Psi \mathrm{sgn}(\sigma)}{\Gamma} > K$) quickly turns around and heads to the sliding surface, and the system response to perturbations is speeded up. On the other hand, when $\sigma \to 0$, the exponential term reduces its value rapidly until it disappears at the sliding surface. Then, after reaching the sliding surface, the overall gain is reduced and the unwanted chattering level is expected to be much more reduced [129].

Remark 6.2. The tuning parameter p introduced in (6.25) (as well as (6.21) and (6.27)) comes from the exponential reaching law (6.20). It affects the response and the attraction region. From (6.21) and the end of the proof of Proposition 6.1, if $\left[\dfrac{1}{\gamma_1}\ln(\dfrac{|\Psi|}{\underline{\Gamma}K_0})\right] > 1$, a large p speeds up the response and improves the accuracy; if $\left[\dfrac{1}{\gamma_1}\ln(\dfrac{|\Psi|}{\underline{\Gamma}K_0})\right] < 1$, a large p slows down the response

and sacrifices accuracy. We choose $p = 1$ in the simulation results of this paper for the sake of simplicity and brevity.

Remark 6.3. It should be noted that the switching gain remains constant after the sliding mode is achieved (*i.e.*, when $\sigma = 0$). Thus, the new algorithm reduces the overall gain with a significant amount and speeds up the system response. In the sense of fast compensation for the uncertainties, the new algorithm exhibits the ability of estimating the perturbations with limited information. In other words, it equips the ability of SMCPE but does not require the information of VHOS. Moreover, one can see, by evaluating the final gain reduction, that the system state is constrained near the sliding surface [129]. Roughly speaking, the final gain reduction is the vanished term, *i.e.*, the exponential term, and the maximum gain reduction can be roughly estimated as

$$\max(K_{reduction}) \approx \gamma_0(e^{\gamma_1 \max|\sigma|^p} - 1) \tag{6.29}$$

From (6.29), one can see that the new algorithm either provides a large gain reduction (if $\max|\sigma|$ is relatively large) or confines $|\sigma|$ not leaving far away from the sliding surface (if $\max|\sigma|$ is small). As a result, the chattering level is reduced. Moreover, while $|\sigma|$ leaves the sliding manifold Σ, the switching gain increases its value quickly and compensates for the lumped perturbation quickly thanks to the added exponential term. Thus, it forces $|\sigma|$ to turn around quickly and start to head to the sliding manifold. As a result, the system state is constrained near the sliding manifold and the system is more robust (not leaving far away from the sliding manifold Σ). In the sense of fast compensation for the uncertainties, the new algorithm exhibits the ability of estimating the perturbations with limited information. In other words, it equips the ability of SMC with perturbation estimation without need for further information of VHOS. In brief, compared to the existing ASMC design (*e.g.*, [11, 14–17, 19, 74]), the new design (6.25) greatly improves the system's robustness and maintains a lower overall gain while the sliding mode is built [129].

6.3.5 Motivational Example

To illustrate the dynamic behavior of the ASMC design using the new gain law introduced in its simple form (6.27) with $K(0) = K_0$, we consider the simple closed-loop dynamics

$$\dot{\sigma} = 1 - K(t)\mathrm{sgn}\cdot(\sigma) \tag{6.30}$$

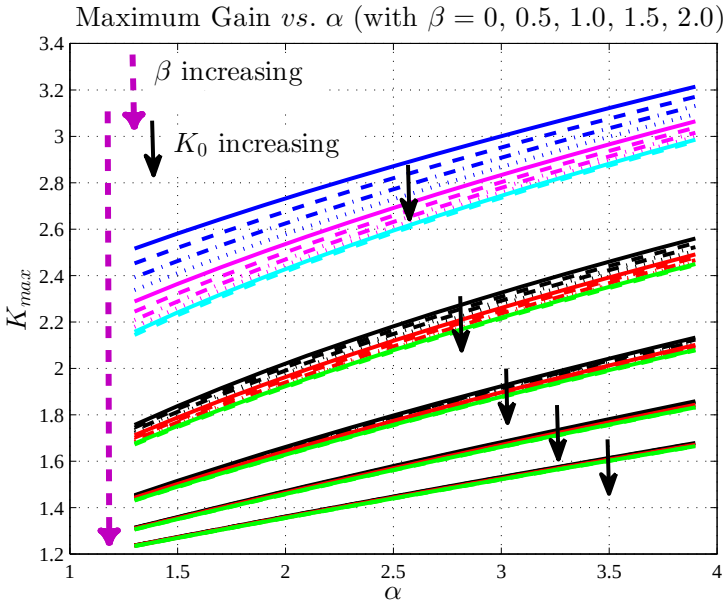

Figure 6.1: Maximum gain performance

Obviously $\sigma \to 0$ in finite time. The performance of these closed-loop dynamics are tested for different values of α, β and $K(0)$. Figures 6.1 and 6.2 show the maximum gain K_{max} reached during the adaptation process and reaching finite time T_c for the different cases [132]. From Figure 6.1, one can see that K_{max} is decreasing when β is increasing or K_0 increasing. However, K_{max} is increasing as α is increasing. In contrast, T_c is decreasing when α and K_0 are increasing, and T_c increasing as β increasing (see Figure 6.2).

6.3.6 Tutorial Example

In the following example, we compare the reaching performance (RTE, and accuracy), the gain evolution and consequently the perturbation estimation of three different gain algorithms: (a) Integral law (6.17), introduced in [14, 16, 19], (b) Exponential reaching law (6.21) and (c) integral-exponential law (6.27). Consider a simple scalar dynamics (with uncertainties) in the form of (6.1). The control objective is to stabilize the state x at the origin, *i.e.*, $x = 0$. The sliding variable is selected as $\sigma = x$ simply. From (6.1), $\Psi = f(t)$ and $\Gamma = g(t)$ are chosen as (recall the equation (5.59) and see Figure 5.2 in

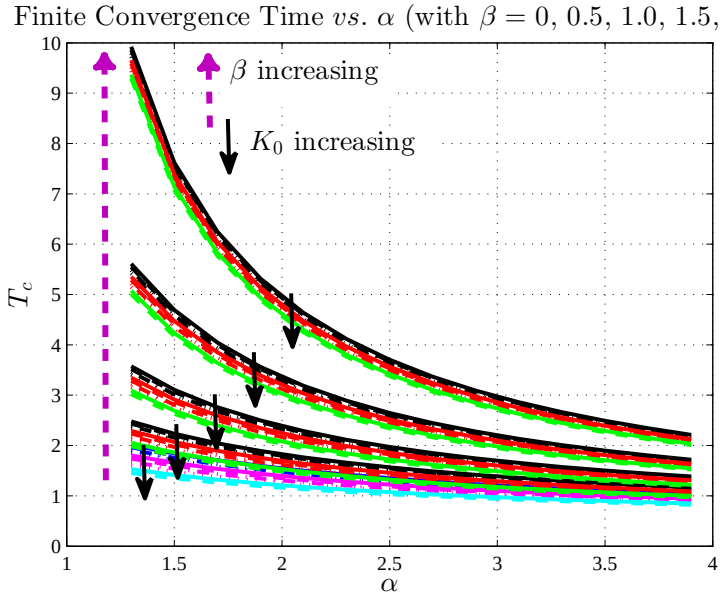

Figure 6.2: Finite time performance

Chapter 5) [129]

$$\Psi = -1.6 + 0.7\delta(t-0.5) + 5.4\delta(t-2.5) + 0.5\delta(t-2.7) - 0.5\delta(t-3.8) + 0.5\delta(t-3.9) - 0.5\delta(t-4.5) + 0.5\delta(t-4.6) - 0.3\delta(t-6.1) \quad (6.31)$$

$$\Gamma = 2 + \sum_{n=0}^{5} \frac{1}{2n+1} \sin\left(\frac{(2n+1)\pi(t-2.5)}{2}\right) \quad (6.32)$$

where $\delta(t-t_i)$ is a shifted unit step function which has a value of 0 up to time instant t_i and 1 thereafter. $K(0) = K_0 = 0.3$ and $\sigma(0) = 0.6$.

One can see that in Figure 6.3 there are three stages of perturbations: first perturbation (negative perturbation, from $t = 0$ to $t \approx 2.5$ sec), second perturbation (positive perturbation, from $t \approx 2.5$ to $t \approx 4.5$ sec) and third perturbation (positive perturbation, from $t \approx 4.5$ to $t \approx 6.5$ sec). These perturbations force σ to swing to the negative side ($\sigma < 0$) and positive side ($\sigma > 0$), respectively. Figure 6.3 also shows that the switching gain $K(t)$ compensates for the lumped perturbation $\frac{\Psi}{\Gamma}$ at time instants $t_{c,1}$, $t_{c,2}$ and $t_{c,3}$ and then reaches the sliding surface at time instants $t_{r,1}$, $t_{r,2}$ and $t_{r,3}$, respectively. One can see in Figure 6.3 that the sliding variable from

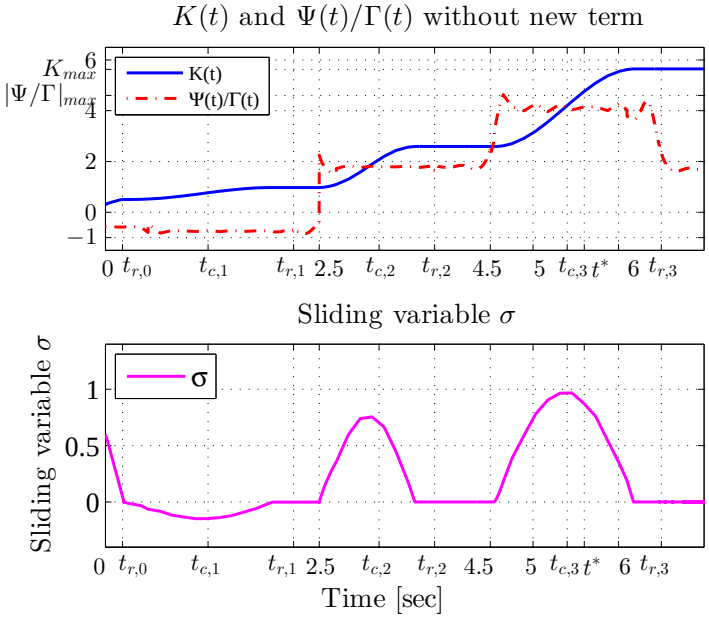

Figure 6.3: Switching gain $K(t)$, lumped perturbation $\dfrac{\Psi}{\Gamma}$ and the resulting sliding variable σ (using algorithm (a): Integral law (6.17) with $\alpha = 3$ [14, 16, 19]).

the positive side converges to the sliding surface ($\sigma = 0$), reaches it at $t_{r,0}$ and moves away to the negative side (*i.e.*, it does not stay on the sliding surface) as the ultimate in compensating phase is not achieved yet. In fact, after that $K(t)$ compensates for the lumped perturbation $\dfrac{\Psi \text{sign}(\sigma)}{\Gamma}$ at the time instant $t_{c,1}$, σ starts to converge to the sliding surface and reaches it at $t_{r,1}$. After a while, the perturbation again exceeds the switching gain at $t \approx 2.5$, σ departs from the sliding surface, and K starts to increase its value to compensate for the new perturbation and forces the sliding variable to reach the sliding surface. This compensating-reaching phase repeats untill the maximum lumped perturbation is completely compensated by the switching gain at $t = t^*$ (see Figure 6.3). Based on the adaptation process, the switching gain $K(t)$ is tuned automatically without *a priori* knowledge of the bounds of Ψ. Also, in Figure 6.3, σ reaches the sliding surface from $t = 0$ to $t = t_{r,0}$ while $K(t) > \dfrac{\Psi \text{sign}(\sigma)}{\Gamma}$ but $K(t) < \dfrac{|\Psi|}{\Gamma}$. It implies that while the sliding

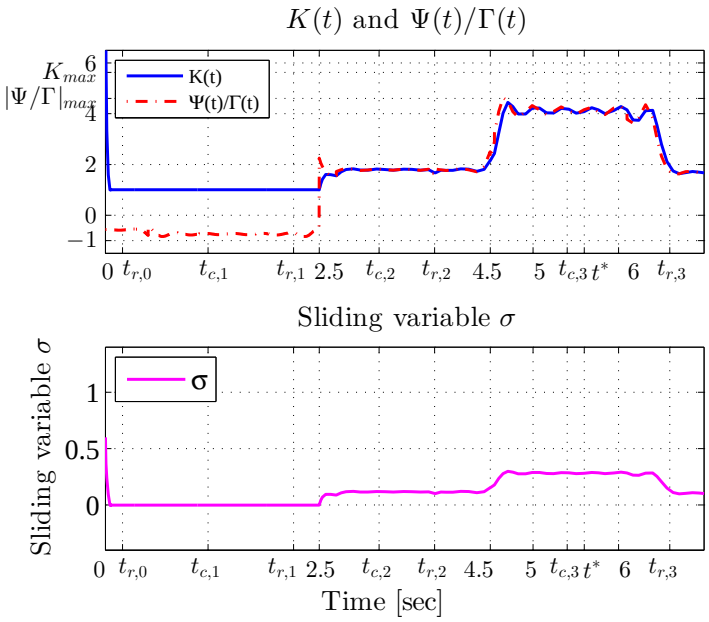

Figure 6.4: Switching gain $K(t)$, lumped perturbation $\dfrac{\Psi}{\Gamma}$ and the resulting sliding variable σ (using algorithm (b): Exponential reaching law (6.21) with $K_0 = 1$, $\gamma_1 = 5$ and $p = 1$).

variable may still approach the sliding surface even $K(t) < \dfrac{|\Psi|}{\Gamma}$ (*i.e.*, even the sufficient condition (4.39) for $\sigma \to 0$ of Lemma 4.3, introduced in Section 4.4 of Chapter 4) does not hold

Figure 6.4 is obtained from exponential reaching law (6.21). It shows that the switching gain $K(t)$ 'almost' follows the lumped perturbation $\dfrac{\Psi}{\Gamma}$ which means that the new exponential reaching law (6.21) provides 'almost' the required gain without the knowledge of the lumped perturbation bounds. This phenomenon also indicates the fast response to any change of uncertainty levels. Moreover, the final gain in Figure 6.4 is reduced by approximately 70% of its corresponding value in Figure 6.3. Thus, the gain overestimation noticed in conventional ASMC is greatly reduced when using (6.21). However, when looking at the behaviour of σ in Figure 6.4, it is only UUB not FTC (σ did not converge to zero). This convergence in a UUB sense phenomenon confirms Proposition 6.1.

Figure 6.5 is obtained under the new adaptation law, integral-exponential

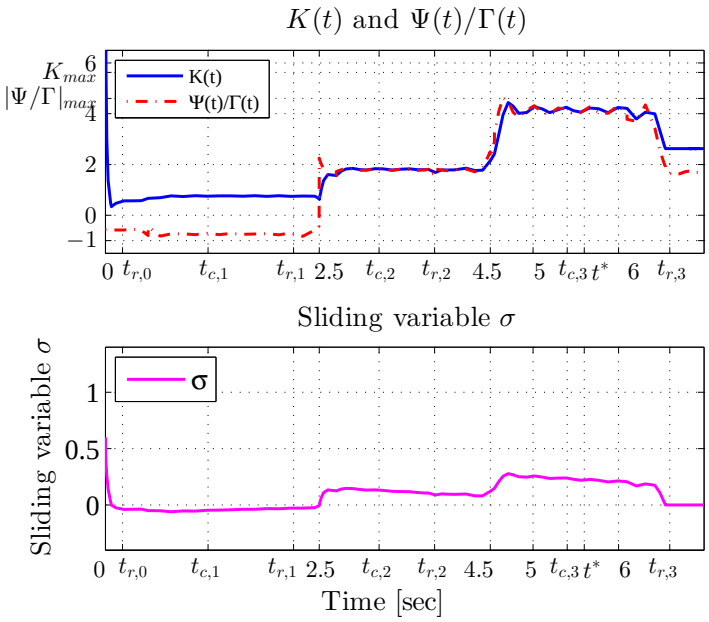

Figure 6.5: Switching gain $K(t)$, lumped perturbation $\dfrac{\Psi}{\Gamma}$ and the resulting sliding variable σ (using new algorithm (c): integral-exponential adaptation law (6.27) with $\alpha = 3$, $\gamma_0 = 1$, $\gamma_1 = 5$ and $p = 1$).

gain (6.27), with $\alpha = 3$, $\gamma_0 = 1$, $\gamma_1 = 5$ and $p = 1$. It shows how the switching gain $K(t)$ follows the lumped perturbation $\dfrac{\Psi}{\Gamma}$, closely. The proposed integral-exponential reaching law (6.27) also provides roughly the required gain without the knowledge of the lumped perturbation bounds. Comparing to Figure 6.3, one can see from Figure 6.5 that, with the new algorithm, the switching gain quickly responds to the perturbation and the variation of σ is greatly suppressed. Moreover, the final switching gain is reduced by approximately 60% of its value given in Figure 6.3. It implies that the gain overestimation is greatly reduced and the chattering level would be suppressed as well. Comparing to Figure 6.4, the sliding variable σ in Figure 6.5 reaches the sliding surface at $t_{r,3}$ which verifies FTC stated by Theorem 6.1.

Thus, with the new algorithm the control objectives, such as the reaching time, the chattering level, the maximum variation of σ and the energy consumed, in ASMC design for nonlinear systems with unknown bounds are relatively optimized and simultaneously achieved.

6.4 integral-exponential Reaching Law for *Real* ASMC Designs

6.4.1 Integral Adaptation Law for Real Sliding

In *real* ASMC techniques [11, 13–17, 19], K is designed to adaptively compensate for the uncertainties. We recall the two similar *boundary-layer*-based approaches

$$\dot{K} = \alpha \cdot |\sigma| \cdot \operatorname{sgn}\big(|\sigma| - \epsilon\big) \tag{6.33}$$

introduced in [16] and

$$\dot{K} = \alpha \cdot \big(|\sigma| - \epsilon\big) \tag{6.34}$$

in [17], respectively. ϵ is the width of the boundary layer. The properties of both designs are very similar. As discussed in Proposition 5.1 (refer to Section 5.5 in Chapter 5), the reaching time is also estimated as $t_r \leq \frac{\pi}{2\sqrt{\underline{\Gamma}\alpha}} + t^*$ (same as the case of ASMC for *ideal sliding*). Thus, it still exhibits relatively slow response at the beginning stage that the sliding variable is leaving the sliding surface forced by perturbations. It also maintains relatively high values after the sliding mode has been built, and thus, produces relatively high chattering levels.

6.4.2 Case of a Single Input

Given the sliding dynamics (6.6) with the switching control (6.14), consider the dynamic gain design

$$\begin{cases} \dot{\breve{K}} &= \alpha\|\sigma\| \cdot \operatorname{sgn}\big(\|\sigma\| - \epsilon\big) \\ K &= \breve{K} + \beta \cdot \big(e^{\|\sigma\|} - 1\big) \end{cases} \tag{6.35}$$

with $\epsilon > 0$ and $\beta > 0$. The reaching law (6.35) is an extension of (6.27) to the real ASMC. In the case of a single input (*i.e.*, $m = 1$), the norm of the variable is simply reduced to its absolute value. We have the following theorem [118].

Theorem 6.2. *Consider the nonlinear uncertain system* (6.1)*, with the sliding variable dynamics* (6.6)*, under Assumptions 6.1-6.4, controlled by* (6.14)*. If the gain $K(t)$ is designed as* (6.35)*, then for any initial condition $|\sigma| > \epsilon$ the sliding variable σ converges to the domain $|\sigma| \leq \epsilon$ and stays on the domain $|\sigma| \leq \delta$, i.e., $x \in \Sigma_\delta$ in finite time.*

Proof. The detailed proof is shown in Appendix A.8. □

6.4.3 Illustrative Example

Consider the following nonlinear scalar dynamics with external disturbance

$$\dot{\sigma} = \cos\sigma + d(t) + bu \tag{6.36}$$

where $b = 1 + 0.1\sin 3t$ is a positive time-varying coefficient of the input u. $d(t) = \big(1+r_1\big)\big(\delta(t-5)-\delta(t-10)\big)+\big(2+r_2\big)\big(\delta(t-10)-\delta(t-15)\big)$, where r_1 and r_2 are random values drawn from the standard uniform distribution on the open interval $\big(0,1\big)$, that is, $d(t)$ is an external disturbance taking a first random value between 1 and 2, exerting on the system at $t = 5$ and disappearing at $t = 10$, then a second random value between 2 and 3, exerting on the system at $t = 10$ and disappearing at $t = 15$. Using the switching control (6.14), the gain K, defined by (6.35), is able to stabilize σ to zero. Taking the parameter $\epsilon = 0.01$, the initial conditions $\sigma(0) = 0$ and $\breve{K}(0) = 0$, and the sampling time $T_s = 5\,\text{ms}$, the simulations have been conducted for different values of α and β. The simulations have been run repeatedly creating a population of results shown in Figures 6.6-6.11. Each iteration corresponds to simulations using one generated random disturbance magnitude (from one pair of (r_1, r_2)). We simulate the closed-loop dynamics using the different adaptation laws and their parameters. Applying multiple iterations, the collected data are summarized in terms of maximum state values $\sigma_{\max}$ depicted during the simulation period of 20 s (see Figures 6.6 and 6.7), steady-state values $|\sigma|_{\min}$ (*i.e.*, absolute state error) during the permanent regime (see Figures 6.8 and 6.9), and maximum switching gain values $K_{\max}$ (see Figures 6.10 and 6.11).

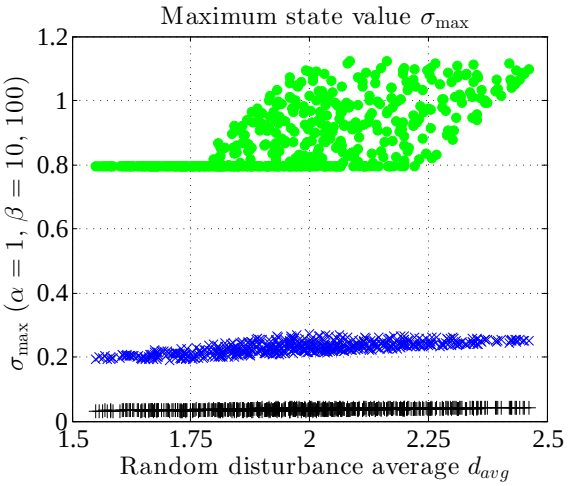

Figure 6.6: Numerical illustration data: Maximum state values $\sigma_{\max}$ obtained for different random disturbances (evaluated in terms of average values). Results using the existing IG-ASMC (7.10) (green dot) and the proposed IEG-ASMC (6.35) (blue cross for $\beta = 10$ and black plus sign for $\beta = 100$) combined with $\alpha = 1$

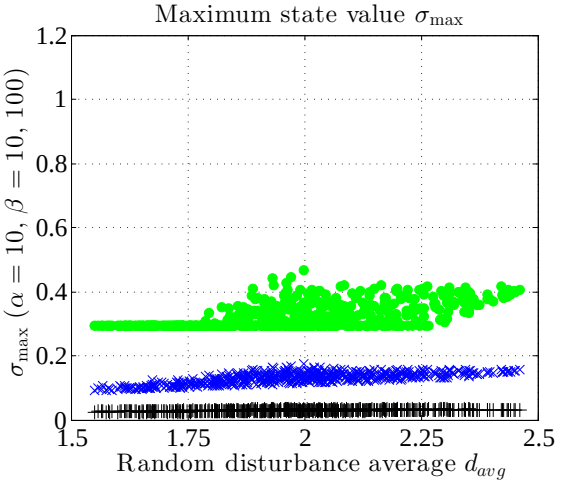

Figure 6.7: Numerical illustration data: Maximum state values $\sigma_{\max}$ obtained for different random disturbances (evaluated in terms of average values). Results using the existing IG-ASMC (7.10) (green dot) and the proposed IEG-ASMC (6.35) (blue cross for $\beta = 10$ and black plus sign for $\beta = 100$) combined with $\alpha = 10$

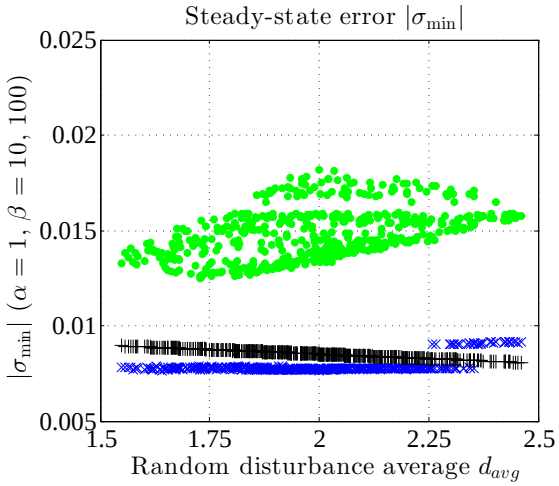

Figure 6.8: Numerical illustration data: Steady-state values $|\sigma|_{\min}$ obtained for different random disturbances (evaluated in terms of average values). Results using the existing IG-ASMC (7.10) (green dot) and the proposed IEG-ASMC (6.35) (blue cross for $\beta = 10$ and black plus sign for $\beta = 100$) combined with $\alpha = 1$

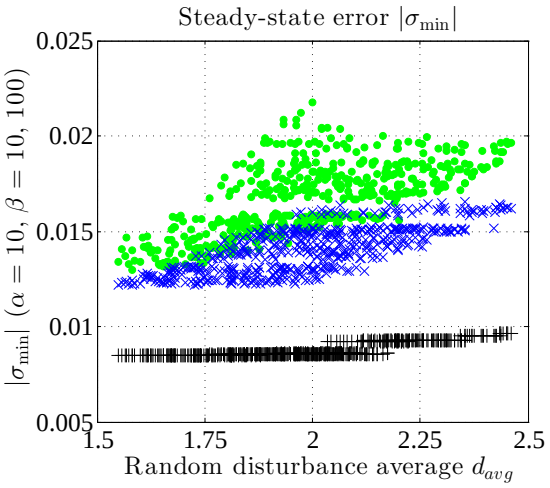

Figure 6.9: Numerical illustration data: Steady-state values $|\sigma|_{\min}$ obtained for different random disturbances (evaluated in terms of average values). Results using the existing IG-ASMC (7.10) (green dot) and the proposed IEG-ASMC (6.35) (blue cross for $\beta = 10$ and black plus sign for $\beta = 100$) combined with $\alpha = 10$

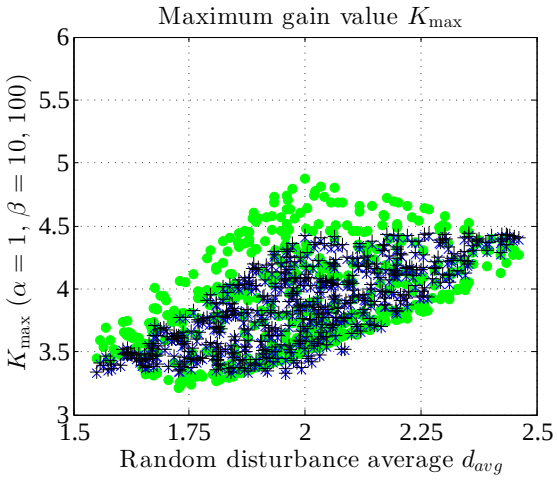

Figure 6.10: Numerical illustration data: Maximum switching gain values $K_{\max}$ obtained for different random disturbances (evaluated in terms of average values). Results using the existing IG-ASMC (7.10) (green dot) and the proposed IEG-ASMC (6.35) (blue cross for $\beta = 10$ and black plus sign for $\beta = 100$) combined with $\alpha = 1$

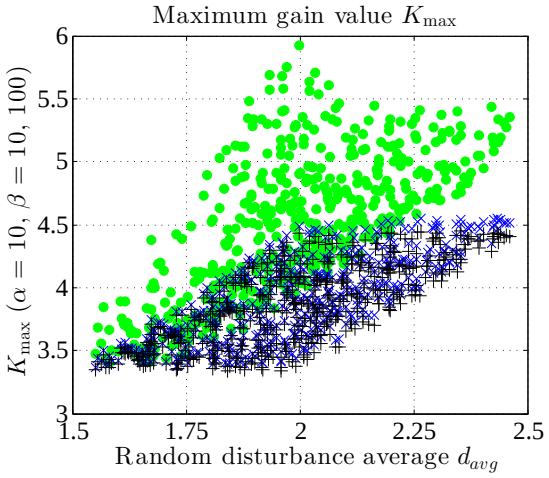

Figure 6.11: Numerical illustration data: Maximum switching gain values $K_{\max}$ obtained for different random disturbances (evaluated in terms of average values). Results using the existing IG-ASMC (7.10) (green dot) and the proposed IEG-ASMC (6.35) (blue cross for $\beta = 10$ and black plus sign for $\beta = 100$) combined with $\alpha = 10$

Figures 6.12-6.17 show a sample depicted from the simulation data described above. The state σ, the input u and the switching gain K under the external disturbance $d(t)$ are given using the existing IG based ASMC (*i.e.*, (6.33)), simply referred to as IG-ASMC in the following, and the proposed IEG-based ASMC (*i.e.*, (6.35)), referred to as IEG-ASMC, for $\alpha = 1$ and $\alpha = 10$, and $\beta = 10$ and $\beta = 100$. From the collected data (refer to Figures 6.6-6.11), we can observe that the results obtained with the existing approach with $\alpha = 1$ and $\alpha = 10$ show higher maximum state values (getting temporarily far from the origin), greater errors and relatively high switching gain values compared to the proposed approach. The samples shown in Figures 6.12-6.17 validate these facts of large states and nondecreasing gains of the IG-ASMC.

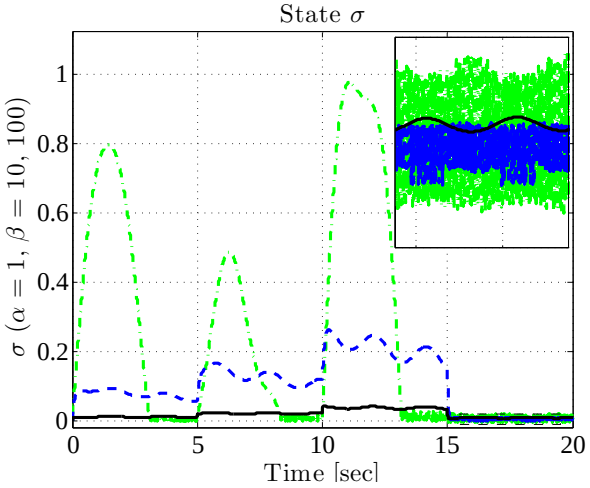

Figure 6.12: Numerical illustration sample: State σ under undetermined bounded external (random) disturbance $d(t)$. Results using the existing IG-ASMC (6.33) (green dot) and the proposed IEG-ASMC (6.35) (blue cross for $\beta = 10$ and black plus sign for $\beta = 100$) combined with $\alpha = 1$

These gains are higher as α increases, while the time evolutions of the state are improved in terms of maximum reachable values. Such performances are improved in terms of large state escape, error performance and switching gain values with different scenarios of IEG-ASMC. In particular, using $\alpha = \beta = 10$ demonstrates the best performances in general regarding all the criteria. One can see that the system compensated by the proposed adaptation law (6.35) responds to the disturbance $d(t)$ faster and constrains the state closer to the sliding surface than with the existing adaptation law (6.33). Moreover, the

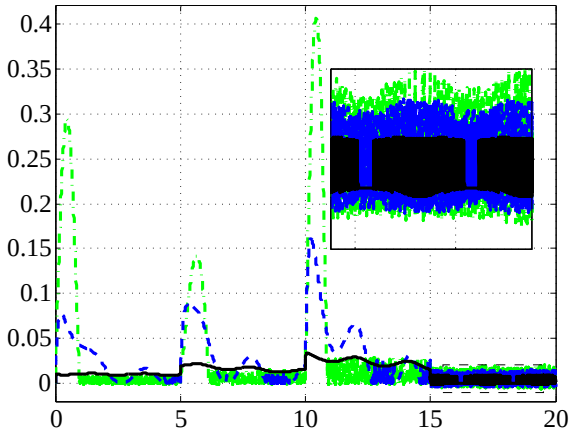

Figure 6.13: Numerical illustration sample: State σ under undetermined bounded external (random) disturbance $d(t)$. Results using the existing IG-ASMC (6.33) (green dot) and the proposed IEG-ASMC (6.35) (blue cross for $\beta = 10$ and black plus sign for $\beta = 100$) combined with $\alpha = 10$

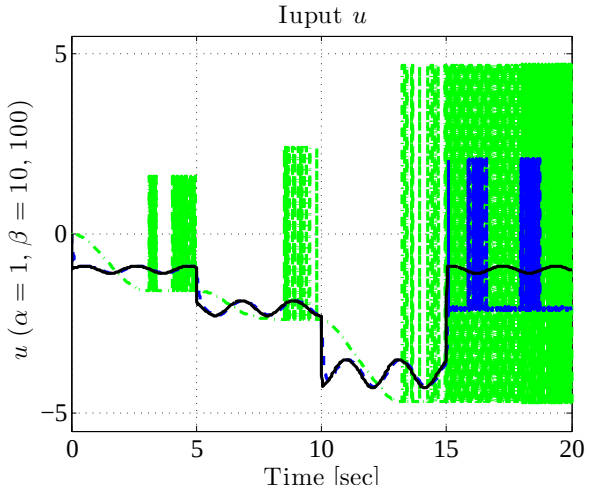

Figure 6.14: Numerical illustration sample: Input u under undetermined bounded external (random) disturbance $d(t)$. Results using the existing IG-ASMC (6.33) (green dot) and the proposed IEG-ASMC (6.35) (blue cross for $\beta = 10$ and black plus sign for $\beta = 100$) combined with $\alpha = 1$

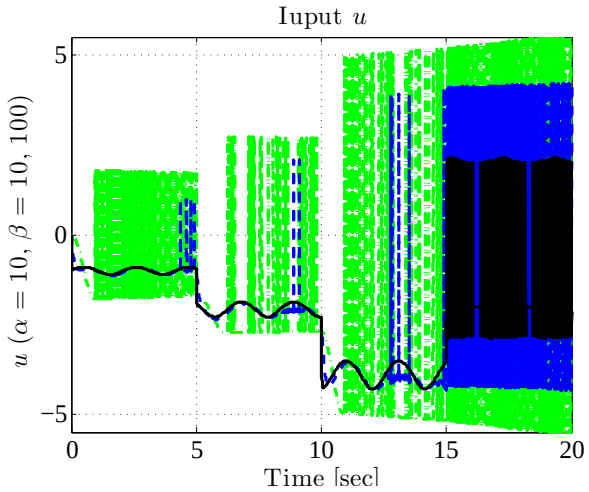

Figure 6.15: Numerical illustration sample: Input u under undetermined bounded external (random) disturbance $d(t)$. Results using the existing IG-ASMC (6.33) (green dot) and the proposed IEG-ASMC (6.35) (blue cross for $\beta = 10$ and black plus sign for $\beta = 100$) combined with $\alpha = 10$

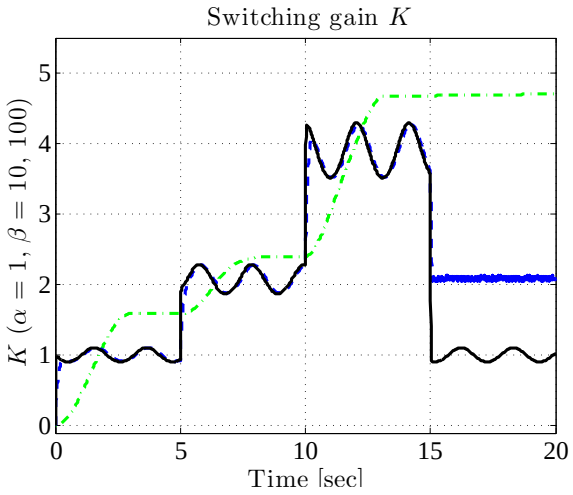

Figure 6.16: Numerical illustration sample: Switching gain K under undetermined bounded external (random) disturbance $d(t)$. Results using the existing IG-ASMC (6.33) (green dot) and the proposed IEG-ASMC (6.35) (blue cross for $\beta = 10$ and black plus sign for $\beta = 100$) combined with $\alpha = 1$

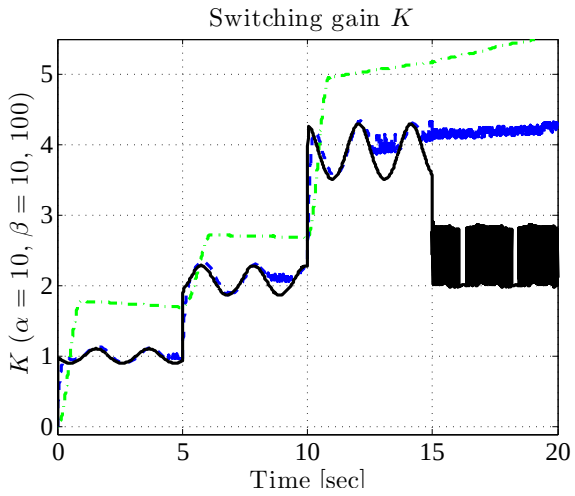

Figure 6.17: Numerical illustration sample: Switching gain K under undetermined bounded external (random) disturbance $d(t)$. Results using the existing IG-ASMC (6.33) (green dot) and the proposed IEG-ASMC (6.35) (blue cross for $\beta = 10$ and black plus sign for $\beta = 100$) combined with $\alpha = 1$

control input using the proposed law has less magnitude and a smaller chattering level than with the existing law. Also, by increasing α from 1 to 10, the error performance of the proposed method does not change. The maximum variation of the state σ by using the existing method is indeed reduced when α increases. However, the existing method simultaneously creates more chattering phenomenon and non-decreasing gains. When $\alpha = 10$, the switching gain K of the existing adapted law (6.33) starts to wind up while the one computed from (6.35) keeps almost the same shape, except the hyper-excited variation with small magnitudes during the steady state regime (see Figures 6.12-6.17). The new algorithm avoids gain overestimation observed when $\max|\sigma|$ is relatively large (refer to Figures 6.12, 6.13, 6.16 and 6.17), confines $|\sigma|$ not leaving far from the sliding surface (see zoomed sections in Figures 6.12 and 6.13) and reduces the control chattering (refer to Figures 6.14 and 6.15). Moreover, while $|\sigma|$ leaves the sliding manifold Σ, the switching gain increases its value quickly and compensates for the lumped perturbation instantaneously thanks to the added *exponential* term (see Figures 6.16-6.17). Thus, it forces $|\sigma|$ to turn around and start to head to the sliding manifold.

6.4.4 Case of MIMO Unit Control with Uncertain Γ

Consider the case of MIMO sliding dynamics (6.6) with the feedback control $u(t) \in \mathbb{R}^m$ defined by [74, 120]

$$u(t) = \begin{cases} -K(t) \cdot \dfrac{\sigma}{\|\sigma\|} & \text{if } \sigma \neq 0 \\ 0 & \text{if } \sigma = 0 \end{cases} \tag{6.37}$$

Substituting (6.37) into (6.6), we obtain for $\sigma \neq 0$

$$\dot{\sigma} = \Psi - \frac{K}{\|\sigma\|}\Gamma \cdot \sigma \tag{6.38}$$

Consider the case $\|\sigma\| > \epsilon$ and the target manifold Σ_δ, We have the following Theorem.

Theorem 6.3. *Consider the nonlinear uncertain system* (6.1)*, with the sliding dynamics* (6.6)*, under Assumptions 6.3–6.4, controlled by* (6.37)*. If the gain* $K(t)$ *is designed as* (6.35)*, then for any initial condition* $\|\sigma\| > \epsilon$*, the sliding variable* σ *converges to the domain* $\|\sigma\| \leq \epsilon$ *and stays on the domain* $\|\sigma\| \leq \delta$*, i.e.,* $x \in \Sigma_\delta$ *in finite time.*

Proof. Let the positive definite function

$$V = \sigma^T \sigma \tag{6.39}$$

be a Lyapunov function candidate. Using (6.38), for $\sigma \neq 0$, the time derivative of V along the system trajectories is

$$\begin{aligned} \dot{V} &= \sigma^T \dot{\sigma} + \dot{\sigma}^T \sigma \\ &= 2\sigma^T \Psi - \frac{K}{\|\sigma\|}(\sigma^T \Gamma \sigma + \sigma^T \Gamma^T \sigma) \end{aligned} \tag{6.40}$$

Using (6.9) and (6.35), we have

$$\begin{aligned} \dot{V} &= 2\|\sigma\|\Big(\frac{\sigma^T \Psi}{\|\sigma\|} - \frac{K}{\|\sigma\|^2}\sigma^T\big[\frac{1}{2}(\Gamma + \Gamma^T)\big]\sigma\Big) \\ &= 2\|\sigma\|\Big(\frac{\sigma^T \Psi}{\|\sigma\|} - K\frac{\sigma^T \Gamma_s \sigma}{\sigma^T \sigma}\Big) \\ &= 2\|\sigma\|\Big(\frac{\sigma^T \Psi}{\|\sigma\|} - \beta\big(e^{\|\sigma\|} - 1\big)\frac{\sigma^T \Gamma_s \sigma}{\sigma^T \sigma} - \breve{K}\frac{\sigma^T \Gamma_s \sigma}{\sigma^T \sigma}\Big) \end{aligned} \tag{6.41}$$

We denote by $\Omega_1(t) = \dfrac{\sigma^T\Psi}{\|\sigma\|} - \beta(e^{\|\sigma\|}-1)\dfrac{\sigma^T\Gamma_s\sigma}{\sigma^T\sigma}$. The scalar $\Omega_1(t)$ is upper-bounded since $\Gamma_s > 0$, $e^{\|\sigma\|}-1 > 0$ and $\|\Psi\| \leq \Psi_M$ (refer to Assumption 6.3). For $\|\sigma\| > \epsilon$, (6.41) can be rewritten as

$$\frac{\dot{V}}{2\sqrt{V}} = \Omega_1(t) - \breve{K}\frac{\sigma^T\Gamma_s\sigma}{\sigma^T\sigma} \tag{6.42}$$

For any $\|\sigma\| > \epsilon$, from (6.35), $\breve{K}$ keeps growing and the positive scalar $\breve{K}\dfrac{\sigma^T\Gamma_s\sigma}{\sigma^T\sigma}$ will eventually compensate for the upper-bounded $\Omega_1(t)$, *i.e.*, $\breve{K}\dfrac{\sigma^T\Gamma_s\sigma}{\sigma^T\sigma} > \Omega_1(t)$. Since this compensating action will occur for any $\|\sigma\| > \epsilon$ and $\Omega_1(t) \geq \breve{K}\dfrac{\sigma^T\Gamma_s\sigma}{\sigma^T\sigma}$ (*i.e.*, $\dfrac{d}{dt}\|\sigma\| \equiv \dfrac{\dot{V}}{2\sqrt{V}} \geq 0$), we conclude that there exist a time instant t^* and a positive scalar ω_1 such that

$$\breve{K}\frac{\sigma^T\Gamma_s\sigma}{\sigma^T\sigma} \geq \Omega_1(t) + \omega_1 \tag{6.43}$$

or, equivalently, using (6.42) for all $t \geq t^*$

$$\frac{d}{dt}\|\sigma\| \leq -\omega_1 \tag{6.44}$$

Now, integrating both sides of the inequality (6.44) between t^* and $t \geq t^*$, we obtain

$$\|\sigma\| \leq -\omega_1 \cdot \left(t - t^*\right) + \|\sigma(t^*)\|$$

Then, $\|\sigma\|$ is decreasing with a rate of at least ω_1 and reaches the domain $\|\sigma\| \leq \epsilon$ in finite time [1]. Moreover, the maximum reaching time t_r is estimated as

$$t_r \leq \frac{\|\sigma(t^*)\| - \epsilon}{\omega_1} + t^* \tag{6.45}$$

for some $t^* \geq 0$, $\epsilon > 0$ and $\omega_1 > 0$. □

As soon as $\|\sigma\|$ reaches the boundary layer, *i.e.*, $\|\sigma\| < \epsilon$, $\breve{K}$ starts to decrease (refer to (6.35)). The decrease of $\breve{K}$ continues until the scalar $\breve{K}\dfrac{\sigma^T\Gamma_s\sigma}{\sigma^T\sigma} \leq \Omega_1(t)$, *i.e.*, $\dot{V} \geq 0$. Then, V (as well as $\|\sigma\|$) starts to increase. So, it is possible that $\|\sigma\|$ increases over ϵ. As soon as $\|\sigma\| > \epsilon$, it turns to the case discussed above. In brief, $\breve{K}$ changes its value around Ω_1 and $\|\sigma\|$ stays around the boundary layer limit $\|\sigma\| = \epsilon$. This also implies that "σ has stable

finite reaching time dynamics with a bounded deviation of σ from the domain Σ during the transient response" [74], *i.e.*, σ keeps in a *real* sliding mode set Σ_δ after reaching the target manifold Σ [16, 74].

Compared to the ASMC law (6.33), the new algorithm (6.35) adds the *exponential* term, $\beta(e^{\|\sigma\|}-1)$, which provides an extra but sufficiently high gain when the state is far away from the sliding surface (*i.e.*, $\|\sigma\|$ is large). Thus, $K\frac{\sigma^T\Gamma_s\sigma}{\sigma^T\sigma}$ (including the *exponential* term) compensates for the perturbation $\frac{\sigma^T\Psi}{\|\sigma\|}$ more quickly than with $\breve{K}$ alone and forces the sliding multi-variable σ initially far away from its desired sliding manifold (because of $\dot{V}>0$, *i.e.*, $\frac{\sigma^T\Psi}{\|\sigma\|} > K\frac{\sigma^T\Gamma_s\sigma}{\sigma^T\sigma}$) to turn around heading to the sliding manifold Σ apace. Moreover, when $\|\sigma\|$ tends to Σ, the *exponential* term reduces its value rapidly. Then, after reaching Σ, the overall gain is reduced and the unwanted chattering level is expected to be much lower since the amplitude of chattering is proportional to the magnitude of the switching gain [61].

Different from the traditional boundary layer ε whose purpose is to smooth out the control discontinuity by replacing the discontinuous *signum* function with a continuous one (*e.g.*, $\frac{\|\sigma\|}{\varepsilon}$) within the layer [49], the boundary layer $\|\sigma\|\leq\epsilon$ introduced in (6.35) is to provide the reduction of switching gain after reaching the layer so that the gain can be gradually reduced to its minimum admissible value (*i.e.*, $K\frac{\sigma^T\Gamma_s\sigma}{\sigma^T\sigma}\approx\frac{\sigma^T\Psi}{\|\sigma\|}$). Moreover, the traditional boundary layer ε is of constant width usually, while ϵ in the proposed ASMC can be either constant if the magnitudes of uncertainties Ψ and Γ are fully unknown, or time-varying (depending on the switching gain K [16, 74]) if some nominal values of Ψ and Γ are known. Indeed, given that the nominal values are greater than the corresponding uncertain values, an ϵ-tuning relation can be applied (see [16] for more details).

6.4.5 Case of an MIMO Unit Control for Indefinite Γ

When the parameter matrix Γ is neither positive definite nor negative definite, the control defined by (6.37) is not appropriate. In this case, it is required that Γ is nonsingular. Moreover, denoting nominal values of Γ by $\hat{\Gamma}$, we consider the following assumption

Assumption 6.5. *The matrix $L(t)$ defined by*

$$L(t) = \hat{\Gamma}^{-1}\Gamma \tag{6.46}$$

for some regular and finite matrix $\hat{\Gamma}$ is positive definite in the wider sense, i.e., the symmetric part $L_s = \frac{1}{2}(L + L^T)$ is positive definite in the regular meaning [130].

Now, we define the control as [120]

$$u(t) = \begin{cases} -K(t) \cdot \dfrac{\hat{\Gamma}^T\sigma}{\|\hat{\Gamma}^T\sigma\|} & \text{if } \sigma \neq 0 \\ 0 & \text{if } \sigma = 0 \end{cases} \tag{6.47}$$

Substituting (6.47) into (6.6), we obtain, for $\sigma \neq 0$

$$\dot{\sigma} = \Psi - \Gamma K(t) \cdot \frac{\hat{\Gamma}^T\sigma}{\|\hat{\Gamma}^T\sigma\|} \tag{6.48}$$

Under Assumption 6.5 and the switching law (6.35), we have the following theorem

Theorem 6.4. *Consider the nonlinear uncertain system* (6.1)*, with the sliding multi-variable dynamics* (6.6)*, under Assumptions 6.3 and 6.5, controlled by* (6.47)*. If the gain $K(t)$ is designed as* (6.35)*, then for any initial condition $\|\sigma\| > \epsilon$ the sliding variable σ converges to the domain $\|\sigma\| \leq \epsilon$ and stays on the domain $\|\sigma\| \leq \delta$, i.e., $x \in \Sigma_\delta$ in finite time.*

Proof. Consider the Lyapunov candidate function (6.39). Let $s = \hat{\Gamma}^T\sigma$ be a new variable. Since $\hat{\Gamma}$ is regular, we have $\sigma^T = s^T\hat{\Gamma}^{-1}$. Using Assumption 6.5, the time derivative of V along the system trajectories is

$$\begin{aligned} \dot{V} &= 2\sigma^T\Big(\Psi - \Gamma K\frac{\Gamma^T\sigma}{\|\Gamma^T\sigma\|}\Big) \\ &= 2\|s\|\Big(\frac{s^T(\hat{\Gamma}^{-1}\Psi)}{\|s\|} - K\frac{s^TL_ss}{\|s\|^2}\Big) \\ &= 2\|s\|\Big(\Omega_2(t) - \breve{K}\frac{s^TL_ss}{\|s\|^2}\Big) \end{aligned} \tag{6.49}$$

with $\Omega_2(t) = \dfrac{s^T\big(\hat{\Gamma}^{-1}\Psi\big)}{\|s\|} - \beta\big(e^{\|\sigma\|}-1\big)\dfrac{s^T L_s s}{\|s\|^2}$. The scalar Ω_2 is upper-bounded for any vector s. For $\|\sigma\| > \epsilon$, $\breve{K}$ will keep growing and eventually the positive scalar $\breve{K}\dfrac{s^T L_s s}{s^T s}$ will compensate for the upper-bounded scalar $\Omega_2(t)$, *i.e.*, $\breve{K}\dfrac{s^T L_s s}{\|s\|^2} > \Omega_2(t)$. Since this compensating action will occur for any $\|\sigma\| > \epsilon$ and $\Omega_2(t) \geq \breve{K}\dfrac{s^T L_s s}{\|s\|^2}$ (*i.e.*, $\dfrac{d}{dt}\|\sigma\| \equiv \dfrac{\dot{V}}{2\sqrt{V}} \geq 0$), we conclude that there exists a time instant t^* and a positive scalar ω_2 such that

$$\breve{K}\frac{s^T L_s s}{\|s\|^2} \geq \Omega_2(t) + \omega_2 \tag{6.50}$$

then, for all $t \geq t^*$

$$\dot{V} \leq -2\omega_2\|s\| \tag{6.51}$$

Since $\|s\|^2 = \sigma^T\hat{\Gamma}\hat{\Gamma}^T\sigma \geq \underline{\lambda}\sigma^T\sigma$ with $\underline{\lambda}$ the minimum eigenvalue of the positive definite matrix $\hat{\Gamma}\hat{\Gamma}^T$, we have $\|s\| \geq \sqrt{\underline{\lambda}}\|\sigma\|$. Then, from (6.51), we obtain

$$\frac{d\sqrt{V}}{dt} \leq -\omega_2\sqrt{\underline{\lambda}} \tag{6.52}$$

Thus, σ converges to the domain $\|\sigma\| \leq \epsilon$ in finite time with a maximum reaching time $t_r \leq \dfrac{\|\sigma(t^*)\| - \epsilon}{\omega_2\sqrt{\underline{\lambda}}} + t^*$ [1]. □

It should be noted that, without completely eliminating the overestimation, the new algorithm reduces the overall gain with a significant amount compared to the existing algorithms (*e.g.*, (6.33) and (6.34) [16,17]). Roughly speaking, the vanishing term, *i.e.*, *exponential* amount, corresponds to the maximum gain reduction when σ reaches the boundary layer. In fact, as previously discussed in the illustrative example, the new algorithm either provides a large gain reduction (if $\max\|\sigma\|$ is relatively large) or confines $\|\sigma\|$ to the sliding surface. As a result, the chattering level is reduced or even eliminated. In addition, out of the sliding manifold Σ, the switching gain increases its value and compensates for the lumped perturbation quickly thanks to the added *exponential* term. Thus, it forces $\|\sigma\|$ to turn around and start to head to the sliding manifold in shorter time. As a result, the system state is constrained near the sliding manifold, and the system is more robust (not leaving far from the sliding manifold Σ). In the sense of fast compensation for the uncertainties, the new algorithm exhibits the ability of estimating the

perturbations with limited information. In other words, it equips the ability of SMC with perturbation estimation without need for further information of very-high-order states. The latter was a fundamental requirement in [11]. In brief, compared to the existing ASMC design (*e.g.*, [11,14–17,19,74]), the new design (6.35) greatly improves the system robustness and maintains a lower overall gain while the sliding mode is built.

6.5 Simulations and Experiments

6.5.1 Simulation Results – Variable-Length Pendulum

We consider the variable-length pendulum dynamic control moving in a vertical plane [18, 59]

$$\ddot{x} = -2\frac{\dot{R}(t)}{R(t)}\dot{x} - \frac{g}{R(t)}\sin x + \frac{1}{mR(t)^2}u \tag{6.53}$$

where $m = 1$ kg is the mass and $g = 9.81$ m/sec^2 the gravity acceleration. u is the input torque, and x, $\dot{x}$ and $\ddot{x}$ are the angle displacement, velocity and acceleration, respectively, for zero initial conditions. The uncertain parameter R is chosen as $R(t) = 1+0.25\sin 4t+0.5\cos t$. The desired angle displacement is given by $x_d = 0.5\sin 0.5t + 0.5\cos t$. The sliding variable is $\sigma = \dot{x} - \dot{x}_d + 2(x - x_d)$. We design the ASMC using three switching gain laws: (a) Integral law (6.17), (b) Exponential reaching law (6.21) and (c) integral-exponential law (6.27). The ASMC parameters are $\alpha = 2$, $K(0) = 4$, $p = 1$, $\gamma_0 = 16$, $\gamma_1 = 1$. The sampling period is $T_s = 10^{-3}$ sec. Results are shown in Figures 6.18-6.21.

From Figure 6.18, one can see that the angle trajectory generated by using the proposed integral-exponential law (c) follows the desired path more accurately than the exponential law (b) and the conventional ASMC law (a). The tracking error by applying the new law (c) is reduced by 80% and 60% of its values obtained with (a) and (b), respectively. It can be also seen from Figure 6.19 that the chattering magnitudes observed with the new law (c) and law (b) are reduced approximately by 30% *w.r.t.* the chattering level generated by law (a).

Figure 6.20 shows that the magnitude of the final (or post-perturbation) switching gains with the proposed integral-exponential algorithm (c) and the exponential one (b) are reduced approximately by 30% compared to the value of the integral one (a).

Comparing the three algorithms of the switching gain, we conclude that the proposed integral-exponential algorithm (c) has simultaneously higher ac-

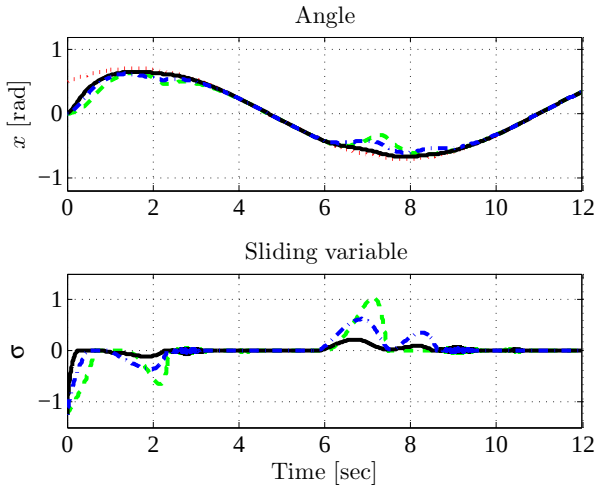

Figure 6.18: Simulation Results for a Variable-length Pendulum: Positions and sliding variables *vs.* time, results with algorithm (a) in green dash line, results with algorithm (b) in blue dash-dot line and results with algorithm (c) in black solid line.

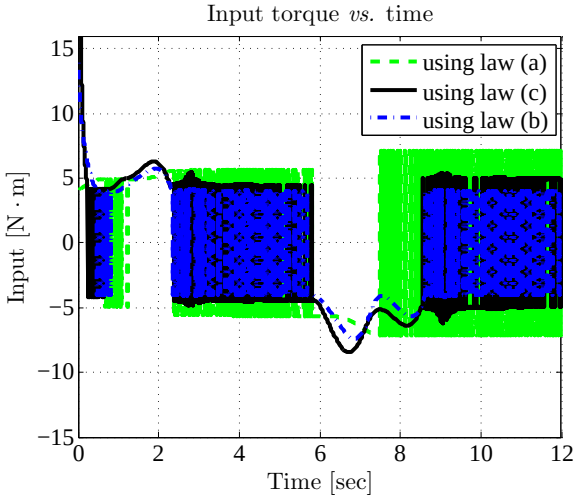

Figure 6.19: Simulation Results for a Variable-length Pendulum: Inputs *vs.* time, results with algorithm (a) in green dash line,results with algorithm (b) in blue dash-dot line and results with algorithm (c) in black solid line.

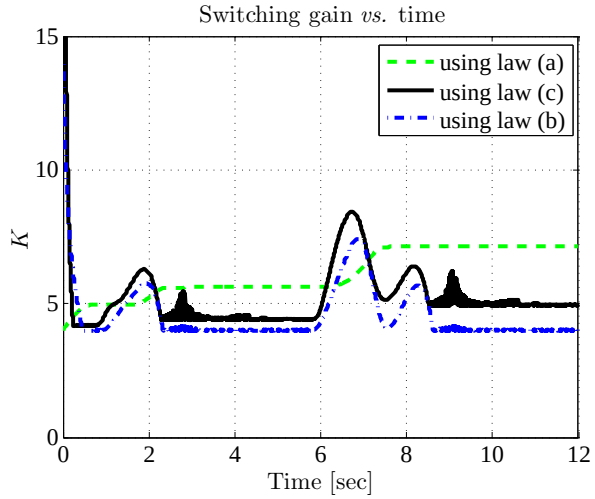

Figure 6.20: Simulation Results for a Variable-length Pendulum: Feedback switching gains *vs.* time, Gain with algorithm (a) in green dash line, results with algorithm (b) in blue dash-dot line, results with algorithm (c) in black solid line and respective lumped uncertainties in red lines.

curacy, quick response, enhanced stability and lower chattering level than traditional ASMC law (a). For almost same level of chattering amplitude, the tracking response is better with the proposed integral-exponential algorithm (c) than the exponential one (b). The algorithm (a) shows a higher level of chattering. The gains of algorithms (b) and (c) are changing dynamically with the magnitude of the lumped uncertainties more than that of the algorithm (a) which keeps increasing with any increase in the magnitude of lumped uncertainties (refer to Figure 6.21). The proposed algorithm (c) is responding more quickly to any change in the uncertainty levels.

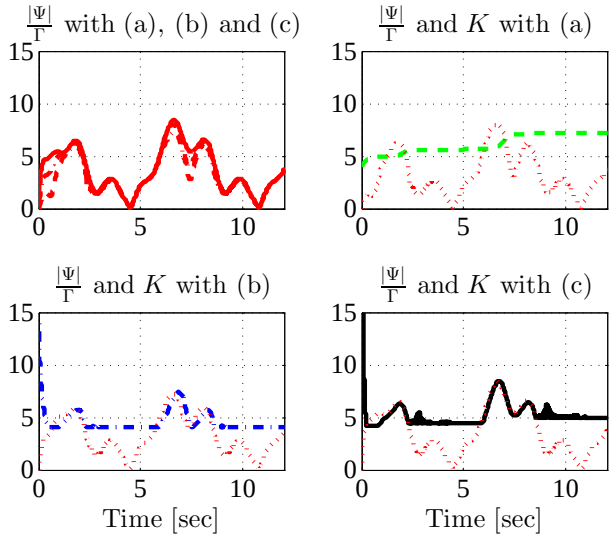

Figure 6.21: Simulation Results for a Variable-length Pendulum: Gains and lumped uncertainties *vs.* time, Gain with algorithm (a) in green dash line, results with algorithm (b) in blue dash-dot line, results with algorithm (c) in black solid line and respective lumped uncertainties in red lines.

6.5.2 Simulation Results for a 2-DOF Experimental Helicopter

We consider the 2-DOF helicopter simulator model actuated with two propellers [21] as shown in Figure 1.1 in Chapter 1 and Figure 3.2 in Chapter 3. Recall its nonlinear dynamic equations (refer to (3.43a) and (3.43b) in Chapter 3)

$$\begin{aligned}\big(J_p + ml^2\big)\ddot{\phi} =& K_{pp}V_p + K_{py}V_y - B_p\dot{\phi} - mgl\cdot\cos\phi \\ & - ml^2\sin\phi\cos\phi\cdot\dot{\psi}^2 \end{aligned} \tag{6.54}$$

$$\big(J_y + ml^2\cos^2\phi\big)\ddot{\psi} = K_{yp}V_p + K_{yy}V_y - B_y\dot{\psi} + 2ml^2\sin\phi\cos\phi\cdot\dot{\phi}\dot{\psi} \tag{6.55}$$

Let $x_1 = \phi$, $x_2 = \psi$, $x_3 = \dot{\phi}$ and $x_4 = \dot{\psi}$ be the measurable states and $u = [u_1 \;\; u_2]^T = [V_p \;\; V_y]^T$. The dynamics (6.54) and (6.55) can be rewritten in the form of (6.1). The expression of $f(x,t)$ and $g(x,t)$ are given by (refer to (3.50)-(3.55) in Chapter 3)

$$f(x,t) = \big[x_3,\; x_4,\; f_1(x),\; f_2(x)\big]^T \tag{6.56}$$

and

$$g(x,t) = \big[g_1(x,t),\; g_2(x,t)\big] \tag{6.57}$$

with

$$f_1(x) = \frac{-B_p x_3 - mgl\cos x_1 - ml^2(\sin x_1\cos x_1)x_4^2}{J_p + ml^2} \tag{6.58}$$

$$f_2(x) = \frac{-B_y x_4 + 2ml^2(\sin x_1\cos x_1)x_3x_4}{J_y + ml^2\cos^2 x_1} \tag{6.59}$$

$$g_1(x,t) = \big(0,\; 0,\; \frac{K_{pp}}{J_p + ml^2},\; \frac{K_{yp}}{J_y + ml^2\cos^2 x_1}\big)^T \tag{6.60}$$

and

$$g_2(x,t) = \big(0,\; 0,\; \frac{K_{py}}{J_p + ml^2},\; \frac{K_{yy}}{J_y + ml^2\cos^2 x_1}\big)^T \tag{6.61}$$

Assuming that the pitch and yaw angles are required to be stabilized to zero exponentially, we design a sliding hyper-surface as $\sigma = \begin{bmatrix} \sigma_1 & \sigma_2 \end{bmatrix}^T$ with $\sigma_i = x_{i+2} + K_P x_i + K_I \int x_i dt$, for $i = 1, 2$ [11]. Then, the sliding dynamics can be written in form (6.6) with

$$\Psi = \begin{pmatrix} \Psi_1 \\ \Psi_2 \end{pmatrix} = \begin{pmatrix} K_P x_3 + K_I x_1 + f_1(x,t) \\ K_P x_4 + K_I x_2 + f_2(x,t) \end{pmatrix} \tag{6.62}$$

Table 6.1: Nominal values of the model parameters [21]

Parameters	Values	Units	Parameters	Values	Units
$\hat{J}_p$	0.038	$\mathrm{kg}\cdot\mathrm{m}^2$	$\hat{J}_y$	0.043	$\mathrm{kg}\cdot\mathrm{m}^2$
$\hat{K}_{pp}$	0.204	$\mathrm{N}\cdot\mathrm{m/V}$	$\hat{K}_{py}$	0.007	$\mathrm{N}\cdot\mathrm{m/V}$
$\hat{K}_{yp}$	0.022	$\mathrm{N}\cdot\mathrm{m/V}$	$\hat{K}_{yy}$	0.072	$\mathrm{N}\cdot\mathrm{m/V}$
$\hat{B}_p$	0.800	N/V	$\hat{B}_y$	0.318	N/V
$\hat{l}$	0.186	m	g	9.810	$\mathrm{m/sec}^2$
$\hat{m}$	1.3872	kg			

and

$$\Gamma = \begin{pmatrix} \Gamma_{11} & \Gamma_{12} \\ \Gamma_{21} & \Gamma_{22} \end{pmatrix} = \begin{pmatrix} \dfrac{K_{pp}}{J_p + ml^2} & \dfrac{K_{py}}{J_p + ml^2} \\ \dfrac{K_{yp}}{J_y + ml^2\cos^2 x_1} & \dfrac{K_{yy}}{J_y + ml^2\cos^2 x_1} \end{pmatrix} \tag{6.63}$$

where $f_1(x,t)$ and $f_2(x,t)$ are given in (6.58) and (6.59), respectively. The nominal parts $\hat{f}_1$ and $\hat{f}_2$ (as well as their corresponding terms $\hat{\Psi}$ and $\hat{\Gamma}$) are obtained using the nominal values of the model parameters provided by Table 6.1 [21] (refer to Table 3.1).

The sampling time $T_s = 5\,\mathrm{ms}$ is picked to be the same as the sensor sampling time of the 2-DOF experimental helicopter. Moreover, we add the following time-varying uncertainties

$$\tilde{\Psi} = 0.1\sin(1.5t)\cdot \begin{pmatrix} \hat{f}_1(x,t) \\ \hat{f}_2(x,t) \end{pmatrix} \tag{6.64}$$

The sliding model dynamics of the setup in the simulations are built based on (6.62) and (6.63) which contain the nominal parts $\hat{\Psi}$ and $\hat{\Gamma}$ and the uncertain part $\tilde{\Psi}$ (6.64). We compare the proposed IEG-ASMC algorithm, with the IG-ASMC one of [16, 74]. The pitch and yaw angles are supposed to be stabilized at the origin. Two control strategies are selected for the following scenarios. First, the parameters provided by [21] are considered inaccurate with uncertain model dynamics. The ASMC controllers are then built based on the assumption that the nominal values of Ψ and Γ are totally unknown, except for the fact that Γ is positive definite. In other words, the bounds of Ψ and Γ in the control are unknown *a priori* (since the nominal terms $\hat{\Psi}$ and $\hat{\Gamma}$, and then, the bounds of $\tilde{\Psi}$ introduced in (6.64) are unknown). We only

consider the positive definiteness of Γ. Thus, in the first set of simulations, the control is defined using (6.37) (refer to Theorem 6.3). The second step of simulations and experiments is conducted using the pitch and yaw dynamics described by (6.54) and (6.55). The values of their parameters introduced above are considered to design the nominal parts of these dynamics. So, an equivalent control is designed based on these nominal dynamics. Then, based on assumption A.6.5 and the nominal term $\hat{\Gamma}$, the switching control is obtained from (6.47) (refer to Theorem 6.4). We use the nominal values of the parameters (and the corresponding terms $\hat{\Psi}$ and $\hat{\Gamma}$) to design the equivalent control (6.12) and the switching control (6.47). However, the bounds of the uncertainties $\tilde{\Psi}$ and $\tilde{\Gamma}$ are unknown *a priori*.

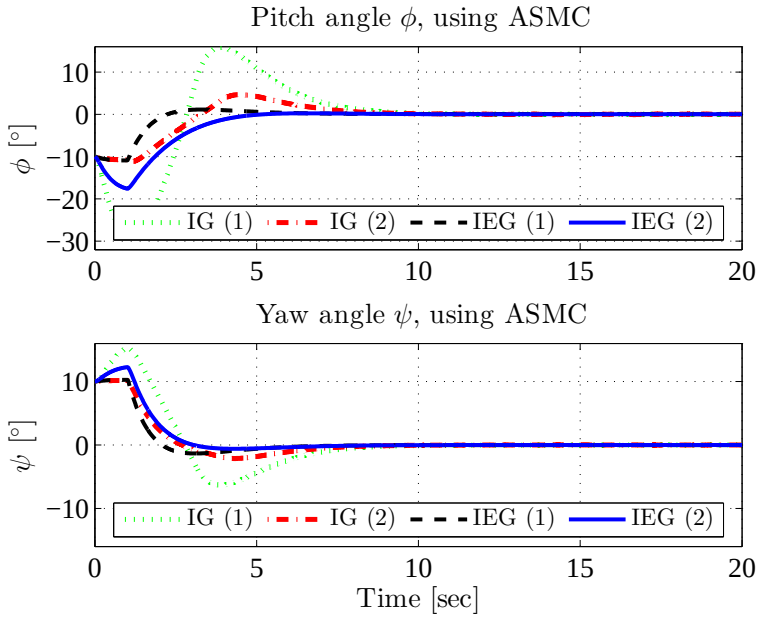

Figure 6.22: Simulation results of ASMC only (*i.e.*, no equivalent control): States ϕ and ψ

First, the terms Ψ and Γ in (6.6) are considered to be uncertain with $\Gamma > 0$ to evaluate properly the proposed algorithm and compare it with the existing ASMC design of [16, 74] exclusively. The sliding surface parameters selected are $K_P = K_I = 1$. The IG and IEG adaptation laws are totally parametrized by the initial condition $\breve{K}(0)$, the target band limit ϵ, and the coefficients α and β (note that $\beta = 0$ in the IG algorithm). The results shown here correspond to two sets of simulations with the IG and IEG laws. The design

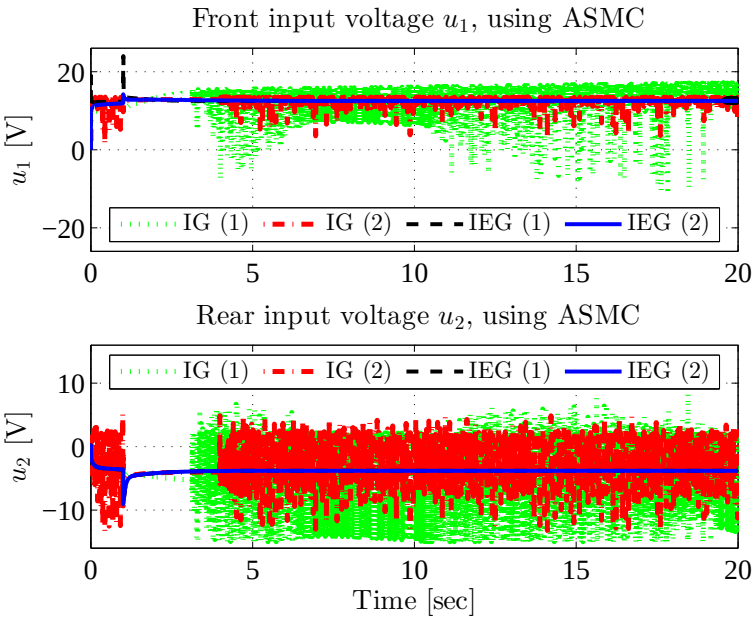

Figure 6.23: Simulation results of ASMC only (*i.e.*, no equivalent control): Inputs u_1 and u_2

(6.35) with the control input (6.37) is deployed using the design parameters shown in Tables 6.2 and 6.3 (refer to second column). The asterisk in Table 6.2 marks the parameters used later for experiments.

The time evolutions of pitch angle ϕ and yaw angle ψ are shown in Figure 6.22. Both angles are stabilized with reduced undershoot and very low overshoot for both pitch and yaw angles, respectively, with the proposed gain law rather than with the existing gain law. The existing IG-ASMC demonstrates more overshoots during the transient period. Figure 6.23 shows the control inputs u_1 and u_2. One can see that with the two IEG cases, the control magnitudes are chattering free whereas the controls with the existing IG-ASMC design show more chattering.

Considering the dynamics (6.38), let $\Omega = \Gamma^{-1}\Psi$ be the lumped perturbation. Figures 6.24 and 6.25 demonstrate how the switching gains of the IEG cases have the minimum required values (*i.e.*, gains just compensating for the lumped perturbations $\|\Omega\|$) [61] while Figures 6.26 and 6.27 show the IG-based switching laws and their corresponding lumped perturbation behaviors. It can be seen that the magnitude of the generated gains are greater and ultimately increasing. Moreover, the new design compensates the lumped

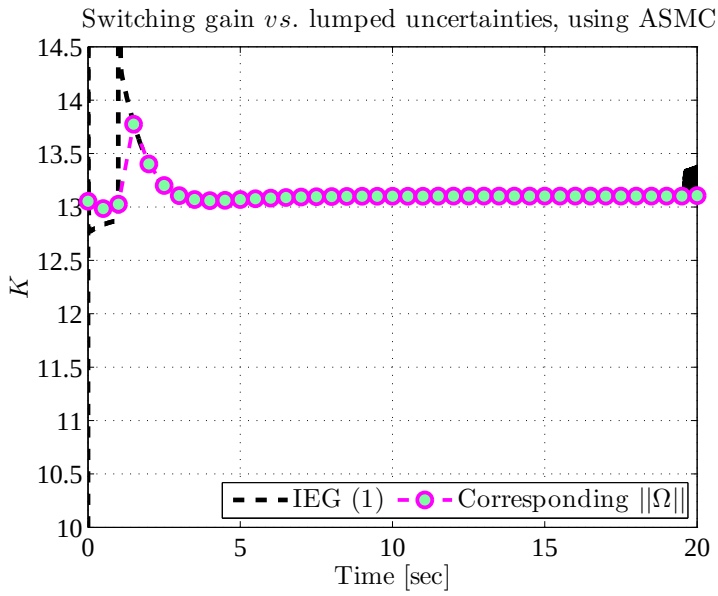

Figure 6.24: Simulation results of ASMC only (*i.e.*, no equivalent control): Corresponding lumped uncertainty $\|\Omega\|$ using IEG (1)

perturbations without overestimation. It works as a 'smart' switching gain being able to compensate for the lumped uncertainties instantaneously. Table 6.2 summarizes the performance of the IG-ASMC and IEG-ASMC techniques in terms of accuracy evaluated by the maximum error (*i.e.*, Peak value) and quadratic mean error (or RMS value).

Table 6.2: Simulation results: Pitch and yaw error (*i.e.*, $\tilde{\phi}$ and $\tilde{\psi}$) performance, in % of maximum displacement, using ASMC with fixed $\epsilon = 10^{-2}$

Gain law method (paramters)		Error peak		Error RMS	
		$\tilde{\phi}$	$\tilde{\psi}$	$\tilde{\phi}$	$\tilde{\psi}$
IG-(1)	$(K(0) = 10,\ \alpha = 2)$	0.33	0.41	**0.12**	0.12
IG-(2)*	$(K(0) = 13.5,\ \alpha = 0.01)$	0.82	0.23	0.33	0.09
IEG-(1)	$(K(0) = 10,\ \alpha = 2,\ \beta = 60)$	0.53	0.17	0.49	0.16
IEG-(2)*	$(K(0) = 10,\ \alpha = 0.01,\ \beta = 5)$	**0.18**	**0.08**	0.18	**0.08**

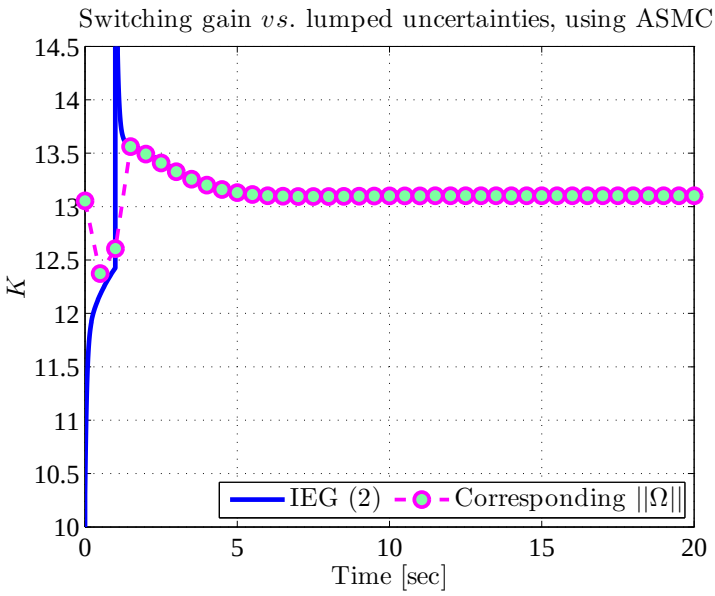

Figure 6.25: Simulation results of ASMC only (*i.e.*, no equivalent control): Switching gain K *vs.* corresponding lumped uncertainty $\|\Omega\|$ using IEG (2)

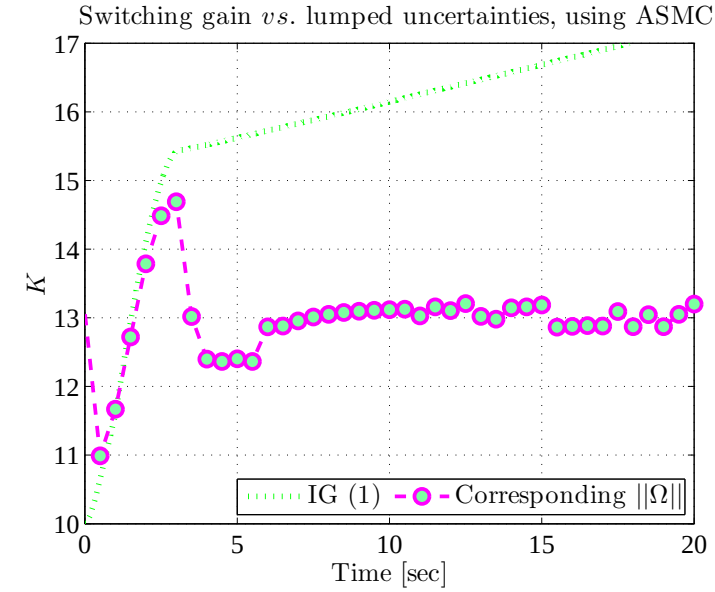

Figure 6.26: Simulation results of ASMC only (*i.e.*, no equivalent control): Switching gain K *vs.* corresponding lumped uncertainty $\|\Omega\|$ using IG

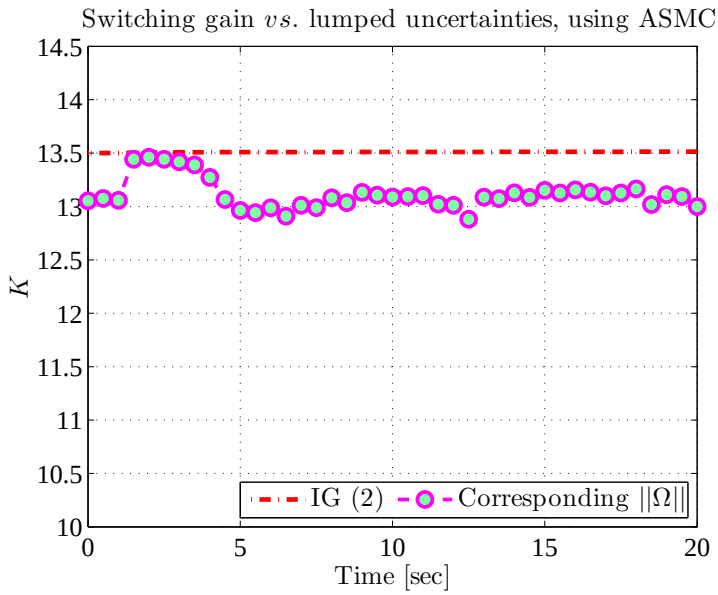

Figure 6.27: Simulation results of ASMC only (*i.e.*, no equivalent control): Switching gain K *vs.* corresponding lumped uncertainty $\|\Omega\|$ using IG (2)

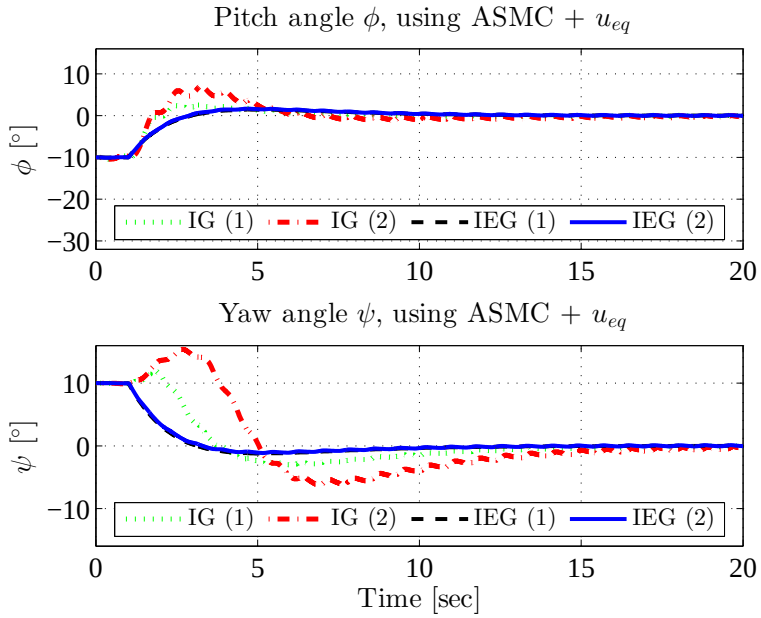

Figure 6.28: Simulation results of ASMC with equivalent control: States ϕ and ψ

In the second simulations, the nominal dynamics of the system is used to design the equivalent control reducing the level of uncertainties. The sliding surface parameters are selected $K_P = 4K_I = 1$. The IG-ASMC and IEG-ASMC designs are computed using α, β and $\breve{K}(0)$ shown in Table 6.3. For these simulations, we use the ϵ-tuning (with $\epsilon = 4T_sK$ [16, 74]). Note that, with the ϵ-tuning, ϵ is time-varying and depending on K. In addition, the design requires Γ to be normalizable (*i.e.*, Assumption 6.5 must be satisfied) [16, 74].

The results of pitch and yaw angles are shown in Figure 6.28. One can see that both angles are stabilized with low overshoot and show improved accuracy with the proposed gain law compared to the existing gain adaptation. Figure 6.29 shows the control signals u_1 and u_2. One can conclude that the magnitudes of the control inputs with the proposed design are less important than those obtained with the existing design. The control magnitudes are limited and non-decreasing now compared to the previous results obtained without equivalent control. The actual switching gains and the magnitude of the lumped uncertainties are shown in Figures 6.30 and 6.31 for the proposed design and Figures 6.32 and 6.33 for the existing gain dynamics. Despite the

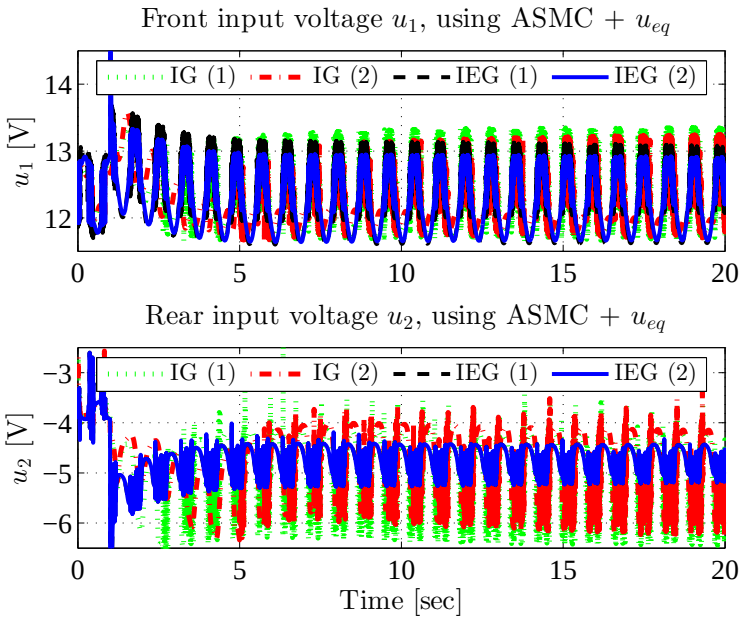

Figure 6.29: Simulation results of ASMC with equivalent control: Inputs u_1 and u_2

pitch and yaw stabilization occurring with the existing design (refer to Figure 6.29), the switching gains in Figures 6.32 and 6.33 are not matching with the changing uncertainties. These gains keep increasing to overcome the actual uncertainty levels. Table 6.3 summarizes the performance of the IG-ASMC and IEG-ASMC with the equivalent control in terms of maximum error and quadratic mean error. These errors are much more reduced with the proposed design.

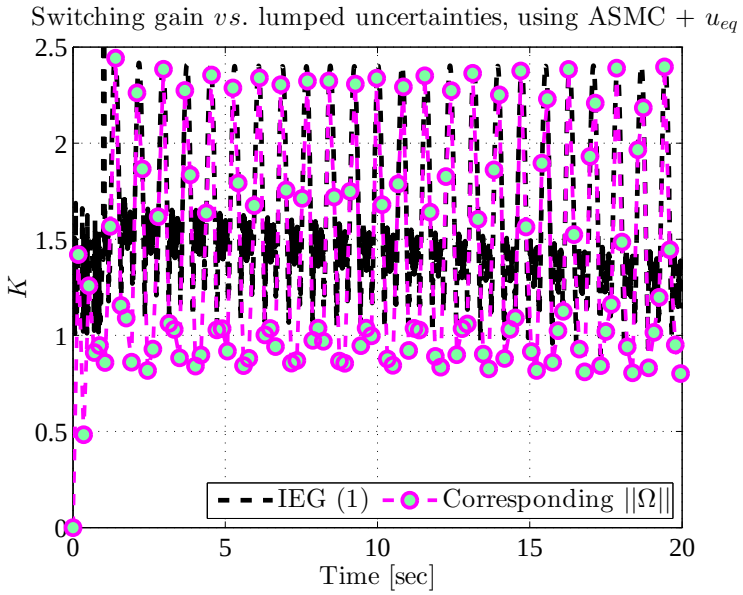

Figure 6.30: Simulation results of ASMC with equivalent control: Switching gain K *vs.* corresponding lumped uncertainty $\|\Omega\|$ using IEG (1)

Table 6.3: Simulation results: Pitch and yaw error (*i.e.*, $\tilde{\phi}$ and $\tilde{\psi}$) performance, in % of maximum displacement, using ASMC + u_{eq} with ϵ-tuning

Gain law method (paramters)		Error peak		Error RMS	
		$\tilde{\phi}$	$\tilde{\psi}$	$\tilde{\phi}$	$\tilde{\psi}$
IG-(1)	$(K(0)=1,\ \alpha=2)$	1.89	3.08	0.97	1.50
IG-(2)*	$(K(0)=1,\ \alpha=0.5)$	6.22	7.45	3.45	4.25
IEG-(1)	$(K(0)=1,\ \alpha=2,\ \beta=120)$	**0.87**	**0.59**	**0.41**	**0.24**
IEG-(2)*	$(K(0)=1,\ \alpha=0.5,\ \beta=40)$	1.58	1.15	0.75	0.63

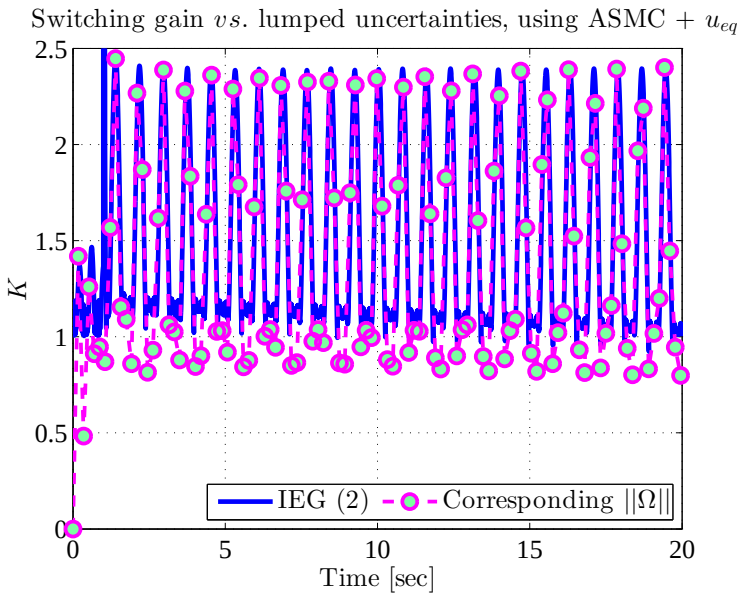

Figure 6.31: Simulation results of ASMC with equivalent control: Switching gain K *vs.* corresponding lumped uncertainty $\|\Omega\|$ using IEG (2)

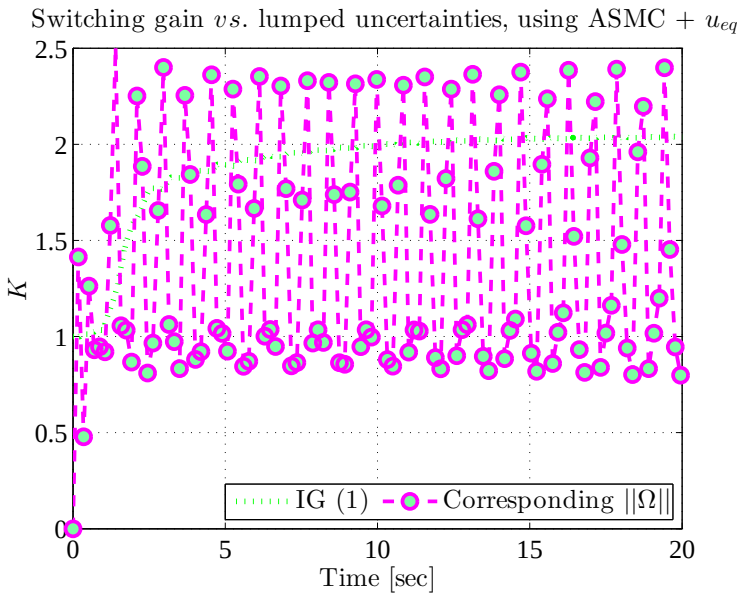

Figure 6.32: Simulation results of ASMC with equivalent control: Switching gain K *vs.* corresponding lumped uncertainty $\|\Omega\|$ using IG (1)

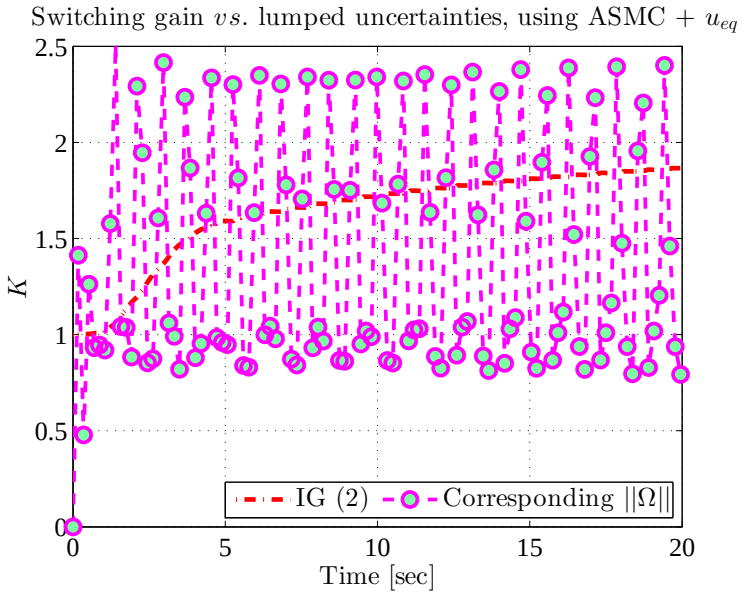

Figure 6.33: Simulation results of ASMC with equivalent control: Switching gain K *vs.* corresponding lumped uncertainty $\|\Omega\|$ using IG (2)

6.5.3 Experimental Results – 2-DOF Helicopter-Model Setup

Note that the input voltages of the front and rear motors are saturated to $\pm 24\,\mathrm{V}$ and $\pm 15\,\mathrm{V}$, respectively [21] (refer to Section 1.6 for further details about the description of this setup). The pitch angle ϕ and yaw angle ψ are still required to stabilize at zero.

First, Ψ and Γ are uncertain. The ASMC controllers are built using the switching control defined by (6.37). The parameters of the sliding dynamics are chosen as $K_P = K_I = 1$. We use a fixed-value $\epsilon = 10^{-2}$, and the ASMC parameters are chosen as $\alpha = 0.01$ and $\beta = 5$ with initial gain $K(0) = 10$ (refer to Table 6.4). The results are shown in Figures 6.34 and 6.35. One can see that, with the proposed integral-exponential algorithm, both pitch and yaw are stabilized to zero in finite time with an acceptable accuracy. The steady-state pitch and yaw angle errors obtained with the proposed design are smaller than those obtained with the existing method (refer to performances of IEG-ASMC and IG-ASMC in Table 6.4). Also, the time response with the proposed method is reduced (see Figure 6.34). Moreover, Figure 6.35 shows that the chattering magnitudes of the control inputs using the proposed algorithm are much lower than those using the existing algorithm. This phenomenon corresponds to the fact that the chattering level is proportional to the magnitude of the switching gain [61].

Table 6.4: Pitch and yaw error (*i.e.*, $\tilde{\phi}$ and $\tilde{\psi}$) performance, in % of maximum displacement, in experiments using ASMC with $\epsilon = 10^{-2}$

Gain law method (paramters)	Error peak		Error RMS	
	$\tilde{\phi}$	$\tilde{\psi}$	$\tilde{\phi}$	$\tilde{\psi}$
IG $(K(0) = 13.5,\ \alpha = 0.01)$	6.0	5.9	2.4	2.0
IEG $(K(0) = 10,\ \alpha = 0.01,\ \beta = 5)$	**3.7**	**2.4**	**1.3**	**0.9**

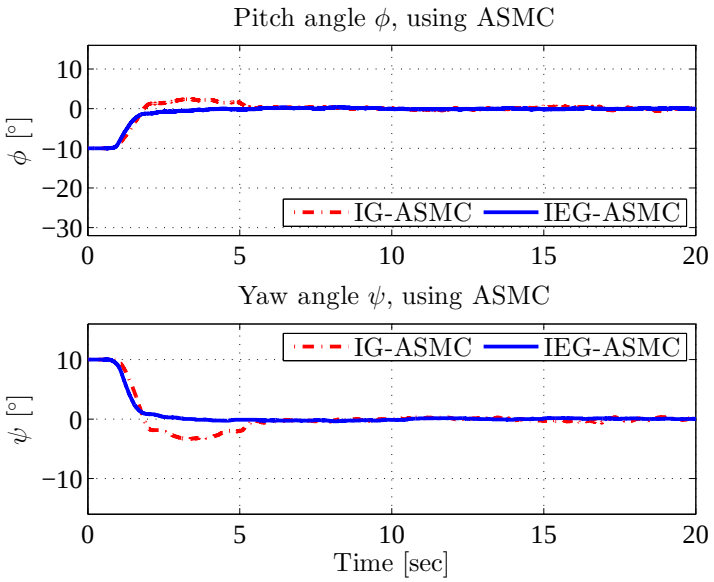

Figure 6.34: Experimental results: ϕ and ψ (left); u_1 and u_2 (right) – Using the proposed IEG-ASMC and the existing IG-ASMC [74]

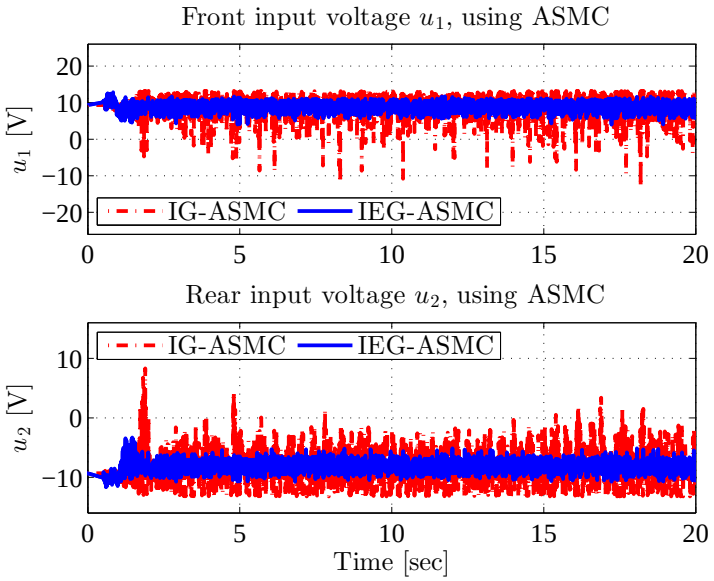

Figure 6.35: Experimental results: ϕ and ψ (left); u_1 and u_2 (right) – Using the proposed IEG-ASMC and the existing IG-ASMC [74]

The second experiments were conducted using the ASMC designs (*i.e.*, IEG-ASMC and IG-ASMC) with the equivalent control obtained from the known nominal dynamics. The parameters of the sliding dynamics were chosen to be $K_P = 4K_I = 1$. The ϵ-tuning (with $\epsilon = 4T_sK$ [16, 74]) was preferred for the IG-ASMC to reduce the chattering levels and improve the overall performance. The ASMC parameters are $\alpha = 0.5$ and $\beta = 40$ with initial gain $K(0) = 1$ (refer to Table 6.5). The results are shown in Figures 6.36 and 6.37. With the proposed algorithm, both pitch and yaw stabilized to the desired static positions at the origin with an acceptable accuracy. In contrast, by using the existing algorithm (6.33), both pitch and yaw oscillated more around the desired trajectories (see Figure 6.36). From Figure 6.37, one can note that the chattering levels of the control inputs using the proposed algorithm are much lower than those using the existing algorithm. Table 6.5 demonstrates the error performance of the different control schemes tested above. Observing all results, we conclude that the proposed algorithm always represents a better behavior in terms of accuracy, time-response and control magnitudes than the existing algorithm. Finally, we note that the inaccuracy of the given nominal dynamics creates some instability when they are used in experiments, in particular with the existing ASMC methods. The performance of the only IG-ASMC and IEG-ASMC is sufficient unless we investigate further the dynamic modeling of the actual setup. In fact, the given results of the ASMC techniques with equivalent control terms are obtained after multiple tests tentatively trying to improve the results.

Table 6.5: Pitch and yaw error (*i.e.*, $\tilde{\phi}$ and $\tilde{\psi}$) performance, in % of maximum displacement, in experiments using ASMC + u_{eq} with ϵ-tuning

Gain law method (paramters)	Error peak		Error RMS	
	$\tilde{\phi}$	$\tilde{\psi}$	$\tilde{\phi}$	$\tilde{\psi}$
IG ($K(0) = 1$, $\alpha = 0.5$)	28.3	13.8	11.5	6.5
IEG ($K(0) = 1$, $\alpha = 0.5$, $\beta = 40$)	**7.7**	**8.1**	**3.1**	**3.4**

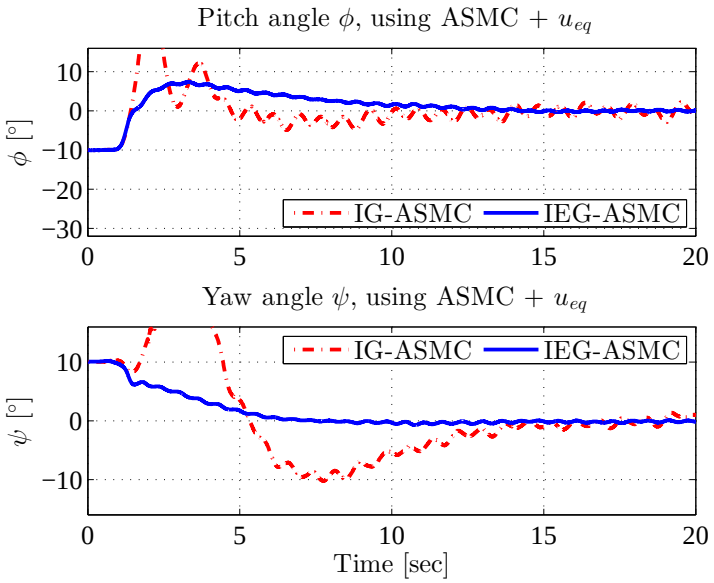

Figure 6.36: Experimental results: ϕ and ψ – Using equivalent control + IEG-ASMC and IG-ASMC

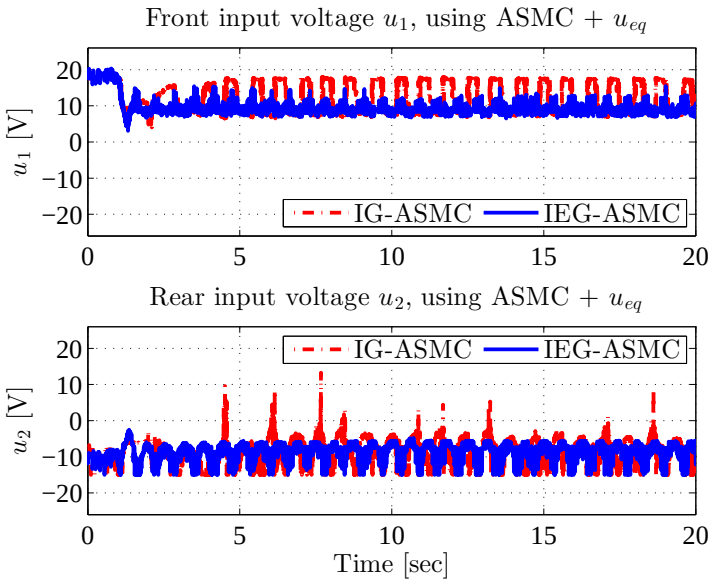

Figure 6.37: Experimental results: u_1 and u_2 – Using equivalent control + IEG-ASMC and IG-ASMC

6.6 Conclusions

The main contribution of this chapter proposes a novel adaptation law called integral-exponential gain law for ASMC. While most existing contributions dealing with ASMC designs address relatively lower response to uncertainties and/or relatively higher switching gain overestimation, the proposed algorithm provides simultaneously 'closely' the required compensating gain without *a prior* knowledge of the lumped uncertainties bounds and greatly reduces final (or post-perturbation) gain. With the proposed algorithm, the closed-loop dynamic system has fast response to perturbations. The gain overestimation is greatly reduced during the adaptation process and, consequently, the chattering level is greatly reduced. A tutorial example shows the compensating phase and the reaching phase during the adaptation process. Simulation results on a variable length pendulum and a 2-DOF helicopter model, and experimental results on the 2-DOF helicopter simulator setup demonstrate the effectiveness of the proposed new design in terms of fast response, enhanced stability and reduced chattering level. More details in terms of motivations, objectives, novelties, pros and cons of this chapter are presented in Table 6.6.

Table 6.6: Chapter 6 Recap

Motivation(s)	- The existing IG-ASMC encounters the problems of gain overestimation, robustness and chattering phenomena.
Objective(s)	- Solving the weakness of the existing IG-ASMC.
Novelty(ies)	- A new simple exponential reaching law is provided. - An ASMC design with new adaptation law, called integral-exponential gain, is proposed - New IEG-ASMC methods for different cases of MIMO systems are provided.
Pro(s)	- Fast response and robustness to perturbations. - Better accuracy. - Greatly reduced switching gain during the adaptation process. - Reduced final gain and greatly reduced chattering level.
Con(s)	- Less aggressive (*i.e.*, reduced) gains lead to relatively long settling time. - Dilemma of chattering *vs.* control performance in some cases. - Comparison to the PID control not provided. - Application to nonlinear systems with unknown polynomial bounds on the norm of the state are not investigated.

7 Application of Adaptive Sliding Mode Control to Nonlinear Systems with Uncertainties of Unknown Polynomial Bounds

In this chapter, we discuss the application of the proposed ASMC design, for a wide class of nonlinear systems with unknown polynomial bounds on uncertainty norm. An FTC-based stability solution is obtained with low chatter on control action and fast transient performance for ASMC handling the nonlinear systems with uncertainties of amplitudes bounded within unknown polynomials in the state vector norm. It prevents the instability issues that encounters the classic integral-gain-law-based ASMC when underestimating its initial gain or gain rate parameter. A simple motivation example will illustrate the convergence of the proposed ASMC. The applications of the proposed ASMC design to a nonlinear spring-mass system (simulation results), a 5-link robotic manipulator (simulation results) and the helicopter-model setup (experimental results) with stabilization and trajectory tracking control will be conducted with comparisons to the existing ASMC designs and the conventional PID control.

7.1 Introduction

In the numerous contributions of the past two decades, the uncertainties are often assumed to be bounded within possibly unknown constant bounds or affine functions. In particular, ASMC design with integral adaptation laws have been widely used in [10, 11, 13, 16, 17, 19, 57, 71, 78]. However, other com-

mon kinds of uncertain systems still exist. For instance, if their parameters are unknown, the Duffing dynamics (*i.e.*, mechanical systems with softening springs) and the tunnel-diode circuit dynamics contain uncertainties bounded by polynomial functions of the state [1]. Moreover, according to Taylor's theorem, most continuous nonlinearities can be approximated by polynomials. The new question then arises: how to control the nonlinear dynamical systems where there exist uncertainties bounded by unknown polynomials. This question motivates the studies of nonlinear systems with polynomially bounded uncertainties. If the bounds and the degree of the polynomial uncertainties are known, the stability region was analyzed in [133] and a polynomial-type dependent gain can be designed [134]. Only given the degree of the polynomial uncertainties, a high order integral-type adaptation law was discussed in [79]. However, in the case where both the degree and the bounds of the polynomial uncertainties are unknown *a priori*, to our best knowledge, no existing control method has been proposed. This chapter discusses the application of the new ASMC design introduced in the previous chapter to such a kind of nonlinear systems. The scalar case and the MIMO structures of ASMC are also provided with a theoretical proof that it has the ability to handle nonlinear systems with uncertainties of unknown polynomial bounds. It will be shown that the new approach constrains the lumped uncertainties bounded by polynomials of unknown parameters. Moreover, it confines the trajectory much close to the sliding surface and greatly reduces the overshoot by reducing the final gain. Then, the stability and robustness are improved, and the chattering is suppressed. Simulation and experimental results will demonstrate the effectiveness of the application of the new algorithm in terms of stability, fast response, smaller trajectory variation and reduced chattering level [135](paper in review, refer to Appendix C.1 for full text).

This chapter is organized as follows. In Section 7.2, we state the control problem and existing ASMC designs. Section 7.3 investigates the integral-exponential adaptation law of ASMC design for polynomial upper-bounds on norm uncertainties. An illustrative example of scalar state dynamics is presented first to motivate the proposed design. Then, theoretic results prove the stability of the closed-loop system. The applications of the proposed ASMC designs to a nonlinear spring-mass system and a robot manipulator model are shown in Sections 7.4 and 7.5, respectively, through simulation results. The application to the 2-DOF helicopter model setup is demonstrated in Section 7.6 comparing experimentally the proposed ASMC with the existing ASMC and the commonly used PID control. Section 7.7 concludes this chapter.

7.2 ASMC Problem and Existing Designs

In this section, we first state the control problem and assumptions for nonlinear systems with uncertainties upper-bounded with polynomials in the norm of the state vector. Then, we recall some existing ASMC tentatively designed.

7.2.1 Problem Statement and Assumptions

Recall the uncertain nonlinear dynamics [135]

$$\dot{x} = f(x,t) + g(x,t) \cdot u \tag{7.1}$$

where $x \in \chi$ is the state vector, with $\chi \subset \mathbb{R}^n$ a domain containing the origin, and $u \in \mathbb{R}^m$ the control input. The vector $f(x,t) \in \mathbb{R}^n$ and the matrix $g(x,t) \in \mathbb{R}^{n \times m}$ are nonlinear time-varying smooth functions containing parametric uncertainties and external disturbances [14, 16, 51, 74, 89, 90]. It is assumed that [135]:

Assumption 7.1. *The norm of the perturbation $f(x,t)$ is upper-bounded with some unknown polynomials in the state vector $x \in \chi$, and the norm of the uncertain term $g(x,t)$ is bounded by some unknown scalars. More specifically,*

$$\|f(x,t)\| \leq \sum_{i=0}^{q} a_i \|x\|^i \tag{7.2}$$

$$0 < \underline{b} \leq \|g(x,t)\| \leq \overline{b} \tag{7.3}$$

where q is an uncertain finite integer, a_i $(i = 0, 1, \cdots, q)$ have uncertain non-negative finite values, $\underline{b}$ and $\overline{b}$ are some unknown positive finite constants.

Assumption 7.1 takes into account a large class of uncertainties, including (but not limited to):

- $a_0 > 0$ and $a_i = 0 \forall i \geq 1$, *i.e.*, $\|f(x,t)\| \leq a_0$, that is, the system uncertainty is regularly bounded by a constant;
- $a_0 > 0$, $a_1 > 0$ and $a_i = 0 \forall i \geq 2$, *i.e.*, $\|f(x,t)\| \leq a_0 + a_1\|x\|$, that is, the system uncertainty is bounded by an affine function in the norm of the system state;
- $a_0 > 0$, $a_1 > 0$, $a_2 > 0$ and $a_i = 0 \forall i \geq 3$,, *i.e.*, $\|f(x,t)\| \leq a_0 + a_1\|x\| + a_2\|x\|^2$, that is, the system uncertainty is constrained by a quadratic function in the norm of the system state vector.

Let $x = 0$ be an equilibrium point for (7.1). Consider a measurable sliding vector $\sigma(x,t) \in \mathbb{R}^m$. We recall the targeted manifolds $\Sigma = \{x \in \chi : \|\sigma(x,t)\| = 0\}$ and $\Sigma_\delta = \{x \in \chi : \|\sigma(x,t)\| \leq \delta\}$ for some $\delta > 0$. Σ and Σ_δ are called "*ideal sliding* mode set" and "*real sliding* mode set" [115], respectively.

Assumption 7.2. *σ is freely designed such that, as soon as the vector $x(t)$ reaches the set Σ (resp. Σ_δ) in finite time $t = t_r > 0$ and belongs to it thereafter, (7.1) has to be stable in the ideal (resp. real) sliding mode. σ is treated as the output of (7.1) [61, 74]. In addition, we assume that there exists finite positive scalars $\gamma_1 > 0$ and $\gamma_2 \geq 0$ s.t.*

$$\|\sigma\| \geq \gamma_1 \cdot \|x\| - \gamma_2 \tag{7.4}$$

Recall the time derivative of σ along the system trajectory

$$\dot{\sigma}(x,t) = \Psi(x,t) + \Gamma(x,t) \cdot u \tag{7.5}$$

with $\Psi(x,t) \in \mathbb{R}^m$ and $\Gamma(x,t) \in \mathbb{R}^{m\times m}$. So, $\sigma(x,t)$ has a relative degree vector of $r = [1,1,\cdots,1]^T_{1\times m}$ [16,74]. Solutions of the dynamics (7.5) with discontinuous right-hand side are defined in the sense of Fillipov [119]. Without loss of generality and based on Assumption 7.1, we consider

Assumption 7.3. *The perturbation vector $\Psi \in \mathbb{R}^m$ is bounded by some unknown polynomials in x, i.e.,*

$$\|\Psi\| \leq \sum_{i=0}^{q} d_i \|x\|^i \tag{7.6}$$

where d_i $(i = 0,1,\cdots,q)$ are unknown finite non-negative constants.

Recall Assumption 6.9.

Assumption 7.4. *The uncertain matrix $\Gamma \in \mathbb{R}^{m\times m}$ is positive definite in the wider sense, i.e., its symmetric part Γ_s defined by*

$$\Gamma_s = \frac{1}{2}(\Gamma + \Gamma^T) \tag{7.7}$$

is positive definite in the regular meaning [130]. In particular, if $m = 1$, the term Γ is lower-bounded as

$$0 < \underline{\Gamma} \leq \Gamma \tag{7.8}$$

where $\underline{\Gamma}$ is a positive, finite, and eventually, unknown constant.

7.2.2 Existing ASMC Laws and Motivation

Given the dynamics (7.5) with uncertainty Ψ fully unknown (refer to Sections 4.3 and 6.2 where we discussed the relaxed scenario when part of these dynamics are known eventually), we recall the control law given by (6.37)) [74, 120]

$$u(t) = \begin{cases} -K \cdot \dfrac{\sigma}{\|\sigma\|} & \text{if } \sigma \neq 0 \\ 0 & \text{if } \sigma = 0 \end{cases} \tag{7.9}$$

where K in ASMC techniques is time-varying to adaptively compensate for the uncertainties [10,11,13–17,19]. In particular, the integral-type adaptation laws

$$\dot{K} = \alpha \cdot \|\sigma\| \tag{7.10}$$

and

$$\dot{K} = \alpha_1 \cdot \|\sigma\| + \alpha_2 \cdot \|x\| \cdot \|\sigma\| \tag{7.11}$$

have been exhaustively discussed in [11, 14, 15, 17, 19, 74, 78] and [10, 81] for the cases of uncertainties bounded by unknown constants and unknown affine functions in the state vector, respectively. The adaptation laws (7.10) and (7.11) are designed for ideal sliding mode, while the real case is treated with slightly modified versions of these forms [10, 16]. The two adaptation laws, for either ideal or real sliding mode, still have relatively large overshoots and chattering phenomena during the adaptation process. In the following, we consider mostly the ideal sliding case analysis for the sake of simplicity.

7.3 integral-exponential Reaching Law-based ASMC Design

To overcome the common weaknesses encountered by most existing ASMC forms, the integral-exponential law has been proposed and widely discussed in the previous chapter. In the following, we will prove that this ASMC design has the ability to handle nonlinear systems with upper-bounds on the norm of uncertainties of unknown polynomials in the norm of the state vector (*i.e.*, written in form (7.1) with uncertainties bounded by (7.2), (7.3) and (7.6)). First, the FTC is shown for the scalar ideal sliding case. Then, the proposed ASMC design will be adapted to the multi-dimensional case, using

the feedback control (7.9). Recall the proposed adaptation law for the ASMC design of the nonlinear systems with fully-unknown uncertainties [129, 135]

$$\dot{\breve{K}} = \alpha \cdot \|\sigma\| \tag{7.12a}$$

$$K = \breve{K} + \beta\big(e^{\|\sigma\|} - 1\big) \tag{7.12b}$$

for some $\alpha > 0$ and $\beta > 0$.

7.3.1 Scalar Case

Let us first consider the case of single-input-single-output sliding scalar dynamics (*i.e.*, $n = 1$) and select $\sigma = x$ trivially, that is, from (7.4), we have $\gamma_1 = 1$ and $\gamma_2 = 0$. Note that the norm of the sliding variable is reduced to its absolute value. Then, the feedback control (7.9) is simply defined as

$$u = -K \cdot \mathrm{sgn}(\sigma) \tag{7.13}$$

where $\mathrm{sgn}(\cdot)$ refers to the real-value signum function.

Motivation Example. Consider the following simple scalar dynamics

$$\dot{\sigma} = c_0 + c_1\sigma + c_2\sigma^2 + u \tag{7.14}$$

The state σ is to be stabilized to zero for unknown (or uncertain) coefficients c_0, c_1 and c_2. Using the switching control (7.13) with the adaptation law (7.12), the state σ of the dynamics (7.14) can be stabilized to zero in finite time for any value of the initial state σ_0 and uncertain c_0, c_1, c_2. To simulate the dynamics (7.14), these parameters are selected as $\sigma_0 = c_0 = c_1 = c_2 = 1$ (corresponding to uncertain condition I) and $\sigma_0 = c_0 = c_1 = c_2 = 5$ (corresponding to uncertain condition II). Figures 7.1-7.4 show the obtained switching gain K and the state σ using the (Old-1) existing gain law (7.10), the (Old-2) existing gain law (7.11) and the (New) proposed gain law (7.12) with the control parameter chosen as $\alpha = \alpha_1 = 2\alpha_2 = 2\beta = 2$ (see Figures 7.1 and 7.2) and $\alpha = \alpha_1 = 2\alpha_2 = 2\beta = 10$ (see Figures 7.3 and 7.4), respectively.

One can see that, by using the proposed integral-exponential gain law (7.12), σ is stabilized to zero in finite time for any initial and uncertain conditions. However, the existing integral-gain-law-based ASMC (*i.e.*, using (7.10)) and modified-integral-gain-law-based ASMC (*i.e.*, using (7.11)) only work for some situations where the control parameters are sufficiently high and the uncertain parameters are small. In fact, when α, α_1 and α_2 are small, the closed-loop dynamics (7.14) diverges. For any other large uncertain values of

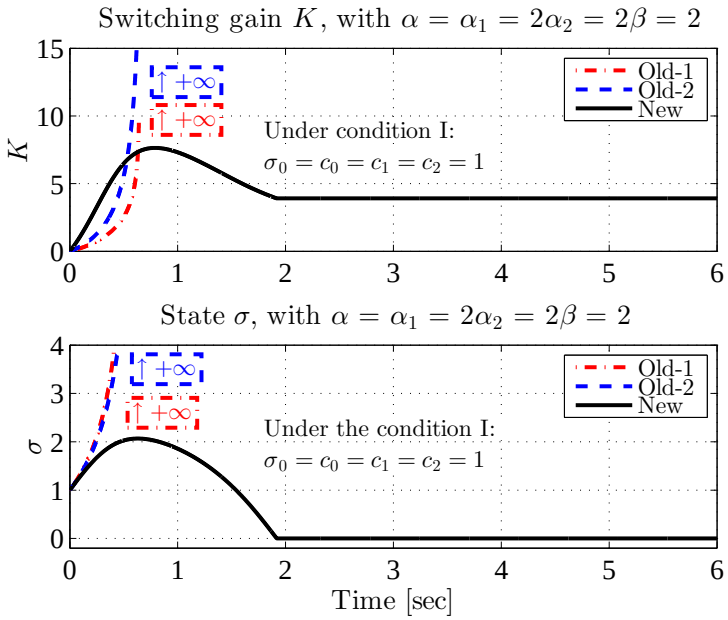

Figure 7.1: Illustrative example using the control parameters $\alpha = \alpha_1 = 2\alpha_2 = 2\beta = 2$: Switching gain K (top) and state σ (bottom) performances of the closed-loop dynamics (7.14) with (7.13) under uncertain conditions I.

σ_0, c_0, c_1, c_2, the proposed method (7.12) works even with small α and β, but the existing ASMC methods (7.10) and (7.11) do not. Furthermore, the switching gain amplitude is ultimately reduced with the new design.

Theorem 7.1. *Consider the nonlinear uncertain system* (7.1)*, with the sliding variable dynamics* (7.5)*, under Assumptions 7.1–7.4, controlled by* (7.13)*. If the gain $K(t)$ is designed as* (7.12)*, then for any initial condition $|\sigma| \neq 0$ the sliding variable σ converges to the hyper-surface $|\sigma| = 0$, i.e., x tends to the domain Σ in finite time.*

Proof. The stability analysis is similar to the case of the ideal ASMC design for bounded uncertainties discussed in Chapter 6 [118, 129]. The main difference will be highlighted in the following to deal with the general case of polynomially bounded uncertainty amounts.

From (7.5), (7.12) and (7.13), the time derivative of $|\sigma|$ along the system

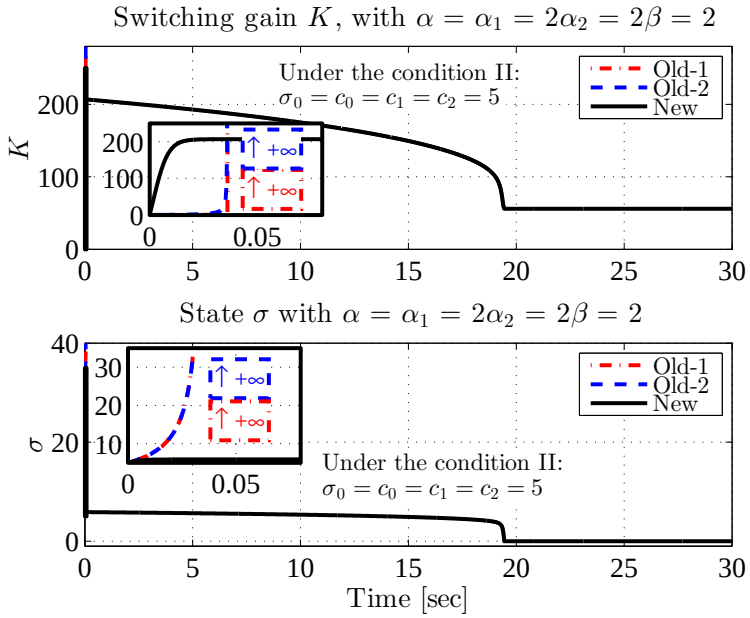

Figure 7.2: Illustrative example using the control parameters $\alpha = \alpha_1 = 2\alpha_2 = 2\beta = 2$: Switching gain K (top) and state σ (bottom) performances of the closed-loop dynamics (7.14) with (7.13) under uncertain conditions II.

trajectory is

$$\begin{aligned}\frac{d}{dt}|\sigma| &= \dot{\sigma} \cdot \operatorname{sgn}(\sigma) \\ &= \Gamma \cdot \big(h(\sigma) - \breve{K}\big)\end{aligned} \tag{7.15}$$

with $h(\sigma) = \dfrac{\Psi \cdot \operatorname{sgn}(\sigma)}{\Gamma} - \beta\big(e^{|\sigma|} - 1\big)$. Note, $h(\sigma)$ is upper-bounded, *i.e.*, there exist finite-values σ^* and $h^* = h(\sigma^*)$ *s.t.*

$$h(\sigma) \leq h^* \tag{7.16}$$

for all $|\sigma| \geq 0$ (see Appendix A.9 for details). Basically, the term $h(\sigma)$ represents a combination of the lumped system uncertainties with the exponential compensating gain of the scalar dynamics (7.5) under the feedback control (7.13) using the reaching law (7.12).

For $\sigma \neq 0$, from (7.12a), $\breve{K}(|\sigma|)$ keeps growing with a rate of, at least, $\alpha|\sigma| > 0$. Thus, the growing state gain $\breve{K}$ will be greater than (eventually

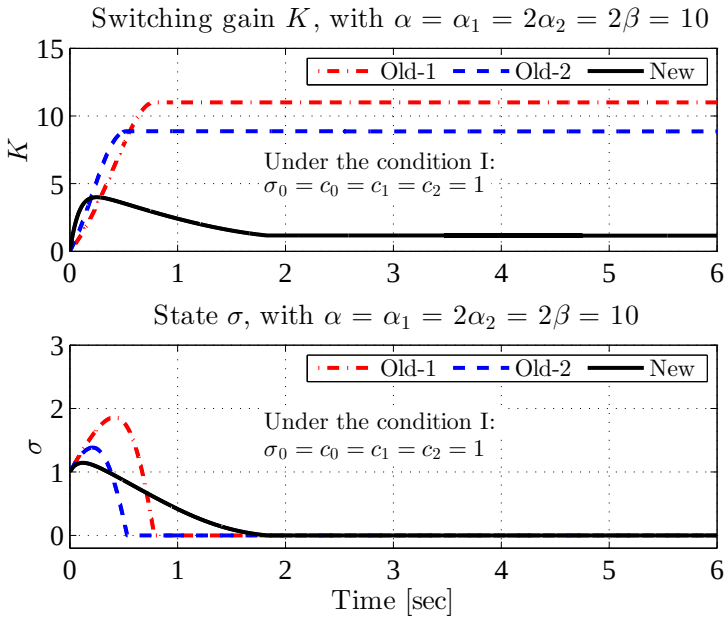

Figure 7.3: Illustrative example using the control parameters $\alpha = \alpha_1 = 2\alpha_2 = \beta = 10$: Switching gain K (top) and state σ (bottom) performances of the closed-loop dynamics (7.14) with (7.13) under uncertain conditions I.

compensate for) the bounded term $h(\sigma)$ in (7.15). Since this compensation action will occur for any $h(\sigma) \geq \breve{K}$ (*i.e.*, $\frac{d}{dt}|\sigma| \geq 0$) and $\sigma \neq 0$, we can conclude that there always exist a positive scalar κ_0 and an ultimate time instant $t^* \geq 0$ *s.t.*

$$h(\sigma) + \kappa_0 < \breve{K} \tag{7.17}$$

for all $t \geq t^*$. Then,

$$\frac{d}{dt}|\sigma| \leq -\Gamma\kappa_0 \leq -\underline{\Gamma}\kappa_0 \tag{7.18}$$

for $t \geq t^*$. We conclude that $|\sigma|$ converges to the domain Σ in finite time [1]. □

Unlike most ASMC designs dealing with bounded uncertainties [11,14–17, 19,78] or affine-function uncertainties [10,61,79–81], this work deals with unknown polynomially bounded uncertainties in the norm of state vector, which are more general than bounded uncertainties and affine-function uncertainties.

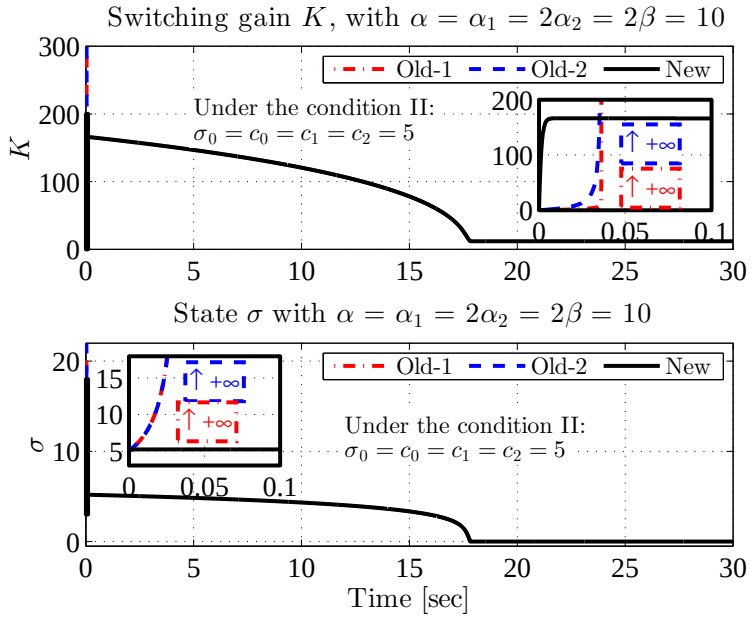

Figure 7.4: Illustrative example using the control parameters $\alpha = \alpha_1 = 2\alpha_2 = \beta = 10$: Switching gain K (top) and state σ (bottom) performances of the closed-loop dynamics (7.14) with (7.13) under uncertain conditions II.

The new design (7.12) provides simultaneous fast response and chattering reduction. The first part, *i.e.*, integration term $\breve{K}$, provides the ability to compensate for uncertainties with unknown polynomial bounds and forces the sliding variable to converge to the domain Σ in finite time. Furthermore, it should be pointed out that the dynamic term (7.12a) remains necessary to guarantee FTC; otherwise, it only guarantees UUB solutions. One can test that, without the integral term (*i.e.*, $\alpha = 0$ in (7.12)), the state is only UUB. The results of the application of the design (7.12) for the illustrative model dynamics (7.14) when $\alpha = 0$ are shown in Appendix B.2.

7.3.2 Multi-dimensional Case

Substituting (7.9) into (7.5), we obtain for $\sigma \neq 0$

$$\dot{\sigma} = \Psi - \frac{K}{\|\sigma\|}\Gamma\sigma \tag{7.19}$$

We state the following theorem [135].

Theorem 7.2. *Consider the nonlinear uncertain system* (7.1)*, with the closed-loop sliding dynamics* (7.19)*, under Assumptions 7.1–7.4. If the gain* $K(t)$ *is designed as* (7.12)*, then for any initial condition* $\|\sigma\| \neq 0$ *the sliding variable* σ *converges to the manifold* $\|\sigma\| = 0$*, i.e.,* $x \in \Sigma$ *in finite time.*

Proof. Let the positive definite function

$$V = \sigma^T \sigma \tag{7.20}$$

be a Lyapunov function candidate. Using (7.7), (7.12) and (7.19), for $\sigma \neq 0$, the time derivative of V along the system trajectories is

$$\begin{aligned} \dot{V} &= 2\sigma^T \dot{\sigma} \\ &= 2\|\sigma\| \Big(\frac{\sigma^T \Psi}{\|\sigma\|} - \beta \big(e^{\|\sigma\|} - 1\big) \frac{\sigma^T \Gamma_s \sigma}{\sigma^T \sigma} - \breve{K} \frac{\sigma^T \Gamma_s \sigma}{\sigma^T \sigma} \Big) \end{aligned} \tag{7.21}$$

We denote by $h_s(\sigma) = \dfrac{\sigma^T \Psi}{\|\sigma\|} - \beta\big(e^{\|\sigma\|} - 1\big) \dfrac{\sigma^T \Gamma_s \sigma}{\sigma^T \sigma}$. For $\sigma \neq 0$, (7.21) can be rewritten as

$$\frac{\dot{V}}{2\sqrt{V}} = h_{\Gamma_s}(\sigma) - \breve{K} \frac{\sigma^T \Gamma_s \sigma}{\sigma^T \sigma} \tag{7.22}$$

Using (7.4) and (7.6), the scalar $h_s(\sigma)$ is upper-bounded. In fact,

$$h_s(\sigma) \leq \sum_{i=0}^{q} d_i \|x\|^i - \beta \big(\frac{e^{\gamma_1 \|x\|}}{e^{\gamma_2}} - 1 \big) \underline{\lambda}(\Gamma_s) \tag{7.23}$$

with $\underline{\lambda}(\Gamma_s)$ denoting the minimum eigenvalue of the symmetric positive definite matrix Γ_s (refer to Assumption 7.4). Note that, a positive exponential function ultimately grows faster than any polynomial (refer to proof shown in Appendix A.9 for more details). For any $\sigma \neq 0$, from (7.12), $\breve{K}$ keeps growing and the positive scalar $\breve{K} \dfrac{\sigma^T \Gamma_s \sigma}{\sigma^T \sigma}$ in (7.22) will eventually compensate for the upper-bounded $h_s(\sigma)$, *i.e.*, $\breve{K} \dfrac{\sigma^T \Gamma_s \sigma}{\sigma^T \sigma} > h_s(\sigma)$. Since this compensating action will occur for any $\|\sigma\| \neq 0$ where $h_s(\sigma) \geq \breve{K} \dfrac{\sigma^T \Gamma_s \sigma}{\sigma^T \sigma}$ (*i.e.*, from (7.21) and (7.23), $\dfrac{d}{dt}\|\sigma\| \equiv \dfrac{\dot{V}}{2\sqrt{V}} \geq 0$), we conclude that there exist a time instant t^* and a positive scalar κ_1 *s.t.*, for $t \geq t^*$

$$\breve{K} \frac{\sigma^T \Gamma_s \sigma}{\sigma^T \sigma} \geq h_s(\sigma) + \kappa_1 \tag{7.24}$$

Thus, from (7.20), (7.21), (7.23) and (7.24), we obtain

$$\frac{d}{dt}\|\sigma\| \leq -\kappa_1 \tag{7.25}$$

for $t \geq t^*$. Now, by integrating both sides of (7.25) between t^* and $t \geq t^*$, we obtain

$$\|\sigma\| \leq -\kappa_1 \cdot \left(t - t^*\right) + \|\sigma(t^*)\|$$

Then, $\|\sigma\|$ is decreasing with a rate κ_1 and reaches the domain $\|\sigma\| = 0$ in finite time [1]. □

The proof discussed above is effectively based on Assumption 7.2. We note that whenever the design condition (7.4) is violated numerically or analytically, a modified version of the switching gain law can still exist to keep the main properties of the proposed integral-exponential design regarding the compensation of uncertainties upper-bounded with polynomials in the norm of the state vector. In fact, substituting $e^{\gamma\|x\|}$ for $e^{\|\sigma\|}$ in (7.12b), for some small positive scalar γ, would keep possible the compensation for the class of perturbations mainly discussed in this paper (refer to Assumptions 7.2 and 7.3).

From the condition (7.8), we note that the uncertain gain matrix Γ matching with the input u in (7.5) does not require any upper-boundedness on its norm magnitude allowing definitely unlimited uncertainty levels of this term as long as it is nonzero (or nonsingular matrix in the wider sense).

Finally, we note that when the parameter matrix Γ is indefinite (*i.e.*, neither positive definite nor negative definite), the control defined by (7.9) is not appropriate. In this case, it is required to define a nonsingular matrix $\hat{\Gamma}$ alluding to the nominal value of Γ. Moreover, we assume that the matrix $L(t) = \hat{\Gamma}^{-1}\Gamma$ is positive definite in the wider sense, *i.e.*, the symmetric part $L_s = \frac{1}{2}(L + L^T)$ is positive definite in the regular meaning [130]. Note that the positiveness of L implies that the value of the nominal matrix $\hat{\Gamma}$ is close to that of its real matrix Γ. Then, by replacing σ with $\hat{\Gamma}^T\sigma$ in the control law (7.9) as [120]

$$u(t) = \begin{cases} -K \cdot \dfrac{\hat{\Gamma}^T\sigma}{\|\hat{\Gamma}^T\sigma\|} & \text{if } \sigma \neq 0 \\ 0 & \text{if } \sigma = 0 \end{cases} \tag{7.26}$$

and applying the adaptation law (7.12), we guarantee the FTC of the states to the targeted manifold Σ. By substituting (7.26) into (7.5), we obtain, for $\sigma \neq 0$

$$\dot{\sigma} = \Psi - \Gamma K(t) \cdot \frac{\hat{\Gamma}^T \sigma}{\|\hat{\Gamma}^T \sigma\|} \tag{7.27}$$

Then, we state the following theorem

Theorem 7.3. *Consider the nonlinear uncertain system* (7.1)*, subject to the closed-loop dynamics* (7.27)*, under Assumptions 7.1–7.3. Given* $L_s = \frac{1}{2}(L + L^T)$ *a symmetric positive definite matrix with* $L(t) = \hat{\Gamma}^{-1}\Gamma$*, if the gain* $K(t)$ *is designed as* (7.12)*, then for any initial condition* $\|\sigma\| \neq 0$ *the sliding variable* σ *converges to the sliding surface* $\|\sigma\| = 0$*, i.e.,* $x \in \Sigma$ *in finite time.*

Proof. See Appendix A.10. □

7.3.3 Case of Real Sliding Mode

To avoid the wind-up phenomenon [16], the ideal ASMC design should be modified for the real implementation. Consider the real sliding set Σ_δ defined in Section 7.2. Recall the dynamic gain design of (6.35) [118, 129]

$$\dot{\breve{K}} = \alpha \|\sigma\| \cdot \operatorname{sgn}\big(\|\sigma\| - \epsilon\big) \tag{7.28a}$$

$$K = \breve{K} + \beta \cdot \big(e^{\|\sigma\|} - 1\big) \tag{7.28b}$$

If $\beta = 0$, then (7.28) is reduced to the integral gain law presented in [74]. We obtain the following theorem in the case of real ASMC design [135].

Theorem 7.4. *Consider the nonlinear uncertain system* (7.1)*, with the sliding dynamics* (7.5)*, under Assumptions 7.1–7.4, controlled by* (7.9)*. If the gain* $K(t)$ *is designed as* (7.28)*, then for any initial condition* $\|\sigma\| > \epsilon$ *the sliding variable* σ *converges to the domain* $\|\sigma\| \leq \epsilon$ *and stays on the domain* $\|\sigma\| \leq \delta$*, i.e.,* $x \in \Sigma_\delta$ *in finite time.*

Proof. It remains drastically identical to the proof of theorem 7.2. □

In the following sections, we validate the effectiveness of the proposed scheme, by considering the dynamics of a nonlinear mass-spring system model as depicted from [136], a five-link robot manipulator with uncertain dynamics and a 2-DOF helicopter simulator model actuated with two propellers [21].

7.4 Applications – Stabilization and Trajectory Tracking Control for a Nonlinear Mass-Spring System

7.4.1 Modelling

The nonlinear mass-spring system consists of two masses m_1 and m_2 connected by a linear-cubic spring. We denote by x_1 and x_2 the positions of the masses. The nonlinear dynamics of the system can be written as [136]

$$m_1\ddot{x}_1 + k_1(x_1 - x_2) + k_2(x_1 - x_2)^3 = u_1 \tag{7.29a}$$

$$m_2\ddot{x}_2 - k_1(x_1 - x_2) - k_2(x_1 - x_2)^3 = u_2 \tag{7.29b}$$

or

$$M\ddot{x} + K_1 x + k_2 f(x) = u \tag{7.30}$$

with $u = \begin{pmatrix} x_1 & x_2 \end{pmatrix}^T$ and $u = \begin{pmatrix} u_1 & u_2 \end{pmatrix}^T$. We have

$$M = \begin{pmatrix} m_1 & 0 \\ 0 & m_2 \end{pmatrix}, \quad K_1 = \begin{pmatrix} k_1 & -k_1 \\ -k_1 & k_1 \end{pmatrix}, \quad f(x) = \begin{pmatrix} (x_1 - x_2)^3 \\ -(x_1 - x_2)^3 \end{pmatrix} \tag{7.31}$$

The mass and spring constant variations are $0.5 < m_1 < 1.5$, $0.5 < m_2 < 1.5$, $0.5 < k_1 < 2$ and $-0.5 < k_2 < 0.2$, with nominal values $\hat{m}_1 = \hat{m}_2 = \hat{k}_1 = 1$ and $\hat{k}_2 = -0.1$ [136]. Note that M is a positive definite diagonal matrix and $f(x)$ is a cubic polynomial in the system states.

7.4.2 Sliding Variable Design

It is desired that the system follows a trajectory x_d. Denote by $\tilde{x} = x - x_d$ the trajectory error. Assuming that the positions and velocities of the two masses are measurable, we design a PID sliding variable [11]

$$\sigma = K_p\tilde{x} + K_i \int \tilde{x} d\tau + K_d\dot{\tilde{x}} \tag{7.32}$$

with K_p, K_i and K_d positive definite matrices of $\mathbb{R}^{2\times 2}$. Taking the time derivative of both sides of (7.32) and substituting (7.30), the sliding variable dynamics can be written as

$$\dot{\sigma} = K_p\dot{\tilde{x}} + K_i\tilde{x} + K_d M^{-1} \cdot \left(u - K_1 x - k_2 f(x) - M\ddot{x}_d\right) \tag{7.33}$$

7.4.3 Equivalent Control

Consider partitions $M = \hat{M} + \tilde{M}$, $K_1 = \hat{K}_1 + \tilde{K}_1$ and $k_2 = \hat{k}_2 + \tilde{k}_2$ where $\hat{M}$, $\hat{K}_1$ and $\hat{k}_2$ are the nominal values of M, K_1 and k_2, and $\tilde{M}$, $\tilde{K}_1$ and $\tilde{k}_2$ their corresponding uncertain values. We apply the equivalent control method where the control input consists of a combination of a smooth nonlinear control input and a switching control input [120], as

$$u = u_{eq} + u_{sw} \tag{7.34}$$

u_{eq} is obtained by assuming that all uncertainties vanish at the permanent sliding regime, *i.e.*, $M = \hat{M}$, $K_1 = \hat{K}_1$, $k_2 = \hat{k}_2$ and $\dot{\sigma} = 0$. We write from (7.33)

$$0 = K_p\dot{\tilde{x}} + K_i\tilde{x} + K_d\hat{M}^{-1} \cdot \left(u_{eq} - \hat{K}_1 x - \hat{k}_2 f(x) - \hat{M}\ddot{x}_d\right) \tag{7.35}$$

that is,

$$u_{eq} = \hat{K}_1 x + \hat{k}_2 f(x) + \hat{M}\ddot{x}_d - \hat{M}K_d^{-1} \cdot \left(K_p\dot{\tilde{x}} + K_i\tilde{x}\right) \tag{7.36}$$

Substituting (7.36) into (7.33), we obtain the sliding variable dynamics in terms of the switching control (refer to the general form (7.5))

$$\dot{\sigma}(x,t) = \Psi(x,t) + \Gamma(x,t) \cdot u_{sw} \tag{7.37}$$

with

$$\begin{aligned}\Psi(x,t) = {} & K_d M^{-1}\tilde{M}K_d^{-1} \cdot \left(K_p\dot{\tilde{x}} + K_i\tilde{x}\right) + \\ & K_d M^{-1} \cdot \left(- \tilde{K}_1 x - \tilde{k}_2 f(x) - \tilde{M}\ddot{x}_d\right)\end{aligned} \tag{7.38}$$

and

$$\Gamma(x,t) = K_d M^{-1} \tag{7.39}$$

Note that $f(x)$ in (7.38) contains a cubic polynomial of the state x and $\tilde{k}_2$ is an uncertain parameter. That is, $\Psi(x,t)$ is an uncertainty bounded within an unknown-coefficient-cubic polynomial. Since the diagonal matrix M and the matrix K_d are positive definite of $\mathbb{R}^{2\times 2}$, then Γ is positive definite. Based on Theorem 7.2, we apply the switching control u_{sw} in form (7.9) with the adaptation law (7.28).

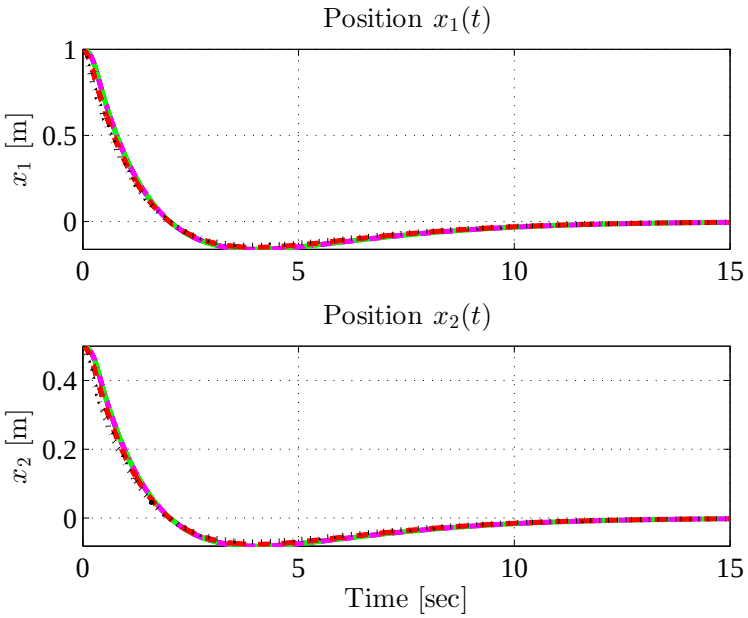

Figure 7.5: Simulation results of nonlinear mass-spring system – Position stabilization. Results in real sliding mode using the existing IG-ASMC, *i.e.*, adaptation law (7.28) with $\beta = 0$ (solid green for fixed ϵ and dash-dot magenta for ϵ–tuning) and proposed IEG-ASMC, *i.e.*, adaptation law (7.28) with $\beta > 0$ (dash red for $\beta = 2$ and dot black for $\beta = 20$).

7.4.4 Simulation Results

First, the two masses m_1 and m_2 are stabilized at the origin. Then, in the second simulations, they are desired to follow trajectories $x_{d1} = \sin(\pi t + \frac{\pi}{2})$ and $x_{d2} = 0.5\sin(\pi t + \frac{\pi}{2})$, respectively. Given, a sampling period $T_s = 5 \cdot 10^{-3}$ and PID matrix gains selected as $K_p = 4K_i = K_d = I_2$, we apply the real ASMC design using the proposed reaching law (7.28) (refer to as IEG-ASMC), with a fixed boundary-layer limit $\epsilon = 10^{-3}$, $\alpha = 10$, and applying $\beta = 2$ and 20. Then, we compare its performance to the existing adaptation gain dynamics discussed in [16, 74] (*i.e.*, (7.28) with $\beta = 0$, refer to as IG-ASMC), using $\alpha = 10$, with boundary-layer limit fixed at $\epsilon = 10^{-3}$, and varying ϵ-tuning [16]. The simulation results are shown in Figures 7.5 to 7.10. From Figure 7.5, one can see that there is no significant difference in terms of stabilization and accuracy for all ASMC implementations. However, the magnitudes and

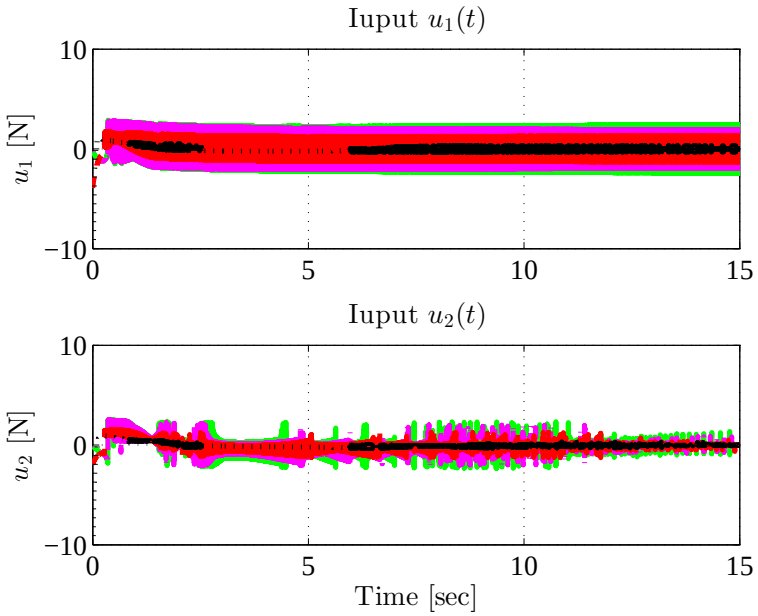

Figure 7.6: Simulation results of nonlinear mass-spring system – Control inputs in position stabilization. Results in real sliding mode using the existing IG-ASMC, *i.e.*, adaptation law (7.28) with $\beta = 0$ (solid green for fixed ϵ and dash-dot magenta for ϵ–tuning) and proposed IEG-ASMC, *i.e.*, adaptation law (7.28) with $\beta > 0$ (dash red for $\beta = 2$ and dot black for $\beta = 20$).

chattering levels of the corresponding control inputs in the proposed IEG-ASMC are much less than those in the existing IG-ASMC (see Figure 7.6). From Figures 7.8 and 7.9, one can see that, compared to those using the existing ASMC, both the trajectory errors and the magnitudes of the control inputs (as well as the chattering levels) when using the proposed ASMC (7.28) are reduced simultaneously. The tracking of the first mass displacement x_1 with the proposed design is much faster than with the existing ones. The switching gain magnitudes are much lower with the proposed design for both position stabilization and trajectory tracking (see Figures 7.7 and 7.10).

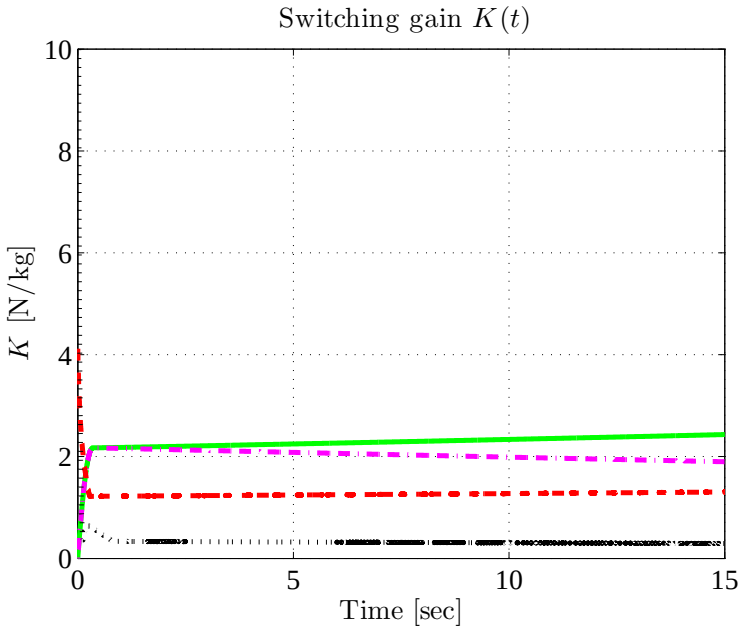

Figure 7.7: Simulation results of nonlinear mass-spring system – Switching gains in position stabilization. Results in real sliding mode using the existing IG-ASMC, *i.e.*, adaptation law (7.28) with $\beta = 0$ (solid green for fixed ϵ and dash-dot magenta for ϵ–tuning) and proposed IEG-ASMC, *i.e.*, adaptation law (7.28) with $\beta > 0$ (dash red for $\beta = 2$ and dot black for $\beta = 20$).

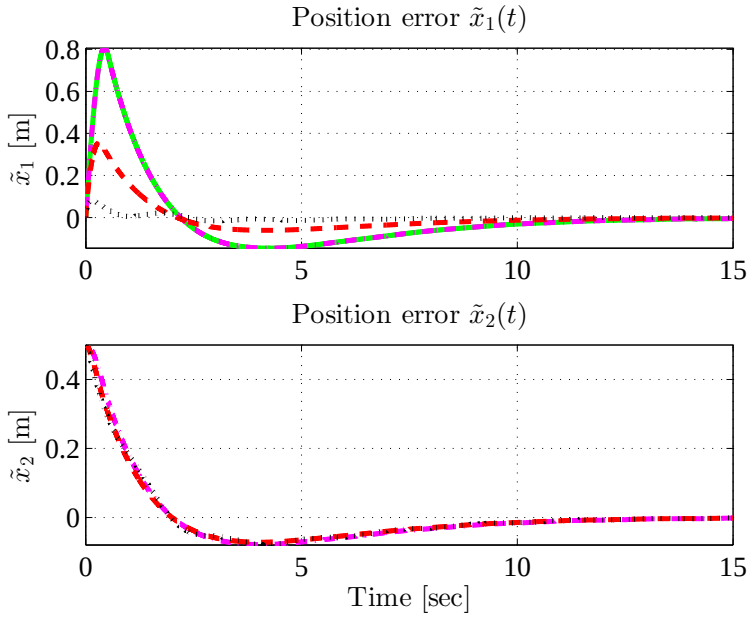

Figure 7.8: Simulation results of nonlinear mass-spring system – Trajectory errors in tracking control of sine waves. Results in real sliding mode using the existing IG-ASMC, *i.e.*, adaptation law (7.28) with $\beta = 0$ (solid green for fixed ϵ and dash-dot magenta for ϵ–tuning) and proposed IEG-ASMC, *i.e.*, adaptation law (7.28) with $\beta > 0$ (dash red for $\beta = 2$ and dot black for $\beta = 20$).

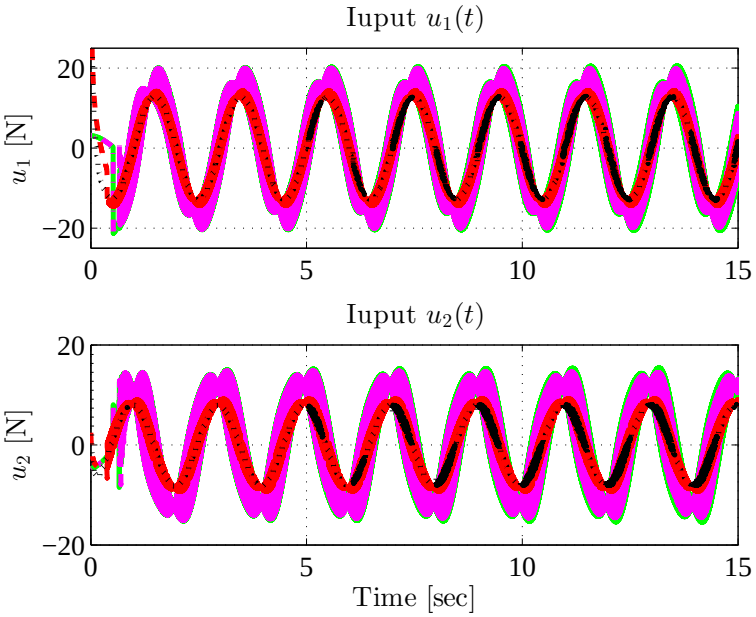

Figure 7.9: Simulation results of nonlinear mass-spring system – Control inputs in tracking control of sine waves. Results in real sliding mode using the existing IG-ASMC, *i.e.*, adaptation law (7.28) with $\beta = 0$ (solid green for fixed ϵ and dash-dot magenta for ϵ–tuning) and proposed IEG-ASMC, *i.e.*, adaptation law (7.28) with $\beta > 0$ (dash red for $\beta = 2$ and dot black for $\beta = 20$).

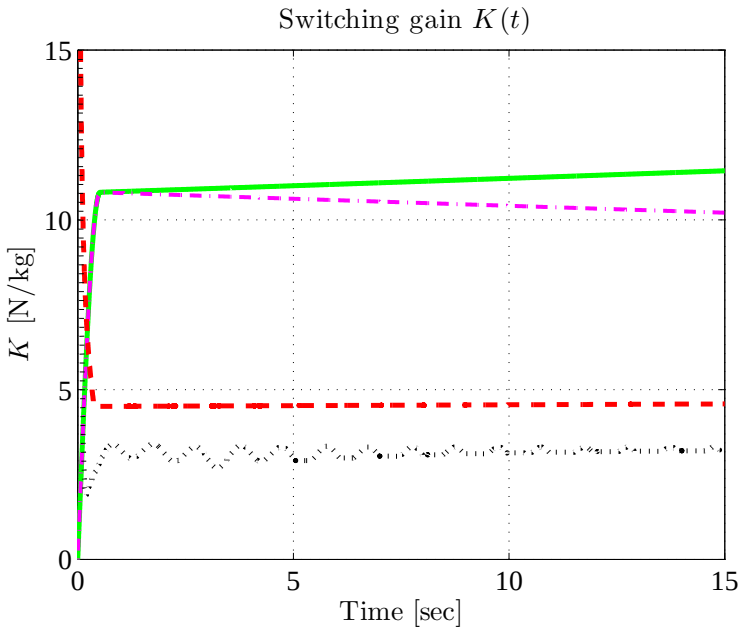

Figure 7.10: Simulation results of nonlinear mass-spring system – Switching gains in trajectory tracking control of sine waves. Results in real sliding mode using the existing IG-ASMC, *i.e.*, adaptation law (7.28) with $\beta = 0$ (solid green for fixed ϵ and dash-dot magenta for ϵ–tuning) and proposed IEG-ASMC, *i.e.*, adaptation law (7.28) with $\beta > 0$ (dash red for $\beta = 2$ and dot black for $\beta = 20$).

7.5 Applications – Trajectory Tracking Control of Robot Manipulators

In the following, we discuss the trajectory tracking control of a five-link robot manipulator with uncertain dynamics by applying the proposed ASMC design with integral-exponential adaptation law.

7.5.1 Robot Model

Consider the dynamics of an $m-$link rigid robotic manipulator [52, 85]

$$M(q)\ddot{q} + C(q,\dot{q})\dot{q} + G(q) = u + d(t) \tag{7.40}$$

where $q \in \mathbb{R}^m$ refers to the $m-$dimensional vector of joint angles, $d(t)$ is the vector of the bounded input disturbance, and $u \in \mathbb{R}^m$ is the applied torque vector. $M(q)$ is the inertia matrix, $C(q,\dot{q})\dot{q}$ the vector of Coriolis and centrifugal forces, and $G(q)$ the vector of gravitational forces [85]. Note that, in most robot systems, Assumption 7.1 is satisfied.

When reliable nominal terms of the robot dynamics are available, the equivalent control method discussed in Chapter 4.3 can be combined with the ASMC to deal with known dynamics in order to reduce the effect of lumped uncertainties. The equivalent control of robot manipulators is shown in Appendix A.11. Here, we consider simply the case where the reliable nominal terms of the robot dynamics are unavailable, *i.e.*, the terms $M(q)$, $C(q,\dot{q})$ and $G(q)$ are fully uncertain except that $M(q)$ is positive definite [52, 85].

7.5.2 Sliding Variable and Sliding Surface Design

The trajectory tracking problem of the robot manipulator can be formulated as follows: given q_d twice differentiable desired bounded trajectory of $\mathbb{R}^m$, define the trajectory error as

$$e = q - q_d \tag{7.41}$$

The error dynamics corresponding to (7.40) is

$$\ddot{e} = -\ddot{q}_d - M^{-1}(C\dot{q} + G) + M^{-1}d(t) + M^{-1}u \tag{7.42}$$

The control objective is to find a feedback control law u such that the output q tracks the desired trajectory q_d, and the tracking error e converges to zero exponentially or in finite time. For this purpose, different schemes of sliding variable dynamics have been presented in [132, 137, 138]. In particular, the

sliding surface design along with comments on the existing TSM methods has been exhaustively discussed in [138]. We define the new state σ as

$$\sigma = \dot{e} + D \cdot e \tag{7.43}$$

Consider the time derivative of σ. By using (7.42) and (7.43), we obtain the sliding variable dynamics

$$\dot{\sigma} = -\ddot{q}_d - M^{-1}(C\dot{q} + G) + M^{-1}d(t) + D \cdot \dot{e} + M^{-1}u \tag{7.44}$$

Based on the fact that the inertia matrix is positive definite (see *e.g.*, [52, 85]) and by assuming the boundedness of the desired trajectories, one can see that the dynamics (7.44) can be written in form (7.5) with

$$\Psi(t) = -\ddot{q}_d - M^{-1}(C\dot{q} + G) + M^{-1}d(t) + D \cdot \dot{e} \tag{7.45}$$

$$\Gamma(t) = M^{-1} > 0 \tag{7.46}$$

Then, we apply the unit control (7.9).

7.5.3 Simulation Results

The five-link robot manipulator to be controlled is designed using Simmechanics (see in Figure 7.11). We compare the performance of the proposed control scheme (7.28) with the existing ASMC (7.11) in real sliding mode, *i.e.*, integral-type adaptation law [79, 80, 83, 139] combined with the boundary layer method

$$\dot{K} = \big(\alpha_1 \cdot \|\sigma\| + \alpha_2 \cdot \|x\| \cdot \|\sigma\|\big) \cdot \mathrm{sgn}\big(\|\sigma\| - \epsilon\big) \tag{7.47}$$

and a simple joint-independent PID control [85]. The parameters for the proposed ASMC (7.28) and the existing ASMC (7.47) are set as $\alpha = \alpha_1 = \alpha_2 = 1$ and $\beta = 50$. For fully uncertainties Ψ and Γ, we use a fixed $\epsilon = 0.1$. The parameters for PID control are chosen from a similar design presented in [140] (see Table 7.1). The trajectories to be followed by each joint are shown in Figure 7.12.

The position errors from link #1 to link #5 and the corresponding control inputs are presented in Figures 7.13-7.17 where ASMC (1) in green dashed lines refers to the results of ASMC by using the existing reaching law (7.47), ASMC (2) in black solid lines refers to the results of ASMC by using the proposed reaching law (7.28), and the magenta dash-dot lines refer to the results of the PID control. It can be seen that the existing ASMC (7.47) has the largest position errors and chatter levels during the ASMC process. The position

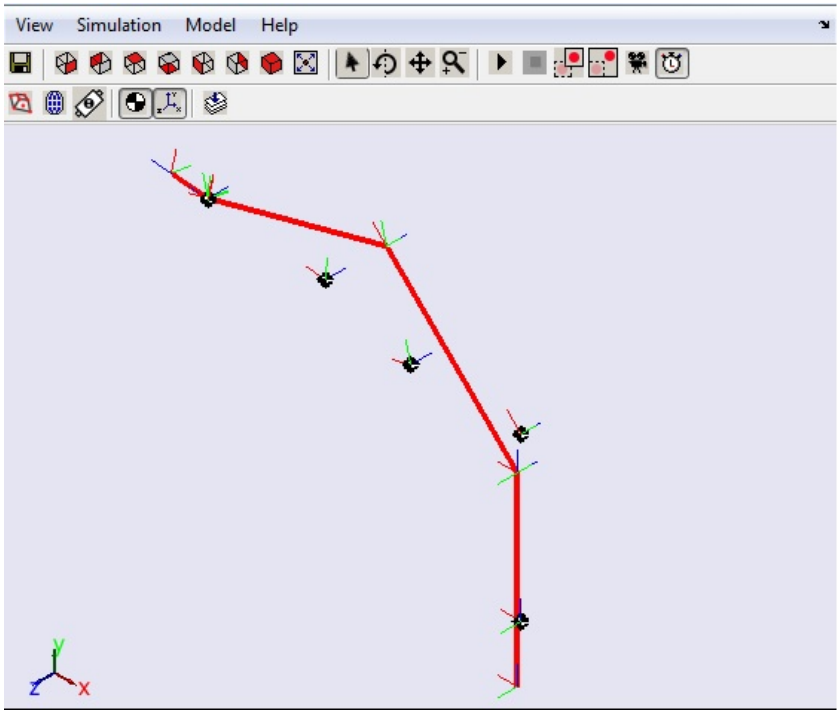

Figure 7.11: Five-link robot manipulator

Table 7.1: Trajectory tracking control on robot manipulators: PID control parameters [140]

Link #	1	2	3	4	5
k_p	81.1	81.1	81.1	81.1	81.1
k_i	20.1	20.1	20.1	20.1	562.4
k_d	15.6	15.6	15.6	15.6	15.6

errors for the existing ASMC (7.47) are also relatively large at the beginning of the ASMC process. The recommended PID control experiences smooth control actions (*i.e.*, low levels of chatter) and, however, relatively large position errors. The proposed ASMC design allows accurate tracking trajectories with reasonably smooth control actions. The results clearly demonstrate that the proposed scheme is capable of solving the robust tracking problem on robotic manipulators. Many advantages can be depicted from the proposed controllers. The resulting closed-loop dynamic system has fast response to

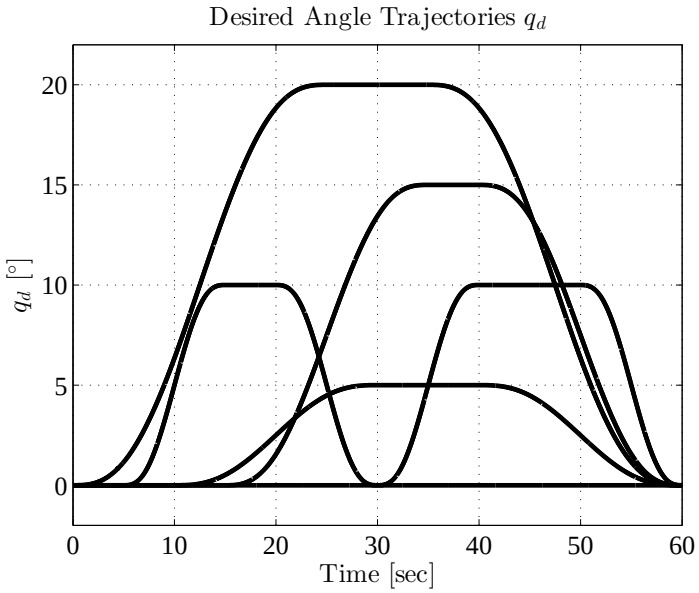

Figure 7.12: Desired trajectories q_{d_i}, for $i = 1 \dots 5$

uncertainties, while the accuracy and stability are well enhanced. The control term does not require the computation of the inverse of the matrix $M(q)$. Skew symmetry, passivity and linearity *w.r.t.* the parameters are not exploited in the proposed design. Knowledge of upper bounds of perturbations, including the input gain matrix, is not required *a priori*.

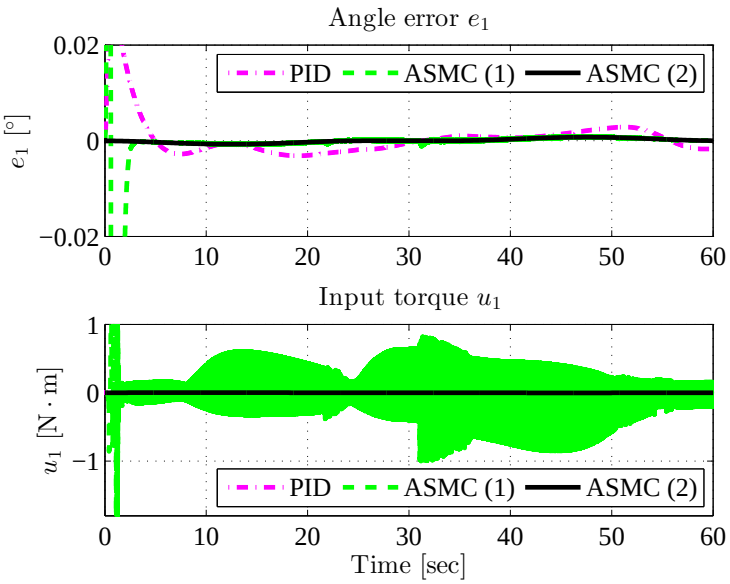

Figure 7.13: Trajectory tracking control on robot manipulators – Angular position error e_1 and control input u_1

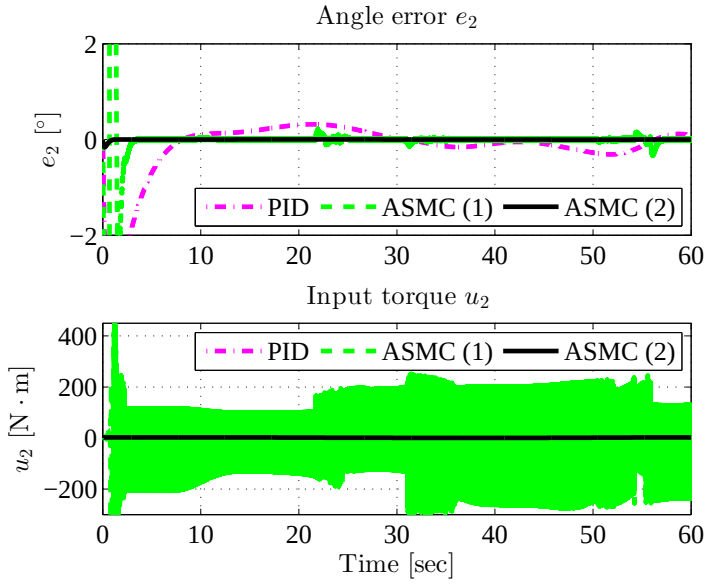

Figure 7.14: Trajectory tracking control on robot manipulators – Angular position error e_2 and control input u_2

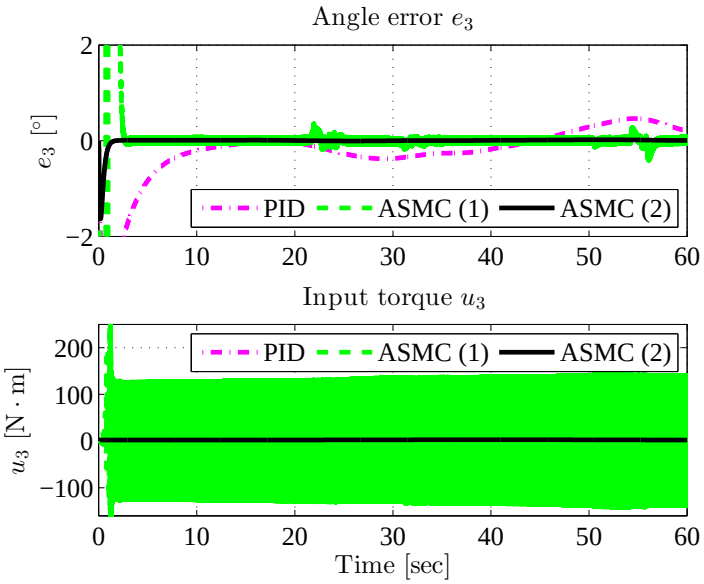

Figure 7.15: Trajectory tracking control on robot manipulators – Angular position error e_3 and control input u_3

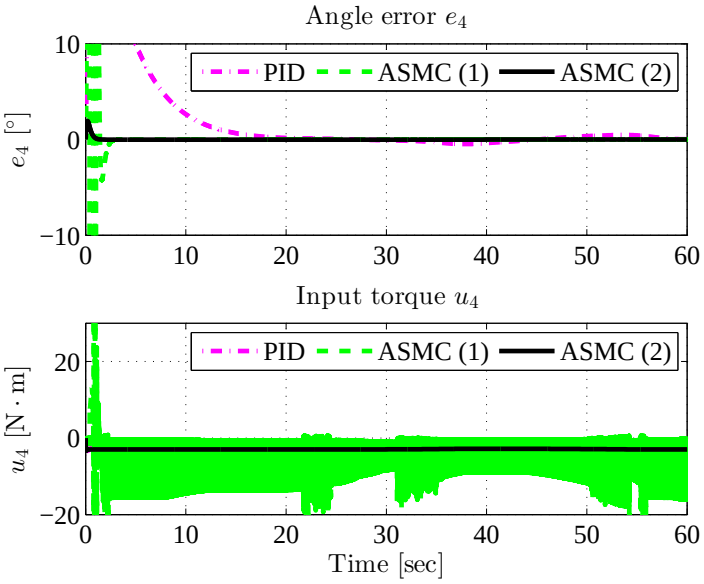

Figure 7.16: Trajectory tracking control on robot manipulators – Angular position error e_4 and control input u_4

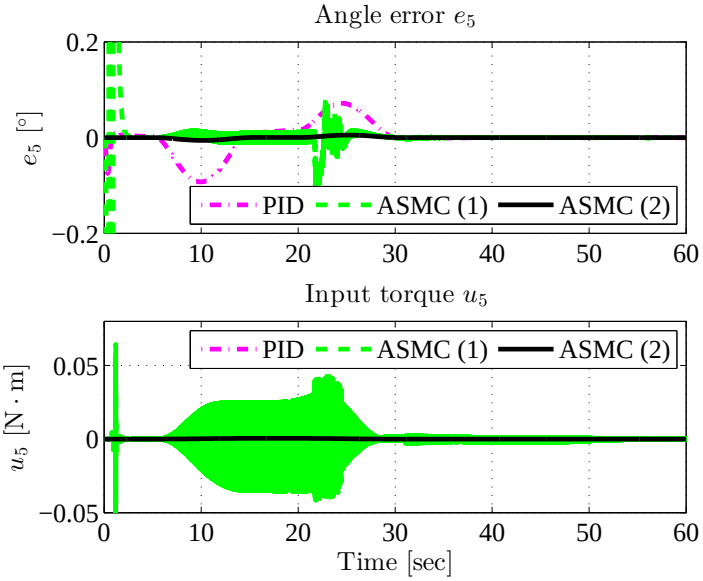

Figure 7.17: Trajectory tracking control on robot manipulators – Angular position error e_5 and control input u_5

7.6 Applications – Stabilization and Trajectory Tracking Control for a 2-DOF Helicopter Model Setup

7.6.1 Modelling

Recall the dynamic equations of the experimental helicopter model [21] discussed in Chapter 3 (refer to, (3.43a) and (3.43b)). Refer to Section 1.6 for further details about the description of this setup.

$$\begin{aligned}\big(J_p + ml^2\big)\ddot{\phi} =& K_{pp}V_p + K_{py}V_y - B_p\dot{\phi} - mgl\cdot\cos\phi \\ & - ml^2\sin\phi\cos\phi\cdot\dot{\psi}^2 \qquad (7.48a)\\ \big(J_y + ml^2\cos^2\phi\big)\ddot{\psi} =& K_{yp}V_p + K_{yy}V_y - B_y\dot{\psi} \\ & + 2ml^2\sin\phi\cos\phi\cdot\dot{\phi}\dot{\psi} \qquad (7.48b)\end{aligned}$$

For any desired trajectories ϕ_d and ψ_d, with their time derivatives $\dot{\phi}_d$ and $\dot{\psi}_d$, let $x_1 = \tilde{\phi} = \phi - \phi_d$, $x_2 = \tilde{\psi} = \psi - \psi_d$, $x_3 = \dot{\tilde{\phi}} = \dot{\phi} - \dot{\phi}_d$ and $x_4 = \dot{\tilde{\psi}} = \dot{\psi} - \dot{\psi}_d$ be the measurable states, and $u = [u_1\ u_2]^T = [V_p\ V_y]^T$ the input vector. Then, dynamics (7.48) can be rewritten in the form of (7.1) where the nonlinear uncertain dynamics are given by

$$f(x,t) = \big[x_3,\ x_4,\ f_1(x),\ f_2(x)\big]^T \qquad (7.49)$$

and

$$g(x,t) = \big[g_1(x,t),\ g_2(x,t)\big] \qquad (7.50)$$

with

$$\begin{aligned}f_1(x) =& \frac{1}{J_p + ml^2}\Big[- B_p(x_3 + \dot{\phi}_d) - mgl\cos(x_1 + \phi_d) \\ & - \frac{1}{2}ml^2(x_4 + \dot{\psi}_d)^2\sin\big(2(x_1 + \phi_d)\big)\Big] + \ddot{\phi}_d \qquad (7.51)\\ f_2(x) =& \frac{-B_y(x_4 + \dot{\psi}_d) + ml^2(x_3 + \dot{\phi}_d)(x_4 + \dot{\psi}_d)\sin\big(2(x_1 + \phi)\big)}{J_y + ml^2\cos^2(x_1 + \phi_d)} - \ddot{\psi}_d \qquad (7.52)\end{aligned}$$

and

$$g_1(x,t) = \big(0,\ 0,\ \frac{K_{pp}}{J_p + ml^2},\ \frac{K_{yp}}{J_y + ml^2\cos^2(x_1 + \phi_d)}\big)^T \qquad (7.53)$$

$$g_2(x,t) = \big(0,\ 0,\ \frac{K_{py}}{J_p + ml^2},\ \frac{K_{yy}}{J_y + ml^2\cos^2(x_1 + \phi_d)}\big)^T \qquad (7.54)$$

For the control design purpose, we consider a PI sliding hyper-surface as [11]

$$\sigma = K_p x + K_i \int x d\tau \tag{7.55}$$

Note that when the system is on the sliding surface ($\sigma = 0$) it has an exponential stability (*i.e.*, $x \to 0$ and $\int x d\tau \to 0$ exponentially). Then, the dynamics of σ can be written in form (7.5) where the uncertainty vector $\Psi(x,t)$ includes affine and quadratic terms in the state variables, in form $a(t)x_4^2$ and $b(t)x_3x_4$ with $a(t)$ and $b(t)$ uncertain bounded coefficients.

We use a fixed-value ϵ instead of ϵ-tuning (*i.e.*, ϵ time-varying and depending on K) which requires that Γ is normalizable [16]. Moreover, by applying the ϵ-tuning, we realize that there is no improvement in the experimental results for the case where all coefficients of (7.48) are unknown. Then, for their consistency, we keep ϵ the same during all the experiments.

We apply the real ASMC design (with a boundary-layer limit $\epsilon = 10^{-2}$ and a sampling period $T_s = 5 \cdot 10^{-3}$) using the proposed reaching law (7.28) and we compare its performance to the existing adaptation gain dynamics discussed in [16, 74] (*i.e.*, (7.28) with $\beta = 0$) and conventional PID controls. Experiments are conducted using different values of α and β.

7.6.2 Experiments – Pitch and Yaw Stabilization at 0° Positions

In the first experiments, we consider the pitch and yaw positions stabilized at the origin (P0Y0), *i.e.*, $\phi_d = \dot{\phi}_d = 0$ and $\psi_d = \dot{\psi}_d = 0$ in (7.49)-(7.54). Then, the helicopter model setup can be roughly considered as a linear dynamic system when the system is close to these desired positions. The initial pitch and yaw positions are set as -40.5° and 10°, respectively.

Figures 7.18 and 7.19 show the experimental results of the pitch and yaw displacements and control inputs, respectively, by using the existing ASMC, referred to as Exst (blue dash) reaching law discussed in [16, 74] (*i.e.*, (7.28) with $\alpha = 0.1$ and $\beta = 0$), PID control (red dash-dot) and proposed ASMC, referred to as Prpsd (black solid line), with $\alpha = 0.1$ and $\beta = 10$, while the experimental results for $\alpha = 0.1$ and $\beta = 20$ are shown in Figures 7.21 and 7.20. The experiments for $\alpha = 0.05$ and $\alpha = 0.2$ combined with $\beta = 10$ and $\beta = 20$ have similar results and are shown in Figures B.17-B.22 in Appendix B.3. The experimental results for $\alpha = 0.05$, $\alpha = 0.1$ and $\alpha = 0.2$ combined with $\beta = 5$ are not shown in the thesis since the results are similar to other combination ones.

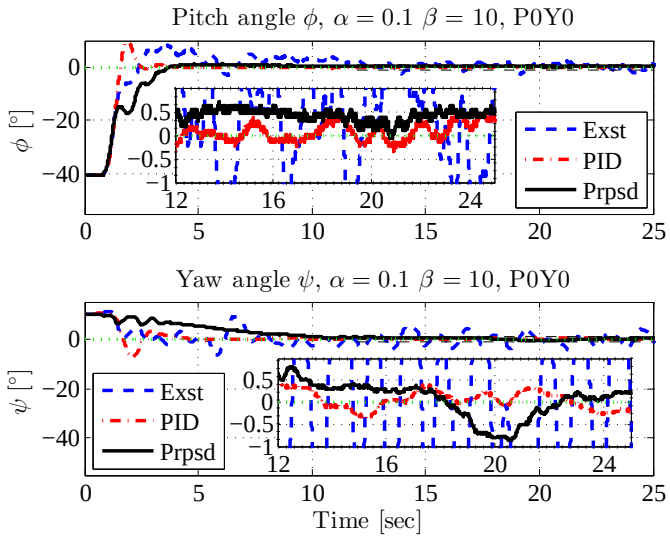

Figure 7.18: Experiment results – Pitch and yaw displacements in regulation problem about 0° using the existing ASMC (blue dash), PID (red dash-dot) and proposed ASMC (black solid line) with $\alpha = 0.1$ and $\beta = 10$.

One can see that the PID control has the best performance in terms of chattering levels, overshoots and accuracies, while the results by using proposed ASMC are also good. However, the results by using the existing ASMC are only acceptable. The experimental results of P0Y0 demonstrate that the PID control is a good choice for linear dynamic systems. Table 7.2 summarizes the experimental results (error peak and RMS performances) for the pitch and yaw stabilization with all combinations of control parameters α and β, *i.e.*, $\alpha = 0.05$, $\alpha = 0.1$ and $\alpha = 0.2$ combined with $\beta = 5$, $\beta = 10$ and $\beta = 20$ where the best results are obtained by PID control and highlighted in bold fonts. The other better results are underlined.

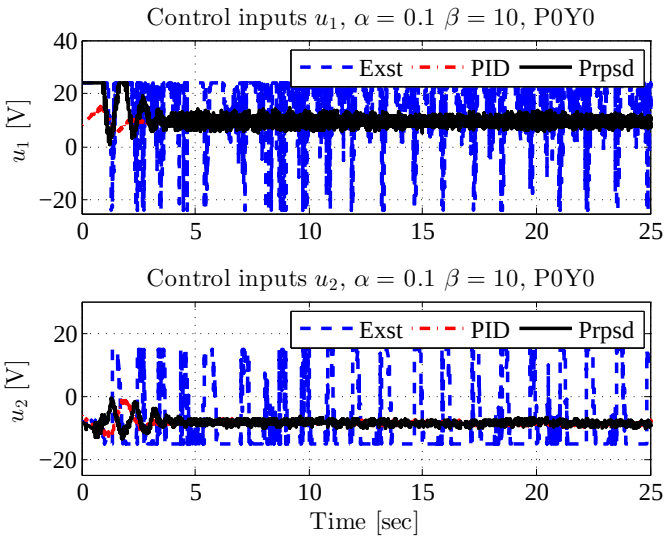

Figure 7.19: Experiment results – Pitch and yaw control inputs in regulation problem about 0° using the existing ASMC (blue dash), PID (red dash-dot) and proposed ASMC (black solid line) with $\alpha = 0.1$ and $\beta = 10$.

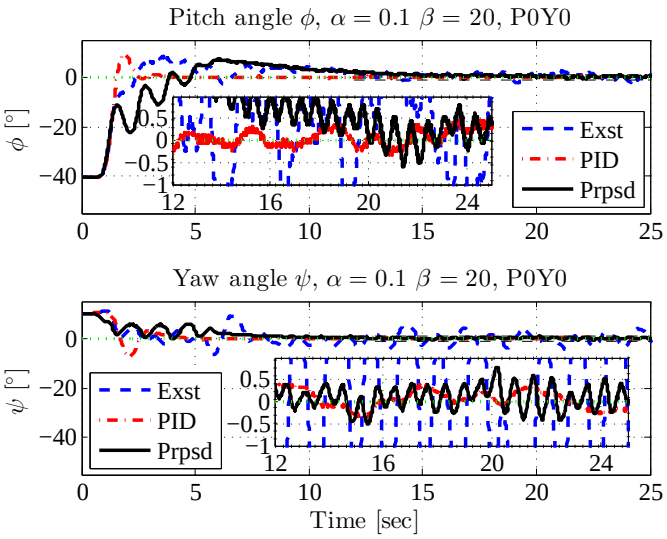

Figure 7.20: Experiment results – Pitch and yaw displacements in regulation problem about 0° using the existing ASMC (blue dash), PID (red dash-dot) and proposed ASMC (black solid line) with $\alpha = 0.1$ and $\beta = 20$.

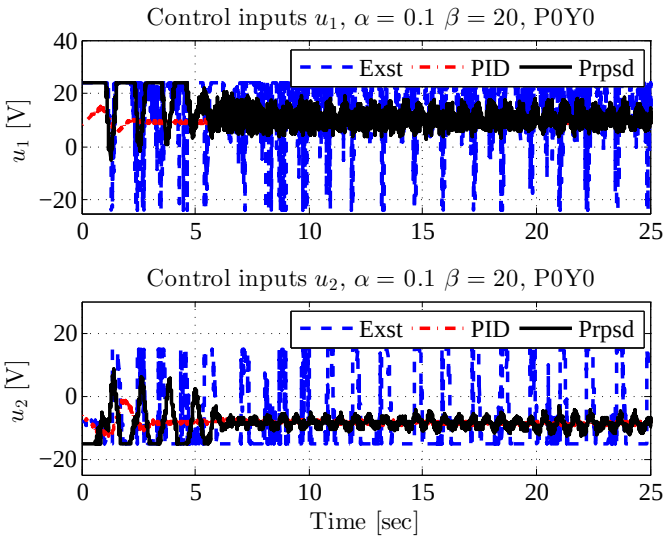

Figure 7.21: Experiment results – Pitch and yaw control inputs in regulation problem about 0° using the existing ASMC (blue dash), PID (red dash-dot) and proposed ASMC (black solid line) with $\alpha = 0.1$ and $\beta = 20$.

Table 7.2: Experimental results recap – Pitch and yaw error (*i.e.*, $\tilde{\phi}$ and $\tilde{\psi}$) performance in position stabilization at 0°. Results are in % of maximum displacement.

P0Y0			Pitch Angle		Yaw Angle	
Method	α	β	RMS	Peak	RMS	Peak
PID			**0.5**	**1.4**	**2.2**	**5.5**
Existing	0.05	0	4.0	15.2	23.3	72.3
Proposed		5	0.9	2.8	6.9	16.5
		10	0.7	1.8	5.7	13.4
		20	1.8	7.0	3.5	12.1
Existing	0.1	0	3.1	10	23.4	53.9
Proposed		5	1.4	2.2	7.0	20.5
		10	1.0	1.8	4.3	9.5
		20	2.3	8.1	2.6	8.2
Existing	0.2	0	3.4	13.4	21.6	57.8
Proposed		5	2.8	4.0	9.7	18.2
		10	1.5	2.7	4.6	9.0
		20	2.2	8.1	3.5	9.9

7.6.3 Experiments – Pitch Stabilization at the Origin 0° and Yaw Sine-Wave Trajectory Tracking

In the experiments of pitch stabilization at the origin and yaw sine-wave trajectory tracking (P0Yv), the pitch is stabilized at $\phi_d = 0^\circ$, and yaw position follows the time-varying trajectory $\psi_d = 10^\circ \sin(0.15\pi t + \frac{\pi}{2})$. The initial pitch and yaw positions are set as -40.5° and 10°, respectively.

Figures 7.22-7.24 show the experimental results of the pitch and yaw displacements, their corresponding errors and the control inputs, respectively, by using the existing ASMC (blue dash) reaching law discussed in [16, 74] (*i.e.*, (7.28) with $\alpha = 0.1$ and $\beta = 0$), PID (red dash-dot) and proposed ASMC (black solid line) reaching law (7.28) with $\alpha = 0.1$ and $\beta = 10$, while the experimental results for $\alpha = 0.1$ and $\beta = 20$ are shown in Figures 7.25-7.27. The experiments for $\alpha = 0.05$ and $\alpha = 0.2$ combined with $\beta = 10$ and $\beta = 20$ have similar results and are shown in Figures B.26-B.34 in Appendix B.4. The experimental results for $\alpha = 0.05$, $\alpha = 0.1$ and $\alpha = 0.2$ combined with $\beta = 5$ are not shown in the thesis since the results are similar. Table 7.3 summarizes the experimental results (in terms of peak and RMS errors) for all combinations of α and β, *i.e.*, $\alpha = 0.05$, $\alpha = 0.1$ and $\alpha = 0.2$ combined with $\beta = 5$, $\beta = 10$ and $\beta = 20$.

In comparison with the existing ASMC, one can see that, by using the proposed gain law, both pitch input u_1 and yaw input u_2 have less chattering levels and smaller magnitude variations than those using the existing one. With ASMC using the existing gain law, the voltages of the rear and front propeller motors are often saturated at their maximum levels of $\pm$15V and $\pm$24V, respectively, while the magnitudes of these values are limited to about 10V with the new design. Simultaneously, the pitch and yaw follow the desired trajectories more accurately by using the proposed gain law than those using the existing one. From Table 7.3, it can be seen that, by using the proposed gain law (*i.e.*, with any $\beta > 0$), the errors are largely reduced compared to those using the existing gain law (*i.e.*, $\beta = 0$). The RMS errors of the pitch angle trajectories with the new design can be reduced by 20%-81% compared to the existing ones and by 29%-83% for yaw angles, while their peak errors can be down by 50%-87% and 45%-82%, respectively.

In comparison with PID, one can see that, by using the proposed ASMC gain law, both pitch input u_1 and yaw input u_2 have almost the same levels as those using the PID. Also, the pitch stabilization errors and yaw trajectory tracking errors are almost same for the proposed ASMC and the PID control. However, the overshoot and peak error of the yaw tracking using the PID are much higher than those obtained using the proposed ASMC.

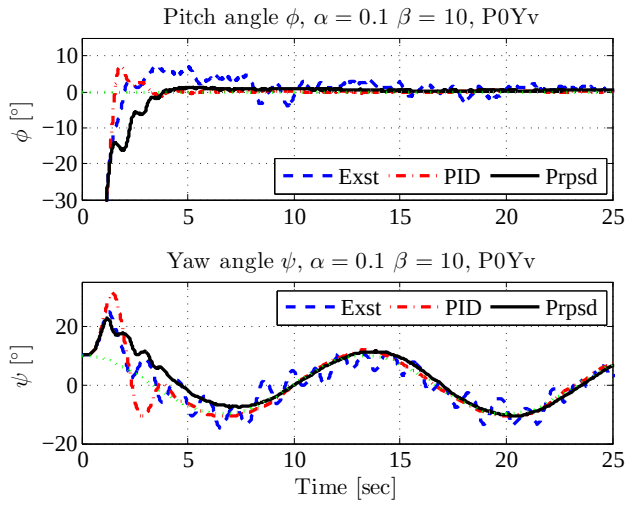

Figure 7.22: Experiment results – Pitch and yaw displacements in pitch regulation and yaw sine wave tracking problem, using the existing ASMC (blue dash), PID (red dash-dot) and proposed ASMC (black solid line) with $\alpha = 0.1$ and $\beta = 10$.

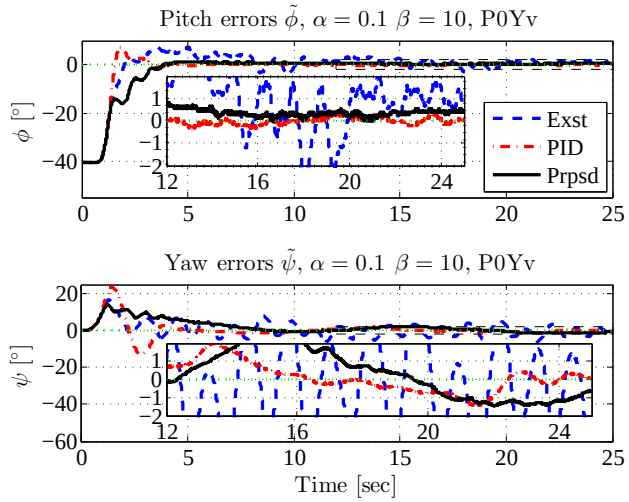

Figure 7.23: Experiment results – Pitch and yaw position errors in pitch regulation and yaw sine wave tracking problem, using the existing ASMC (blue dash), PID (red dash-dot) and proposed ASMC (black solid line) with $\alpha = 0.1$ and $\beta = 10$.

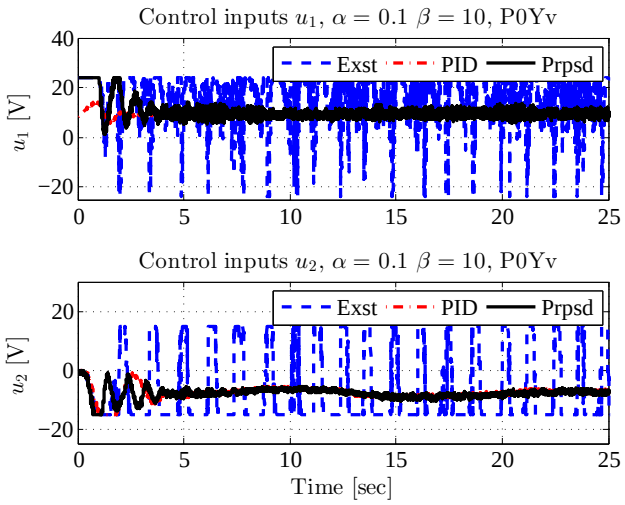

Figure 7.24: Experiment results – Pitch and yaw control inputs in pitch regulation and yaw sine wave tracking problem, using the existing ASMC (blue dash), PID (red dash-dot) and proposed ASMC (black solid line) with $\alpha = 0.1$ and $\beta = 10$.

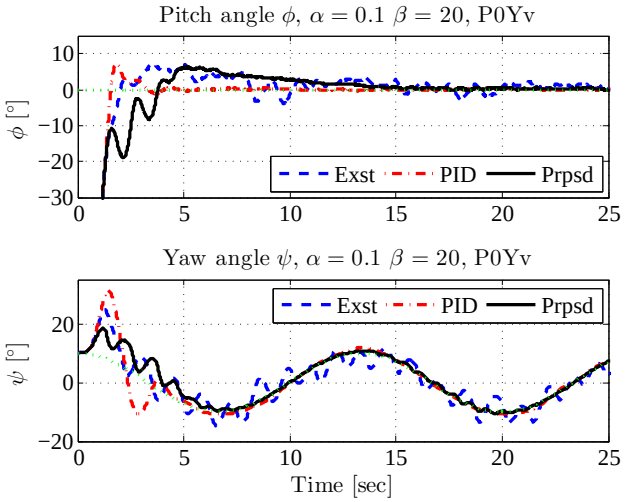

Figure 7.25: Experiment results – Pitch and yaw displacements in pitch regulation and yaw sine wave tracking problem, using the existing ASMC (blue dash), PID (red dash-dot) and proposed ASMC (black solid line) with $\alpha = 0.1$ and $\beta = 20$.

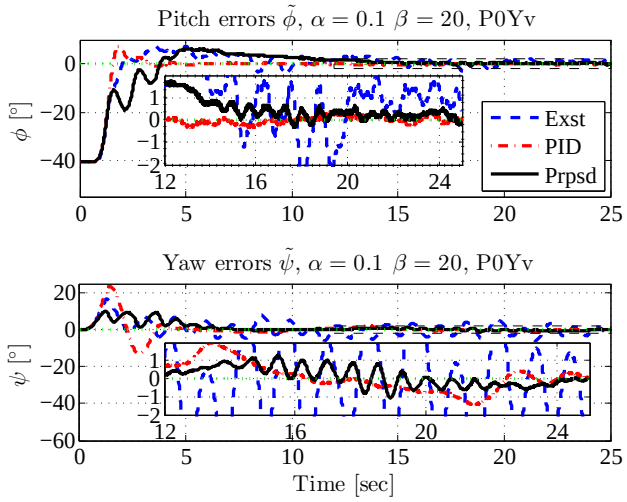

Figure 7.26: Experiment results – Pitch and yaw position errors in pitch regulation and yaw sine wave tracking problem, using the existing ASMC (blue dash), PID (red dash-dot) and proposed ASMC (black solid line) with $\alpha = 0.1$ and $\beta = 20$.

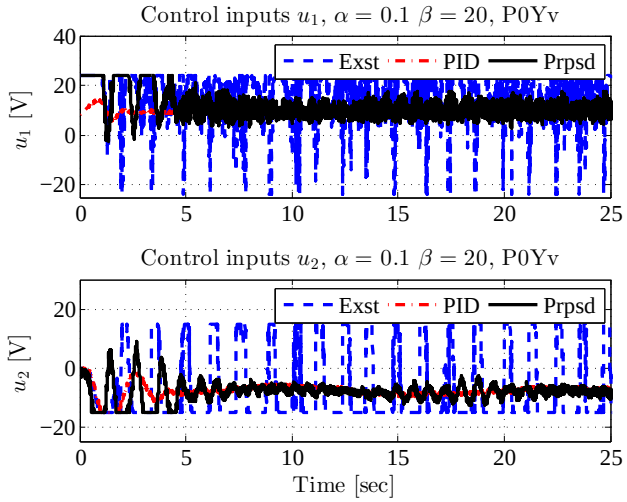

Figure 7.27: Experiment results – Pitch and yaw control inputs in pitch regulation and yaw sine wave tracking problem, using the existing ASMC (blue dash), PID (red dash-dot) and proposed ASMC (black solid line) with $\alpha = 0.1$ and $\beta = 20$.

Table 7.3: Experimental results recap – Pitch and yaw error (*i.e.*, $\tilde{\phi}$ and $\tilde{\psi}$) performance in pitch position stabilization and yaw trajectory tracking. Results are in % of maximum displacement.

P0Yv			Pitch Angle		Yaw Angle	
Method	α	β	RMS	Peak	RMS	Peak
PID			**0.5**	**1.7**	7.1	19.9
Existing	0.05	0	3.7	14.1	26.4	63.0
Proposed		5	1.1	3.9	19.0	34.9
		10	0.7	1.8	12.7	26.9
		20	1.5	5.5	5.7	15.2
Existing	0.1	0	3.2	8.4	25.7	62.5
Proposed		5	1.6	2.9	14.6	31.4
		10	1.0	2.0	10.2	23.9
		20	1.8	7.0	**4.4**	12.9
Existing	0.2	0	3.2	10.8	26.2	62.9
Proposed		5	2.9	4.8	18.2	32.6
		10	1.8	3.1	11.6	25.3
		20	1.8	7.0	4.7	**11.3**

7.6.4 Experiments – Pitch Sine-Wave Trajectory Tracking and Yaw Stabilization at the Origin 0°

In the experiments of pitch sine-wave trajectory tracking and yaw stabilization at the origin (PvY0), the pitch follows the time-varying trajectory, $\phi_d = 10^\circ \sin(0.4\pi t - \frac{\pi}{2})$, and yaw is stabilized at $\psi_d = 0^\circ$. The initial pitch and yaw positions are set as -40.5° and 10°, respectively.

Figures 7.28-7.30 show the experimental results of the pitch and yaw displacements, their corresponding position errors and the control inputs, respectively, by using the existing ASMC (blue dash) reaching law discussed in [16, 74] (*i.e.*, (7.28) with $\alpha = 0.1$ and $\beta = 0$), PID (red dash-dot) and proposed ASMC (black solid line) reaching law (7.28) with $\alpha = 0.1$ and $\beta = 10$, while the experimental results for $\alpha = 0.1$ and $\beta = 20$ are shown in Figures 7.31-7.33. The experiments for $\alpha = 0.05$ and $\alpha = 0.2$ combined with $\beta = 10$ and $\beta = 20$ have similar results and are shown in Figures B.36-B.47 in Appendix B.5. The experimental results for $\alpha = 0.05$, $\alpha = 0.1$ and $\alpha = 0.2$ combined with $\beta = 5$ are not shown in the thesis since the results are similar to other combination ones. Table 7.4 summarizes the experimental results (in terms of error performances) for all combinations of α and β, *i.e.*, $\alpha = 0.05$, $\alpha = 0.1$ and $\alpha = 0.2$ combined with $\beta = 5$, $\beta = 10$ and $\beta = 20$.

In comparison with the existing ASMC, one can see that, by using the proposed gain law, both pitch input u_1 and yaw input u_2 have less chattering levels and smaller magnitude variations than those using the existing one. With ASMC using the existing gain law, the voltages of both propeller motors are often saturated, while the magnitudes of these values are limited to about 10V with the new design. Simultaneously, the pitch and yaw follow the desired trajectories more accurately by using the proposed gain law than those using the existing one. From Table 7.4, it can be seen that, by using the proposed gain law (*i.e.*, with any $\beta > 0$), the errors are largely reduced compared to those using the existing gain law (*i.e.*, $\beta = 0$). The RMS errors of the pitch angle trajectories with the new design can be reduced by 68%-83% compared to the existing ones and by 73%-93% for yaw angles, while their peak errors can be down by 70%-89% and 85%-92%, respectively.

In comparison with PID, one can see that, by using the proposed ASMC gain law, both pitch input u_1 and yaw input u_2 have almost the same levels as those obtained using the PID. Also, the pitch trajectory tracking errors and yaw stabilization errors are almost same for the proposed ASMC and the PID control.

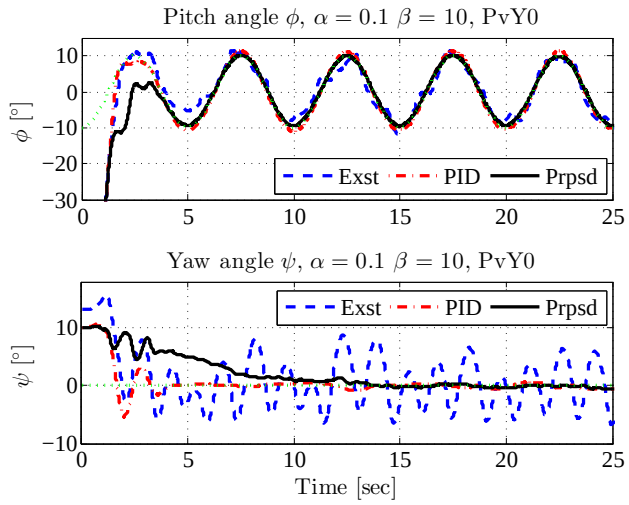

Figure 7.28: Experiment results – Pitch and yaw displacements in pitch sine wave tracking control and yaw regulation, using the existing ASMC (blue dash), PID (red dash-dot) and proposed ASMC (black solid line) with $\alpha = 0.1$ and $\beta = 10$.

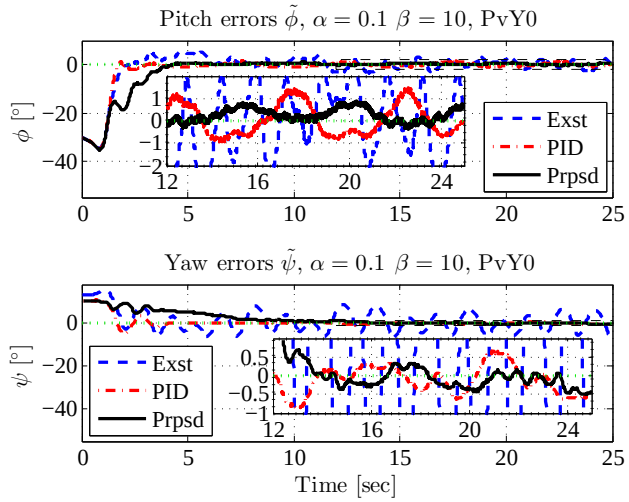

Figure 7.29: Experiment results – Pitch and yaw position errors in pitch sine wave tracking control and yaw regulation, using the existing ASMC (blue dash), PID (red dash-dot) and proposed ASMC (black solid line) with $\alpha = 0.1$ and $\beta = 10$.

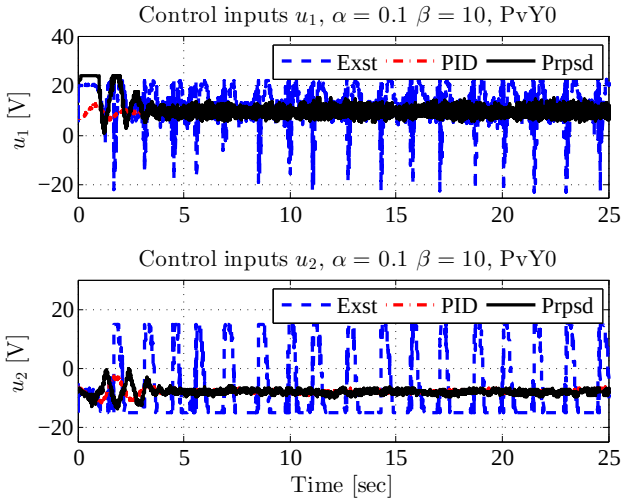

Figure 7.30: Experiment results – Pitch and yaw control inputs in pitch sine wave tracking control and yaw regulation, using the existing ASMC (blue dash), PID (red dash-dot) and proposed ASMC (black solid line) with $\alpha = 0.1$ and $\beta = 10$.

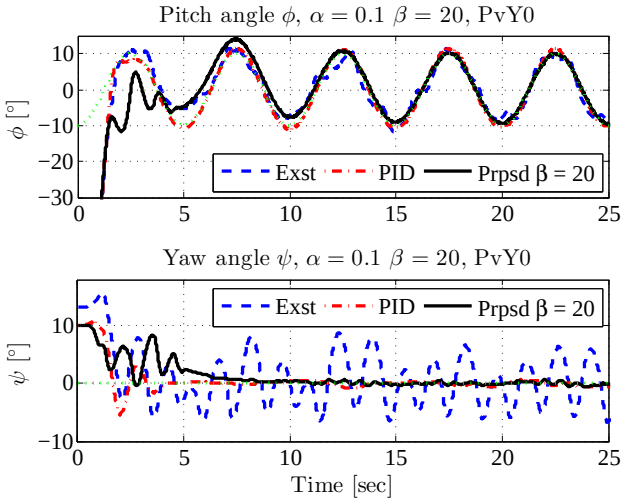

Figure 7.31: Experiment results – Pitch and yaw displacements in pitch sine wave tracking control and yaw regulation, using the existing ASMC (blue dash), PID (red dash-dot) and proposed ASMC (black solid line) with $\alpha = 0.1$ and $\beta = 20$.

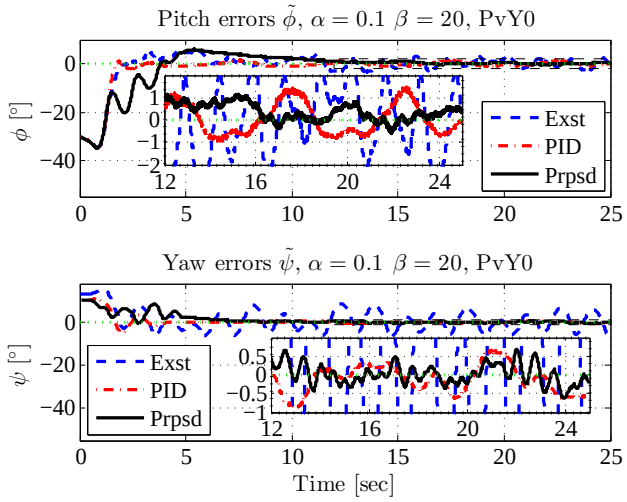

Figure 7.32: Experiment results – Pitch and yaw position errors in pitch sine wave tracking control and yaw regulation, using the existing ASMC (blue dash), PID (red dash-dot) and proposed ASMC (black solid line) with $\alpha = 0.1$ and $\beta = 20$.

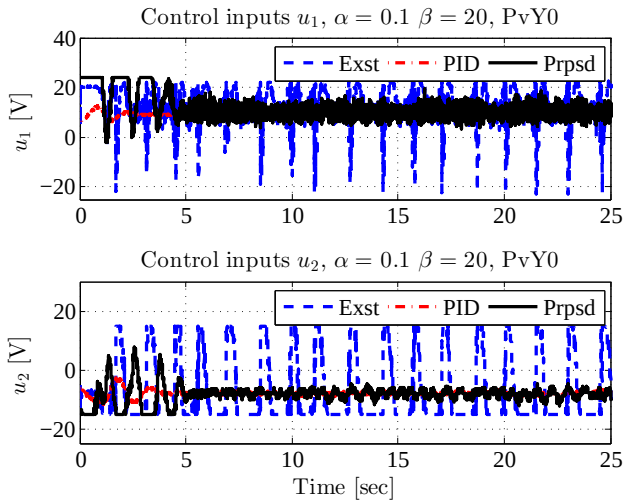

Figure 7.33: Experiment results – Pitch and yaw control inputs in pitch sine wave tracking control and yaw regulation, using the existing ASMC (blue dash), PID (red dash-dot) and proposed ASMC (black solid line) with $\alpha = 0.1$ and $\beta = 20$.

Table 7.4: Experimental results recap – Pitch and yaw error (*i.e.*, $\tilde{\phi}$ and $\tilde{\psi}$) performance in pitch trajectory tracking and yaw position stabilization. Results are in % of maximum displacement.

PvY0			Pitch Angle		Yaw Angle	
Method	α	β	RMS	Peak	RMS	Peak
PID			7.2	19.8	4.7	11.8
Existing	0.05	0	19.5	79.9	34.2	100.4
Proposed		5	4.0	11.2	5.9	17.4
		10	**3.3**	**8.5**	4.0	10.8
		20	5.1	21.1	2.9	9.0
Existing	0.1	0	15.2	39.2	27.6	66.3
Proposed		5	6.2	12.3	5.3	12.5
		10	4.1	9.8	4.0	13.9
		20	6.1	23.7	**2.8**	9.0
Existing	0.2	0	15.4	36.6	36.8	112.3
Proposed		5	11.3	18.4	9.8	15.6
		10	6.0	11.8	3.4	**8.0**
		20	6.0	20.6	3.9	10.8

7.6.5 Experiments – Pitch and Yaw Stabilization at 10° Position

In the experiments of pitch and yaw stabilization at 10° (P10Y10), we consider the pitch and yaw positions stabilized at the desired angle, *i.e.*, $\phi_d = \psi_d = 10^\circ$ in (7.49)-(7.54). The initial pitch and yaw positions are set as -40.5° and 0°, respectively.

Figures 7.34 and 7.35 show the experimental results of the pitch and yaw displacements and the control inputs, respectively, by using the existing ASMC (blue dash) reaching law discussed in [16, 74] (*i.e.*, (7.28) with $\alpha = 0.1$ and $\beta = 0$), PID (red dash-dot) and proposed ASMC (black solid line) reaching law (7.28) with $\alpha = 0.1$ and $\beta = 10$, while the experimental results for $\alpha = 0.1$ and $\beta = 20$ are shown in Figures 7.36 and 7.37. The experiments for $\alpha = 0.05$ and $\alpha = 0.2$ combined with $\beta = 10$ and $\beta = 20$ have similar results and are shown in Figures B.48-B.51 in Appendix B.6. The experimental results for $\alpha = 0.05$, $\alpha = 0.1$ and $\alpha = 0.2$ combined with $\beta = 5$ are not shown in the thesis since the results are similar to other combination ones. Table 7.5 summarizes the experimental results of the pitch and yaw stabilization errors for all combinations of control parameters α and β, *i.e.*, $\alpha = 0.05$, $\alpha = 0.1$ and $\alpha = 0.2$ combined with $\beta = 5$, $\beta = 10$ and $\beta = 20$.

One can see that the proposed ASMC has the best performance in terms of robustness, smoothness and accuracy, while the results using existing ASMC are acceptable. However, the results using PID control are unacceptable (unstable). In Table 7.5, the best results are highlighted in bold fonts, and the second better performances are underlined. Since the setup at pitch and yaw positions of 10° is a typical highly coupled nonlinear system, the results indicate that the PID control may not be a good choice for nonlinear dynamic systems (system unstable). In contrast, the proposed ASMC might be a good choice.

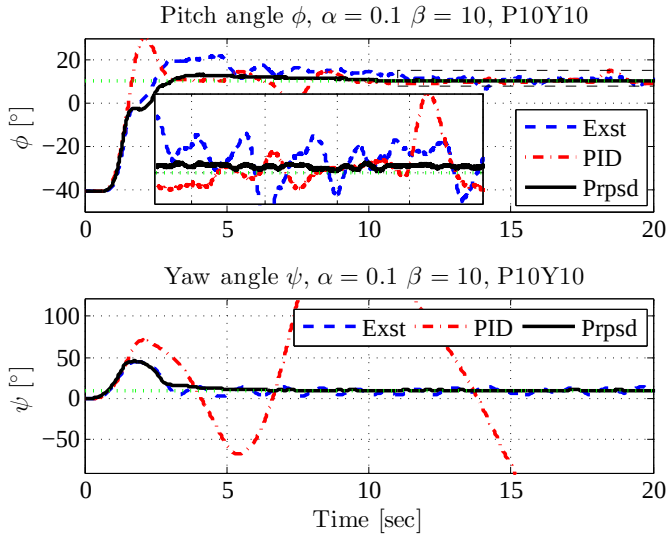

Figure 7.34: Experiment results – Pitch and yaw displacements in regulation problem about 0° using the existing ASMC (blue dash), PID (red dash-dot) and proposed ASMC (black solid line) with $\alpha = 0.1$ and $\beta = 10$.

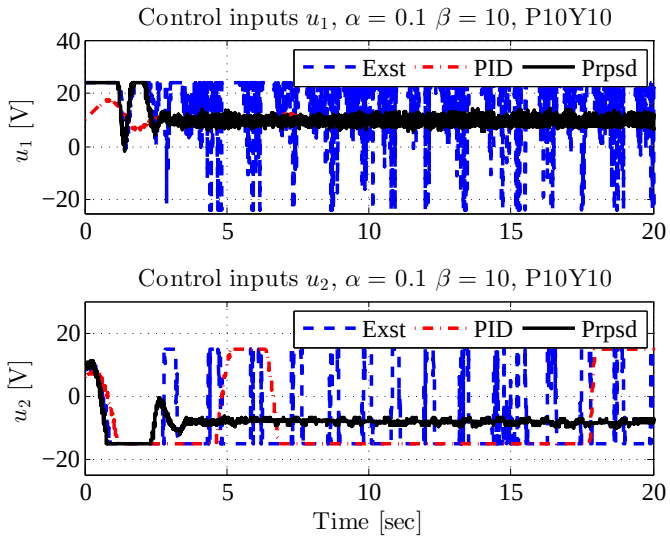

Figure 7.35: Experiment results – Pitch and yaw control inputs in regulation problem about 0° using the existing ASMC (blue dash), PID (red dash-dot) and proposed ASMC (black solid line) with $\alpha = 0.1$ and $\beta = 10$.

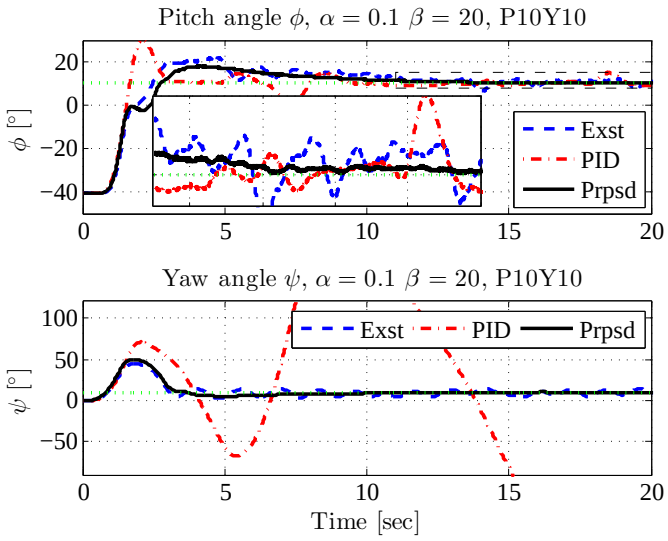

Figure 7.36: Experiment results – Pitch and yaw displacements in regulation problem about 0° using the existing ASMC (blue dash), PID (red dash-dot) and proposed ASMC (black solid line) with $\alpha = 0.1$ and $\beta = 20$.

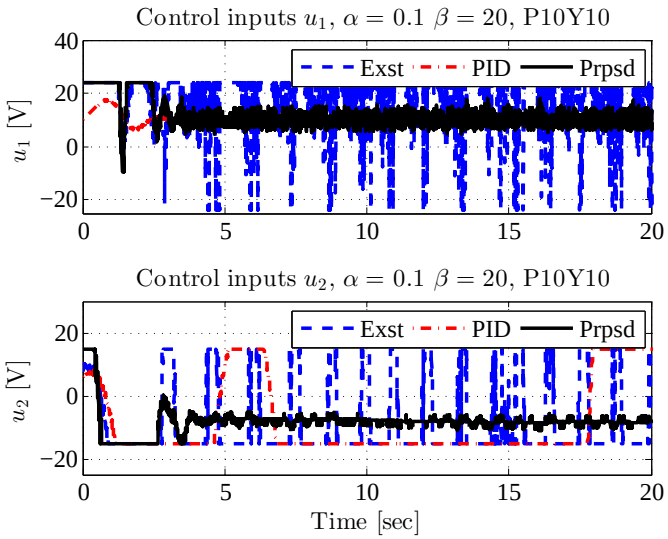

Figure 7.37: Experiment results – Pitch and yaw control inputs in regulation problem about 0° using the existing ASMC (blue dash), PID (red dash-dot) and proposed ASMC (black solid line) with $\alpha = 0.1$ and $\beta = 20$.

Table 7.5: Experimental results recap – Pitch and yaw error (*i.e.*, $\tilde{\phi}$ and $\tilde{\psi}$) performance in positions stabilization at 10°. Results are in % of maximum displacement.

P10Y10			Pitch Angle		Yaw Angle	
Method	α	β	RMS	Peak	RMS	Peak
PID			13.2	50.47	1597.24	2631.25
Existing	0.05	0	21.0	67.3	28.5	18.9
Proposed		5	3.3	**8.4**	5.8	16.1
		10	**3.0**	9.2	**3.1**	**10.4**
		20	5.0	21.5	3.2	13.0
Existing	0.1	0	15.4	48.0	25.8	61.3
Proposed		5	6.0	9.2	7.2	16.1
		10	**3.9**	**7.4**	3.9	**9.5**
		20	4.7	18.0	**3.3**	12.6
Existing	0.2	0	17.9	60.3	29.3	69.7
Proposed		5	12.3	18.0	11.7	21.3
		10	6.9	**13.6**	5.3	**12.6**
		20	**5.7**	18.8	**4.7**	15.6

7.6.6 Experiments – Pitch and Yaw Trajectory Tracking Control

In the experiments of pitch and yaw trajectories tracking control, the pitch and yaw positions follow the time-varying trajectories, $\phi_d = 10^\circ \sin(0.4\pi t - \frac{\pi}{2}) = -10^\circ \cos 0.4\pi t$ and $\psi_d = 10^\circ \sin(0.15\pi t + \frac{\pi}{2}) = 10^\circ \cos 0.15\pi t$, respectively. The initial pitch and yaw positions are set as -40.5° and 10°, respectively.

Figures 7.38-7.40 show the experimental results of the pitch and yaw displacements, the position errors, and the control inputs, respectively, using the existing ASMC (blue dash) reaching law discussed in [16, 74] (*i.e.*, reaching law (7.28) with $\alpha = 0.1$ and $\beta = 0$), PID (red dash-dot) and proposed ASMC (black solid line) reaching law (7.28) with $\alpha = 0.1$ and $\beta = 10$, while the experimental results for $\alpha = 0.1$ and $\beta = 20$ are shown in Figures 7.41-7.43. The experiments for $\alpha = 0.05$ and $\alpha = 0.2$ combined with $\beta = 10$ and $\beta = 20$ have similar results and are shown in Figures B.56-B.67 in Appendix B.7. The experimental results for $\alpha = 0.05$, $\alpha = 0.1$ and $\alpha = 0.2$ combined with $\beta = 5$ are not shown in the thesis since the results are similar to other combination ones. Table 7.6 summarizes the experimental results for all combinations of α and β, *i.e.*, $\alpha = 0.05$, $\alpha = 0.1$ and $\alpha = 0.2$ combined with $\beta = 5$, $\beta = 10$ and $\beta = 20$.

In comparison with the existing ASMC, one can see that, by using the proposed IEG-ASMC, both pitch and yaw inputs have less chattering levels and smaller magnitude variations than those using the existing IG-ASMC. With IG-ASMC, the voltages of both the front and rear propeller motors are often saturated at their maximum levels of $\pm$24V and $\pm$15V, respectively, while these values are limited to about 10V with the new design. Simultaneously, the pitch and yaw follow the desired trajectories more accurately when using the proposed gain law than with those using the existing one. From Table 7.6, it can be seen that, by using the proposed IEG-ASMC, the errors are largely reduced compared to those by using the existing gain law (*i.e.*, $\beta = 0$). The RMS errors of the pitch angle trajectories with the new design can be reduced by up to 72% compared to the existing ones and by up to 80% for yaw angles, while their peak errors can be down by 43%-76% and 50%-83%, respectively.

In comparison with PID, it can be seen that, by using the proposed gain law, the pitch follows the desired trajectories more accurately than when using the PID. Though the accuracy of the yaw tracking by using the PID has the same level of those using the proposed gain law, the overshoot and peak error of the yaw tracking using the PID is much higher than those using the proposed ASMC. Simultaneously, both pitch input u_1 and yaw input u_2 have almost

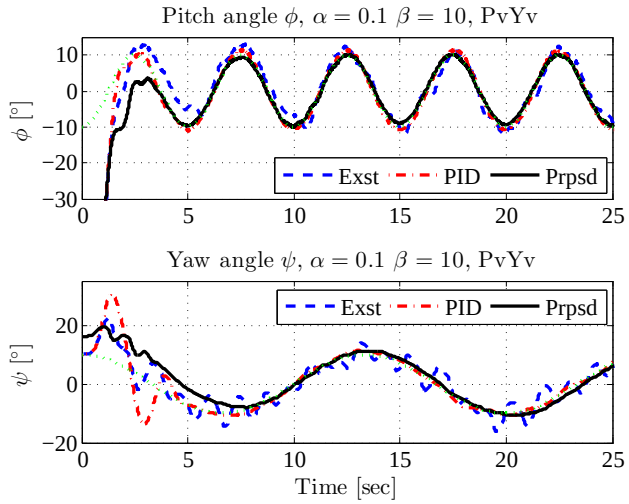

Figure 7.38: Experiment results – Pitch and yaw displacements in sine wave tracking for both pitch and yaw angles, using the existing ASMC (blue dash), PID (red dash-dot) and proposed ASMC (black solid line) with $\alpha = 0.1$ and $\beta = 10$.

the same levels for the proposed IEG-ASMC and PID.

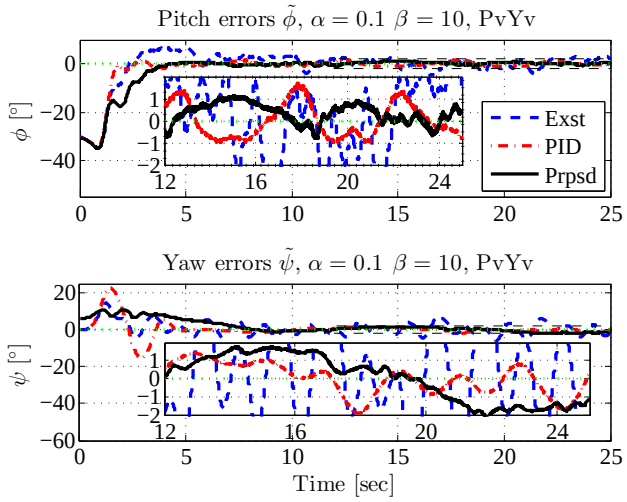

Figure 7.39: Experiment results – Pitch and yaw position errors in sine wave tracking for both pitch and yaw angles, using the existing ASMC (blue dash), PID (red dash-dot) and proposed ASMC (black solid line) with $\alpha = 0.1$ and $\beta = 10$.

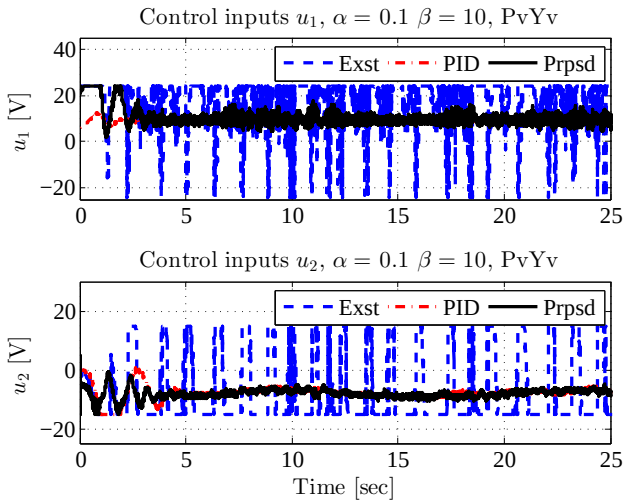

Figure 7.40: Experiment results – Pitch and yaw control inputs in sine wave tracking for both pitch and yaw angles, using the existing ASMC (blue dash), PID (red dash-dot) and proposed ASMC (black solid line) with $\alpha = 0.1$ and $\beta = 10$.

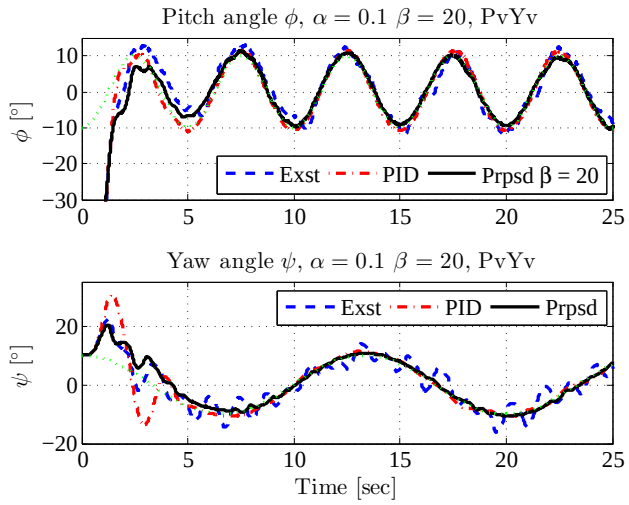

Figure 7.41: Experiment results – Pitch and yaw displacements in sine wave tracking for both pitch and yaw angles, using the existing ASMC (blue dash), PID (red dash-dot) and proposed ASMC (black solid line) with $\alpha = 0.1$ and $\beta = 20$.

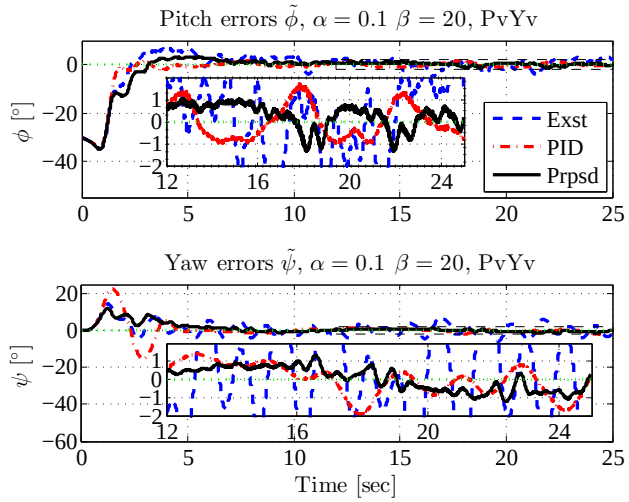

Figure 7.42: Experiment results – Pitch and yaw position errors in sine wave tracking for both pitch and yaw angles, using the existing ASMC (blue dash), PID (red dash-dot) and proposed ASMC (black solid line) with $\alpha = 0.1$ and $\beta = 20$.

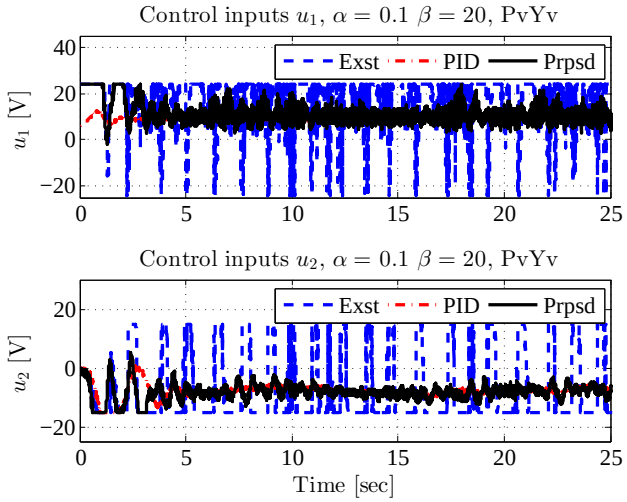

Figure 7.43: Experiment results – Pitch and yaw control inputs in sine wave tracking for both pitch and yaw angles, using the existing ASMC (blue dash), PID (red dash-dot) and proposed ASMC (black solid line) with $\alpha = 0.1$ and $\beta = 20$.

Table 7.6: Experimental results recap – Pitch and yaw error (*i.e.*, $\tilde{\phi}$ and $\tilde{\psi}$) performance in tracking control of sine wave trajectories. Results are in % of maximum displacement.

PvYv			Pitch Angle		Yaw Angle	
Method	α	β	RMS	Peak	RMS	Peak
PID			8.0	18.1	8.1	19.4
Existing	0.05	0	14.6	36.1	27.8	73.7
Proposed		5	**4.7**	**14.9**	15.4	36.0
		10	<u>5.6</u>	20.0	10.9	21.8
		20	5.8	19.8	**6.3**	**12.6**
Existing	0.1	0	16.9	48.0	27.6	65.7
Proposed		5	8.1	<u>16.2</u>	15.2	27.8
		10	**5.4**	**11.6**	11.5	25.8
		20	<u>6.0</u>	16.9	**6.3**	**13.3**
Existing	0.2	0	15.3	35.8	30.0	68.1
Proposed		5	13.2	27.2	16.5	36.6
		10	**7.3**	**13.1**	9.5	23.0
		20	**7.3**	<u>17.6</u>	**6.0**	**15.3**

7.6.7 Experimental results recap – Comments on the Proposed ASMC, Existing ASMC and PID

The performance of all the experimental results are summarized in Table 7.7. One can see that when the pitch of the helicopter-model setup is stabilized at the origin 0° where the system is roughly linear, the PID control has the best performance. However, when the pitch of the helicopter-model setup is stabilized at the origin 10° where the system is highly nonlinear, the PID control has the worst performance. In contrast, the proposed ASMC design has good performance for pitch stabilization at the origin 0° and the best performance for stabilization at 10° and trajectory tracking.

Table 7.7: Experimental results recap – Comments on the three control methods, proposed ASMC (*i.e.*, IEG-ASMC), existing ASMC (*i.e.*, IE-ASMC) and PID

Control Objectives	Best	Good	Occasionally Acceptable	Not Acceptable
P0Y0	PID	IEG-ASMC	IG-ASMC	
P0Yv	IEG-ASMC	PID	IG-ASMC	
PvY0	IEG-ASMC	PID		IG-ASMC
P10Y10	IEG-ASMC		IG-ASMC	PID
PvYv	IEG-ASMC	PID	IG-ASMC	

7.7 Conclusions

The application of the proposed ASMC techniques to a large class of nonlinear systems with unknown polynomial uncertainties are investigated. While most existing papers on ASMC designs deal with uncertainties bounded by constants or affine functions, the proposed design with integral-exponential gain law successfully handles the uncertainties bounded by unknown polynomials in the norm of system state vector. Moreover, the new algorithm provides simultaneously the required compensating gain "almost" and greatly reduced the final (or post-perturbation) gain. With the proposed algorithm, the closed-loop dynamic system has fast response to uncertainties, the accuracy and stability are enhanced, and a much lower level of gain overestimation reduces the chattering level eventually. A simple motivation example illustrates the feasibility of the proposed ASMC. The applications, including simulations and experiments, of the proposed ASMC design on a nonlinear mass-spring system, a 5-link robotic manipulator and the helicopter-model setup with stabilization and trajectory tracking control are conducted with comparisons to the existing ASMC design and the conventional PID control. The simulation and experimental results demonstrate the effectiveness of the proposed design in terms of stability, chattering reduction and error performances for handling nonlinear systems with unknown polynomial (and more general) uncertainties. Also, the simulation results on the 5-link robot manipulator and the experimental results on the 2-DOF helicopter-model setup show that the PID control is a good choice for linear uncertain systems, but may not be a good choice for nonlinear uncertain systems. In contrast, the proposed ASMC is a good choice or the best choice for nonlinear uncertain systems and most situations.

The extension of the improved adaptation law discussed in this chapter can be easily adapted to a large class of uncertain dynamics with uneven upper-bounds on the norm of uncertainties. Such bounds can be modelled by any real-value function, in the state norm, provided that its output does not exceed any exponential-based model. This requirement remains fundamental to keep the design parameters of the proposed method independent of the uncertainty levels (*i.e.*, that can be freely selected as most of ASMC gain laws).

More details in terms of motivations, objectives, novelties, pros and cons of this chapter are presented in Table 7.8.

Table 7.8: Chapter 7 Recap

Motivation(s)	- Many dynamic systems encounter nonlinear (mostly, polynomial) terms with unknown parameters.
Objective(s)	- Application of the new ASMC techniques to the nonlinear systems with uncertainties bounded by unknown polynomial in the norm of the states. - Further investigation of the new ASMC.
Novelty(ies)	- The application of the new IEG-ASMC is provided for systems with uncertainties of unknown polynomial bounds . - The stabilities of the new ASMC methods for different cases of MIMO systems with unknown polynomial uncertainties are proven.
Pro(s)	- The new ASMC successfully handles the nonlinear systems with uncertainties of unknown polynomial bounds in the norm of the states. - In practice, we show better performance than the existing IG-ASMC for any situation and better performance than PID control for nonlinear situations.
Con(s)	- No significant improvement compared to the PID control when systems in linear mode. - Extension of the proposed IEG-ASMC to high-order ASMC not investigated.

8 Conclusion

The dissertation focuses on the analysis, design and applications of robust adaptive controllers to the nonlinear systems with uncertainties of unknown bounds. In particular, ASMC techniques with integral or modified integral adaptation laws introduced for two decades have been thoroughly analysed. Through analysis of the existence of FTC in ASMC, new necessary and sufficient conditions, different from the existing analyses, are provided with the conclusion that any positive definite function of the sliding variable can be used in the integral adaptation law. Moreover, a special type of function is proposed to smooth the chattering.

The dissertation then investigates the convergence and boundedness in the existing classic IG-ASMC techniques. The applications of a new Lyapunov approach and a new majorant curve approach successfully prove the FTC of sliding variable and UUB of the switching gain. Moreover, a new formula for RTE is deduced showing the relationship that the reaching time is inverse-proportional to the square root of the designed integral parameter. The explicit relationship indicates that the classic ASMC techniques cannot achieve fast response and lower chattering simultaneously. Thus, it reveals the inherent reason of the slow response existing in the classic ASMC techniques with integral adaptation laws.

In order to thoroughly resolve the trade-offs involved in system response to the uncertainties and chattering attenuation, a new adaptation formula, called integral-exponential reaching law, of first order ASMC is proposed. The new algorithm combines the classic integral reaching law with an exponential term. With the newly added exponential term, the system responds to the uncertainties quickly. Simultaneously, it reduces the final switching gain and lower chattering levels are achieved. The stability of the new IEG-ASMC designs are proven based on the Lyapunov theorems.

Further investigations show that the new design not only deals with nonlinear systems with the uncertainties bounded by unknown constants, but also successfully handles the uncertainties bounded by unknown polynomials in the

norm of system state vector. Since the upper-bounds of most uncertainties can be modelled by some unknown polynomials, the proposed IEG-ASMC can be easily adapted to a large class of uncertain dynamics with uneven upper-bounds. This requirement also remains fundamental to keep the design parameters of the proposed method independent of the uncertainty levels.

The proposed designs are numerically verified upon different nonlinear dynamic systems: a variable-length pendulum, a 2-DOF experimental helicopter and a 5-link robotic manipulator. The experiments are conducted on the 2-DOF experimental helicopter compared with the existing ASMC designs and the general PID designs. Both numerical and experimental results show that the new proposed ASMC designs for nonlinear dynamic systems of uncertainties of unknown bounds can significantly improve the system's robustness and reduce the chattering level compared to currently existing ASMC designs. Compared to PID control, the proposed IEG-ASMC shows notable improvement in terms of robustness and accuracy when systems are in nonlinear mode. However, when the system is in linear mode (*i.e.*, about the equilibium), the ASMC techniques do not show any significant improvement compared to PID controllers. The proposed IEG-ASMC is designed for nonlinear uncertain systems with limited input measurements (*e.g.*, only position signals are available). For the nonlinear uncertain systems with full input measurements (*e.g.*, other than positions, velocities and/or accelerations are also available), the proposed IEG-ASMC may not be the best or optimal control method. New questions arise:

- How to borrow the idea of IEG-ASMC to develop a high-performance control algorithm for nonlinear systems with full input measurements?
- Combination/implementation of the proposed algorithm presented in this thesis with robust differentiator tools.
- How to apply the proposed IEG-ASMC to the control of a more complex structure of any robotic system or a UAV flying through a snow storm?

These questions motivate the future research: the implementation of the proposed IEG-ASMC in a real industrial product (*e.g.*, robot arms, a UAV with high stability performance in a snow storm, *etc.*).

Bibliography

[1] H. Khalil. *Nonlinear Systems*. Prentice-Hall, NY, 3rd ed. edition, 2002.

[2] M. Berger. *Perspective in Nonlinearity: an Introduction to Nonlinear Analysis*. W. A. Benjamin, NY, 1st edition, 1968.

[3] D. P. Atherton. *Stability of Nonlinear Systems*. John Wiley, NY, 1st edition, 1981.

[4] J. Guckenheimer and P. Holmes. *Nonlinear Oscillations, Dynamical Systems and Bifurcations of Vector Fields*. Springer Verlag, NY, 1st edition, 1983.

[5] W. Gao and J.-C. Hung. Variable Structure Control of Nonlinear Systems: A New Approach. *IEEE Transactions on Industrial Electronics*, 40(1):45–55, 1993.

[6] P. Ioannou and J. Sun. *Robust Adaptive Control*. Prentice-Hall, NY, 2nd ed. edition, 2003.

[7] B. D. O. Anderson, R. R. Bitmead, C. R. Johnson, P. V. Kokotovic, R. L. Kosut, I. Mareels, L. Praly, and B. D. Riedle. *Stability of Adaptive Systems*. M.I.T. Press, Cambridge, Massachusetts, 1st edition, 1986.

[8] B. Yao. *Adaptive Robust Control of Nonlinear Systems with Application to Control of Mechanical Systems*. PhD thesis, University of California at Berkeley, 1996.

[9] M. T. Hagan and H. B. Demuth. Neural Networks for Control, July 2013.

[10] G. Wheeler, C.-Y. Su, and Y. Stepanenko. A Sliding Mode Controller with Improved Adaptation Laws for the Upper Bounds on the Norm of Uncertainties. *Automatica*, 34(12):1657–1661, 1998.

[11] Y. Li and Q. Xu. Adaptive Sliding Model Control with Perturbation Estimation and PID Sliding Surface for Motion Tracking of a Piezo-Driven Micromanipulator. *IEEE Transactions on Control Systems Technology*, 18(4):798–810, 2010.

[12] J. Han. From PID to Active Disturbance Rejection Control. *IEEE Transactions on Industrial Electronics*, 56(3):2–22, 2009.

[13] H. Lee and V. I. Utkin. Chattering Suppression Methods in Sliding Mode Control Systems. *Annual Reviews in Control*, 31(1):179–188, 2007.

[14] Y. Huang, T. Kuo, and S. Chang. Adaptive Sliding-Mode Control for Nonlinear Systems with Uncertain Parameters. *IEEE Transactions on Systems, Man and Cybernetics–Part B: Cybernetics*, 38(2):534–539, 2008.

[15] M.-C. Pai. Observer-Based Adaptive Sliding Mode Control for Robust Tracking and Mode Following. *International Journal of Control, Automation, and Systems*, 11(2):225–232, 2013.

[16] F. Plestan, Y. Shtessel, V. Bregeault, and A. Poznyak. New Methodologies for Adaptive Sliding Mode Control. *International Journal of Control*, 83(9):1907–1919, 2010.

[17] B.-L. Cong, Z. Chen, and X.-D. Liu. On Adaptive Sliding Mode Control Without Switching Gain Overestimation. *International Journal of Robust and Nonlinear Control*, 1(1):001–017, 2012.

[18] P. Li and Z.-Q. Zheng. Robust Adaptive Second-Order Sliding-Mode Control with Fast Transient Performance. *IET Control Theory and Applications*, 6(2):305–312, 2012.

[19] V. I. Utkin and A. Poznyak. *Advances in Sliding Mode Control – Concept, Theory and Implementation*. Springer, Heidelberg, NY, 1st edition, 2013.

[20] J. J. E. Slotine and W. Li. Composite Adaptive Control of Robot Manipulators. *Automatica*, 24(1):509–520, 1989.

[21] Quanser. *2-DOF Helicopter Reference Manual*, revision 2.0 edition, 2006. Document Number 658.

[22] S. Boyd and S. Sastry. Necessary and Sufficient Conditions for Parameter Convergence in Adaptive Control. *Automatica*, 22(6):629–639, 1986.

[23] D. E. Miller and E. J. Davison. Robust Adaptive Control in the Presence of Bounded Disturbances. *IEEE Transactions on Automatic Control*, 31(4):306–315, 1986.

[24] P. A. Ioannou and G. Tao. Dominant Richness and Improvement of Performance of Robust Adaptive Control. *Automatica*, 25(2):287–291, 1989.

[25] G. Kreisselmeier. An Indirect Adaptive Controller with a Self-Excitation Capability. *IEEE Transactions on Automatic Control*, 34(5):524–528, 1989.

[26] A. S. Morse. Towards a Unified Theory of Parameter Adaptive Control: Tunability. *IEEE Transactions on Automatic Control*, 35(9):1002–1012, 1990.

[27] D. E. Miller and E. J. Davison. An Adaptive Control which Provides an Arbitrarily Good Transient and Steady-State Response. *IEEE Transactions on Automatic Control*, 36(1):68–81, 1991.

[28] K. S. Tsakalis. Robustness of Model Reference Adaptive Controllers: An Input-Output Approach. *IEEE Transactions on Automatic Control*, 37(5):556–565, 1992.

[29] A. Isidori. *Nonlinear Control Systems II*. Springer Verlag, London, 3rd ed. edition, 1999.

[30] P. Kokotovic and M. Arcak. Constructive Nonlinear Control: A Historical Perspective. *Automatica*, 37(1):637–662, 1995.

[31] Y. Zhai, M. Nounou, H. Nounou, and Y. Al-Hamidi. Model Predictive Control of a 3-DOF Helicopter System Using Successive Linearization. *International Journal of Engineering. Science and Technology*, 2(10):9–19, 2010.

[32] R. E. Kalman and J. E. Bertram. Control Systems Analysis and Design via the 'Second Method' of Lyapunov. *Journal of Basic Engineering*, 82(1):371–392, 1960.

[33] P. V. Osburn, A. P. Whitaker, and A. Kezer. New Developments in the Design of Model Reference Adaptive Control Systems. Technical report, Institute of the Aerospace Sciences, Institute of the Aerospace Sciences, 1961.

[34] A. A. Fel'dbaum. Dual Control Theory, Parts I and II, July 2013.

[35] R. E. Bellman. *Adaptive Control Processes: A Guided Tour*. Princeton University Press, Princeton, NJ, 1st edition, 1961.

[36] G. Tao and P.A. Ioannou. Robust Stability and Performance Improvement of Multivariable Adaptive Control Systems. *International Journal of Control*, 50(5):1835–1855, 1989.

[37] A. S. Morse. Global Stability of Parameter Adaptive Control Systems. *IEEE Transactions on Automatic Control*, 25(1):433–439, 1980.

[38] C. E. Rohrs, L. Valavani, M. Athans, and G. Stein. Robustness of Continuous-Time Adaptive Control Algorithms in the Presence of Unmodeled Dynamics. *IEEE Transactions on Automatic Control*, 30(9):881–889, 1985.

[39] K. D. Young, V. I. Utkin, and U. Ozguner. A Control Engineer's Guide to Sliding Mode Control. *IEEE Transactions on Control Systems Technology*, 7(3):328–342, 1999.

[40] P. A. Ioannou and P. V. Kokotovic. Instability Analysis and Improvement of Robustness of Adaptive Control. *Automatica*, 20(5):583–594, 1984.

[41] A. Jnifene and A. Fahim. A Computed Torque/Time Delay Approach to the End-Point Control of a One-Link Flexible Manipulator. *Journal of Dynamics and Control*, 7(2):171–189, 1997.

[42] J. J. Craig, P. Hsu, and S. S. Sastry. Adaptive Control of Mechanical Manipulators. *International Journal of Robotics Research*, 6(2):16–28, 1987.

[43] N. Sadegh and R. Horowitz. Stability and Robustness Analysis of a Class of Adaptive Controllers for Robot Manipulators. *International Journal of Robotic Research*, 9(3):74–92, 1990.

[44] D. Taylor, P. V. Kokotovic, R. Marino, and I. Kanellakopoulos. Adaptive Regulation of Nonlinear Systems with Unmodeled Dynamics. *IEEE Transactions on Automatic Control*, 34(4):405–415, 1989.

[45] L. Praly, G. Bastin, J.B. Pomet, and Z.P. Jiang. *Adaptive Stabilization of Nonlinear Systems*. Springer-Verlag, Berlin, 1st edition, 1991.

[46] J. B. Pomet and L. Praly. Adaptive Nonlinear Regulation: Estimation from the Lyapunov Equation. *IEEE Transactions on Automatic Control*, 37(1):729–740, 1991.

[47] R. Marino and P. Tomei. Global Adaptive Output-Feedback Control of Nonlinear Systems, Part I: Linear Parameterization; Part II: Nonlinear Parameterization. *IEEE Transactions on Automatic Control*, 38(1):17–49, 1993.

[48] I. Kanellakopoulos, P. V. Kokotovic, and A. S. Morse. Systematic Design of Adaptive Controllers for Feedback Linearizqable Systems. *IEEE Transactions on Automatic Control*, 36(1):1241–1253, 1991.

[49] V. I. Utkin. *Sliding Modes in Control and Optimization*. Springer-Verlag, NY, 1st edition, 1992.

[50] Y. B. Shtessel, I. A. Shkolnilov, and M. D. J. Brown. An Asymptotic Second-Order Smooth Sliding Mode Control. *Asian Journal of Control*, 5(4):498–504, 2003.

[51] M. Taleb, F. Plestan, and B. Bououlid. An Adaptive Solution for Robust Control Based on Integral High-Order Sliding Mode Concept. *International Journal of Robust and Nonlinear Control*, 25(8):1201–1213, 2015.

[52] J.-J. E. Slotine and W. Li. *Applied Nonlinear Control*. Prentice Hall, Englewood Cliffs, NJ, 1991.

[53] A. Levant. Sliding Oder and Sliding Accuracy in Sliding Mode Control. *International Journal of Control*, 58(6):1247–1263, 1993.

[54] G. Bartolini, L. Fridman, A. Pisano, and E. Usai. *Modern Slidng Mode Control Theory - New Perspectives and Aplications*. Springer, Heidelberg, NY, 1st edition, 2008.

[55] T. Floquet, S. K. Spurgeon, and C. Edwards. An Output Feedback Sliding Mode Control Strategy for MIMO Systems of Arbitrary Relative Degree. *International Journal of Robust and Nonlinear Control*, 21(2):119–133, 2010.

[56] C. J. Fallaha, M. Saad, H. Y. Kanaan, and K. Al-Haddad. Sliding-Mode Robot Control with Exponential Reaching Law. *IEEE Transactions on Industrial Electronics*, 58(2):600–610, 2011.

[57] A. H. Mazinan, M. F. Kazemi, and H. Shirzad. An Efficient Robust Adaptive Sliding Mode Control Approach with Its Application to Secure Communications in the Presence of Uncertainties, External Disturbance and Unknown Parameters . *Transactions of the Institute of Measurement and Control*, 36(2):164–174, 2014.

[58] X. Chen. Adaptive Sliding Mode Control for Discrete-Time Multi-Input Multi-Output Systems. *IEEE Transactions on Automatic Control*, 1(42):427–435, 2006.

[59] A. Levant. Principles of Two-Sliding Mode Design. *Automatica*, 43(43):576–586, 2007.

[60] S. Yu, X. Yu, B. Shirinzadeh, and Z. Man. Continuous Finite-Time Control for Robotic Manipulators with Terminal Sliding Mode. *Automatica*, 41:1957–1964, 2005.

[61] V. I. Utkin and A. S. Poznyak. Adaptive Siding Mode Control with Application to Super-Twist Algorithm: Equivalent Control Method. *Automatica*, 1(49):39–47, 2013.

[62] C.-M. Lin and H.-Y. Li. Adaptive Dynamic Sliding-Mode Fuzzy CMAC for Voice Coil Motor Using Asymmetric Gaussian Membership Function. *IEEE Transactions on Industrial Electronics*, 61(10):5662–5671, 2014.

[63] S. M. Yang and S. J. Ke. Performance Evaluation of a Velocity Observer for Accurate Velocity Estimation of Servo Motor Drives. *IEEE Transactions on Industry Applications*, 36(1):98–104, 2000.

[64] H. Ghafarirada, S. M. Rezaeia, A. Abdullaha, M. Zareinejada, and M. Saadat. Observer-Based Sliding Mode Control with Adaptive Perturbation Estimation for Micropositioning Actuators. *Precision Engineering*, 35(1):271–281, 2011.

[65] C. Kravaris, V. Sotiropoulosa, C. Georgioua, N. Kazantzisb, M. Xiao, and A.J. Krener. Nonlinear Observer Design for State and Disturbance Estimation. *Systems and Control Letters*, 56(1):730–735, 2007.

[66] J.-T. Fei, M.-Y. Xin, and W.-R. Juan. Adaptive Fuzzy Sliding Mode Control Using Adaptive Sliding Gain for MEMS Gyroscope . *Transactions of the Institute of Measurement and Control*, 35(4):551–558, 2012.

[67] M. J. Mahmoodabadi, M. Taherkhorsandi, M. Talebipour, and K. K. Castilo-Vilar. Adaptive Robust PID Control Subject to Supervisory Decoupled Sliding Mode Control Based upon Genetic Algorithm Optimization. *Transactions of the Institute of Measurement and Control*, 70(1):001–010, 2014.

[68] H. Nourisola and B. Ahmadi. Robust Adaptive Sliding Mode Control Sased on Wavelet Kernel Principal Component for Offshore Steel Jacket Platforms Subject to Nonlinear Wave-Induced Force. *Transactions of the Insitute of Measurement and Control*, 22(15):3299–3311, 2014.

[69] A. Bartoszewicz and P. Latosinski. Discrete Time Sliding Mode Control with Reduced Switching – A New Reaching Law Approach. *International Journal of Robust and Nonlinear Control*, 26(1):47–68, 2014.

[70] B. Jakovljevic, A. Pisano, M. R. Rapaic, and E. Usai. On the Sliding-Mode control of Fractional-Order Nonlinear Uncertain Dynamics. *International Journal of Robust and Nonlinear Control*, 26(4):782–798, 2015.

[71] N. Ullah, S. Han, and M. I. Khattak. Adaptive Fuzzy Fractional Sliding Mode controller for a Class of Dynamical Systems with Uncertainty. *Transactions of the Insitute of Measurement and Control*, 38(4):402–413, 2016.

[72] K. Khayati. Multivariable Adaptive Sliding-Mode Observer-Based Control for Mechanical Systems. *Canadian Journal of Electrical and Computer Engineering*, 38(3):253–265, 2015.

[73] J. Zhu and K. Khayati. Adaptive Sliding Mode Control – Convergence and Gain Boundedness Revisited. *International Journal of Control*, 89(4):801–814, 2016.

[74] F. Plestan, Y. Shtessel, V. Bregeault, and A. Poznyak. Sliding Mode Control with Gain Adaptation – Application to an Electropneumatic Actuator. *Control Engineering Practice*, 21(21):679–688, 2013.

[75] A. Fazeli, M. Zeinali, and A. Khajepour. Application of Adaptive Sliding Mode Control for Regenerative Braking Torque Control. *IEEE/ASME Transactions on Mechatronics*, 17(4):745–755, 2012.

[76] O. Barambones and P. Alkorta. Position Control of the Induction Motor Using an Adaptive Sliding-Mode Controller and Observers. *IEEE Transactions on Industry Electronics*, 61(12):6556–6565, 2014.

[77] R. Pupadubsin, N. Chayopitak, D. G. Taylor, N. Nulek, S. Kachapornkul, P. Jitkreeyarn, P. Somsiri, and K. Tungpimolrut. Adaptive Integral Sliding-Mode Position Control of a Coupled-Phase Linear Variable Reluctance Motor for High-Precision Applications. *IEEE Transactions on Industrial Electronics*, 48(4):1353–1363, 2012.

[78] J.-H. Zhang and W.-X. Zheng. Design of Adaptive Sliding Mode Controllers for Linear Systems via Output Feedback. *IEEE Transactions on Industrial Electronics*, 61(7):3553–3562, 2014.

[79] C.-C. Cheng, S.-H. Chien, and F.-C. Shih. Design of Robust Adaptive Variable Structure Tracking Controllers with Application to Rigid Robot Manipulators. *IET Control Theory and Applications*, 4(9):1655–1664, 2010.

[80] M. B. R. Neila and D. Tarak. Adaptive Terminal Sliding Mode Control for Rigid Robotic Manipulators. *International Journal of Automation and Computing*, 8(2):215–220, 2011.

[81] H. Li, J. Yu, C. Hilton, and H. Liu. Adaptive Sliding-Mode Control for Nonlinear Active Suspension Vehicle Systems Using T–S Fuzzy Approach. *IEEE Transactions on Industrial Electronics*, 60(8):3328–3338, 2013.

[82] Jean-Jacques E. Slotine and Mark W. Spong. Robust robot control with bounded input torques. *Journal of Robotic Systems*, 2(4):329–352, 1985.

[83] C.-Y. Su. Adaptive Sliding Mode Control of Nonlinear Robotic Systems with Time-Varying Parameters. *Systems and Control Letters*, 23(1):509–520, 1994.

[84] Yury Stepanenko, Yong Cao, and Chun-Yi Su. Variable structure control of robotic manipulator with PID sliding surfaces. *International Journal of Robust and Nonlinear Control*, 8(1):79–90, 1998.

[85] M. W. Spong, S. Hutchinson, and M. Vidyasagar. *Robot Modeling and Control*. Wiley, NJ, 2006.

[86] S. Islam and X. Liu. Robust Sliding Mode Control for Robot Manipulators. *IEEE Transactions on Industrial Electronics*, 58(6):2444–2453, 2011.

[87] Y. Feng, X.-H. Yu, and Z.-H. Man. Non-Singular Terminal Sliding Mode Control of Rigid Manipulators. *Automaica*, 38(1):2159–2167, 2002.

[88] S.-H. Yu, X.-H. Yu, B. Shirinzadeh, and Z.-H. Man. Continuous Finite-Time Control for Robotic Manipulators with Terminal Sliding Mode. *Automatica*, 41(1):1957–1964, 2005.

[89] A. Levant. High-Order Sliding Modes, Differentiation and Ouput Feedback Control. *International Journal of Control*, 76(9):924–941, 2003.

[90] Y. Shtessel, M. Taleb, and F. Plestan. A Novel Adaptive-Gain Supertwisting Sliding Mode Controller: Methodology and application. *Automatica*, 48(4):759–769, 2012.

[91] B. Fernandez and J. K. Hedrick. Control of Multivariable Nonlinear Systems by the Sliding Mode Method. *International Journal of Control*, 46(3):1019–1040, 1987.

[92] K. Khayati and J. Zhu. Nonlinear Adaptive Observers for Electromechanical Systems – Asymptotic and Exponential Stability Designs. *International Journal of Adaptive Control and Signal Processing*, 2016. In review.

[93] J. J. Craig. *Introduction to Robotics Mechanics and Control*. Pearson Education, Upper Saddle River, NJ, 3rd ed. edition, 2005.

[94] NASA. Aircraft Rotations, July 2016.

[95] W. F. Phillips. *Mechanics of Flight*. John Wiley & Sons, Hoboken, New Jersey, 2nd edition, 2009.

[96] C. M. Close, D. K. Frederick, and J. C. Newell. *Modeling and Analysis of Dynamic Systems*. John Wiley & Sons, Princeton, NJ, 3rd ed. edition, 2001.

[97] J. Zhu and K. Khayati. Adaptive Observer for a Class of Second Order Nonlinear Systems. In *International Conference on Communications, Computing and Control Applications*, Hammamet, Tunisia, 2011.

[98] K. Khayati and J. Zhu. Nonlinear Adaptive Observer Design for an Electromechanical Rotative Plant. In *23rd Canadian Congress of Applied Mechanics*, Vancouver, Canada, 2011.

[99] J. Zhu and K. Khayati. On Robust Nonlinear Adaptive Observer – LMI Design. In *International Conference on Mechanical Engineering and Mechatronics*, Ottawa, Canada, 2012.

[100] J. Zhu and K. Khayati. LMI-Based Adaptive Observers for Nonlinear Systems. *International Journal of Mechanical Engineering and Mechatronics*, pages 50–60, 2012. doi:10.11159/ijmem.2012.006.

[101] K. Khayati and J. Zhu. On Exponentially Stable Nonlinear Adaptive Observer. In *International Conference on Mechanical Engineering and Mechatronics*, Ottawa, Canada, 2012.

[102] K. Khayati and J. Zhu. Adaptive Observer for a Large Class of Nonlinear System with Exponential Convergence of Parameter Estimation. In *International Conference on Control, Decision and Information Technologies*, Hammamet, Tunisia, 2013.

[103] R. Marino and P. Tomei. Adaptive Observers with Arbitrary Exponential Rate of Convergence for Nonlinear Systems. *IEEE Transactions on Automatic Control*, 40(7):1300–1304, 1995.

[104] Y.-M. Cho and R. Rajamani. A Systematic Approach to Adaptive Observer Synthesis for Nonlinear Systems. *IEEE Transactions on Automatic Control*, 42(4):534–537, 1997.

[105] P. Ioannou and B. Fidan. Adaptive Control Tutorial. In *SIAM Studies in Applied Mathematics*. Society for Industrial and Applied Mathematics, Philadelphia, PA, 2006.

[106] Y.-L. Dong and S.-W. Mei. Adaptive Observer for a Class of Nonlinear Systems. *Acta Automatica Sinica*, 33(10):1081–1084, 2007.

[107] T. Maatoug, M. Farza, M. M'Saad, Y. Koubaa, and M. Kamoun. Adaptive Observer Design for a Class of Nonlinear Systems with Coupled Structures. *International Journal of Sciences and Techniques of Automatic Control and Computer Engineering*, 2(1):484–499, 2008.

[108] P. Ioannou and B. Fidan. *Adaptive Control Tutorial: Part of Advances in Design and Control*. The Society for Industrial and Applied Mathematics, PA, 2007.

[109] P. Gahinet, A. Nemirovskii, A. J. Laub, and M. Chilali. MATLAB LMI Control Toolbox. MathWorks Inc., Natick, MA, 1995.

[110] A. Zemouche and M. Boutayeba. A Unified Adaptive Observer Synthesis Method for a Class of Systems with Both Lipschitz and Monotone Nonlinearities. *Systems and Control Letters*, 58(4):282–288, 2009.

[111] Y. Liu. Robust Adaptive Observer for Nonlinear Systems with Unmodeled Dynamics. *Automatica*, 45:1891–1895, 2009.

[112] G. Besançon. Remarks on Nonlinear Adaptive Observer Design. *Systems and Control Letters*, 41:271–280, 2000.

[113] O. N. Stamnes, J. Zhu., O. M. Aamo, and G. O. Kaasa. Adaptive Observer Design for Nonlinear Systems with Parametric Uncertainties in Unmeasured State Dynamics. In *IEEE Conference on Decision and Control and Chinese Control Conference*, pages 4414–4419, Shanghai, China, 2009.

[114] M. Pourgholi and V. J. Majd. A Nonlinear Adaptive Resilient Observer Design for a Class of Lipschitz Systems using LMI. *Journal of Circuits, Systems, and Signal Processing*, 30(6):1401–1415, 2011.

[115] A. Levant. Universal Single-Input-Single-Output (SISO) Sliding-Mode Controllers with Finite-Time Convergence. *IEEE Transactions on Automatic Control*, 46(9):1447–1451, 2001.

[116] J. Zhu and K. Khayati. On Adaptive Sliding Mode Control Switching Gain Comments and Alternative Design. In *Canadian Society for Mechanical Engineering International Congress*, pages 1–6, Toronto, Canada, 2014.

[117] J. Zhu and K. Khayati. Adaptive Sliding Mode Control with Smooth Switching Gain. In *IEEE 27th Annual Canadian Conference on Electrical and Computer Engineering*, pages 893–898, Toronto, Canada, 2014.

[118] J. Zhu and K. Khayati. A New Approach for Adaptive Sliding Mode control: Integral/Exponential Gain Law. *Transactions of the Insitute of Measurement and Control*, 38(4):385–394, 2016.

[119] A. F. Fillippov. *Differential Equations with Discontinuous Right Hand Side*. Kluwer Academic Publisher, Dordrecht, Netherlands, 1988.

[120] V. I. Utkin, J. Guldner, and J. Shi. *Sliding Modes in Electromechanical Systems*. Taylor and Francis, London, 1st edition, 1999.

[121] K.-M. Zhou and J. C. Doyle. *Essentials of Robust Control*. Prentice Hall, Upper Saddle River, New Jersey, 1st edition, 1997.

[122] Wikipedia. Sliding Mode Control, July 2013.

[123] S. P. Bhat and D. S. Bernstein. Finite-Time Stability of Continuous Autonomous Systems. *SIAM Journal on Control and Optimization*, 38(3):751–766, 2000.

[124] A. Polyakov and A. Poznyak. Reaching Time Estimation for "Super-Twisting" Second Order Sliding Mode Controller via Lyapunov Function Designing. *IEEE Transactions on Automatic Control*, 54(8):1951–1955, 2009.

[125] J. Zhu and K. Khayati. New Algorithms of Adaptive Switching Gain for Sliding Mode Control: Part I – Ideal Case. In *IEEE International Conference on Control, Decision and Information Technologies*, pages 441–446, Metz, France, 2014.

[126] J. Zhu and K. Khayati. New Algorithms of Adaptive Switching Gain for Sliding Mode Control: Part II – Real Case. In *IEEE 2nd International Conference on Control, Decision and Information Technologies*, pages 447–452, Metz, France, 2014.

[127] C.-C. Cheng and Y. Chang. Design of Decentralised Adaptive Sliding Mode Controllers for Large-Scale Systems with Mismatched Perturbations. *International Journal of Control*, 81(10):1507–1518, 2008.

[128] M. Harmouche, S. Laghrouche, and Y. Chitour. Robust and Adaptive Higher Order Sliding Mode Controllers. In *51st IEEE Conference on Decision and Control*, Maui, Hawaii, USA, 2012.

[129] J. Zhu and K. Khayati. On New Adaptive Sliding Mode Control for MIMO Nonlinear Systems with Uncertainties of Unknown Bounds. *International Journal of Robust and Nonlinear Control*, 2016. doi: 10.1002/rnc.3608.

[130] M. Marcus and H. Minc. *A Survey of Matrix Theory and Matrix Inequalities*. Dover Publications, NY, 1st edition, 2010.

[131] J. Y. Hung, W. Gao, and J.-C. Hung. Variable Structure Control: A Survey. *IEEE Transactions on Industrial Electronics*, 40(1):2–22, 1993.

[132] J. Zhu and K. Khayati. Robust, Smooth and Fast ASMC - Applications to Robot Manipulators. In *24th International Congress of Theoretical and Applied Mechanics*, Montreal, Canada, 2016.

[133] U. Topuc and A. Packard. Stability Region Analysis for Uncertain Nonlinear Systems. pages 1693–1698, 2007.

[134] M. C. Han and Y. H. Chen. Polynomial Robust Control Design for Uncertain Systems. *Automatica*, 28(4):809–814, 1992.

[135] J. Zhu and K. Khayati. Application of Adaptive Sliding Mode Control for Nonlinear Systems with Unknown Polynomial Bounded Uncertainties. *Transactions of the Institute of Measurement and Control*, 2016. In review.

[136] Q. Wang and R. F. Stengel. Robust Control of Nonlinear Systems with Parametric Uncertainty. *Automatica*, 38(1):1591–1559, 2002.

[137] J. Zhu and K. Khayati. On ASMC Design for Robotic Manipulators. In *IEEE 29th Annual Canadian Conference on Electrical and Computer Engineering*, Vancouver, Canada, 2016.

[138] J. Zhu and K. Khayati. Application of Adaptive Sliding Mode Control with Integral/Exponential Adaptation Law to Mechanical Manipulators. In *IEEE 3rd International Conference on Control, Decision and Information Technologies*, Saint Julian's, Malta, 2016.

[139] X. Kong, X. Zhang, X. Chen, B. Wen, and B. Wang. Synchronization Analysis and Control of Three Eccentric Rotors in a Vibrating System Using Adaptive Sliding Mode Control Algorithm. *Mechanical Systems and Signal Processing*, DOI:10.1016/j.ymssp.2015.11.007, 2015.

[140] Quanser. *Quanser/Thermo Electron Special Plants, CRS CataLyst-5T Robot System - Open-Architecture Control Manual*. Quanser, 1.2 edition, 2014.

[141] G. Teschl. *Ordinary Differential Equations and Dynamical Systems*. American Mathematical Society, Providence, Rhode Island, 1st edition, 2012.

[142] M. OSearcoid. *Matric Spaces*. Springer, NY, 1st edition, 2006.

[143] A. Levant. Homogeneity Approach to High-Order Sliding-Mode Design. *Automatica*, 41(41):823–830, 2005.

[144] S. G. Krantz. *A Handbook of Real Variables – With Applications to Differential Equations and Fourier Analysis*. Birkhäuser Boston Inc., Boston, MA, 1st edition, 2004.

Appendices

A Basic Definitions, Teorems and Proofs

A.1 Dynamic Systems and Equilibrium

Definition A.1. [1] When the input u does not present explicitly in (3.1) or (3.2), we obtain the *unforced state equation*

$$\dot{x} = f(x, t) \tag{A.1}$$

Note, the input u is not required to be zero for an unforced system. In fact, substituting the input $u = \gamma(x, t)$ into (3.2) yields an unforced state equation.

Definition A.2. [1] When the function a does not depend explicitly on time t, the system (A.1) is said to be *autonomous* or *time invariant*, *i.e.*,

$$\dot{x} = f(x) \tag{A.2}$$

If the system is not autonomous, then it is called *non-autonomous or time-varying.*

The concept of equilibrium points plays an important role in analysing the dynamic system (A.1).

Definition A.3. [1] A point $x = x_e$ in the state space is called an *equilibrium point* of (A.1) if it has the property that whenever the state of the system starts at x_e, it will remain at x_e for all future time.

Without loss of generality, we state all definitions and theorems for the case when the equilibrium point is at the origin, *i.e.*, $x_e = 0$. Therefore, we will always study the stability of the origin $x = 0$.

A.2 Fundamental Properties of Ordinary Differential Equations

Since the dynamic system (A.1) is essentially a system of ordinary differential equations (ODE), we introduce some fundamental properties of ODE. In the theory of differential equations, the Lipschitz continuity is the central condition of the Picard–Lindelöf theorem [141] which guarantees the existence and uniqueness of the solution to an initial value problem.

Definition A.4. [142] Given two metric spaces (X, d_X) and (Y, d_Y), where d_X denotes the metric on the set X and d_Y is the metric on set Y (for example, Y might be the set of real numbers $\mathbb{R}$ with the metric $d_Y(X, Y) = |X - Y|$, and X might be a subset of $\mathbb{R}$), a function $f : X \to Y$ is called *Lipschitz continuous* if there exists a real constant $L \geq 0$ *s.t.*, for all x_1 and x_2 in X,

$$d_Y(f(x_1), f(x_2)) \leq L \cdot d_X(x_1, x_2) \tag{A.3}$$

Since the metric space considered in most engineering area is $n-$dimensional Euclidean space $(\mathbb{R}^n)$, we call that the system (A.1) with initial condition $x(t_0) = x_0$ satisfies *Lipschitz Condition* if there exist a real constant $L \geq 0$ *s.t.*, for all (x, t) and (y, t) in some neighbourhood of (x_0, t_0), [1]

$$\|f(x, t) - f(y, t)\| \leq L\|x - y\| \tag{A.4}$$

where $\|\cdot\|$ denotes an Euclidean norm and the constant L is called a *Lipschitz Constant*. A function satisfying (A.4) is said to be *Lipschitz* in x. The Lipschitz property is stronger than continuity and weaker than continuous differentiability. By applying the Lipschitz condition, we have the following theorem for the local existence and uniqueness.

Theorem A.1. *[1] Given $r > 0$. Let $f(x, t)$ be piecewise continuous in t and satisfy the Lipschitz condition* (A.4) *$\forall x, y \in X = \{x \in R^n : \|x - x_0\| \leq r\}$. Then, there exists some $\delta > 0$ such that the state equation* (A.1) *with initial condition $x(t_0) = x_0$ has a unique solution over $[t_0, t_0 + \delta]$.*

Mostly, $f(x, t)$ in (3.2) is considered to be Lipschitz in x on $[a, b] \times \chi \subset \mathbb{R} \times \mathbb{R}^n$. If $f(x, t)$ is bounded by some polynomial function of degree greater than 1 in $\mathbb{R} \times \mathbb{R}^n$, then f is not Lipschitz globally. In the later of the thesis, the non-Lipschitz condition will be considered and a solution to stabilize the nonlinear system (3.2) will be given.

Since the vector $f(x, t) \in \mathbb{R}^n$ and the matrix $g(x, t) \in \mathbb{R}^{n \times m}$ of the nonlinear system (3.2) are nonlinear time-varying smooth functions containing

parametric uncertainties and external disturbances, they are usually considered to be bounded by some functions. Consider the state equation $\dot{x} = f(x,t)$ as the unforced form of (3.2) with the uncertain function $f(x,t)$ bounded by $F(x,t)$, *i.e.*,

$$\dot{x} \leq F(x,t) \tag{A.5}$$

The Comparison Lemma is commonly used to deal with this differential inequality.

Lemma A.1 (**Comparison Lemma**). *[1] Consider the scalar differential equation*

$$\dot{v} = F(v,t), \quad v(t_0) = v_0 \tag{A.6}$$

where $F(v,t)$ is continuous in t and locally Lipschitz in v for all $(t,v) \in \mathbb{R} \times \chi$. Let $[t_0, T)$ be the maximal interval of existence of the solution $v(t)$, and suppose $v(t) \in \chi$ for all $t \in [t_0, T)$. Let $x(t)$ be a continuous function whose upper right-hand derivative $D^+x(t)$ satisfies the differential inequality

$$D^+x(t) = f(x,t) \leq F(x,t), \quad x(t_0) = v_0 \tag{A.7}$$

with $x(t) \in \chi$ for all $t \in [t_0, T)$. Then, $x(t) \leq v(t)$ for all $t \in [t_0, T)$.

The Comparison Lemma states that the state (or trajectory) $x(t)$ of the uncertain system $\dot{x} = f(x,t)$ is governed (or upper-bounded) by the solution of the explicit system $\dot{x} = F(x,t)$.

A.3 Stability

A.3.1 Definitions

Consider the autonomous system (A.2) where $f(x)$ is Locally Lipschitz map from a domain $\chi \subset \mathbb{R}^n$ into $\mathbb{R}^n$.

Definition A.5. [1] [123] The equilibrium $x = 0$ is

- *stable* if, for each $\varepsilon > 0$, there exist $\delta = \delta(\varepsilon) > 0$ such that

$$\|x(0)\| < \delta \Rightarrow \|x(t)\| < \varepsilon, \quad \forall t \geq 0 \tag{A.8}$$

- *unstable* if it is not stable
- *asymptotically stable* if it is stable and δ can be chosen such that

$$\|x(0)\| < \delta \Rightarrow \lim_{t \to \infty} x(t) = 0 \tag{A.9}$$

- *finite-time stable* if it is stable, there exists finite time $T \in [0, \infty)$, and δ can be chosen such that,

$$\|x(0)\| < \delta \Rightarrow \lim_{t \to T} x(t) = 0 \tag{A.10}$$

Consider the non-autonomous system (A.1) where $f(x,t)$ is a map from a domain $[0,\infty) \times \chi$ into $\mathbb{R}^n$ and $\chi \subset \mathbb{R}^n$ is a domain containing the origin. Assuming that $f(x,t)$ is locally Lipschitz in x

Definition A.6. [1] [123] The equilibrium $x = 0$ of (A.1) is

- stable if, for each $\varepsilon > 0$, there exist $\delta = \delta(\varepsilon, t_0) > 0$ such that

$$\|x(0)\| < \delta \Rightarrow \|x(t)\| < \varepsilon, \quad \forall t \geq t_0 \geq 0 \tag{A.11}$$

- *uniformly stable* if, for each $\varepsilon > 0$, there exist $\delta = \delta(\varepsilon) > 0$, independent of t_0 such that (A.11) is satisfied.
- *unstable* if it is not stable
- *asymptotically stable* if it is stable and there exists a positive constant $c = c(t_0)$ such that $x(t) \to 0$ as $t \to \infty$, for all $x(t_0) \leq c$.
- *finite-time stable* if it is stable and there exist positive constant $c = c(t_0)$ and T such that $x(t) \to 0$ as $t \to T$, for all $x(t_0) \leq c$.

Definition A.7. [1] [123] The solution of (A.1) is

- *uniformly bounded* if there exists a positive constant c, independent of $t_0 \geq 0$, and for every $a \in (0, c)$, there exist $\beta = \beta(a) > 0$ independent of t_0, such that

$$\|x(t_0)\| < a \Rightarrow \|x(t)\| < \beta, \quad \forall t \geq t_0 \geq 0 \tag{A.12}$$

- *globally uniformly bounded* if (A.12) holds for arbitrarily large a.
- *uniformly ultimately bounded* with an ultimate bound b if there exist positive constants b and c, independent of $t_0 \geq 0$, and for every $a \in (0, c)$, there exists $T = T(a, b) \geq 0$ independent of t_0, such that

$$\|x(t_0)\| < a \Rightarrow \|x(t)\| < b, \quad \forall t \geq t_0 + T \tag{A.13}$$

- *globally uniformly ultimately bounded* if (A.13) holds for arbitrarily large a.

Given a dynamic system $\dot{\mathbf{x}} = f(\mathbf{x})$ where f is continuous on any open domain $\chi \subseteq \mathbb{R}^n$ comprising the origin which is an equilibrium of this dynamics, we have

Definition A.8. (refer to [123, 143]) The equilibrium $\mathbf{x} = 0$ is *asymptotically convergent* if there exists an open neighborhood $U \subseteq \chi$ of the origin such that the solution trajectory $\mathbf{x}(t, \mathbf{x}_0)$ starting from initial point $\mathbf{x}_0 \in U\backslash\{0\}$ is well-defined and unique in forward time for $t \in \mathbb{R}$ and $\mathbf{x}(t, \mathbf{x}_0) \to 0$ as $t \to \infty$.

Definition A.9. (refer to [18, 123]) The equilibrium $\mathbf{x} = 0$ is *finite-time convergent* if there exists an open neighborhood $U \subseteq \chi$ of the origin and a function $t_{\mathbf{x}} : U\backslash\{0\} \to \mathbb{R}\backslash\{0\}$, such that the solution trajectory $\mathbf{x}(t, \mathbf{x}_0)$ starting from initial point $x_0 \in U\backslash\{0\}$ is well-defined and unique in forward time for $t \in [0, t_{\mathbf{x}}(\mathbf{x}_0))$ and $\mathbf{x}(t, \mathbf{x}_0) \to 0$ as $t \to t_{\mathbf{x}}(\mathbf{x}_0)$.

A.3.2 Stability Theorems

For the nonlinear systems with uncertainties, the stability analysis is mainly based on Lyapunov's Stability Theorem and its extensions such as Barbalat's Lemma, LaSalle's Invariance Principle, Comparison Lemma, Fillipov Integration, *etc.* [1].

A.4 Proof of Lemma 4.5

Proof. Refer to Lemma 2 of [16]. The proof is based on Lyapunov stability criterion. Consider the following Lyapunov candidate function

$$V = \frac{1}{2}\sigma^2 \tag{A.14}$$

The time derivative of V is

$$\begin{aligned} \dot{V} &= \sigma\dot{\sigma} \\ &= \sigma(\Psi - \Gamma K \mathrm{sgn}(\sigma)) \\ &= [\Psi \mathrm{sgn}(\sigma) - \Gamma K]|\sigma| \end{aligned} \tag{A.15}$$

Note that $\Psi\mathrm{sgn}(\sigma)$ is bounded, $\Gamma > 0$ and K is an monotonically increasing function. There exist a $K(t^*) = K^*$ large enough and a positive scalar $\kappa > 0$ *s.t.* $\forall t \geq t^*$

$$\begin{aligned} \dot{V} &\leq -\kappa|\sigma| \\ &\leq -\kappa\sqrt{2V} \end{aligned} \tag{A.16}$$

That is,

$$\frac{d}{dt}\sqrt{V} \leq -\frac{\kappa}{\sqrt{2}} \tag{A.17}$$

The inequality (A.17) implies that the positive $\sqrt{V}$ will decrease with a rate at least $\frac{\kappa}{\sqrt{2}}$ and reaches zero in finite time and stay on zero thereafter [1]. Denote the finite time as t_f. Then $\sqrt{V} = |\sigma| = 0$ for all $t \geq t^* + t_f$. From (4.47), we conclude that K stops increasing for all $t \geq t^* + t_f$ and thus K is upper bounded. □

A.5 Proof of Theorem 4.1

Proof. Refer to Theorem 3 of [16]. The proof is based on Lyapunov stability criterion. Define the switching gain adaptation error $\tilde{K} = K - K^*$, where K^* is an upper bound value of K defined in (4.48). Indeed, from Lemma 4.5, there always exists a constant K^* *s.t.* $\tilde{K} < 0\ \forall t > 0$, *i.e.*, $\tilde{K} = -|\tilde{K}|$. Given the closed-loop system (4.37) with (4.47), consider the following Lyapunov candidate function

$$V = \frac{1}{2}\sigma^2 + \frac{1}{2\gamma}\tilde{K}^2 \tag{A.18}$$

with $\gamma > 0$. Since Ψ and Γ are bounded, there exist $\bar{\Psi}$ and $\underline{\Gamma}$ *s.t.* $\big|\Psi\big| \leq \bar{\Psi}$ and $\underline{\Gamma} \leq \Gamma$ (refer to (4.24) and (4.25)). Noting that K^* is constant and $K(t) > 0 \forall t$, the time derivative of V is

$$\begin{aligned}
\dot{V} &= \sigma\dot{\sigma} + \frac{1}{\gamma}\tilde{K}\dot{K} \\
&= \sigma\big[\Psi - \Gamma K \mathrm{sgn}(\sigma)\big] + \frac{1}{\gamma}\tilde{K}\alpha\cdot|\sigma| \\
&\leq |\sigma|(\bar{\Psi} - \underline{\Gamma}K) + \frac{1}{\gamma}\tilde{K}\alpha\cdot|\sigma| + |\sigma|\underline{\Gamma}K^* - |\sigma|\underline{\Gamma}K^* \\
&\leq -|\sigma|\big[-\bar{\Psi} + \underline{\Gamma}K^*\big] + \frac{1}{\gamma}\tilde{K}\alpha\cdot|\sigma| - |\sigma|\underline{\Gamma}\tilde{K} \\
&\leq -|\sigma|\big[-\bar{\Psi} + \underline{\Gamma}K^*\big] - |\tilde{K}|\cdot\big[\frac{\alpha}{\gamma}\cdot|\sigma| - |\sigma|\underline{\Gamma}\big]
\end{aligned} \tag{A.19}$$

Note that there always exists K^* and $\gamma > 0$ small *s.t.* $\beta_\sigma \triangleq -\bar{\Psi} + \underline{\Gamma}K^* > 0$, $0 < \gamma < \frac{\alpha}{\underline{\Gamma}}$ and $\beta_k = \big(-\underline{\Gamma} + \frac{\alpha}{\gamma}\big)\cdot|\sigma| > 0$ [16]. Then,

$$\dot{V} \leq -\beta_\sigma|\sigma| - \beta_k|\tilde{K}| \tag{A.20}$$

Then

$$\dot{V} \leq -\beta\cdot(2V)^{1/2} \tag{A.21}$$

with $\beta = \min(\beta_\sigma, \beta_K\sqrt{\gamma})$. Therefore, a finite time convergence to a domain $|\sigma| \leq \epsilon$ is guaranteed from any initial condition $|\sigma(0)| > \epsilon > 0$, and the reaching time can be estimated [1]

$$t_F \leq \frac{\sqrt{2}V(0)^{1/2}}{\beta} \tag{A.22}$$

□

A.6 Example of a System Verifying Lemma 5.1

The following is an example of a system varifying Lemma 5.1 that it does not show FTC.

Given the perturbed system

$$\dot{x} = -2x \tag{A.23a}$$
$$\dot{y} = -x - y + d \tag{A.23b}$$

with $y(0) > x(0) \geq 0$ and $d > 0$ unknown positive constant satisfying $y(0) - x(0) - d > 0$. We have

$$x(t) = e^{-2t}x(0) \tag{A.24a}$$
$$y(t) = x(t) + e^{-t}\big(y(0) - x(0) - d\big) + d \tag{A.24b}$$

Obviously, $x(t) \to 0$ (exponentially) and $y(t) \to d$ (bounded) as $t \to \infty$. Taking the time derivative of (A.24b), we have

$$\dot{y} = -2x - \big(y(0) - x(0) - d\big)e^{-t} \tag{A.25}$$

Noting that $\big(y(0) - x(0) - d\big)e^{-t} > 0$ and $y(t) > 0$, we have

$$\begin{aligned} y\dot{y} &\leq -2xy \\ &\leq -2dx \end{aligned} \tag{A.26}$$

Given $V = x^2 + y^2$ which satisfies (5.2) and noting that $x(t) > 0$, we have, $\forall X = (x, y) \in \chi \subset \mathbb{R}^2$,

$$\begin{aligned} \dot{V} &= 2x\dot{x} + 2y\dot{y} \\ &\leq -4x^2 - 4dx \\ &\leq -4d\|x\| \end{aligned} \tag{A.27}$$

which verifies Lemma 5.1 without any FTC. In stead, x is ES and y UUB.

A.7 Proof of Proposition 5.1

Proof. The proofs for adaptation laws (5.53) or (5.55) are similar and are derived from their ideal case discussed in [118]. We briefly show the FTC proof of adaptation law (5.55) for the sake of simplicity. Basically, it is separated into two steps. First, we prove that there exists a *compensating phase* for any $|\sigma| > \epsilon$. At the end of the compensating phase, the lumped perturbation will be eventually compensated by the switching gain. Then, we prove that there exists a finite time *reaching phase*. During this second phase, the switching gain is always greater than the lumped perturbation, *i.e.*, the time derivative of $|\sigma|$ is always negative. Thus the sliding variable reaches the domain $|\sigma| \leq \epsilon$ from any $|\sigma| > \epsilon$ in finite time. In fact, we have

***Compensating phase*:** Recall the closed-loop dynamics (5.17)

$$\dot{\sigma} = \Psi - \Gamma K \text{sgn}(\sigma) \tag{A.28}$$

with the dynamic gain law introduced in (5.19)

$$\dot{K} = \alpha|\sigma| \cdot (|\sigma| - \varepsilon) \tag{A.29}$$

For *any* perturbation $\dfrac{\Psi \cdot \text{sgn}(\sigma)}{\Gamma}$ no less than the actual switching gain K, *i.e.*,

$$\frac{\Psi \cdot \text{sgn}(\sigma)}{\Gamma} \geq K(t) \tag{A.30}$$

We have, from (A.28)

$$\begin{aligned} \frac{d}{dt}|\sigma| &= \Psi \cdot \text{sgn}(\sigma) - \Gamma K \\ &\geq 0 \end{aligned} \tag{A.31}$$

Thus, $|\sigma|$ is non-decreasing and from (A.29), $K(t)$ keeps increasing. Noting that $\dfrac{\Psi \cdot \text{sgn}(\sigma)}{\Gamma}$ is bounded, the gain $K(t)$ will eventually compensate for the lumped uncertainties $\dfrac{\Psi \cdot \text{sgn}(\sigma)}{\Gamma}$. Since the non-decreasing switching gain $K(t)$ reacts and compensates for *any* perturbation $\dfrac{\Psi \cdot \text{sgn}(\sigma)}{\Gamma}$, we state that there always exists a time instant $t^* \geq 0$ so that $K(t^*)$ compensates for $\dfrac{\Psi \cdot \text{sgn}(\sigma)}{\Gamma}$, *i.e.*, for all $t \geq t^*$

$$K(t^*) \geq \frac{\Psi \cdot \text{sgn}(\sigma)}{\Gamma} \tag{A.32}$$

The discussion of the compensating phase is dealing with the two different cases $\sigma > \epsilon > 0$ and $\sigma < \epsilon < 0$, simultaneously.

***Reaching phase*:** After the compensating phase, the system trajectory moves into the *reaching phase*. We integrate (A.29) between t^* and any instant $t \geq t^*$ to obtain

$$K(t) = K(t^*) + \int_{t^*}^{t} \alpha \cdot (|\sigma| - \epsilon) d\tau \tag{A.33}$$

From (A.28) and (A.33), we have, for $|\sigma| > \epsilon > 0$,

$$\frac{d}{dt}(|\sigma| - \epsilon) = \Psi \mathrm{sgn}(\sigma) - \Gamma K(t^*) - \Gamma \int_{t^*}^{t} \alpha \cdot (|\sigma| - \epsilon) d\tau$$

Noting (A.32) and $\Gamma \geq \underline{\Gamma} > 0$, we have

$$\frac{d}{dt}(|\sigma| - \epsilon) \leq -\alpha \underline{\Gamma} \int_{t^*}^{t} (|\sigma| - \epsilon) d\tau \tag{A.34}$$

The above differential inequality shows that the positive amount $(|\sigma| - \epsilon)$ is decreasing with a time-varying rate of at least $\alpha \underline{\Gamma} \int_{t^*}^{t} (|\sigma| - \epsilon) d\tau$. From (A.34), we derive the following limit case (*i.e.*, the worst in terms of response rate) for the time evolution of σ during the reaching phase with the initial condition stated at the instant t^* (*i.e.*, the end of the compensating phase). In fact, the trajectory of $(|\sigma| - \epsilon)$ geometrically lies below the majorant curve [53, 89] of $(|\sigma| - \epsilon)$ governed by

$$\frac{d\big(|\sigma| - \epsilon\big)}{dt} = -\alpha \underline{\Gamma} \int_{t^*}^{t} \big(|\sigma| - \epsilon\big) d\tau \tag{A.35}$$

Then, the reaching time can be generically estimated by solving (A.35) with the limit conditions $|\sigma(t^*)| = |\sigma^*|$ and $|\dot{\sigma}(t^*)| = 0$. We write the explicit formula of the majorant curve as

$$|\sigma(t)| - \epsilon = \big(|\sigma^*| - \epsilon\big) \cdot \cos\big(\sqrt{\underline{\Gamma}\alpha} \cdot (t - t^*)\big) \tag{A.36}$$

which reaches the domain $|\sigma| \leq \epsilon$ when the argument of the cosine function in (A.36) reaches $\frac{\pi}{2}$ from 0 (*i.e.*, initial value corresponding to $t = t^*$), that is, $\sqrt{\underline{\Gamma}\alpha} \cdot (t - t^*) = \frac{\pi}{2}$. Thus, the upper-bound of the reaching time is estimated as

$$t_r - t^* \leq \frac{\pi}{2\sqrt{\underline{\Gamma}\alpha}} \tag{A.37}$$

where t^* is the compensating time. $t^* + \frac{\pi}{2\sqrt{\underline{\Gamma}\alpha}}$ represents an estimate of the total FTC of the sliding variable to the domain $|\sigma| \leq \epsilon$. □

A.8 Proof of Theorem 6.2

Proof. In this new design, there still exists a compensating phase and a reaching phase. Thus, the proof is similar to Theorem 1 in the case of bounded uncertainties for the ideal ASMC design introduced in [118].

Compensating phase: Recall the scalar sliding variable dynamics (6.6)

$$\dot{\sigma}(x,t) = \Psi(x,t) + \Gamma(x,t)u \tag{A.38}$$

controlled by the switching control

$$u(t) = -K(t)\cdot \mathrm{sgn}(\sigma) \tag{A.39}$$

with the adaptation gain law (6.25)

$$\begin{cases} \dot{\breve{K}}(\sigma) & = \alpha|\sigma| \\ K(\sigma) & = \breve{K}(\sigma) + \beta(e^{|\sigma|}-1) \end{cases} \tag{A.40}$$

For *any* perturbation no less than the switching gain, *i.e.*,

$$\frac{\Psi\cdot\mathrm{sgn}(\sigma)}{\Gamma} \geq K(t) \tag{A.41}$$

we have, from (A.38)

$$\begin{aligned} \frac{d}{dt}|\sigma| &= \Gamma\Big(\frac{\Psi\cdot\mathrm{sgn}(\sigma)}{\Gamma} - K\Big) \\ &\geq 0 \end{aligned} \tag{A.42}$$

Then, $|\sigma|$ is non-decreasing. Using (A.40) and $\Gamma > 0$, the above inequality is equivalent to

$$\breve{K}(|\sigma|) \leq \frac{\Psi\cdot\mathrm{sgn}(\sigma)}{\Gamma} - \beta\big(e^{|\sigma|}-1\big) \tag{A.43}$$

Since $|\sigma|$ is non-decreasing, from (A.40), $\breve{K}(|\sigma|)$ keeps growing with a rate of at least $\alpha|\sigma| > 0$. Thus, the growing state gain $\breve{K}$ of the left side of (A.43) will eventually compensate for the upper bounded right side of (A.43). Consequently, the growing K will consequently completely compensate for the perturbation $\dfrac{\Psi\cdot\mathrm{sgn}(\sigma)}{\Gamma}$ in (A.41) at some time instant t^*. In other words, for any perturbations and bounded uncertain terms Ψ and Γ by assumptions 6.3

and 6.4 (refer to Section 6.2 of Chapter 6), respectively, and for any $|\sigma| > \epsilon$, there always exists an ultimate time instant $t^* \geq 0$ such that

$$\breve{K}(|\sigma|) > \frac{\Psi \cdot \mathrm{sgn}(\sigma)}{\Gamma} - \beta\big(e^{|\sigma|} - 1\big) \tag{A.44}$$

and, equivalently,

$$K(t) > \frac{\Psi \cdot \mathrm{sgn}(\sigma)}{\Gamma} \tag{A.45}$$

for all $t \geq t^*$. If the perturbation exceeds the switching gain in the future, the state gain $\breve{K}(t)$ and the switching again $K(t)$ react and compensate for the perturbation again. So, there always exists such a time instant $t^* \geq 0$. Since $\breve{K}(|\sigma|)$ still keeps increasing for any $|\sigma| > \epsilon$, without loss of generality, there exists $\kappa > 0$ and $\delta t > 0$ such that

$$\breve{K}(|\sigma|) \geq \frac{\Psi \cdot \mathrm{sgn}(\sigma)}{\Gamma} - \beta(e^{|\sigma|} - 1) + \kappa \tag{A.46}$$

and, equivalently,

$$K(t) \geq \frac{\Psi \cdot \mathrm{sgn}(\sigma)}{\Gamma} + \kappa \tag{A.47}$$

for all $t \geq t^* + \delta t$.

Reaching phase: After the compensating phase, the system trajectory moves ultimately into the *reaching phase*. This statement happens when $\breve{K}$ is large enough to compensate for the compound uncertainties independently of the exponential term. Prior to this ultimate regime, the exponential term of the switching gain (A.40) could intermittently increase and decrease depending on the fact that the instantaneous total switching gain is compensating or not for the lumped uncertainties (*i.e.*, $\dfrac{d|\sigma|}{dt} < 0$ or $\dfrac{d|\sigma|}{dt} > 0$), while the integral term, *i.e.*, $\breve{K}$, is always increasing as far as $|\sigma| > \epsilon$. Now, we consider the following Lyapunov candidate function

$$V = \sigma^2 \tag{A.48}$$

We have, from (A.47), for all $t \geq t^* + \delta t$,

$$\begin{aligned} \dot{V} &= 2|\sigma| \cdot \mathrm{sgn}(\sigma)\dot{\sigma} \\ &= 2\sqrt{V} \cdot [\Psi \mathrm{sgn}(\sigma) - \Gamma K] \\ &\leq -2\sqrt{V} \cdot \underline{\Gamma}\kappa \end{aligned}$$

That is,

$$d\sqrt{V} \leq -\underline{\Gamma}\kappa \cdot dt \tag{A.49}$$

Integrating both sides of (A.49) between $t^* + \delta t$ and $t \geq t^* + \delta t$, we conclude that the positive definite function V, as well as $|\sigma|$, converges to the domain $|\sigma| \leq \epsilon$ in finite time [1]. □

A.9 Upper-Boundedness of Combined Lumped Uncertainties with Exponential Gain – Scalar Dynamics Case

In the following, we demonstrate the upper-boundedness of term $h(\sigma)$ introduced in (7.15) (*i.e.*, Proof of (7.16)).

Proof. Note here that $\sigma = x$. From assumptions 7.2 – 7.4, we have for any $\sigma \in \mathbb{R}$

$$\begin{aligned} h(\sigma) &= \frac{\Psi \cdot \mathrm{sgn}(\sigma)}{\Gamma} - \beta(e^{|\sigma|} - 1) \\ &\leq \big(\beta + \frac{d_0}{\Gamma}\big) + \sum_{i=1}^{q} \frac{d_i}{\Gamma}|\sigma|^i - \beta e^{|\sigma|} \end{aligned} \tag{A.50}$$

Given scalars $\beta > 0$ and $d_i \geq 0$ $(i = 0, \cdots, q)$, there always exist a positive integer r, real scalars $\delta_0 \geq 0$ and $\delta \geq 0$ *s.t.*

$$h(\sigma) \leq \delta_0 + \delta|\sigma|^r - \beta e^{|\sigma|} \tag{A.51}$$

The two terms $\delta_0 + \delta|\sigma|^r$ and $\beta e^{|\sigma|}$ of the right side of (A.51) are continuously monotonically increasing as $|\sigma|$ increases on $[0, +\infty)$. However, by applying L'Hopital's rule repeatedly [144], we obtain

$$\lim_{|\sigma| \to \infty} \frac{\delta_0 + \delta|\sigma|^r}{\beta e^{|\sigma|}} = 0 \tag{A.52}$$

That is, the polynomial term $\delta_0 + \delta|\sigma|^r$ grows with a slower rate than the exponential term $\beta e^{|\sigma|}$. In other words, there exists $h^* \in \mathbb{R}$ *s.t.*, for all $|\sigma| \neq 0$,

$$h(\sigma) \leq h^* = \sup_{|\sigma|} \Big(\delta_0 + \delta|\sigma|^r - \beta e^{|\sigma|}\Big) \tag{A.53}$$

Note that h^* is a finite value. □

A.10 Switching Control in the Case of Indefinite Parameter Matrix Γ

In the following, we demonstrate the FTC problem of theorem 6.4.

Proof. Recall the closed-loop dynamics (6.48)

$$\dot{\sigma} = \Psi - \Gamma K(t) \cdot \frac{\hat{\Gamma}^T \sigma}{\|\hat{\Gamma}^T \sigma\|} \tag{A.54}$$

Consider the Lyapunov function candidate $V = \sigma^T \sigma$. Let $s = \hat{\Gamma}^T \sigma$. Using $L(t) = \hat{\Gamma}^{-1}\Gamma$, $L_s = \frac{1}{2}(L + L^T)$ and (A.54), the time derivative of V along the system trajectories is

$$\begin{aligned} \dot{V} &= 2\|s\| \Big(\frac{s^T(\hat{\Gamma}^{-1}\Psi)}{\|s\|} - K \frac{s^T L_s s}{\|s\|^2} \Big) \\ &= 2\|s\| \Big(h_{L_s}(\sigma) - \breve{K} \frac{s^T L_s s}{\|s\|^2} \Big) \end{aligned} \tag{A.55}$$

with $h_{L_s}(\sigma) = \dfrac{s^T\big(\hat{\Gamma}^{-1}\Psi\big)}{\|s\|} - \beta\big(e^{\|\sigma\|} - 1\big)\dfrac{s^T L_s s}{\|s\|^2}$. The scalar $h_{L_s}(\sigma)$ is upper-bounded for any value of σ. For any $\|\sigma\| > \epsilon$, $\breve{K}$ will keep growing and eventually the positive scalar $\breve{K}\dfrac{s^T L_s s}{s^T s}$ will compensate for the upper-bounded scalar $h_{L_s}(\sigma)$, *i.e.*, $\breve{K}\dfrac{s^T L_s s}{\|s\|^2} > h_{L_s}(\sigma)$. Since this compensating action will occur for any $\|\sigma\| > \epsilon$ where $h_{L_s}(\sigma) \geq \breve{K}\dfrac{s^T L_s s}{\|s\|^2}$ (*i.e.*, $\dfrac{d}{dt}\|\sigma\| \equiv \dfrac{\dot{V}}{2\sqrt{V}} \geq 0$), we conclude that there exists a time instant t^* and a positive scalar κ_2 such that

$$\breve{K}\frac{s^T L_s s}{\|s\|^2} \geq h_{L_s}(\sigma) + \kappa_2 \tag{A.56}$$

for $t \geq t^*$. Then,

$$\dot{V} \leq -2\kappa_2 \|s\| \tag{A.57}$$

for $t \geq t^*$. Since $\|s\|^2 = \sigma^T \hat{\Gamma}\hat{\Gamma}^T \sigma \geq \underline{\lambda}(\hat{\Gamma})^2 \sigma^T \sigma$ with $\underline{\lambda}(\hat{\Gamma}) > 0$ the minimum singular value of the matrix $\hat{\Gamma}$, we have $\|s\| \geq \underline{\lambda}(\hat{\Gamma})\|\sigma\|$. Then, from (6.51), we obtain

$$\frac{d\sqrt{V}}{dt} \leq -\kappa_2 \underline{\lambda}(\hat{\Gamma}) \tag{A.58}$$

Thus, σ converges to the domain $\|\sigma\| \leq \epsilon$ in finite time with a maximum reaching time $t_r \leq \dfrac{\|\sigma(t^*)\| - \epsilon}{\kappa_2 \underline{\lambda}(\hat{\Gamma})} + t^*$ [1]. □

A.11 Equivalent Control of Robot Manipulators

When reliable nominal terms of the robot dynamics are available, the equivalent control method can be combined with the ASMC to deal with known dynamics in order to reduce the effect of lumped uncertainties. In this case, the uncertain elements $M(q)$, $C(q, \dot{q})$ and $G(q)$ defined in (7.40) will be replaced by the corresponding modeling errors, parameter variations and unknown loads in the dynamic model of rigid manipulator (7.40) as

$$M(q) = \hat{M}(q) + \tilde{M}(q) \tag{A.59a}$$

$$C(q, \dot{q}) = \hat{C}(q, \dot{q}) + \tilde{C}(q, \dot{q}) \tag{A.59b}$$

$$G(q) = \hat{G}(q) + \tilde{G}(q) \tag{A.59c}$$

where $\hat{M}(q)$, $\hat{C}(q, \dot{q})$ and $\hat{G}(q)$ represent the nominal values and $\tilde{M}(q)$, $\tilde{C}(q, \dot{q})$ and $\tilde{G}(q)$ the uncertain values. Then, from (A.59), the dynamics (7.40) can be written as

$$\hat{M}(q)\ddot{q} + \hat{C}(q, \dot{q})\dot{q} + \hat{G}(q) = u + \rho(t) \tag{A.60}$$

where $\rho(t)$ is the lumped uncertainty.

$$\rho(t) = -\tilde{M}\ddot{q} - \tilde{C}\dot{q} - \tilde{G} + d(t) \tag{A.61}$$

Note that, in most robot systems, Assumption 7.1 is satisfied.

Given q_d twice differentiable desired bounded trajectory of $\mathbb{R}^n$, consider the trajectory error (7.41)

$$e = q - q_d \tag{A.62}$$

The error dynamics corresponding to (A.60) is

$$\ddot{e} = -\ddot{q}_d - \hat{M}^{-1}(\hat{C}\dot{q} + \hat{G}) + \hat{M}^{-1}u + \hat{M}^{-1}\rho(t) \tag{A.63}$$

Noting the sliding variable defined by (7.43), the sliding variable dynamics is written as the time derivative of (7.43)

$$\dot{\sigma} = -\ddot{q}_d - \hat{M}^{-1}(\hat{C}\dot{q} + \hat{G}) + \hat{M}^{-1}u + \hat{M}^{-1}\rho(t) + D \cdot \dot{e} \tag{A.64}$$

The equivalent control applied to the rigid robotic manipulator consists of two parts as

$$u = u_{eq} + u_s \tag{A.65}$$

The smooth control u_{eq} is used to maintain the movement of the system on the sliding surface and the discontinuous switching control u_s drives the system trajectory to reach the sliding surface. The equivalent control can be determined, in the absence of uncertainties (*i.e.*, $\tilde{M} = 0$, $\tilde{C} = 0$, $\tilde{G} = 0$ and $d(t) = 0$), from

$$\dot{\sigma} = 0 \tag{A.66}$$

That is, letting $\rho(t) = 0$ and replacing u with u_{eq} in (A.64), we have from (7.43)

$$-\ddot{q}_d - \hat{M}^{-1}(\hat{C}\dot{q} + \hat{G}) + \hat{M}^{-1}u_{eq} + D \cdot \dot{e} = 0$$

The expression of the equivalent control is then obtained by solving the above equation in the variable u_{eq} as

$$u_{eq} = (\hat{C}\dot{q} + \hat{G}) + \hat{M}\big(\ddot{q}_d - D \cdot \dot{e}\big) \tag{A.67}$$

Substituting (A.65) into (A.64) with u_{eq} defined by (A.67), we obtain the sliding variable dynamics in terms of the switching control u_s

$$\dot{\sigma} = \hat{M}^{-1}u_s + \hat{M}^{-1}\rho(t) \tag{A.68}$$

Defining the new lumped uncertainty $\Psi = \hat{M}^{-1}\rho(t)$, the sliding variable dynamics can be written as

$$\dot{\sigma} = \Psi(t) + \hat{M}^{-1}u_s \tag{A.69}$$

Noting that $\hat{M}^{-1}$ is known and positive definite, we define the unit switching control as [120, 138]

$$u_s = \begin{cases} -K \cdot \dfrac{\hat{M}^{-T}\sigma}{\|\hat{M}^{-T}\sigma\|} & \text{if } \sigma \neq 0 \\ 0 & \text{if } \sigma = 0 \end{cases} \tag{A.70}$$

where $K > 0$ is the switching gain. Applying the adaptation law (7.28), we guarantee the FTC of the states to the targeted manifold Σ_δ [138].

B Further Simulation and Experiment Results

B.1 Experimental Results of ESAO Design

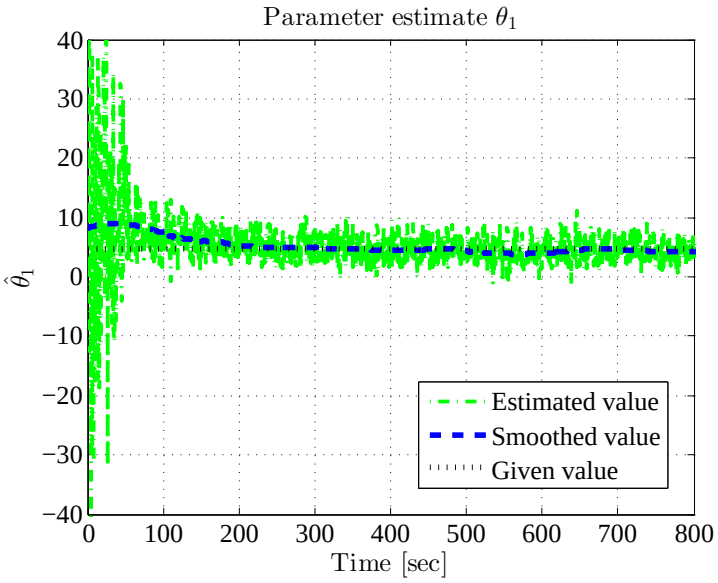

Figure B.1: Experimental Results – Estimate of parameter θ_1

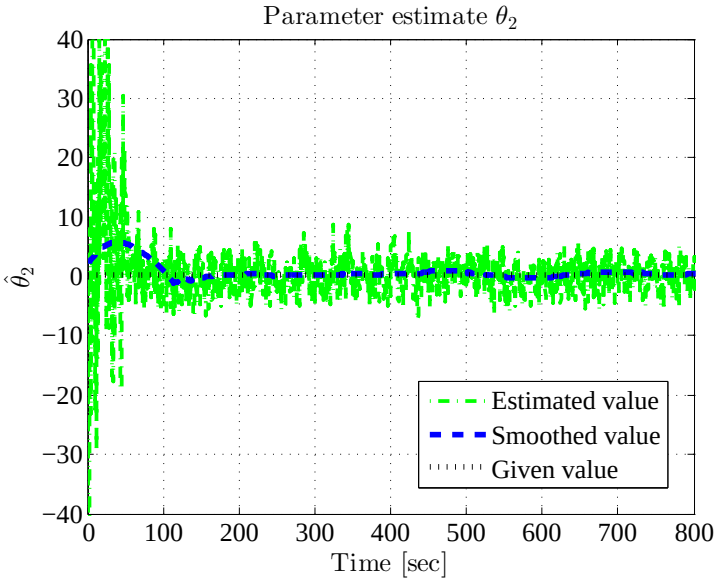

Figure B.2: Experimental Results – Estimate of parameter θ_2

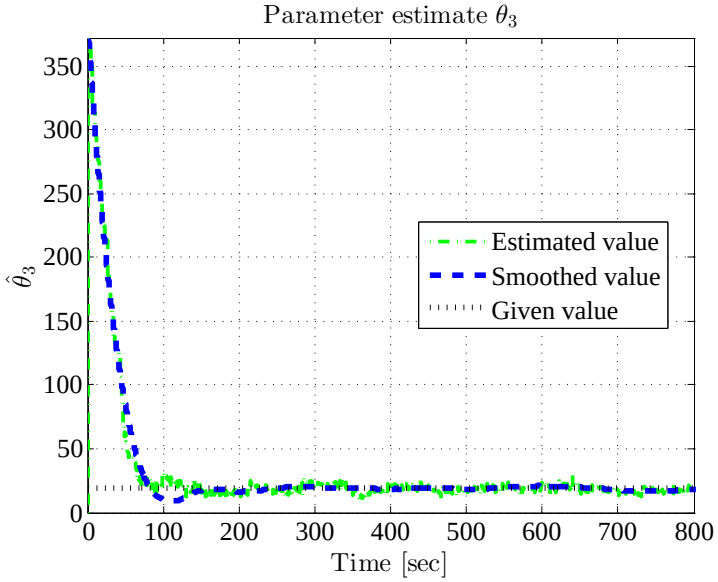

Figure B.3: Experimental Results – Estimate of parameter θ_3

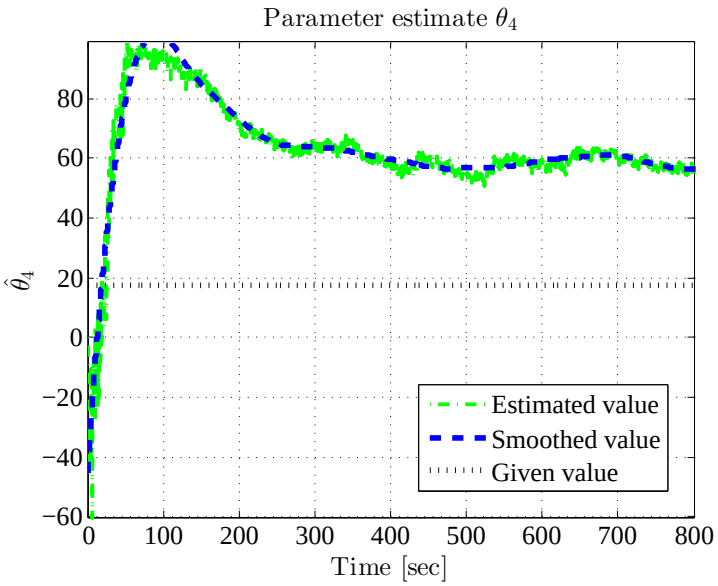

Figure B.4: Experimental Results – Estimate of parameter θ_4

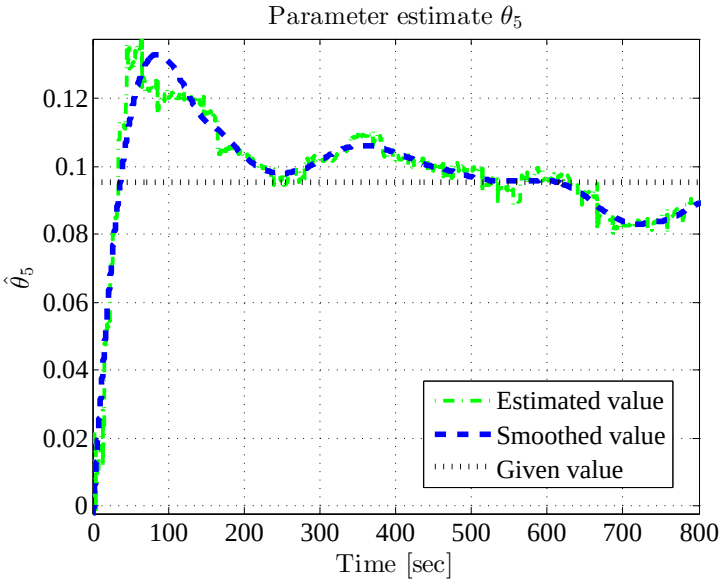

Figure B.5: Experimental Results – Experimental Results – Estimate of parameter θ_5

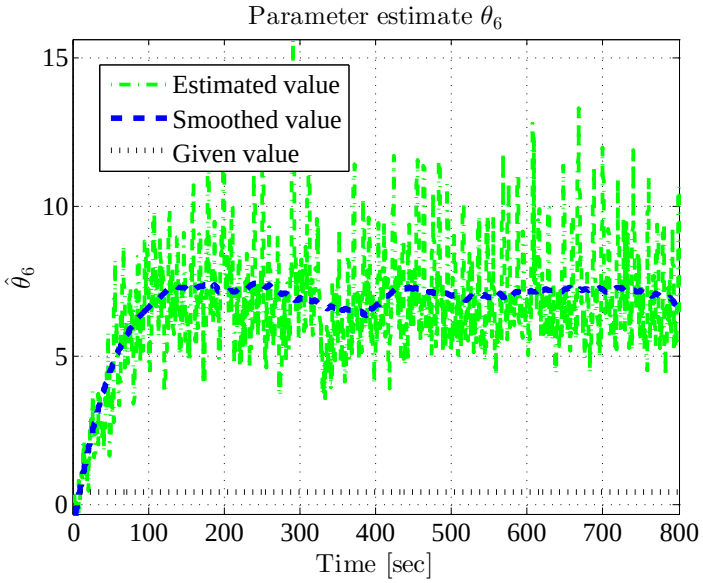

Figure B.6: Experimental Results – Estimate of parameter θ_6

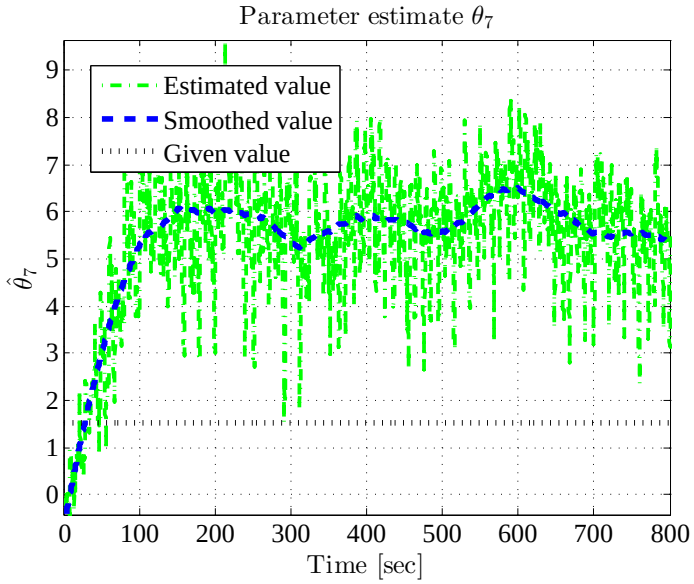

Figure B.7: Experimental Results – Estimate of parameter θ_7

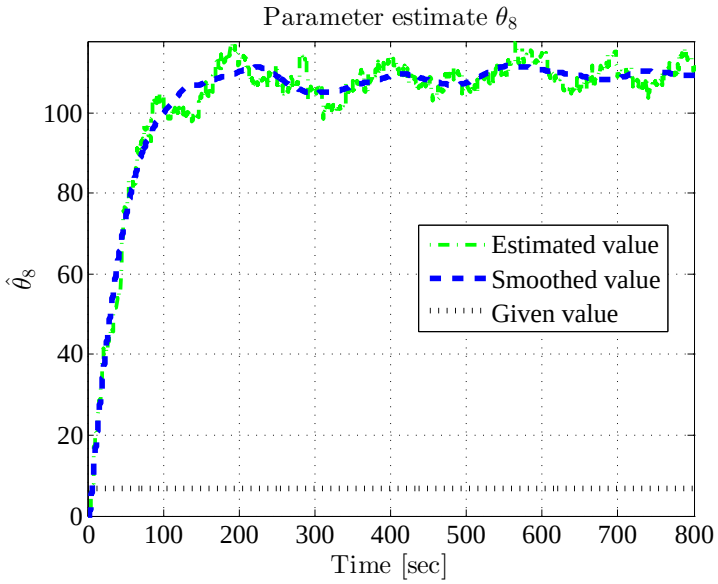

Figure B.8: Experimental Results – Estimate of parameter θ_8

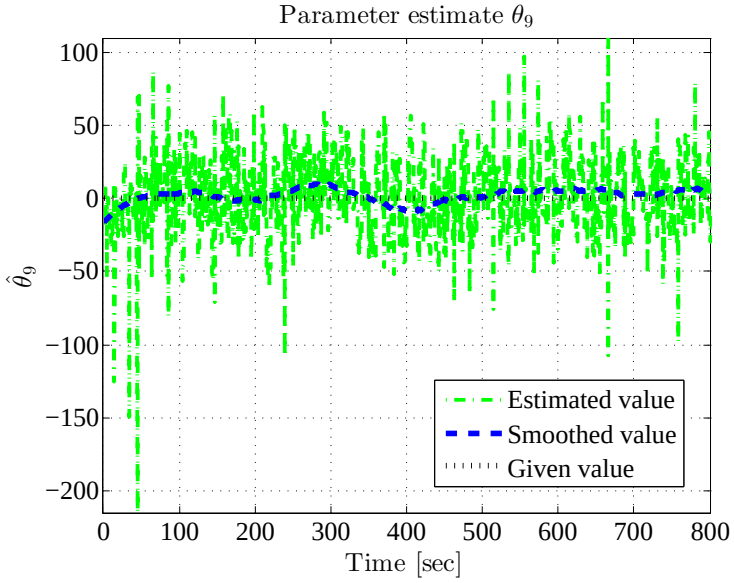

Figure B.9: Experimental Results – Estimate of parameter θ_9

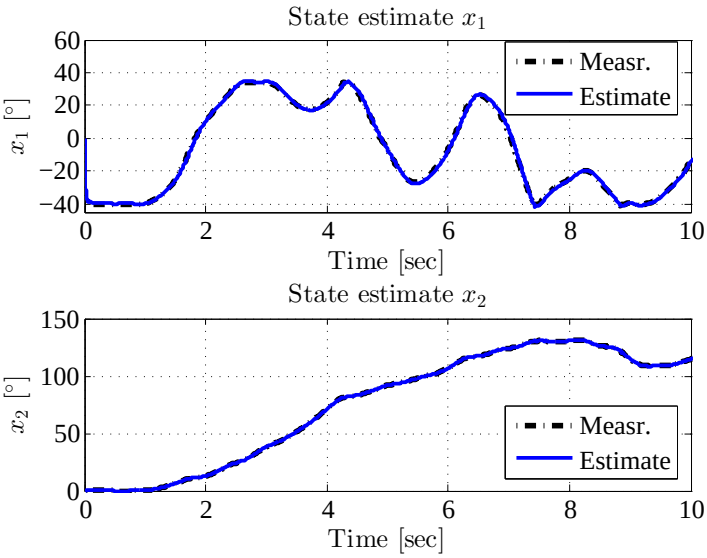

Figure B.10: Experimental Results – State estimate errors x_1 and x_2

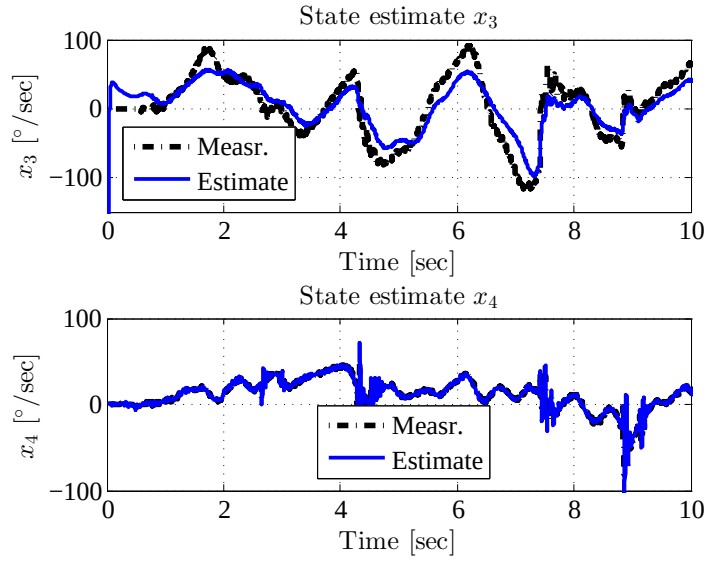

Figure B.11: Experimental Results – State estimate errors of x_3 and x_4

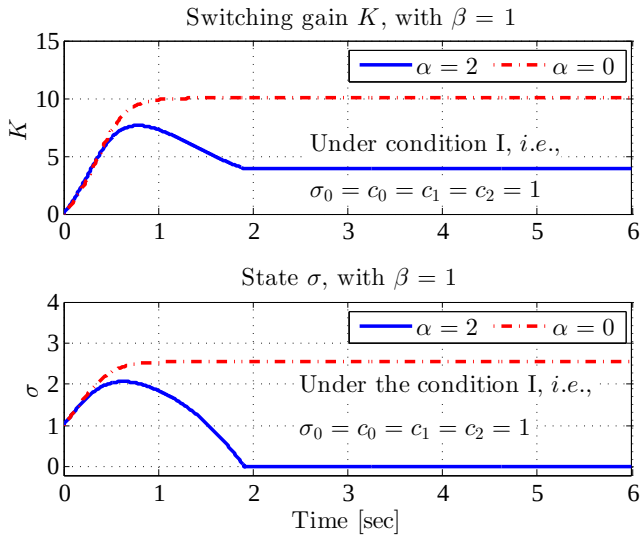

Figure B.12: Illustrative example using the control parameters $\alpha = 0$ and $\alpha = 2$ with $\beta = 1$: Switching gain K (top) and state σ (bottom) performances of the closed-loop dynamics (7.14) with (7.13) under uncertain conditions I.

B.2 Results of the Illustrative Model Dynamics (7.14) When $\alpha = 0$ in Chapter 7

The results of the application of the design (7.12) for the illustrative model dynamics (7.14) when $\alpha = 0$ are shown in Figures B.12-B.15

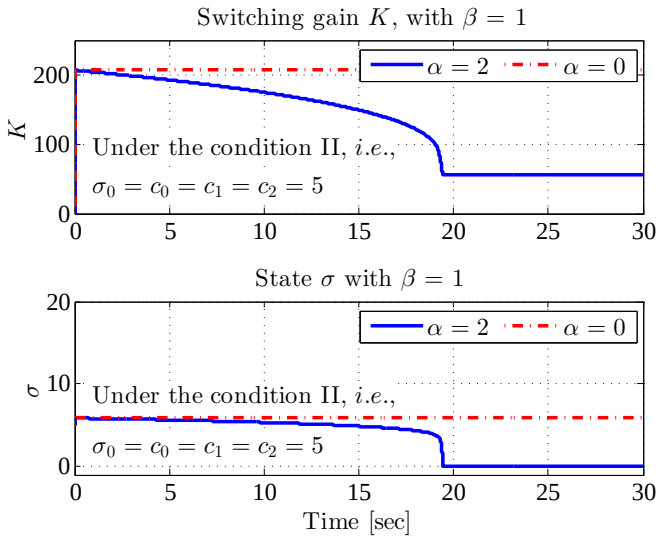

Figure B.13: Illustrative example using the control parameters $\alpha = 0$ and $\alpha = 2$ with $\beta = 1$: Switching gain K (top) and state σ (bottom) performances of the closed-loop dynamics (7.14) with (7.13) under uncertain conditions II.

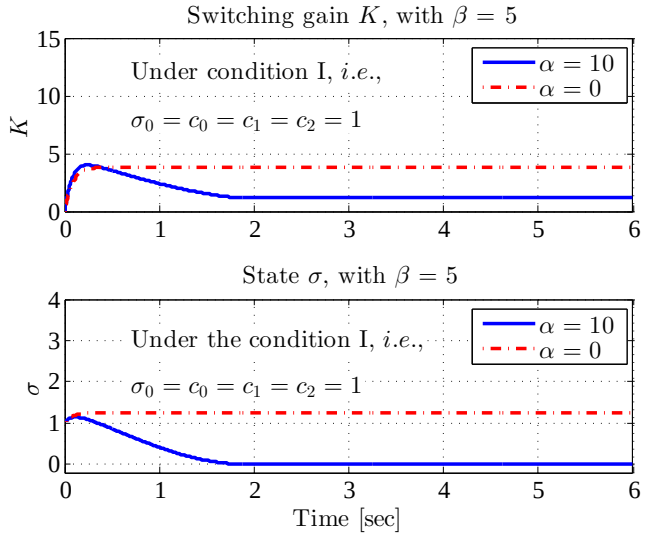

Figure B.14: Illustrative example using the control parameters $\alpha = 0$ and $\alpha = 10$ with $\beta = 5$: Switching gain K (top) and state σ (bottom) performances of the closed-loop dynamics (7.14) with (7.13) under uncertain conditions I.

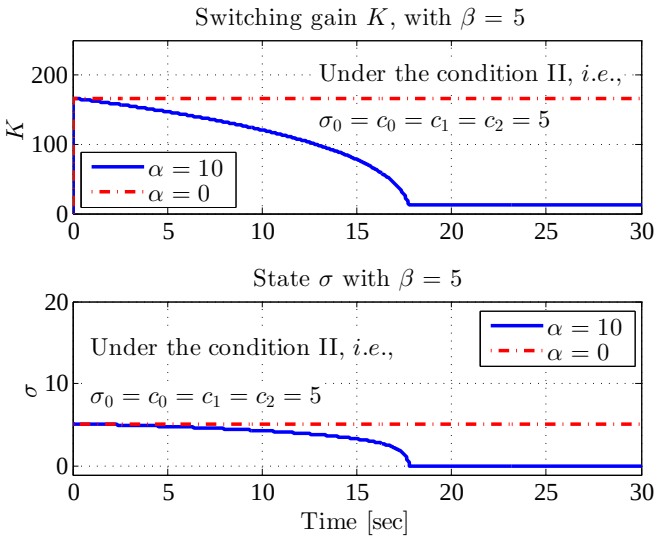

Figure B.15: Illustrative example using the control parameters $\alpha = 0$ and $\alpha = 10$ with $\beta = 5$: Switching gain K (top) and state σ (bottom) performances of the closed-loop dynamics (7.14) with (7.13) under uncertain conditions II.

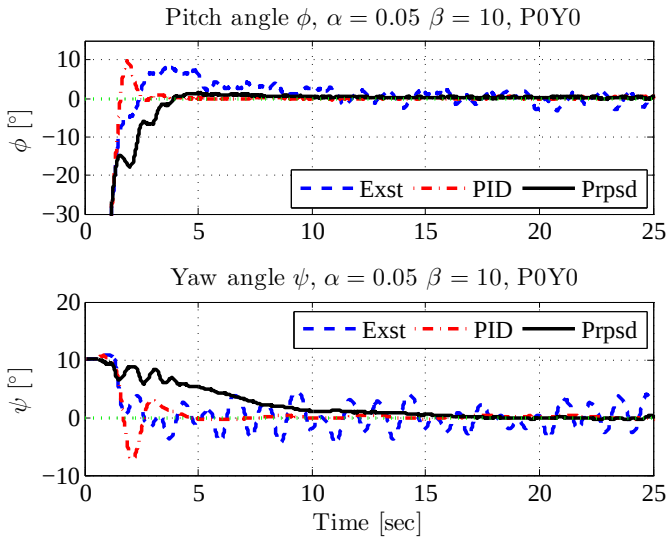

Figure B.16: Experiment results – Pitch and yaw displacements in regulation problem about 0° using the existing ASMC (blue dash), PID (red dash-dot) and proposed ASMC (black solid line) with $\alpha = 0.05$ and $\beta = 10$.

B.3 Experimental Results of P0Y0 for $\alpha = 0.05$, $\alpha = 0.2$, $\beta = 10$ and $\beta = 20$

The experimental results for $\alpha = 0.05$, $\alpha = 0.2$, $\beta = 10$ and $\beta = 20$ are shown here as the supplement to the subsection 7.6.3 in Chapter 7. Figures B.16 and B.17 show the experimental results of the pitch and yaw displacements and the control inputs, respectively, using the existing ASMC (blue dash) reaching law discussed in [16,74] (*i.e.*, (7.28) with $\alpha = 0.05$ and $\beta = 0$), PID (red dash-dot) and proposed ASMC (black solid line) reaching law (7.28) with $\alpha = 0.05$ and $\beta = 10$, while the results for $\alpha = 0.05$ and $\beta = 20$ are shown in Figures B.18 and B.19, $\alpha = 0.2$ and $\beta = 10$ in Figures B.20 and B.21, and $\alpha = 0.2$ and $\beta = 20$ in Figures B.22 and B.23.

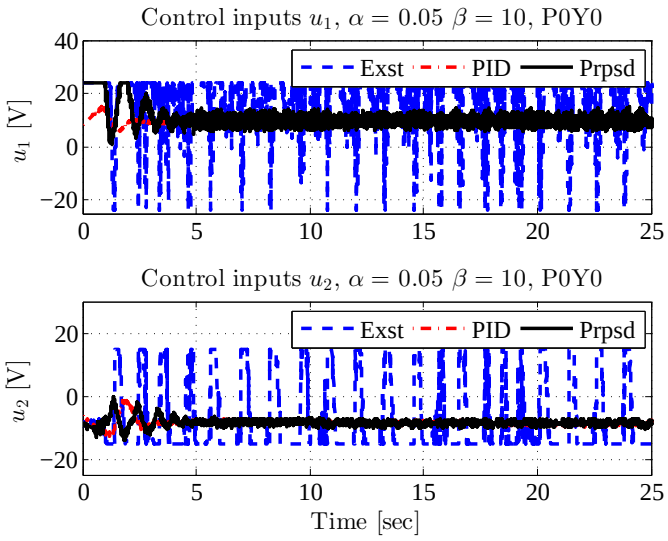

Figure B.17: Experiment results – Pitch and yaw control inputs in regulation problem about 0° using the existing ASMC (blue dash), PID (red dash-dot) and proposed ASMC (black solid line) with $\alpha = 0.05$ and $\beta = 10$.

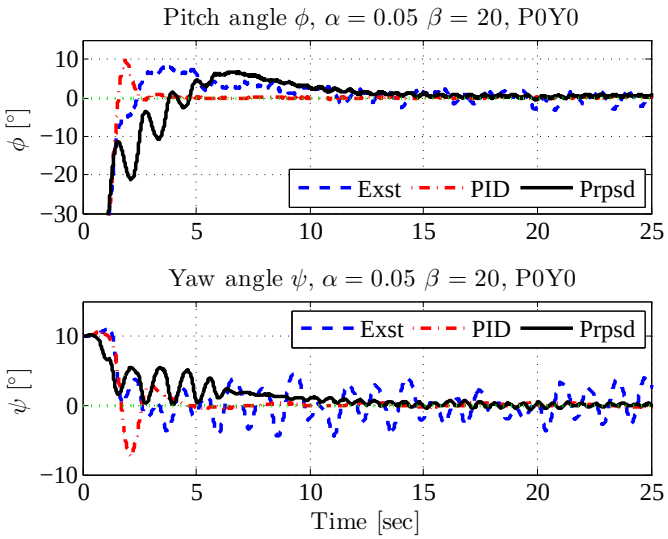

Figure B.18: Experiment results – Pitch and yaw displacements in regulation problem about 0° using the existing ASMC (blue dash), PID (red dash-dot) and proposed ASMC (black solid line) with $\alpha = 0.05$ and $\beta = 20$.

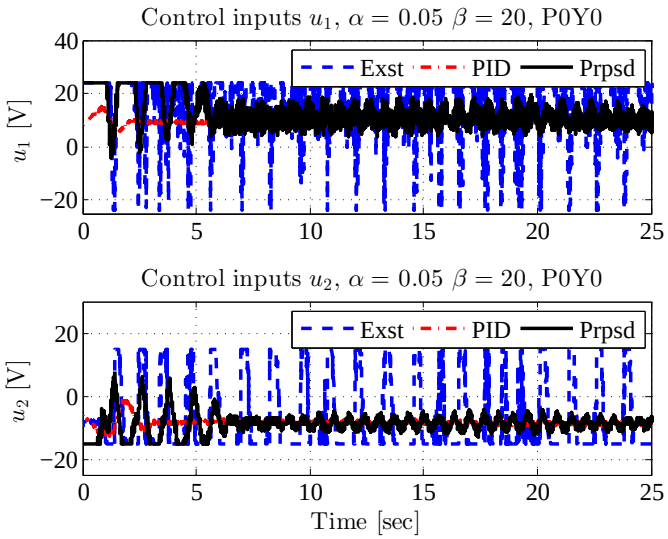

Figure B.19: Experiment results – Pitch and yaw control inputs in regulation problem about 0° using the existing ASMC (blue dash), PID (red dash-dot) and proposed ASMC (black solid line) with $\alpha = 0.05$ and $\beta = 20$.

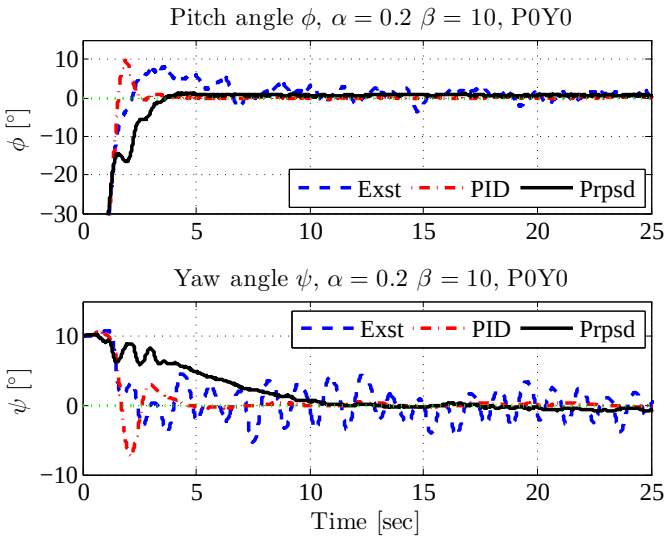

Figure B.20: Experiment results – Pitch and yaw displacements in regulation problem about 0° using the existing ASMC (blue dash), PID (red dash-dot) and proposed ASMC (black solid line) with $\alpha = 0.2$ and $\beta = 10$.

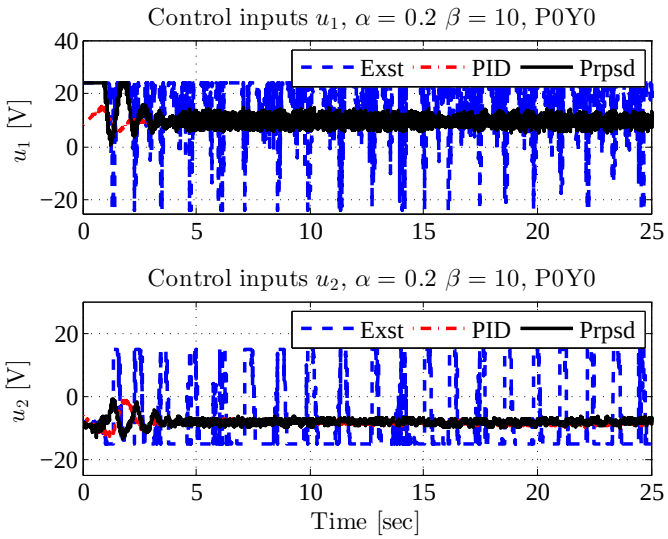

Figure B.21: Experiment results – Pitch and yaw control inputs in regulation problem about 0° using the existing ASMC (blue dash), PID (red dash-dot) and proposed ASMC (black solid line) with $\alpha = 0.2$ and $\beta = 10$.

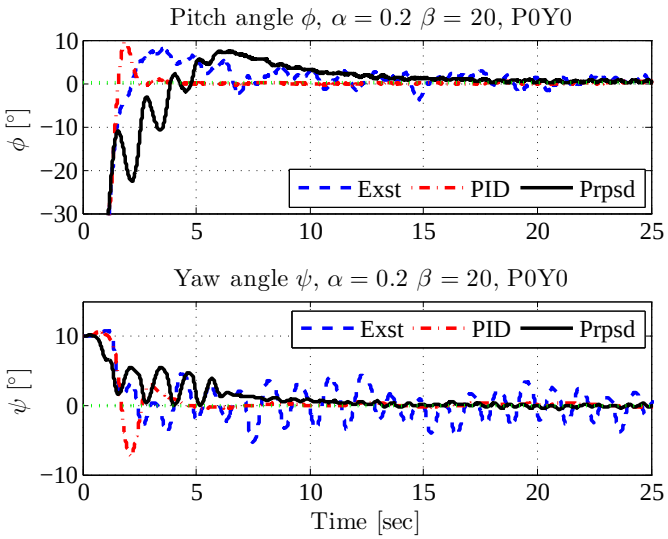

Figure B.22: Experiment results – Pitch and yaw displacements in regulation problem about 0° using the existing ASMC (blue dash), PID (red dash-dot) and proposed ASMC (black solid line) with $\alpha = 0.2$ and $\beta = 20$.

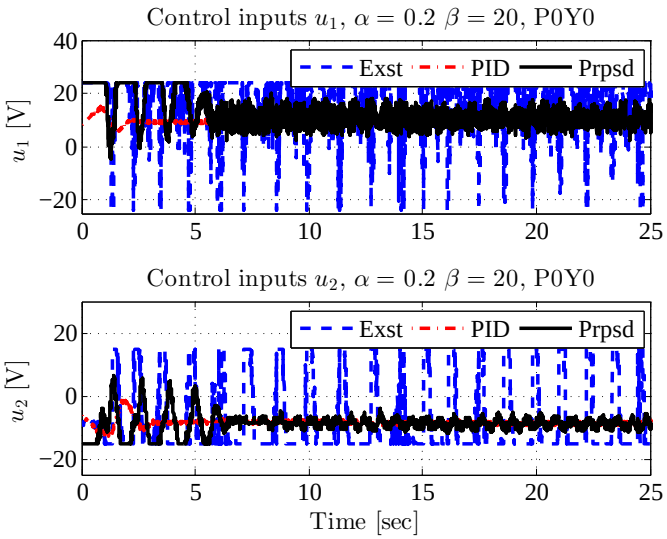

Figure B.23: Experiment results – Pitch and yaw control inputs in regulation problem about 0° using the existing ASMC (blue dash), PID (red dash-dot) and proposed ASMC (black solid line) with $\alpha = 0.2$ and $\beta = 20$.

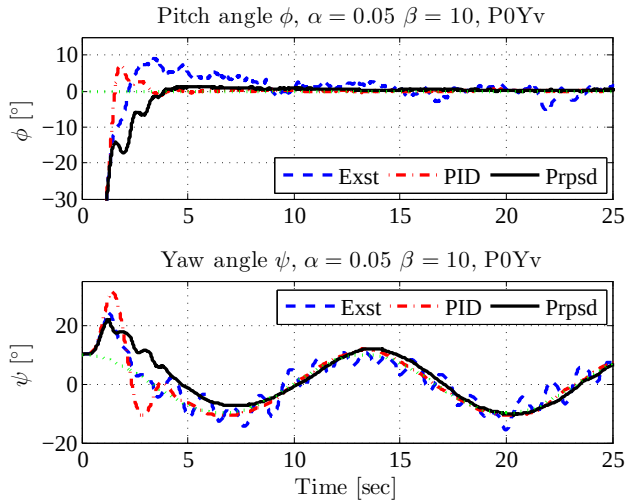

Figure B.24: Experiment results – Pitch and yaw displacements in pitch regulation and yaw sine wave tracking problem, using the existing ASMC (blue dash), PID (red dash-dot) and proposed ASMC (black solid line) with $\alpha = 0.05$ and $\beta = 10$.

B.4 Experiment Results of P0Yv for $\alpha = 0.05$, $\alpha = 0.2$, $\beta = 10$ and $\beta = 20$

The experimental results for $\alpha = 0.05$, $\alpha = 0.2$, $\beta = 10$ and $\beta = 20$ are shown here as the supplement to the subsection 7.6.3 in Chapter 7. Figures B.24-B.26 show the experimental results of the pitch and yaw displacements, the position errors, and the control inputs, respectively, using the existing ASMC (blue dash) reaching law discussed in [16, 74] (*i.e.*, (7.28) with $\alpha = 0.05$ and $\beta = 0$), PID (red dash-dot) and proposed ASMC (black solid line) reaching law (7.28) with $\alpha = 0.05$ and $\beta = 10$, while the results for $\alpha = 0.05$ and $\beta = 20$ are shown in Figures B.27-B.29, $\alpha = 0.2$ and $\beta = 10$ in Figures B.30-B.32, and $\alpha = 0.2$ and $\beta = 20$ in Figures B.33-B.35.

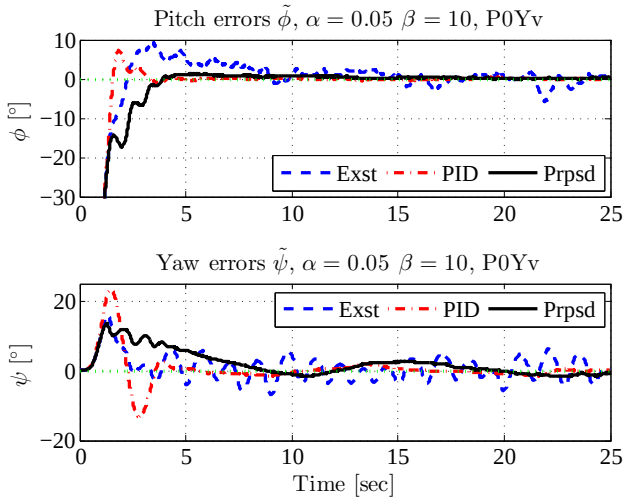

Figure B.25: Experiment results – Pitch and yaw position errors in pitch regulation and yaw sine wave tracking problem, using the existing ASMC (blue dash), PID (red dash-dot) and proposed ASMC (black solid line) with $\alpha = 0.05$ and $\beta = 10$.

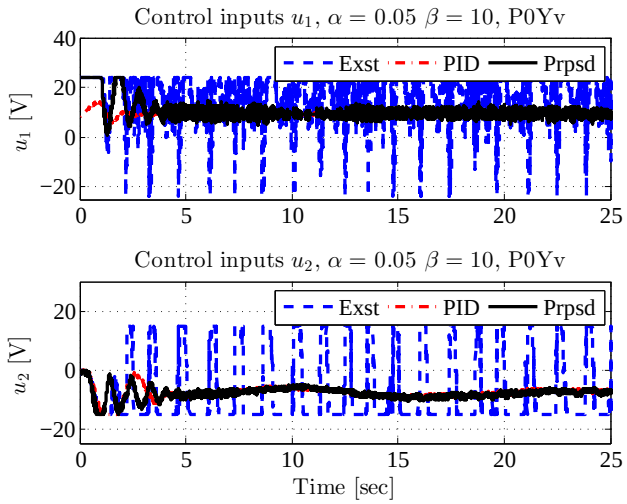

Figure B.26: Experiment results – Pitch and yaw control inputs in pitch regulation and yaw sine wave tracking problem, using the existing ASMC (blue dash), PID (red dash-dot) and proposed ASMC (black solid line) with $\alpha = 0.05$ and $\beta = 10$.

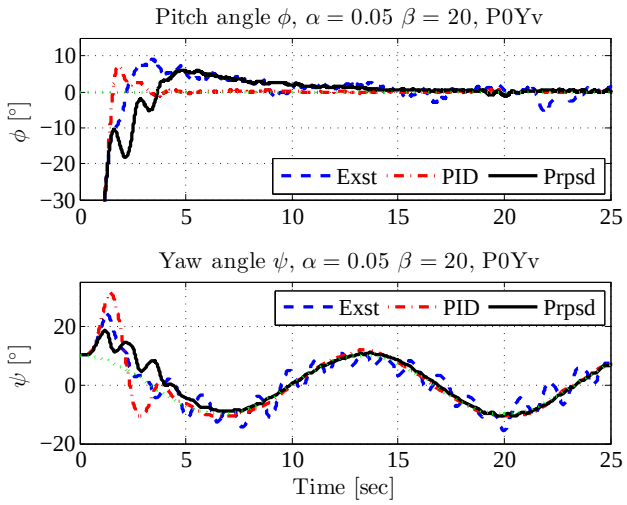

Figure B.27: Experiment results – Pitch and yaw displacements in pitch regulation and yaw sine wave tracking problem, using the existing ASMC (blue dash), PID (red dash-dot) and proposed ASMC (black solid line) with $\alpha = 0.05$ and $\beta = 20$.

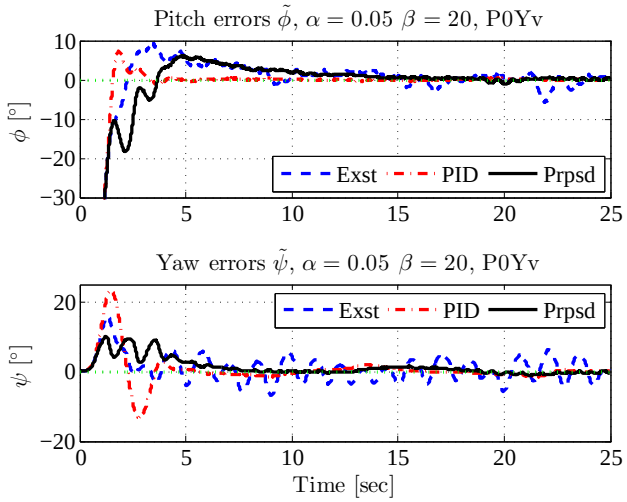

Figure B.28: Experiment results – Pitch and yaw position errors in pitch regulation and yaw sine wave tracking problem, using the existing ASMC (blue dash), PID (red dash-dot) and proposed ASMC (black solid line) with $\alpha = 0.05$ and $\beta = 20$.

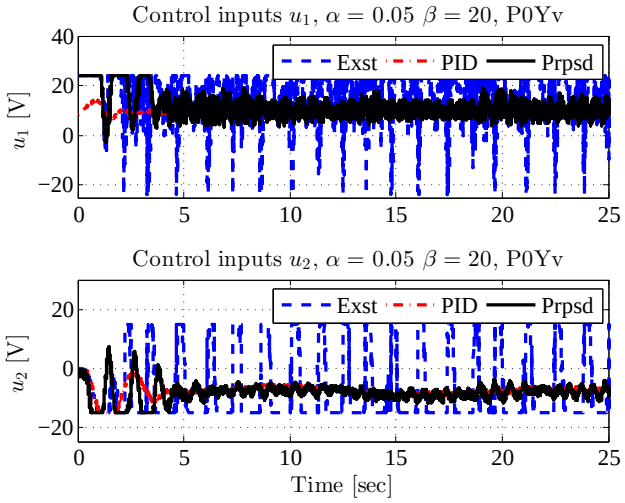

Figure B.29: Experiment results – Pitch and yaw control inputs in pitch regulation and yaw sine wave tracking problem, using the existing ASMC (blue dash), PID (red dash-dot) and proposed ASMC (black solid line) with $\alpha = 0.05$ and $\beta = 20$.

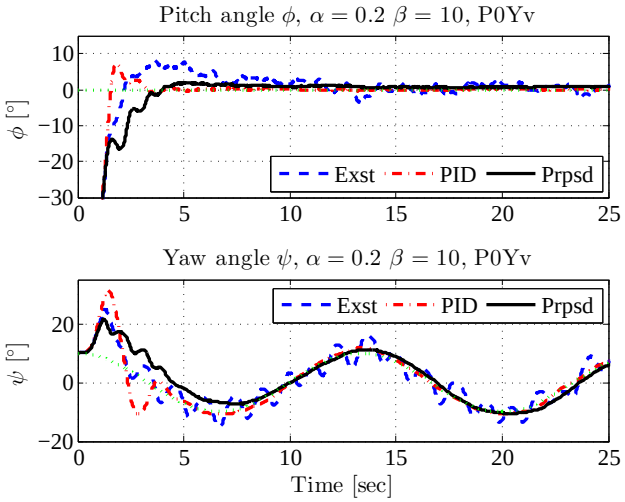

Figure B.30: Experiment results – Pitch and yaw displacements in pitch regulation and yaw sine wave tracking problem, using the existing ASMC (blue dash), PID (red dash-dot) and proposed ASMC (black solid line) with $\alpha = 0.2$ and $\beta = 10$.

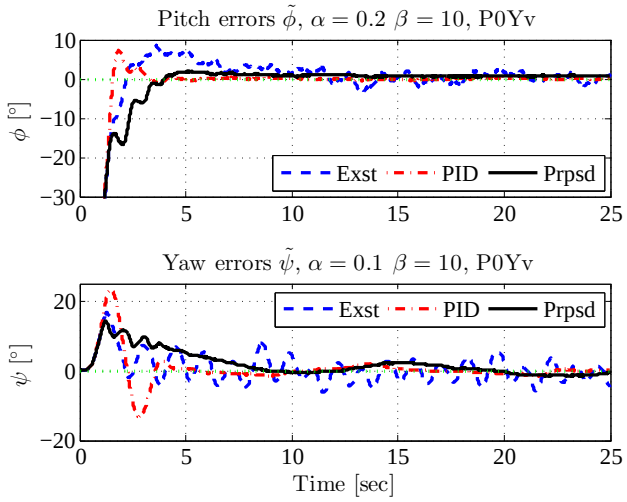

Figure B.31: Experiment results – Pitch and yaw position errors in pitch regulation and yaw sine wave tracking problem, using the existing ASMC (blue dash), PID (red dash-dot) and proposed ASMC (black solid line) with $\alpha = 0.2$ and $\beta = 10$.

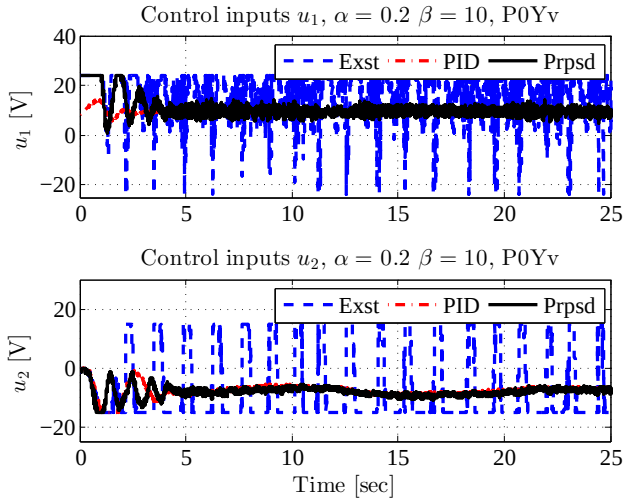

Figure B.32: Experiment results – Pitch and yaw control inputs in pitch regulation and yaw sine wave tracking problem, using the existing ASMC (blue dash), PID (red dash-dot) and proposed ASMC (black solid line) with $\alpha = 0.2$ and $\beta = 10$.

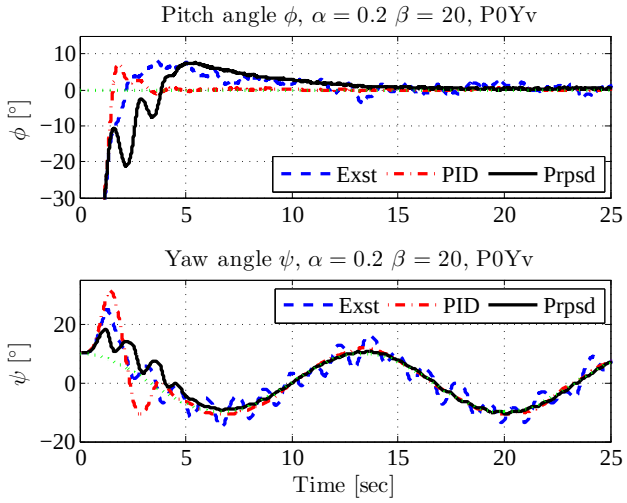

Figure B.33: Experiment results – Pitch and yaw displacements in pitch regulation and yaw sine wave tracking problem, using the existing ASMC (blue dash), PID (red dash-dot) and proposed ASMC (black solid line) with $\alpha = 0.2$ and $\beta = 20$.

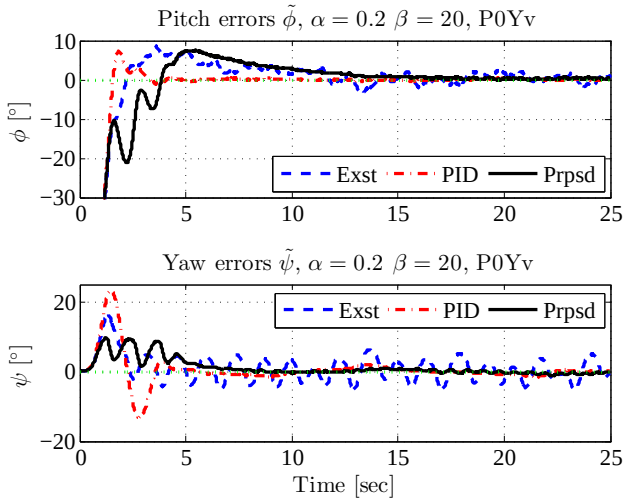

Figure B.34: Experiment results – Pitch and yaw position errors in pitch regulation and yaw sine wave tracking problem, using the existing ASMC (blue dash), PID (red dash-dot) and proposed ASMC (black solid line) with $\alpha = 0.2$ and $\beta = 20$.

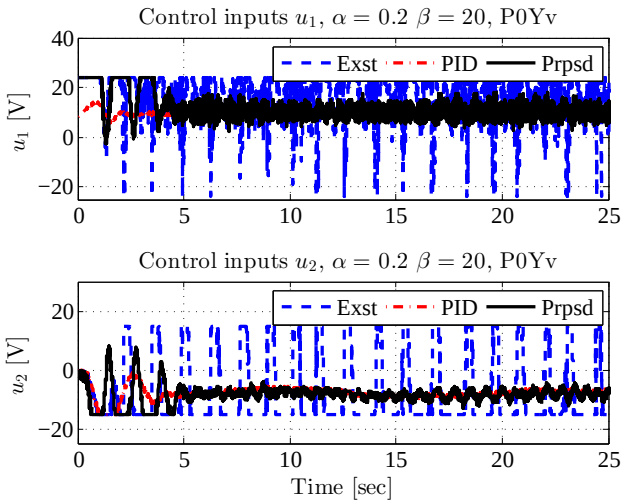

Figure B.35: Experiment results – Pitch and yaw control inputs in pitch regulation and yaw sine wave tracking problem, using the existing ASMC (blue dash), PID (red dash-dot) and proposed ASMC (black solid line) with $\alpha = 0.2$ and $\beta = 20$.

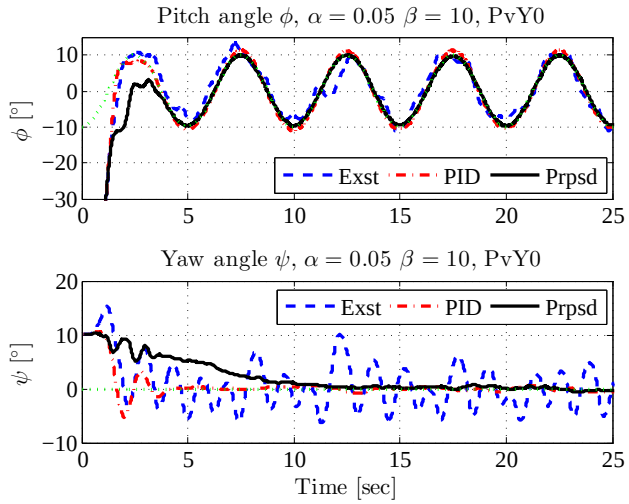

Figure B.36: Experiment results – Pitch and yaw displacements in pitch sine wave tracking control and yaw regulation, using the existing ASMC (blue dash), PID (red dash-dot) and proposed ASMC (black solid line) with $\alpha = 0.05$ and $\beta = 10$.

B.5 Experiment Results of PvY0 for $\alpha = 0.05$, $\alpha = 0.2$, $\beta = 10$ and $\beta = 20$

The experimental results for $\alpha = 0.05$, $\alpha = 0.2$, $\beta = 10$ and $\beta = 20$ are shown here as the supplement to the subsection 7.6.4 in Chapter 7. Figures B.36-B.38 show the experimental results of the pitch and yaw displacements, the position errors, and the control inputs, respectively, using the existing ASMC (blue dash) reaching law discussed in [16, 74] (*i.e.*, (7.28) with $\alpha = 0.05$ and $\beta = 0$), PID (red dash-dot) and proposed ASMC (black solid line) reaching law (7.28) with $\alpha = 0.05$ and $\beta = 10$, while the results for $\alpha = 0.05$ and $\beta = 20$ are shown in Figures B.39-B.41, $\alpha = 0.2$ and $\beta = 10$ in Figures B.42-B.44, and $\alpha = 0.2$ and $\beta = 20$ in Figures B.45-B.47.

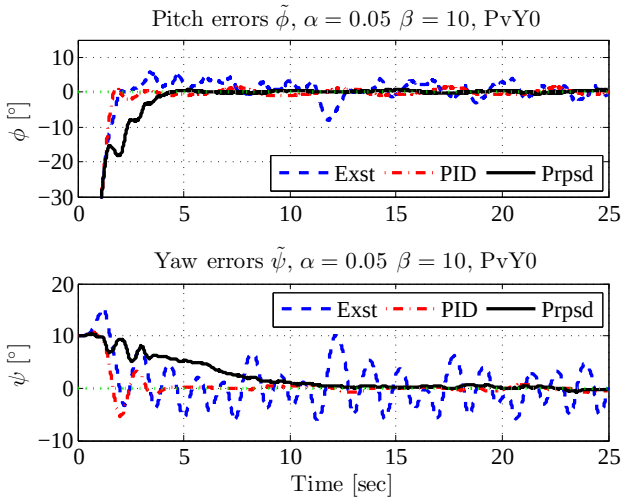

Figure B.37: Experiment results – Pitch and yaw position errors in pitch sine wave tracking control and yaw regulation, using the existing ASMC (blue dash), PID (red dash-dot) and proposed ASMC (black solid line) with $\alpha = 0.05$ and $\beta = 10$.

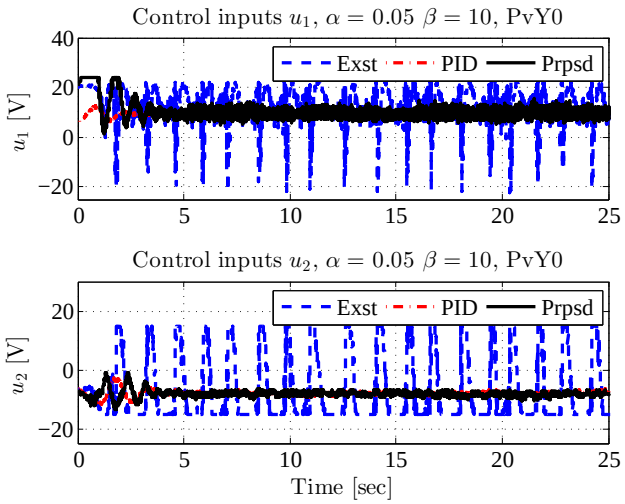

Figure B.38: Experiment results – Pitch and yaw control inputs in pitch sine wave tracking control and yaw regulation, using the existing ASMC (blue dash), PID (red dash-dot) and proposed ASMC (black solid line) with $\alpha = 0.05$ and $\beta = 10$.

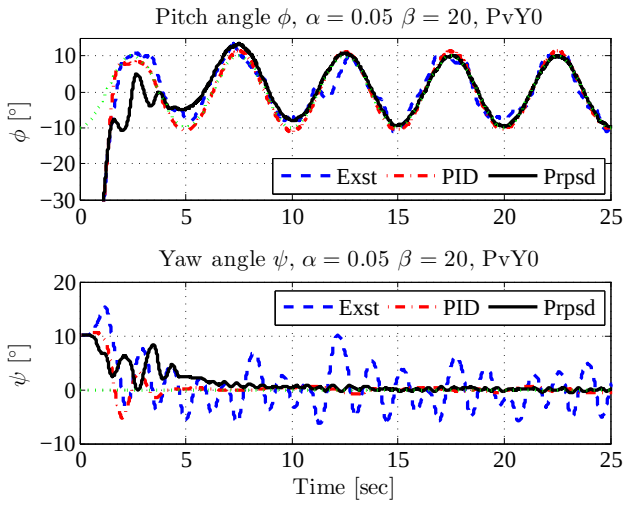

Figure B.39: Experiment results – Pitch and yaw displacements in pitch sine wave tracking control and yaw regulation, using the existing ASMC (blue dash), PID (red dash-dot) and proposed ASMC (black solid line) with $\alpha = 0.05$ and $\beta = 20$.

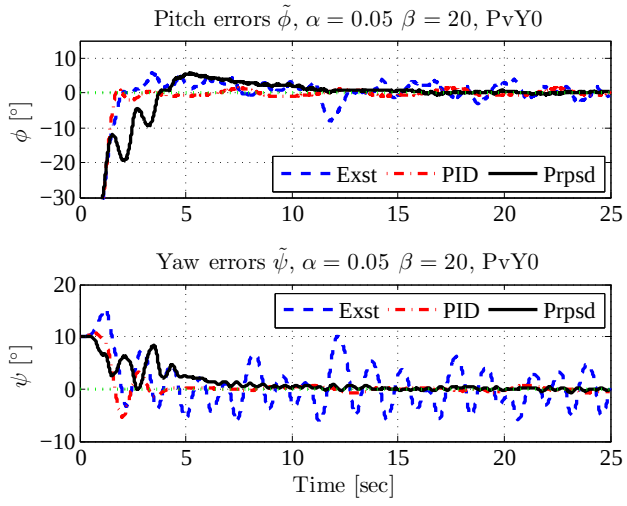

Figure B.40: Experiment results – Pitch and yaw position errors in pitch sine wave tracking control and yaw regulation, using the existing ASMC (blue dash), PID (red dash-dot) and proposed ASMC (black solid line) with $\alpha = 0.05$ and $\beta = 20$.

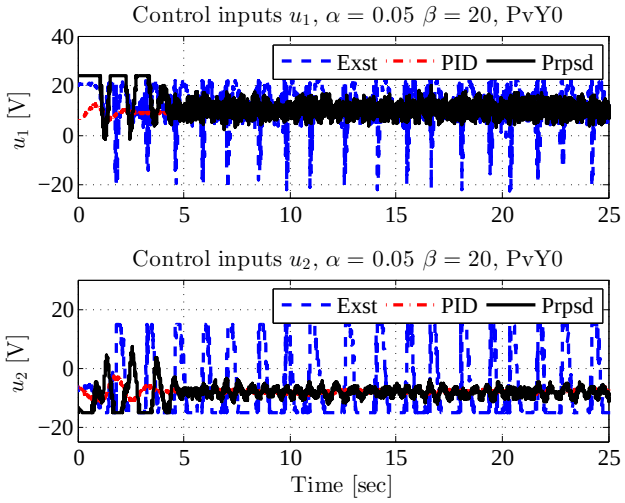

Figure B.41: Experiment results – Pitch and yaw control inputs in pitch sine wave tracking control and yaw regulation, using the existing ASMC (blue dash), PID (red dash-dot) and proposed ASMC (black solid line) with $\alpha = 0.05$ and $\beta = 20$.

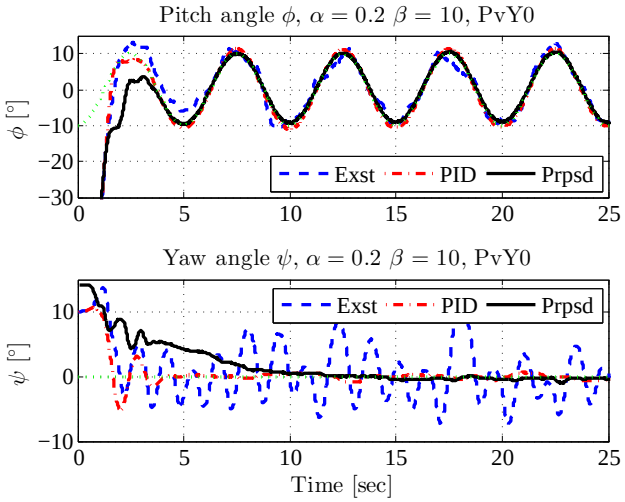

Figure B.42: Experiment results – Pitch and yaw displacements in pitch sine wave tracking control and yaw regulation, using the existing ASMC (blue dash), PID (red dash-dot) and proposed ASMC (black solid line) with $\alpha = 0.2$ and $\beta = 10$.

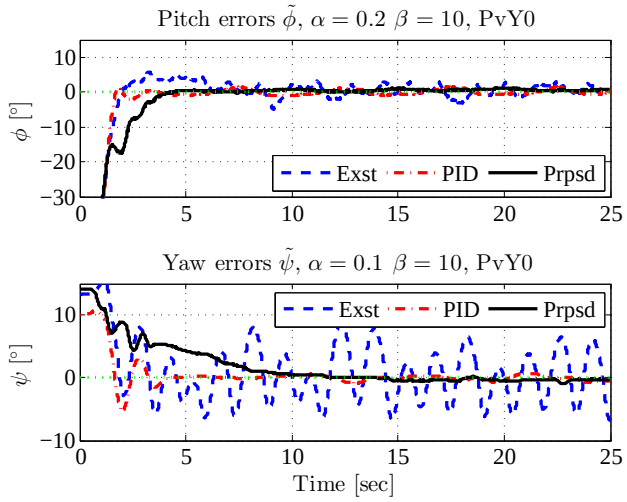

Figure B.43: Experiment results – Pitch and yaw position errors in pitch sine wave tracking control and yaw regulation, using the existing ASMC (blue dash), PID (red dash-dot) and proposed ASMC (black solid line) with $\alpha = 0.2$ and $\beta = 10$.

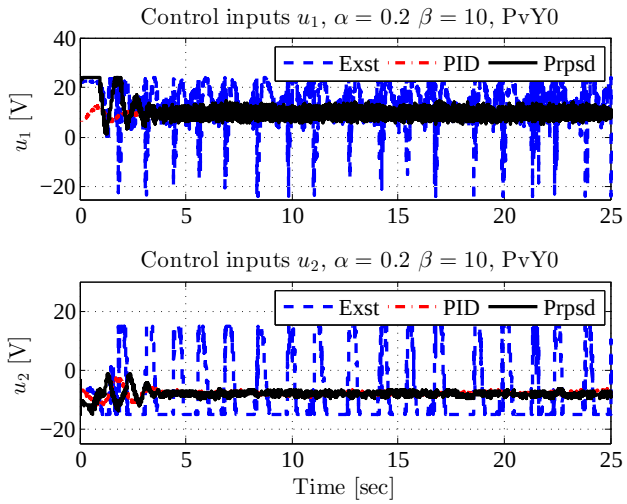

Figure B.44: Experiment results – Pitch and yaw control inputs in pitch sine wave tracking control and yaw regulation, using the existing ASMC (blue dash), PID (red dash-dot) and proposed ASMC (black solid line) with $\alpha = 0.2$ and $\beta = 10$.

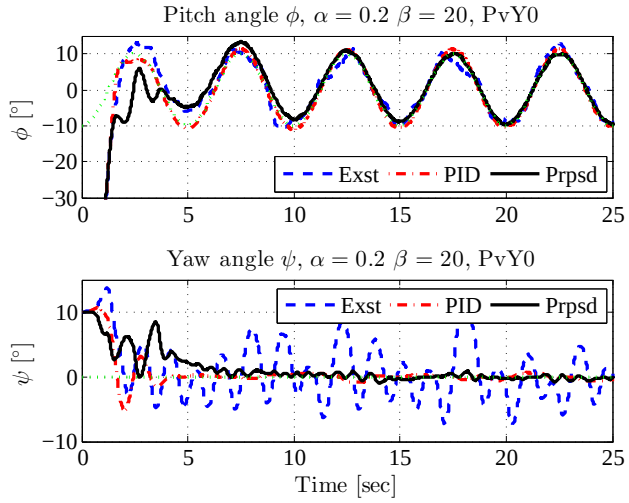

Figure B.45: Experiment results – Pitch and yaw displacements in pitch sine wave tracking control and yaw regulation, using the existing ASMC (blue dash), PID (red dash-dot) and proposed ASMC (black solid line) with $\alpha = 0.2$ and $\beta = 20$.

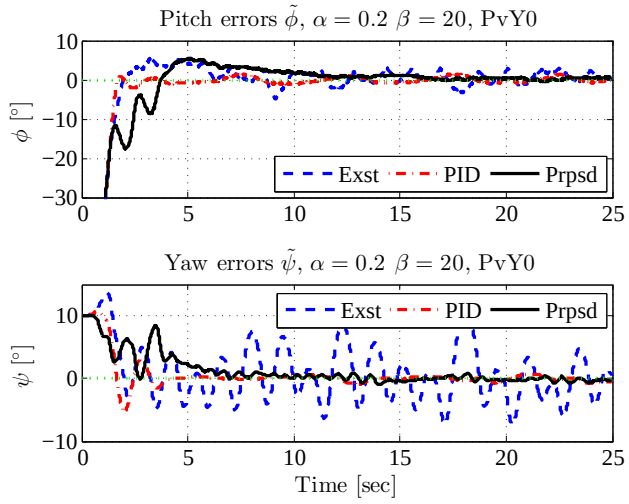

Figure B.46: Experiment results – Pitch and yaw position errors in pitch sine wave tracking control and yaw regulation, using the existing ASMC (blue dash), PID (red dash-dot) and proposed ASMC (black solid line) with $\alpha = 0.2$ and $\beta = 20$.

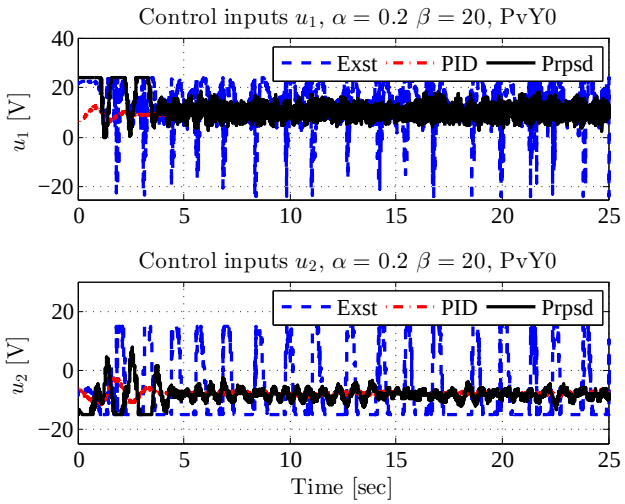

Figure B.47: Experiment results – Pitch and yaw control inputs in pitch sine wave tracking control and yaw regulation, using the existing ASMC (blue dash), PID (red dash-dot) and proposed ASMC (black solid line) with $\alpha = 0.2$ and $\beta = 20$.

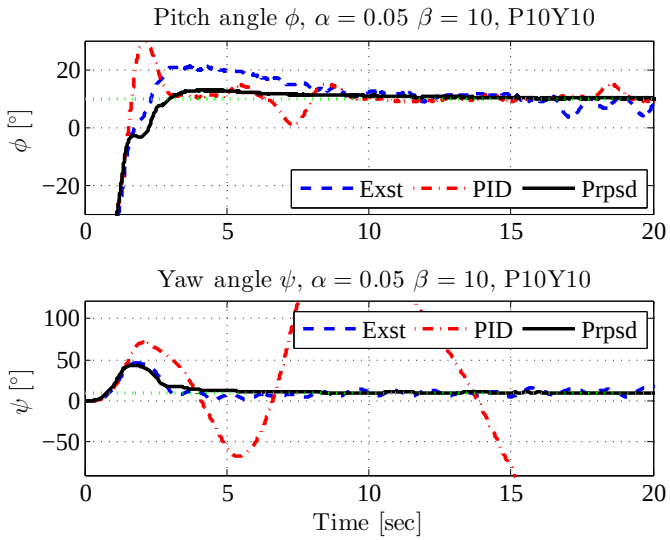

Figure B.48: Experiment results – Pitch and yaw displacements in regulation problem about 10° using the existing ASMC (blue dash), PID (red dash-dot) and proposed ASMC (black solid line) with $\alpha = 0.05$ and $\beta = 10$.

B.6 Experiment Results of P10Y10 for $\alpha = 0.05$, $\alpha = 0.2$, $\beta = 10$ and $\beta = 20$

The experimental results for $\alpha = 0.05$, $\alpha = 0.2$, $\beta = 10$ and $\beta = 20$ are shown here as the supplement to the subsection 7.6.5 in Chapter 7. Figures B.48 and B.49 show the experimental results of the pitch and yaw displacements and the control inputs, respectively, using the existing ASMC (blue dash) reaching law discussed in [16,74] (*i.e.*, (7.28) with $\alpha = 0.05$ and $\beta = 0$), PID (red dash-dot) and proposed ASMC (black solid line) reaching law (7.28) with $\alpha = 0.05$ and $\beta = 10$, while the results for $\alpha = 0.05$ and $\beta = 20$ are shown in Figures B.50 and B.51, $\alpha = 0.2$ and $\beta = 10$ in Figures B.52 and B.53, and $\alpha = 0.2$ and $\beta = 20$ in Figures B.54 and B.55.

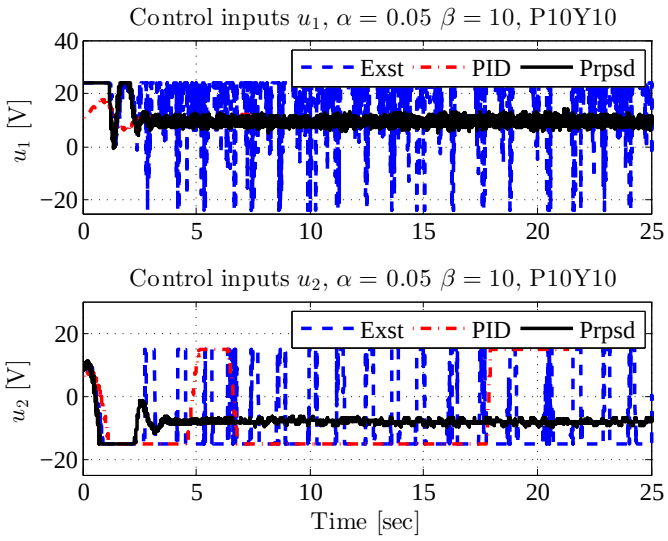

Figure B.49: Experiment results – Pitch and yaw control inputs in regulation problem about 10° using the existing ASMC (blue dash), PID (red dash-dot) and proposed ASMC (black solid line) with $\alpha = 0.05$ and $\beta = 10$.

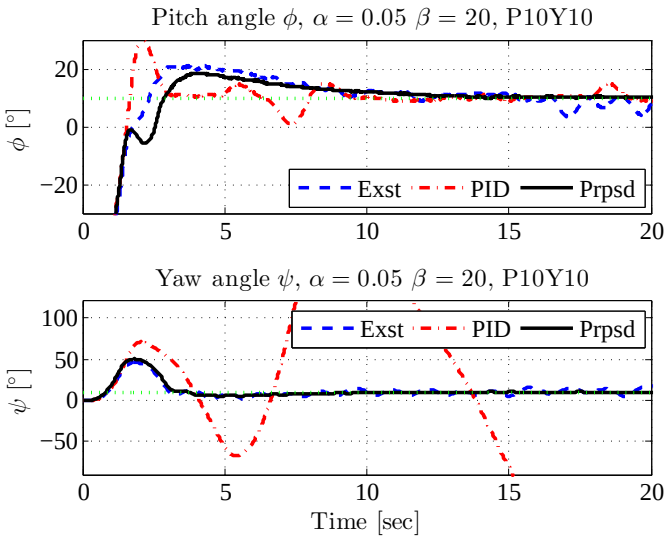

Figure B.50: Experiment results – Pitch and yaw displacements in regulation problem about 10° using the existing ASMC (blue dash), PID (red dash-dot) and proposed ASMC (black solid line) with $\alpha = 0.05$ and $\beta = 20$.

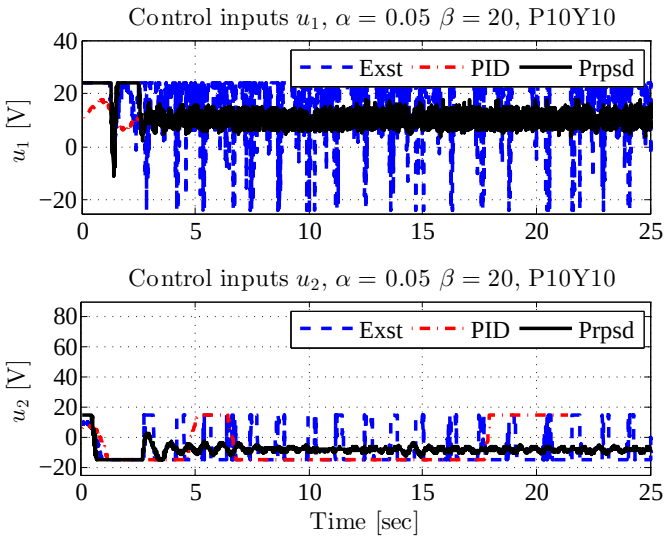

Figure B.51: Experiment results – Pitch and yaw control inputs in regulation problem about 10° using the existing ASMC (blue dash), PID (red dash-dot) and proposed ASMC (black solid line) with $\alpha = 0.05$ and $\beta = 20$.

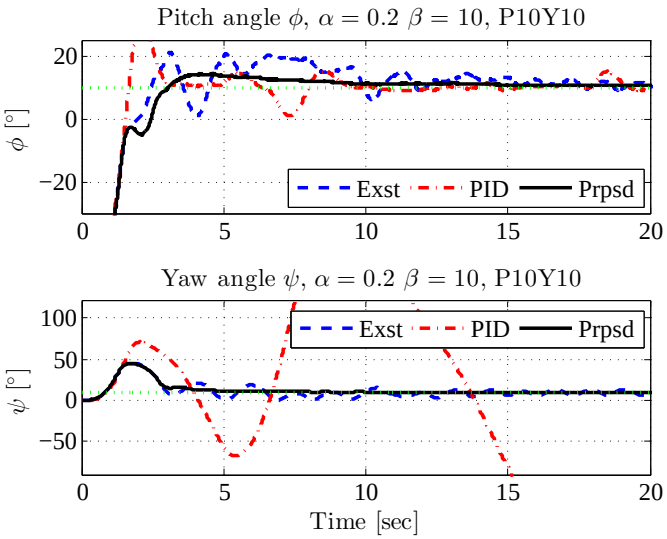

Figure B.52: Experiment results – Pitch and yaw displacements in regulation problem about 10° using the existing ASMC (blue dash), PID (red dash-dot) and proposed ASMC (black solid line) with $\alpha = 0.2$ and $\beta = 10$.

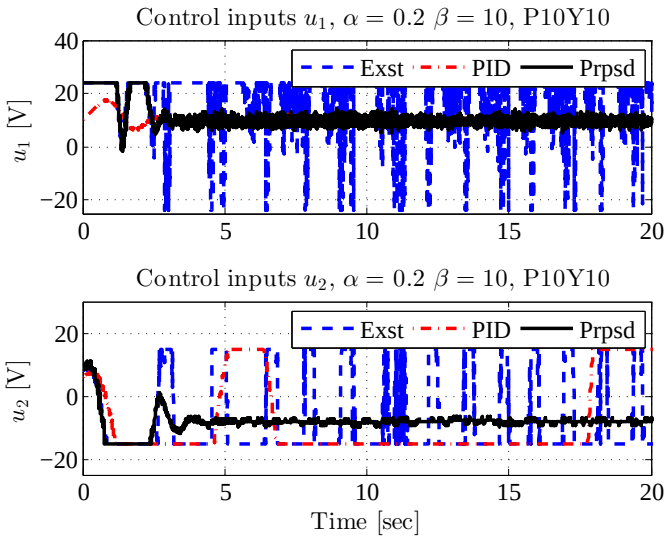

Figure B.53: Experiment results – Pitch and yaw control inputs in regulation problem about 10° using the existing ASMC (blue dash), PID (red dash-dot) and proposed ASMC (black solid line) with $\alpha = 0.2$ and $\beta = 10$.

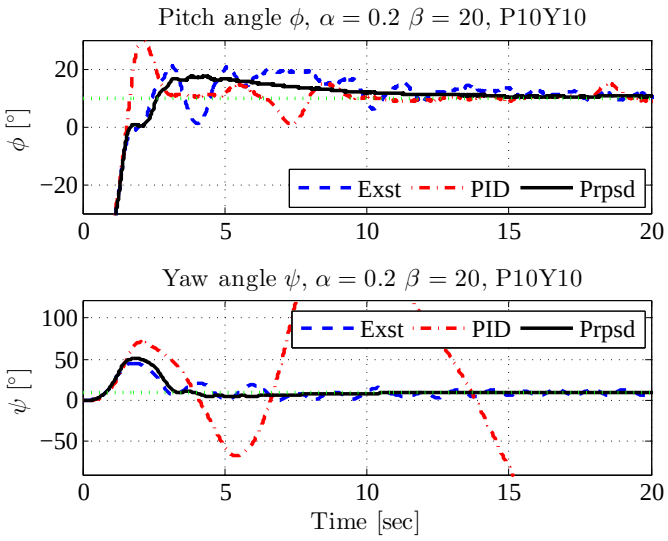

Figure B.54: Experiment results – Pitch and yaw displacements in regulation problem about 10° using the existing ASMC (blue dash), PID (red dash-dot) and proposed ASMC (black solid line) with $\alpha = 0.2$ and $\beta = 20$.

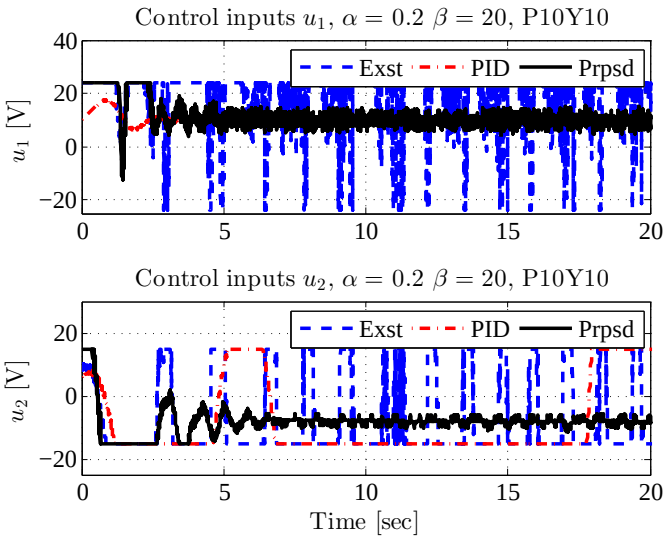

Figure B.55: Experiment results – Pitch and yaw control inputs in regulation problem about 10° using the existing ASMC (blue dash), PID (red dash-dot) and proposed ASMC (black solid line) with $\alpha = 0.2$ and $\beta = 20$.

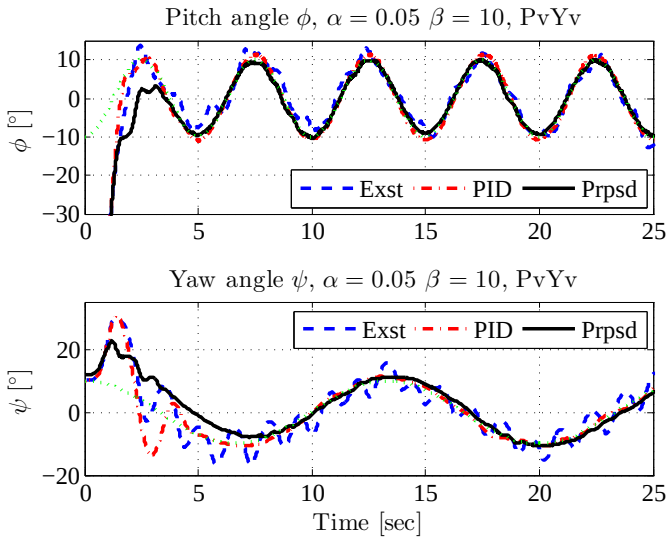

Figure B.56: Experiment results – Pitch and yaw displacements in sine waves tracking control, using the existing ASMC (blue dash), PID (red dash-dot) and proposed ASMC (black solid line) with $\alpha = 0.05$ and $\beta = 10$.

B.7 Experiment Results of PvYv for $\alpha = 0.05$, $\alpha = 0.2$, $\beta = 10$ and $\beta = 20$

The experimental results for $\alpha = 0.05$, $\alpha = 0.2$, $\beta = 10$ and $\beta = 20$ are shown here as the supplement to the subsection 7.6.6 in Chapter 7. Figures B.56-B.58 show the experimental results of the pitch and yaw displacements, the position errors, and the control inputs, respectively, using the existing ASMC (blue dash) reaching law discussed in [16, 74] (*i.e.*, (7.28) with $\alpha = 0.05$ and $\beta = 0$), PID (red dash-dot) and proposed ASMC (black solid line) reaching law (7.28) with $\alpha = 0.05$ and $\beta = 10$, while the results for $\alpha = 0.05$ and $\beta = 20$ are shown in Figures B.59-B.61, $\alpha = 0.2$ and $\beta = 10$ in Figures B.62-B.64, and $\alpha = 0.2$ and $\beta = 20$ in Figures B.65-B.67.

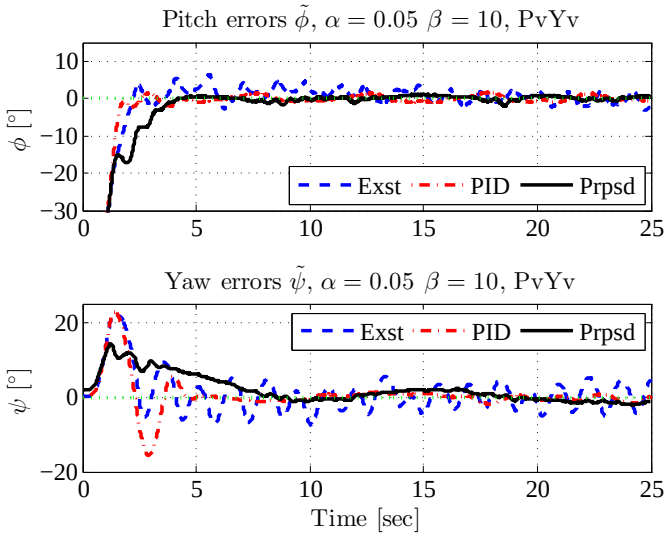

Figure B.57: Experiment results – Pitch and yaw position errors in sine waves tracking control, using the existing ASMC (blue dash), PID (red dash-dot) and proposed ASMC (black solid line) with $\alpha = 0.05$ and $\beta = 10$.

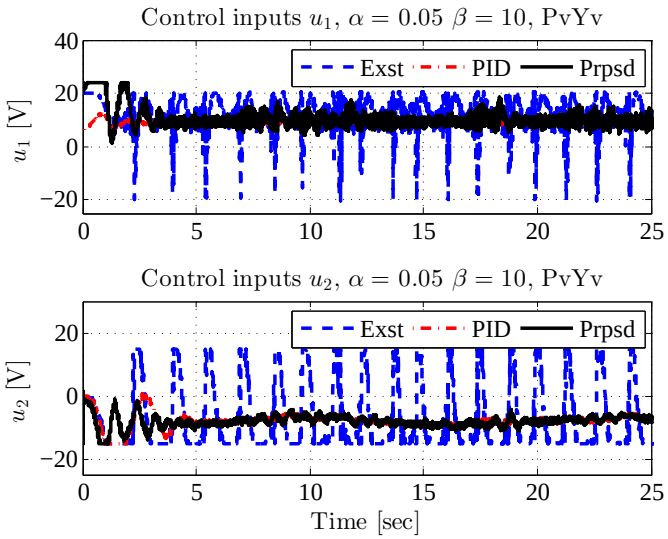

Figure B.58: Experiment results – Pitch and yaw control inputs in sine waves tracking control, using the existing ASMC (blue dash), PID (red dash-dot) and proposed ASMC (black solid line) with $\alpha = 0.05$ and $\beta = 10$.

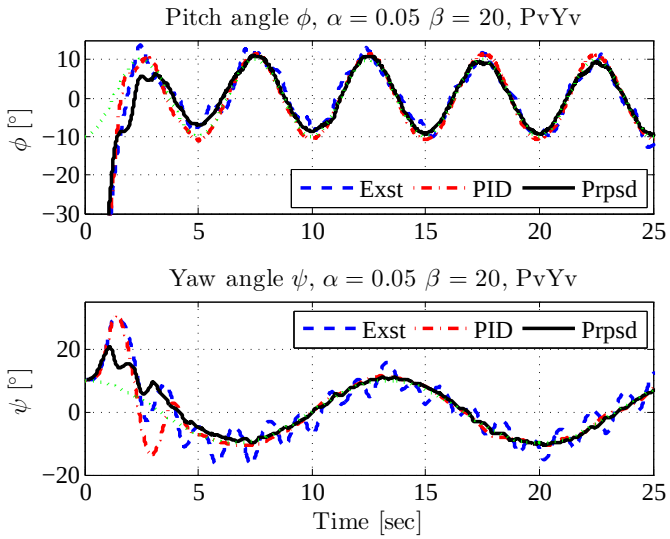

Figure B.59: Experiment results – Pitch and yaw displacements in sine waves tracking control, using the existing ASMC (blue dash), PID (red dash-dot) and proposed ASMC (black solid line) with $\alpha = 0.05$ and $\beta = 20$.

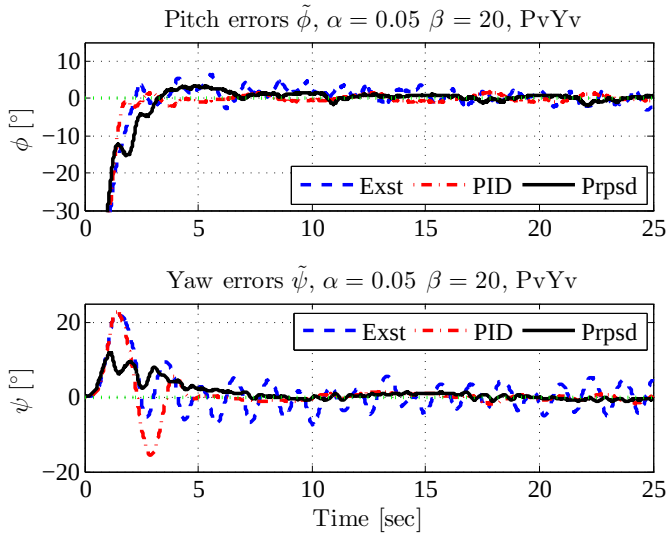

Figure B.60: Experiment results – Pitch and yaw position errors in sine waves tracking control, using the existing ASMC (blue dash), PID (red dash-dot) and proposed ASMC (black solid line) with $\alpha = 0.05$ and $\beta = 20$.

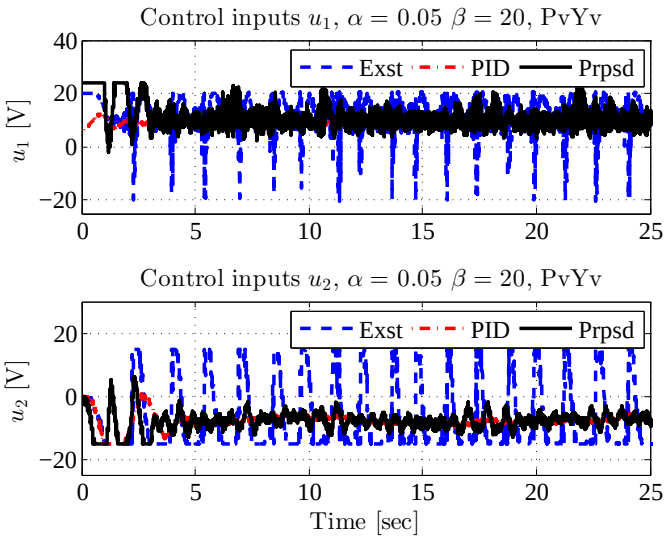

Figure B.61: Experiment results – Pitch and yaw control inputs in sine waves tracking control, using the existing ASMC (blue dash), PID (red dash-dot) and proposed ASMC (black solid line) with $\alpha = 0.05$ and $\beta = 20$.

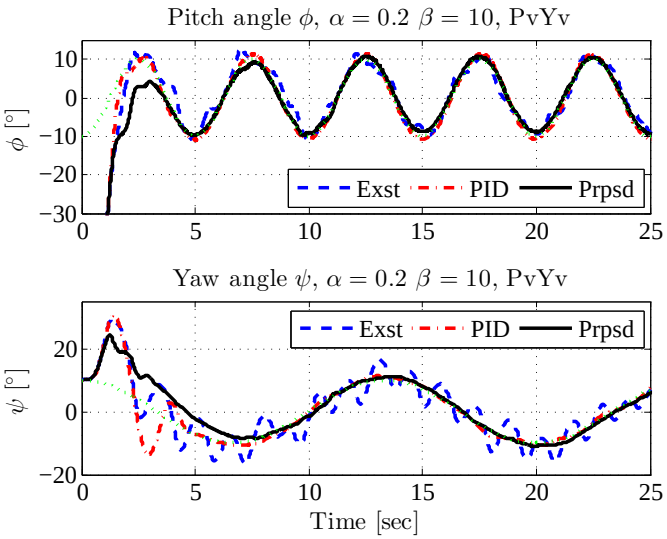

Figure B.62: Experiment results – Pitch and yaw displacements in sine waves tracking control, using the existing ASMC (blue dash), PID (red dash-dot) and proposed ASMC (black solid line) with $\alpha = 0.2$ and $\beta = 10$.

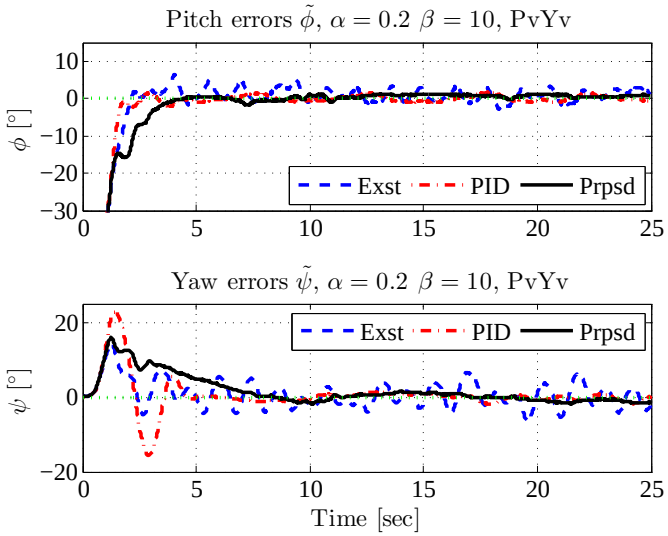

Figure B.63: Experiment results – Pitch and yaw position errors in sine waves tracking control, using the existing ASMC (blue dash), PID (red dash-dot) and proposed ASMC (black solid line) with $\alpha = 0.2$ and $\beta = 10$.

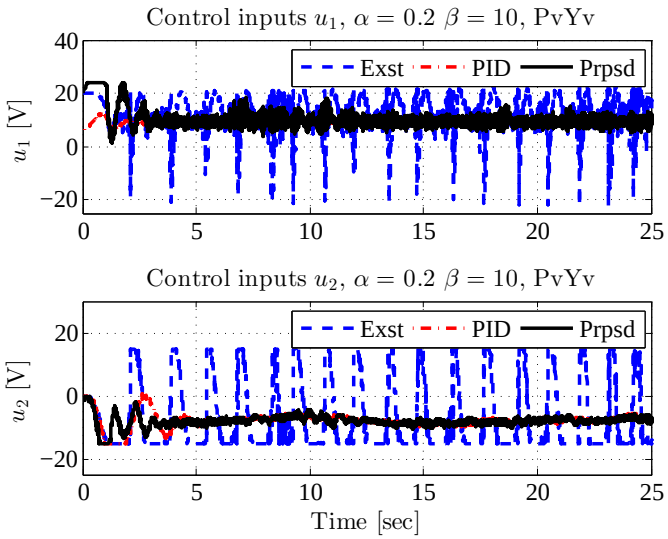

Figure B.64: Experiment results – Pitch and yaw control inputs in sine waves tracking control, using the existing ASMC (blue dash), PID (red dash-dot) and proposed ASMC (black solid line) with $\alpha = 0.2$ and $\beta = 10$.

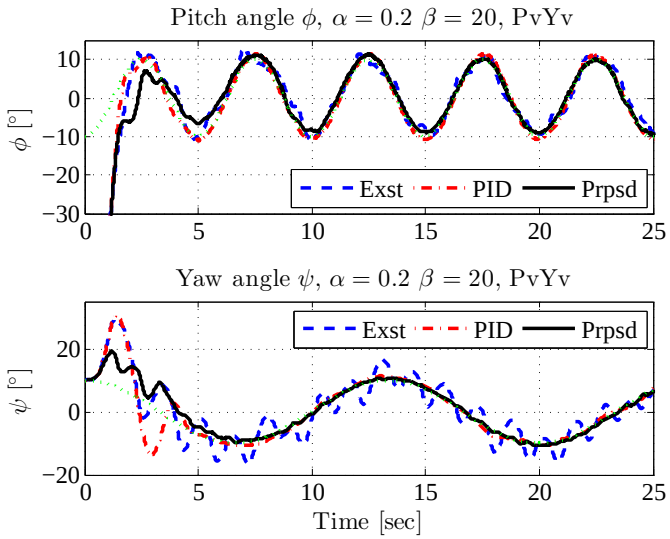

Figure B.65: Experiment results – Pitch and yaw displacements in sine waves tracking control, using the existing ASMC (blue dash), PID (red dash-dot) and proposed ASMC (black solid line) with $\alpha = 0.2$ and $\beta = 20$.

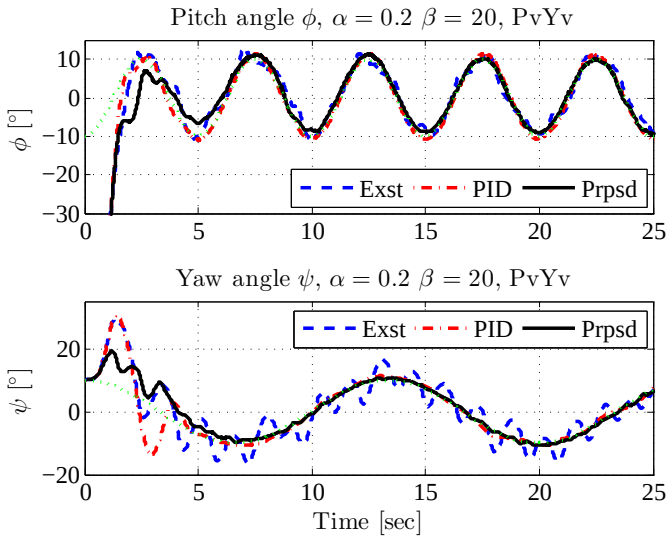

Figure B.66: Experiment results – Pitch and yaw position errors in sine waves tracking control, using the existing ASMC (blue dash), PID (red dash-dot) and proposed ASMC (black solid line) with $\alpha = 0.2$ and $\beta = 20$.

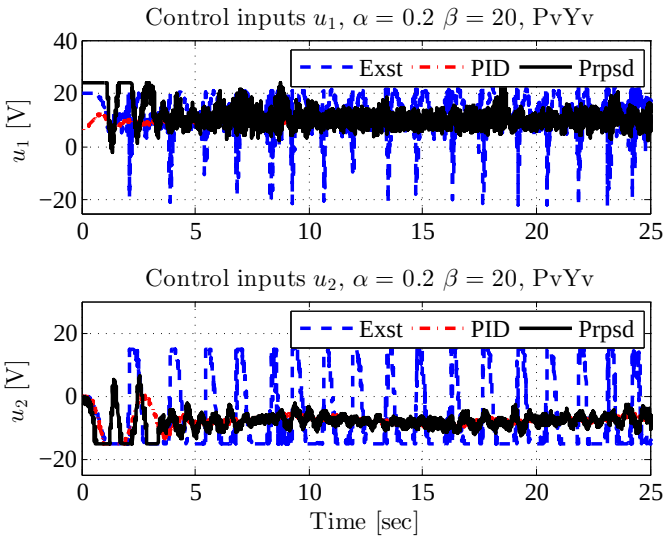

Figure B.67: Experiment results – Pitch and yaw control inputs in sine waves tracking control, using the existing ASMC (blue dash), PID (red dash-dot) and proposed ASMC (black solid line) with $\alpha = 0.2$ and $\beta = 20$.

C Papers in Review in Journals

C.1 Application of Adaptive Sliding Mode Control to Nonlinear Systems with Unknown Polynomial Bounded Uncertainties

Jiang Zhu and Karim Khayati. Application of Adaptive Sliding Mode Control to Nonlinear Systems with Unknown Polynomial Bounded Uncertainties. In review in *Transactions of the Institute of Measurement and Control*, 2016.

To appear in the *Transactions of the Institute of Measurement and Control*

Vol. 00, No. 00, Month 20XX, 1–33

Application of Adaptive Sliding Mode Control for Nonlinear Systems with Unknown Polynomial Bounded Uncertainties

Jiang Zhu[a] and Karim Khayati[a] *

[a] *Department of Mechanical and Aerospace Engineering, Royal Military College of Canada, Kingston, Ontario, K7K 7B4, Canada*

(*v1.0 released December 2014*)

In this paper, we discuss the application of a novel switching gain law – integral/exponential adaptation law, recently proposed for adaptive sliding mode control (ASMC) design, for a wide class of nonlinear systems with unknown polynomial bounds on uncertainty norm. A robust finite time convergence (FTC), *i.e.*, stability solution, is obtained with low chatter on control action and fast transient performance for ASMC handling the multi-input multi output (MIMO) nonlinear systems with uncertainties of amplitudes bounded within unknown polynomials in the state vector norm. The exponential term of the proposed adaptation law targets the reduction of the chatter levels of the sliding mode by significantly reducing the gain overestimation while simultaneously suppressing the overshoot by speeding up the system response to the uncertainties. It also prevents the instability issues that encounters the classic integral-gain-law-based ASMC when underestimating its initial gain or gain rate parameter. A simple example illustrates the motivation and feasibility of the proposed ASMC. The applications on a nonlinear mass-spring system

*Corresponding author. Email: karim.khayati@rmc.ca; phone: +1(613)-541-6000 ext. 8407

and on a two-degree-of-freedom (2-DOF) electromechanical rotative plant demonstrate the effectiveness of the proposed design.

Keywords: nonlinear systems, polynomially bounded uncertainties, adaptive sliding mode control, finite time convergence, integral/exponential adaptation law, chattering reduction.

1. Introduction

Control theory for linear systems has been developed for a long time. In the real world, however, most control systems are nonlinear. Moreover, the nonlinear systems often withstand parameter uncertainties (*e.g.*, the loading or unloading action of a helicopter changes its mass and moment of inertia) and external disturbances (*e.g.*, unmanned-aerial-vehicle flying through a snow storm). The control techniques developed for linear dynamical systems are not always suitable for nonlinear systems, particularly for those with uncertainties. Such uncertainties are often assumed to be bounded (Ullah, Han, & Khattak, 2016; Utkin & Poznyak, 2013b; Mazinan, Kazemi, & Shirzad, 2014; Y. Li & Xu, 2010; Plestan, Shtessel, Brgeault, & Poznyak, 2010; Wang & Stengel, 2002; Khalil, 2002; Slotine & Li, 1991). Most conventional linear and nonlinear robust control techniques such as H-infinity control, conventional sliding mode control (SMC) and high-order SMC are designed based on the knowledge of the bounds of uncertainties. In fact, the designed feedback gain must be greater than the bounds of the lumped uncertainties to ultimately compensates for these uncertainties (Utkin & Poznyak, 2013b; Khalil, 2002; Slotine & Li, 1991; Levant, 2001; Young, Utkin, & Ozguner, 1999). However, in most cases, such perturbation bounds are unknown and rarely estimated *a priori*. Thus, the conventional control algorithms face a dilemma: If the designed feedback gain is based on underestimated bounds of the actual uncertainties, the system may become unstable, and, if the designed feedback gain is based on an overestimation of the

actual uncertainty bounds, the system may encounter high chattering and consume "unnecessary" high energy. To solve the problem of nonlinear systems with uncertainties of unknown bounds, techniques of perturbation-estimation-SMC (Y. Li & Xu, 2010) and active disturbance rejection control (J. Han, 2009) were proposed to estimate the bounds of uncertainties and then reject them. Both techniques require a differentiator to obtain the knowledge of the system's high order state (*e.g.*, acceleration). The differentiator required for these methods also amplifies the noisy input signals and may create further uncertainties and large errors. Without using differentiators, another nonlinear control technique, the adaptive sliding mode control (ASMC), has been introduced during the past decade to design a feedback gain adaptively compensating for the lumped uncertainties (Wheeler, Su, & Stepanenko, 1998; Lee & Utkin, 2007; Cheng, Chien, & Shih, 2010; Y. Li & Xu, 2010; Plestan et al., 2010; Cong, Chen, & Liu, 2012; Utkin & Poznyak, 2013b; Nourisola & Ahmadi, 2014; Lin, 2014). The chattering attenuation and the trajectory accuracy in the existing ASMC methods are acceptable after the end of the adaptation process. The efficiency of this sliding mode structure has been demonstrated using an observer-based control design for mechanical systems with uncertainties reducing significantly the levels of chatter and improving the accuracy (Khayati, 2015). However, the overshoot is still large at the beginning of the adaptation process and the chattering still exists in the control input and the system trajectories before the end of the adaptation process (Zhu & Khayati, 2016a). To improve the overshoot and chattering levels during the adaptation process, time-varying boundary-layer-based gain law for real ASMC (Plestan et al., 2010) and improved forms of the switching gain near the boundary-layer (Zhu & Khayati, 2014a, 2014b) have been proposed and tested accordingly. More recently, an integral/exponential gain law has been introduced in (Zhu & Khayati, 2016b). This new algorithm provides instantaneously "almost" the required compensating gain without *a prior* knowledge of the lumped uncertainty

C.1. Application of Adaptive Sliding Mode Control to Nonlinear Systems with Unknown Polynomial Bounded Uncertainties

bounds.

In the numerous contributions of the past two decades, the uncertainties are often assumed to be bounded within possibly unknown constant bounds or affine functions. In particular, ASMC design with integral adaptation laws (Zhang & Zheng, 2014; Utkin & Poznyak, 2013b; Cong et al., 2012; Y. Li & Xu, 2010; Plestan et al., 2010; Lee & Utkin, 2007; Wheeler et al., 1998) have been widely used. However, other common kinds uncertain systems still exist. For instance, if their parameters are unknown, the Duffing dynamics (*i.e.*, mechanical systems with softening springs) and the tunnel-diode circuit dynamics contain uncertainties bounded by polynomial functions of the state (Khalil, 2002). Moreover, according to Taylor's theorem, most continuous nonlinearities can be approximated by polynomials. The new question then arises: how to control the nonlinear dynamical systems where there exist uncertainties bounded by unknown polynomials. The question motivates the studies of nonlinear systems with polynomially bounded uncertainties. If the bounds and the maximum order of the polynomial uncertainties are known, the stability region was analyzed in (Topuc & Packard, 2007) and a polynomial-type dependent gain can be designed (M. C. Han & Chen, 1992). Only given the maximum order of the polynomial uncertainties, a high order integral-type adaptation law was discussed in (Cheng et al., 2010). In the case that both the order and the bounds of the polynomial uncertainties are unknown *a priori*, however, to our best knowledge, no existing control method has been proposed. This paper discusses the application of the recently developed ASMC (Zhu & Khayati, 2016b) to such kind of nonlinear systems. Slightly different from the ASMC design in (Zhu & Khayati, 2016b), the ASMC structure proposed in this paper has less tuning parameters. In addition the scalar ASMC in (Zhu & Khayati, 2016b), the MIMO structures of ASMC are provided in this paper with theoretical proof that it has the ability to handle nonlinear systems with uncertainties of unknown polynomial bounds. It

will be shown that the new approach constrains the lumped uncertainties bounded by polynomials of unknown parameters. Moreover, it confines the trajectory much close to the sliding surface and greatly reduces the overshoot by reducing the final gain. Then, the stability and robustness are improved, and the chattering is suppressed. Simulation and experimental results will demonstrate the effectiveness of the application of the new algorithm in terms of stability, fast response, smaller trajectory variation and reduced chattering level.

This paper is organized as follows. In Section 2, we state the control problem and existing ASMC designs. Section 3 proposes the integral/exponential adaptation law of ASMC design for polynomial upper-bounds on norm uncertainties. An simple example of scalar dynamics is presented first to illustrate the proposed design. Then, theoretic results prove the stability of the closed-loop MIMO system. Applications of the proposed ASMC on a nonlinear mass-spring system and a 2-DOF helicopter setup are shown in Section 4, while Section 5 concludes this work.

2. ASMC Problem and Existing Designs

In this section, we first state the control problem and assumptions for nonlinear systems with uncertainties of unknown bounds. Then, we recall some existing ASMC designs.

2.1 *Problem Statement and Assumptions*

Consider the uncertain nonlinear dynamics

$$\dot{x} = f(x,t) + g(x,t) \cdot u \tag{1}$$

where $x \in \chi$ is the state vector in a domain $\chi \subset \mathrm{R}^n$ containing the origin, and $u \in \mathrm{R}^m$ the control input. The vector $f(x,t) \in \mathrm{R}^n$ and the matrix $g(x,t) \in \mathrm{R}^{n \times m}$ are nonlinear time-varying smooth

functions containing parametric uncertainties and external disturbances (Levant, 2003; Plestan et al., 2010; Plestan, Shtessel, Bregeault, & Poznyak, 2013; Shtessel, Taleb, & Plestan, 2012; Taleb, Plestan, & Bououlid, 2015). It is assumed that

Assumption 1: *The norm of the perturbation $f(x,t)$ is upper-bounded with some unknown polynomials in the state vector $x \in \chi$, and the norm of the uncertain term $g(x,t)$ is bounded by some unknown scalars. More specifically,*

$$\|f(x,t)\| \leq c_0 + \sum_{i=1}^{q} c_i \|x\|^i \tag{2}$$

$$0 < \underline{b} \leq \|g(x,t)\| \leq \overline{b} \tag{3}$$

where q is a finite uncertain integer, c_0 and c_i $(i = 1, 2, \cdots, q)$ have finite uncertain non-negative values, $\underline{b}$ and $\overline{b}$ are unknown positive finite constants.

The assumption A.1 takes into account a large class of uncertainties, including (but not limited to) the following cases:

- $c_0 > 0$ and $c_1 = c_2 = \cdots = 0$, *i.e.*, $\|f(x,t)\| \leq c_0$, that is, the system uncertainty is regularly bounded;
- $c_0 > 0$, $c_1 > 0$ and $c_2 = c_3 = \cdots = 0$, *i.e.*, $\|f(x,t)\| \leq c_0 + c_1\|x\|$, that is, the system uncertainty is bounded by an affine function of the system state vector;
- $c_0 > 0$, $c_1 > 0$, $c_2 > 0$ and $c_3 = a_4 = \cdots = 0$, *i.e.*, $\|f(x,t)\| \leq c_0 + c_1\|x\| + c_2\|x\|^2$, that is, the system uncertainty is constrained by a quadratic function in the norm of the system state vector.

Let $x = 0$ be an equilibrium point for (1). Consider a measurable sliding vector $\sigma(x,t) \in \mathrm{R}^m$. We define the targeted manifolds $\Sigma = \{x \in \chi : \|\sigma(x,t)\| = 0\}$ and $\Sigma_\epsilon = \{x \in \chi : \|\sigma(x,t)\| \leq \epsilon\}$ for

some $\epsilon > 0$. Σ and Σ_ϵ are called "*ideal sliding* mode set" and "*real sliding* mode set", respectively (Levant, 2001).

Assumption 2: *σ is freely designed such that, as soon as the vector $x(t)$ reaches the set Σ (resp. Σ_ϵ) in finite time $t_r > 0$ and belongs to it thereafter, the dynamics (1) have to be stable in the ideal (resp. real) sliding mode. σ is its output (Plestan et al., 2013; Utkin & Poznyak, 2013a). In addition, we assume that there exists finite positive scalars γ_1 and γ_2 s.t.*

$$\|\sigma\| \geq \gamma_1 \cdot \|x\| - \gamma_2 \tag{4}$$

Consider the time derivative of σ along the system trajectory

$$\dot{\sigma}(x,t) = \Psi(x,t) + \Gamma(x,t) \cdot u \tag{5}$$

with $\Psi(x,t) \in \mathrm{R}^m$ and $\Gamma(x,t) \in \mathrm{R}^{m\times m}$, that is, $\sigma(x,t)$ has a vector relative degree of $r = [1,1,\cdots,1]^T_{1\times m}$ (Plestan et al., 2013; Levant, 2003). Solutions of the dynamics (5) with discontinuous right-hand side are defined in the sense of Fillipov (Fillippov, 1988). In the following, the arguments x and t of these functions will be omitted for simplicity. Moreover, without loss of generality and based on assumption A.1, we consider

Assumption 3: *The perturbation vector $\Psi \in \mathrm{R}^m$ is bounded by unknown polynomials in x,* i.e.*,*

$$\|\Psi\| \leq d_0 + \sum_{i=1}^{q} d_i \|x\|^i \tag{6}$$

where d_0 and d_i $(i = 1,2,\cdots,q)$ are unknown finite non-negative constants.

Assumption 4: *The uncertain matrix $\Gamma \in \mathrm{R}^{m\times m}$ is positive definite in the wider sense, i.e., its*

symmetric part Γ_s *defined by*

$$\Gamma_s = \frac{1}{2}(\Gamma + \Gamma^T) \tag{7}$$

is positive definite in the regular meaning (Marcus & Minc, 2010). In particular, if $m = 1$*, the term* Γ *is lower-bounded by a positive constant* $\underline{\Gamma}$*, a priori unknown,* i.e.*,*

$$0 < \underline{\Gamma} \leq \Gamma \tag{8}$$

2.2 *Existing ASMC Laws and Motivation*

Given the dynamics (5), we consider the control law (Utkin, Guldner, & Shi, 1999; Plestan et al., 2013)

$$u(t) = \begin{cases} -K \cdot \dfrac{\sigma}{\|\sigma\|} & \text{if } \sigma \neq 0 \\ 0 & \text{if } \sigma = 0 \end{cases} \tag{9}$$

For classic SMC design, the gain K is a constant scalar which is designed to be sufficiently large so that it can compensate for the lumped uncertainties (Young et al., 1999; Slotine & Li, 1991). To deal with uncertainties of unknown bounds, K in ASMC techniques is time-varying to adaptively compensate for the uncertainties (Wheeler et al., 1998; Lee & Utkin, 2007; Y. Li & Xu, 2010; Plestan et al., 2010; Cong et al., 2012; Utkin & Poznyak, 2013b). In particular, adaptation laws in form

$$\dot{K} = \alpha \cdot \|\sigma\| \tag{10}$$

and

$$\dot{K} = \alpha_1 \cdot \|\sigma\| + \alpha_2 \cdot \|x\| \cdot \|\sigma\| \tag{11}$$

have been exhaustively proposed in (Y. Li & Xu, 2010; Cong et al., 2012; Utkin & Poznyak, 2013b; Plestan et al., 2013; Zhang & Zheng, 2014; Wheeler et al., 1998; H. Li, Yu, Hilton, & Liu, 2013) for uncertainties bounded by unknown constants and unknown affine functions in the state vector, respectively. The adaptation laws (10) and (11) are designed for ideal sliding mode, while the real case is treated with slightly modified versions of these forms (Plestan et al., 2010; Wheeler et al., 1998). The two adaptation laws, for either ideal or real sliding mode, still have relatively large overshoots and chattering phenomena during the adaptation process. In the following, we consider mostly the ideal sliding case analysis for the sake of simplicity.

3. Integral/Exponential Reaching Law-based ASMC Design

To overcome the common weaknesses encountered by most existing ASMC forms, an integral/exponential law was proposed in (Zhu & Khayati, 2016b) for uncertainties of unknown bounds. In the following, we will prove that this ASMC design has the ability to handle nonlinear systems with uncertainties of unknown polynomial bounds in the norm of the state vector (*i.e.*, refer to the model (1) with the sliding dynamics (5) under assumptions A.1–A.4). The new ASMC design (slightly different from that introduced in (Zhu & Khayati, 2016b)) will follow for the multi-dimensional case, using the feedback control (9), as

$$\dot{\breve{K}} = \alpha \cdot \|\sigma\| \tag{12a}$$

$$K = \breve{K} + \beta\big(e^{\|\sigma\|} - 1\big) \tag{12b}$$

for some $\alpha > 0$ and $\beta > 0$.

3.1 *Scalar Case*

Let us first consider the case of single-input-single-output sliding scalar dynamics, *i.e.*, $n = 1$, and select $\sigma = x$ trivially (that is, from (4), $\gamma_1 = 1$ and $\gamma_2 = 0$). The norm of the sliding variable is reduced to its absolute value. Then, the feedback control (9) is simply defined as

$$u = -K \cdot \mathrm{sgn}(\sigma) \tag{13}$$

where $\mathrm{sgn}(\cdot)$ refers to the real-valued signum function.

Motivation Example. Consider the following simple scalar dynamics

$$\dot{\sigma} = c_0 + c_1\sigma + c_2\sigma^2 + u \tag{14}$$

The state σ is to be stabilized to zero for unknown (or uncertain) coefficients c_0, c_1 and c_2. Using the switching control (13) with the adaptation law (12), the state σ of the dynamics (14) can be stabilized to zero in finite time for any values of the initial state σ_0 and uncertain c_0, c_1, c_2. To simulate the dynamics (14), these parameters are selected as $\sigma_0 = c_0 = c_1 = c_2 = 1$ (under uncertain condition I) and $\sigma_0 = c_0 = c_1 = c_2 = 5$ (under uncertain condition II). Figures 1 and 2 show the obtained switching gain K and the state σ using the (Old-1) existing gain law (10), the (Old-2) existing gain law (11) and the (New) proposed gain law (12) with the control parameter chosen as $\alpha = \alpha_1 = 2\alpha_2 = 2\beta = 2$ and $\alpha = \alpha_1 = 2\alpha_2 = 2\beta = 10$, respectively.

One can see that, by using the proposed integral/exponential gain law (12), σ is stabilized to zero in finite time for any initial and uncertain conditions. However, the existing integral-gain-law-based

July 29, 2016 Transactions of the Institute of Measurement and Control ASMC˙TIMC˙poly2
Page 11 of 33 Transactions of the Institute of Measurement and Control

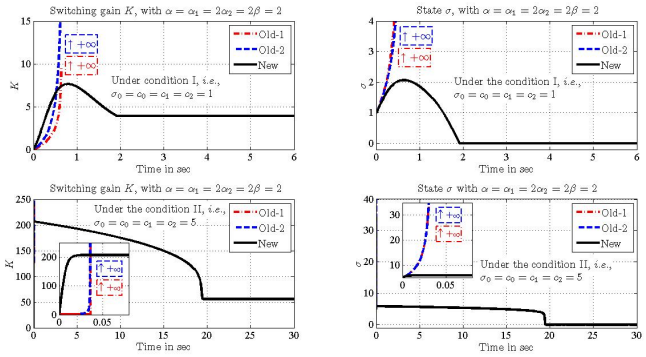

Figure 1. Illustrative example using the control parameters $\alpha = \alpha_1 = 2\alpha_2 = 2\beta = 2$: Switching gain K (left) and state σ (right) performances of the closed-loop dynamics (14) with (13) under different uncertain conditions.

ASMC (*i.e.*, using (10)) and modified-integral-gain-law-based ASMC (*i.e.*, using (11)) only work for some situations when the control parameters are sufficiently high and the uncertain parameters are small. Otherwise (when α, α_1 and α_2 are small), the dynamics (14) diverges. For any other large uncertain values of σ_0, c_0, c_1, c_2, the proposed method (12) also works even with small α and β, but the existing ASMC methods (10) and (11) do not. Furthermore, the switching gain amplitude is ultimately reduced with the new design.

Theorem 1: *Consider the nonlinear uncertain system* (1)*, with the sliding variable dynamics* (5)*, under assumptions A.1–A.4, controlled by* (13)*. If the gain $K(t)$ is designed as* (12)*, then for any initial condition $|\sigma| \neq 0$ the sliding variable σ converges to the domain Σ in finite time.*

Proof. The ASMC design for bounded uncertainties discussed in (Zhu & Khayati, 2016b) inspired

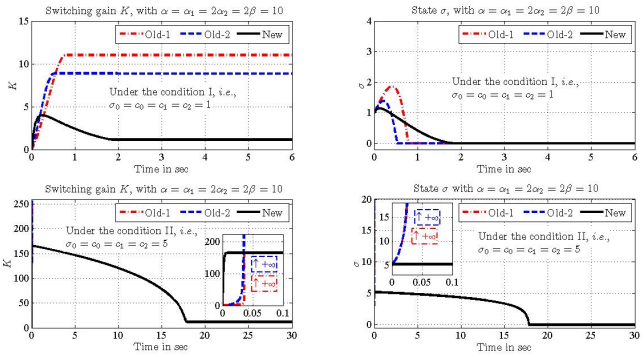

Figure 2. Illustrative example using the control parameters $\alpha = \alpha_1 = 2\alpha_2 = \beta = 10$: Switching gain K (left) and state σ (right) performances of the closed-loop dynamics (14) with (13) under different uncertain conditions.

us to deal with the general case of polynomially bounded uncertainty amounts.

From (5), (12) and (13), the time derivative of $|\sigma|$ along the system trajectory is

$$\begin{aligned}\frac{d}{dt}|\sigma| &= \dot{\sigma} \cdot \operatorname{sgn}(\sigma) \\ &= \Gamma\big(h(\sigma) - \breve{K}\big)\end{aligned} \tag{15}$$

with $h(\sigma) = \dfrac{\Psi \cdot \operatorname{sgn}(\sigma)}{\Gamma} - \beta\big(e^{|\sigma|} - 1\big)$. Note, $h(\sigma)$ is upper-bounded, *i.e.*, there exist finite values σ^* and $h^* = h(\sigma^*)$, *s.t.*,

$$h(\sigma) \leq h^* \tag{16}$$

for all $|\sigma| \geq 0$ (see Appendix 6.1 for details). Basically, the term $h(\sigma)$ represents a combination of the lumped system uncertainties with the exponential compensating gain of the dynamics (5)

(considering the scalar case) under the feedback control (13) using the reaching law (12).

For $\sigma \neq 0$, from (12a), $\breve{K}(|\sigma|)$ keeps growing with a rate of, at least, $\alpha|\sigma| > 0$. Thus, the growing state gain $\breve{K}$ will eventually compensate for (*i.e.*, be greater than) the bounded $h(\sigma)$ in (15). Since this compensation action will occur for any $h(\sigma) \geq \breve{K}$ (*i.e.*, $\frac{d}{dt}|\sigma| \geq 0$) and $\sigma \neq 0$, we can conclude that there will always exist a positive scalar κ_0 and an ultimate time instant $t^* \geq 0$, *s.t.*,

$$h(\sigma) + \kappa_0 \leq \breve{K} \tag{17}$$

for all $t \geq t^*$. Then, we obtain from (15)

$$\frac{d}{dt}|\sigma| \leq -\Gamma\kappa_0 \leq -\underline{\Gamma}\kappa_0 \tag{18}$$

for all $t \geq t^*$. We conclude that $|\sigma|$ converges to the domain Σ in finite time (Khalil, 2002). □

Unlike most ASMC designs dealing with bounded uncertainties (Plestan et al., 2010) or affine-function uncertainties (Wheeler et al., 1998), this work deals with unknown polynomial bounded uncertainties which are more than bounded uncertainties and affine-function uncertainties. In addition, the new design (12) provides simultaneously fast response and chattering reduction. The first part, integration state term $\breve{K}$, provides the ability to compensate for uncertainties with unknown polynomial bounds and forces the sliding variable to converge to the domain Σ in finite time. Furthermore, it should be pointed out that the integral term (12a) guarantees the FTC; otherwise, the exponential term only guarantees ultimately uniformly bounded (UUB) solutions. One can test that, without the integral term (*i.e.*, $\alpha = 0$ in (12)), the state is only UUB. The results of the application of the design (12) for the illustrative model dynamics (14) when $\alpha = 0$ are omitted here due to lack of space.

Comparing to the ASMC laws (10) and (11), the new algorithm (12) adds the exponential term

$\beta\left(e^{|\sigma|}-1\right)$, which provides an extra but sufficiently high gain to compensate for the lumped perturbation $\Gamma^{-1}\Psi\text{sgn}(\sigma)$ (which is possibly bounded by unknown polynomial) when the state is far (*i.e.*, $|\sigma|$ is large) from the sliding surface. Thus, K (with the exponential term) forces the sliding variable σ, if it is far from its desired sliding manifold Σ, to quickly turn around and be heading to the sliding surface. Moreover, when $|\sigma|$ tends to Σ, the exponential term reduces its value rapidly. Then, after reaching the sliding surface, the overall gain is reduced and the unwanted chattering level is expected to be much lower.

3.2 *Multi-dimensional Case*

Substituting (12) and (9) into (5), we obtain for $\sigma \neq 0$

$$\dot{\sigma} = \Psi - \frac{K}{\|\sigma\|}\Gamma\sigma \tag{19}$$

Then, we state the following theorem.

Theorem 2: *Consider the nonlinear uncertain system* (1)*, with the sliding dynamics* (5)*, under assumptions A.1–A.4, controlled by* (9)*. If the gain* $K(t)$ *is designed as* (12)*, then for any initial condition* $\|\sigma\| \neq 0$ *the sliding variable* σ *converges to the manifold* $\|\sigma\| = 0$*, i.e.,* $x \in \Sigma$ *in finite time.*

Proof. Let the positive definite function

$$V = \sigma^T\sigma \tag{20}$$

be a Lyapunov function candidate. Using (7), (12) and (19), for $\sigma \neq 0$, the time derivative of V

July 29, 2016 Transactions of the Institute of Measurement and Control ASMC˙TIMC˙poly2
Page 15 of 33 Transactions of the Institute of Measurement and Control

along the system trajectories is

$$\begin{aligned}\dot{V} &= 2\sigma^T\dot{\sigma} \\ &= 2\|\sigma\|\Big(\frac{\sigma^T\Psi}{\|\sigma\|} - \beta\big(e^{\|\sigma\|}-1\big)\frac{\sigma^T\Gamma_s\sigma}{\sigma^T\sigma} - \breve{K}\frac{\sigma^T\Gamma_s\sigma}{\sigma^T\sigma}\Big)\end{aligned} \tag{21}$$

We denote by $h_\Gamma(\sigma) = \dfrac{\sigma^T\Psi}{\|\sigma\|} - \beta\big(e^{\|\sigma\|}-1\big)\dfrac{\sigma^T\Gamma_s\sigma}{\sigma^T\sigma}$. For $\sigma \neq 0$, (21) can be rewritten as

$$\frac{\dot{V}}{2\sqrt{V}} = h_\Gamma(\sigma) - \breve{K}\frac{\sigma^T\Gamma_s\sigma}{\sigma^T\sigma} \tag{22}$$

Using (4) and (6), the scalar $h_\Gamma(\sigma)$ is upper-bounded. In fact,

$$h_\Gamma(\sigma) \leq d_0 + \sum_{i=1}^{q} d_i\|x\|^i - \beta\big(e^{\gamma_1\|x\|-\gamma_2}-1\big)\underline{\lambda}(\Gamma_s) \tag{23}$$

with $\underline{\lambda}(\Gamma_s)$ denoting the minimum eigenvalue of the symmetric positive definite Γ_s (refer to assumption A.4). Then, a positive exponential function ultimately grows faster than any polynomial (refer to the proof shown in Appendix 6.1 for more details).

For any $\sigma \neq 0$, from (12), $\breve{K}$ keeps growing and the positive scalar $\breve{K}\dfrac{\sigma^T\Gamma_s\sigma}{\sigma^T\sigma}$ in (22) will eventually compensate for the upper-bounded $h_\Gamma(\sigma)$, *i.e.*, $\breve{K}\dfrac{\sigma^T\Gamma_s\sigma}{\sigma^T\sigma} > h_\Gamma(\sigma)$. Since this compensating action will occur for any $\|\sigma\| \neq 0$ where $h_\Gamma(\sigma) \geq \breve{K}\dfrac{\sigma^T\Gamma_s\sigma}{\sigma^T\sigma}$ (*i.e.*, from (21) and (23), $\dfrac{d}{dt}\|\sigma\| \triangleq \dfrac{\dot{V}}{2\sqrt{V}} \geq 0$), we conclude that there exist a time instant t^* and a positive scalar κ_1, *s.t.*, for $t \geq t^*$

$$\breve{K}\frac{\sigma^T\Gamma_s\sigma}{\sigma^T\sigma} \geq h_\Gamma(\sigma) + \kappa_1 \tag{24}$$

Thus, from (20), (21), (23) and (24), we obtain

$$\frac{d}{dt}\|\sigma\| \leq -\kappa_1 \tag{25}$$

for $\|\sigma \neq 0\|$ and $t \geq t^*$. Now, by integrating both sides of (25) between t^* and $t \geq t^*$, we obtain

$$\|\sigma\| \leq -\kappa_1 \cdot \left(t - t^*\right) + \|\sigma(t^*)\|$$

Then, $\|\sigma\|$ is decreasing with a rate κ_1 and reaches the domain $\|\sigma\| = 0$ in finite time (Khalil, 2002). □

The proof discussed above is effectively based on assumption A.2. We note that whenever the design condition (4) is violated numerically or analytically, a modified version of the switching gain law can still exist to maintain the integral/exponential form. In fact, substituting $e^{\gamma\|x\|}$ for $e^{\|\sigma\|}$ in (12b), for some small positive scalar γ, would keep possible the compensation for the class of perturbations mainly discussed in this paper (refer to assumptions A.2 and A.3).

From the condition (8), we note that the uncertain gain matrix Γ matching with the input u in (5) does not require any upper-boundedness on its norm magnitude allowing definitely unlimited uncertainty levels of this term as long as it is nonzero (or nonsingular matrix in the wider sense).

Finally, we note that when the parameter matrix Γ is indefinite (*i.e.*, neither positive definite nor negative definite), the control defined by (9) is not appropriate. In this case, it is required to define a nonsingular matrix $\hat{\Gamma}$ alluding to the nominal value of Γ. Moreover, we assume that the matrix $L(t) = \hat{\Gamma}^{-1}\Gamma$ is positive definite in the wider sense, *i.e.*, the symmetric part $L_s = \frac{1}{2}(L + L^T)$ is positive definite in the regular meaning (Marcus & Minc, 2010). Note that the positiveness of L implies that the value of the nominal matrix $\hat{\Gamma}$ is close to that of its real matrix Γ. Then, by replacing σ with $\hat{\Gamma}^T\sigma$ in the control law (9) as (Utkin et al., 1999)

$$u(t) = \begin{cases} -K \cdot \dfrac{\hat{\Gamma}^T\sigma}{\|\hat{\Gamma}^T\sigma\|} & \text{if } \sigma \neq 0 \\ 0 & \text{if } \sigma = 0 \end{cases} \tag{26}$$

and applying the adaptation law (12), we guarantee the FTC of the states to the targeted manifold Σ. In deed, substituting (26) into (5), we obtain, for $\sigma \neq 0$

$$\dot{\sigma} = \Psi - \Gamma K(t) \cdot \frac{\hat{\Gamma}^T \sigma}{\|\hat{\Gamma}^T \sigma\|} \tag{27}$$

Then, we state the following theorem

Theorem 3: *Consider the nonlinear uncertain system* (1)*, subject to the closed-loop dynamics* (27)*, under assumptions A.1–A.3. Given* $L_s = \frac{1}{2}(L + L^T)$ *a symmetric positive definite matrix with* $L(t) = \hat{\Gamma}^{-1}\Gamma$*, if the gain* $K(t)$ *is designed as* (12)*, then for any initial condition* $\|\sigma\| \neq 0$ *the sliding variable* σ *converges to the sliding surface* $\|\sigma\| = 0$*, i.e.,* $x \in \Sigma$ *in finite time.*

Proof. See Appendix 6.2. □

3.3 *Case of Real Sliding Mode*

Different from the ideal sliding mode, where the sliding variable is constrained perfectly on the sliding surface after reaching the targeted manifold Σ, the sliding variable σ in the real sliding mode is generally non-zero due to measurement and computation imperfections. In other words, σ may be nonzero though it has reached the aimed manifold. As a result, the use of the adaptation law of ideal case to the real sliding mode has the risk of resulting in a permanently increasing and unbounded switching gain K. Thus, the ideal ASMC design should be modified for the real implementation. Consider the real sliding set Σ_ϵ defined in Section 2. The dynamic gain design is

defined as

$$\dot{\breve{K}} = \alpha \|\sigma\| \cdot \operatorname{sgn}\big(\|\sigma\| - \epsilon\big) \tag{28a}$$

$$K = \breve{K} + \beta \cdot \big(e^{\|\sigma\|} - 1\big) \tag{28b}$$

If $\beta = 0$, then (28) is reduced to the integral gain law presented in (Plestan et al., 2013). We obtain the following theorem of real ASMC design.

Theorem 4: *Consider the nonlinear uncertain system* (1)*, with the sliding dynamics* (5)*, under assumptions A.1–A.4, controlled by* (9)*. If the gain* $K(t)$ *is designed as* (28)*, then for any initial condition* $\|\sigma\| > \epsilon$ *the sliding variable* σ *converges to the domain* $\|\sigma\| \leq \epsilon$*, i.e.,* $x \in \Sigma_\epsilon$ *in finite time.*

Proof. It is similar to the proof of theorem 2 and is omitted here. □

4. Applications

To validate the effectiveness of the proposed scheme, we consider a nonlinear mass-spring system model depicted from (Wang & Stengel, 2002) and a 2-DOF helicopter simulator model actuated with two propellers (Quanser, 2006).

4.1 *Control of a Nonlinear Mass-Spring System*

4.1.1 Modelling

The nonlinear mass-spring system consists of two masses m_1 and m_2 connected by a linear-cubic spring. We denote by x_1 and x_2 the positions of the masses. The nonlinear dynamics of the system

can be written as

$$m_1\ddot{x}_1 + k_1(x_1 - x_2) + k_2(x_1 - x_2)^3 = u_1 \tag{29a}$$

$$m_2\ddot{x}_2 - k_1(x_1 - x_2) - k_2(x_1 - x_2)^3 = u_2 \tag{29b}$$

or

$$M\ddot{x} + K_1 x + k_2 f(x) = u \tag{30}$$

where $u = \begin{pmatrix} x_1 & x_2 \end{pmatrix}^T$ and $u = \begin{pmatrix} u_1 & u_2 \end{pmatrix}^T$. We have

$$M = \begin{pmatrix} m_1 & 0 \\ 0 & m_2 \end{pmatrix}, \quad K_1 = \begin{pmatrix} k_1 & -k_1 \\ -k_1 & k_1 \end{pmatrix}, \quad f(x) = \begin{pmatrix} (x_1 - x_2)^3 \\ -(x_1 - x_2)^3 \end{pmatrix} \tag{31}$$

The mass and spring constant variations are $0.5 < m_1 < 1.5$, $0.5 < m_2 < 1.5$, $0.5 < k_1 < 2$ and $-0.5 < k_2 < 0.2$, with nominal values as $\hat{m}_1 = \hat{m}_2 = \hat{k}_1 = 1$ and $\hat{k}_2 = -0.1$ (Wang & Stengel, 2002). Note that M is a positive definite diagonal matrix and $f(x)$ is a cubic polynomial in the system states.

4.1.2 Sliding variable design

It is desired that the system follows a trajectory x_d. Denote by $\tilde{x} = x - x_d$ the trajectory error. Assuming that the positions and velocities of the two masses are measurable, we design a PID sliding variable (Y. Li & Xu, 2010)

$$\sigma = K_p\tilde{x} + K_i \int \tilde{x} d\tau + K_d\dot{\tilde{x}} \tag{32}$$

with K_p, K_i and K_d positive definite matrices of $\mathbb{R}^{2\times 2}$. Taking the time derivative of the both sides of (32) and substituting (30), the sliding variable dynamics can be written as

$$\dot{\sigma} = K_p\dot{\tilde{x}} + K_i\tilde{x} + K_dM^{-1}\cdot\left(u - K_1x - k_2f(x) - M\ddot{x}_d\right) \tag{33}$$

4.1.3 Equivalent control

Consider $M = \hat{M} + \tilde{M}$, $K_1 = \hat{K}_1 + \tilde{K}_1$ and $k_2 = \hat{k}_2 + \tilde{k}_2$ where $\hat{M}$, $\hat{K}_1$ and $\hat{k}_2$ are given nominal values of M, K_1 and k_2, and $\tilde{M}$, $\tilde{K}_1$ and $\tilde{k}_2$ their corresponding uncertain values. We apply the equivalent control method where the control input consists of a combination of an equivalent control input and a switching control input (Utkin et al., 1999), as

$$u = u_{eq} + u_{sw} \tag{34}$$

u_{eq} is obtained by assuming that all uncertainties vanish at the permanent sliding regime, *i.e.*, $M = \hat{M}$, $K_1 = \hat{K}_1$, $k_2 = \hat{k}_2$ and $\dot{\sigma} = 0$. We have

$$0 = K_p\dot{\tilde{x}} + K_i\tilde{x} + K_d\hat{M}^{-1}\cdot\left(u_{eq} - \hat{K}_1x - \hat{k}_2f(x) - \hat{M}\ddot{x}_d\right) \tag{35}$$

That is,

$$u_{eq} = \hat{K}_1x + \hat{k}_2f(x) + \hat{M}\ddot{x}_d - \hat{M}K_d^{-1}\cdot\left(K_p\dot{\tilde{x}} + K_i\tilde{x}\right) \tag{36}$$

Substituting (36) into (33), we obtain the sliding variable dynamics in terms of the switching control (refer to (5))

$$\dot{\sigma}(x,t) = \Psi(x,t) + \Gamma(x,t)\cdot u_{sw} \tag{37}$$

with

$$\Psi(x,t) = K_d M^{-1} \tilde{M} K_d^{-1} \cdot \left(K_p \dot{\tilde{x}} + K_i \tilde{x}\right) + K_d M^{-1} \cdot \left(- \tilde{K}_1 x - \tilde{k}_2 f(x) - \tilde{M} \ddot{x}_d\right) \tag{38}$$

and

$$\Gamma(x,t) = K_d M^{-1} \tag{39}$$

Note that $f(x)$ in (38) contains a cubic polynomial of the state x and $\tilde{k}_2$ is an uncertain parameter. That is, $\Psi(x,t)$ is an uncertainty bounded within an unknown-coefficient-cubic polynomial. Since the diagonal matrix M and the matrix K_d are positive definite of $\mathbb{R}^{2\times 2}$, then Γ is positive definite. Based on Theorem 2, we apply the switching control u_{sw} in form (9) with the adaptation law (28).

4.1.4 Simulation results

First, the two masses m_1 and m_2 are stabilized at the equilibrium positions. Then, in the second simulations, they are desired to follow trajectories $x_{d1} = \sin(\pi t + \frac{\pi}{2})$ and $x_{d2} = 0.5\sin(\pi t + \frac{\pi}{2})$, respectively. Given, a sampling period $T_s = 5 \cdot 10^{-3}$ and PID matrix gains selected as $K_p = 4K_i = K_d = I_2$, we apply the real ASMC design using the (Proposed) reaching law (28), with a fixed boundary-layer limit $\epsilon = 10^{-3}$, $\alpha = 10$, and applying $\beta = 2$ and 20. Then, we compare its performance to the (Existing) adaptation gain dynamics discussed in (Plestan et al., 2013, 2010) (*i.e.*, (28) with $\beta = 0$), using $\alpha = 10$, with boundary-layer limit fixed at $\epsilon = 10^{-3}$, and varying ϵ-tuning (Plestan et al., 2010). The simulation results are shown in Figures 3 to 5. From Figure 3, one can see that there is no significant difference in terms of stabilization and accuracy for all ASMC implementations. However, the magnitudes and chattering levels of the corresponding control inputs in the proposed ASMC are much less than those in the existing ASMC. From Figure

4, one can see that, comparing to those using the existing ASMC, both the trajectory errors and the magnitudes of the control inputs (as well as the chattering levels) by using the proposed ASMC (28) are reduced simultaneously. The tracking of the first mass displacement $\tilde{x}_1$ with the proposed design is much faster than with the existing ones. The switching gain magnitudes are much lower with the proposed design (see Figure 5).

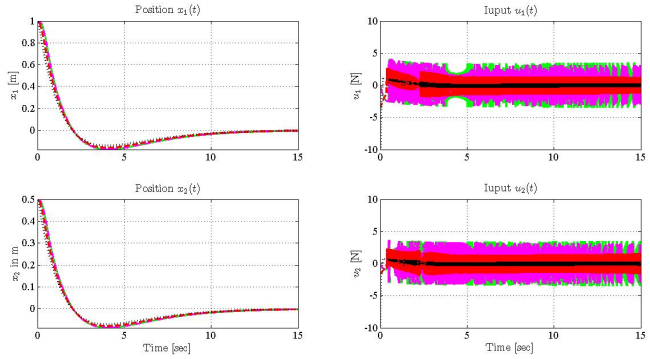

Figure 3. Simulation results of nonlinear spring-mass system – Position stabilizations and the corresponding control inputs. Results in real sliding mode using the existing IG-ASMC, *i.e.*, adaptation law (28) with $\beta = 0$ (solid green for fixed ϵ and dash-dot magenta for ϵ–tuning) and proposed IEG-ASMC, *i.e.*, adaptation law (28) with $\beta > 0$ (dash red for $\beta = 2$ and dot black for $\beta = 20$).

4.2 *Control of a 2-DOF Helicopter-Model Setup*

The 2-DOF helicopter simulator model, built by Quanser Inc., is actuated with two propellers (Quanser, 2006). The front propeller controls the elevation of the helicopter nose about the pitch

July 29, 2016 Transactions of the Institute of Measurement and Control ASMC˙TIMC˙poly2
Page 23 of 33 Transactions of the Institute of Measurement and Control

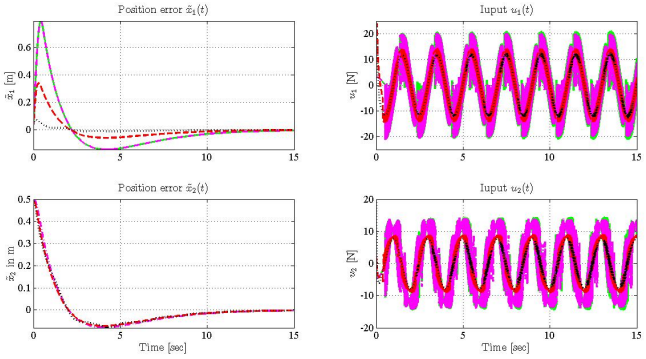

Figure 4. Simulation results of nonlinear spring-mass system – Trajectory errors of sine waves and the corresponding control inputs. Results in real sliding mode using the existing IG-ASMC, *i.e.*, adaptation law (28) with $\beta = 0$ (solid green for fixed ϵ and dash-dot magenta for ϵ–tuning) and proposed IEG-ASMC, *i.e.*, adaptation law (28) with $\beta > 0$ (dash red for $\beta = 2$ and dot black for $\beta = 20$).

axis and the back propeller controls the side to side motions of the helicopter about the yaw axis. We define (Quanser, 2006)

$$\left(J_p + ml^2\right)\ddot{\phi} = K_{pp}V_p + K_{py}V_y - B_p\dot{\phi} - mgl \cdot \cos\phi - ml^2 \sin\phi\cos\phi \cdot \dot{\psi}^2 \tag{40a}$$

$$\left(J_y + ml^2\cos^2\phi\right)\ddot{\psi} = K_{yp}V_p + K_{yy}V_y - B_y\dot{\psi} + 2ml^2 \sin\phi\cos\phi \cdot \dot{\phi}\dot{\psi} \tag{40b}$$

where V_p and V_y are the applied voltages, ϕ the pitch angle position, ψ the yaw angle position, $\dot{\phi}$ and $\dot{\psi}$ the pitch and yaw angular velocities, respectively. B_p (*resp.* B_y) is the viscous damping about pitch (*resp.* yaw) axis, J_p (*resp.* J_y) the moment of inertia about pitch (*resp.* yaw) pivot, K_{pp} (*resp.* K_{py}) the thrust torque constant acting on pitch axis from pitch (*resp.* yaw) motor/propeller, K_{yy}

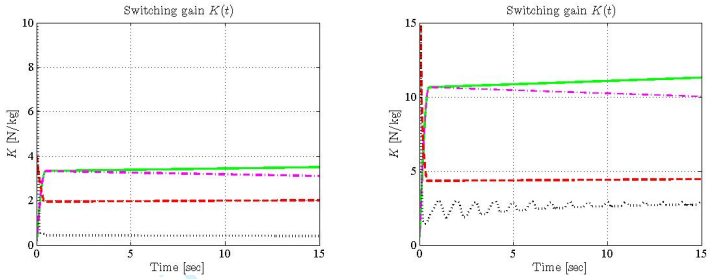

Figure 5. Simulation results of nonlinear spring-mass system – the switching gains in position stabilization (left sub-figure) and the switching gains in trajectory tracking control (right sub-figure). Results in real sliding mode using the existing IG-ASMC, *i.e.*, adaptation law (28) with $\beta = 0$ (solid green for fixed ϵ and dash-dot magenta for ϵ–tuning) and proposed IEG-ASMC, *i.e.*, adaptation law (28) with $\beta > 0$ (dash red for $\beta = 2$ and dot black for $\beta = 20$).

(*resp.* K_{yp}) the thrust torque constant acting on yaw axis from yaw (*resp.* pitch) motor/propeller, l the center-of-mass length along the helicopter body from pitch axis, m the mass of the helicopter and g the gravitational acceleration. The voltage of the front and rear propeller motors are limited to $\pm$25V and $\pm$15V, respectively (Quanser, 2006).

It is desired that the helicopter follows trajectories ϕ_d, ψ_d with their time derivatives $\dot{\phi}_d$, $\dot{\psi}_d$. Let $x_1 \triangleq \phi - \phi_d$, $x_2 \triangleq \psi - \psi_d$, $x_3 \triangleq \dot{\phi} - \dot{\phi}_d$ and $x_4 \triangleq \dot{\psi} - \dot{\psi}_d$ be the measurable states, and $u = [u_1 \ u_2]^T \triangleq [V_p \ V_y]^T$ the input vector. Assuming all parameters of the dynamics (40) are unknown, the latter can be rewritten in the form of (1). For the control design purpose, we consider a proportional-integral sliding hyper-surface as $\sigma \triangleq K_p x + K_i \int x d\tau$ (Y. Li & Xu, 2010). Note when the system is on the sliding surface ($\sigma = 0$) it has an exponential stability, *i.e.*, $x \to 0$ and $\int x d\tau \to 0$ exponentially. Then, the dynamics of σ can be written in form (5) where the uncertainty vector

$\Psi(x,t)$ shows affine and quadratic terms in the state variables, in form $a(t)x_2^2$ and $b(t)x_1x_2$ with $a(t)$ and $b(t)$ uncertain bounded coefficients.

During the experiments, the pitch and yaw positions are supposed to follow the time-varying trajectories, $\phi_d = -10^\circ \cos 0.4\pi t$ and $\psi_d = 10^\circ \cos 0.15\pi t$, respectively. We apply the real ASMC design (with a boundary-layer limit $\epsilon = 10^{-2}$ and a sampling period $T_s = 5 \cdot 10^{-3}$) using the (Proposed) reaching law (28) and we compare its performance to the (Existing) adaptation gain dynamics discussed in (Plestan et al., 2013, 2010) (*i.e.*, (28) with $\beta = 0$). The experiments are conducted using different values of α and β. We use a fixed-value ϵ instead of ϵ-tuning (*i.e.*, ϵ time-varying and depending on K) which requires that Γ is normalizable (Plestan et al., 2010). Moreover, by applying the ϵ-tuning, we realize that there is no improvement in the experimental results. Then, for their consistency we keep ϵ the same during all the experiments. Figures 6 and 7 show results obtained with $\alpha = 0.2$, $\beta = 20$ and $\alpha = 0.05$, $\beta = 5$, respectively. The other results are omitted here to save space. Table 1 shows the summary of the tracking errors in terms of root-mean-square (RMS) and peak (*i.e.*, maximum absolute value) for these experiments. One can see that, by using the proposed gain law, both pitch input u_1 and yaw input u_2 have less chattering levels and smaller magnitude variations than those using the existing one. With ASMC using the existing gain law, the voltages of the rear propeller motor are often saturated at their minimum and maximum levels of ± 15V, respectively, while these values are limited about -10V with the new design. For the front motor, the input voltages oscillate within ± 20V with the existing design, while the new design requires voltages of about 10V with $\alpha = 0.05$, $\beta = 5$ and up to 20V with $\alpha = 0.2$, $\beta = 20$. Simultaneously, the pitch and yaw angles follow the desired trajectories more accurately by using the proposed gain law than those using the existing one. From Table 1, it can be seen that, by using the proposed gain law (*i.e.*, with any $\beta > 0$), the errors are largely reduced

July 29, 2016 Transactions of the Institute of Measurement and Control ASMC˙TIMC˙poly2
Transactions of the Institute of Measurement and Control

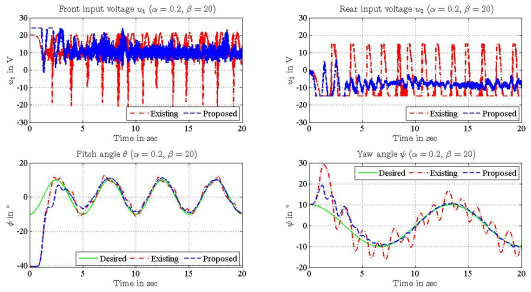

Figure 6. Input voltages (in volt) and angular positions (in degree) for $\alpha = 0.2$ and $\beta = 20$.

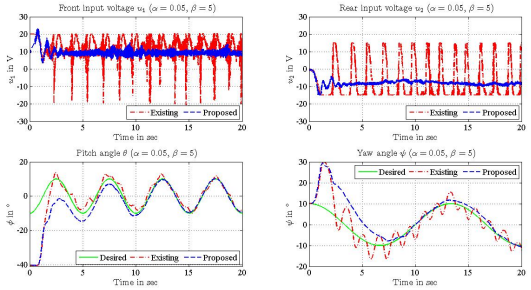

Figure 7. Input voltages (in volt) and angular positions (in degree) for $\alpha = 0.05$ and $\beta = 5$.

compared to those obtained by using the existing gain law (*i.e.*, $\beta = 0$). The RMS errors of the pitch angle trajectories with the new design can be reduced by 70% compared to the existing ones and by 80% for yaw angles, while their peak errors can be down by 70% and more than 50%, respectively.

Table 1. Recap – Error RMS and Peak Values in % of Maximum Displacement

			Pitch Angle		Yaw Angle	
Method	α	β	RMS	Peak	RMS	Peak
Existing	0.05	0	14.6	36.1	27.8	73.7
Proposed		5	**4.7**	**14.9**	15.4	36.0
		10	5.6	20.0	10.9	21.8
		20	5.8	19.8	**6.3**	**12.6**
Existing	0.1	0	16.9	48.0	27.6	65.7
Proposed		5	8.1	16.2	15.2	27.8
		10	**5.4**	**11.6**	11.5	25.8
		20	6.0	16.9	**6.3**	**13.3**
Existing	0.2	0	15.3	35.8	30.0	68.1
Proposed		5	13.2	27.2	16.5	36.6
		10	**7.3**	**13.1**	9.5	23.0
		20	**7.3**	17.6	**6.0**	**15.3**

5. Conclusions

The application of a newly developed ASMC for nonlinear systems with unknown polynomial uncertainties are presented. While most existing papers on ASMC designs deal with uncertainties bounded by constants or affine functions, the recently proposed design with integral/exponential

gain law successfully handles the uncertainties bounded by unknown polynomials in the norm of system state vector. Moreover, the new algorithm provides simultaneously the "almost" required compensating gain and the greatly reduced final (or post-perturbation) gain. With the proposed algorithm, the closed-loop dynamic system has fast response to uncertainties, the accuracy and stability are enhanced, and a much lower level of gain reduces the chattering level eventually. A simple example illustrates the feasibility of the proposed ASMC. The applications on a nonlinear mass-spring system and on a 2-DOF electromechanical rotative plant demonstrate the effectiveness of the proposed design in terms of stability, chattering reduction and error performances for handling nonlinear systems with unknown polynomial uncertainties. This requirement remains fundamental to keep the design parameters of the proposed method independent of the initial conditions and the uncertainty levels (*i.e.*, that can be freely selected as most of ASMC gain laws).

References

Arfken, G. (1985). *Mathematical Methods for Physicists* (3rd ed. ed.). Orlando, FL: Academic Press.

Cheng, C. C., Chien, S.-H., & Shih, F.-C. (2010). Design of robust adaptive variable structure tracking controllers with application to rigid robot manipulators. *IET Control Theory and Applications*, *4*(9), 1655–1664.

Cong, B., Chen, Z., & Liu, X. (2012). On Adaptive Sliding Mode Control Without Switching Gain Overestimation. *International Journal of Robust and Nonlinear Control*, *1*(1), 001–017.

Fillippov, A. (1988). *Differential Equations with Discontinuous Right Hand Side.* Dordrecht, Netherlands: Kluwer Academic Publisher.

Han, J. (2009). From PID to Active Distirbance Rejection Control. *IEEE Transactions on Industrial Electronics*, *56*(3), 2–22.

Han, M. C., & Chen, Y. H. (1992). Polynomial robust control design for uncertain systems. *Automatica*, *28*(4), 809–814.

Khalil, H. (2002). *Nonlinear Systems* (3rd ed. ed.). NY: Prentice-Hall.

Khayati, K. (2015). Multivariable Adaptive Sliding-Mode Observer-Based Control for Mechanical Systems. *Canadian Journal of Electrical and Computer Engineering*, *38*(3), 253–265. doi:

Lee, H., & Utkin, V. (2007). Chattering Suppression Methods in Sliding Mode Control Systems. *Annual Reviews in Control*, *31*(1), 179–188.

Levant, A. (2001). Universal Single-Input-Single-Output (SISO) Sliding-Mode Controllers with Finite-Time Convergence. *IEEE Transactions on Automatic Control*, *46*(9), 1447–1451.

Levant, A. (2003). High-Order Sliding Modes, Differentiation and Ouput Feedback Control. *International Journal of Control*, *76*(9), 924–941.

Li, H., Yu, J., Hilton, C., & Liu, H. (2013). Adaptive Sliding-Mode Control for Nonlinear Active Suspension Vehicle Systems Using TS Fuzzy Approach. *IEEE Transactions on Industrial Electronics*, *60*(8), 3328–3338.

Li, Y., & Xu, Q. (2010). Adaptive Sliding Model Control with Perturbation Estimation and PID Sliding Surface for Motion Tracking of a Piezo-Driven Micromanipulator. *IEEE Transactions on Control Systems Technology*, *18*(4), 798–810.

Lin, K.-J. (2014). Adaptive Sliding Model Control Design for a Class of Uncertain Singularly Perturbed Nonlinear Systems. *International Journal of Control*, *87*(2), 432–439.

Marcus, M., & Minc, H. (2010). *A Survey of Matrix Theory and Matrix Inequalities* (1st ed. ed.). NY: Dover Publications.

Mazinan, A., Kazemi, M., & Shirzad, H. (2014). An efficient robust adaptive sliding mode control approach with its application to secure communications in the presence of uncertainties, external disturbance and unknown parameters . *Transactions of the Institute of Measurement and Control*, *36*(2), 164–174.

Nourisola, H., & Ahmadi, B. (2014). Robust Adaptive Sliding Mode Control Sased on Wavelet Kernel

Principal Component for Offshore Steel Jacket Platforms Subject to Nonlinear Wave-induced Force. *Transactions of the Insitute of Measurement and Control*, *22*(15), 3299–3311.

Plestan, F., Shtessel, Y., Bregeault, V., & Poznyak, A. (2013). Sliding Mode Control with Gain Adaptation – Application to an Electropneumatic Actuator. *Control Engineering Practice*, *21*(21), 679–688.

Plestan, F., Shtessel, Y., Brgeault, V., & Poznyak, A. (2010). New Methodologies for Adaptive Sliding Mode Control. *International Journal of Control*, *83*(9), 1907–1919.

Quanser. (2006). 2 DOF Helicopter User and Control Manual [Computer software manual].

Shtessel, Y., Taleb, M., & Plestan, F. (2012). A Novel Adaptive Gain Supertwisting Sliding Mode Controller: Methodology and Application. *Automatica*, *48*(4), 759–769.

Slotine, J.-J., & Li, W. (1991). *Applied Nonlinear Control*. Englewood Cliffs, NJ: Prentice Hall.

Taleb, M., Plestan, F., & Bououlid, B. (2015). An Adaptive Solution for Robust Control based on Integral High-Order Sliding Mode Concept. *International Journal of Robust and Nonlinear Control*, *25*(8), 1201–1213.

Topuc, U., & Packard, A. (2007). Stability Region Analysis for Uncertain Nonlinear Systems. , 1693–1698.

Ullah, N., Han, S., & Khattak, M. (2016). Adaptive Fuzzy Fractional Sliding Mode controller for a Class of Dynamical Systems with Uncertainty. *Transactions of the Insitute of Measurement and Control*, *38*(4), 402–413.

Utkin, V., Guldner, J., & Shi, J. (1999). *Sliding Modes in Electromechanical Systems* (1st ed. ed.). London: Taylor and Francis.

Utkin, V., & Poznyak, A. (2013a). Adaptive Siding Mode Control with Application to Super-Twist Algorithm: Equivalent Control Method. *Automatica*, *1*(49), 39–47.

Utkin, V., & Poznyak, A. (2013b). *Advances in Sliding Mode Control – Concept, Theory and Implementation* (1st ed. ed.). Heidelberg, NY: Springer.

Wang, Q., & Stengel, R. F. (2002). Robust control of nonlinear systems with parametric uncertainty. *Automatica*, *38*(1), 1591–1559.

Wheeler, G., Su, C.-Y., & Stepanenko, Y. (1998). A Sliding Mode Controller with Improved Adaptation Laws for the Upper Bounds on the Norm of Uncertainties. *Automatica*, *34*(12), 1657–1661.

Young, K., Utkin, V., & Ozguner, U. (1999). A Control Engineer's Guide to Sliding Mode Control. *IEEE Transactions on Control Systems Technology*, *7*(3), 328–342.

Zhang, J., & Zheng, W. X. (2014). Design of Adaptive Sliding Mode Controllers for Linear Systems via Output Feedback. *IEEE Transactions on Industrial Electronics*, *61*(7), 3553–3562.

Zhu, J., & Khayati, K. (2014a). Adaptive Sliding Mode Control with Smooth Switching Gain. In *Ieee 27th annual canadian conference on electrical and computer engineering* (pp. 893–898). Toronto, Canada: IEEE.

Zhu, J., & Khayati, K. (2014b). New Algorithms of Adaptive Switching Gain for Sliding Mode Control: Part I – Ideal Case. In *Ieee international conference on control, decision and information technologies* (pp. 441–446). Metz, France: IEEE.

Zhu, J., & Khayati, K. (2016a). Adaptive Sliding Mode Control – Convergence and Gain Boundedness Revisited. *International Journal of Control*, *89*(4), 801–814.

Zhu, J., & Khayati, K. (2016b). A New Approach for Adaptive Sliding Mode control: Integral/Exponential Gain Law. *Transactions of the Insitute of Measurement and Control*, *38*(4), 385–394.

6. Appendices

6.1 *Upper-Boundedness of Combined Lumped Uncertainties with Exponential Gain – Scalar Dynamics Case*

In the following, we demonstrate the upper-boundedness of term $h(\sigma)$ introduced in (15) (*i.e.*, Proof of (16)).

Proof. From (4), (6) and (8), we have for any $\sigma \in \mathrm{R}$

$$h(\sigma) = \frac{\Psi \cdot \mathrm{sgn}(\sigma)}{\Gamma} - \beta(e^{|\sigma|} - 1)$$
$$\leq (\beta + \frac{d_0}{\Gamma}) + \sum_{i=1}^{q} \frac{d_i}{\Gamma}|\sigma|^i - \beta e^{|\sigma|} \tag{41}$$

Given scalars $\beta > 0$, $d_0 \geq 0$, $d_i \geq 0$ and $i > 0$ $(i = 1, \cdots, q)$, there always exist a positive integer r, real scalars $\delta_0 \geq 0$ and $\delta \geq 0$, *s.t.*,

$$h(\sigma) \leq \delta_0 + \delta|\sigma|^r - \beta e^{|\sigma|} \tag{42}$$

The two terms $\delta_0 + \delta|\sigma|^r$ and $\beta e^{\gamma|\sigma|}$ of the right side of (42) are continuously monotonically increasing as $|\sigma|$ increases on $[0, +\infty)$. However, by applying L'Hopital's rule (Arfken, 1985) repeatedly, we have

$$\lim_{|\sigma| \to \infty} \frac{\delta_0 + \delta|\sigma|^r}{\beta e^{|\sigma|}} = 0 \tag{43}$$

Thus, the polynomial term $\delta_0 + \delta|\sigma|^r$ grows with a slower rate than the exponential term $\beta e^{|\sigma|}$. In other words, there exists a finite value $h^* \in \mathrm{R}$, *s.t.*, for all $|\sigma| \neq 0$,

$$h(\sigma) \leq h^* \triangleq \sup_{|\sigma|} \left(\delta_0 + \delta|\sigma|^r - \beta e^{|\sigma|}\right) \tag{44}$$

That is, $h(\sigma)$ is upper-bounded. □

6.2 *Switching Control in the Case of Indefinite Parameter Matrix* Γ

In the following, we demonstrate the FTC problem of theorem 3.

Proof. Consider the Lyapunov function candidate $V = \sigma^T\sigma$. Given $s = \hat{\Gamma}^T\sigma$, using $L(t) = \hat{\Gamma}^{-1}\Gamma$,

$L_s = \frac{1}{2}(L + L^T)$ and (27), the time derivative of V along the system trajectories is

$$\dot{V} = 2\|s\|\Big(\frac{s^T(\hat{\Gamma}^{-1}\Psi)}{\|s\|} - K\frac{s^T L_s s}{\|s\|^2}\Big)$$
$$= 2\|s\|\Big(h_L(\sigma) - \check{K}\frac{s^T L_s s}{\|s\|^2}\Big) \tag{45}$$

with $h_L(\sigma) = \frac{s^T(\hat{\Gamma}^{-1}\Psi)}{\|s\|} - \beta\big(e^{\|\sigma\|} - 1\big)\frac{s^T L_s s}{\|s\|^2}$. The scalar $h_L(\sigma)$ is upper-bounded for any value of σ. For $\|\sigma\| > \epsilon$, $\check{K}$ will keep growing and eventually the positive scalar $\check{K}\frac{s^T L_s s}{s^T s}$ will compensate for the upper-bounded scalar $h_L(\sigma)$, *i.e.*, $\check{K}\frac{s^T L_s s}{\|s\|^2} > h_L(\sigma)$. Since this compensating action will occur for any $\|\sigma\| > \epsilon$ where $h_L(\sigma) \geq \check{K}\frac{s^T L_s s}{\|s\|^2}$ (*i.e.*, $\frac{d}{dt}\|\sigma\| \triangleq \frac{\dot{V}}{2\sqrt{V}} \geq 0$), we conclude that there exist a time instant t^* and a positive scalar κ_2, *s.t.*,

$$\check{K}\frac{s^T L_s s}{\|s\|^2} \geq h_L(\sigma) + \kappa_2 \tag{46}$$

for $t \geq t^*$. Then,

$$\dot{V} \leq -2\kappa_2\|s\| \tag{47}$$

for $t \geq t^*$. Since $\|s\|^2 = \sigma^T\hat{\Gamma}\hat{\Gamma}^T\sigma \geq \underline{\lambda}(\hat{\Gamma})^2\sigma^T\sigma$ with $\underline{\lambda}(\hat{\Gamma}) > 0$ the minimum singular value of the matrix $\hat{\Gamma}$, we have $\|s\| \geq \underline{\lambda}(\hat{\Gamma})\|\sigma\|$. Then, from (47), we obtain

$$\frac{d\sqrt{V}}{dt} \leq -\kappa_2\underline{\lambda}(\hat{\Gamma}) \tag{48}$$

Thus, σ converges to the domain $\|\sigma\| \leq \epsilon$ in finite time with a maximum reaching time $t_r \leq \frac{\|\sigma(t^*)\| - \epsilon}{\kappa_2\underline{\lambda}(\hat{\Gamma})} + t^*$ (Khalil, 2002). □

C.2 Nonlinear Adaptive Observer for Electromechanical Systems – Asymptotic and Exponential Stability Designs

Karim Khayati and **Jiang Zhu**. Nonlinear Adaptive Observer for Electromechanical Systems – Asymptotic and Exponential Stability Designs. In review in *International Journal of Adaptive Control and Signal Proccessing*, 2016.

INTERNATIONAL JOURNAL OF ADAPTIVE CONTROL AND SIGNAL PROCESSING

Int. J. Adapt. Control Signal Process. 2016; **00**:1–35

Published online in Wiley InterScience (www.interscience.wiley.com). DOI: 10.1002/acs

Nonlinear Adaptive Observers for Electromechanical Systems – Asymptotic and Exponential Stability Designs

K. Khayati and J. Zhu*

Department of Mechanical and Aerospace Engineering, Royal Military College of Canada, Kingston, ON

SUMMARY

In this paper, a comprehensive review of the literature of the adaptive observers is presented. Then, we investigate the design of adaptive observers for a large class of nonlinear systems with linearly dependent parameters that are joined with unmeasured regression dynamics. Asymptotic and exponential stabilities of both the state and parameter estimates are developed. The calculus of the observer gains and the adaptation law parameters are cast as linear matrix inequality (LMI) feasibility problems. Simulation results are shown to demonstrate the effectiveness of the proposed estimating patterns. Copyright © 2016 John Wiley & Sons, Ltd.

Received …

KEY WORDS: Nonlinear Systems; Adaptive Observer; Asymptotic Stability; Exponential Stability

1. INTRODUCTION

Over the past few decades, numerous adaptive observers have been proposed, in linear forms (*e.g.* proportional-integral-like) and in nonlinear gain shapes, estimating the unmeasurable states for different classes of nonlinear systems [1–7]. The discussed schemes are continuously adapted to

*Correspondence to: Zhu, PhD student, Department of Mechanical and Aerospace Engineering, Royal Military College of Canada, 19 General Crerar Cr., Room 2117, PO Box 17000, Station Forces,Kingston, K7K 7B4, ON, Tel. +1-613-541-6000 # 6370, Fax +1-613-542-8612. E-mail: jiang.zhu@rmc.ca

guarantee a uniformly bounded and convergent observation error. However, such observers do not estimate the parameter uncertainties and the adaptation law may be complicated. For linear systems and nonlinear systems that are linearly transformable, the well-known Luenburger and the switched mode observers including sliding mode observers and Kalman filters have been widely used [6, 7]. However, the high gains eventually required for such techniques lead to peaking phenomena that make the initial error amplified to probably unsafe levels when implemented within any closed-loop control design.

For nonlinear systems where all states are measurable, the gradient algorithm and the least square algorithm have been applied for the parameter identification problem [8]. Also, for nonlinear dynamics satisfying the Lipschitz condition [9], a high gain observer is designed in [10], whereas the adaptive observer design that can be applied for both Lipschitz and monotone nonlinearities (that are not necessarily Lipschitz) is presented in [11]. However, the alleviation of the limitation on monotonic nonlinearities needs more investigation. And withal, Luenberger-like observers have been applied for nonlinear systems with unknown states and uncertain parameters, where nonlinearities are measurable [12, 13]. In the case where nonlinear terms are dependent on unmeasured states, various observers are designed in [13–17] under the so-called matching condition. This condition has been essentially revisited in [18], and then, to relax it, the authors have introduced a new LMI-based adaptive observer which successfully estimates the unknown parameters and the unmeasured nonlinearity with an asymptotic convergence [18, 19]. This work has been extended to estimate both the states and the parameters of a large class of perturbed and noisy nonlinear systems with a regressor matrix function of unknown states [20, 21]. Noting that some nonlinearly dependent parameter systems can be transformed into parameter affine dynamics (*i.e.* linearly dependent on unknown parameters) [16], the author has applied an adaptive observer to nonlinear parameterized systems which estimates the states only with a uniformly bounded error performance. Furthermore, an adaptive observer has been developed for linear time-varying systems which comprise unknown parameters in the output equation. The realization of such dynamic

Prepared using acsauth.cls http://mc.manuscriptcentral.com/acsp-wiley DOI: 10.1002/acs

models is assumed to be uniformly completely observable [22]. These systems can refer indeed to nonlinear dynamics with known nonlinearities (in particular the regressor terms) [22].

In most nonlinear observer design techniques, the stability analysis is based on the Lyapunov criteria guaranteeing the asymptotic convergence. This feature is often based on the strict-positive-real (SPR) property (widely defined in the literature, see *e.g.* [9]) of the relationship between the parameter matching nonlinearities and a sub-set of the measurable states [23–25]. Recently, in [26], the authors consider the more general problem of asymptotic reconstruction of the state and parameter values in dynamic systems with nonlinearly parameterized terms. However, all the results proposed therein are basically dependent on the restrictive SPR assumption. In addition, it has been shown in [27] that subject to the linear part of the most natural dynamics is observable, there is a time-varying parameter-dependent coordinate transformation such that in new coordinates the SPR condition is satisfied [26]. Nonetheless, the design of a global state-space diffeomorphism transforming any system into the required form could be either unfeasible or discordant with the investigated system representation.

A unifying adaptive observer form is proposed in [28] based on the property of the parameter-independent detectability, known later as the passivity-like condition, in addition to the appropriate and common persistent excitation (PE) condition. The author discusses this generic adaptive design for nonlinear dynamics with unknown parameters matching only with the measurable state sub-system (*i.e.*, the dynamics of the unmeasurable signals are independent of the unknown parameters). In [29], the authors redesign an adaptive observer by solving a partial differential equation instead of applying the SPR property, even though this differential equation is hard to be solved in practice. However, in [30], the authors use the Lyapunov analysis and a nonlinear transformation to design the adaptive observers for nonlinear dynamics where the unknown parameters are only present in the unmeasurable state dynamics. This method requires a sector condition on the nonlinear matching terms related to the unknown parameters [9]. The state and parameter estimation dynamics are uniformly globally asymptotically stable while the corresponding linearized form is uniformly locally exponentially stable. Noting that the asymptotical stability is characterized by a relatively

DOI: 10.1002/acs

slow rate of convergence compared to the exponential stability, adaptive observers with exponential convergence have been investigated [31,32]. The exponential convergence of the parameter estimate has been guaranteed by using appropriate gradient and least square algorithms when all the states are measureable [8, 33]. However, in most cases the states are not completely measurable. In [32], the authors characterize the use of filtered transformations to obtain a canonical form of the adaptive observer where the unknown parameters are joined to the measured nonlinearities only. The method introduced in [11] applies the differential mean value theorem to design an LMI-based H_∞ adaptive observer capable of estimating the unmeasured nonlinearities and unknown parameters, where the equality constraint in terms of matching conditions is not required. This method illustrates an exponential convergence of the state estimation and an asymptotical convergence of the parameter estimation. More recently, [34] uses a converse Lyapunov-like theorem with sufficient gain conditions. This approach aims to apply a parameter and state estimator with an exponential convergence rate to an adaptive controller using a nonlinear damping term. Moreover, an exponentially stable nonlinear adaptive observer for a large class of nonlinear systems, with a regressor matrix function of both measurable and unmeasurable states, has been discussed in [31]. The authors have set up a stability feature based on a memoryless nonlinear mapping satisfying a sector condition with respect to the parameter estimate error. The latter remains a conservative condition regarding the implementation purpose. In fact, the concerned nonlinear mapping is particularly dependent on the state estimates, which makes the required condition hard to predict and needs excessively high adaptation gains.

The objective of this paper is to build an asymptotically stable adaptive observer (ASAO) and an exponentially stable adaptive observers (ESAO) for nonlinear systems with unmeasured regression terms (*i.e.*, nonlinearities coupled with unknown parameters) based on common requirements such as Lipschitz and bounded nonlinearities. The design uses the same technique developed in [18,19,31] to eliminate the passivity-like equality condition on the Lyapunov matrix gain. Thus, the design will be based essentially on LMIs to determine the Lyapunov, observer and adaptation gain matrices, and independently on further algebraic matrix equations and Hurwitz constraints applied

Prepared using acsauth.cls http://mc.manuscriptcentral.com/acsp-wiley DOI: 10.1002/acs

to the remaining variables that lead to the exponential stability. It represents an extension of the observer dynamics, discussed in [20, 21, 35], by adding coupling terms along with the algorithm improvement to achieve the requirements of the exponential stability of the estimates (of both the states and the parameters). The paper is organized as follows. Section 2 is devoted to the presentation of the nonlinear dynamics. The asymptotic stability for the observer design is first introduced in Section 3. In Section 4, the adaptive observer scheme showing an exponential convergence of the parameter and state estimates is then developed. Finally, in order to illustrate the proposed techniques, numerical results are presented in Section 5, while Section 6 concludes this work.

2. NONLINEAR DYNAMIC MODELS

The proposed observers in this paper are based essentially on nominal dynamical systems with linearly parameterized unknown continuous nonlinearities. An adaptation law will be designed to estimate the unknown parameters. The term "unknown nonlinearities" refers here to the nonlinearities matching with the parameters and depending on the unmeasurable states.

2.1. Problem Statement and Assumptions

We consider the following nonlinear dynamics

$$\dot{x} = Ax + f_m(y,u) + B\big[f_u(x,u) + f(x,u)\theta\big] \quad (1)$$

$$y = Cx \quad (2)$$

with $A \in \mathbb{R}^{n\times n}$, $B \in \mathbb{R}^{n\times p}$ and $C \in \mathbb{R}^{m\times n}$. $x \in \mathbb{R}^n$ designates the state vector, $u \in \mathbb{R}^k$ the input vector, $y \in \mathbb{R}^m$ the output, and $\theta \in \mathbb{R}^q$ the vector of unknown constant parameters. $f_m(y,u)$, $f_u(x,u)$ and $f(x,u)$ are nonlinear functions in $\mathbb{R}^n$, $\mathbb{R}^p$ and $\mathbb{R}^{p\times q}$, respectively. For the forthcoming designs, we consider the following assumptions:

(A1) The matrix B is a *strict* full-column-rank matrix, that is $\mathrm{rk}(B) = p < n$, the output vector y does not recover the whole states of x, that is $m < n$, and the pair (A, C) is observable.

Prepared using acsauth.cls http://mc.manuscriptcentral.com/acsp-wiley DOI: 10.1002/acs

(A2) There exist matrices Φ and Ψ of $\mathbb{R}^{n\times m}$ chosen, *s.t.*

$$\Psi CB = 0 \tag{3}$$

and

$$\Phi C + \Psi CA = I_n \tag{4}$$

(A3) The vector of unknown constant parameters θ is bounded with

$$\|\theta\| < \beta_0 \tag{5}$$

(A4) The functions f_u and f are continuously bounded and Lipschitz in x, with

$$\|f_u(x,u) - f_u(\hat{x},u)\| \leq \beta_u \|x - \hat{x}\| \tag{6}$$

and

$$\|f(x,u) - f(\hat{x},u)\| \leq \beta \|x - \hat{x}\| \tag{7}$$

(A5) The input vector u is of class $\mathcal{C}_1$ (*i.e.*, continuous and differentiable function having continuous derivatives). In addition, u is required to fulfill the PE condition.

These hypotheses are commonly used in related works and can characterize adequately many real plants [4, 17, 18, 32, 36]. In particular, by setting up assumptions A1 and A2, one can neutralize the following inappropriate observer forms: form 1, where B is right invertible (*i.e.*, B regular square matrix or full-row-rank), and form 2, where C is a full-column rank matrix. In fact, with form 1, there always exists a transformation reducing the number of channels within the parameter matching term $Bf(x,u)\theta$, by reducing and/or combining the elements of $f(x,u)\theta$ to lower p under the number of states n, while with form 2, the output vector y would recover the whole state vector x. Moreover, we notice, from (3) of assumption A2, that in the case where the columns of B lie in the null space of C, *i.e.*, $CB = 0$, then Ψ and Φ will be selected based on the equality requirement (4) only. However, when $CB \neq 0$, the assumption A2 requires the selection of a matrix Ψ in the null space of C, *i.e.*, $\Psi C = 0$, then we select Φ *s.t.* $\Phi C = I$. This statement remains strenuous. Otherwise, we select Ψ simply in the null space of CB, *i.e.*, $\Psi \cdot (CB) = 0$, and Φ *s.t.* (4) holds. Later in this paper, where

Prepared using acsauth.cls http://mc.manuscriptcentral.com/acsp-wiley DOI: 10.1002/acs

we deal with the ESAO design, the condition (4) of assumption A2 will be slightly relaxed from [19, 21, 35] enrolling wider set of dynamics. In fact, we substitute the following conditions for the constraint (4), as

(A2.*s*) There exist matrices Φ and Ψ of $\mathbb{R}^{n\times m}$ chosen, *s.t.* (3) holds and $\tilde{B} = \big(\Phi C + \Psi CA\big)B$ is full-column rank.

Note that, from assumptions A1 and A2.*s*, $\big(\Phi C + \Psi CA\big)$ can be either regular (that is, there exist Φ and Ψ *s.t.* (4) holds), or singular.

Finally, we notice that the representation (1) and (2) can be reduced, without loss of generality, to the system model discussed in [35] as

$$\dot{x} = Ax + f_m(y,u) + Bf(x,u)\theta \tag{8}$$

$$y = Cx \tag{9}$$

In fact, disregarding the unmeasurable state function and reducing the non-matching nonlinearity to the term $f_m(y,u)$ do not limit the use of algorithms that will be discussed in this paper. The further term in the form of $f_u(x,u)$ could be combined with the matching nonlinearities $Bf(x,u)$ and the parameter vector θ could be augmented to consider such a combination, as far as the matching matrix B remains of full-column-rank [35]. The model (1) and (2) considered above, with the assumptions A1 and A2, represents a wide class of nonlinear dynamics called *adaptive observer forms* and gathers most of the forms discussed in literature.

2.2. *Further General Models*

The proposed designs respond appropriately in the case of systems where the condition (3) (refer to assumption A2) holds and the eventual global state-space diffeomorphism discussed in [27] fails. Among these models, we recall the observer form [37, 38]

$$\dot{y} = z \tag{10}$$

$$\dot{z} = f_1(q,z,u) + f(q,z,u)\theta = \mathcal{M}^{-1}(q)\big(u - \mathcal{C}(q,z)z - \mathcal{G}(q)\big) \tag{11}$$

Prepared using acsauth.cls http://mc.manuscriptcentral.com/acsp-wiley DOI: 10.1002/acs

with $z = \dot{q}$ and $y = q$, obtained from the robot equation [39]

$$\mathcal{M}(q)\ddot{q} + \mathcal{C}(q,\dot{q})\dot{q} + \mathcal{G}(q) = u \tag{12}$$

where only the positions q are available through measurement and u is the input. We note that the systematic approach introduced in [4, 40, 41] cannot be applied for such dynamics. The main result provided therein is based on some restrictive equality condition regarding the Lyapunov design matrix [41]. Fundamentally, the realization of the system between the unknown parameters and some of the measured outputs have to be strictly positive [9]. This condition has been also discussed in more recent works dealing with the stability of the observer error dynamics [13, 42]. In order to solve the problem with only strict inequalities, the authors propose in [40] to find a set of matrices P such that $B^T P C^\dagger = 0$; $C^\dagger$ is in null space of C. This subset is then used to solve the feasibility of the proposed matrix inequality problem in the remaining unknown decision variables of P. In [19], the authors have cited evidence and motivated the redesign of the adaptive observer for the class of nonlinear systems introduced above, by showing analytical examples of dynamic representations with unknown parameters lacking the required condition of passivity, $PB \neq C_1^T$ for all $P > 0$ and C_1 in span (*i.e.*, row space) of C. The algorithms that will be discussed in this paper represent a redesign of adaptive observers revoking both the limited sector condition of the nonlinear regression term (matching with unknown parameter vector) required in [30, 31] and the hardly achievable design of [40] (when dealing with models investigated in [20, 21]). A forward general form including (10) and (11) as

$$\dot{y} = A_1 x + f_1(y,u) \tag{13}$$

$$\dot{z} = A_2 x + f_{21}(y,u) + f_{22}(z,t) + f(x,u)\theta \tag{14}$$

can be directly referred to as of (1) and (2), where $y \in \mathbb{R}^m$ is the measurable state vector, $z \in \mathbb{R}^{n-m}$ the unmeasurable state vector, $x = (y^T, z^T)^T \in \mathbb{R}^n$ the overall state vector, u the input and $\theta \in \mathbb{R}^q$ the vector of constant uncertain parameters. The further condition $n \leq 2m$ on the partition of the measurable and unmeasurable states is relevant for the validation of (4). Then, more generally, the

Prepared using acsauth.cls http://mc.manuscriptcentral.com/acsp-wiley DOI: 10.1002/acs

dynamic form [29, 30]

$$\dot{y} = A_{11}y + A_{12}z + f_{11}(y,u) + f_{12}(z,t) \quad (15)$$

$$\dot{z} = A_2x + f_{21}(y,u) + f_{22}(z,t) + f(x,u)\theta \quad (16)$$

with f_{12} continuously differentiable *w.r.t.* time, can be transformed into the set of equations (13) and (14) by either adjoining part of the dynamics of y that acquires $f_{12}(z,u)$ from (15) to (16), as far as $n \leq 2m$ remains valid (to let (4) hold for some Φ and Ψ), or by applying some appropriate change of variable $z' \triangleq z - B_2 f_{12}(z,t)$.

Finally, we note that the nonlinear adaptive observer form enclosing the unknown parameter vector within the measurable state dynamics as [28]

$$\dot{y} = f_1(y,z,u,t) + f(y,z,u,t)\theta \quad (17)$$

$$\dot{z} = f_2(y,z,u,t) \quad (18)$$

is not directly covered by the proposed model (1) and (2). An algorithm of the corresponding adaptive observer is discussed in [28]. It is based on the Lipschitz property of the nonlinear functions f_1, f_2 and f of the states and the input signals, and requires the existence of a candidate nonlinear Lyapunov function respecting appropriate conditions as given therein. The explicit form of such a Lyapunov function is not shown, and only an artificial design is proposed based on the hypothetic conditions of this function [28, 43]. However, we notice that the approach of [4, 41] could be appropriately concordant with the model (17) and (18) whenever the equality condition on the Lyapunov positive definite matrix (referred as the SPR) is valid.

2.3. *Useful Notations and Properties*

$\mathcal{L}_2$ and $\mathcal{L}_\infty$ represent the classes of finite ∞-norm and 2-norm time-vector-functions, respectively. In this paper, we denote by I_i the identity matrix of order i. $\lambda(\cdot)$, $\underline{\lambda}(\cdot)$ and $\overline{\lambda}(\cdot)$ represent any eigenvalue, minimal and maximal eigenvalues of any matrix, respectively. For simplicity, we denote by $\tilde{x} \triangleq x - \hat{x}$ the state estimate error, $\tilde{\theta} \triangleq \theta - \hat{\theta}$ the parameter estimate error, $f_u \triangleq f_u(x,u)$ (*resp.* $f \triangleq f(x,u)$) the unmeasured nonlinearity (*resp.* the nonlinear regression term), $\hat{f}_u \triangleq f_u(\hat{x},u)$ (*resp.*

Prepared using acsauth.cls http://mc.manuscriptcentral.com/acsp-wiley DOI: 10.1002/acs

$\hat{f} \triangleq f(\hat{x}, u)$) the estimated unmeasured nonlinearity (*resp.* the estimated nonlinear regression term) and $\tilde{f}_u \triangleq f_u - \hat{f}_u$ (*resp.* $\tilde{f} \triangleq f - \hat{f}$) the estimate errors of the nonlinear terms.

3. ADAPTIVE OBSERVER WITH ASYMPTOTIC STABILITY

In this section, we present the design of a nonlinear adaptive observer for the nonlinear dynamics, generalizing a previous one introduced in [19,21]. The detailed proof of the asymptotic stability of the overall scheme is discussed using an appropriate Lyapunov function. Based on the dynamics (1) and (2), we propose the following full-order nonlinear observer

$$\dot{\hat{x}} = A\hat{x} + f_m(y,u) + B\big[f_u(\hat{x},u) + f(\hat{x},u)\hat{\theta}\big] + L\big(y - C\hat{x}\big) \tag{19}$$

coupled with the adaptation law

$$\dot{\hat{\theta}} = \big[G(t)^T P\big(\Phi + \Psi CL\big) - \dot{G}(t)^T P\Psi\big] \cdot \big(y - C\hat{x}\big) \tag{20}$$

$$\hat{\theta} = \breve{\theta} + G(t)^T P\Psi \cdot \big(y - C\hat{x}\big) \tag{21}$$

with

$$G(t) = Bf(\hat{x},u)Q \tag{22}$$

where $Q = Q^T > 0$ and L are matrices of $\mathbb{R}^{q\times q}$ and $\mathbb{R}^{n\times m}$, respectively. Φ and Ψ are matrices of $\mathbb{R}^{n\times m}$, and $\dot{G}(t)$ the total time derivative of G. The following result discusses the conditions that guarantee the convergence of the estimates of both states and parameters to their actual values.

Proposition 1 (LMI-based ASAO Design)

Under assumptions A1–A5, for $\delta = \beta_u + \beta_0\beta > 0$, if there exist matrices $P = P^T > 0$ in $\mathbb{R}^{n\times n}$ and W in $\mathbb{R}^{n\times m}$, *s.t.*

$$\begin{pmatrix} PA + A^TP - WC - C^TW^T & PB & I_n \\ B^TP & -\frac{1}{\delta}I_p & 0 \\ I_n & 0 & -\frac{1}{\delta}I_n \end{pmatrix} < 0 \tag{23}$$

and if $Bf(x,u)$ respects the PE condition, that is, there exist positive scalars α_1, α_2 and t_0, *s.t.* $\forall t$

$$\alpha_1 I_q \leq \int_t^{t_0+t} f^T(u,x)B^TBf(x,u)d\tau \leq \alpha_2 I_q \tag{24}$$

DOI: 10.1002/acs

then the adaptive observer (19)–(22) for the system (1) and (2), with the observer gain matrix $L = P^{-1}W$, is asymptotically stable, that is, the state estimate error $\tilde{x}$ and the parameter estimate error $\tilde{\theta}$ tend both to zero as $t \to \infty$.

Proof

This proof is updated from [21]. Given $\tilde{x} = x - \hat{x}$ and noting $\tilde{f}_u = f_u - \hat{f}_u$, the estimation error dynamics are obtained from (1), (2) and (19)

$$\dot{\tilde{x}} = \big(A - LC\big)\tilde{x} + B\big(\tilde{f}_u + f\theta - \hat{f}\hat{\theta}\big) \tag{25}$$

Using the adaptation law (20) and (21), and the estimation error dynamics (25), we obtain

$$\dot{\hat{\theta}} = G(t)^T P \cdot \Big[\big(\Phi + \Psi CL\big)C + \Psi C\big(A - LC\big)\Big]\tilde{x} + G(t)^T P \Psi C B\big(\tilde{f}_u + f\theta - \hat{f}\hat{\theta}\big) \tag{26}$$

Given $\tilde{\theta} = \theta - \hat{\theta}$ and based on assumption A3, we have $\dot{\tilde{\theta}} = -\dot{\hat{\theta}}$. Then, using (3), (4) and (22), we derive the adaptation error dynamics

$$\dot{\tilde{\theta}} = -Q\hat{f}^T B^T P\tilde{x} \tag{27}$$

Now, to investigate the stability, consider the Lyapunov candidate function

$$V_a(t) = \tilde{x}^T P\tilde{x} + \tilde{\theta}^T Q^{-1}\tilde{\theta} \tag{28}$$

with $P = P^T > 0$ and $Q = Q^T > 0$. Using (25) and (27) and noting $\tilde{\theta} = \theta - \hat{\theta}$, $\tilde{f}_u = f_u - \hat{f}_u$ and $\tilde{f} = f - \hat{f}$, the time derivative of V_a is

$$\begin{aligned} \dot{V}_a &= 2\tilde{x}^T P\dot{\tilde{x}} + 2\tilde{\theta}^T Q^{-1}\dot{\tilde{\theta}} \\ &= 2\tilde{x}^T P \cdot \Big[\big(A - LC\big)\tilde{x} + B\big(\tilde{f}_u + \tilde{f}\theta\big)\Big] \end{aligned} \tag{29}$$

Noting $W = PL$ and based on assumptions A3 and A4, we have

$$\dot{V}_a \le \tilde{x}^T\big(PA + A^T P - WC - C^T W^T\big)\tilde{x} + 2\big(\beta_u + \beta_0\beta\big)\big\|B^T P\tilde{x}\big\|\|\tilde{x}\| \tag{30}$$

Denoting by $\delta = \beta_u + \beta_0\beta > 0$ the total Lipschitz constant, we write

$$2\delta\big\|B^T P\tilde{x}\big\|\|\tilde{x}\| \le \delta \cdot \big(\tilde{x}^T PBB^T P\tilde{x} + \tilde{x}^T\tilde{x}\big) \tag{31}$$

Prepared using acsauth.cls http://mc.manuscriptcentral.com/acsp-wiley DOI: 10.1002/acs

From (30) and (31), we obtain

$$\dot{V}_a \leq \tilde{x}^T \Big[PA + A^T P - WC - C^T W^T + \delta\big(PBB^T P + I_n\big) \Big] \tilde{x} \tag{32}$$

The right member of the inequality (32) is negative definite if

$$PA + A^T P - WC - C^T W^T + \delta \cdot \big(PBB^T P + I_n\big) < 0 \tag{33}$$

We use the Schur complement [44] to transform the nonlinear inequality (33) into the LMI (23) in the decision variables P and W. From (33), $\exists \varepsilon > 0$, *s.t.* $PA + A^T P - WC - C^T W^T + \delta\big(PBB^T P + I_n\big) < -\varepsilon I_n$. Thus,

$$\dot{V}_a < -\varepsilon \|\tilde{x}\|^2 \tag{34}$$

This implies $V_a(t) \in \mathcal{L}_\infty$ (*i.e.*, time-function of finite ∞-norm), and then, using Theorem 4.18 of [9], we show that $\tilde{x} \in \mathcal{L}_\infty$ and $\tilde{\theta} \in \mathcal{L}_\infty$. Integrating (34) leads to $V_a(t) \leq V_a(0) - \varepsilon \int_0^t \|\tilde{x}\|^2 dt$. Since $V_a(0)$ is finite, we obtain $\tilde{x} \in \mathcal{L}_2$. From (25), we have $\dot{\tilde{x}} \in \mathcal{L}_\infty$. Therefore, by applying Theorem 8.4 of [9] based on Barbalat's Lemma, $\hat{x} \to x$ when $t \to \infty$. Now, note that $\int_0^\infty \dot{\tilde{x}} dt = -\tilde{x}(0)$ is bounded, f is Lipschitz continuous, and $\dot{\theta}$ continuous. From (25), $\dot{\tilde{x}}$ is uniformly continuous [9]. Then, according to Barbalat's Lemma, we have $\dot{\tilde{x}} \to 0$. Also, from (25) and (29), we have $B\big(f\theta - \hat{f}\hat{\theta}\big) \to 0$. Now, using assumptions A3 and A4 and noting that $\tilde{x} \to 0$, we have $B\tilde{f}\theta \to 0$. Then, from $\tilde{\theta} = \theta - \hat{\theta} \in \mathcal{L}_\infty$ and A3, we obtain $B\hat{f}\tilde{\theta} \to 0$ and $Bf\tilde{\theta} \to 0$ as $t \to \infty$. Hence, since f is bounded (refer to A4), $f^T B^T Bf\tilde{\theta} \to 0$ as $t \to \infty$. In the following, we apply the property of PE to obtain $\tilde{\theta}(t) \to 0$ [36, 45]. Define $h(t_0) \triangleq \int_t^{t_0} f^T B^T Bf d\tau$. Note that $h(t) = 0$. Using integration by parts, we obtain

$$\int_t^{t_0+t} f^T B^T Bf\tilde{\theta}(\tau) d\tau = h(t_0+t) \cdot \tilde{\theta}(t_0+t) - \int_t^{t_0+t} h(\tau)\dot{\tilde{\theta}}(\tau) d\tau \tag{35}$$

Since $f^T B^T Bf\tilde{\theta} \to 0$, then, for any finite t_0, we have $\int_t^{t_0+t} f^T\ B^T Bf\tilde{\theta}(\tau) d\tau \to 0$ as $t \to \infty$. Now, based on assumption A4 and since $\tilde{x} \to 0$ and $\hat{f}$ is bounded, we have from (27), $\dot{\tilde{\theta}} \to 0$, and then, $\int_t^{t_0+t} h(\tau)\dot{\tilde{\theta}}(\tau) d\tau \to 0$ as $t \to \infty$. Thus, we obtain $h(t_0+t)\tilde{\theta}(t_0+t) \to 0$ as $t \to \infty$. From (24), *i.e.*, $\alpha_1 I_q \leq h(t_0+t) \leq \alpha_2 I_q$ for some $\alpha_1 > 0$ and $\alpha_2 > 0$, we obtain $\tilde{\theta}(t_0+t) \to 0$, implying $\tilde{\theta}(t) \to 0$ [36]. □

Prepared using acsauth.cls http://mc.manuscriptcentral.com/acsp-wiley DOI: 10.1002/acs

The matching condition in terms of the equality constraint on the Lyapunov matrix (*i.e.*, $B^T P C^\perp = 0$ where $C C^\perp = 0$) required in several previous works (*e.g.* [4, 13, 16, 36]) is not necessary anymore in the proposed scheme, neutralizing the conservative SPR condition on the design Lyapunov matrix P [11, 31].

The proof of the proposed design is presented in a recent contribution of the authors [21]. However, because of the few changes brought into the LMI (23) compared to the equivalent form shown in Proposition 1 of [21], we present here the detailed proof of such a result. The discussion of the parameter estimate convergence based on the PE condition is more exhaustively analyzed in the proof shown above. The observer gain synthesis of the nonlinear ASAO introduced in this section is slightly different from the one discussed in previous works, *e.g.* [19, 20, 31]. In fact, the transformation of the quadratic amount into separated terms of PB and $B^T P$ in the LMI (23) (refer to the proof of Proposition 1 for more details) is relaxing the LMI condition *w.r.t.* the Lipschitz constant (in terms of feasible magnitude limit on δ), as compared to the decomposition used in many of the previous works [4, 20, 21] where the Lipschitz constant is more restrictive. It has been tested that the maximum value of δ for which the LMI (23) holds is much higher than the one obtained with the LMI syntheis of the Proposition 1 of [21]. Moreover, we notice that (30) (which leads to (23)) holds for some $0 < \delta \leq \beta_u + \beta_0 \beta$. In practice, this coefficient can be obtained directly from $\|\tilde{f}_u + \tilde{f}\theta\| \leq \delta \|\tilde{x}\|$, replacing the combined assumptions A3 and A4, to relax the LMI explicitly depending on δ. In fact, large values of δ may result in high gains L or even infeasible LMIs. Actually, δ is chosen as small as possible under the constraint $\|\tilde{f}_u + \tilde{f}\theta\| \leq \delta \|\tilde{x}\|$. Various scenarios can be investigated to overcome the possible large values of δ if the solution of the decision variables for the LMI (23) vanishes. In [19], we have designed the observer gains for particular second order nonlinear systems using an analytical solution based on the negativeness of the unmeasurable state-dependent matching function. This property has allowed the existence of a solution for the nonlinear adaptive observer in form (19)–(22), where the LMI synthesis has been reduced to simply placing the closed-loop poles of the linear part $(A - LC)$, whereas the nonlinear matching term has been treated using a further designed gain (refer to [19]). In a more general context, less conservative

Prepared using acsauth.cls http://mc.manuscriptcentral.com/acsp-wiley DOI: 10.1002/acs

Lipschitz conditions have been proposed in [46]. These new conditions defined here as

$$\left\|f_u(x,u) - f_u(\hat{x},u)\right\| \leq \left\|F_u \cdot (x-\hat{x})\right\| \tag{36}$$

and

$$\left\|f(x,u) - f(\hat{x},u)\right\| \leq \left\|F \cdot (x-\hat{x})\right\| \tag{37}$$

for some sparely populated matrices F_u and F [46], can be used to make $\left\|F_u \cdot (x-\hat{x})\right\|$ (*resp.* $\left\|F \cdot (x-\hat{x})\right\|$) much smaller than $\beta_u\|x-\hat{x}\|$ (*resp.* $\beta\|x-\hat{x}\|$), introduced earlier in (6) and (7) for the same nonlinear functions, eventually. Moreover, from the LMI (23), not only do we need the pair (A,C) to be observable, but also need its "distance to unobservability" to be large. In fact, it could not be enough to place the eigenvalues of $(A-LC)$ far into the left half-plane [41].

Moreover, from the LMI problem presented above (refer to Proposition 1), we can estimate the "maximum" upper-bound values of δ for which the LMI (23) hold by solving these LMIs in P, (eventually R), W and minimizing $\zeta \triangleq \frac{1}{\delta} > 0$. This strategy can validate the feasibility of the LMI problem discussed above (and also those discussed in the following) and its limits in terms of Lipschitz conditions.

The time-varying gain matrix $G(t)$ of the adaptation dynamics (20) and (21) would be high enough to achieve a better convergence rate of the parameter estimate. Thus, (22) requires the matrix Q to be of large weighting values (*e.g.*, any diagonal matrix with large coefficients).

Finally, we note that the term $\dot{G}$, introduced in (20), can be actually computed using the expression of $\dot{\hat{x}}$, introduced in (19), where all the terms are known, as

$$\dot{G}(t) = B\frac{df}{dt}(u,\hat{x})Q \tag{38}$$

The terms $\frac{df_{ij}}{dt}(u,\hat{x})$, $i=1,\ldots,p$ and $j=1,\ldots,q$, of the time-derivative of the regression matrix $f(\hat{x},u)$ are implemented using the continuously bounded and differentiable input u (refer to assumption A5), $\hat{x}$ and their derivatives $\dot{u}$ and $\dot{\hat{x}}$ as

$$\frac{df_{ij}}{dt}(u,\hat{x}) = \frac{\partial f_{ij}}{\partial \hat{x}}(u,\hat{x})\dot{\hat{x}} + \frac{\partial f_{ij}}{\partial u}(u,\hat{x})\dot{u} \tag{39}$$

In the following section, we will overcome such extra computations of the time derivatives within the design of the ESAO.

DOI: 10.1002/acs

4. ADAPTIVE OBSERVER WITH EXPONENTIAL STABILITY

In this section, we present the design of a nonlinear adaptive observer for the nonlinear dynamics. The detailed proof of the exponential stability of the overall scheme is based on the Lyapunov theory. We consider the model dynamics (1) and (2). We modify the previous adaptive observer scheme to ensure the exponential convergence of both the state and parameter estimates. We use appropriate change of variables and Lyapunov function candidates to extend the scenario introduced first in [35] and subdue the weaknesses depicted therein.

We propose the following full-order nonlinear observer

$$\dot{\breve{x}} = A\hat{x} + f_m(u,y) + B\big[f_u(\hat{x},u) - \Lambda\Gamma(t)\hat{\theta}\big] + L\big(y - C\hat{x}\big) \tag{40}$$

$$\hat{x} = \breve{x} + B\Gamma(t)\hat{\theta} \tag{41}$$

where $\Gamma(t) \in \mathbb{R}^{p\times q}$ is defined as

$$\dot{\Gamma} = \Lambda\Gamma + f(\hat{x},u) \tag{42}$$

with $\Lambda \in \mathbb{R}^{p\times p}$ any Hurwitz matrix, coupled with the adaptation law

$$\dot{\breve{\theta}} = \Big[G(t)^T P\big(\Phi + \Psi CL\big) - \dot{G}(t)^T P\Psi\Big]\cdot\big(y - C\hat{x}\big) \tag{43}$$

$$\hat{\theta} = \breve{\theta} + G(t)^T P\Psi\cdot\big(y - C\hat{x}\big) \tag{44}$$

where $P = P^T > 0$ is a matrix of $\mathbb{R}^{n\times n}$, L, Φ and Ψ matrices of $\mathbb{R}^{n\times m}$, and $G(t) \in \mathbb{R}^{n\times q}$ is defined by

$$G(t) = P^{-1}\Upsilon\bar{B}\Gamma(t)Q \tag{45}$$

with $\Upsilon = \Upsilon^T > 0$ in $\mathbb{R}^{n\times n}$, $Q = Q^T > 0$ in $\mathbb{R}^{q\times q}$ and $\bar{B} = \big(\Phi C + \Psi CA\big)B$. Finally, $\dot{G}(t)$ denotes the total time derivative of G.

Proposition 2 (LMI-based ESAO Design – Form 1)

Under assumptions A1, A2.*s*, A3–A5, if there exist matrices $P = P^T > 0$, $\Upsilon = \Upsilon^T > 0$ in $\mathbb{R}^{n\times n}$,

Prepared using acsauth.cls http://mc.manuscriptcentral.com/acsp-wiley DOI: 10.1002/acs

$W \in \mathbb{R}^{n\times m}$, *s.t.*

$$\begin{pmatrix} \mathcal{T}(P,W) & \mathcal{S}_\Lambda(P,W,\Upsilon) & PB & I_n & 0 \\ \mathcal{S}_\Lambda^T(P,W,\Upsilon) & -2\tilde{B}^T\Upsilon\tilde{B} & 0 & 0 & B^T \\ B^TP & 0 & -\frac{1}{2\delta}I_p & 0 & 0 \\ I_n & 0 & 0 & -\frac{1}{\delta}I_n & 0 \\ 0 & B & 0 & 0 & -\frac{1}{\delta}I_n \end{pmatrix} < 0 \tag{46}$$

with $\mathcal{T}(P,W) = PA + A^TP - WC - C^TW^T$, $\mathcal{S}_\Lambda(P,W,\Upsilon) = PAB - WCB - PB\Lambda - \big(\Phi C + \Psi CA\big)^T\Upsilon\tilde{B}$, Φ and Ψ in $\mathbb{R}^{n\times m}$, $\Lambda \in \mathbb{R}^{p\times p}$ any Hurwitz matrix, $\delta = \beta_u + \beta_0\beta > 0$, and if Γ is PE, that is, there exist positive scalars α_0 and t_0, *s.t.* $\forall t$ [17, 36, 47]

$$\alpha_0 t_0 I_q \leq \int_t^{t+t_0} \Gamma(\tau)^T\Gamma(\tau)d\tau \tag{47}$$

then the state estimation error vector $\tilde{x}$ and the parameter estimate error vector $\tilde{\theta}$ of the nonlinear adaptive observer (40)–(45), designed for the nonlinear system (1) and (2), tend to zero exponentially as $t \to \infty$. The closed-loop observer gain matrix L is computed as $L = P^{-1}W$.

Proof

Given $\tilde{x} = x - \hat{x}$ and noting that $\tilde{f}_u = f_u - \hat{f}_u$, we derive from (1), (2), (40)–(42) the state estimation error dynamics

$$\dot{\tilde{x}} = \big(A - LC\big)\tilde{x} + B\big(\tilde{f}_u + f\theta - \hat{f}\hat{\theta} - \Gamma\dot{\hat{\theta}}\big) \tag{48}$$

Given $\tilde{\theta} = \theta - \hat{\theta}$, we introduce the new variable vector $\chi \triangleq \tilde{x} - B\Gamma\tilde{\theta}$, *i.e.*, $\tilde{x} = \chi + B\Gamma\tilde{\theta}$. Denote by $\bar{B} \triangleq \big(A - LC\big)B - B\Lambda$ and $\tilde{f} = f - \hat{f}$, and notice from A3 that $\dot{\hat{\theta}} = -\dot{\tilde{\theta}}$. By using (42) and (48), we derive

$$\begin{aligned} \dot{\chi} &= \dot{\tilde{x}} - B\dot{\Gamma}\tilde{\theta} - B\Gamma\dot{\tilde{\theta}} \\ &= \big(A - LC\big)\chi + B\big(\tilde{f}_u + \tilde{f}\theta\big) + \bar{B}\Gamma\tilde{\theta} \end{aligned} \tag{49}$$

From the parameter estimate dynamics (43) and (44), we use (3) and (48) to obtain

$$\begin{aligned} \dot{\tilde{\theta}} &= \dot{\tilde{\theta}} + \dot{G}(t)^TP\Psi C\tilde{x} + G(t)^TP\Psi C\dot{\tilde{x}} \\ &= G(t)^TP\cdot\big(\Phi C + \Psi CA\big)\tilde{x} \end{aligned} \tag{50}$$

Prepared using acsauth.cls http://mc.manuscriptcentral.com/acsp-wiley DOI: 10.1002/acs

Based on $\dot{\tilde{\theta}} = -\dot{\hat{\theta}}$, using $\tilde{x} = \chi + B\Gamma\tilde{\theta}$ and $\tilde{B} = \big(\Phi C + \Psi CA\big)B$, and applying A2.*s*, we substitute (45) into (50)

$$\dot{\tilde{\theta}} = -Q\Gamma^T\tilde{B}^T\Upsilon\tilde{B}\Gamma\tilde{\theta} - Q\Gamma^T\tilde{B}^T\Upsilon\big(\Phi C + \Psi CA\big)\chi \tag{51}$$

Now, consider the Lyapunov candidate function

$$V_e(t) = \chi^T P\chi + \tilde{\theta}^T Q^{-1}\tilde{\theta} \tag{52}$$

We have

$$k_1 \cdot \big(\|\chi\|^2 + \|\tilde{\theta}\|^2\big) \leq V_e(t) \leq k_2 \cdot \big(\|\chi\|^2 + \|\tilde{\theta}\|^2\big) \tag{53}$$

with $k_1 \triangleq \min\big(\underline{\lambda}(P), \underline{\lambda}(Q^{-1})\big) > 0$ and $k_2 \triangleq \max\big(\overline{\lambda}(P), \overline{\lambda}(Q^{-1})\big) > 0$. Using (49) and (51), the time derivative of (52) is

$$\begin{aligned}\dot{V}_e(t) &= 2\chi^T P\dot{\chi} + 2\tilde{\theta}^T Q^{-1}\dot{\tilde{\theta}} \\ &= \chi^T\Big[P\big(A - LC\big) + \big(A - LC\big)^T P\Big]\chi + 2\chi^T PB\big(\tilde{f}_u + \tilde{f}\theta\big) + 2\chi^T P\tilde{B}\Gamma\tilde{\theta} - \\ &\quad 2\tilde{\theta}^T\Gamma^T\tilde{B}^T\Upsilon\tilde{B}\Gamma\tilde{\theta} - 2\tilde{\theta}^T\Gamma^T\tilde{B}^T\Upsilon\big(\Phi C + \Psi CA\big)\chi\end{aligned} \tag{54}$$

Noting $\delta = \beta_u + \beta_0\beta$, based on the inequalities (5)–(7), and substituting $\tilde{x} = \chi + B\Gamma\tilde{\theta}$, we have

$$\begin{aligned}2\chi^T PB\big(\tilde{f}_u + \tilde{f}\theta\big) &\leq 2\big\|\chi^T PB\big\| \cdot \big(\|\tilde{f}_u\| + \|\tilde{f}\| \cdot \|\theta\|\big) \\ &\leq 2\delta\big\|\chi^T PB\big\| \cdot \|\tilde{x}\| \\ &\leq \delta\big(2\chi^T PBB^T P\chi + \chi^T\chi + \tilde{\theta}^T\Gamma^T B^T B\Gamma\tilde{\theta}\big)\end{aligned} \tag{55}$$

Using $W = PL$, we deduce from (54) and (55)

$$\begin{aligned}\dot{V}_e(t) \leq\ & \chi^T\big(PA + A^T P - WC - C^T W^T\big)\chi + 2\delta\chi^T PBB^T P\chi + \delta\chi^T\chi + \delta\tilde{\theta}^T\Gamma^T B^T B\Gamma\tilde{\theta} + \\ & 2\chi^T P\tilde{B}\Gamma\tilde{\theta} - 2\tilde{\theta}^T\Gamma^T\tilde{B}^T\Upsilon\big(\Phi C + \Psi CA\big)\chi - 2\tilde{\theta}^T\Gamma^T\tilde{B}^T\Upsilon\tilde{B}\Gamma\tilde{\theta}\end{aligned} \tag{56}$$

Recall $\bar{B} \triangleq \big(A - LC\big)B - B\Lambda$. Noting $\mathcal{T}(P, W) = PA + A^T P - WC - C^T W^T$ and $\mathcal{S}_\Lambda(P, W, \Upsilon) = PAB - WCB - PB\Lambda - \big(\Phi C + \Psi CA\big)^T\Upsilon\tilde{B}$, if the inequality

$$\begin{pmatrix} \mathcal{T}(P, W) + 2\delta PBB^T P + \delta I_n & \mathcal{S}_\Lambda(P, W, \Upsilon) \\ \mathcal{S}_\Lambda^T(P, W, \Upsilon) & \delta B^T B - 2\tilde{B}^T\Upsilon\tilde{B} \end{pmatrix} < 0 \tag{57}$$

Prepared using acsauth.cls http://mc.manuscriptcentral.com/acsp-wiley DOI: 10.1002/acs

holds, then the right member of the inequality (56) is negative. Given any Hurwitz matrix Λ and the matrices Φ and Ψ respecting A2.*s*, using the Schur complement [44], the LMI (46) is equivalent to (57), and, there exists a positive scalar ε *s.t.*

$$\dot{V}_e(t) \leq -\varepsilon \chi^T \chi - \varepsilon \tilde{\theta}^T \Gamma^T \Gamma \tilde{\theta} \tag{58}$$

Then, $\chi \in \mathcal{L}_2$, $\chi \in \mathcal{L}_\infty$ and $\tilde{\theta} \in \mathcal{L}_\infty$, that is $V_e(t) \in \mathcal{L}_\infty$ [9]. Moreover, we have $\chi \to 0$, as $t \to \infty$. In particular, from (58), we have $\dot{V}_e(t) \leq -\varepsilon \chi^T \chi$, then we obtain

$$V_e(t) \leq V_e(0) - \varepsilon \int_0^t \chi^T \chi d\tau \tag{59}$$

Noting $V_e(t) \in \mathcal{L}_\infty$, $V_e(0)$ is finite and $\chi \in \mathcal{L}_2$, from (49) we obtain $\dot{\chi} \in \mathcal{L}_\infty$. Because $\chi \to 0$ as $t \to \infty$, we have $\int_0^\infty \dot{\chi} dt = \chi(\infty) - \chi(0) = -\chi(0)$ bounded. By (49), using the Lipschitz continuity of f_u and f (refer to assumption A4), $\dot{\chi}$ is uniformly continuous [36]. Thus, using Barbalat's lemma, we obtain $\dot{\chi} \to 0$ [9], and then, $\tilde{f} \in \mathcal{L}_\infty$ (*resp.* $\hat{f} \in \mathcal{L}_\infty$), as f is bounded. In addition, given Λ a finite Hurwitz matrix of (42), we obtain $\Gamma \in \mathcal{L}_\infty$, *i.e.*, Γ is finite. Alternatively, the boundedness of Γ can be obtained from (49) using Micaelli and Samson Lemma [48].

Now, let us introduce the following lemma that will be used in the sequel.

Lemma 1

Assume that $\Gamma(t)$ is PE, that is $\exists \alpha_0 > 0$ and $t_0 > 0$ *s.t.* (47) holds [17, 36, 47]. Then, there exists $0 < \epsilon_0 < \frac{k_2}{\varepsilon}$ *s.t.*

$$\int_t^{t+t_0} \left(\chi^T \chi + \tilde{\theta}^T \Gamma^T \Gamma \tilde{\theta}\right) d\tau \geq \epsilon_0 \cdot \left(\chi(t)^T \chi(t) + \tilde{\theta}(t)^T \tilde{\theta}(t)\right) \tag{60}$$

Proof

See Appendix A. □

We integrate (58) between t and $t + t_0$ and we use (60) to obtain

$$\begin{aligned} V_e(t+t_0) - V_e(t) &\leq -\varepsilon \int_t^{t+t_0} \left(\chi^T \chi + \tilde{\theta}^T \Gamma^T \Gamma \tilde{\theta}\right) d\tau \\ &\leq -\varepsilon \epsilon_0 \cdot \left(\chi(t)^T \chi(t) + \tilde{\theta}(t)^T \tilde{\theta}(t)\right) \end{aligned} \tag{61}$$

Prepared using acsauth.cls http://mc.manuscriptcentral.com/acsp-wiley DOI: 10.1002/acs

Using (53), we write

$$V_e(t+t_0) - V_e(t) \leq -\frac{\varepsilon\epsilon_0}{k_2} V_e(t) \tag{62}$$

Noting the fact that $\epsilon_0 < \frac{k_2}{\varepsilon}$, we have obviously $0 < \frac{\varepsilon\epsilon_0}{k_2} < 1$. Thus, $V_e(t+t_0) \leq \big(1 - \frac{\varepsilon\epsilon_0}{k_2}\big) V_e(t)$. Hence, $V_e(t) \to 0$ as $t \to \infty$ exponentially fast, and $\chi \to 0$ and $\tilde{\theta} \to 0$ as $t \to \infty$ [9]. Finally, as $\Gamma \in \mathcal{L}_\infty$, we obtain $\tilde{x} = \chi + B\Gamma\tilde{\theta} \to 0$ exponentially as $t \to \infty$. □

The state representation (40) and (41) with (42) is simply equivalent to

$$\dot{\hat{x}} = A\hat{x} + f_m(u,y) + B\big[f_u(\hat{x},u) + f(\hat{x},u)\hat{\theta}\big] + L(y - C\hat{x}) + B\Gamma(t)\dot{\hat{\theta}} \tag{63}$$

However, for the implementation purpose, we use (40) and (41) computed from known terms instead of the combined form (63) which may induce an algebraic loop by the calculation of $\dot{\hat{\theta}}$ from (44).

The adaptation dynamics (43)–(45) of the proposed ESAO uses basically the same structure of the ASAO scheme (compare the pair (20) and (21) *v.s.* (43) and (44)) to deal with the nonlinear matching term in the state estimate dynamics and its connection with the adaptation error dynamics. The parameters P, Υ and Q of the time-varying gain are introduced carefully in (45). In fact, the term $P^{-1}\Upsilon$ is used to eliminate the Lyapunov matrix P from the parameter estimate dynamics and replace it by the positive definite matrix Υ. This parametrization would make the LMI design (46) relaxed by the new decision variable Υ. In fact, if we replace (45) by $G(t) = \tilde{B}\Gamma(t)Q$ simply, we substitute the variable Υ for the matrix P in the LMI (46), which will reduce the feasibility range of this LMI in the decision variables P and W compared to the same LMI in P, W and Υ. The parameters of the positive definite matrix Q can be freely selected to adjust the parameter estimate rates.

In (43), the term $\dot{G}$ is much easier to compute analytically, from (42), than the one required for the algorithm (20) of the ASAO discussed in the previous section, and is given by

$$\dot{G}(t) = P^{-1}\Upsilon\tilde{B}\dot{\Gamma}(t)Q = P^{-1}\Upsilon\tilde{B}\Lambda\Gamma Q + P^{-1}\Upsilon\tilde{B}f(\hat{x},u)Q \tag{64}$$

where all terms are well-known.

The PE condition of $\Gamma(t)$, required in Proposition 2, depends on the estimated nonlinearity $f(\hat{x},u)$ (equivalently, $f(x,u)$ required to be PE *a priori*), and therefore depends on the input signal u. Thus,

Prepared using acsauth.cls http://mc.manuscriptcentral.com/acsp-wiley DOI: 10.1002/acs

a sufficiently rich input signal guarantees the PE condition that is typically required for parameter estimation problems.

The techniques proposed in this paper are roughly built around the same observer and adaptation dynamics discussed in [18,31], and are also based on the LMI frameworks, to determine the observer and adaptation gain matrices, independently of the additional equality and Hurwitz constraints applied to the remaining variables (*i.e.*, Φ, Ψ and Λ). Compared to [31], the scheme introduced above shows a difference corresponding to the use of the extra coupling dynamics (42) adding a mutual link between the observer dynamics and the adaptation law matching with the Lyapunov function. Inspired from ideas dealing with the exponential stability (see *e.g.* [22, 23] and references cited therein), this coupling represents the key-element of the exponential stability of both the state and parameter estimates. The ESAO design proposed in this paper extends the algorithm introduced in [35] treating the more general case where $\bar{B} \triangleq (A-LC)B - B\Lambda \neq 0$. The main difference between the two cases can be depicted by the reduction of the term $\mathcal{S}_\Lambda(P,W,\Upsilon) = PAB - WCB - PB\Lambda - \big(\Phi C + \Psi CA\big)^T \Upsilon \bar{B}$ from (46). In addition, the computation of the term $\big(\Phi C + \Psi CA\big)$ is relaxed from [35] (refer to assumptions A2 *v.s.* A2.*s*). Literally, if $CB = 0$, then $\mathcal{S}_\Lambda(P,W,\Upsilon)$ is explicitly independent of W and L.

Basically, the condition Λ Hurwitz [9] makes the coupling matrix dynamics (42) stable. In the LMI (46), this matrix is selected *a priori*, eliminating the nonlinear term $PB\Lambda$, then leading to a sensitive trial-by-error procedure. Nonetheless, it is still possible to include the Hurwitz matrix Λ in the set of decision variables. Denoting by $R = PB\Lambda$ a new variable where B is full-column rank, the computation of the Hurwitz matrix Λ can be obtained from the following LMI problem.

Corollary 1 to Proposition 2 (LMI-based ESAO Design – Form 2)

Under assumptions A1, A2.*s*, A3–A5, if there exist matrices $P = P^T > 0$, $\Upsilon = \Upsilon^T > 0$ in $\mathbb{R}^{n\times n}$,

Prepared using acsauth.cls http://mc.manuscriptcentral.com/acsp-wiley DOI: 10.1002/acs

$R \in \mathbb{R}^{n\times p}$ and $W \in \mathbb{R}^{n\times m}$, *s.t.*

$$\begin{pmatrix} \mathcal{T}(P,W) & \mathcal{S}(P,R,W,\Upsilon) & PB & I_n & 0 \\ \mathcal{S}^T(P,R,W,\Upsilon) & -2\tilde{B}^T\Upsilon\tilde{B} & 0 & 0 & B^T \\ B^TP & 0 & -\frac{1}{2\delta}I_p & 0 & 0 \\ I_n & 0 & 0 & -\frac{1}{\delta}I_n & 0 \\ 0 & B & 0 & 0 & -\frac{1}{\delta}I_n \end{pmatrix} < 0 \tag{65}$$

and

$$B^TR + R^TB < 0 \tag{66}$$

with $\tilde{B} = \big(\Phi C + \Psi CA\big)B$, $\mathcal{T}(P,W) = PA + A^TP - WC - C^TW^T$, $\mathcal{S}(P,R,W,\Upsilon) = PAB - WCB - R - \big(\Phi C + \Psi CA\big)^T\Upsilon\tilde{B}$, Φ and Ψ in $\mathbb{R}^{n\times m}$, $\delta = \beta_u + \beta_0\beta > 0$, and if Γ is PE, then the state estimation error vector $\tilde{x}$ and the parameter estimate error vector $\tilde{\theta}$ of the nonlinear adaptive observer (40)–(45), designed for the nonlinear system (1) and (2), tend to zero exponentially as $t \to \infty$. The closed-loop observer gain matrix L is computed as $L = P^{-1}W$ and the Hurwitz matrix $\Lambda = \big(B^TPB\big)^{-1}B^TR \in \mathbb{R}^{p\times p}$ exists for any full-column rank matrix B and $P = P^T > 0$. $Q = Q^T > 0$ is selected freely in $\mathbb{R}^{q\times q}$.

Proof

It is similar to Proposition 2. Noting that the matrix B is of full-column rank, we denote by $R = PB\Lambda$ the additional decision variable. □

Definitely, the term $\mathcal{S}_\Lambda^T(P,W,\Upsilon)$ in (46) which is nonlinear in the unknown matrix Λ is now replaced by the term $\mathcal{S}(P,R,W,\Upsilon)$ linear in the new decision variables. The LMI (66) represents a conservative condition that is proposed to guarantee the convexity of the LMI problem by seeking a common Lypunov matrix P for the LMI (65) and the Hurwitz condition (66) simultaneously. In fact, we note that seeking a single Lyapunov matrix to investigate multiple constraints has been widely used in scientific literature (see [49] and references cited therein).

Alternatively, if $CB \neq 0$, we denote by $R = B^TPB\Lambda$ the new variable. Then, we can set up the following result:

Prepared using acsauth.cls http://mc.manuscriptcentral.com/acsp-wiley DOI: 10.1002/acs

Corollary 2 to Proposition 2 (LMI-based ESAO Design – Form 3)

Under assumptions A1, A2.*s*, A3–A5, if there exist matrices $P = P^T > 0$, $\Upsilon = \Upsilon^T > 0$ in $\mathbb{R}^{n\times n}$, $R \in \mathbb{R}^{p\times p}$ and $W \in \mathbb{R}^{n\times m}$, *s.t.*

$$\begin{pmatrix} B^T\mathcal{T}(P,W)B & \mathcal{S}(P,R,W,\Upsilon) & B^TPB & B^T & 0 \\ \mathcal{S}^T(P,R,W,\Upsilon) & -2\tilde{B}^T\Upsilon\tilde{B} & 0 & 0 & B^T \\ B^TPB & 0 & -\frac{1}{2\delta}I_p & 0 & 0 \\ B & 0 & 0 & -\frac{1}{\delta}I_n & 0 \\ 0 & B & 0 & 0 & -\frac{1}{\delta}I_n \end{pmatrix} < 0 \tag{67}$$

and

$$R + R^T < 0 \tag{68}$$

with $\tilde{B} = \big(\Phi C + \Psi CA\big)B$, $\mathcal{T}(P,W) = PA + A^TP - WC - C^TW^T$, $\mathcal{S}(P,R,W,\Upsilon) = B^TPAB - B^TWCB - R - \tilde{B}^T\Upsilon\tilde{B}$, Φ and Ψ in $\mathbb{R}^{n\times m}$, $\delta = \beta_u + \beta_0\beta > 0$, and if Γ is PE, then the state estimation error vector $\tilde{x}$ and the parameter estimate error vector $\tilde{\theta}$ of the nonlinear adaptive observer (40)–(45), designed for the nonlinear system (1) and (2), tend to zero exponentially as $t \to \infty$. The closed-loop observer gain matrix L is computed as $L = P^{-1}W$ and the Hurwitz matrix $\Lambda = \big(B^TPB\big)^{-1}R \in \mathbb{R}^{p\times p}$ exists for any full-column rank matrix B and $P = P^T > 0$. $Q = Q^T > 0$ can be freely in $\mathbb{R}^{q\times q}$.

Proof

It is similar to Proposition 2. In addition, noting that the matrix B is of full-column rank and denoting by $R = B^TPB\Lambda$, we substitute the nonlinear inequality (46), in Λ, P and W, by the new form (67) obtained from the pre-multiplication and post-multiplication of (46) by the block-diagonal matrices $\mathrm{diag}(B^T, I_p, I_p, I_n, I_n)$ and $\mathrm{diag}(B, I_p, I_p, I_n, I_n)$, respectively. □

5. ILLUSTRATIVE EXAMPLE

In this section, we present the example that motivates the techniques discussed in this paper. We consider a two-degree-of-freedom helicopter simulator model actuated with two propellers [50].

DOI: 10.1002/acs

The front propeller controls the elevation of the helicopter nose about the pitch axis and the back propeller controls the side to side motions of the helicopter about the yaw axis. We define [50]

$$\left(J_p + ml^2\right)\ddot{\phi} = K_{pp}u_p + K_{py}u_y - B_p\dot{\phi} - mgl \cdot \cos\phi - ml^2 \sin\phi \cos\phi \cdot \dot{\psi}^2 \tag{69}$$

and

$$\left(J_y + ml^2 \cos^2\phi\right)\ddot{\psi} = K_{yp}u_p + K_{yy}u_y - B_y\dot{\psi} + 2ml^2 \sin\phi \cos\phi \cdot \dot{\phi}\dot{\psi} \tag{70}$$

where u_p and u_y are the applied forces, ϕ the pitch angle position, ψ the yaw angle position, $\dot{\phi}$ and $\dot{\psi}$ the pitch and yaw angular velocities. B_p (*resp.* B_y) is the viscous damping about pitch (*resp.* yaw) axis, J_p (*resp.* J_y) the moment of inertia about pitch (*resp.* yaw) pivot, K_{pp} (*resp.* K_{py}) the thrust torque constant acting on pitch axis from pitch (*resp.* yaw) motor/propeller, K_{yy} (*resp.* K_{yp}) the thrust torque constant acting on yaw axis from yaw (*resp.* pitch) motor/propeller, l the center-of-mass length along the helicopter body from pitch axis, m the mass of the helicopter and g the gravitational acceleration. We assume that only the pitch and yaw angles are measured. Let $x_1 = \phi$, $x_2 = \psi$, $x_3 = \dot{\phi}$ and $x_4 = \dot{\psi}$ be the states, $u = \begin{bmatrix} V_{m,p} & V_{m,y} \end{bmatrix}^T$ the input vector and $y = \begin{bmatrix} x_1 & x_2 \end{bmatrix}^T$ the output vector.

To deal with the nonlinear parametrization depicted in (70) when we tend to write the corresponding state representation, an approximation technique resulting in uncertain bounded terms is used to develop the modeling scheme. Denote $a = \frac{1}{J_y + ml^2}$. Noting that $ml^2a^2 \sin^2\phi \ll 1$, we apply the Taylor series decomposition to the nonlinear parameter dependent term $\frac{1}{J_y + ml^2\cos^2\phi}$ as $\frac{1}{J_y + ml^2\cos^2\phi} = \frac{a}{1 - ml^2a\sin^2\phi} = a + \mathcal{O}(\sin^2\phi)$ where $\mathcal{O}(\sin^2\phi) \triangleq ml^2a^2\sin^2\phi + m^2l^4a^3\sin^4\phi + m^3l^6a^4\sin^6\phi + \ldots$ is very small. We use this approximation to linearize the yaw dynamics (70) *w.r.t.* its independent parameters. We can also use a second order extended form of the approximation instead of the reduced approximation (limited to the constant $a = \frac{1}{J_y + ml^2}$) for the sake of accuracy. The plant (69) and (70) can be considered as nonlinear dynamics (1)–(2) subject to assumptions A1–A5 (and A2.*s*), where $x \in \mathbb{R}^4$ is the state vector, $u \in \mathbb{R}^2$ the input vector, $y \in \mathbb{R}^2$ the output and $\theta \in \mathbb{R}^9$ vector of unknown constant parameters. From (69) and (70), the components of the unknown parameter vector are $\theta_1 = \frac{K_{pp}}{J_p + ml^2}$, $\theta_2 =$

Prepared using acsauth.cls http://mc.manuscriptcentral.com/acsp-wiley DOI: 10.1002/acs

$\frac{K_{py}}{J_p+ml^2}, \theta_3 = \frac{B_p}{J_p+ml^2}, \theta_4 = \frac{mgl}{J_p+ml^2}, \theta_5 = \frac{ml^2}{J_p+ml^2}, \theta_6 = aK_{yp}, \theta_7 = aK_{yy}, \theta_8 = aB_y$ and $\theta_9 = aml^2$, respectively. The matrices A, B and C are given by:

$$A = \begin{pmatrix} 0 & 0 & 1 & 0 \\ 0 & 0 & 0 & 1 \\ 0 & 0 & 0 & 0 \\ 0 & 0 & 0 & 0 \end{pmatrix}, \; B = \begin{pmatrix} 0 & 0 \\ 0 & 0 \\ 1 & 0 \\ 0 & 1 \end{pmatrix}, \; C = \begin{pmatrix} 1 & 0 & 0 & 0 \\ 0 & 1 & 0 & 0 \end{pmatrix} \tag{71}$$

$f_m(y,u) = 0$, $f_u(x,u) = 0$ and $f(x,u) \in \mathbb{R}^{2\times 13}$ can be easily depicted from (69)–(70), according to the parameter vector θ defined above. Note that the matrices A, B and C respect in particular the equality conditions (3) and (4) of assumption A2, as well as assumption A2.*s*. We assume that all the input and state signals are bounded. The values of the actual parameters characterizing the simulated helicopter-based dynamics are determined in [50]. Moreover, the terms $\sin\phi\cos\phi\cdot\dot{\psi}^2$, $\sin\phi\cos\phi\cdot\dot{\phi}\dot{\psi}$, shown in (69) and (70) respectively, are not globally Lipschitz functions in the state variables (any function, which is not globally Lipschitz, can be referred to as a weak Lipschitz function if it is bounded). Nevertheless, we consider the terms depicted above as Lipschitz since in practice they are bounded (based on the boundedness of the states). The matrices Φ and Ψ are simply computed from the matrix equality (4) as

$$\Phi = \begin{pmatrix} 1 & 0 \\ 0 & 1 \\ 0 & 0 \\ 0 & 0 \end{pmatrix}, \; \Psi = \begin{pmatrix} 0 & 0 \\ 0 & 0 \\ 1 & 0 \\ 0 & 1 \end{pmatrix} \tag{72}$$

The computation of the ASAO gains L and P is based on the LMI design of the asymptotic stability (refer to Proposition 1). Meanwhile, the observer gains L, P, Υ and Λ of the ESAO scheme are computed based on the exponential stability (refer to Corollary 2 to Proposition 2, *i.e.*, ESAO –

Prepared using acsauth.cls http://mc.manuscriptcentral.com/acsp-wiley DOI: 10.1002/acs

Form 2). The observer and adaptation law parameters of the ASAO (19)–(22) are

$$P = \begin{pmatrix} 4471.1 & 0 & -25.6 & 0 \\ 0 & 4471.1 & 0 & -25.6 \\ -25.6 & 0 & 1.2 & 0 \\ 0 & -25.6 & 0 & 1.2 \end{pmatrix}, \; L = \begin{pmatrix} 23.9 & 0 \\ 0 & 23.9 \\ 3984.2 & 0 \\ 0 & 3984.2 \end{pmatrix} \tag{73}$$

The observer and adaptation law parameters of the ESAO (40)–(45) are therefore selected as

$$P = \begin{pmatrix} 6595.9 & 0 & -20.6 & 0 \\ 0 & 6595.9 & 0 & -20.6 \\ -20.6 & 0 & 0.8 & 0 \\ 0 & -20.6 & 0 & 0.8 \end{pmatrix}, \; L = \begin{pmatrix} 28.4 & 0 \\ 0 & 28.4 \\ 8776.3 & 0 \\ 0 & 8776.3 \end{pmatrix} \tag{74}$$

$$\Lambda = \begin{pmatrix} -4395.6 & 0 \\ 0 & -4395.6 \end{pmatrix}, \; \Upsilon = \begin{pmatrix} 6061.6 & 0 & 0 & 0 \\ 0 & 6061.6 & 0 & 0 \\ 0 & 0 & 3425.9 & 0 \\ 0 & 0 & 0 & 3425.9 \end{pmatrix} \tag{75}$$

and

$$Q = \mathrm{diag}(20,\ 20,\ 20,\ 20,\ 400,\ 20,\ 400,\ 2000,\ 200) \tag{76}$$

for both ASAO and ESAO schemes. The computation of the observer gains, in both cases, are cast as LMI problems which can easily be solved by using the interior point optimization method implemented in the MATLAB software using the LMI control toolbox [51]. While the selection of the adaptation matrix Q, which is significant for the algorithms proposed in this paper regarding the parameter estimation performance (rate and accuracy), is freely adjusted, it is reduced to a positive diagonal matrix (more simply, can be any positive scalar multiplying the identity matrix). In fact, the parametrization and the implementation of the proposed algorithms remain moderately easier (less laborious) than many other algorithms for the similar adaptive observer problems (see *e.g.* [11, 16, 17, 28, 30, 52]).

Consider the input signals $u_1 = 3.4 + 2.7\sin(4.3\pi t) + 4.0\sin(3.0\pi t + 0.4\pi) + 3.7\sin(2.0\pi t + 0.4\pi) + 3.2\sin(0.4\pi t) + 1.9\sin(0.3\pi t)$ and $u_2 = 1.0 + 3.1\sin(5.1\pi t - 0.25\pi) + 2.7\sin(3.1\pi t -$

Prepared using acsauth.cls http://mc.manuscriptcentral.com/acsp-wiley DOI: 10.1002/acs

$0.5\pi) + 2.5\sin(1.7\pi t + 0.4\pi) + 3.3\sin(\pi t + 0.5\pi) + 2.3\sin(0.6\pi t + 0.5\pi)$ which result in sufficiently PE signals. The simulation results for the estimation of the parameters and states are shown in Fig. 1–6. It can be seen that both the state and the parameter estimates converge to their actual values accurately. However, the transient responses of the ESAO design are more satisfactory than those of the ASAO (see Fig. 1–5). The estimation errors of the states are demonstrated within a very short time (see Fig. 6). Indeed, their convergences are much faster than the parameter estimate. We notice that we use the ASAO and ESAO schemes by considering the effect of the uncertainty approximations negligible. It should be pointed out that the effect of the approximation uncertainty due to the nonlinear parameter dependency within the yaw dynamics is well rejected and cannot be distinguished in the different estimation graphics shown. However, to deal with any external perturbation or any modeling uncertainty, given by $d(x,t)$ added to the system dynamics, the different adaptive observers discussed above can be extended to robust ASAO and ESAO designs based on any H_∞ minimization of the loop transfer from the lumped uncertainty amount $d(x,t)$ to the estimate errors (for instance, $\tilde{x}$). In addition, such multi-objective designs can be investigated under further LMI constraints encountering specific transient performances and robustness properties.

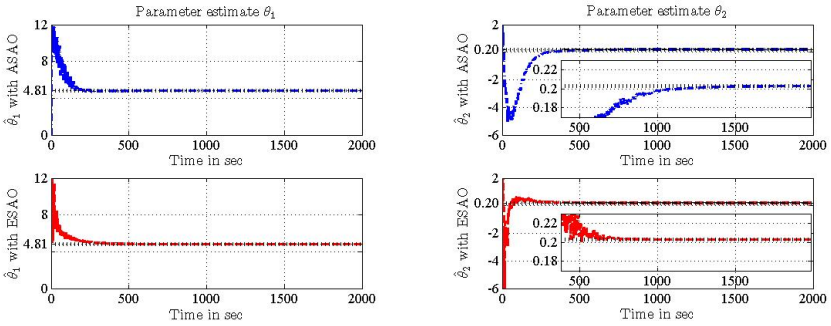

Figure 1. Estimate of parameters θ_1 and θ_2

Prepared using acsauth.cls http://mc.manuscriptcentral.com/acsp-wiley DOI: 10.1002/acs

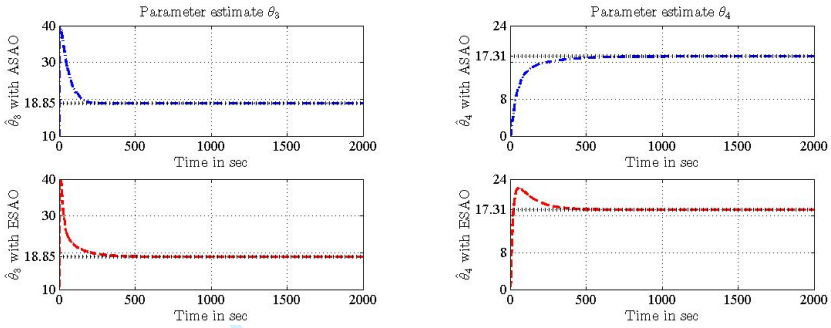

Figure 2. Estimate of parameters θ_3 and θ_4

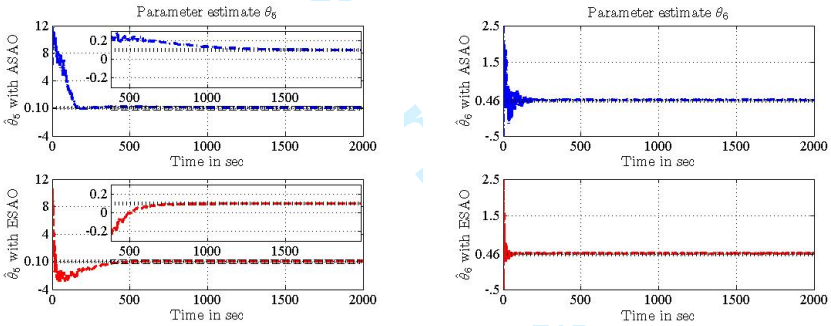

Figure 3. Estimate of parameters θ_5 and θ_6

6. CONCLUSIONS

In this paper, we propose the design of adaptive observers with asymptotic and exponential parameter estimation convergence for a general nonlinear system with unmeasured regressor matrix based on common Lipschitz and boundedness requirements. An example of a multi-input-multi-output dynamics is tested through simulation results that successfully demonstrate the effectiveness of the proposed algorithms which exhibit a satisfactory convergence of both the states and the

Prepared using acsauth.cls http://mc.manuscriptcentral.com/acsp-wiley DOI: 10.1002/acs

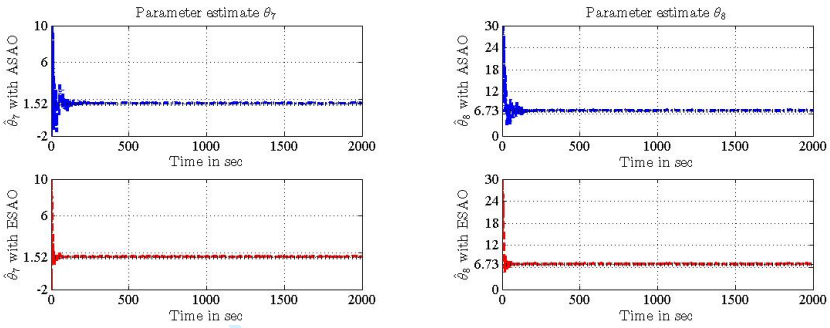

Figure 4. Estimate of parameters θ_7 and θ_8

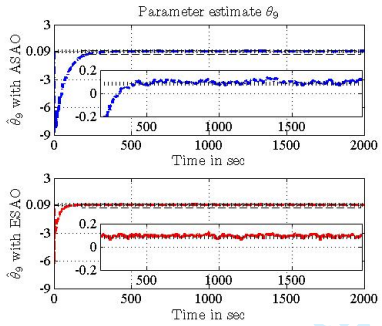

Figure 5. Estimate of parameter θ_9

parameters to the actual values. These results show an adequate comparison between the ASAO and ESAO performances.

REFERENCES

1. Marino R, Tomei P. Robust Adaptive Observers for Unknown Linear Exosystems. *International Journal of Adaptive Control and Signal Processing* 2013; **27**:35–45.

DOI: 10.1002/acs

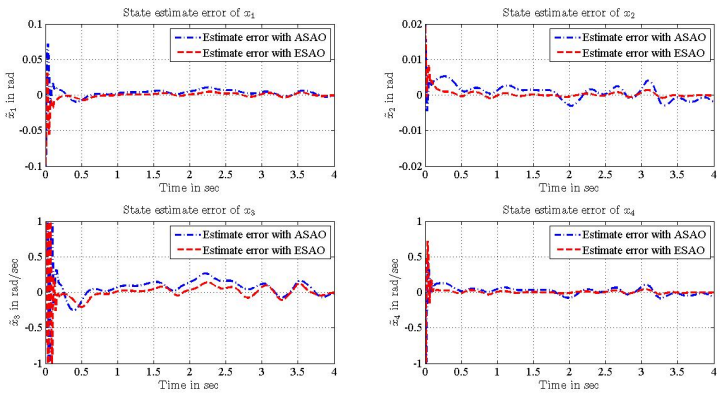

Figure 6. State estimate errors

2. Farza M, M'Saad M, Rossignol L. Observer Design for a Class of MIMO Nonlinear Systems. *Automatica* 2004; **40**:135–143.
3. Vargas J, Hemerly E. Adaptive Observers for Unknown General Nonlinear Systems. *IEEE Transactions on Systems, Man and Cybernetics – Part B* 2001; **31**(5):683–690.
4. Cho Y, Rajamani R. A Systematic Approach to Adaptive Observer Synthesis for Nonlinear Systems. *IEEE Transactions on Automatic Control* 1997; **42**(4):534–537.
5. Yaz E, Azemi A. Sliding Mode Observers for Nonlinear Models with Unbounded Noise and Measurement Uncertainties. *Journal of Dynamics and Control* 1993; **3**(3):217–235.
6. Luenberger D. An Introduction to Observers. *IEEE Transactions on Automatic Control* 1971; **16**(6):596–602.
7. Kalman R. A New Approach to Linear Filtering and Prediction Problems. *Journal of Basic Engineering* 1960; **82**:35–45.
8. Ioannou P, Fidan B. Adaptive Control Tutorial. *SIAM Studies in Applied Mathematics*. Society for Industrial and Applied Mathematics: Philadelphia, PA, 2006.
9. Khalil H. *Nonlinear Systems*. 3rd edn., Prentice-Hall: NY, 2002.
10. Khalil H. High-Gain Observers in Nonlinear Feedback Control. *IEEE International Conference on Control and Automation*, Christchurch, New Zealand, 2009; 1527–1528.
11. Zemouche A, Boutayeba M. A Unified Adaptive Observer Synthesis Method for a Class of Systems with Both Lipschitz and Monotone Nonlinearities. *Systems and Control Letters* 2009; **58**(4):282–288.

Prepared using acsauth.cls http://mc.manuscriptcentral.com/acsp-wiley DOI: 10.1002/acs

12. Paesa D, Franco C, Llorente S, Lopez-Nicolas G, Sagues C. On Robust PI Adaptive Observers for Nonlinear Uncertain Systems with Bounded Disturbances. *18th Mediterranean Conference on Control and Automation*, Marrakech, Morocco, 2010; 1031–1036.
13. Marino R, Santosuosso G, Tomei P. Robust Adaptive Observers for Nonlinear Systems with Bounded Disturbances. *IEEE Transactions on Automatic Control* 2001; **46**(6):967–972.
14. Ekramian M, Sheikholeslam F, Hosseinnia S, Yazdanpanah M. Adaptive State Observer for Lipschitz Nonlinear Systems. *Systems and Control Letters* 2013; **62**(3):319–323.
15. Mondal S, Chung W. Adaptive Observer for a Class of Nonlinear Systems with Time-Varying Delays. *International Journal of Adaptive Control and Signal Processing* 2012; Doi:10.1002/acs.2331.
16. Liu Y. Robust Adaptive Observer for Nonlinear Systems with Unmodeled Dynamics. *Automatica* 2009; **45**:1891–1895.
17. Maatoug T, Farza M, M'Saad M, Koubaa Y, Kamoun M. Adaptive Observer Design for a Class of Nonlinear Systems with Coupled Structures. *International Journal of Sciences and Techniques of Automatic Control and Computer Engineering* 2008; **2**(1):484–499.
18. Khayati K, Zhu J. Nonlinear Adaptive Observer Design for an Electromechanical Rotative Plant. *23rd Canadian Congress of Applied Mechanics*, Vancouver, Canada, 2011.
19. Zhu J, Khayati K. Adaptive Observer for a Class of Second Order Nonlinear Systems. *International Conference on Communications, Computing and Control Applications*, Hammamet, Tunisia, 2011.
20. Zhu J, Khayati K. On Robust Nonlinear Adaptive Observer – LMI Design. *International Conference on Mechanical Engineering and Mechatronics*, Ottawa, Canada, 2012.
21. Zhu J, Khayati K. LMI-based Adaptive Observers for Nonlinear Systems. *International Journal of Mechanical Engineering and Mechatronics* 2012; :50–60Doi:10.11159/ijmem.2012.006.
22. Li X, Zhang Q, Su H. An Adaptive Observer for Joint Estimation of States and Parameters in Both State and Output Equations. *International Journal of Adaptive Control and Signal Processing* 2011; **25**:831–842.
23. Zhao Z, Xie WF, Hong H, Zhang Y. A Disturbance Decoupled Adaptive Observer and Its Application to Faulty Parameters Estimation of a Hydraulically Driven Elevator. *International Journal of Adaptive Control and Signal Processing* 2011; **25**:519–534.
24. Zhang Q. Adaptive Observer for Multiple-Input-Multiple-Output (MIMO) Linear Time-Varying Systems. *IEEE Transactions on Automatic Control* 2002; **47**(3):525–529.
25. Bobtsov A, Efimov D, Pyrkin A. Hybrid Adaptive Observers for Locally Lipschitz Systems. *International Journal of Adaptive Control and Signal Processing* 2011; **25**:33–47.
26. Tyukin I, Steur E, Nijmeijer H, Leeuwen C. Adaptive Observers and Parameter Estimation for a Class of Systems Nonlinear in the Parameters. *Automatica* 2013; **49**(8):2409–2423.
27. Marino R, Tomei P. Global Adaptive Observers for Nonlinear Systems via Filtered Transformations. *IEEE Transactions on Automatic Control* 1992; **37**(8):1239–1245.
28. Besanon G. Remarks on Nonlinear Adaptive Observer Design. *Systems and Control Letters* 2000; **41**:271–280.

Prepared using acsauth.cls http://mc.manuscriptcentral.com/acsp-wiley DOI: 10.1002/acs

29. Stamnes O, Aamo O, Kaasa G. Adaptive Redesign of Nonlinear Observers. *IEEE Transactions on Automatic Control* 2001; **56**(5):1152–1157.
30. Stamnes O, Zhu J, Aamo O, Kaasa G. Adaptive Observer Design for Nonlinear Systems with Parametric Uncertainties in Unmeasured State Dynamics. *IEEE Conference on Decision and Control and Chinese Control Conference*, Shanghai, China, 2009; 4414–4419.
31. Khayati K, Zhu J. Exponentially Stable Nonlinear Adaptive Observer – LMI Design. *International Conference on Mechanical Engineering and Mechatronics*, Ottawa, Canada, 2012.
32. Marino R, Tomei P. Adaptive Observers with Arbitrary Exponential Rate of Convergence for Nonlinear Systems. *IEEE Transactions on Automatic Control* 1995; **40**(7):1300–1304.
33. Cao L, Schwartz H. Exponential Convergence of the Kalman Filter-Based Parameter Estimation Algorithm. *International Journal of Adaptive Control and Signal Processing* 2003; **17**:763–783.
34. Patre P, Joshi S. On Using Exponential Parameters with an Adaptive Controller. *Technical Report*, NASA, Hampton 2011. Technical Report.
35. Khayati K, Zhu J. Adaptive Observer for a Large Class of Nonlinear System with Exponential Convergence of Parameter Estimation. *International Conference on Control, Decision and Information Technologies*, Hammamet, Tunisia, 2013.
36. Dong Y, Mei S. Adaptive Observer for a Class of Nonlinear Systems. *Acta Automatica Sinica* 2007; **33**(10):1081–1084.
37. Erlic M, Lu WS. A Reduced Order Adaptive Velocity Observer Synthesis for Manipulator Control. *IEEE Transactions on Robotics and Automation* 1995; **11**(2):293–303.
38. Zhu Y, Pagilla P. Adaptive Controller and Observer Design for a Class of Nonlinear Systems. *Transactions of the ASME* 2006; **128**:712–717.
39. Spong M, Hutchinson S, Vidyasagar M. *Robot Modeling and Control*. John Wiley & Sons Inc.: NY, 2005.
40. Rajamani R, Hedrick J. Adaptive Observers for Active Automotive Suspensions: Theory and Experiment. *IEEE Transactions on Control Systems Technology* 1995; **3**(1):86–93.
41. Rajamani R. Observers for Lipschitz for Nonlinear Systems. *IEEE Transactions on Automatic Control* 1998; **43**(3):397–401.
42. Stepanyan V, Hovakimyan N. Robust Adaptive Observer Design for Uncertain Systems with Bounded Disturbances. *IEEE Conference on Decision and Control and 2005 European Control Conference*, Seville, Spain, 2005; 7750–7755.
43. Besanon G, Zhang Q. Further Developments on Adaptive Observers for Nonlinear Systems with Application in Fault Detection. *15th Triennial World Congress*, vol. 15, Barcelona, Spain, 2002; 732–735.
44. Boyd S, El-Ghaoui L, Feron E, Balakrishnan V. Linear Matrix Inequalities in Systems and Control Theory. *SIAM Studies in Applied Mathematics*, vol. 15. Society for Industrial and Applied Mathematics: Philadelphia, PA, 1994.
45. Ioannou P, Sun J. *Robust Adaptive Control*. 2nd edn., Prentice-Hall: NY, 2003.

Prepared using acsauth.cls http://mc.manuscriptcentral.com/acsp-wiley DOI: 10.1002/acs

46. Phanomchoeng G, Rajamani R. Observer Design for Lipschitz Nonlinear Systems using Riccati Equations. *American Control Conference*, Baltimore, MD, 2010; 6060–6065.
47. Ioannou P, Fidan B. *Adaptive Control Tutorial: Part of Advances in Design and Control*. The Society for Industrial and Applied Mathematics: PA, 2007.
48. Micaelli A, Samson C. Trajectory Tracking for Unicycle-Type and two-Steering-Wheels Mobile Robots. *Technical Report*, INRIA, Sophia-Antipolis, France 1993. Technical Report.
49. Chilali M, Gahinet P. H_∞ Design with Pole Placement Constraints: An LMI Approach. *IEEE Transactions on Automatic Control* 1996; **41**(3):358–367.
50. Quanser. *2 DOF Helicopter User and Control Manual*. Quanser 2006.
51. Gahinet P, Nemirovskii A, Laub A, Chilali M. MATLAB LMI Control Toolbox. MathWorks Inc., 1995.
52. Pourgholi M, Majd V. A Nonlinear Adaptive Resilient Observer Design for a Class of Lipschitz Systems using LMI. *Journal of Circuits, Systems, and Signal Processing* 2011; **30**(6):1401–1415.

APPENDIX A – PROOF OF LEMMA 1

We recall the following inequality

$$(x+y)^2 \geq \frac{1}{2}x^2 - y^2 \tag{A-1}$$

First, using the inequality (A-1), we write, for $\tau > 0$ and $t > 0$

$$\begin{aligned}\tilde{\theta}(\tau)^T\Gamma(\tau)^T\Gamma(\tau)\tilde{\theta}(\tau) &= \Big[\tilde{\theta}(t)+\big(\tilde{\theta}(\tau)-\tilde{\theta}(t)\big)\Big]^T\Gamma(\tau)^T\Gamma(\tau)\Big[\tilde{\theta}(t)+\big(\tilde{\theta}(\tau)-\tilde{\theta}(t)\big)\Big]\\ &\geq \frac{1}{2}\big(\Gamma(\tau)\tilde{\theta}(t)\big)^T\big(\Gamma(\tau)\tilde{\theta}(t)\big) - \big(\tilde{\theta}(\tau)-\tilde{\theta}(t)\big)^T\Gamma(\tau)^T\\ &\quad \Gamma(\tau)\big(\tilde{\theta}(\tau)-\tilde{\theta}(t)\big)\end{aligned} \tag{A-2}$$

From (47), we have, for $t > 0$ and $t_0 > 0$

$$\begin{aligned}\frac{1}{2}\int_t^{t+t_0}\big(\Gamma(\tau)\tilde{\theta}(t)\big)^T\big(\Gamma(\tau)\tilde{\theta}(t)\big)d\tau &= \frac{1}{2}\int_t^{t+t_0}\tilde{\theta}(t)^T\Gamma(\tau)^T\Gamma(\tau)\tilde{\theta}(t)d\tau\\ &= \frac{1}{2}\tilde{\theta}(t)^T\int_t^{t+t_0}\Gamma(\tau)^T\Gamma(\tau)d\tau\tilde{\theta}(t)\\ &\geq \frac{\alpha_0 t_0}{2}\tilde{\theta}(t)^T\tilde{\theta}(t)\end{aligned} \tag{A-3}$$

Now, we note that

$$\tilde{\theta}(\tau)-\tilde{\theta}(t) = \int_t^\tau \dot{\tilde{\theta}}(s)ds \tag{A-4}$$

Prepared using acsauth.cls http://mc.manuscriptcentral.com/acsp-wiley DOI: 10.1002/acs

Using the Schwartz inequality [45], we have

$$\begin{aligned}\int_t^{t+t_0}\big(\tilde\theta(\tau)-\tilde\theta(t)\big)^T\Gamma(\tau)^T\Gamma(\tau)\big(\tilde\theta(\tau)-\tilde\theta(t)\big)d\tau &= \int_t^{t+t_0}\Big[\int_t^\tau\dot{\tilde\theta}(s)ds\Big]^T\Gamma(\tau)^T\Gamma(\tau)\Big[\int_t^\tau\dot{\tilde\theta}(s)ds\Big]d\tau\\ &\le \int_t^{t+t_0}\Big[\int_t^\tau\Gamma(\tau)\dot{\tilde\theta}(s)ds\Big]^T\Big[\int_t^\tau\Gamma(\tau)\dot{\tilde\theta}(s)ds\Big]d\tau\\ &\le \int_t^{t+t_0}\int_t^\tau\|\Gamma(\tau)\|^2ds\cdot\int_t^\tau\|\dot{\tilde\theta}(s)\|^2dsd\tau \qquad \text{(A-5)}\end{aligned}$$

Since $\Gamma\in\mathcal{L}_\infty$, *i.e.*, $\rho_2=\sup_{\tau\ge0}\|\Gamma(\tau)\|$ is a finite constant, we have

$$\int_t^{t+t_0}\big(\tilde\theta(\tau)-\tilde\theta(t)\big)^T\Gamma(\tau)^T\Gamma(\tau)\big(\tilde\theta(\tau)-\tilde\theta(t)\big)d\tau\le\int_t^{t+t_0}(\tau-t)\rho_2^2\cdot\int_t^\tau\|\dot{\tilde\theta}(s)\|^2dsd\tau \qquad \text{(A-6)}$$

Then, using the integration by parts, we obtain

$$\begin{aligned}\int_t^{t+t_0}\big(\tilde\theta(\tau)-\tilde\theta(t)\big)^T\Gamma(\tau)^T\Gamma(\tau)\big(\tilde\theta(\tau)-\tilde\theta(t)\big)d\tau &\le \rho_2^2\int_t^{t+t_0}\|\dot{\tilde\theta}(\tau)\|^2\cdot\int_\tau^{t+t_0}(s-t)dsd\tau\\ &\le \rho_2^2\int_t^{t+t_0}\|\dot{\tilde\theta}(\tau)\|^2\cdot\big(\frac{t_0^2}{2}-\frac{(\tau-t)^2}{2}\big)d\tau\\ &\le \rho_2^2\frac{t_0^2}{2}\int_t^{t+t_0}\|\dot{\tilde\theta}(\tau)\|^2d\tau\\ &\le \rho_2^2\frac{t_0^2}{2}\int_t^{t+t_0}\|G(\tau)^TP\|^2\|\tilde x\|^2d\tau \qquad \text{(A-7)}\end{aligned}$$

From (45), we note that $G\in\mathcal{L}_\infty$, *i.e.*, $\rho_3=\sup_{\tau\ge0}\|G(\tau)^TP\|$ is a finite positive constant. Then, using $\tilde x=\chi+B\Gamma\tilde\theta$, we have

$$\int_t^{t+t_0}\big(\tilde\theta(\tau)-\tilde\theta(t)\big)^T\Gamma(\tau)^T\Gamma(\tau)\big(\tilde\theta(\tau)-\tilde\theta(t)\big)d\tau\le\rho_2^2\rho_3^2\frac{t_0^2}{2}\int_t^{t+t_0}\big(\|\chi\|^2+\|B\Gamma\tilde\theta\|^2\big)d\tau \qquad \text{(A-8)}$$

Now, using $\|B\Gamma\tilde\theta\|\le\rho_4\|\Gamma\tilde\theta\|$ with $\rho_4=\|B\|>0$, we obtain from (A-8)

$$\int_t^{t+t_0}\big(\tilde\theta(\tau)-\tilde\theta(t)\big)^T\Gamma(\tau)^T\Gamma(\tau)\big(\tilde\theta(\tau)-\tilde\theta(t)\big)d\tau\le\rho_2^2\rho_3^2\frac{t_0^2}{2}\int_t^{t+t_0}\big(\|\chi\|^2+\rho_4^2\|\Gamma\tilde\theta\|^2\big)d\tau \qquad \text{(A-9)}$$

Integrating (A-2) between t and $t+t_0$, and using (A-3) and (A-9), we have

$$\begin{aligned}\int_t^{t+t_0}\tilde\theta^T\Gamma^T\Gamma\tilde\theta d\tau &\ge \frac12\int_t^{t+t_0}\big(\Gamma(\tau)\tilde\theta(t)\big)^T\big(\Gamma(\tau)\tilde\theta(t)\big)d\tau-\\ &\quad\int_t^{t+t_0}\big(\tilde\theta(\tau)-\tilde\theta(t)\big)^T\Gamma(\tau)^T\Gamma(\tau)\big(\tilde\theta(\tau)-\tilde\theta(t)\big)d\tau\\ &\ge \frac{\alpha_0t_0}{2}\tilde\theta(t)^T\tilde\theta(t)-\rho_2^2\rho_3^2\frac{t_0^2}{2}\int_t^{t+t_0}\big(\|\chi\|^2+\rho_4^2\|\Gamma\tilde\theta\|^2\big)d\tau \qquad \text{(A-10)}\end{aligned}$$

Thus, we have

$$\eta_2\int_t^{t+t_0}\chi^T\chi d\tau+\eta_3\int_t^{t+t_0}\tilde\theta^T\Gamma^T\Gamma\tilde\theta d\tau\ge\frac{\alpha_0t_0}{2}\tilde\theta(t)^T\tilde\theta(t) \qquad \text{(A-11)}$$

Prepared using acsauth.cls http://mc.manuscriptcentral.com/acsp-wiley DOI: 10.1002/acs

with $\eta_2 = \rho_2^2\rho_3^2\frac{t_0^2}{2}$ and $\eta_3 = 1 + \rho_2^2\rho_3^2\rho_4^2\frac{t_0^2}{2}$.

Second, using the inequality (A-1), we write, for $\tau > 0$ and $t > 0$

$$\begin{aligned}\chi^T(\tau)\chi(\tau) &= \Big[\chi(t) + \big(\chi(\tau) - \chi(t)\big)\Big]^T\Big[\chi(t) + \big(\chi(\tau) - \chi(t)\big)\Big] \\ &\geq \frac{1}{2}\chi(t)^T\chi(t) - \big(\chi(\tau) - \chi(t)\big)^T\big(\chi(\tau) - \chi(t)\big) \qquad \text{(A-12)}\end{aligned}$$

Noting that

$$\chi(\tau) - \chi(t) = \int_t^\tau \dot{\chi}(s)ds \qquad \text{(A-13)}$$

and using the Schwartz inequality [45], we obtain

$$\begin{aligned}\int_t^{t+t_0}\big(\chi(\tau) - \chi(t)\big)^T\big(\chi(\tau) - \chi(t)\big)d\tau &= \int_t^{t+t_0}\Big[\int_t^\tau \dot{\chi}(s)ds\Big]^T\Big[\int_t^\tau \dot{\chi}(s)ds\Big]d\tau \\ &\leq \int_t^{t+t_0}\|\int_t^\tau \dot{\chi}(s)ds\|^2 d\tau \\ &\leq \int_t^{t+t_0}\Big(\int_t^\tau ds\Big)\Big(\int_t^\tau \|\dot{\chi}(s)\|^2 ds\Big)d\tau \\ &\leq \int_t^{t+t_0}(\tau - t)\Big(\int_t^\tau \|\dot{\chi}(s)\|^2 ds\Big)d\tau \qquad \text{(A-14)}\end{aligned}$$

Then, using the integration by parts, we obtain

$$\begin{aligned}\int_t^{t+t_0}\big(\chi(\tau) - \chi(t)\big)^T\big(\chi(\tau) - \chi(t)\big)d\tau &\leq \int_t^{t+t_0}\|\dot{\chi}(\tau)\|^2\cdot\Big(\int_\tau^{t+t_0}(s-t)ds\Big)d\tau \\ &\leq \int_t^{t+t_0}\|\dot{\chi}(\tau)\|^2\cdot\big(\frac{t_0^2}{2} - \frac{(\tau-t)^2}{2}\big)d\tau \\ &\leq \frac{t_0^2}{2}\int_t^{t+t_0}\|\dot{\chi}(\tau)\|^2 d\tau \qquad \text{(A-15)}\end{aligned}$$

From (49), using (5)–(7), we have

$$\begin{aligned}\|\dot{\chi}\|^2 &\leq \|A - LC\|^2\|\chi\|^2 + \|B\|^2\big(\|\tilde{f}_u\|^2 + \|\tilde{f}\|^2\|\theta\|^2\big)\|\tilde{x}\|^2 + \|\bar{B}\|^2\|\Gamma\tilde{\theta}\|^2 \\ &\leq \|A - LC\|^2\|\chi\|^2 + \rho_4^2\big(\beta_u^2 + \beta^2\beta_0^2\big)\big(\|\chi\|^2 + \|B\|^2\|\Gamma\tilde{\theta}\|^2\big) + \|\bar{B}\|^2\|\Gamma\tilde{\theta}\|^2 \\ &\leq \Big(\rho_4^2\big(\beta_u^2 + \beta^2\beta_0^2\big) + \rho_5^2\Big)\|\chi\|^2 + \Big(\rho_4^4\big(\beta_u^2 + \beta^2\beta_0^2\big) + \rho_6^2\Big)\|\Gamma\tilde{\theta}\|^2 \qquad \text{(A-16)}\end{aligned}$$

with $\rho_5 = \|A - LC\|$ and $\rho_6 = \|\bar{B}\|$. Then,

$$\begin{aligned}\int_t^{t+t_0}\big(\chi(\tau) - \chi(t)\big)^T\big(\chi(\tau) - \chi(t)\big)d\tau \leq \Big(\rho_4^2\big(\beta_u^2 + \beta^2\beta_0^2\big) + \rho_5^2\Big)\frac{t_0^2}{2}\int_t^{t+t_0}\|\chi\|^2 d\tau + \\ \Big(\rho_4^4\big(\beta_u^2 + \beta^2\beta_0^2\big) + \rho_6^2\Big)\frac{t_0^2}{2}\int_t^{t+t_0}\|\Gamma\tilde{\theta}\|^2 d\tau \qquad \text{(A-17)}\end{aligned}$$

Prepared using acsauth.cls http://mc.manuscriptcentral.com/acsp-wiley DOI: 10.1002/acs

Integrating (A-12) between t and $t+t_0$, and using (A-15) and (A-17), we obtain

$$\int_t^{t+t_0} \chi^T(\tau)\chi(\tau)d\tau \geq \frac{t_0}{2}\chi(t)^T\chi(t) - \left(\rho_4^2\left(\beta_u^2+\beta^2\beta_0^2\right)+\rho_5^2\right)\frac{t_0^2}{2}\int_t^{t+t_0}\chi^T\chi d\tau - \left(\rho_4^4\left(\beta_u^2+\beta^2\beta_0^2\right)+\rho_6^2\right)\frac{t_0^2}{2}\int_t^{t+t_0}\|\Gamma\tilde{\theta}\|^2 d\tau \quad \text{(A-18)}$$

Thus, we have

$$\eta_4\int_t^{t+t_0}\chi^T(\tau)\chi(\tau)d\tau + \eta_5\int_t^{t+t_0}\tilde{\theta}^T\Gamma^T\Gamma\tilde{\theta}d\tau \geq \frac{t_0}{2}\chi(t)^T\chi(t) \quad \text{(A-19)}$$

with $\eta_4 = 1+\rho_4^2\left(\beta_u^2+\beta^2\beta_0^2\right)\frac{t_0^2}{2}+\rho_5^2\frac{t_0^2}{2}$ and $\eta_5 = \left(\rho_4^4\left(\beta_u^2+\beta^2\beta_0^2\right)+\rho_6^2\right)\frac{t_0^2}{2}$

Now, combine (A-11) and (A-19)

$$\left(\eta_2+\eta_4\right)\int_t^{t+t_0}\chi^T\chi d\tau + \left(\eta_3+\eta_5\right)\int_t^{t+t_0}\tilde{\theta}^T\Gamma^T\Gamma\tilde{\theta}d\tau \geq \frac{t_0}{2}\chi(t)^T\chi(t) + \frac{\alpha_0 t_0}{2}\tilde{\theta}(t)^T\tilde{\theta}(t) \quad \text{(A-20)}$$

Then, given $\bar{\eta} = \max\left(\eta_2+\eta_4, \eta_3+\eta_5\right)$, we have

$$\int_t^{t+t_0}\chi^T\chi d\tau + \int_t^{t+t_0}\tilde{\theta}^T\Gamma^T\Gamma\tilde{\theta}d\tau \geq \frac{t_0}{2\bar{\eta}}\chi(t)^T\chi(t) + \frac{\alpha_0 t_0}{2\bar{\eta}}\tilde{\theta}(t)^T\tilde{\theta}(t) \geq \epsilon_0\left(\chi(t)^T\chi(t)+\tilde{\theta}(t)^T\tilde{\theta}(t)\right) \quad \text{(A-21)}$$

with $\epsilon_0 = \min\left(\frac{t_0}{2\bar{\eta}}, \frac{t_0\alpha_0}{2\bar{\eta}}\right) > 0$. Moreover, ϵ_0 can be selected as $\epsilon_0 < \min\left(\frac{t_0}{2\bar{\eta}}, \frac{t_0\alpha_0}{2\bar{\eta}}, \frac{k_2}{\varepsilon}\right)$ where k_2 and ε are introduced in (53) and (34), respectively.

Prepared using acsauth.cls http://mc.manuscriptcentral.com/acsp-wiley DOI: 10.1002/acs